13th International Conference on Coasts, Ports and Marine Structures

26th - 28th November 2018 | Olympic Hotel, Tehran, Iran

ICOPMAS 2018

CONFERENCE PROCEEDINGS

ICOPMAS
2018

ICOPMAS 2018

13th International Conference on Coasts, Ports, and Marine Structures PROCEEDINGS

پیام محمد راستاد، معاون وزیر راه و شهرسازی و مدیرعامل سازمان بنادر و دریانوردی به سیزدهمین همایش بین‌المللی سواحل، بنادر و سازه‌های دریایی (ICOPMAS 2018)

همایش دوسالانه بین‌المللی سواحل، بنادر و سازه‌های دریایی (ICOPMAS) یکی از ممتازترین رویدادهای علمی، پژوهشی و کاربردی در کشور و منطقه است که طی ۲۸ سال گذشته با برگزاری منظم و موثر، بستری مناسب برای تبادل نظر و انتقال تجربیات میان جامعه متخصصین و فرهیختگان دریایی کشور با دانشمندان و نخبگان ملی و بین‌المللی فراهم کرده است.

سیزدهمین دوره این رویداد علمی موسوم به (ICOPMAS 2018) در حالی تازه‌ترین یافته‌ها و دستاوردهای علمی در حوزه هیدرودینامیک و رسوب، مدیریت بنادر، مهندسی ساحل و فراساحل، مهندسی خطوط لوله، محیط‌زیست دریایی و ایمنی را با دانشجویان، استادان دانشگاه و نخبگان دریایی و بندری به اشتراک می‌گذارد که بر «فرهنگ‌سازی در بهره‌برداری پایدار از سواحل و دریا» به‌عنوان یکی از مهم‌ترین رویکردهای این نشست علمی تاکید شده است.

همایش سواحل، بنادر و سازه‌های دریایی ضمن تداوم پیوند دانش مهندسی بنادر و سواحل ایران با پیشگامان علمی جهان در این عرصه، گویای عزم جدی سازمان بنادر و دریانوردی به‌عنوان مرجع دریایی کشور در ارتقای علوم و فنون مدیریت سواحل و مهندسی بندری و سازه‌های دریایی است.

اندیشگاه ICOPMAS با عرضه و ارائه یافته‌ها و دست‌آوردهای علمی، تجربی و فنی جامعه مهندسان دریایی در زمینه سواحل، بنادر و سازه‌های دریایی در سطح بین‌المللی، عرصه‌ای برای تلاش مجدانه سازمان بنادر و دریانوردی و سایر ارگان‌های مرتبط دریایی کشور و ایفای مسئولیت اجتماعی آنها در برابر کلیه شهروندان از جمله ساحل‌نشینان قلمداد می‌شود تا پاسخی برای پرسش‌ها، نیازها و ضرورت‌های توسعه دریایی فراهم سازد.

نزدیک به سه دهه است که این همایش با حضور چهره‌های صاحب‌نظر علمی از شرکت‌ها و دانشگاه‌های معتبر جهان به‌عنوان یک رخداد پایدار و انکارناپذیر در ایجاد ارتباط مستحکم بین‌المللی و تبادل علم و دانش و تجربه میان دانشمندان، اندیشمندان، صاحب‌نظران و پژوهشگران کشورهای قدرتمند و مطرح دریایی، نقش بسیار موثری در ارتقای جایگاه جمهوری اسلامی ایران در همکاری‌های منطقه‌ای و بین‌المللی ایفا نموده است.

به دنبال تحولات صورت گرفته در حوزه‌های اقتصاد سیاسی بین‌الملل و ارتقای ظرفیت بندری و پسکرانه‌ای جمهوری اسلامی ایران طی دو سال گذشته، هم‌اکنون رویکرد توسعه‌گرایانه به همایش ICOPMAS ، این فرصت گران‌بها را پیش روی جامعه دریایی کشور قرار داده تا کلیه متخصصان، اندیشمندان و ارگان‌های مختلف دریایی بتوانند همپای اساتید برجسته این رشته و نهادهای بین‌المللی ذی‌ربط، مباحث و موضوعات مختلف تخصصی را در این کانون مهم علم و تجربه از دانش فنی و تخصصی دریایی مطرح و رهیافت‌های موثر و مفیدی را در جهت توسعه و ارتقای این علوم در پاسخ به نیازهای کنونی و آینده جوامع بشری و توسعه پایدار ملی و منطقه‌ای ترسیم نمایند.

از آنجا که سیزدهمین همایش سواحل، بنادر و سازه‌های دریایی (ICOPMAS 2018) راهی برای دستیابی به منابع و بازارهای جهانی و باقی ماندن در فضای رقابت فراهم می‌سازد، انتظار می‌رود گردهمایی متخصصان، دانشمندان و مهندسان دریایی و بندری، اتاق فکری جهت ارتقای دانش مهندسی سواحل و بنادر ایجاد کرده و عرصه‌های بین‌المللی را برای نمایان ساختن توانمندی‌های محققین و متخصصین داخلی جهت همکاری‌های آتی فراهم آورد.

همچنین پیش‌بینی می‌شود، بستر لازم جهت بهینه‌سازی طرح‌های زیربنایی، بکارگیری راهکارها و رویکردهای جدید جهت ارتقای سیستم‌های نوین مدیریتی و استفاده از فناوری‌های به روز و بهینه در حوزه سواحل، بنادر و سازه‌های دریایی نیز با برگزاری این همایش مهیا شود؛ در این ارتباط ظرفیت‌های قانونی مناسبی در کشور فراهم شده و حمایت‌های قابل‌توجهی توسط سازمان‌ها و نهادهای دولتی مرتبط انجام می‌شود تا انتقال سریع یافته‌های علمی و نوآوری‌ها به مرحله تولید و عملیات تحقق یابد و رقابت‌پذیری و پایداری این صنعت تسهیل شود.

امیدوارم برگزاری همایش بین‌المللی سواحل، بنادر و سازه‌های دریایی، ضمن «زمینه‌سازی و برنامه‌ریزی جهت توسعه همکاری‌های کارفرمایان، مهندسان مشاور، پیمانکاران و دیگر متقاضیان ارائه خدمات با جامعه بین‌المللی»، جایگاه بنادر به عنوان پل ارتباطی با اقتصاد جهانی و ایجاد فرصت‌های متنوع اشتغال و کارآفرینی را ارتقاء دهد.

در پایان، توفیق روزافزون همگان را از درگاه خداوند متعال خواستارم.

تحقق اقتصاد دریاپایه در سایه آیکوپمس

پیام محمدرضا الهیار، معاون مهندسی و توسعه امور زیربنایی سازمان بنادر و دریانوردی و قائم‌مقام رئیس به سیزدهمین همایش بینالمللی سواحل، بنادر و سازه‌های دریایی (ICOPMAS 2018)

گستردگی سواحل کشور در شمال و جنوب، دسترسی به آب‌های آزاد، وجود جزایر متعدد با قابلیت‌های مختلف و... فرصت بی‌نظیری را در اختیار کشور قرار داده تا با بهره‌برداری مناسب، پایدار و متوازن از ظرفیت‌های دریا و سواحل در کاربری‌های مختلفی چون صنعتی، نفتی، شیلاتی، سفر دریایی، تجاری و بازرگانی و گردشگری و تفریحی بتوان به رشد و توسعه کشور کمک نمود. البته نباید در کنار این ظرفیت‌ها از موقعیت استراتژیک و ژئوپلیتیک کشور و قرار گرفتن ایران در چهارراه شرق - غرب و جنوب - شمال غافل بود که فرصت کم‌نظیری را برای کشور مهیا کرده است تا پیشگام صنعت حمل‌ونقل و خصوصاً تجارت دریایی در منطقه باشد.

پرواضح است پیش‌نیاز استفاده از این نعمت خدادادی داشتن برنامه‌ای مناسب، هوشمند و جامع مبتنی بر تجارب جهانی با تکیه بر دانش بومی و ملی است. اما به اعتقاد اندیشمندان و نظریه‌پردازان دانش روز، ابتدایی‌ترین مرحله تدوین این برنامه، داشتن اطلاعات پایه دریایی، شناخت پدیده‌ها و مشخصه‌های اقلیمی و محیطی و تحلیل رفتار و اثر این پدیده‌ها بر مناطق ساحلی و ساخت‌وسازهای دریایی در مقیاسِ فراساحل، بندری و ساحلی است. از آنجا که دانش مهندسی و مدیریت سواحل، نسبت به سایر رشته‌های علمی و تخصصی دیگر، رشته‌ای جوان محسوب شده و از قدمت کمتری برخوردار است، ضرورت دارد یافته‌ها و دستاوردهای مجامع علمی جهان به اشتراک گذاشته شده و متخصصان مرتبط در راستای مدیریت دانش و انتقال تجربیات، دستاوردهای خود را در اختیار دیگران قرار دهند. اهمیت این هم‌آوایی علمی و تخصصی وقتی دوچندان می‌شود که دریابیم، با وجود جوان بودن این شاخه از علوم مهندسی، در سال‌های اخیر شاهد رشد فزایندهای در حوزه علمی و عملی مهندسی و مدیریت سواحل بوده‌ایم.

همایش دوسالانه سواحل، بنادر و سازه‌های دریایی از سال ۱۳۶۹ تا به‌حال کوشیده نه تنها زمینه‌ساز حضور دانشمندان و اساتید بزرگی از مجموعه‌های اجرایی، موسسات علمی و دانشگاه‌های سراسر دنیا جهت کمک به رشد و تعالی دانش مهندسی و مدیریت سواحل و

بنـادر، محیط‌زیسـت دریایـی، مهندسـی فراسـاحل و... گـردد، بلکـه تـلاش کـرده فرصتـی را بـرای عرضـه توانمندی‌هـای متخصصـان و دانش‌پژوهـان داخلـی در عرصـه بین‌الملـل فراهـم سـازد؛ فرصتـی کـه گروه‌هـای مختلـف بتواننـد آخریـن یافته‌هـا و دسـتاوردهای خـود را بـا یکدیگـر بـه اشـتراک بگذارنـد و از تجـارب یکدیگـر جهـت رفـع چالش‌هـا و معضـلات اجرایـی بهره‌منـد گردنـد.

خوشبختانه درحال‌حاضر جمهوری اسلامی ایران از ظرفیت‌های بسیار مناسبی در حوزه مدیریت و مهندسی سواحل برخوردار است و با داشتن تعداد کثیری از متخصصان جوان و علاقه‌مند و وجود موسسات علمی، مراکز دانش‌بنیان و شرکت‌های مهندسین مشاور و پیمانکار، توانسته در بین کشورهای منطقه، جایگاهِ ممتازی داشته باشد. همین امر سبب گردیده که جمهوری اسلامی ایران به عنوان تنها کشور خاورمیانه به عضویت قدیمی‌ترین و معتبرترین انجمن مهندسی دریایی جهان، یعنی انجمن دریایی زیرساخت‌های حمل‌ونقل آبی (پیانک) درآید. ضمن اینکه این انجمن یکی از دوره‌های همایش آیکوپمس را به عنوان بزرگترین اجتماع متخصصان مهندسی دریایی در جهان (در سال ۲۰۱۴) معرفی کرد.

ذکر این نکته نیز ضروری است که برگزاری مستمر و رو به رشد این همایش در ادوار گوناگون، باعث شده که آیکوپمس یکی از کلیدی‌ترین همایش‌های جهانی در حوزه مهندسی دریا باشد تا جایی که انجمن دریایی زیرساخت‌های حمل‌ونقل آبی، جمهوری اسلامی ایران را میزبان همایش بین‌المللی مهندسی سواحل در کشورهای در حال توسعه معرفی کرد.

در پایان لازم می‌دانم از همه دست‌اندرکاران برگزاری این دوره از همایش از جمله سازمان‌های بین‌المللی که حامیان معنوی آیکوپمس ۲۱۰۸ هستند و دیگر سازمان‌ها، نهادها، دانشگاه‌ها، شرکت‌های مشاور و پیمانکار و تامین‌کنندگان تجهیزات، اعضای خارجی و داخلی کمیته علمی و کمیته اجرایی کمال تشکر و قدردانی را داشته باشم. امید است در سایه الطاف الهی و با بهره‌گیری هرچه بهتر از ظرفیت‌ها و توان تخصصی متخصصان ایرانی، روزبه‌روز شاهد رشد و توسعه متوازن و پایدار مناطق ساحلی کشور و تحقق اقتصاد دریاپایه باشیم.

Introduction

The Ports and Maritime Organization of Iran is going to hold the 13th International Conference on Coasts, Ports and Marine Structures (ICOPMAS 2018) in cooperation with International Maritime Associations, domestic and foreign organizations, universities, contractors and consulting engineers in the Twenty-Eighth anniversary of holding the first Conference. The Conference emphasizes on invigorating technical and specialized cooperation among all countries, especially coastal neighboring countries.

In this respect, ICOPMAS secretariat recommends interested students, experts and scientists to visit the website for more detailed information: http://icopmas.pmo.ir

History of the Conference

On 27 may 1990, the first International Conference on Ports & Marine Structures was held in Tehran University and in the Twenty-Sixth year of holding this conference, the Twelfth International Biennial Conference on Coasts, Ports and Marine Structures (ICOPMAS 2018) was held on 31st Oct. – 2nd Nov. 2016 at Tehran Olympic Hotel with participation of more than 1300 related experts and scientists from 37 countries.

Objectives

As one of the most important technical and scientific events in Iran, ICOPMAS aims to provide an appropriate ground to exchange the latest scientific innovations and technical executive achievements. The Conference affords a forum to promote the coastal and marine engineering science and opens up new horizons for related experts to preset their capabilities to the world. In addition, this conference leads to using new methods and modern devices in marine industry to promote innovative management systems, strategic and economical technology and preparing the required ground for future cooperation among employers, investors and consultant engineers.

It should be also mentioned that the next ICOPMAS Conference will be held simultaneously with 10th International Conference on Coastal and Port Engineering in Developing Countries (PIANC-COPEDEC X) on summer 2020 in Kish Island, Iran.

IMPORTANT DATES

Procedure	Deadline
Extended abstract deadline	22nd June 2018
Notification accepted abstracts	7th Aug. 2018
Closure early bird registration	7th Sept. 2018
Conference	26th - 28th Nov. 2018

Language

The official language of the conference is English.

Venue

OLYMPIC HOTEL, TEHRAN, IRAN

26th – 28th Nov. 2018

Tel: (9821) 44739300
Fax: (9821) 44739191
info@olympichotel.ir
www.olympichotel.ir

Keynote Speakers

Aliakbar Aghakouchak
Tarbiat Modarres University - I.R. Iran
Topic: Analysis, design and assessment of offshore platforms in the Persian Gulf; past experience and future challenges

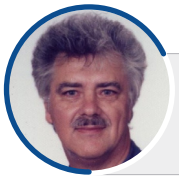

Robert Kirby
Ravensrodd Consultants Ltd. - U.K.
Topic: Challenges of Restoring Polluted Industrialized NW European Estuaries

Magnus Larson
Lund University – Sweden
Topic: A Semi-Analytic Model of Coastal Inlet Evolution

Ioan Nistor
University of Ottawa – Canada
Topic: Debris Loading on Infrastructure in Extreme Coastal Flood Events: Field, Experimental and Numerical Investigations

Dano Roelvink
UNESCO-IHE - The Netherlands
Topic: Process-Based Modeling of Beaches and Dunes; Towards Decadal Timescales

Ahmad Sana
Soltan Qaboos University – Oman
Topic: Two-EquationTurbulence Modelling of Wave Boundary Layers

Tomoya Shibayama
Waseda University – Japan
Topic: Recent Studies on Coastal Disaster Mitigation

Marcel Stive
TU Delft University – Netherlands
Topic: An Alternative to Saving Our Beaches from Sea Level Rise: The Sand Engine

Michael Risk
McMaster University - Canada
Topic: Approaches to Carrying Capacity of Aquaculture in the Persian Gulf: Monitoring Data, Modelling and Concerns

Themes

1. Hydrodynamic and Sediment

- Waves and Currents
- Tropical Storms and Tsunami
- Sediment Transport, Erosion and Geomorphology
- Metocean Measurements and Analysis
- Marine Renewable Energy

2. Port and Coastal Management

- Integrated Coastal Zone Management (ICZM)
- Crisis Management of Marine Hazards
- GIS and Remote Sensing
- Port's Technologies and Management
- Coastal and Marine Tourism

3. Port Engineering and Coastal Structures

- Planning and Design of Ports
- Design and Construction of Coastal Structures
- Maintenance, Inspection and Repair of Coastal Structures
- New Equipment and Materials for Construction of Coastal Structures
- Hydrography and Dredging

4. Offshore and Pipeline Engineering

- Design and Construction of Offshore Structures
- Maintenance, Inspection and Repair of Offshore Structures
- Planning and Construction of Submarine Pipelines
- Marine Geotechnics

5. Marine Environment and Safety

- Ports and Maritime Safety Management
- International Convention, Regulations and Rules
- Pollution and Environmental Impacts of Structures and Marine Transportation
- Coastal and Marine Ecosystems

Board of Directors

No.	Organization
1	Deputy Minister of Roads and Urban Development and the Managing Director of Ports and Maritime Organization (Conference President)
2	Commander of the Navy of Islamic Republic of Iran Army
3	Commander of the Navy of the Army of the Guardians of the Islamic Revolution
4	Vice president and Head of Environmental Protection Organization
5	Vice president and Head of Cultural Heritage and Tourism Organization
6	Deputy Minister of Defense and Armed Forces Logistics and President of Geographical Organization
7	Deputy Minister of Defense and Armed Forces Logistics and President of Marine Industries Organization
8	Deputy Minister of Energy and President of Renewable Energy and energy Efficiency Organization
9	Deputy Minister of Industry, Mining and Business and President of Geological Survey and Exploration
10	Deputy Minister of Roads and Urban Development and Meteorological Organization
11	Deputy Minister of Agriculture and President of Iran's Fishery Organization
12	President of National Cartographic Center
13	President of Iranian Offshore Engineering and Construction Company
14	President of the Supreme Council of Iran's Free Trade, Industrial and Special Economic Zone
15	Managing Director of Development and Management Company of Kish Free Zone's Ports and Airports
16	Managing Director of Islamic Republic Of Iran Shipping Lines
17	Managing Director of Iranian Oil Terminals Company
18	Managing Director of Iranian Offshore Oil Company
19	President of Tehran University
20	President of Sharif Industrial University
21	President of Tarbiat Modarres University
22	President of AmirKabir University of Technology
23	President of K.N. Toosi University of Technology
24	President of Iran University of Science and Technology
25	President of Islamic Azad University
26	Governor of Guilan Province of Iran
27	Governor of Khuzestan Province of Iran

Scientific Committee

Chair of Scientific Committee: Mohsen Soltanpour
K.N. Toosi University of Technology - Iran

No.	Name	Affiliation
1	Hamidreza Abaei	Ports and Maritime Organization - Iran
2	Aliakbar Aghakouchak	Tarbiat Modarres University - Iran
3	Reza Ahmadian	Islamic Azad University - Iran
4	Mohammad Reza Alam	University of California - USA
5	Ali Asghar Ale Sheikh	K.N. Toosi University of Technology – Iran
6	Issa Alharthy	Soltan Qaboos University - Oman
7	Abbas Ali Aliakbari Bidokhti	Institute of Geophysics - Iran
8	Mohammad Reza Allahyar	Ports and Maritime Organization - Iran
9	Behrooz Asgarian	K.N. Toosi University of Technology - Iran
10	Mahad Baawain	Soltan Qaboos University - Oman
11	Seyed Peyman Badiee	University of Tehran - Iran
12	Mohammad Reza Bahari	Consulting Engineer - Iran
13	Babak Banijamali	Consulting Engineer - Iran
14	Vahid Chegini	Iranian Society of Marine Sciences
15	Mohammad Daghigh	Consulting Engineer - Iran
16	Afshin Danekar	University of Tehran - Iran
17	Mohammad Dibajnia	Baird Company - Canada
18	Seyed Ali Estiri	Consulting Engineer - Iran
19	Amir Farshad Etemad shahidi	University of Science and Industry - Iran
20	Mojtaba Ezam	Islamic Azad University, Science & Research Branch of Tehran - Iran
21	Sarmad Ghader	University of Tehran - Iran
22	Ali Asghar Golshani	Islamic Azad University - Iran
23	Naser Hajizadeh Zaker	University of Tehran - Iran

No.	Name	Affiliation
24	Habib Hakimzadeh	Sahand University of technology - Iran
25	Kourosh Hejazi	K.N. Toosi University of Technology - Iran
26	Gerald Higelin	University of Applied Science Furtwangen - Germany
27	Majid Jandaghi Alaei	Consulting Engineer - Iran
28	Reza Kamalian	Ministry of Energy , Water Research Institute - Iran
29	Alireza Karbasi	University of Tehran - Iran
30	Alireza Kebriaee	Consulting Engineer - Iran
31	Robert Kirby	Ravensrodd Consultants Ltd - England
32	Mohammad Javad Ketabdari	Amirkabir University of Technology - Iran
33	Abbas Khayyer	Kyoto University - Japan
34	Mohammad Reza Khedmati	Amirkabir University of Technology - Iran
35	Homayoun Khoshravan	Water Research Institute/Caspian Sea Research Center - Iran
36	Razieh Lak	Geological Survey and Mineral Exploration of Iran
37	Magnus Larson	Lund University - Sweden
38	Han Ligteringen	Delft University of Technology and UNESCO IHE - Netherland
39	Majid Makhdoum	University of Tehran - Iran
40	Saeid Mazaheri	Iranian National Institute for Oceanography and Atmospheric Science
41	Ahmadreza Mostafa Ghar-abaghi	Sahand University of technology - Iran
42	David Nemazie	University of Maryland Center for Environmental Science - USA
43	Ioan Nistor	University of Ottawa - Canada
44	Charitha Bandula Pattiaratchi	The University of Western Australia - Australia
45	Saeid Pirasteh	Waterlo Institute - Canada
46	Hamid Rahimipour	Consulting Engineer - Iran

No.	Name	Affiliation
47	MD. Ataur Rahman	Bangladesh University of Engineering and Technology (BUET)- Bangladesh
48	Iraj Rahmani	Building and Housing Research Center - Iran
49	Ali Akbar Ramezanianpour	Amirkabir University of Technology - Iran
50	Abdolkarim Razazan	Ports and Maritime Organization - Iran
51	Michael J. Risk	McMaster University - Canada
52	Dano Roelvink	UNESCO-IHE - The Netherlands
53	Irene Rosberg	Copenhagen - Denmark
54	Kabir Sadeghi	Near East University - Cyprus
55	Ahmad Sana	Soltan Qaboos University - Oman
56	Jun Sasaki	The University of Tokyo - Japan
57	Mehdi Shafiee Far	Tarbiat Modarres University - Iran
58	Siavosh Shayan	Tarbiat Modares University - Iran
59	Tomoya Shibayama	Waseda University - Japan
60	Mohsen Soltanpour	K.N. Toosi University of Technology - Iran
61	Marcel Stive	TU Delft University - Netherland
62	Neelamani Subramaniam	Kuwait Institute for Scientific Research - KUWAIT
63	Seyede Masoome Sadaghi	Road, Housing & Urban Development Research Center
64	Danling Tang	South China Sea Institute of Oceanology, Guangzhou - China
65	Giuseppe Roberto Tomasicchio	University of Salento - Italy
66	Klaas Van Breugel	TU Delft University - Netherland
67	Jenste Van Der Meer	Delft University of Technology and UNESCO IHE - Netherland
68	Tiedo Vellinga	TU Delft University - Netherlands
69	Han Winterwerp	TU Delft University - Netherland
70	Abbas Yeganeh Bakhtiari	University and Science Technology - Iran
71	Homayoun Zaker	Consulting Engineer - Iran


13th International Conference on
Coasts, Ports and Marine Structures
2018
ICOPMAS

Exhibition Plan

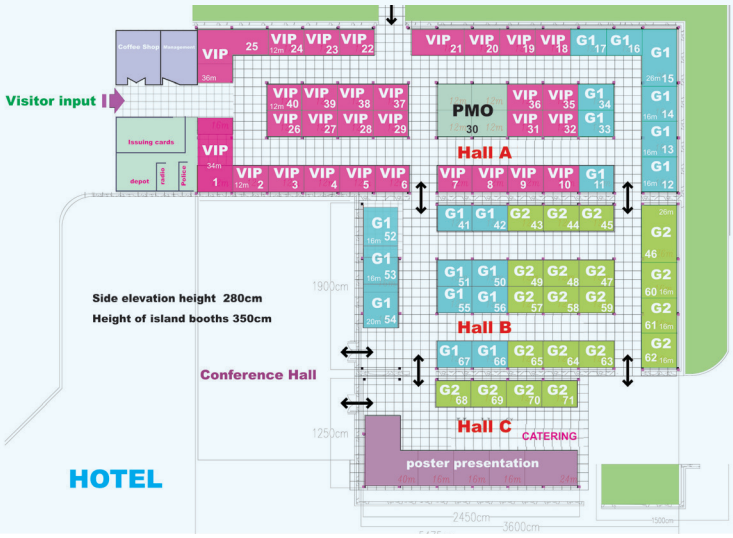

For further enquiries please contact the secretariat via Tel: +982184932272 or email: icopmas@pmo.ir & icopmas@yahoo.com

Registration fees (Euro)

	Before 7th September	After 7th September
Authors of the accepted papers	200 €	200 €
Professors	300 €	400 €
Students	150 €	200 €
Other participants	500 €	600 €
Accompanying Persons	250 €	350 €

Note

- Registration fees cover the conference certificate and materials, lunch and coffee break, and admission to all sessions of the conference.
- To register for ICOPMAS 2018, please Visit http://icopmas.pmo.ir or contact the secretariat via email: icopmas@pmo.ir & icopmas@yahoo.com
- All of the fees should be paid on desk. There would be no online payment.

Organization

Mohammad Rastad — President

Mohammad Reza Allahyar — Vice-President

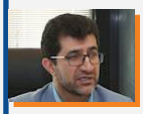

Hamid Khalili — Secretary

Mohsen Soltanpour — Chair of Scientific Committee

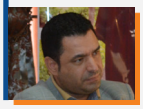

Behzad Alvand — Chair of Executive Committee

Executive committee

No.	Name	Designation
1	Vahid Komasi	In charge of Secretariat
2	Hamed Mohammadnejad	Website Expert
3	Zahra Ranji	International Affairs Expert
4	Farzad Kalantari	Coordinator & Formalities
5	Farshid Zandinejad	Coordinator
6	Mehdi Monadi	EDI Expert
7	Hamed Asgari	Hardware Expert
8	Asghar Lak Aliabadi	Public Relation Expert
9	Mehrdad Aziminia	Coordinator
10	Mohammad Reza Khezri	Accounting Experts

Moral Sponsors

The World Association for Waterborne Transport Infrastructure (PIANC)

International Association of Ports and Harbors (IAPH)

International Association for Hydro-Environment Engineering and Research (IAHR)

World Meteorological Organization (WMO)

International Association of Marine Aids to Navigation and Lighthouse Authorities (IALA –AISM)

International Hydrographic Organization (IHO)

Coordinating Committee on Hydrometeorology & Pollution Monitoring of the Caspian Sea (CASPCOM)

Iranian National Commission for UNESCO

Iranian Coastal & Marine Structural Engineering Association (ICOMSEA)

Iranian National Institute for Oceanography and Atmospheric Science

Iranian Association of Geomorphology

Iranian Association of Naval Architecture and Marine Engineering

Shipping Association of Iran

Iranian Society of Marine Science and Technology

Iranian Hydraulic Association

Iranian Society of Structural Engineering

Islamic World Science Citation Center

TABLE OF CONTENT

Keynote Lectures

Hydrodynamics and Sediment

Port and Coastal Management

Port Engineering and Coastal Structures

Offshore and Pipeline Engineering

Marine Environment and Safety

index

KEYNOTE LECTURES

ANALYSIS, DESIGN AND ASSESSMENT OF OFFSHORE PLATFORMS IN THE PERSIAN GULF; PAST EXPERIENCE AND FUTURE CHALLENGES

Ali Akbar Aghakouchak

Faculty of Civil and Environmental Engineering, Tarbiat Modares University, Tehran, Iran
a_agha@modares.ac.ir

1. Introduction

In Iran, installation of offshore platforms in the Persian Gulf began in 1960s in Bahreganser field. Till 1979, tens of platforms were installed in four operational fields namely Bahregansar, Khark, Lavan and Sirri.

After the revolution, South Pars field was also developed. Nowadays about two hundred platforms are in operation in Iranian waters of the Persian Gulf.

This key note lecture reviews the practice for design of these structures in the past. Challenges, which have been overcome and the experiences gained will be discussed. On the other hand, given the number and the age of the existing platforms, the challenges, which the technical community may face in the future with regard to assessment of these structures either to decommission them or to extend their service life will be presented.

2. Design of New Platforms

Usually offshore platform in Iran are designed based on API-RP 2A code of practice. Similar to other design guide and standards, this document has undergone revisions during past decades. As the results of these revisions, more sophisticated methods of analysis and design must now be used. These structures are normally designed for several load combinations, which generally fall into two categories:

-In-service conditions
-pre-service conditions

The most important types of analysis, which need to be carried for In-service conditions, are as follows:

- In-place analysis
- Fatigue analysis
- Seismic analysis
- Ship impact analysis

Design life of these platforms is usually between 25 to 30 years. The design life directly affects the fatigue design of structure and indirectly affects the design environmental conditions. The design environmental criteria should be developed from the environmental information and/or a risk analysis.

The difficulties that the designers have been facing in the past for gathering the information, selecting the design parameters and modelling the structures, for the purpose of analysis and design will be discussed in this lecture.

The most important types of analysis, which need to be carried for Pre-service conditions, are as follows:

- Load out analysis
- Transportation analysis
- Lift/Launch analysis
- Un-piled stability analysis
- Pile driving analysis

In this phase of operations some incidents and/or accidents have happened in the past. Some of them have had major financial consequences. Some have been attributed to wrong operations and some to shortcomings in design procedures and assumptions. The problems that the designers have been facing in this regard will also be discussed in this lecture.

3. Assessment of Existing Platforms

Currently there are many platforms in operation in the Persian Gulf. Design life of quite a number of theses platforms has already expired. Taking into account the assets installed on topsides of these platforms, they worth hundreds of millions of Dollars.

Mechanisms that may reduce the structural capacity of a platform during its operational life, are as follows:

- Dropped objects
- Vessel collision
- Corrosion
- Fatigue
- Installation damage
- Fabrication flaws
- Seabed scour or seabed build-up
- Overload

-Accidents such as fire and explosion.

Therefore, apart from a good practice in design, construction and installation, in order to ensure that a platform can serve its design life, a proper maintenance program is necessary. Even if a proper maintenance program is implemented, when the design life of a platform is expired, the whole structure needs to undergo an assessment process.

Previously a chapter of API-RP 2A code of practice was devoted to the subject of assessment of existing platforms. However due to its growing importance recently a separate document called API-RP 2SIM has been developed for this purpose.

Structural Integrity Management, SIM, is a continuous process, which can be used for demonstrating the fitness-for-purpose of an offshore structure from installation through to decommissioning. SIM provides the process for understanding the effects of deterioration, damage, changes in loading, and accidental overloading. In addition, SIM provides a framework for inspection planning, maintenance, and repair of a platform or group of platforms. Application of SIM requires different types of analytical procedures and more realistic information and data regarding site environmental, seismic hazard and soil conditions.

So far only a few platforms have undergone this process, mostly using the provisions of previous editions of API-RP 2A. Challenges facing the engineers in futures, with regard to assessment of old existing platforms will form the second part of this lecture.

PROCESS-BASED MODELLING OF BEACHES AND DUNES: TOWARDS DECADAL TIMESCALES

Dano Roelvink[1,3], Susana Costas[2], Ahmed Elghandour[1,2] and Bas Huisman[3,4]

1) Water Science and Engineering, IHE Delft, Delft, the Netherlands, d.roelvink@un-ihe.org
2) CIMA, Universidad do Algarve, Faro, Portugal, scotero@ualg.pt
3) Marine and Coastal Systems, Deltares, Delft, the Netherlands, bas.huisman@deltares.nl
4) Faculty of Civil Engineering, Delft University of Technology, Delft, the Netherlands

1. Introduction

The evolution of sandy, often human-impacted coasts over decades is of great interest to coastal scientists, engineers and managers. Existing modeling approaches focus on the plan-view development of the coastline, on the evolution and variability of the beach and dune profile, or try to simulate the evolution of the complex bathymetry and topography of the beach-dune system; however, the state of the art of existing models is not up to what is expected of them.

2. Shoreline: A New Coastline Modelling Concept

In coastline plan view modeling, existing model approaches only allow for incremental coastal evolution relative to a fixed reference line. This does not allow the evolution of important features such as spits and sandy hooks, tombolo's and migrating islands. We have recently developed a new coastline model, ShorelineS [1], that has abandoned the fixed shoreline grid approach in favor of a completely free description where the coast is schematized to strings of grid points that can move about freely and interact with each other.

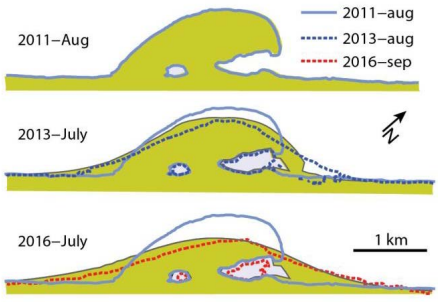

Figure 1. Validation of ShorelineS model for the Sand Motor, Delfland, the Netherlands

The freedom of this approach allows an easy definition of the model domain and input wave climate or time series. We recently added approaches to represent diffraction behind breakwaters the full evolution to a (series of) salient and tombolos can be simulated.

3. Applying XBeach for Longer Timescales

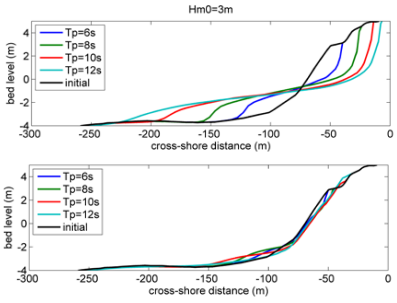

Figure 2. Effect of 'bermslope' effect on nearshore profile evolution; bottom panel: with, top panel: without.

A limitation of XBeach for longer-term applications is the fact that, especially for reflective and semi-reflective beaches, XBeach tends to grossly overpredict erosion at the water line, since it does not resolve the small-scale and highly dynamic swash processes there. While efforts toimprove this situation are ongoing using the non-hydrostatic mode, here we apply a pragmatic approach outlined in [2], where the profile in a very limited area near the water line is 'nudged' towards a given 'bermslope', using an upslope transport process. This simple modification has a dramatic effect on the behaviour of steep beaches (see example in Figure 2) and allows the full range of scarping to berm building, maintaining the general shape of the intertidal beach through erosive and accretive sequences.

4. Including Wind-Blown Processes

A new model, Duna [3], coupled with XBeach, simulates the evolution of dunes as a result of input conditions (e.g. wind, vegetation cover, moisture) that can change over time and interact with the dune topography. The model computes and updates the horizontal distribution of the cross-shore and longshore wind velocity, the velocity thresholds of sand movement, the growth and the coverage of the vegetation, and the sediment transport. The results from each time step allow the update of the dune topography and vegetation cover. The coupled XBeach-Duna system was calibrated to represent the evolution of two beach-dune profiles in Praia de Faro, Portugal, over a 2-year period.

5. Effects of Longshore Transport Gradients

In profile models usually the total cross-sectional area of the profile is conserved, limiting the application to situations where the profile moves around a quasi-equilibrium. This can be overcome by assuming that the longshore transport gradient, responsible for structural erosion or accretion, is proportional to the longshore transport itself, divided by a typical length scale. In such a way long simulations can be carried out where, amid intra-annual variations, the coastal profile, including the dune, retreats or advances while the location of the accretion or erosion in the profile is simulated realistically. Figure 3 shows an example 10-year simulation for seriously eroding, relatively stable and strongly accretive profile evolution.

The model captures a balance between longshore gradients and cross-shore processes in the surf zone, competing effects of moderate conditions and storms in the intertidal area and between build-up by storm waves and aeolian transport on the berm. Vegetation behaviour is shown to play a key role in the development of the shape of the foredunes. The relation between progradation or recession rate and foredune height as often reported in literature is reproduced.

6. The Dream: Hybrid Modelling of Complex Areas

While efforts will continue to simulate long-term evolution of complex areas with detailed morphodynamic area models, we see a large scope for considerably faster concepts that combine simplified but effective models of coastline behaviour and profile response, or coastline models with area models that do not need to resolve the wave-driven processes. This will bring much-needed simulations over decades to centuries, needed to assess impacts of increasingly alarming climate change scenarios, to within acceptable computation times.

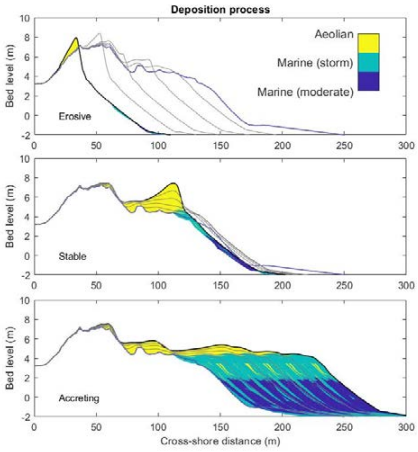

Figure 3. Profile and stratigraphy evolution over a 10-year period for a strongly erosive (top panel), approximately stable (middle panel) and strongly accretive case.

7. References

[1] Dano Roelvink, Bas Huisman, Ahmed Elghandour (2018). Efficient modelling of complex coastal evolution at monthly to century time scales. Sixth International Conference on Estuaries and Coasts (ICEC-2018), August 20-23, 2018, Caen, France

[2] Dano Roelvink, Susana Costas, 2017. Beach berms as an essential link between subaqueous and subaerial beach/dune profiles. Geo-Temas 17 79-82.

[3] Dano Roelvink and Susana Costas, 2018. Coupling nearshore and aeolian processes: XBeach and Duna process-based models. Subm. Env. Modelling and Software.

APPROACHES TO CARRYING CAPACITY OF AQUACULTURE IN THE PERSIAN GULF: MONITORING DATA, MODELLING AND CONCERNS

Michael John Risk[1], S. Abbas Haghshenas[2] and Hamid Rezaei[3]

1) PO Box 1195, Durham ON Canada, riskmj@mcmaster.ca
2) Institute of Geophysics – University of Tehran, sahaghshenas@ut.ac.ir
3) Darya Negar Institute of, rezaihamid1@yahoo.com

1. Introduction

At the 2016 ICOPMAS, we presented the results of a hydrodynamic model of water movement in the Persian Gulf, added the projected nutrient discharges from proposed mariculture installations, and warned that the increased nutrients could threaten coral reefs and artisanal fisheries in the Gulf. There are now several fish farms established in the Gulf, and some monitoring data are available to allow some highly tentative conclusions to be drawn.

These results are important for Iran, because of issues of food security and environmental maintenance. Excessive nutrient inputs will lead to Red Tides, possible sulfide toxicity, and damage to surrounding ecosystems. If aquaculture activities are found to overload the natural absorptive capacity of the sea bed, then either operations will need to be curtailed, or land-based systems considered.

2. The Slippery Concept of Carrying Capacity

There are many definitions of carrying capacity in use: 1) Physical carrying capacity-the number of fish farms that can fit in a given space. 2) Production carrying capacity is the stocking density at which production is maximised. 3) Ecological carrying capacity is that density above which unacceptable damage results to the ecosystem, and finally 4) Social carrying capacity is the level at which the aquaculture operations do not cause societal disruption.

The most important of these is ecological carrying capacity, which we define as that level of aquaculture activity that does not result in permanent or long-standing change to the environment. Most of the damage from open-net fish farms results from the organic discharges, and we will focus on that herein. This means that any organic matter deposited by a fish farm needs to be oxidised as rapidly as it accumulates [1].

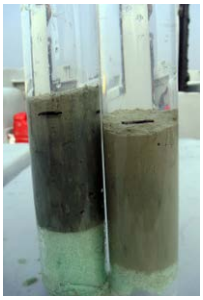

Figure 1: Two cores from under a cage operation near Kish Is., after less than a year. The core on the left has already begun to generate anoxic conditions.

3. Previous Research and Present Situation

Our paper at the previous ICOPMAS noted that the value of the coral reefs of Kish Is. Was about US$100 million, or $200,000/ha, and that the artisanal fishery (much of which depends on reef areas) had a market value of $200 million and employed about 20,000 people. Our model suggested that, with the projected number of fish farms operating, after one year all the reefs around Qeshm and Kish Is. would be killed, and that-in addition-there would be serious trans-boundary issues.

At time of writing, there are a few fish farms operating in Iranian waters, most around Kish Is. There is a limited amount of data available from monitoring programs.

Table 1: Monitoring data from a cage farm near Kish Is., showing progressive deterioration in sediment quality.

Time (Mos.)	Control	Control	Near Cage	Near Cage
	Eh	Sulfide	Eh	Sulfide
2	133	3	-31	20
4	50	20	-250	80
5	40	50	-130	180

4. Sustainability

We suggest that, for operations to be sustainable, the sediment conditions under the fish pens show always show: pH>8; Eh 0 to -50, DO >2ml/l, and (perhaps the most important) sedimentary sulfide levels <1,000µM. Much of the labile N in the organic deposits is capable of being transported over large areas [2], so the OM under the cages should not increase, nor should there be accumulation of material [3].

5. Preliminary Results

Examination of the limited monitoring data shows that Eh is often at unacceptable levels, and sedimentary sulfide levels are starting to creep up to the boundary between Acceptable and Unacceptable. Refining the hydrodynamic model shows the potential for spreading organic pollution to other areas, as we suggested earlier.

6. Conclusions and Suggestions

Some of the farms are operating beyond the absorptive capacity of the environment. Stock reductions or fallowing are possible ways to remedy this. Continuation of the monitoring to a variety of fish farm operations should allow a rough estimate of carrying capacity of the Iranian side of the Gulf. In any event, the organic pollution from fish farms may become such a problem that land-based operations will have to be considered.

7. References

[1] Grant, J. and Hargrave B. T. (1987) Benthic metabolism and the quality of sediment organic carbon, *Biological Oceanography, 4:3, 243-264*

[2] Nguyen, H. K., Kristensen E. and L. C. Lund-Hansen (2012) Benthic metabolism and nitrogen transformations affected by fish cage farming in the tropical Nha Phu estuary (Vietnam), *Mar. Freshwater Res. 63, 887-897.*

[3] Stigebrandt, A., J. Aure, A. Ervik and P. K. Hansen. (2004) Regulating the local environmental impact of intensive marine fish farming III. A model for estimating the holding capacity on the Modelling-Ongrowing fish farm-Monitoring system *Aquaculture 234 239-261.*

CHALLENGES OF RESTORING POLLUTED INDUSTRIALISED NW EUROPEAN ESTUARIES

Robert Kirby

Ravensrodd Consultants Ltd., Liverpool, England, robkirby@globalnet.co.uk

It is now well established that a number of important commercial muddy estuaries, Loire, Scheldt, Ems, Weser and reaches of the Elbe have become severely degraded due to a combination of marginal reclamation coupled with gross-scale over-deepening to facilitate passage of modern deep-draughted trading vessels. If the Gironde, Seine and Rhine have been similarly managed and investigated such studies are not, as yet, publicly available. Degradation manifests itself as a shift to much greater flood tide dominance, together with import of mud from a down-estuary direction and resulting in hyper-turbid, fluid mud, conditions. Estuary reaches affected have severely impaired ecosystems, whilst ground water effects in marginal land areas have manifested themselves in differential ground movements and subsidence of buildings etc.

Appreciation of these detrimental changes has led to intense studies of how to reverse this degradation?

It is already clear that this will require many years of effort along with a high cost. Early attempts to reduce the enhanced fine sediment load in the Inner Ems by creating backshore ponds accessed via deep, narrow cuttings aimed at siphoning off and capturing the fluid mud have proved impractical for the moment. Similarly suggestions to restrict up-estuary advection of fluid mud in the Loire by installing upstanding cross-channel cills or by use of cross-channel air bubble curtains have been dismissed as overly expensive and impractical.

Alternative and more readily reached-for options involve much wider application of the KSIS principal (Keep Sediment In the System) and the Ems Estuary could be a candidate for the worlds first sustainably managed cohesive sediment estuary. There are three objectives, port sediment, muddy fairway sediment and polluted sediment. The three significant muddy ports, Emden, Delfzijl and Leer along with Husum just outside already apply one or more generic SMS's (Sediment Management Systems). These are total as opposed to partial solutions; implying fine cohesive sediment is no longer dredged, removed and dumped outside this estuary. Secondly, repeat experiments applying Active Nautical Depth in the Inner Ems fairway have proved successful; the engineered aerobic fluid mud cloud created allows ships to pass through it. At the same time the induced fluid mud advects short distances up and down the channel due to flood and ebb shear stress, so providing a significant degree of flood tide retardation. This assists in reducing excessive induced flood phase advective transport into the inner reaches of the Ems. Thirdly, it is well-established that aerobic suspensions created by Active Nautical Depth have the added side-benefit of destroying the contaminant TBT in situ. Since 1990 no TBT-contaminated mud has needed to be dredged and stored outside the Ems Estuary. Research is currently in progress to investigate whether this natural phenomenon can be enhanced into a viable industrial process – 'in-situ bio-remediation'. Studies involve both laboratory and field tests seeking the dominant communities of natural aerobes most adept at this destruction. Lab tests on cold-stored mud samples are now being complemented by mesocosm experiments in impounded docks in Port of Liverpool, UK, most contaminated with TBT.

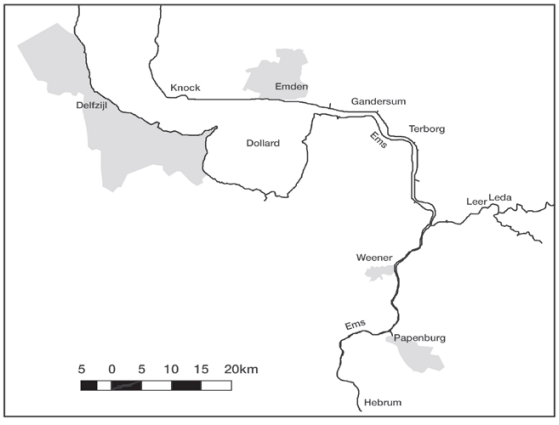

Figure 1. Cluster of ports in Ems region managing fine sediment in sustainable manner.

Attached graphs show conceptually how contrasted degrees of oxygenation and water temperature accelerate the process. This topic area remains, for now, in its infancy.

These novel strategies, altering port mud attributes to facilitate ship passage, permitting 'Conditioned' aerobic mud to lie in fairways and 'in-situ bio-remediation' each contribute to sustainability, whilst permitting maritime economic activity to continue.

Days	TBT w/ O_2	TBT w/ O_2	DBT w/ O_2	MBT w/ O_2
1	2000	2000	0	50
3	1975	1600	100	300
5	1950	1200	150	650
7	1925	800	200	1000
9	1900	400	250	1350
12	1875	0	300	1700
15	1850	0	0	2000

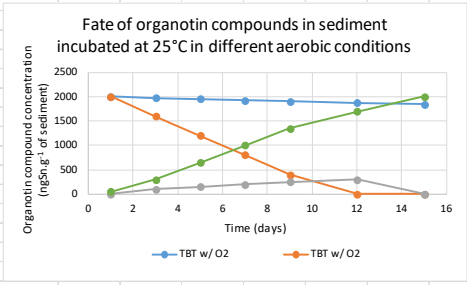

Days	10°C	15°C	20°C
1	800	800	800
3	750	700	600
5	700	600	400
7	650	500	200
9	600	400	0
12	550	300	0
15	500	200	0

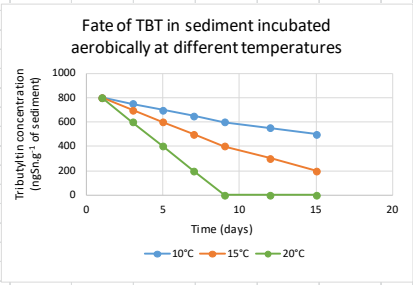

References

[1] Kirby R (in press) Challenges of Restoring Polluted Industrialised NW-European Estuaries. In: Muddy Coasts and Estuaries: The Future. Publ:- Elsevier.

[2] Polrot AK, Kirby JR, Birkett JW, Jenkinson I and Sharples GP (in press) Steps towards the sustainable management of sediment in ports and harbours. In:- Coastal Transitions: Towards Sustainability and Resilience in the Coastal Zone. Publ:- Taylor and Francis Inc.

A SEMI-ANALYTIC MODEL OF COASTAL INLET EVOLUTION

Magnus Larson[1], Almir Nunes[1], and Hitoshi Tanaka[2]

1) Water Resources Engineering, Lund University, Lund, Sweden; magnus.larson@tvrl.lth.se
2) Department of Civil Engineering, Tohoku University, Sendai, Japan

1. Introduction

The water exchange between the sea and a lagoon or bay through an inlet due to tides is a classical topic that has been investigated in a large number of studies [1, 3, 4, 6]. Initial efforts to calculate the inlet flow involved simplified governing equations that were solved in terms of non-dimensional variables, implying that key parameters could be displayed efficiently in diagram form [2]. Subsequently, numerical approaches have been taken that may include more general forcing, initial, and boundary conditions employing governing equations that involve less restrictions However, the simplified approaches still have their use for making approximate estimates in the initial stage of a project or for smaller studies where available resources prevent large-scale numerical modelling. Also, in coupling inlet flow models to sediment transport and morphological change simulations, it may be advantageous to employ simpler models to achieve robust and reliable results at reasonable computational efforts.

The main objective of this paper is to derive a simple semi-analytic model of the flow induced by tides through an inlet connecting the sea to a lagoon or bay that can be used to develop explicit expression for key parameters associated with this type of flow, such as bay water level amplitude, tidal prism, maximum inlet velocity, and retention (mixing) time. The word semi-analytic is used to denote an approach that does not exactly solve the governing equation, but only satisfies it in an overall sense according to a specific criterion. Also, the inlet flow model is employed to explore inlet equilibrium and stability as well as inlet cross-sectional area evolution by using a sediment transport relationship together with a sediment balance equation for the inlet.

2. Model of Inlet Flow

The flow through an inlet connecting a lagoon (or bay) to the sea was described by [4] using the continuity equation for the lagoon together with the momentum equation for the inlet channel, resulting in,

$$\frac{d\eta_B}{dt} = \frac{A_I}{A_B}\sqrt{\frac{2g}{K_I}}\sqrt{|\eta_o - \eta_B|}\,\mathrm{sgn}(\eta_o - \eta_B) \qquad (1)$$

where A_B is the bay surface area, η_B the bay water level, A_I the inlet cross-sectional area, η_o the sea level, g the acceleration due to gravity, K_I a friction coefficient, and t time. Assuming a sinusoidal sea level variation with amplitude a_o and period T, and introducing non-dimensional quantities, the repletion coefficient emerges as the main parameter controlling the inlet flow, defined as $K = (A_I / A_B)\sqrt{2ga_o / K_I}\,(T / 2\pi a_o)$. Figure 1 shows the non-dimensional water level variation in a lagoon for different values on K at quasi-steady conditions obtained by numerically solving Eq. 1.

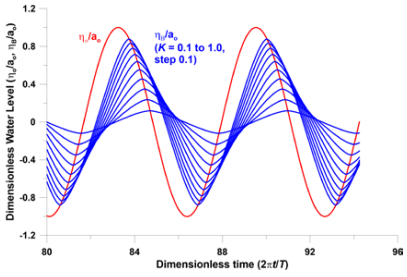

Figure 1. Water level variation in a lagoon for different values on the repletion coefficient (K).

A semi-analytical approach can be taken to solve Eq. 1 using different matching conditions; for several such conditions the following solution is obtained,

$$\frac{a_B}{a_o} = \left(1 - \frac{(C_M K)^4}{4}\left(\sqrt{1 + \frac{4}{(C_M K)^4}} - 1\right)^2\right)^{1/2} \qquad (2)$$

where a_B is the bay amplitude and C_M is a matching coefficient equal to 1.23.

3. Inlet Flow Properties

Based on the semi-analytic solution, different inlet flow properties can be calculated and expressed in non-dimensional form. A common parameter employed to quantify the water exchange is the tidal prism, which expresses the volume of water that is transported into and from to the bay during a tidal cycle. The tidal prism is given by $P = 2a_B A_B$; if $P_{\max} = 2a_o A_B$, then the non-dimensional tidal prism is $\hat{P} = P / P_{\max} = a_B / a_o$, which is given by Eq. 2. Other quantities that can be determined in a similar manner is the maximum and mean inlet velocity, and the bay retention time. In many studies on inlets a

strong connection between the inlet cross-sectional area and the tidal prism has been established. The present solution yields $A_I / A_o = \hat{P} / \left(1 - \hat{P}^2\right)^{1/4}$, where $A_o = \pi P_{\max} / T u_{\max}$ with u_{max} being the maximum possible velocity through the inlet.

4. Model of Morphological Evolution

The semi-analytical solution can be employed to investigate tidal inlet area evolution. A sediment balance for the inlet involving the longshore sediment and inlet channel transport defines this evolution. The governing equation is given by [5, 7],

$$B\frac{dA_I}{dt} = \frac{K_w}{g}\left(u_I^2 - u_{cr}^2\right)u_I W - m_L \qquad (3)$$

where B is the barrier island width, K_w a transport coefficient, u_I the inlet velocity, u_{cr} the critical inlet velocity for sediment movement, W the inlet width (related to A_I through assumptions about the cross-sectional shape), and m_L the longshore sediment transport. For steady forcing conditions, Eq. 3 approaches equilibrium, which may imply a stable, open inlet or one that experiences closure. Figure 2 displays the solution to Eq. 3 in non-dimensional form for dA_I/dt = 0, using different critical velocities and longshore transport rates (self-similar shape for A_I). The semi-analytic solution was employed to calculate u_I and Eq. 3 was solved in terms of the equilibrium repletion coefficient (K_E). The curves shown are analogous to the ones proposed by [3], indicating whether an inlet is stable or not.

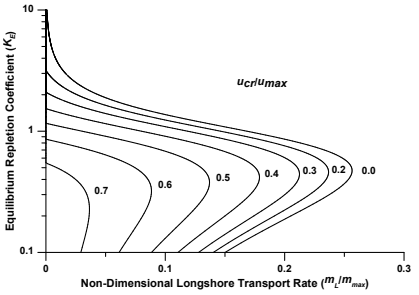

Figure 2. Equilibrium repletion coefficient for different critical velocities and longshore transport rates.

5. Simulation of Inlet Area Evolution

In order to describe the time evolution of the inlet cross-sectional area, Eq. 3 must be solved with the proper initial conditions; this is done numerically, even for schematic cases, since the equation exhibits a complex nonlinear relationship involving K and other variables. Several simulation cases were investigated to demonstrate the behavior of an inlet under different initial and forcing conditions. As an example, Figure 3 shows the response to an increase or decrease in the LST transport rate with regard to the initial transport conditions in equilibrium, where both equilibrium situations (above and below maximum K_E) are considered. Small perturbations of the initial transport conditions lead to quite different responses, whether the initial repletion coefficient (K_{in}) is in the stable or unstable region. In the latter case closure may occur.

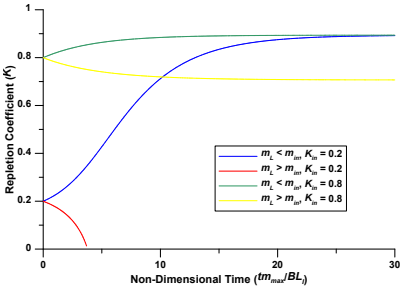

Figure 3. Inlet area evolution for different sediment transport rates and initial repletion coefficient values.

6. Concluding Remarks

In this study the basic properties of the coupled inlet hydraulics and morphological evolution models were investigated, and by a using semi-analytic approach these properties could be expressed in a compact manner through non-dimensional quantities. Asymptotic and equilibrium behavior could be established. The next step is to investigate the ability of the model to simulate the inlet evolution under more realistic conditions. A numerical approach will then be taken and comparison with field data will be performed.

7. References

[1] Brown , E.I. 1928. Inlets on Sandy Coasts. *Proceedings of the American Society of Civil Engineers*, Vol. LIV, 505-553.

[2] Dean, R.G. and Dalrymple, R.A. 2002. Coastal processes with engineering applications. Cambridge University Press, Cambridge, UK.

[3] Escoffier, F.F. 1977. Hydraulics and stability of tidal inlets. GITI Report 13, US Army Corps of Engineers, Waterways Experiment Station, Vicksburg, MS.

[4] Keulegan, G.H. 1967. Tidal flow in entrances. Water-level fluctuations of basins in communication with seas. Technical Bulletin No. 14, US Army Corps of Engineers, Vicksburg, MS.

[5] Kraus, N.C. 2010. Engineering of tidal inlets and morphologic consequences. Handbook of Coastal and Ocean Engineering, Ed: Kim, Y.C., World Scientific, Chapter 31, 867-900.

[6] O'Brien, M.P. and Dean, R.G. 1972. Hydraulics and sedimentary stability of tidal inlets. *Proceedings of the 13th International Coastal Engineering Conference*, ASCE, 761-780.

[7] Ogawa, Y., Fujita, Y., and Shuto, N. 1984. Change in the cross-sectional area and topography at river mouth. *Coastal Engineering in Japan*, 27, 233-247.

DEBRIS LOADING ON INFRASTRUCTURE IN EXTREME COASTAL FLOOD EVENTS: FIELD AND EXPERIMENTAL INVESTIGATIONS

Ioan Nistor[1]

1) Department of Civil Engineering, University of Ottawa, Ottawa, Canada, inistor@uottawa.ca

1. Introduction

Catastrophic coastal flooding generated by the 2004 Indian Ocean Tsunami or the 2011 Tohoku Tsunami as well as by the 2005 Katrina and 2012 Sandy hurricanes have shown that, hydrodynamic loading aside, debris loading is a major contributor to the extreme damage experienced by coastal infrastructure. While extreme hydrodynamic loading due to coastal flooding events has been the object of intense research during the past decade, few studies dealing with debris impact and loading due to coastal flooding have been conducted. Post-tsunami forensic engineering field investigations conducted by the author of this paper (Nistor et al. 2005, Nistor et al. 2010, Nistor et al. 2011) and other researchers (Sato et al. 2014, Chock et al. 2012) revealed that debris loading and debris damming have a significant effect on the structural integrity of buildings and infrastructure in general, especially in high density urban areas. The new ASCE-7 Tsunami Loads and Effects Committee (of which the author is a Voting Member) has recognized the significant importance of debris loading and proposed several prescriptions pertaining to debris loading as well as debris spatial distribution during a tsunami-induced flood event. These prescriptions are based on limited data collected from field investigations (Chock et al. 2012, Naito et al. 2014,) and have yet to be validated as previous prescriptions often resulted in conservative estimations of debris spatial spreading and an inaccurate estimation of associated loading. The few experimental tests (Shafiei et al. 2014, Rueben et al. 2014) showed that accurate tracking of debris is complicated: hence, this study is geared towards investigating and tracking the spatial and temporal displacement of floating debris due to rapid coastal flooding in a built-in port environment.

2. Field Investigations

The author was part of several major international posts-tsunami forensic engineering surveys: (1) Thailand (Phuket) and Indonesia (Banda Aceh) following the December 2004 Indian Ocean Tsunami; (2) 2010 Chile Earthquake and Tsunami and (3) 2011 Tohoku Japan Tsunami. As part of these field surveys the effect of debris impact was analyzed in detail to asses in detail their impact on built infrastructure and to estimate the loading induced by them. Fig, 1 and 2 show examples of debris loading during the 2011 Tohoku Tsunami.

Fig. 1 Debris impact on structures following the 2011 Tohoku Japan Tsunami (Nistor, 2011).

3. Experimental Investigations

This experimental program was conducted in two facilities: the Tsunami Wave Basin at the Coastal Engineering Laboratory at Waseda University in Tokyo, Japan (Shibayama, 2014) which is shown in Fig. 2 as well as in the Hydraulic Laboratory in the Department of Civil Engineering at the University of Ottawa, Canada.

Figure 2: Waseda Tsunami Wave Basin and experimental setup

The experimental program comprised of 12 preliminary (calibration and trial) runs and 48 further runs employing various combinations of "smart debris". During tests, debris were placed parallel to the edge of the apron on either one or three rows, in single layer or two-layer stacked configuration. Additionally, to investigate the spatial motion of debris within a built-in environment of a port with warehouses and various constructions, one and

two rows of structures were installed on the horizontal apron, right behind the smart debris' initial location

For this particular experimental program, the authors designed and constructed a horizontal apron which simulated a horizontal quay (apron) with an adjacent port area. The vacuum-controlled wave maker has the capability to generate a solitary wave which broke at the edge of the apron further generating a hydraulic bore which propagated over its entire length.

Wave gages were located in the deep water section of the basin while some others were located at the inner edge of the apron and at the middle of the apron, respectively. An ECM (electromagnetic current meter) was placed close to the edge of the apron recorded the time-history of flow velocities. The experiments used a novel method to track the spatial motion of "smart" debris using (1) a wireless tracking device employing Bluetooth low energy technology (BLE) and (2) a motion sensor. A third (3), stereo video-analysis system combined with a newly developed algorithm helped further validate the accuracy of the "smart debris" tracking system.

The debris were scaled-down 20' shipping containers and were manufactured from polyethylene (PE-HMW, 0.92 g/cm³) to simulate an average prototype container weight, W = 14,400 kg. Each debris was equipped with a BLE tag and a motion sensor which recorded the three-dimensional position and orientation, hence the term "smart" debris. The coordinate system and the debris rotation angles are shown in Figure 3.

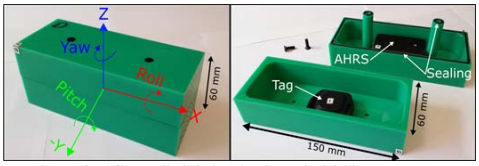

Figure3: "Smart" debris -1:40 scaled 20' prototype containers with tracking devices installed

Tracking data were recorded with a combination of different carefully synchronized data acquisition systems. A software-based video frame grabber was used to record images at 24 Hz. A Linux-based system drove the positioning engine to determine the (x,y,z)-positions in space with a sampling rate which was dependent on the number of debris used in each test. Sampling rates of 25 Hz were attained during the tests with 18 debris units. In addition to the positioning engine, a network time protocol server (NTP) was operated on the Linux-PC which broadcasted the current computer clock time into the network that connected the DAQ computer. According to the NTP-server output, synchronization accuracy in the order of 30 ms was achieved during the tests. Finally, a third computer, also connected to the NTP-synchronization network, was used to setup and read-out the motion sensors.

4. Results

The main goal of this experimental study was to assess the validity and accuracy of the prescriptions of the upcoming ASCE-7 Tsunami Effects and Loads chapter (Chock et al. 2015). The spreading angle and the longitudinal displacement of multiple "smart" debris were measured and processed for each test run. Stereo-images were processed using a color thresholding method in order to isolate the shapes/contours of the debris within each image frame. This allowed results from the BLE tags and the motion sensors to be compared with results from the stereo-imaging. This allowed to assess the performance of the "smart" debris tracking systems.

Figure 4 shows some of the results in terms of the trajectories of debris from their initial position on the horizontal bottom apron with the presence of structures, respectively. For all tests, debris trajectories remained bounded within the ±22.5° envelope suggested by the new ASCE-7 Tsunami Loads and Effects chapter (Chock et al. 2015). However, an increase in the number of "smart debris" was found to result in a decrease in their longitudinal trajectory length, which was confirmed also by Reuben et al. (2015).

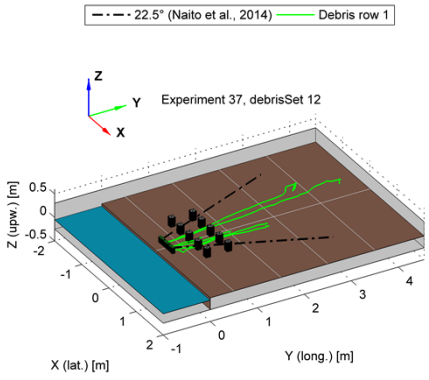

Figure4: Time-history of "smart debris" trajectories – with two rows of fixed structures

5. Conclusions

This field and experimental comprehensive study presents novel results and analysis of the time history of the spatial motion of multiple "smart debris" displaced by overland tsunami bores. This work was conducted with the ultimate goal of assessing the validity of debris motion prescriptions made by the ASCE-7 Tsunami Loads and Effects Committee. An important component of this work was the development of laboratory measurement system capable of simultaneously recording the 6 degree-of-freedom of multiple debris as an alternative to previously used video-camera-based systems

6. References

Due to space limitations, references mentioned are not listed herein.

TWO-EQUATION TURBULENCE MODELLING OF WAVE BOUNDARY LAYERS

Ahmad Sana[1] and Hitoshi Tanaka[2]

1) Department of Civil and Arch. Engineering, Sultan Qaboos University, Muscat, Oman, sana@squ.edu.om
2) Department of Civil Engineering, Tohoku University, Sendai, Japan, hitoshi.tanaka.b7@tohoku.ac.jp

1. Introduction

Different turbulence models of variable complexity based on the user's requirements are used to analyze turbulence boundary layers. The governing (Navier-Stokes) equation is a nonlinear, time-dependent, three-dimensional partial differential equation. The actual solutions of this equation are few and only applicable to laminar flow. At high Reynolds numbers, which is the case for most of the practical applications, the laminar flow undergoes instabilities, generally referred as turbulence. Since these instabilities generate three-dimensional features, no satisfactory 2D approximations for turbulent phenomena are available. In addition, turbulence being random process in time, the deterministic approach is not fully applicable. The turbulent flows contain small fluctuations, which can be resolved by choosing very fine grids and time steps, such that a direct simulation is not feasible for high Reynolds numbers.

Using Reynolds Averaged Navier-Stokes (RANS) models, the computational costs are significantly reduced, however, it requires closure assumptions for the higher moments. Large Eddy Simulation (LES) aims to reduce the dependence on the turbulence model by simulating the major portion of the flow without any models, resolving by the grid. Only the scales smaller than the resolution of the grid are simulated by a model. Such a computational strategy makes LES approach computationally more demanding than RANS. It is estimated that RANS models have a computing time of about 5% of the LES whereas, LES has a computing time of about 10% of DNS [1].

Owing to the computational economy and reasonable accuracy of RANS models, various practical flow phenomena have been simulated using different types of models. In this paper, a brief review of some of the applications of two-equation turbulence models in different types of wave boundary layers is presented. Such a review may be helpful in selecting an appropriate turbulence model for relevant field applications.

2. Types of RANS Models

Generally, RANS models are classified based on the number of transport equations of turbulent quantities employed in the model. Therefore, the names one-equation (using the transport equation of turbulent kinetic energy only) and two-equation (utilizing the transport equations of turbulent kinetic energy and another turbulent quantity such as the dissipation rate) are used in the literature. General availability of sufficient computational power has made the utilization of two-equation turbulence models more convenient than three decades earlier.

The most popular two-equation models are k-ε and k-ω models, which have been used a large number of field applications [2].

3. Two-Equation Models and Wave BL

Originally, the two-equation models were developed for steady boundary layers. Later, these models were applied to various complex flows including the boundary layers under unsteady flow. However, using two-equation models for simulating wave boundary layers started in late 70s and became more popular in 90s. Since then, various types of wave boundary layers have been analyzed using two-equation models [3-8].

3.1. Sinusoidal Wave Boundary Layers

A total of five k-ε model versions were applied to sinusoidal wave boundary layers and the model predictions were compared with the available DNS data [3]. It was found that the original model by Jones and Launder [9] performed better in predicting the transition, whereas the version by Myong and Kasagi[10] proved to be superior in predicting turbulent kinetic energy.

Another study employed three versions of k-ε and three versions of k-ω models to analyze sinusoidal wave boundary layers. The comparison with the DNS data showed that the newer versions of k-ε model showed overall better performance, whereas the k-ω model by Wilcox [11] showed better results for bottom shear stress.

3.2. Cnoidal Wave Boundary Layers

Cnoidal wave theory describes an asymmetric wave profile with a sharp crest and flat trough. In coastal environments, such type of waves exist in the vicinity of the breaking point. Figure 1 shows the k-ε model results of temporal variation of the bottom shear stress in a wave cycle for various Reynolds Numbers ranging from laminar to turbulent condition [6]. For laminar flow, the computed and the analytical solution show almost perfect agreement. The time variation of the shear stress under asymmetric wave shows significantly different behavior than that in sinusoidal wave BL.

3.3. Saw-tooth Wave Boundary Layers

The saw-tooth waves occur at the breaking point in the coastal environments. The *k-ω* model results of acceleration parameter (Fig. 2) with the experimental data as a function of the wave skew-ness parameter, α, show quite good agreement [7].

3.4. Irregular Wave Boundary Layers

Figure 3 shows the wall shear stress with the *k-ω* model predictions. The three versions show a good comparison of wall shear stress with the experimental data. However, the peak values of the shear stress, except the highest one, are underestimated [5].

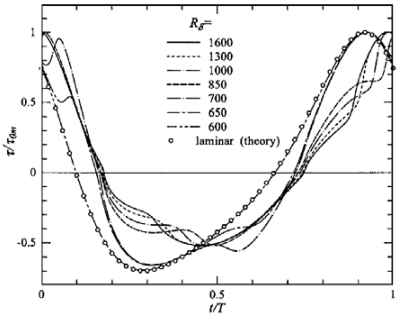

***Figure 1. Bottom sheat stress under cnoidal wave with As=0.6* [6]**

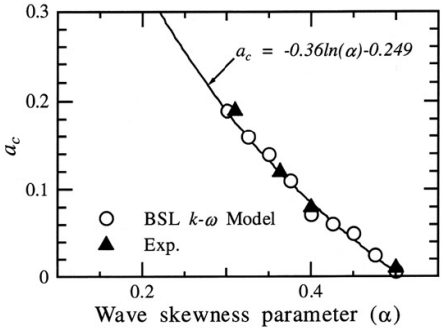

***Figure 2. Acceleration and wave skewness parameters in saw-tooth wave BL* [7]**

4. Future Research

The ongoing research deals with the solitary wave boundary layers, wave-current combined motion, shear stress and sediment transport modeling under tsunami and other long waves. Although, LES and DNS simulations of wave boundary layers are becoming more popular owing to the availability of powerful computing facilities, the two-equation models are more popular among the practicing engineers by virtue of their simplicity and computational economy with reasonable accuracy.

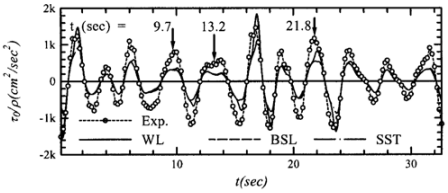

***Figure 3. Bottom shear stress under irregular waves* [5]**

5. References

[1] Sodja, J., Turbulence models in CFD, University of Ljubljana, Department of physics, Ljubljana, 2007. (http://mafija.fmf.uni-lj.si/seminar/files/2006_2007/Turbulence_models_in_CFD.pdf)

[2] Nichols, R. H. *Turbulence Models and Their Application to Complex Flows*, University of Alabama at Birmingham, USA, 2014(https://overflow.larc.nasa.gov/files/2014/06/Turbulence_Guide_v4.01.pdf)

[3] Sana, A. and Tanaka, H., "Review of k-e model to analyze oscillatory boundary layers*", Journal of Hydraulic Engineering (ASCE)*, 2000, 126, 9, 701-710.

[4] Sana, A. and Shuy, E. B., "Two-Equation turbulence models for smooth oscillatory boundary layers", *Journal of Waterway, Port, Coastal and Ocean Engineering (ASCE)*, 2002, 128, 1, 38-45.

[5] Sana, A., Tanaka, H. and Suzuki, T., "Experimental and numerical study of irregular wave boundary layers on a rough bottom", *Proceedings, International Conference on Coastal Engineering (ASCE)*, Lisbon, Portugal, 2004, 1, pp.521-528.

[6] Sana, A., Tanaka, H., Yamaji, H. and Kawamura, I., "Hydrodynamic Behavior of Asymmetric Oscillatory Boundary Layers at Low Reynolds Numbers", *Journal of Hydraulic Engineering (ASCE)*, 2006, 132, 10, 1086-1096.

[7] Suntoyo, Tanaka, H. and Sana, A., "Characteristics of turbulent boundary layers over a rough bed under saw-tooth waves and its application to sediment transport", *Coastal Engineering*, Elsevier, 2008, 55, 12, 1102-1112.

[8] Sana, A. and Tanaka, H., "Two-Equation turbulence modeling of an oscillatory boundary layer under steep pressure gradient", *Canadian Journal of Civil Engineering*, 2010, 37, 4, 648-656.

[9] Jones, W. P., and Launder, B. E., "The prediction of laminarization with a two-equation model of turbulence", *Int. J. Heat Mass Transfer*, 1972, 15, 301–314.

[10] Myong, H. K., and Kasagi, N., "A new approach to the improvement of *k-ε* turbulence model for wall-bounded shear flows", *JMSE Int. J., Tokyo, Series II*, 1990, 33, 1, 63–72.

[11] Wilcox, D. C., "Reassessment of the scale-determining equation for advanced turbulence models", *AIAA J.*, 1988, 26, 11, 1299–1310.

RECENT STUDIES ON COASTAL DISASTER MITIGATION

Tomoya Shibayama[1]

Department of Civil and Environmental Engineering, Waseda University, Tokyo, Japan
shibayama@waseda.jp

1. Introduction

There have been significant storm surge and high wind wave attacks over the world in the past fifteen years. Hurricane Katrina (USA) in 2005, Cyclone Sidr (Bangladesh) in 2007, Cyclone Nargis (Myanmar) in 2008 and Typhoon Haiyan (Philippines) in 2013 are some of the most recent important examples. To predict the behaviours of storms and resultant surges or waves, numerical simulation models are proposed and examined in recent times. The model still has shortcomings, but it is now possible to conduct accurate predictions. The model is composed of three sub-models: climate, storm surge and wind wave. They are applied for cases in the Philippines and Japan. The model limitations are also discussed.

2. Framework of Prediction Models

2.1. Storm Surge

The storm surge prediction model is composed of the Weather Research and Forecasting model, WRF [1], and the Unstructured Grid Finite Volume Coastal Ocean Model, FVCOM [2]. Figure 1 shows the general flow of the model elements. In order to predict the storm surge heights with good accuracy, it is necessary to capture the wind and pressure fields of strong typhoons with high precision.

2.2. Wave

The wave prediction model is a combination of WRF and the third generation wave forecast model, SWAN [3]. Figure 2 shows the general flow of the model elements. Here as well, the accurate wind field predictions under low pressure conditions are the most important factors for high precision results.

3. Real-world Applications

3.1. Storm Surge Model - Haiyan (2013)

Figure 3 shows the comparison of measured and predicted values by the present model system for the storm surge heights in Leyte bay during the attack of Typhoon Haiyan in 2013. In the figure, we also draw the predicted values corresponding to the conditions after global warming (2100 RCP8.5). In general, the agreements between the predicted and the measured values are not very good. In order to get better estimations, it is necessary to try the calculations in parallel by changing physics models or given conditions and calculate ensemble means of the results.

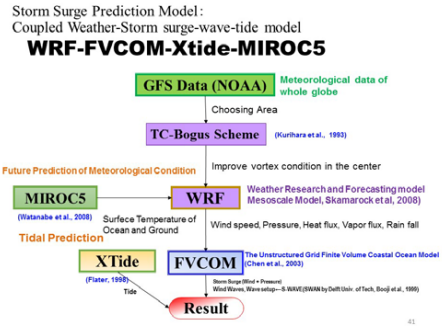

Figure 1. Diagram for storm surge prediction [4].

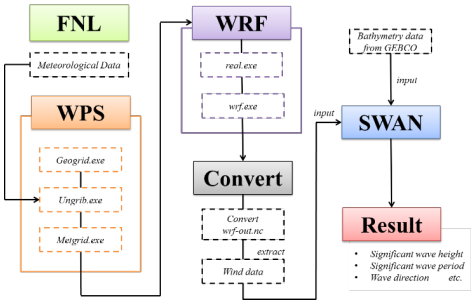

Figure 2. Diagram for wind wave surge prediction [5].

3.2. Wave Model - Japan Coast

Hindcast simulations are conducted to evaluate the wave climate in Japanese islands for the whole year of 2014. In the area, typhoons pass the Pacific coast side frequently during the summer season. The calculation results of wave heights are highly dependent on typhoon route. This results in the difficulty to continuously calculate the wave conditions for a whole month period during summer. Instead, we calculate by changing the

duration of one prediction appropriately, typically less than one month, and combine the results for the whole year in order to improve the accuracy of calculated waves. From the comparison of the hindcast and measured values, we can judge that the calculation results give good agreements after the justification of calculation duration by using trials and errors.

4. Conclusions

The present forecasting models composed of climate, storm surge and wind waves sub-models give good estimation by considering the precise physical processes. However, if they are applied to real phenomena under typhoon attack, there are discrepancies for typhoon route and intensity. In order to improve the accuracy of the models, it is necessary to use ensemble prediction by calculating several cases. For wind-wave prediction, it is necessary to modify calculation durations for long-term predictions.

5. Acknowledgements

The present work was performed as a part of activities of Research Institute of Sustainable Future Society, Waseda Research Institute for Science and Engineering, Waseda University. Also, funding was provided by Penta-Ocean Construction Co., Ltd.

6. References

[1] Skamarock, W. C., Klemp, J. B. (2008): A time-split nonhydrostatic atmospheric model for weather research and forecasting applications, Journal of Computational Physics, 227(7), 3465-3485.

[2] Chen C, Liu H and Beardsley RC (2003) An Unstructured Grid , Finite-Volume , Three-Dimensional , Primitive Equations Ocean Model: Application to Coastal Ocean and Estuaries. Journal of Atmospheric and Oceanic Technology 20:159-186.

[3] Booij, N. R. R. C., Ris, R. C., Holthuijsen, L. H. (1999): A third-generation wave model for coastal regions: 1. Model description and validation, Journal of geophysical research: Oceans, 104(C4), 7649-7666.

[4] Nakamura, R., Shibayama, T., Esteban, M., & Iwamoto, T.: Future Typhoon and Storm Surges under Different Global Warming Scenarios: Case Study of Typhoon Haiyan (2013), Natural Hazards, 82(3), 1645-1681, 2016.

[5] Nishizaki, S., Shibayama, T., Takabatake, T. & Nakamura, R. (2017): Hindcasting of wave climate along the pacific coast of Japan in October 2014, Proceeding of the 9th International Conference on Asian and Pacific Coasts, 129-138, 2017.

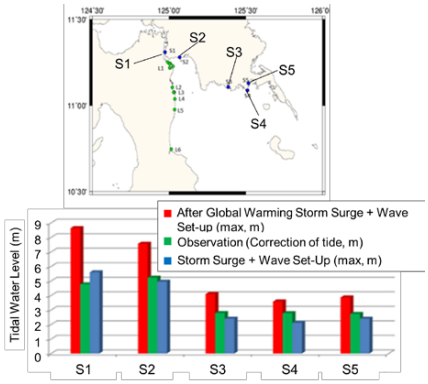

Figure 3. Comparison of storm surge height for Typhoon Haiyan [4].

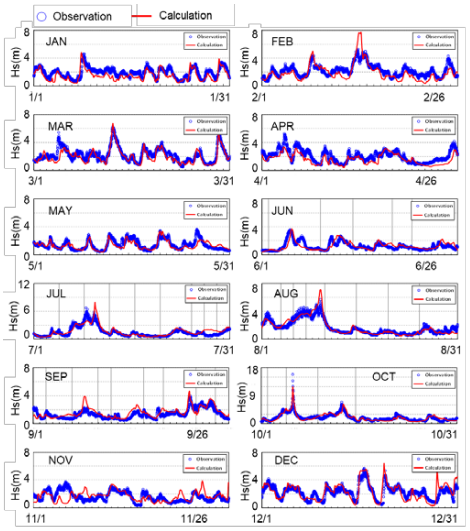

Figure 4. Comparison of significant wave height at Omaezaki, Japan [5].

AN ALTERNATIVE TO SAVING OUR BEACHES FROM SEA LEVEL RISE: THE SAND ENGINE

Marcel Stive[1], Matthieu de Schipper[1], Sierd de Vries[1], Arjen Luijendijk[2], Stefan Aarninkhof[1] and Jaap van Thiel deVries[3]

1) Delft University of Technology, Civil Enineering, Delft, The Netherlands, m.j.f.stive@tudelft.nl
2) Deltares, Delft, The Netherlands, arjen.luijendijk@deltares.nl
3) Royal Boskalis, Papendrecht, The Netherlands, j.v.thiel.de.vries@boskalis.com

1. Introduction

The Netherlands has recently adopted a boldly innovative intervention approach named "The Sand Engine". The Sand Engine is a very large, locally concentrated sand nourishment of 21.5 Mm^3, aiming to provide safety against flooding in combination with new spatial values. Such an approach could provide useful elements for other low-lying areas around the globe. The Sand Engine nourishment initially spans the coastal system over a 2.4 km stretch, and extends up to 1 km offshore following a specific shape (Figure 1). The main expectation is that the Sand Engine will stabilize the coastline at its present position and feed the adjacent coastal sections over an extended length of time (20 years) and space (order of 10 km). Here, for the first time, we describe the thinking behind this world-first climate change adaptation strategy and present numerical model predictions of its long-term evolution along with the observed natural evolution of the Sand Engine during its first year of existence. However, implementing far-reaching interventions like the Sand Engine in the modern reflective society requires a paradigm shift that is necessary to implement such interventions in the light of possibly accelerated climate change.

Figure 1. Aerial photograph of the Sand Engine after completion (September 2011) looking southward. Picture courtesy of Rijkswaterstaat/Joop van Houdt.

2. Paradigm shift

The paradigm shift in the approach of water and coastal management that is observable during the last decades represents a major challenge for the coming century. Where in the past the challenge was formulated as to "fight" the forces of nature, today's approach recognises the many issues other than protection against flooding and especially the multiple ecological forces that have to be accommodated and can help the processes of protection. While this issue has received attention in the western world since about two decades, it is increasingly also being recognized by the non-western world, notably the growth countries. This implies that water and coastal management have become interdisciplinary as well as transdisciplinary [1]. Some of the issues and dilemmas involved in this challenge are illustrated by the following examples.

In a critical evaluation of the morphological, ecological and socio-economic effects of large number human interventions in the Dutch Delta project (following the 1953 flood disaster), Saeijs et al. [2] advocate working with nature in any future flood protection project in estuarine and coastal environments. A number of their recommendations exemplify this: " …(1) If there is still is a choice, leave untouched estuaries and deltas alone. … (2) If there is already a history of human intervention, try to adopt the most flexible approaches to safety and development. …(3) Reversible and local measures within the limits of the natural processes are preferable….".

The recommendations of [2] regarding working with nature are in line with today's policy (cf. the coastal policy to maintain the coastline with "soft" solutions rather than hard (concrete) barriers). Nevertheless implementing the recommendations appears to be complex. For instance, sea revetments may hamper natural processes, but from an economic viewpoint it is generally not justifiable to remove revetments, let alone from a socio-emotional perspective. The complexity may be further illustrated by the conclusions of Jonkman et al. [3] drawing lessons for the Dutch from the New Orleans flood disaster of 2005. These authors observe a tendency in Dutch policy to head towards the US model of mitigating the consequences instead of strengthening the flood defences, while prevention of floods is receiving gradually and relatively

less attention. Then, arguing that (1) the protection standards are over 40 years old and have not evolved with the increase of economic value of the protected area over time, and that (2) the societal risks associated with flood defences on a national scale are larger than in other domains of the Dutch society (Ten Brinke and Bannink, 2004), these authors concluded that a fundamental debate on the required safety levels of Dutch flood defences is necessary. This will undoubtedly lead to the need for stronger flood defences challenging the proponents of soft solutions to fulfil safety requirements as well as incorporating ecological and societal aspects in an evaluation of a design.

Coping with these dilemmas, is an example of the major challenge for the near future. It illustrates that "building with nature" (De Vriend and Van Koningsveld, [4]) not simply implies the use of methods from natural sciences, but involves a range of different disciplines and asks for a transdisciplinary approach. This paradigm shift is very prominent in Dutch coastal zone management and it is within this context that the Sand Engine concept was developed.

3. The Sand Engine

The above discussion and context calls for adaptation strategies that are unprecedented; both in form and magnitude. Recognizing this need, policymakers in the Netherlands, in close collaboration with the scientific community, have recently adopted an innovative intervention approach named "The Sand Engine" (*Zand Motor,* www.zandmotor.nl) to address the potentially massive threat of flooding in the low lying coastal zone of the Netherlands from projected Sea Level Rise (SLR). The Sand Engine is a very large sand nourishment of 21.5 Mm^3: a nourishment magnitude for defence against flooding that is unprecedented anywhere on the globe.

The initial nourishment spans the coastal system over a 2.4 km stretch, and extends up to 1 km offshore following a specific shape (Figure 1). The shape of the nourishment was largely inspired by the potential to provide areas for nature and recreation. It consists of a large hook-shaped peninsula attached to the shoreline by a base of ~ 1 km and including a small (7.5 ha) lake (Figure 1). The curved tip of the peninsula provides shelter from waves and the shallow artificial lagoon formed behind the tip is expected to offer habitats for flatfish and other organisms.

The responsible decision makers found this solution attractive and approved the mega-nourishment of 21.5 Mm^3 at Ter Heijde coast in the province of South Holland. The Sand Engine was, to a large extent, constructed between March and July 2011 using sand mined from approximately 10 km offshore, with some additional work in early 2012. It presents a world-first research site as well as a practical demonstration of total coastal management system linking a coastal engineering construction with environmental, ecological and social considerations. To date, the project has received a very positive response by the general public and especially by recreational beach users, notably wave, wind and kite surfers.

The main expectation is that the Sand Engine will perturb the coastal system such that the coastline will, as a minimum, be stabilized at its present position over an extended length of time (20 years) and space (10 km). An anticipated secondary benefit is the creation of environmentally and recreationally attractive space in this strongly urbanized coastal stretch.

4. Conclusions

A boldly innovative soft engineering intervention, comprising an unprecedented 21.5 Mm^3 sand nourishment known as the Sand Engine, has been recently implemented in the Netherlands. The Sand Engine is a pilot project to test the efficacy of local mega-nourishments as a counter measure for the anticipated enhanced coastal recession due to accelerated sea level rise in the 21st century. This single mega-nourishment is expected to be more efficient and economical in the long term than traditional shoreface nourishments that are presently being used to negate coastal recession. Preliminary numerical model results indicate that this nourishment will result in the widening of the beach along an 8 km stretch of the coastline, and a beach area gain of 200 ha over a 20 yr period. First observations show indeed a redistribution of the sand, feeding the adjacent coasts, roughly 40% towards the south and 60% towards the north. While the jury is still out on this globally unique intervention, if proven successful, it may well become a global generic solution for combating sea level rise driven coastal recession on open coasts.

5. References

[1] Waterman, R.E. *Integrated Coastal Policy via Building with Nature.* 2nd edn. The Hague, 2008, 449 p. (www.ronaldwaterman.com)

[2] Saeijs, H.L.F., Smits, A.J.M., Overmars, W, and Willems, D. (eds). *Changing Estuaries, Changing Views*. Erasmus University Rotterdam, Radboud University, Nijmegen, 2004, 53 p (http://repub.eur.nl/res/pub/1850/ESM-2004-005.pdf)

[3] Jonkman, S.N., Stive, M.J.F. and Vrijling, J.K. (2005). New Orleans is a lesson to the Dutch, Editorial. *Journal of Coastal Research*, 21(6) November 2005; xi-xii

[4] De Vriend and Van Koningsveld (2012). Building with Nature. Thinking, acting and interacting differently. *EcoShape, ISBN 978-94-6190-957-2*

BUILDING WITH NATURE IN THE COASTAL ZONE

Johan C. Winterwerp (and many colleagues)

Delft University of Technology and Wetlands International, the Netherlands, j.c.winterwerp@tudelft.nl

The scale at which humankind interferes in coastal systems is growing exponentially, owing to demographic developments, urbanization and the size of constructions. Adverse effects, such as coastal erosion, poor water quality and degraded ecosystems are visible across the world. Losses of sediment in upstream reservoirs or across the continental shelf (New Orleans), large scale sand mining, subsidence and climate change further threaten coastal communities and ecosystems. Reasons for these adverse effects are well-known and range from uneducated/uninformed interventions to mono-disciplinary management.

In particular, violating the physical laws of nature can be extremely harmful, whereas nature can be a strong ally of mankind, when treated with respect. This is the basic idea behind Building with Nature (BwN), which promotes to use the power of nature to achieve societal goals, rather than working against nature. The philosophy behind BwN contains the following elements:

1. Integration of all interests – refrain from mono-disciplinary solutions,
2. Involve all stakeholders from the very beginning,
3. Use natural processes to achieve one's goals,
4. Obey the inherent time scales of natural processes in the management of coastal systems,
5. Follow a flexible and adaptive design and construction strategy, which allows learning-by-doing and learning-from-mistakes.
6. Respect, and where possible, enforce local ecosystems in order to maintain ecosystem services.

As many problems in coastal systems are the result of uninformed and uneducated interventions, education and communication form an important aspect of all BwN projects.

Letting nature do the work for you of course requires a thorough understanding of the natural system and its forces and possibilities. Development of knowledge and know-how is too often categorized as costs, whereas they generally provide a very high return-on-investment. As such, BwN is often an economic alternative for practices developed in the course of the 20th century – economic on both short term and in in particular in the long term.

The management of the Dutch coastal zone is a typical example on how knowledge and know-how steered the evolution of an ever more reliable and at the same time cheaper and less offensive strategy. The current zenith of this approach is the installation of the Sand Motor, details of which are presented in another presentation by Prof. Stive.

BwN is a design and construction philosophy and does not provide a "one size fits all" – solutions are always site-specific. What works at one location, not necessarily works elsewhere. But our experience with BwN can give guidelines. As an example, Figure 1 presents an array of solutions, depending on available space and hydrodynamic forcings.

Figure 1: Array of BwN solutions

In this presentation we elaborate on our BwN experience in muddy-mangrove coasts. These coasts contain important ecosystems, which may be provide many USD 10,000/ha worth of ecosystem services. The basic scientific background for the BwN works in these coastal systems is fairly simple (equation (1)):

coastal development = deposition – erosion (1)

Of course, if there is more erosion than deposition, the coastline will retreat, and vice versa. However, the important observation is that the two gross terms on the right hand side of equation (1) are many orders of magnitude larger than the net coastal development. This implies that small changes in deposition and/or erosion rates may have very large effects on the net coastal development. In our presentation, we show how net erosion rates of many 10s to 100 m/yr are induced by small changes in deposition rates, and how BwN works can stop and reverse this erosion.

Our example refers to Demak, Indonesia, which suffers from coastal erosion rates of over 100 m/yr. The trigger to this erosion is large scale cutting of mangroves in favor of aquaculture ponds. This case is exemplary for 10,000s km of mangrove coastline across the world in Asia, Africa and South and Latin America. Our philosophy is to stop/reverse coastal erosion by restoring the protecting mangrove green belt, which is achieved by restoring the mangrove habitat, which is accomplished by restoring the local sediment balance.

In Indonesia, conversion of mangrove forest to aquaculture ponds is done because of mono-interest management of the coastal zone, i.e. earn much money in a brief period. However, the ponds are productive for a few years only, upon which local communities lose their land and fall back into poverty. The Indonesian government estimates the annual loss in economic growth due to land erosion in Indonesia at three billion USD. Our BwN project therefore also includes a strong socio-economic component, teaching local communities techniques for sustainable aquaculture and other means of income from the mangrove forest.

1

HYDRODYNAMICS AND SEDIMENT

CASPIAN RAPID SEA LEVEL CHANGING IMPACT on GORGAN BAY MORPHOLOGIC DEFORMATION

Homayoun Khoshravan[1] and Tahereh Alinejhad-Tabrizi[2]

1) Head of Environment research management Group (EMRIRAN), Science research and Technology ministry of Iran , Mazandaran, Iran, h_khoshravan@yahoo.com
2) Senior expert of scientific collaboration and international affairs, Environment research management Group (EMRIRAN), Science research and Technology ministry of Iran, n.alinejhad.t@gmail.com

1. Introduction

The Caspian rapid Sea level changing has direct impact on the marginal basin. Morphologic and environment condition of many bays of the Caspian Sea have been affected during the last century. Ghara- Boghaz Gol as the biggest Bay of the Caspian Sea had experienced full drought condition in 1984 while the Caspian Sea level decreased about 3 meters during 1930- 1978[1]. Gorgan Bay is the other main marginal basin in the south-eastern of the Caspian Sea which has same vulnerability response to the sea level changing. Nowadays the Gorgan bay has lost vast parts of its water supplies due to Caspian Sea level decrease and its morphological consideration has changed obviously [2]. Therefore, the main objective of this paper is the evaluation of morphological changing of Gorgan bay due to sea level fluctuation of the Caspian Sea.

2. The Study Area

The Gorgan bay watershed is one of the most important southern catchments of Caspian Sea basin with an area about 15000 Km^2 which consists of mountainous, sub mountain regions, and coastal plains [3]. The Gorgan bay is located at the southeastern part of Caspian Sea and lies in west-east direction parallel with shoreline (fig. 1). At the moment, the length of the bay is 54 Km and it's width at the widest section is about 12 Km. the area of Gorgan bay is 360 Km^2 and its maximum water depth is evaluated about 2.5 m [4].

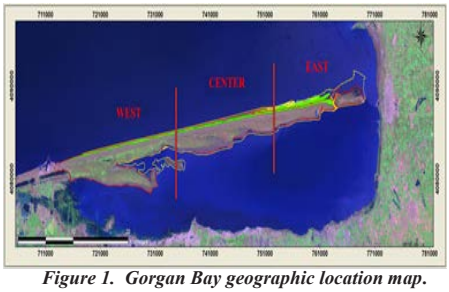

Figure 1. Gorgan Bay geographic location map.

3. Methods and Materials

The deformation of Gorgan bay morphological condition has been evaluated by comparing the satellite pictures (Land sat- TM images). The morphology and sedimentary condition of Gorgan Bay have been studied by field measuring and laboratory tests. By selecting 4 monitoring transects in the western, central and eastern part of Gorgan Bay, 23 sediment samples have been collected in coastal zone and beach structure and geometry have been measured by cartographical survey. Then main results have been analyzed for Gorgan bay morphological classification and beach response to rapid sea level changing.

4. Results

4.1. Gorgan Bay Morphology Classification

Three morphological zones have been determined which have different response to Caspian Sea level changing. The steepness of beach, berm wide and sediment varied from west to East of Gorgan Bay. The maximum deep of basin is located in the central part of Gorgan bay and the steepness of shore has decreased gradually toward western part. So the most vulnerable zone of Gorgan Bay to Caspian Sea level fluctuation has spread in the western part. The comparison between historical satellite pictures (1977- 1995 -2017) showed that the reaction of Miankaleh peninsula and Gorgan bay shoreline are so different towards Caspian Sea water level variations (fig. 2). The maximum shoreline displacement due to Caspian Sea water level increment has been appeared in western and at the end of eastern north of Gorgan bay overlooking to the north of Ashooradeh Island. The Gorgan bay area is now reduced up to 360 Km^2, while it was about 450 Km^2 in 1995 year. The area of outlet channels have been reduced from 15.4 Km^2 at 1995 to 9.3 Km^2 nowadays, and the island with an area about 0.1 Km^2 has been exposed from water between Ashooradeh and Chopoghli channels (fig. 2).

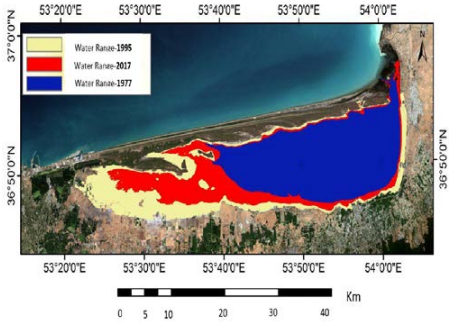

Figure 2. The Gorgan Bay area changing between 1977- 2017 years.

4.2. The Classification of Sedimentary Environments of Gorgan Bay

The field studies have shown the various sedimentary environments in Gorgan bay as follow mentioned:

- Marsh sediments, including dark clays with high organic materials, full of Mollusks lime shells (gastropods and bivalves)
- Sandy spit sediments, including well sorted brown reddish sands, with bivalve shells
- Marine sediments, fine well sorted sandy materials along with microorganisms and marine mollusks lime crusts
- Sand dunes and Aeolians, including fine light brown well sorted sands and iron oxide without marine shells

The study of 17 sediment samples showed us that the sediments texture has been changed from east to west of Gorgan Bay and the percent of very fine sediments have different amount in each transects (fig. 3). The clay and silt are frequent in the lagoon environment and mud flats and the sand sediments have been deposited more near to North central to North Eastern of Gorgan bay.

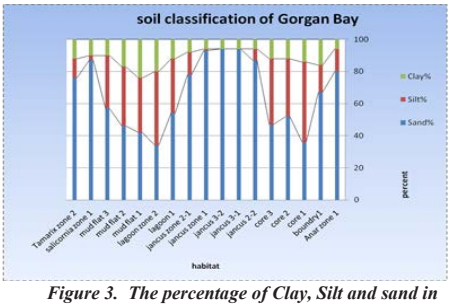

Figure 3. The percentage of Clay, Silt and sand in the sediments of Gorgan bay.

5. Conclusion

The Caspian Sea water level has experienced about 3 m shrinkage between 1930-1978 and has reached to -28 m water level, and as a result the huge parts of Gorgan bay have been dried out. The maximum drought vulnerability has been observed in western areas of Gorgan bay and the complete obstruction of Ashooradeh, Chopoghli and Khoozini channels inlets have caused the blockage of water to the Gorgan bay. the morphologic response of Gorgan bay are sensitive to rapid fluctuations of Caspian Sea, and the maximum bay area has been happened at -26 m sea level in 1995 years. As a result the pendulous acceleration of water level variations during downfall and development periods may cause serious challenges for related water bodies, just as the current events in Gorgan bay and Miankaleh wetland.

6. Acknowledgment

This research project has been supported by INSF (Iranian National Science Foundation) and it is vital pleasure to thank all colleagues who were participated and collaborated in field survey and monitoring.

7. References

[1] Kakroodi, A. A., Kroonenberg, S. B., Hoogendoorn, R. M., Mohammd Khani, H., Yamani, M., Ghassemi, M. R. & Lahijani, H. A. K., "Rapid Holocene sea level changes along the Iranian Caspian coast", Quaternary International, 263, 2012b, pp: 93-103.

[2] Sharbati, S., Ghanghermeh, A., "the forcasting of Caspian Sea level decreasing impact on Gorgan Bay", the Journal of science and technology of environment, 17, No. 4, 2015, pp: 33-45.

[3] Alizadeh, H., "sedimentology and geochemistry index of Gorgan Bay", the journal of oceanography, 1, 2010, pp: 45- 55.

[4] Khoshravan, H., "Caspian Sea morphodynamic classification", the Journal of Earth and Space, Geophysic survey of Tehran University, 3, 2011, V. 37.

PARAMETRIC STUDY OF DEGREE OF BENDING IN TUBULAR KT-JOINTS UNDER THE IPB LOADING

Esmaeil Zavvar[1] and Hamid Ahmadi[2]

1) Faculty of Civil Engineering, University of Tabriz, Tabriz, Iran, esmaeilzavvar@gmail.com
2) Faculty of Civil Engineering, University of Tabriz, Tabriz, Iran, h-ahmadi@tabrizu.ac.ir

1. Introduction

Until now, offshore steel platform structures have used for exploration of gas and oil to meet energy requirements. Structural platforms are fabricated from Circular Hollow Sections. In particular, circular hollow sections have proved to be suitable for structural elements. Due to their shape, circular hollow sections have low drag coefficients and therefore are the most favorite choice for elements subjected to the wind and wave loading. Thanks to low cyclic loading, they are susceptible to fatigue damage.

Tubular welded joints have more complex geometry than other plated joints. Due to the variety of geometries that tubular joint may have, the classification approach is not useful for the design of such joints. One approach, for designing weld details from the viewpoint of potential failure from the weld toe, is the so-called hot-spot stress method [1].

The non-linear distribution around the weld-toe stress concentration area is contingent on the weld toe geometry and is difficult to estimate during the design of tubular welded joints. Nevertheless, it would have little effect for a deep crack [2]. Consequently, the stress distribution throughout the wall thickness is presumed to be a linear combination of membrane stresses and bending stresses. It can be characterized by the degree of bending (DoB), i.e. DoB expressed as DoB = $\frac{\sigma_B}{\sigma_B+\sigma_M}$. Where $\sigma_B$the bending is stress component, and σ_M is membrane stress components.

The degree of bending is a significant input parameter for the estimation of fatigue crack growth in tubular joints, and the high degree of bending in conjunction with the load-shedding mechanism, make the performance of fatigue crack growth in tubular joints different from other types of welded steel joints. The analyzes indicated that not only does the fatigue life of the tubular welded joint dependent on the HSS, but also it is dramatically influenced by the throughout-the-thickness stress distribution. Consideration of load shedding makes the effect of DoB on fatigue life more pronounced as shedding of membrane stresses due to crack growth occurs at a considerably slower rate relative to the shedding of bending stresses in the same hot-spot section [2].

The degree-of-bending value throughout the weld toe of a tubular welded joint subject to any types of loading condition is predicted by the joint geometry. In order to study the behaviour of tubular welded joints and to easily correlate this behaviour to the geometrical features of the joint, a set of dimensionless geometrical parameters has been defined.

The tubular KT-joint is a common joint type found in offshore steel platform structures. Nevertheless, notwithstanding the significant role of the DoB in assessing the fatigue performance of tubular welded joints, DoB values in KT-joints exposed to in-plane bending (IPB) moment loads have not been investigated so far and no any design equation is available to predict DoB values for IPB-loaded joints of this type.

In this paper, the results of analyzing the tubular KT-joints are used to present general remarks on the effect of geometrical parameters including τ, β, γ, and θ. Based on the results of KT-joint finite element models, a new set of DoB parametric formulas was established.

2. Finite Element Modeling

In the present program, the welding size throughout the brace/chord intersection satisfies the AWS D 1.1 [4] is widely discussed in Ahmadi et al. [5]. Details of weld profile modeling performed according to AWS D1.1 [4]

For modeling KT-joints with weld profiles, ANSYS element type SOLID95 was used. These elements have compatible displacements and are well-suited to model curved boundaries. The element is defined by 20 nodes having three degrees of freedom per node and may have any spatial orientation. In order to ensure the mesh quality, a sub-zone mesh generation method is used during the finite element modeling. In this method, the whole structure is divided into several zones according to the computational requirements. The mesh of each zone is generated separately and then by merging the meshes of all the sub-zones are united. Quality and quantity of the mesh can easily control by this method. The mesh generated by this method for a tubular KT-joint is shown in Figure 2.

3. Effect of Geometrical Parameters on the KT-Joints Dobs

In this part, the effect of the parameter β on the tubular KT-joint with different values of the parameter γ is studied. The parameter β is defined as follows: the ratio of the brace diameter to the chord diameter ($\beta = d/D$). Many

comparative charts were used to investigate the influence of the parameter β and only one of them are shown here for the sake of brevity (Figure 3 depicts the change of DoB at the heel in outer brace).

4. Parametric Design Formula for the DoB

Geometrically parametric DoB equations were derived based on multiple non-linear regression analyses performed by the statistical software package, SPSS. The Values which imported in SPSS are dependent variable (i.e. DoB) and independent variables (i.e. β, γ, τ, and θ) constitute the input data imported in the form of a matrix. Each row of this matrix involves the information about the DoB value at the critical positions on the weld toe of the central/outer brace in a tubular KT-joints having specific geometrical characteristics.

The objective was to investigate the effects of dimensionless geometrical parameters on the chord-side DoBs at the at the crown, toe and heel positions. The saddle positions were not studied, since at those positions, the nominal stress at the saddle position is nearly zero and hence the determination of DoB is not necessary. Design formulas met all the acceptance criteria recommended by the UK Department of Energy (DoE) [3]

$$DoB_{CB\ Crown} = (0.743\tau^{-0.023}\gamma^{-0.037}\beta^{-1.116}\theta^{0.219})(1.507\beta + 0.008\tau - 0.119\theta - 0.047\beta\tau) \quad (1)$$
$$, R^2 = 0.916$$

$$DoB_{CB\ Crown} = (0.583\tau^{-0.036}\gamma^{-0.038}\beta^{-0.329}\theta^{-0.084}) \quad (2)$$
$$, R^2 = 0.972$$

$$DoB_{CB\ Crown} = (-0.153\tau^{0.044}\gamma^{-0.064}\beta^{-0.568}\theta^{-1.249})(0.372\beta + 0.621\tau - 3.311\theta - 1.012\beta\tau) \quad (3)$$
$$, R^2 = 0.956$$

5. Conclusion

In the present research, results extracted from the stress analysis of finite element models were used to study the DoBs in tubular KT-joints subjected to in-plane bending load. A geometrically parametric investigation was conducted and then followed by a set of nonlinear regression analyses to derive a DoB parametric equation for the fatigue analysis and design.

6. References

[1] Niemi E, Fricke W, Maddox SJ. Structural hot-spot stress approach to fatigue analysis of welded components. IIW doc. 2000;13:1819-00.

[2] Chang E, Dover WD. Prediction of degree of bending in tubular X and DT joints. International Journal of Fatigue. 1999 Feb 1;21(2):147-61.

[3] UK Department of Energy. Background notes to the fatigue guidance of offshore tubular joints. London, UK; 1983.

[4] American Welding Society (AWS). Structural welding code: AWS D 1.1. Miami (FL), US; 2002.

[5] Ahmadi H, Zavvar E. The effect of multi-planarity on the SCFs in offshore tubular KT-joints subjected to in-plane and out-of-plane bending loads. Thin-Walled Structures. 2016 Sep 1;106:148-65.

Figure 1. The considered in-plane bending (IPB) load case applied to KT-joints

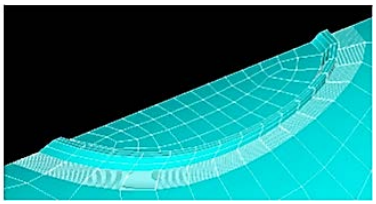

Figure 2. The mesh generated by the sub-zone method for the region between the weld toe and the second extrapolation point

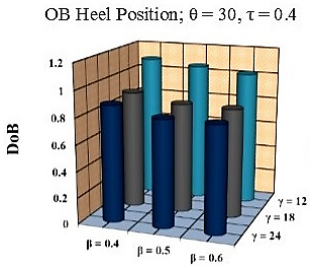

Figure 3. Effect of the β on the DoBs at the heel position in the KT-joint subjected to the IPB loading condition: θ = 30°, τ = 0.4

TIDAL ASYMMETRY IN THE NORTHWESTERN COASTS OF THE PERSIAN GULF

Seyed Taleb Hosseini[1] and Seyed Masoud Mahmoudof[2]

1) Iranian National Institute for Oceanography and Atmospheric Science, sthosseini@gmail.com
2) Iranian National Institute for Oceanography and Atmospheric Science, m_mahmoudof@inio.ac.ir

1. Introduction

The interaction of the astronomical tide and shallow water components results in tidal asymmetry. In such conditions, if the ebb duration (the time period between crest and next trough) is longer than the flood duration, the mass continuity dictates higher velocities during flooding, and the condition is referred to as "flood-dominance". Advancing (delaying) of low water (high water) results in the opposite pattern, known as "ebb-dominance". A representative parameter to describe the tidal asymmetry in shallow estuaries was suggested based on estuarine geometry [1]:

$$f = \frac{a}{\langle d \rangle} - \frac{1}{2}\frac{\Delta w}{\langle w \rangle} \quad (1)$$

where $\langle w \rangle$ and Δw are mean width of tidal channel and its change from low to high tide, respectively. The first term is the ratio of tidal amplitude (a) to mean water depth ($\langle d \rangle$).This parameter describes the relative importance of changes in total water depth and in wet area over a tidal cycle. The values of $f > 0$ or $f < 0$ signifies the flood or ebb-dominance condition respectively [1].

The asymmetric tidal duration using the skewness parameter was discussed as follows [3]:

$$A = \frac{m_3}{m_2^{3/2}} \quad (2)$$

where the i-th moment about mean value is defined as

$$m_i = \frac{1}{J-1}\sum_{j=1}^{J}(n_j)^i \quad (3)$$

and $J$is the number of samples n_j. In this paper the skewness parameter defined in equation (2) is used to quantify duration asymmetry in the rise and fall of water level A^{ε_t} is quantified by substituting $n = \varepsilon_t \equiv \frac{\partial \varepsilon}{\partial t}$ in equation (3) in which ε is water level. The duration of falling water is shorter than rising water when $A^{\varepsilon_t} < 0$ and longer when $A^{\varepsilon_t} > 0$.

To examine the tidal triad asymmetry, the frequencies of the three principal constituents O_1, K_1 and M_2 in terms of their Doodson frequencies [2], is expressed as follows:

$$S_{O_1} = a_{O_1}\cos[(\omega_1 - \omega_2)t - \theta_{O_1}] \quad (4)$$

$$S_{K_1} = a_{K_1}\cos[(\omega_1 + \omega_2)t - \theta_{K_1}] \quad (5)$$

$$S_{M_2} = a_{M_2}\cos(2\omega_1 t - \theta_{M_2}) \quad (6)$$

where, S, can be tidal fluctuation [2]. $2\pi/\omega_1$ is the period of the mean lunar day (24.84 hours) and $2\pi/\omega_2$ the sidereal month (27.32 mean solar days). Using trigonometric identities, it is possible to combine K_1 and O_1 terms into a single equation as follows:

$$S_D = S_{O_1} + S_{K_1} = a_D(t)\cos[\omega_1 t - \theta_D(t)] \quad (7)$$

where,

$$a_D(t) = [a_{O_1}^2 + a_{K_1}^2 + 2a_{O_1}a_{K_1}\cos(2\omega_2 t + \theta_{O_1} - \theta_{K_1})]^{1/2} \quad (8)$$

and

$$\theta_D t = -\arctan\left[\frac{a_{K_1}\sin(\omega_2 t - \theta_{K_1}) - a_{O_1}\sin(\omega_2 t + \theta_{O_1})}{a_{K_1}\cos(\omega_2 t - \theta_{K_1}) + a_{O_1}\cos(\omega_2 t + \theta_{O_1})}\right] \quad (9)$$

Now the intensity of tidal asymmetry can be evaluated by the amplitude ratio, a_D/a_{M_2}; and its direction can be described by $2\theta_D - \theta_{M_2}$ [2].

2. Study Area

The study area consists of five stations on the head of the Persian Gulf (Figure 1), so that three estuarine stations of Khoramshahr, Choebdeh and Hendijan situate in the upstream directions of Arvandrud, Bahmanshir and Zohreh estuaries, respectively. Also, Khowr-e Musa and Bandar-e Emam stations are selected in the mouth and the upstream channel of the Khowr-e Musa Creek, respectively.

Figure 1. The study area and the locations of 5 shallow water estuarine stations (yellow points).

The tide recorder stations (NCC-Iran) show that the mixed and mainly semidiurnal tidal regimes are dominant at 5 studied points with the form number, $[F = (a_{O_1} + a_{K_1})/(a_{M_2} + a_{S_2})]$, between 0.4 and 0.8, (see Table 1).

3. Methods

In this study, time series of Water level fluctuations are analyzed at five stations (see Figure 1 for locations of stations) from 1-Dec- 2016 to 29-Dec- 2016. Data recorded

by NCC-Iran with 30 minutes time step, are implemented for harmonic analysis.

4. Results and Discussion

4.1. Asymmetry from Nonlinearities

The tidal amplitudes from four principal constituents (M2, S2, K1 and O1) and the strongest higher harmonics (overtide and compound tide) are presented in Table 1. These results are derived from harmonics analysis of water level time series with length of 28 days.

Table 1. The amplitudes of four main tidal constituents and the strongest shallow water components.

Station		H	Khowr	B	Ch	Kh
F		0.5	0.76	0.42	0.53	0.62
4 Main Cons.	O_1	24.5	28.8	16.5	18.7	2.3
	K_1	24.6	60.0	60.3	32.0	17.7
	M_2	69.7	89.3	141.1	69.6	27.3
	S_2	28.8	28.1	40.4	25.7	5.0
OverT	M_4	10.7	2.2	15.9	10.5	2.2
Comp. T	MS_4	10.1		10.3		
	MK_3		4.5		7.9	4.2

The maximum and minimum tidal amplitudes occurred at Bandar-e Emam and Khoramshahr stations, respectively (Table 1). The lunar semidiurnal constituent (M_2) was the most important component while the lunar diurnal constituent (O_1) was approximately the weakest tide among four main components at all stations.

At all of five stations, the M_4 was the most important overtide. Also, the strongest compound constituent was MS_4 at Hendijan and Bandar-e Emam stations and MK_3 at three other stations during these 28-day time series of water level fluctuation.

The amplitudes of all main constituents, except O_1, and higher harmonics increased as the direction moved landward within the creek from Khowr-e Musa Station to Bandar-e Emam Station (see Table 1). The increments of tidal amplitudes for higher harmonics induced by nonlinearities were also considerable at three other stations located in the upstream of estuarine embayments.

Based on the morphologic asymmetry factor, (equation 1), nonlinearities imposed by local geometry enforce the ebb-dominance regime where the tidal variation of width is significant. On the other hand, the nonlinearities can alter the asymmetry to flood-dominance due to high convergent effects.

4.2. Asymmetry from Triad K_1-O_1-M_2 and from (K_1-O_1-M_2)-Nonlinearities Interaction

The asymmetry imposed by the triad constituents is ebb-dominance during spring tide and weak flood-dominance during neap tide at all stations (see the open rectangles in Figure 2.a). Although ebb-dominance duration asymmetry is observed over complete length of data recording (see the straight dashed lines in Figure 2.a).

The maximum values of a_D/a_{M_2} occur when the difference between $\theta_{O_1}+\theta_{K_1}-\theta_{M_2}$ line and time-series of $2\theta_D-\theta_{M_2}$ is minimum (see Figures 2.a and 2.b) as confirmed by the results of [2].

The interaction between asymmetries from triad K_1-O_1-M_2 and higher harmonics at five stations are investigated with comparing K_1-O_1-M_2 driven A^{ε_t} and the corresponding value induced by all harmonics.

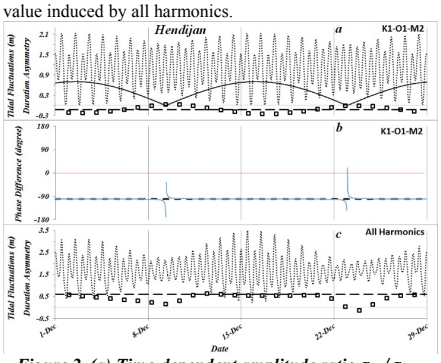

Figure 2. (a) Time-dependent amplitude ratio α_D/α_{M_2} (solid line), triad K_1-O_1-M_2 driven tidal fluctuations (point line) and duration asymmetry computed with both one-lunar-day window (open rectangular) and the full records of 28 days (dashed line) at Hendijan Station, (b) time-dependent phase difference $2\theta_D-\theta_{M_2}$ (narrow blue line), compared with phase differences $\theta_{O_1}+\theta_{K_1}-\theta_{M_2}$ (dashed line) at Hendijan Station during 28 days in December 2016, (c) tidal fluctuations and duration asymmetry similar to (a) but induced by all harmonics.

5. Conclusion

The ebb-dominance from triad K_1-O_1-M_2 is augmented (weakened) by nonlinearities of local geometry where the intertidal storages are (not) considerable. Therefore, the ebb-dominance regime at Khowr-e Musa Station was strengthened at Bandar-e Emam Station. At the estuarine stations of Hendijan, Choebdeh and Khoramshahr, the periodic asymmetry from K_1-O_1-M_2 (ebb-dominance in spring tide and flood-dominance in neap tide) was overcome by higher harmonics due to high convergent effects, so flood-dominance conditions were observed at these stations.

6. References

[1] Friedrichs, C. T., Barotropic tides in channelized estuaries. in Valle-Levinson A (ed) Contemporary issues in estuarine physics. Cambridge University Press 27 – 61, 2010.

[2] Nidzieko, N. J., Tidal asymmetry in estuaries with mixed semidiurnal/diurnal tides. J. Geophys. Res.: Oceans 115(C8), 2010.

[3] Nidzieko, N. J., and Ralston, D. K., Tidal asymmetry and velocity skew over tidal flats and shallow channels within a macrotidal river delta. J. Geophys. Res.: Oceans 117(C3), 2012.

REFLECTION OF IRREGULAR WAVES FROM VERTICAL POROUS SEAWALLS

Mehdi Esmaeili[1*] and Maryam Rahbani[2]

1) Faculty of Marine Sciences, Chabahar Maritime University, Chabahar, Iran, Email: esmaeili@cmu.ac.ir
2) Faculty of Marine Science and Technology, University of Hormozgan, Bandar Abbas, Iran, Email: maryamrahbani@yahoo.com

1. Introduction

Porous seawalls are common shore protection structures around the world. They can dissipate the incident wave energy and reduce the reflected wave height. Vertical porous seawalls are considered as effective replacement for traditional impermeable seawalls, especially for the reduction of wave energy in harbors and fishing ports. The amount of wave energy dissipation depends on the porosity of the seawall. In addition, the shore side of the vertical porous seawall can be used for vessel berthing activities.

Many experimental studies have been conducted on different hydrodynamic aspects of waves, such as reflection, transmission, and dissipation, and their effects on various seawall structures. From the literature survey, it was concluded that nearly no investigation has been carried out on the mechanism of wave reflection from vertical caisson-type porous and semi-porous seawalls.

The present study is based on experimental investigations on wave interactions with vertical porous and semi-porous seawalls in order to estimate the reflection coefficient of the wave against these seawalls. The aim of this research is to better understand the performance of vertical porous and semi-porous seawalls in front of sea waves and to increase the knowledge about this type of coastal structures. To achieve this aim, some laboratory tests were conducted on vertical seawalls for a wide range of hydrodynamic conditions and for different water depths (d= 0.165, 0.270 and 0.375 m). The exact experiments were conducted for plane, semi-porous, and porous seawalls in order to obtain the best performance with regard to the reflection coefficients and to determine an empirical formula for the reflection coefficient, K_r, of each type of seawall.

2. Experimental Set-up and Methods

2.1 Wave Flume

In this experiment, a wave flume with dimensions of 33 m (length) × 5.5 m (width) × 1.5 m (height) was used. The wave flume was provided by the Soil Conservation and Watershed Management Research Institute, Tehran, Iran (Figure 1). It was equipped with a modern DHI wave generating system and included paddle, power pack, hardware, and software components.

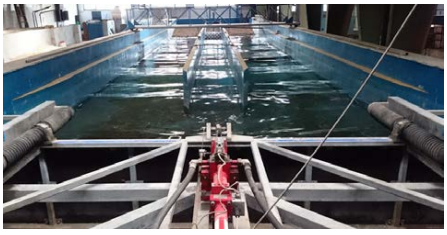

Figure 1. A view of the SCWMRI wave flume.

2.2 Seawall Details

A caisson-type seawall prototype was used in the installation of the wave flume. The dimension of each caisson was 0.1 m × 0.1 m × 0.1 m, and it was made from a 1-cm thick Plexiglas sheet. To obtain a semicircular shape to reduce the reflection of the wave, a semi cylinder Plexiglas with an outer radius of 5 cm and inner radius of 1.5 cm was connected to one of the uncovered sides of the box. The next step involved affixing 50 blocks to a rigid frame in the flume in two formats; one as a totally porous seawall (Figure 2a) and the other as a semi-porous seawall (Figure 2b).

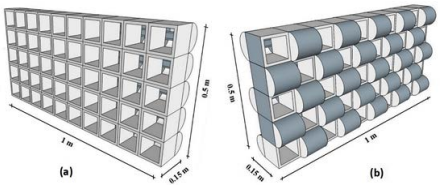

Figure 2. A schematic view of (a) the porous, and (b) the semi- porous seawall.

2.3 Characteristics of the Waves

This experiment involved the use of waves with heights ranging from 0.03 m to 0.15 m and wave periods ranging from 1.6 s to 2.8 s, which, according to the Froude scale (1:10), correspond in actual situations to wave heights of 0.3 m to 1.5 m and wave periods of 5.05 s to 8.85 s, respectively. A total of 120 tests were conducted to measure the reflection coefficient of the irregular waves,

and they were conducted using plane, semi-porous, and porous seawalls. The amount of wave reflection is described by the reflection coefficient K_r, defined in terms of incident and reflected wave heights, H_i and H_r, respectively:

$$K_r = \frac{H_r}{H_i} \quad (1)$$

3. Experimental Results and Discussion

The effect of wave height in terms of wave steepness (H_s/L_p), and wave period in terms of relative water depth (d/L_p), on the reflection coefficient (K_r) was investigated for plane, semi-porous, and porous seawalls. A set of tests were carried out for three different depths: 0.375 m, 0.270 m, and 0.165 m. As the results were quite similar for the different depths, the results relevant to the depth of 0.375 m are presented here.

Figure 3 represents the effect of wave height on the reflection coefficient for different wave periods on the vertical porous seawalls. The reflection coefficients from the plane seawall is relatively high for all H_s/L_p and d/L_p, with values over 0.89. This value for the semi-porous seawall ranged from 0.66 to 0.90, whereas for the porous seawall, it ranged from 0.53 to 0.86. These sets of tests show that the porous and semi-porous seawalls cause a decrease in wave reflection of about 33% and 21%, respectively, in comparison with that for the plane seawall. It is obvious that porous and semi-porous seawalls are better in reducing the wave reflection in comparison to the plane seawall.

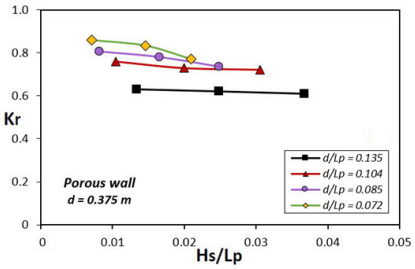

Figure 3. K_r versus H_s/L_p on the porous seawall for different d/L_p in water depths 0.375 m.

Figure 4 shows the variation of K_r with d/L_p on the porous seawalls in water depths of 0.270 m. It is found that the K_r decreases with increasing relative water depth for all the plane, semi-porous, and porous seawalls, for all the depths considered. A comparison of the results for identical input conditions shows that the reduction in K_r for the porous seawall is about 30–42%, and for the semi-porous seawall, it is about 20–25%, when compared with the plane seawall. It is obvious from the plots that porous and semi-porous seawalls are better in reducing the wave reflection in comparison to the plane seawall.

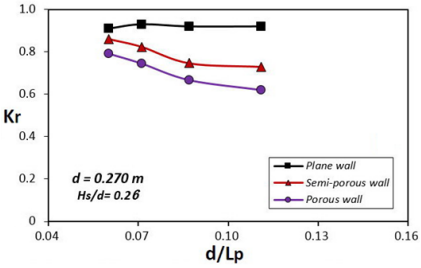

Figure 3. K_r versus d/L_p for porous seawall in water depth 0.260 m.

The results derived from the experimental tests involving irregular waves confirmed that the value of K_r decreases with increasing H_s/L_p and d/L_p, which is in consistent with the results presented by Neelamani and Sandhya (2003), Koraim and Rageh (2013) and Koraim et al. (2014) [1, 2, 3]. Based on the laboratory measurements and multiple regression analysis, predictive equations for the reflection coefficient were obtained [4]. The proposed equations for the plane, semi-porous, and porous seawalls are listed in Table 1.

Table 1. Proposed equations to calculate wave reflection for different seawall types.

Type of seawall	Proposed equation	R^2
Plane	$K_r = 0.86\,(d/L)^{0.026}\,(H_s/L)^{-0.039}$	0.78
Semi-porous	$K_r = 0.45\,(d/L)^{-0.075}\,(H_s/L)^{-0.101}$	0.74
Porous	$K_r = 0.29\,(d/L)^{-0.088}\,(H_s/L)^{-0.176}$	0.76

The results derived from the proposed equations show reasonable agreement with similar tests performed by other researchers.

5. References

[1] Koraim, A. S., Heikal, E. M., and Abo Zaid, A. A., 2014. "Hydrodynamic characteristics of porous seawall protected by submerged breakwater", *Applied Ocean Research*, 46, February 2014, pp. 1-14.

[2] Koraim, A., and Rageh, O., "Hydrodynamic performance of vertical porous structures under regular waves", *China Ocean Engineering*, 4, 27, January 2013, pp. 451-468.

[3] Neelamani, S., and Sandhya, N., "Wave reflection characteristics of plane, dentated and serrated seawalls", *Ocean Engineering*, 30, 12, August 2003, pp. 1507-1533.

[4] Negm, A., and Nassar, K., "Determination of Wave Reflection Formulae for Vertical and Sloped Seawalls Via Experimental Modelling", *Procedia Engineering*, 154, August 2016, pp. 919-927.

A COMBINED WAVE ABSORBER METHOD FOR SPH MODELS

Ali Pooyarad [1] and Hasan Akbari [2]

1) MSc Student, Department of Civil and Environmental Engineering, Tarbiat Modares University, Tehran, Iran, ali.pooyarad@modares.ac.ir
2) Assistant professor, Department of Civil and Environmental Engineering, Tarbiat Modares University, Tehran, Iran, Akbari.h@modares.ac.ir

1. Introduction

It is necessary to model a long computational domain in SPH (Smooth Particle Hydrodynamics) methods. to prevent reflection from solid boundaries. This increases computational cost and it is not cost-effective especially for mesh-free methods. One solution is using a wave absorber to shorten the domain and minimize probable reflections. Wave absorber system is located at the end of the computational domain and reduces the wave energy gradually along the damper length. The use of wave absorption allows modeling long time series of sea waves in relatively short domains with negligible wave reflection. As an initial effort, Larsen and Dancy [1] used an exponential function for damping Boussinesq waves. In an Incompressible SPH model, Xu [2] presented a simple exponential absorbing zone to damp linear wave reflection, in which the absorbing length was 2 times the wave length. Later, Shibata et al.[3] presented a wave absorbing method and they assigned a large viscosity value to the fluid particle in the absorbing region with dimension of 1.98~2.83 times the wave length. Besides, Molteni et al.[4] developed a matched layer approach for the shallow wave damping, in which a shorter damping distance of 1.5 wave length was used. In this paper, two damping systems including a sloping surface at the end of the domain and a velocity reduction system are proposed. The efficiency of each system is analyzed and an effective wave absorber is introduced finally.

2. Governing Equations

Navier Stokes equations in Lagrangian coordinate are solved in SPH model. Following Monaghan [5], the discrete form of these equation in weakly compressible scheme of SPH system is

$$\frac{d\rho_a}{dt} = \sum_b m_b \mathbf{v}_{ab} \cdot \nabla_a W_{ab} \tag{1}$$

$$\frac{d\mathbf{v}_a}{dt} = -\sum_b m_b \left(\frac{P_a + P_b}{\rho_a \cdot \rho_b} + \Pi_{ab} \right) \nabla_a W_{ab} + \mathbf{g} \tag{2}$$

$$\frac{dr_a}{dt} = \mathbf{v}_a \tag{3}$$

Where, r, v and p denote particle position, velocity and pressure, respectively. ρ and m are density and mass of each particle and g is the gravitational acceleration. Particles interact with each other through a Kernel function W_{ab} its value depends on the distance between particles a and b. Π_{ab} is the artificial viscous term as proposed by Monaghan[5]. An equation of state is applied to calculate the pressure via Tait's equation.

3. The Proposed Wave Damper

Two types of dampers are introduced and applied in this study. In the first method, a sloping beach is utilized at the end of the model to absorb wave energy via breaking and run up processes. In the second one, particle velocities decrease gradually inside a damping zone. In this method, velocity of each particle at each time step is modified based on its location via:

$$v = v_0 . f(x) \tag{4}$$

Where, v_0 is the calculated velocity of the particle i , v is the corrected velocity and f(x) is the reduction function defined as

$$f(x) = 1 - \alpha . \left(\frac{x - x_0}{x_1 - x_0} \right)^{\beta} \tag{5}$$

Where, x is position of particles, x_0 and x_1 are the start and end positions of the damping zone, respectively. In this study, values of α=1, β=4 are used in all simulation after sensitivity analysis.

4. Results and Discussion

4.1. Model Configuration

Specifications of different cases are presented in Table1. Sketch of the wave flume and the location of wave absorber are depicted in Figure 1. L_t is domain length and L_d is absorbing region length. In all simulation, wave height, period and length are 0.14m, 2.0s and 4.5m, respectively. Initial water depth is 0.64m. A case with domain length of 10 times of wave length is also modeled, in which no wave reflection occurs. The surface elevation is extracted at the depicted point in Figure 1. Error of each case is calculated by comparing the simulated surface elevation with case 0 and it is normalized by wave height as reported in Table 1.

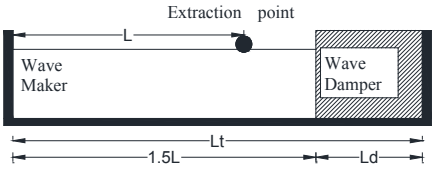

Figure 1. Sketch of the wave flume configuration

Table 1. Cases and condition of dampers

	Damper Length (Ld)	Slope (V:H)	Total length (Lt)	Number of particles	Error %
Case 0	-	-	10L	118148	0
Case 1	-	-	1.5L	19532	36
Case 2	-	1 : 2	1.92L	21422	12.8
Case 3	-	1 : 3	2.13L	22377	3.02
Case 4	-	1 : 4	2.34L	23322	1.95
Case 5	L	-	2.5L	32432	1.22
Case 6	2L	-	3.5L	45332	0.74
Case 7	L	1 : 4	2.5L	25317	1.39

4.2. Wave Absorbing Via Sloped Beach

Different slopes as 1:2 and 1:3 and 1:4 are applied at the end of the model. The results in Figure 2 as well as the reported errors in Table 1 show that the milder slopes can better damp out the waves. However, changing wave characteristics may change the results. Large errors can be detected in case of using no damper (Case 1).

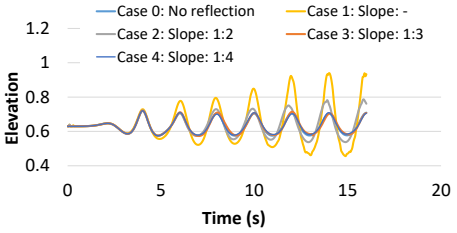

Figure 2. Elevation of water surface at x=L for slope dampers

4.3. Wave Absorbing Via Velocity Damper

Velocity damper with lengths of L and 2L are modeled as Case 5 and 6. The results are shown in Figure 3. According to the results, the latter case outperforms the former one in wave absorption. On the other hand, the wave is even absorbed efficiently by means of a velocity damper with the length equal to the wave length. In contrast to the slope damper, the results of velocity damper are valid for any wave length and therefore it is preferred to slope damper.

Although velocity damper can be applied properly for wave energy absorption, making use of both slope and velocity dampers can results in acceptable errors while less number of particles will be contributed due to sloped beach (Case 7).

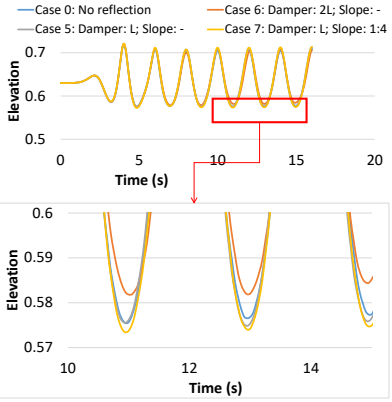

Figure 3. Elevation of water surface at x=L for velocity dampers

5. Conclusion

- Wave energy can be dissipated by means of slope and velocity dampers. However, the latter scheme outperforms the other one and can be applied to different wave conditions.
- Wave can be absorbed properly using a velocity damper with a length equal to the wave length
- To reduce the computational cost, a combination of two methods (velocity and slope dampers) can be used at the end of the model.

6. References

[1] Larsen, J. and H. Dancy, *Open boundaries in short wave simulations—a new approach.* Coastal Engineering, 1983. 7(3): p. 285-297.

[2] Xu, R., *An improved incompressible smoothed particle hydrodynamics method and its application in free-surface simulations*. 2010, University of Manchester.

[3] Shibata, K., et al., *Transparent boundary condition for simulating nonlinear water waves by a particle method.* Ocean Engineering, 2011. 38(16): p. 1839-1848.

[4] Molteni, D., R. Grammauta, and E. Vitanza, *Simple absorbing layer conditions for shallow wave simulations with Smoothed Particle Hydrodynamics.* Ocean Engineering, 2013. 62: p. 78-90.

[5] Gingold, R.A. and J.J. Monaghan, *Smoothed particle hydrodynamics: theory and application to non-spherical stars.* Monthly notices of the royal astronomical society, 1977. 181(3): p. 375-389.

NUMERICAL MODELING OF WAVES BY NONLINEAR FINITE ELEMENT METHOD

Sajedeh Farmani[1], Mahnaz Ghaeini-Hessaroeyeh[2] and Saleh Hamzehei-Javaran[3],

1) Department of Civil Engineering, Faculty of Engineering, Shahid Bahonar University of Kerman, Kerman, Iran, sajedeh.farmani@eng.uk.ac.ir
2) Department of Civil Engineering, Faculty of Engineering, Shahid Bahonar University of Kerman, Kerman, Iran, mghaeini@uk.ac.ir
3) Department of Civil Engineering, Faculty of Engineering, Shahid Bahonar University of Kerman, Kerman, Iran, s.hamzehijavaran@uk.ac.ir

1. Introduction

In this research, a nonlinear Finite Element Method (FEM) is developed for numerical modeling of water wave sloshing in 2D tank. The oscillation motion of liquid in a tank due to an external force is called sloshing phenomenon [1]. In this study, the water wave height is calculated using the present model for the wave maker problem and the numerical results are compared with the available analytical solutions. In the following, the modeling procedure is stated.

2. Governing Equations and Modeling Algorithm

To model the sloshing wave in a tank, it is assumed that the liquid is incompressible, irrotational and inviscid. Therefore, the potential flow theory is governed [1-4]. Relation (1) shows the Laplace equation for potential flow. Boundary conditions also include the velocity potential on the free surface and the normal velocity at the tank walls (Dirichlet and Neumann boundary conditions).

$$\nabla^2\phi = 0 \tag{1}$$

in which, ϕ denotes the velocity potential. At the initial of time step, the velocity potential at the free surface is known and for all modeling in this study is considered equal to zero. While, for next time steps, it is needed to be found, and therefore it can be computed by the dynamic condition. Also, the free surface elevation at the initial time step is known and in the other time steps it is calculated by the kinematic condition [1]. Relations (2) and (3) indicate these conditions.

$$\frac{\partial\phi}{\partial t} + \frac{1}{2}\nabla\phi.\nabla\phi + g\eta = 0 \tag{2}$$

$$\frac{\partial\eta}{\partial t} + \frac{\partial\phi}{\partial t}.\frac{\partial\eta}{\partial x} - \frac{\partial\phi}{\partial y} = 0 \tag{3}$$

Where, η shows the free surface elevation and g and t are the gravitational acceleration and time, respectively.

The above relations can be written in the Lagrangian form, then:

$$\frac{d\phi}{dt} = \frac{1}{2}\nabla\phi.\nabla\phi - g\eta \tag{4}$$

$$\frac{dx}{dt} = \frac{\partial\phi}{\partial x}, \quad \frac{\partial y}{\partial t} = \frac{\partial\phi}{\partial y} \tag{5}$$

By employing the FEM for solving the Laplace equation, relation (6) can be obtained:

$$K\phi = 0, \quad K = \int_\Gamma (\nabla N)^T (\nabla N)\, d\Gamma \tag{6}$$

where N is the interpolation (shape) function and K indicates the coefficient matrix.

After calculating the velocity potential using FEM, the horizontal and vertical velocities can be obtained. For this purpose, the cubic spline approximation is used [4]. Then, the velocity potential at the free surface and the height of free surface are updated by relations (4) and (5) for the next time step. It should be noted that, the fourth-order Rung-Kutta method is utilized for updating in this study [1, 3].

After several time steps, the free surface nodes may be placed into a steep gradient and this causes the numerical instability. In order to prevent this problem, the smoothing and regridding techniques are needed for the free surface nodes [1, 3, 5]. In this research, the cubic spline is applied for smoothing.

3. Validation

In order to validate and investigate the accuracy of the present model, a numerical test is considered in this section.

3.1. The Wave Maker Problem

The dimensions of tank and also the location of wave maker are shown in Figure 1. For this problem, the computational domain is meshed with 1000 elements (Figure 2). Figures 3 and 4 show the numerical results obtained from the present model and comparison with the analytical solutions of [6].

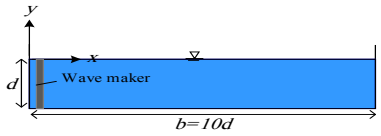

Figure 1. The geometry of wave maker problem.

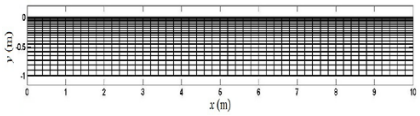

Figure 2. Meshed domain for wave maker problem.

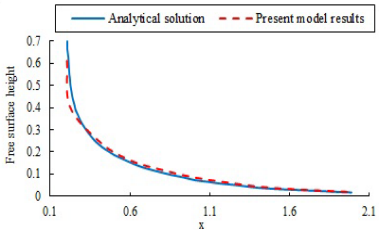

Figure 3. Free surface height at t=0.2 s after beginning the wave maker

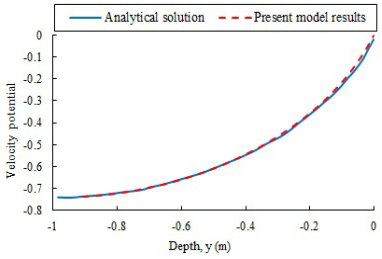

Figure 4. Velocity potential on the wave maker at $t = 0^+$

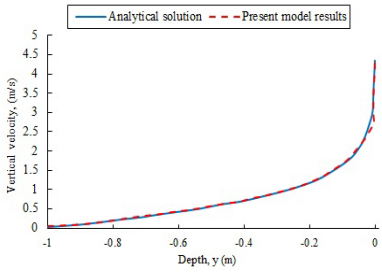

Figure 5. Vertical velocity on the wave maker at $t = 0^+$

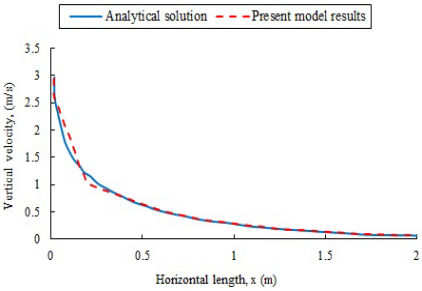

Figure 6. Vertical velocity on the free surface

4. Conclusion

In this study, waves in a tank containing liquid with the wave maker were investigated. For this purpose, a numerical model based on nonlinear finite element method was developed. The results included the free surface height at t=0.2 s, velocity potential and vertical velocity on the wave maker and vertical velocity on the free surface. Then, these results were compared with the analytical solutions. The comparison indicated that the present model presented the results with good accuracy.

5. References

[1] Kolukula, S.S., Chellapandi, P., "Nonlinear Finite Element Analysis of Sloshing" *Adv. Numer. Anal.,* Article ID 571528, 2013, 10 pages.

[2] Kolukula, S.S, Chellapandi, P., "Finite element simulation of dynamic stability of plan free-surface of a liquid under vertical excitation". *Model Simul. Eng.*; Article ID 252760, 2013, 13 pages.

[3] Sriram, V., Sannasasiraj, S.A., Sundar, V., "Numerical simulation of 2D sloshing waves due to horizontal and vertical random excitation". *Appl. Ocean. Res.,* 28, 2006, pp. 19-32.

[4] Sriram, V., Sannasiraj, S.A., Sundar, V., "Simulation of 2-D nonlinear waves using finite element method with cubic spline approximation". *J. Fluids. Struct.* 22, 2006, pp. 663-681.

[5] Wu, G.X., Taylor, R.E., "Finite element analysis of two-dimensional non-linear transient water waves". *Appl. Ocean. Res.,* 16, 1994, pp. 363-372.

[6] Peregrine, D.H., "Flow due to vertical plate moving in a channel". Unpublished note, Department of Mathematics, University of Bristol, 1972.

PROGRADATION AND TRANSGRESSION OF SHORELINE IN THE ARVAND DELTA (IRANIAN PART) FROM THE LAST 9,000 YEARS TO PRESENT

Maryam Rahmati[1], Raziye Lak[2], Siavash Shayan[3], Zahra Hajikarimi[4] and Zahra Dadashzade[5]

1) Geomorphology Instructor, Lorestan University, Khoramabad, Mary.Rahmati88@gmail.com
2) Sedimentary Associate Professor, Research Institute for earth sciences, Geological Survey of Iran, Tehran, Lak_ir@yahoo.com
3) Geomorphology Associate Professor, Tarbiat Modares University, Tehran, Shayan314@yahoo.com
4) Graduated of Geomorphology, Tarbiat Modares University, Tehran, elahe.hajikarimi@gmail.com
5) Ph. D Student of Geomorphology, Tarbiat Modares University, Tehran, z.dadashzade@yahoo.com

1. Introduction

Deltas are the most dynamic geomorphological landforms which simultaneously affected by the sea and land processes. Arvand delta is located in southwest of Iran and northwest of Persian Gulf. This delta due to the very low slope in foreshore during the last period of the Quaternary to the present influenced the eustatic changes of Persian Gulf and river sedimentation has experienced many changes [2-4] that from foundation – applied geomorphology point of view so far has not been studied. The aim of this study is to achieve the changes and evolution of the Arvand delta.

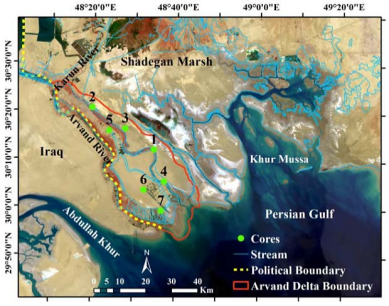

Figure 1. Location of the study area and cores

2. Materials and Methods

Accordingly, seismic data, debit and sediment Ahvaz (Karun) hydrometric stations statistics, tidal data, wave rose, wind rose and current rose, Cartosat (2011), Landsat (1973, 1982, 1994, 2002, 2016) satellite imagery and aerial photographs (1955) had used to study the effective processes on delta's changes at present and geochemistry, granulometery (in the Geological Survey of Iran Laboratory) and dating results (in Beta Analytic Radiocarbon Dating Laboratory (Florida)) of sediments obtained from the 7 cores, for studying the delta morphogenesis processes during the Holocene (Figure 1).

3. Results and Discussions

The results of historical sources, geodynamic station data of Abadan - Ahwaz and the distribution of the earthquakes above the 4 Richter in relation to the distance of active and important faults, in order to investigate the effect of tectonic movements on river channel avulsion and evolution delta, indication of the low mobility and influence of the earth crust on the displacement and changes of the delta landforms in the past and present. Study the rate and direction of shoreline displacement during the past 60 years, in relation to human activities (particularly damming) via technique Digital Shoreline Analysis System (DSAS) represents delta progressing equivalent of 3/8 Km (Figure 2). The most operations of delta-making have been during the period of time 1955-1973. The greatest amount of progressing in the mentioned period has reverse relationship with damming activity in the upstream region.

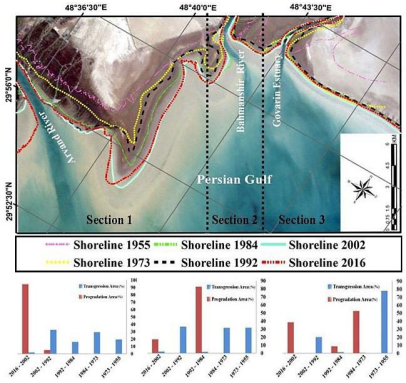

Figure 2. Shorelines position of Arvand delta during years 1955-2016

Longshore currents as an indirect factor and tidal currents as a direct factor were recognized as the main

factors in the creation and transformation of coastal landforms. Separation of sedimentary environments initially was carried out and 3 sedimentary environments, respectively (from up to down) were identified, 3 sedimentary environments fluvial plain, brackish–freshwater marsh and marine (tidal). The variation and sequence of sedimentary environments from the fluvial to the marine is in 3 meters depth on average. Granulometry analysis of 47 sedimentary samples shows study of granulometery cannot correctly do the analysis the sedimentation processes of delta. Elemental analysis of samples shows the amounts of aluminum, chromium, manganese and barium (terrigenous origin) are inversely related to the changes in sea level in this region. Also, change trend in the elements of calcium and strontium (ocean basin) conforms to sea level changes trend. Mineralogy results of samples showed due to the crossing of major rivers flowing to the Arvand delta, especially Karun river from carbonate formations in the Zagros mountains and the geographic location of the Persian Gulf in the semi-tropical climate, the amount of calcium carbonate in the form of calcite, dolomite and aragonite is more than 50% of the total amount of sediment. Evaluation of the dating results after calibration of samples and depth - age graph in the core MR.7 (the southernmost core in the delta distal) shows the average of delta sedimentation rate has been 2.9 mm / yr in 2500 years ago.

4. Conclusion

Water and sediment transport dynamic of Arvand river to the shoreline, has been introduced as main factor of progradation in this part of Persian Gulf shoreline during 1955-2016. Delta-making process had been largest area between the years 1955-1973 .This progradation has been associated with one of the highest peaks of water and sediment flow to Arvand river. Marine currents with direction of east to west have a major role and are responsible in shaping of shoreline convexity and development of spits to the west. The results of this part have been conformed with findings of Some researchers [6].

Also the results of sedimentary paleoenvironments reconstruction and delta morphogenesis processes in relation to Persian Gulf sea level changes has shown geochemical analysis (elemental and mineralogy analysis) of sedimentary samples compared to granulometry analysis can be show better determine the relationship between sea-level changes with delta progressing in this area. Results of carbon isotope analysis (in order to time reconstruction of sedimentation process) and the isotope of oxygen (in order to reconstruction of past climatic conditions) along with other previous studies [1-5, 7] showed Arvand delta due to the interference of active fluvial processes (about 2300 years ago) with progradation and transgression of sea (about 9,000 to 2300 years ago) is formed. Arvand river about 2,300 years ago when the weather was colder than present (-2 /75 °) in response to gradual dropping of sea level had tried to reach itself to the lower basic level (Persian Gulf) with the rate of 3/19 mm/yr (Figure 3).

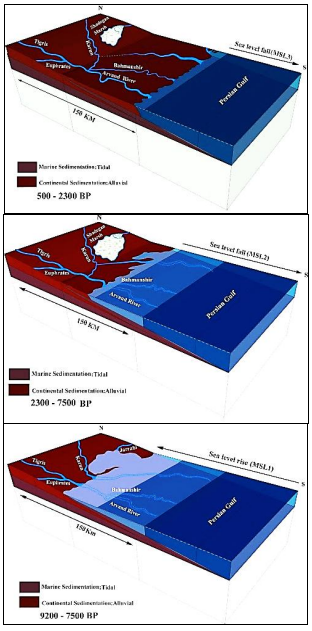

Figure 3. Evolution of Arvand delta during 9000-500 BP

5. References

[1] Aqrawi A. A. M., "Stratigraphic signatures of climatic change during the Holocene evolution of the Tigris–Euphrates delta, lower Mesopotamia", *Global and Planetary Change*, 28, 2001, pp. 267–283.

[2] Bogemans, F., Janssens, R., and C, Baeteman, C., "Depositional evolution of the Lower Khuzestan plain (SW Iran) since the end of the Late Pleistocene", *Quaternary Science Reviews*, 171, 2017, pp.154-165.

[3] Heyvaert, V.M.A., and Baeteman, C.," Holocene Sedimentary Evolution and Palaeocoastlines of the Lower Khuzestan Plain (Southwest Iran)", *Marine Geology*, 242 (1-3), 2007, pp. 83–108.

[4] Lambeck, K., "Shoreline reconstructions for the Persian Gulf since the last glacial maximum", *Earth and Planetary Science Letters*, 142 (1-2), 1996, pp. 43-57.

[5] Purser, B. H., *The Persian Gulf Holocene Carbonate Sedimentation and Diagenesis in a Shallow Epicontinental Sea*, Springer-Verlag, New York, 1973.

[6] Ranjbar, M., and Iranmanesh, F., "Coastal morphodynamic and cyclical changes in the north of Oman sea", *Geography*, 31, 2011, pp. 245-235.

[7] Shahbazi, R., *Study of Quaternary sedimentary changes for recognition of natural patterns of desertification in Shadegan marshes and sabkhas*, Tehran University, Tehran, Iran, Doctoral Thesis, 2016.

COASTAL CURRENTS ON THE NORTHERN OMANI SHELF

Gerd Bruss[1], Andy Kwarteng[2], Mahad Baawain[3], Ahmad Sana[3], Prerana Chitrakar[3], Farid Al-Abdali[1] and Harib Al-Habsi[1]

[1] College of Agricultural and Marine Sciences, Sultan Qaboos University, Muscat, Oman, gerd@squ.edu.com
[2] Remote Sensing and GIS Center, Sultan Qaboos University, Muscat, Oman
[3] Department of Civil and Architectural Engineering, Sultan Qaboos University, Muscat, Oman

1. Introduction

Coastal currents affect morphology, ecology and economy of the coastal zone. The main controlling factors for coastal currents are shelf topography, terrestrial discharges, tides, wind and motions imposed from the open ocean [1]. Since all these factors depend on specific local conditions, coastal currents must be studied locally. Currently, the hydrodynamics along Oman's northern coasts are not well understood. Concepts about currents on the shelf are mainly derived from studies on open ocean processes within the Sea of Oman. The relative importance of tides, wind and mesoscale dynamics on the coastal circulation has not been studied. Nearshore currents remain unclear, largely owing to missing high resolution models and local field data. Here we study coastal flow in the vicinity of Muscat, based on ADCP measurements. Our principal research question was: what are the general patterns and the main drivers of the local circulation?

2. Site Description

The Sea of Oman connects the Arabian/Persian Gulf with the north western Indian Ocean. Several studies on regional ocean circulation describe the slope current of the Persian Gulf Water (PGW) , propagating southwards at 150 - 350 m depth [2] and a system of energetic mesoscale eddies occasionally impinging on the Omani shelf [3, 4]. In this study we focus on the coastal region around Muscat. Tide gauge records at Muscat show a mixed, mainly semidiurnal tide with an average (maximum) tidal range of 1.5 m (3.3 m). Local winds are variable and seldom exceed 10 knots at 10 m height. Local coastal upwelling appears as short irregular events [5].

3. Methods

We measured flow between Ras Al Hamra and Jazirat Al Fahal (Figure 1). A 600 kHz RDI Workhorse Sentinel ADCP was deployed upwards looking at a depth of 20 m. Data was recorded every minute for 76 days during Sep.-Dec. 2017 at a vertical resolution of 1 m. Here we present hourly filtered horizontal current velocities. Records from the tide gauge at Port Sultan Qaboos and wind data measured at Muscat Airport, both in vicinity of the ADCP location, are included in the study. Tidal analysis was performed with the UTide Matlab routines [6]. Rotary spectra using Slepian tapers and wavelet analysis using Morse wavelets were computed following the methods described in [7]. Principal axes and the ratio of the variances along them are determined by principal component analysis.

4. Results

Figure 1 shows the scatter (east vs. north) of all hourly current components. The depth and time averaged flow goes to the east (84°) at 15 cm/s (white arrow Fig.1). The first principal component axis of the scatter, indicating the direction of the highest variance, is also directed to the east (88°). The major and minor axes (black lines in Figure 1) are scaled by 5 times the standard deviation and have an eccentricity of about 4.

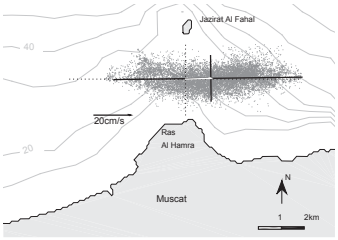

Figure 1. Scatter of east vs. northward current velocity components; residual flow vector (white) and principal component axes (black).

Figure 2 shows the rotary spectra for the surface and bottom layers and for the wind data. All three spectra show distinct diurnal (d) and semidiurnal (sd) peaks. The diurnal band is dominant in the wind and the upper water column. In the upper water layer a second peak appears for clockwise rotation at inertial frequency (f, ~29 h). Inertial and diurnal components decrease towards the sea floor. A weaker peak shows in the rotary spectra over the entire water column at periods between 5 and 30 days.

Figure 3 shows the time series of the current vectors and their wavelet transform. In the time series of the dominant eastward current the diurnal and semidiurnal fluctuations are superimposed by larger low frequency variations. The wavelet transform shows a series of events at periods around 5 days. A longer event around periods of 20 days shifts energy to periods around 5 days on 15. Nov.

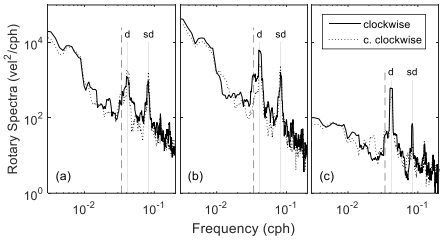

Figure 2. Rotary spectra of currents in cm/s, 2 m above the sea floor (a) and 3 m below the sea surface (b); wind in m/s at 10 m above the sea surface (c).

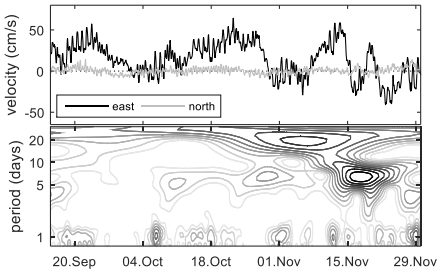

Figure 3. Top: time series of east and northward depth averaged current components. Bottom: wavelet transform of the currents using Morse wavelets.

The wind record mainly correlates to currents in the upper water column. Near the sea surface a maximal correlation of r = 0.48 was found for a time lag of 1 h (wind leading) and an angle of 18° between wind and current vectors. Below the sea surface, wind influence decreases with depth at increasing time lags and changing angles to a correlation of r ~ 0.1 at 3 m depth. Tidal analysis of the flow below the wind influenced layers gives 35 significant harmonics of which K1, M2, OO1 and S2 are the most important ones. MSF and MM were excluded as not realistic (see discussion). The K1/M2 energy % ratio is 50/10 3 m below the surface and 30/16 close to the sea floor. Predicted tidal currents, using the 33 components, correlate to the high pass filtered (period < 1.15d) measurements at r = 0.9. Tidal flow is oriented in east-west direction with an average eccentricity of major/minor axes of 3 and average magnitudes of 10 cm/s.

5. Discussion

The observed currents show high energy in semidiurnal, diurnal and longer period bands. Tides account for about 80% (r^2) of the variation in the semidiurnal and diurnal bands below the wind influenced layers. The local wind also peaks at these two frequencies giving evidence to a pronounced sea breeze. The vertical influence of the wind is however restricted to near surface layers reducing the potential smearing of tidal analysis for lower layers. Possible reasons for the shallow influence of the wind are its strong diurnal and semidiurnal variations and generally low wind speeds. The influence of the diurnal and inertial bands decreases with water depth as has been observed by others [1]. The most energetic currents of up to 60 cm/s are linked to easterly low frequency pulses. When including fortnightly and monthly constituents (MSF + MM) in the tidal analysis some of the low frequency variation can be resolved but this results in an over dominance of these harmonics (combined > 70%). Also, monthly harmonics are insignificant for the local sea level tides and therefore not considered realistic. The isolated pulses identified in the wavelet transform furthermore suggest nonstationary processes. Low pass filtered wind correlates to surface currents but no to the depth averaged low frequency flow and can therefore also not account for this variability.

6. Conclusions

Based on the analysis of ADCP data and local wind and tide gauge records we could determine general patterns of the local circulation on the Muscat shelf. Wind influence is mostly restricted to the upper water column while tidal flow accounts for most of the super inertial variation within the lower water column. Tidal currents are oriented in east-west direction with magnitudes ranging up to 15 cm/s. Sub inertial variations appear as irregular easterly pulses of up to 60 cm/s. Possible drivers for these energetic low frequency pulses are oceanic processes such as PGW flow, mesoscale eddies or alongshore barotropic gradients and coastal trapped waves. Ongoing research aims at understanding the low frequency dynamics and their general impact on the local shelf currents.

7. Acknowledgments

This study was funded by Sultan Qaboos University internal grant IG/AGR/FISH/17/02.

8. References

[1] Churchill, J.H., Lentz, S.J., Farrar, J.T. & Abualnaja, Y. 2014. Properties of Red Sea coastal currents. *Continental Shelf Research*, Volume 78, 51-61.

[2] Bower, A. S., Hunt, H. D., & Price, J. F. 2000. Character and dynamics of the Red Sea and Persian Gulf outflows. *Journal of Geophysical Research*, 105(C3), 6387–6414.

[3] L'Hégaret, P., Lacour, L. & Carton, X. 2013. A seasonal dipolar eddy near Ras Al Hamra (Sea of Oman). *Ocean Dynamics*, 63: 633.

[4] Vic, C., Roullet, G., Capet, X., Carton, X., Molemaker, M. J., & Gula, J. 2015. Eddy-topography interactions and the fate of the Persian Gulf outflow. *Journal of Geophysical Research*: Oceans, 120, 6700–6717

[5] Watanabe, T., Watanabe, T., Yamazaki, A., Pfeiffer, M., Garbe-Schönberg D. and Claereboudt, M. 2017. Past summer upwelling events in the Gulf of Oman derived from a coral geochemical record. *Scientific Reports*. 7.

[6] Codiga, D.L. 2011. Unified Tidal Analysis and Prediction Using the UTide Matlab Functions. Technical Report 2011-01. *Graduate School of Oceanography, University of Rhode Island, Narragansett*, RI. 59pp.

[7] Lilly, J. M. 2017. jLab: A data analysis package for Matlab, v. 1.6.5., http://www.jmlilly.net/jmlsoft.html

ASSESSMENT OF LAND CHARACTERISTICS IMPACT ON TROPICAL CYCLONE FRESHWATER FLOOD VULNERABILITY

Mehdi Rezapour[1] and Tom E. Baldock[2]

1) Assistant professor, Department of Civil Engineering, Chabahar Maritime University, Iran.
2) Professor, School of Civil Engineering, University of Queensland, Australia.

1. Introduction

Although coastal zones are attractive for people to live, they are impacted by different natural phenomena, mostly of hydro-meteorological origin, such as waves, wind, tides, and rainfall which can reach extraordinary magnitudes during the occurrence of severe events such as tropical cyclones and tsunami [3,4,5,6].

2. Methodology and Databases

The impact of rainfall within the catchment has been divided into three main steps (Figure 1); the transformation of rainfall into a runoff; the resulting flood flows corresponding to the runoff and the losses arising from the flood flows.

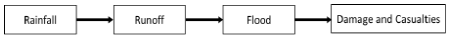

Figure 1. Physical process steps.

The vulnerability is a product of the hazards and exposure to the hazards [1]. Consequently, to develop a rainfall vulnerability index, it is necessary to firstly identify the effective factors, secondly to create indicators that represent the effects of the selected factors and finally to develop a mathematical equation for those indicators as an index [2], (Figure 2).

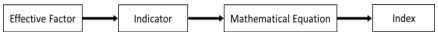

Figure 2. Process steps to develop a general index.

2.1. Land Databases

The 2011 National Land Cover Dataset (NLCD) provided by the Multi-Resolution Land Characteristics (MRLC) consortium has been selected as the Land Use map. The Gridded Soil Survey Geographic (gSSURGO) database that was used in this study is derived from the Soil Survey Geographic (version 2.2) database dated December 1, 2014. The Gridded Population of the World, Version 3 (GPWv3) was selected to quantify the population in the impacted areas. The Shuttle Radar Topographic Mission (STRM) 30m Digital Elevation Data for the continental U.S.A was chosen as the DEM for the study. The impacted areas for each storm have been extracted using the total rainfall map provided by Weather Prediction Center (WPC). Arcmap 10.1 and HEC GeoHMS was used to extract the required result.

3. Hurricanes Jeane versus Frances

Category 2 (SSHS) hurricane Frances (2004) caused 12 billion U.S. dollar worth of damage and led to 49 fatalities, compared with category 3 Hurricane Jeanne (2004), with 7 billion USD of damage and 5 fatalities, in the United States, even though both made landfall at almost the same location, just 2 miles apart in Florida (Table 1). Further, the other existing hurricane scales (SSHS, HII, HHI, and HIS) also do not classify properly the differing impact of these hurricanes (Table 1).

Table 1: Hurricanes Frances and Jeanne.

Characteristics	Frances	Jeanne	Note
Sustained wind (kt)	90	105	At landfall
Radius of max wind (n mi)	29	39	At landfall
Forward Speed (kt)	10	10.5	At landfall
Max surge (ft)	6	5-6	
Landfall location	Florida	Florida	(2 mi apart)
U.S. damage (billion USD)	12	7	2004 values
U.S. death toll	49	5	
SSHS	2	3	
HII	2	2.7	Kantha (2006)
HHI	5.1	7.5	Kantha (2006)
HSI	26	29	Hebert et al. (2010)

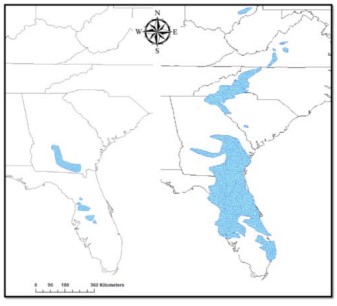

Figure 3. Hurricane Frances impacted areas versus Hurricane Jeanne impacted areas.

Table 2. Hurricanes Jeanne and Frances estimated polygon areas, population and Curve Number.

Hurricane Jeanne 2005			
Polygon Number	Area(A) km^2	Curve Number	Population
1	8885	78.1	41,905
2	174	61.1	10,118
3	287	55.3	33,826
4	1850	70	74,673
5	114	77.8	219,795
6	252	69.7	17,199
7	1663	82.6	56,187
Total	14251	76.8	453,703

Hurricane Frances 2005				
Polygon Number		Area(A) km^2	Curve Number	Population
1		36779	75.9	2,276316
2	1	62400	79.5	7,705,617
	2		78.2	
3		268	64.8	5,374
4	1	18140	64.3	1,222,865
	2		68.3	
	3		63.2	
5		1405	65.8	112,736
6		139	71.2	5,420
7		545	64.3	49,977
8		339	68.3	3,816
9		820	74	11,213
Total		87738	73.7	11,393,334

4. Hurricane Rita (2005) Versus Hurricane Irene (2011)

Table 3. A comparison of the characteristics of hurricanes Rita (2005) and Irene (2011).

Characteristics	Rita (2005)	Irene (2011)	Note
Sustained wind (kt)	96	80	At landfall
Radius of max wind (n mi)	16	20	At landfall
Forward Speed (kt)	16	32	At landfall
Landfall location	Between Texas and Louisiana	North Carolina	
SSHS	3	2	
U.S. damage (billion USD)	14.3	16.1	2013 USD
Fresh water flooding death toll	1	21	
Impacted area $(km)^2$	51,805	82,182	
Impacted population	1,642,000	19,672,000	
Curve Number	84	78	

5. Conclusion and Discussion

Two comparison examples have been presented to explain the role of the land characteristics on vulnerability; hurricane Frances (2004) versus hurricane Jeanne (2004), and hurricane Rita (2005) versus hurricane Irene (2011).

These results show that the impacted area Curve Number of hurricanes Frances and Jeanne are approximately the same which is logically predictable due to their similar trajectories. The reason for differences between their damage and death toll despite the differences in their rainfall characteristics might be due to the significant difference in the number of residents at risk (impacted population). Hurricane Frances affected more than 11 million residents with a population density of 130 people per square kilometre versus approximately half a million residents with a population density of 32 people per square kilometre for Jeanne.

The same calculations have been performed for CAT3 hurricane Rita and CAT2 hurricane Irene to support the theory that population at risk is the most important indicator of freshwater flood vulnerability, between those indicators which were considered in this study. These results indicate that the areas impacted by Rita have greater runoff potential than Irene. However, ignoring any differences in emergency management decisions and evacuation systems, the degree of exposure might also be the reason, since Irene impacted more than 19 million residents versus 1.6 million exposed in hurricane Rita.

References

[1] Alwang, J., Siegel, P. B. & JORGENSEN, S. L. 2001. Vulnerability: a view from different disciplines. Social protection discussion paper series.

[2] Davidson, R. & LAMBERT, K. 2001. Comparing the Hurricane Disaster Risk of U.S. Coastal Counties. *Natural Hazards Review,* 2, 132-142.

[3] Escudero Castillo, M., Mendoza Baldwin, E., Silva Casarin, R., Posada Vanegas, G. & Arganis Juarez, M. 2012. Characterization of Risks in Coastal Zones: A Review. *Clean - Soil, Air, Water,* 40, 894-905.

[4] Rezapour, M. & Baldock, T. E. 2014. Classification of Hurricane Hazards: The Importance of Rainfall. Weather and Forecasting, 29, 1319-1331.

[5] Tran, P. & Shaw, R. 2007. Towards an integrated approach of disaster and environment management: A case study of Thua Thien Hue province, central Viet Nam. *Environmental Hazards,* 7, 271-282.

[6] Van Der Weide, J. 1993. A systems view of integrated coastal management. *Ocean and Coastal Management,* 21, 129-148.

THE CABBELING INSTABILITY IN THE HIGH LATITUDE SEA AND ITS IMPLICATIONS TO THE IRANIAN SEA

Javad Babagoli Matikolaei[1] and Abbasali Aliakbari Bidokhti [1]

1) Institute of Geophysics, University of Tehran, Tehran, Iran, javadbabagoli@ut.ac.ir

1. Introduction

The physical properties of water have a significant effect on the ocean phenomena. Distribution of temperature, salinity, and density are the most important tools to develop physical insight into the structure of water column. The study of these physical oceanography quantities become more substantial in the area where different water mass are combined under different physical conditions (temperature and salinity). Among this region, Greenland Sea is the most important example of this area because the formation of water mass includes 9 water type according to swift and Aagaard (1981). In the course of water mass formation, some Physical phenomena can occur such as double diffusion and cabbeling. Double diffusion is as a result of the difference between salinity and temperature distribution coefficients (Ruddick, 1983). Cabbeling occurs when two separate water parcels mix to form a third which sinks below both parcels. The combined water parcel is denser than the original two water parcels (Foster, 1972). There are many surveys to investigate the cabbeling and double diffusion due to the importance of these phenomena in oceanography. Study of double-diffusive and cabbeling in an environment of the Arctic front by Cottier and Venables (2007), Thermobaricity, cabbeling, and water-mass conversion by Mcdougal (1987) are some of these research. Kasajima and Johannessen (2009) investigate the Role of cabbeling in water densification in the Greenland Basin. Present work concentrates on the effect of cabbeling on the densification in high latitude sea (Greenland, Iceland, and the Norwegian Sea). To evaluate the stability of water column, the Brunt-Vaisala Frequency N and stability ratio $R\rho$ is calculated by following equation (Eq.1).

$$N^2 = \frac{1}{g}\alpha^\theta \theta_z - \beta^\theta \partial S_A / \partial Z\big|_{x,y} = \alpha^\Theta \Theta_Z - \beta^\Theta \partial S_A / \partial z\big|_{x,y} \qquad (1)$$

$$R_\rho = \frac{\alpha^\Theta \Theta_Z}{\beta^\Theta (S_A)_Z}$$

The first step to study of cabbeling is the estimation of thermal expansion α^θ and haline contraction coefficients β^θ. To calculate α^θ and β^θ, the Eq. 2 is used (McDougall et al., 2009).

$$\alpha^\theta = \alpha^\theta(S_A,t,p,p_r) = -\frac{1}{\rho}\frac{\partial \rho}{\partial \theta}\Big|_{S_A,p} = \frac{1}{v}\frac{\partial v}{\partial \theta}\Big|_{S_A,p} = \frac{g_{p\pi}}{g_p}\frac{g_{\pi\pi}(S_A,\theta,p_r)}{g_{\pi\pi}} \qquad (2)$$

$$\beta^\theta = \beta^\theta(S_A,t,p,p_r) = \frac{1}{\rho}\frac{\partial \rho}{\partial S_A}\Big|_{\theta,p} = -\frac{1}{v}\frac{\partial v}{\partial S_A}\Big|_{\theta,p} = \frac{g_{\pi\pi}\left[g_{S_A,T} - g_{S_A,T}(S_A,\theta,P_r\right] - g_{\pi\pi}g_{S_A,p}}{g_p g_{\pi\pi}}$$

Where g Gibbs function of seawater (under different condition based on its index), Θ Conservative Temperature, t situ temperature, p pressure, p_r the reference pressure of the potential temperature, v volume of seawater, S_A absolute Salinity. The cabbeling coefficient quantifies the rate at which dianeutral advection occurs as a result of mixing of heat and salt along the neutral tangent plane. With respect to potential temperature θ, the cabbeling coefficient is (McDougall (1987b))

$$C_b^\Theta = C_b^\Theta(S_A,t,p) = \frac{\partial \alpha\Theta}{\partial \Theta}\Big|_{S_A,P} + 2\frac{\alpha^\Theta}{\beta^\Theta}\frac{\partial \alpha^\Theta}{\partial S_A}\Big|_{\Theta,P} \qquad (3)$$

$$-\left(\frac{\alpha^\Theta}{\beta^\Theta}\right)^2 \frac{\partial \beta^\Theta}{\partial S_A}\Big|_{\Theta,P}$$

2. Hydrography and Method of Research

In March hydrographic observations were performed by ICES (extract from http://www.noaa.gov/). This data is collected in 189 stations in the Greenland Sea, Norwegian and Iceland Sea. Considering the data distribution, the stations cover almost entire areas. The Figure 1 shows the location of reign and the stations.

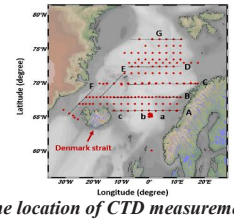

Figure 1. The location of CTD measurements in winter, the geographic position of transects and the bottom topography.

Based on the data, the profile of physical property of water and also many transects is plotted to investigate this area. Among transects, in transects A, B the Atlantic water(AW) and Norwegian Atlantic water (NWAW) mass are the remarkably observed due to high salinity and temperature. To evaluate the effect of cabbeling (and also double diffusion) *T-S* diagrams are plotted. The mixing line between water mass (in *T-S* dia.) and a transect of cabbeling coefficient are plotted (Figure 3). The density ratio for typical profiles of T and S, cabbeling coefficient, and Brunt-Vaisala Frequency, thermal expansion α^θ and haline contraction coefficients β^θ are calculated in all stations.

3. Results and Conclusion

This paper is profound with a thermodynamic view to physical phenomena in water mass formation. We found some of the fronts due to the resolution of our data and being remarkable to distinguish. After this step, we concentrate to warm and saline water which is formed by Atlantic Water (AW) and Norwegian Atlantic Water (NWAW). These fronts were easily found in stations because of the main features of this water mass presented in previous studies.

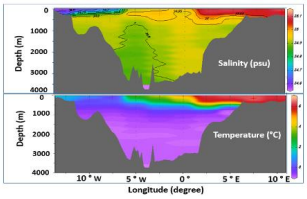

Figure 2. CTD measurements along transect A for temperature, salinity.

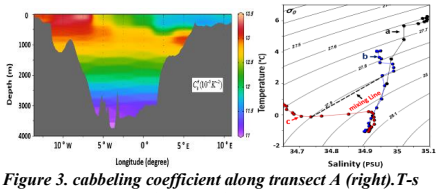

Figure 3. cabbeling coefficient along transect A (right).T-s diagram of a, b, and c (see Fig. 1) mixing line between b and c is plotted.

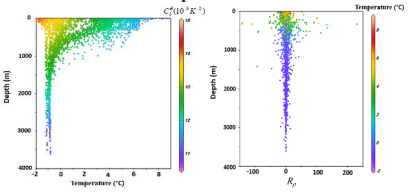

Figure 4. Vertical profiles of cabbeling coefficient (left) and density ratio (right) corresponding to all stations.

In terms of physical properties, the range of temperature and salinity for AW are 6-8 °C and 35.1-35.3 PSU respectively. This values for NWAW are T >3 and S >35(Swift and Aagaard 1981). Based on the result of present work, the width and the thickness of warm and saline water is 400 km and 250 - 300 m respectively (estimated in transect A). Based on these dimensions, the area of this water mass is estimated about 1.2×10^8 m^2. To begin discuss the cabbeling effect, the thermal expansion coefficient and saline contraction coefficient are estimated and plotted profile of each quantities in all stations. For the stations located on the warm and saline water, the α^θ decrease from surface up to 1000 m and after that the α^θ increase with depth. For example in station b, the α^θ decline from 1.20×10^{-4} 1/k (near surface) to 7.5×10^{-5} 1/k (1000 m). After this depth, it enhance linearly up to 1.5×10^{-4} 1/k (3500 m). However α^θ increase linearly from surface to bottom in the stations located 10-20° W. Due to Figure 1, the stations exactly locate the eastern Greenland Current(EGC). It indicates that as the surface temperature rises, the thermal expansion coefficient increases, however after a certain depth the effect of depth can be more important. When it comes to saline contraction coefficient β^θ, it rises to a depth of 700-800 meters and then decreases linearly particularly in the area of saline and warm water. However for the rest of the stations is steadily declining with depth. The typical value for β^θ is between 0.74-0.79 $\times10^{-3}$ kg/g. To investigate the cabbeling effects, it is used the T-S diagram. In some transects such as A and B, the cabbeling phenomena is remarkably observed between isopycnals 28 and 28.1 kg/m^3. For this sections, the cabbeling coefficient is about 10.5-13 $\times10^{-6}$ k^{-2}. The stations located on the Denmark Strait show the cabbeling effect on the outflow which cause that the dense water sink more depth. Due to Whitehead, 1998, this phenomena can affect the overflow speed. The cabbeling cause the increase the column water, sinking, and also a decrease in potential energy (Kasajima and Johannessen, 2009). In terms of instability, the results show that the Brunt-Vaisala frequency is between -4 and 6 cycle/h for all stations. Most of statistic instability is observed near the surface (0-500 m). The density ratio $R\rho$ have a different value in the stations hence salt finger and thermohaline convective layering of the diffusive type can are favorable. We can conclude that cabbeling and double diffusion instability can occur in this area and water mass formation. In terms of implication in Iranian sea, this phenomenon is likely to be found in the gravity current from northern to southern the Caspian Sea water where the flow is colder and low saltier rather than the surrounding water. On the other hand, in the Persian Gulf Outflow (PGO) where enter and move on the Oman Sea it can happen due to being high temperature and salinity rather than surrounding. It may be an important reason for the sinking of water at high depths in winter. From an ecological point of view, water falls into deeper part of basins and it gives the possibility to live for living organisms at greater depths due to its ability to carry oxygen and nutrients.We choose this area to study because we can simultaneously investigate the cabbeling effect under physical condition of the Iranian sea for warm and saline water mass (similar to PGO) and cold and low saline water (similar to the Caspian Sea overflow) although the scale of the phenomena is much more in Greenland sea.

4. References

[1] Cottier, F. R., & Venables, E. J. (2007). On the double-diffusive and cabbeling environment of the Arctic Front, West Spitsbergen. Polar Research, 26(2), 152-159.

[2] Foster, T. D. (1972). An analysis of the cabbeling instability in sea water. *Journal of Physical Oceanography*, *2*(3), 294-301.

[3]Kasajima, Y., & Johannessen, T. (2009). Role of cabbeling in water densification in the Greenland Basin. *Ocean Science*, *5*(3), 247-257.

INVESTIGATION ON THE EFFECTS OF SUBMERGED BREAKWATER ON TSUNAMI RUN-UP

Masih honarmand[1], Ahmad shanehsazzadeh[2*], Mahdi zandi[3] and Arman vahida[4]

1) Department of Civil and Transportation Engineering, University of Isfahan, Isfahan, Iran, honarmand.masih@yahoo.com
2*) Department of Civil and Transportation Engineering, University of Isfahan, Isfahan, Iran, a.shanehsazzadeh@eng.ui.ac.ir
3) Department of Civil and Transportation Engineering, University of Isfahan, Isfahan, Iran, s.m.zandi@eng.ui.ac.ir
4) Department of Civil and Transportation Engineering, University of Isfahan, Isfahan, Iran, armanvahida@yahoo.com

1. Introduction

Owing to casualties and extensive damage caused by tsunami, the recognition of tsunami propagation, ways to tackle it and reducing its run up height are subject of extensive studies. A number of methods such as coastal walls, armor segments, coastal forests, and breakwaters have been used in order to conquer tsunami-related damage and reduce its run up. The application of submerged breakwater is recently considered as one of the effective methods for the reduction of tsunami run up, the advantage is that the near shore activities does not affect and the landscape beauty intact is preserved [1]. In this article the effect of submerged obstacles on the Tsunami run-up is numerically and experimentally investigated. Solitary waves are considered as the model for tsunami. OpenFOAM computational fluid dynamics (CFD) open source software is adopted for numerical simulation of propagation and run-up of tsunami waves in different conditions, with and without submerged breakwater. In order to verify the numerical simulation results, the experimental study is conducted in the hydraulic laboratory of the University of Isfahan.

2. Numerical Method

The governing equations include the continuity equation:

$$\frac{\partial \rho}{\partial t} + \nabla \cdot (\rho \mathbf{u}) = 0 \qquad (1)$$

Where ρ is the density and $\mathbf{u} = \langle u \;\; v \rangle^T$ is the velocity vector and the Navier-Stokes equation:

$$\frac{D\mathbf{u}}{Dt} = -\frac{1}{\rho}\nabla p + \nu \nabla^2 \mathbf{u} + \mathbf{g} \nabla h \qquad (2)$$

Where p is particle pressure, $\mathbf{g}$ is gravitational acceleration, and ν is laminar kinematic viscosity, and h is fluid height from the mean sea level. OpenFOAM is adopted to discrete the equations governing. OpenFOAM includes hundreds of robust CFD applications built from the software developing kits, which can be extended and customized, quickly and conveniently. The applications are used to create CFD simulations across all fields of engineering and science. The algorithm used to discrete the equations governing in the OpenFOAM software is the Pressure Implicit with Splitting of Operator (PISO) [2]. The cross section of experimental set up and corresponding numerical domain is shown in Figure 1. The optimum number of meshes for numerical simulation is 5000 and 400 for x and z directions, respectively.

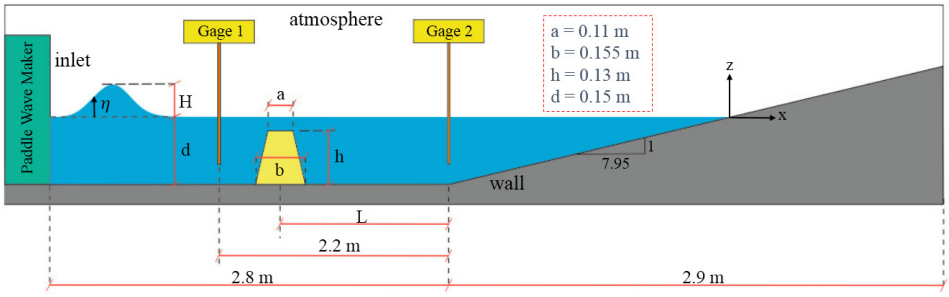

Figure 1. Experimental set up and corresponding numerical domain

3. Experimental Set up

In order to investigate the validity of the results of numerical simulation of wave propagation and run-up on the sloping beach with and without the existence of submerges breakwater, 15 sets of experiment are conducted. The experiments include: one without the obstacle and the others with obstacle for four distances (L) from the slope. For each condition three H/d is examined, where H is wave height and d the water depth. The velocity time series of the solitary shape wave generated by the wave maker at gage 1 are shown in Figure 2.

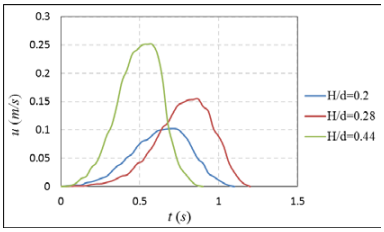

Figure 2. Incident wave generated by wave maker

An example of the water surface elevation at gage 2 predicted by OpenFOAM and that of the measurement are compared in Figure 3, which indicate the extensive accuracy of the numerical simulation.

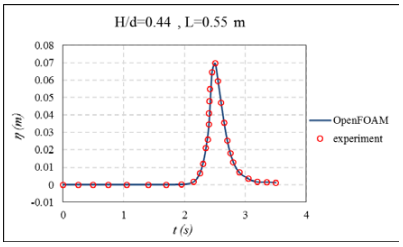

Figure 3. Water surface elevation at gage 2

The results of experimental and numerical simulation for 15 experimental sets are summarized in Table 1. In the table, R/d is relative run-up height.

The percentage of discrepancies presented in the table with the maximum of 2.3%, indicate the accuracy of the model in prediction of run-up height at the present of submerged breakwater. In the left side column of Table 1 the reduction of the run-up height due to the submerged breakwater is shown. As presented in the table, the run-up is reduced up to 20% for the present case study, which is a considerable value.

Table 1. Observations and predictions of maximum solitary wave run-up

Experiment Number	L (m)	H/d	R/d		Percentage of discrepancies	Reduction in run-up height
			Observed	Simulated		
1	Without the Obstacle	0.2	0.71	0.7	2.1	-
2		0.28	1.02	0.99	2.2	-
3		0.44	1.25	1.22	2.3	-
4	0.15	0.2	0.6	0.59	2.3	15 %
5		0.28	0.93	0.91	2.1	9 %
6		0.44	1.16	1.14	1.9	7 %
7	0.55	0.2	0.59	0.58	1.8	17 %
8		0.28	0.9	0.89	1.9	12 %
9		0.44	1.1	1.09	1.8	12 %
10	0.95	0.2	0.58	0.57	1.6	18 %
11		0.28	0.86	0.85	1.5	16 %
12		0.44	1.06	1.05	1.7	15 %
13	1.35	0.2	0.57	0.56	1.4	20 %
14		0.28	0.85	0.83	1.6	17 %
15		0.44	1.03	1.01	1.5	18 %

4. Conclusions

In this research the effects of submerged breakwater on the tsunami run-up height is investigated, experimentally and through numerical simulation. OpenFOAM CFD open source platform is applied for numerical simulation. 15 sets of experiments are carried out for verification of the numerical predictions. The results show that the numerical model predicts the water surface elevation and run-up height with extensive level of accuracy, less than 2.3% discrepancy. The preliminary investigation of the present study shows that the submerged breakwater can diminish the run-up height up to 20%, which is considered as a significant efficiency.

5. References

[1] Irtem, E., Seyfioglu, E. and Kabdasli, S., 2011. Experimental investigation on the effects of submerged breakwaters on tsunami run-up height. Journal of Coastal Research, (64), p.516.

[2] OpenFOAM Programmer's Guide. (2012). Version 2.1.1, 16th May.

PRELIMINARY ASSESSMENT OF WATER QUALITY IN THE COAST OF MUSCAT, OMAN

Prerana Chitrakar[1], Ahmad Sana[1], Mahad Baawain[1], Abdullah Al-Mamun[1], Gerd Bruss[2] and Andy Kwarteng[3]

1) Department of Civil and Architectural Engineering, Sultan Qaboos University, Al-Khoud, Oman, p099279@student.squ.edu.om
2) College of Agricultural and Marine Sciences, Sultan Qaboos University, Muscat, Oman
3) Remote Sensing and GIS Center, Sultan Qaboos University, Muscat, Oman

1. Introduction

The Sea of Oman is the semi-enclosed basin that connects to Arabian Gulf in north by Strait of Hormuz and opens to Arabian Sea in the south. It is located in subtropical zone and experience arid climate. The average sea surface temperature in summer is 31.4 ºC and ranges from 22.6 to 23 ºC in winter [1]. The water circulation in the region is highly governed by the salinity gradient, stratification in water column, wind and tide effects and excess evaporation with limited precipitation. This research aims to measure and study the dynamic water quality parameter along the coast of Muscat, Oman. The coastline highly varies in its character with presence of habitation, ports, refinery, desalination plants and, existence of natural cliffs and harbors. The paper outlines the field measurements including temperature, salinity, dissolve oxygen, chlorophyll-a, and current data. The assessed data helps to understand the physical oceanographic condition. The measurements are also aimed to be used in numerical modeling for assessment and combating marine pollutant effects in the studied area.

2. Study Area

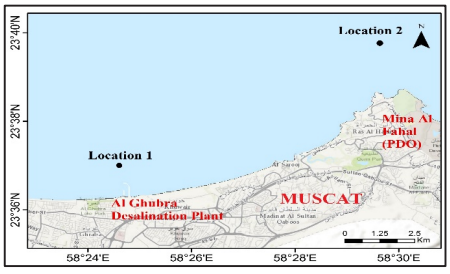

Figure 1. Monitoring Stations along the coast of Muscat

The study was carried out at two important coastal locations of Muscat at Ghubrah and Mina Al Fahal as shown in Figure 1. The study location 1 (23.621°N, 58.407°E) was situated approximately 1.8 km from the Al Ghubrah Desalination Plant and the location 2 (23.659°N, 58.499°E) was situated approximately 3 km from the Petroleum Development Oman in Mina Al Fahal.

3. Methodology

In this study, Sultan Qaboos University (SQU) research vessel Al-Jamiah equipped with ADCP (Acoustic Doppler Current Profiler), CTD (Conductivity-Temperature-Depth), GPS (Global Positioning System) and sampling apparatuses was used for the field location and measurements. Nortek ADCP (Model AWAC AST 600 kHz) was used for measurement of current over the water depth. AWAC was deployed for 132 days at Mina Al Fahal from November 2017 to April 2018. The current data were obtained at every 10 min profile interval. Velocities were sampled with the vertical bin resolution of 1 m and blanking distance of 0.5 m along the water column. RINKO CTD profiler (Model AAQ177) was used to measure the in-situ water quality. The probe was equipped with the sensor to measure the basic water parameter including electric conductivity, temperature, pressure, salinity, dissolve oxygen and chlorophyll-a. The CTD measurements were carried at Mina Al Fahal on December 27, 2017, and on March 6, 2018, and, at Ghubrah on March 6, 2018.

4. Result and Discussion

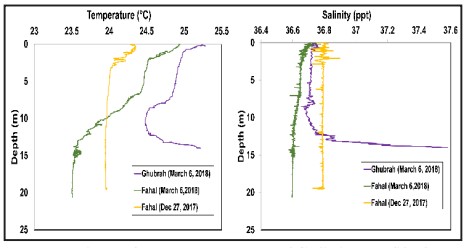

Figure 2. Temperature and Salinity profile for Ghubrah and Mina Al Fahal.

Temperature and salinity profile at Mina Al Fahal (December 2017 and March 2018) and at Ghubrah (March 2018) station are shown in Figure 2. The temperature profile at the Mina Al Fahal on December 2017 did not show any significant stratification and variation of temperature between top and bottom water surface.

However, in March 2018 approximately 1.5 and 1 ºC of the temperature difference was observed between the top and bottom layers at Mina Al Fahal and Ghubrah respectively with thermocline depth ranging from 5 to 13 m of water depth. Salinity profile at Mina Al Fahal Station did not show any major variation between top and bottom layers in both December (winter) and March (spring). At Ghubrah station, halocline was observed with higher salinity at the lower level as compared to upper water surface during spring. This increment of salinity at the lower depth could be attributed by the effect of brine disposal from the Ghubrah Desalination plant.

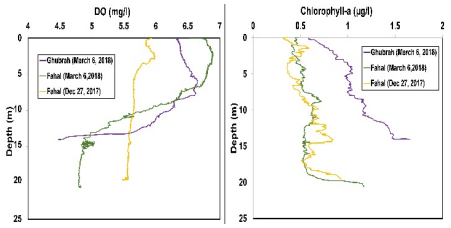

Figure 3. Dissolve Oxygen and Chlorophyll-a profile for Ghubrah and Mina Al Fahal.

Figure 3 shows the dissolved oxygen and chlorophyll- a profiles at Mina Al Fahal (December 2017 and March 2018) and at Ghubrah (March 2018). At Mina Al Fahal no significant variation in dissolved oxygen was noticed during winter with an average concentration of 5.6 mg/l. However, during spring notable difference in dissolved oxygen concentration was observed in top and bottom water level. Dissolved oxygen ranged from 6.9 to 4.8 mg/l at Mina Al Fahal, and from 6.7 to 4.5 mg/l at Ghubrah. Chlorophyll-a profile for Mina Al Fahal does not shows much variation in its concentration between upper and lower sea depths for both December and March study. However, at Ghubrah the trend of increment in chlorophyll-a concentration with respect to the depth was observed with difference of approximately 1 µg/l between the upper and lower depth reading.

Marine lives are most stressed with the decreased dissolved oxygen (below 5 mg/l). The decrease in dissolved oxygen concentration below 2 mg/l for few hours can lead to large fish kill events [2]. Also, chlorophyll-a is an essential indicator for the existence and growth of phytoplankton. Both rise and decrease in the concentration of chlorophyll-a in the sea may result in the fluctuation of nutrient (basically Nitrogen and Phosphorous), causing the adverse effect in marine ecosystem [3]. The growth of phytoplankton reduces the dissolve oxygen leading to the mass mortality of aquatic lives. Therefore, the lower dissolved oxygen and higher chlorophyll-a at the lower sea level noticed at the study locations (especially Ghubrah) indicates the necessity of regular monitoring of these water quality parameter to protect marine ecosystem in the sea.

Figure 4 shows the vertical distribution of average velocity in the water column during the spring and neap tide in December 2017 and March 2018 at Mina Al Fahal Station. All the velocity profiles illustrate similar trend of fluctuation from the sea surface to bottom depth. Sea surface illustrates the higher velocity with smooth transition as compared to the lower bed velocity. At the sea surface, highest velocity of 0.76 m/s and 0.66 m/s was observed during the spring tide event in December 2017 and March 2018 respectively. In addition, the velocities during the spring tide event were marginally more as compared to the velocities at neap tide event for both winter and spring measurement.

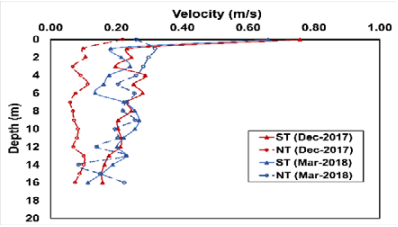

Figure 4. Velocity Profile at Mina Al Fahal. During spring and neap tide events.

5. Conclusion

Water quality parameters including temperature, salinity, dissolve oxygen and chlorophyll-a in coastal locations of Muscat were measured by using CTD probe. In addition, currents measurement from the initial deployment of ADCP were also presented in this study. Temperature and salinity distribution along the water column showed some stratification during spring season. The concentration of dissolved oxygen less than 5 mg/l was observed with increment of chlorophyll-a at the bottom sea surface of studied location. Low dissolved oxygen and high fluctuation in the nutrient in the sea water can adversely impact the lives of aquatic species. Therefore, the study indicates the requirement of regular monitoring of such water quality parameters in the coast of Muscat to safeguard the marine ecosystem.

6. Acknowledgment

The authors would like to acknowledge the financial support provided by the Ministry of Environment and Climate Affairs, Sultanate of Oman, through the research project (CR/DVC/CESAR/15/02).

7. References

[1] Kwarteng, A. Y. and Mozumder, C. "Monitoring chlorophyll-a and sea surface temperature variations in SE Arabian Gulf and NW Sea of Oman from MODIS Aqua data", in *Proceedings 37th Asian Conference on Remote Sensing (ACRS2016)*, Colombo, Sri Lanka, 2016, pp. 1572-1577.

[2] Duxbury, A.B., Duxbury, A.C., and Sverdrup, K.A., *Fundamentals of Oceanography, 4th Ed*, McGraw-Hill, 2002

[3] Jamshidi, S., and Abu Bakar, N.B.,"A study on distribution of chlorophyll-a in the coastal waters of Anzali Port, south Caspian Sea", *Ocean Science Discussions*, 8, 2011, pp. 435-451.

MODELING OF POLLUTANT VARIATION BY SEDIMENT TRANSPORT BASED ON APPLIED NUMERICAL SOLUTION WITH FINITE VOLUME METHOD (CASE STUDY ANZALI PORT)

Seyed Arman Hashemi Monfared[1], Seyed Reza Elyas Langaran[2] and Behrang Ghalamzan[3]

1) Civil Eng. Department, University of Sistan &Baluchestan, Zahedan, Iran, hashemi@eng.usb.ac.ir
2) Civil Eng. Department, University of Sistan &Baluchestan, Zahedan, Iran, sr.elyas@gmail.com
3) Civil Eng. Department, University of Tabriz, Tabriz, Iran, ghalamzan@azaranind.com

1. Introduction

The simulation of hydrodynamics and transport of different substances in lakes and reservoirs is a developing tool in order to predict their internal processes and interactions. Modeling of pollutant in order to predict their variation and keeping them under the criteria limitation plays a key role in ongoing environmental projects [1]. This study focus on concentration changes of water pollutant in basis of applied numerical solution by using MIKE21 software in which compatible for eco-lab hydrodynamic with sediment transport in two dimensional scopes. Time series data's such as wind velocity and direction, eddy viscosity, water ph., water velocity, etc. gathered to treat model. In accordance to high qualified calibration the data's trending precisely checked and the software applied in soft run mode [2]. Boundary condition compiled with three sources that interact inlet and outlet of water quantity due to pollutant changes. At last, verification of the results discussed in comparison of the observed and computed data's.

1.1. Numerical Solution

The discretization in solution domain is performed using a finite volume method in the two dimensional.

1.2. Shallow Water Equations

Integration of the horizontal momentum equations and the continuity equation (1) over depth the two – dimensional shallow water equations obtained

$$\frac{\partial h}{\partial t}+\frac{\partial h\bar{u}}{\partial x}+\frac{\partial h\bar{v}}{\partial y}=hS \qquad (1)$$

Where (u,) $\bar{v}$ is the depth – averaged velocities defined by (2) respectively

$$h\bar{u}=\int_{-d}^{\eta}udz.\quad h\bar{v}=\int_{-d}^{\eta}vdz \qquad (2)$$

The integral form of the system of shallow water equations can in general form be written as (3).

$$\frac{\partial U}{\partial t}+\nabla.\mathrm{F(U)}=\mathrm{S(U)} \qquad (3)$$

Where U is the vector of conserved variables, F is the flux vector function and S is the vector of source terms. All these terms are considered in hydrodynamic section [3].

2. Case Study

The case study is located in Gilan province, Iran. Area of this study is descripted due to $49^o26'$ to $49^o29'$ longitude and 37^o26 to $37^o28'$ Latitude.

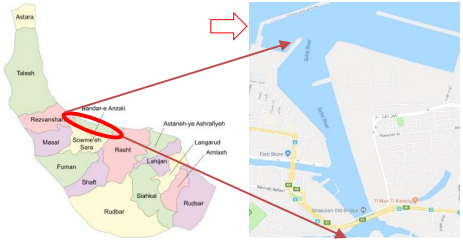

Figure 1. Location of case study and geographical position of Anzali port **[5]**

Anzali port has high range of annual precipitation in which this quantity can affect the flow of sediment into the port and effectively contaminant (Figure 1).

3. Bathymetry

Anzali port is processes with Mike21 software package depend on pollutant concentration variation that simulated in the software based on mesh generator (Figure 2).

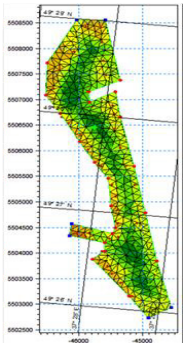

Figure 2. Anzali port mesh generator pollutant changes in the modeling

The model is based on flexible mesh approach, in which it can generate and handle of unstructured meshes including the definition and edition of boundaries [4, 6, 7].

4. Simulation

Observation stations are: 1- North, 2- West and 3- South. Each data's that gathered from these stations are evaluated for any gaps in registration, then by comparison of data information trends, the appropriate nonlinear equation in time series interpolation of the software has used in which it operates as soft start in the simulation [3,4,7]. Table 1, shows the stations longitude and latitude coordinates positions.

Table1. Stations of 1 to 3 and their geographical coordinates

No of Stations	Longitude	Latitude
1- North	$49^0 27' 22"$	$37^0 28' 58"$
2- West	$49^0 27' 16"$	$37^0 28' 11"$
3- South	$49^0 28' 32"$	$37^0 27' 36"$

Figure 3. Location of the stations [5]

Modeling of the parameters due to simulation are consisting of hydrodynamic characteristics. Parameters such as wind direction and angle, velocity profiles, eddy viscosity, humidity in time series format were done and constant items such as manning number in regard of bed river condition entered in the simulation [4, 7].

5. Results and Conclusion

By considering the simulation, accurate outcome for inlet of North and West branch observed beside the outlet of South station. Variation of concentrations for pollutant Zn is shown in figure 4 that demonstrate compatibility of observed data and outcome of the simulation. After the first year of time step these errors are reach closest to zero as it vivid in November for Pb variation in Anzali port area, there are no errors after the fourth month of the time step till the end of the year simulation reaches high compatibility [4,7].

6. Prediction of Pollutant

As it shown in Figure 5 during the month of March – May model compatibility is accordance with observation. The gap during the month of May-June is because of data interpolation in reliance upon shortage of information due to data's trending. In hot season of July-August the model shows precise adaptability depending on pollutant variation.

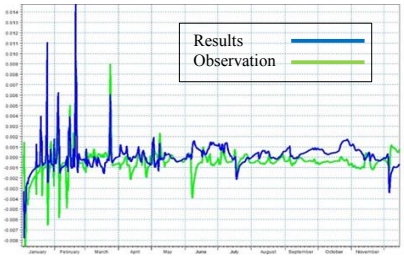

Figure 4. Pb concentration changes in water (ppm)

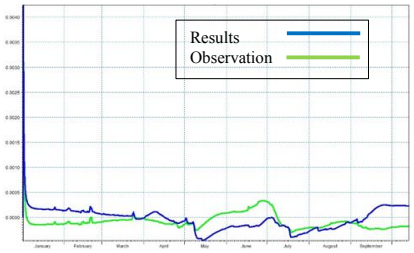

Figure 5. Prediction of sediment pollutant transport

7. References

[1] Elyas Langaran, S. Reza., "*Modeling of heavy metal concentration changes in reservoirs case study Zyqlab dam*", Master of Science Thesis, February 2011.

[2] Hashemi Monfared, S. Arman., Elyas Langaran, S. Reza., *"Fluid dynamics modeling for concentration variation in Kondok tributary using MIKE11"*, 7th National Congress on civil Engineering, Zahedan, Iran

[3] Danish Hydraulic Institute, MIKE collection software manual, scientific document. 2007 edition

[4] Hashemi Monfared, S.A, Elyas Langaran, S.R, "*Applied Modeling of Computational Fluid Dynamic for Eco-Lab concentration changes with sediment transport (Case Study Shadegan Lake)"* The 10th International Conference on Coasts, Ports and Marine Structures ICOPMAS 2012.

[5] http://earth.google.com.

[6] Akbari, Gholamhossein., Elyas Langaran, S. Reza., "*Risk of contaminants modelling errors in Middle East waters*", Technical Journal of Engineering and Applied Sciences, TJEAS Journal-2013-3-14/1441-1446

[7] Hashemi Monfared, S.A, Elyas Langaran, S.R, "*Modeling of heavy metal pollutant in Sarbaz tributary with finite volume method (case study Pishin Dam)"* The 12th International Conference on Coasts, Ports and Marine Structures, ICOPMAS 2016

EXPERIMENTAL STUDY OF WAVE HEIGHT EFFECT ON EFFICEINCY OF AN OFFSHORE FIXED FLOATING OWC

Milad Zabihi[1], Said Mazaheri[2], Masoud Montazeri Namin[3] and Taghi AliAkbari[4]

1) Iranian National Institute for Oceanography and Atmospheric Science, Tehran, Iran, milad.zabihi@inio.ac.ir
2) Iranian National Institute for Oceanography and Atmospheric Science, Tehran, Iran, said.mazaheri@inio.ac.ir
3) Tehran University, Tehran, Iran, mnamin@ut.ac.ir
4) National Iranian Marine Laboratory (NIMALA), Tehran, Iran, taghi.aliakbari@gmail.com

1. Introduction

Renewable energy is one the most interesting marine issues researchers have studied in the last two decades. Considering fossil energy limited resources and their pollutant nature, it is indispensable to find a solution for world future energy demand. Among different kinds of marine renewable energies, wave energy is one of the best resources as it includes higher energy density. Oscillating Water Column is a wave energy converter consisting of a chamber which can be built as a fixed shore or nearshore device or can be a floating one.

The mechanism of OWC working includes wave induced water fluctuation inside a chamber followed by air compressing or decompressing. The pressurized air passes through a vent or nozzle to drive a turbine installed to the chamber. Although there are a lot of studies on OWCs, they are not fully commercialized due to their sophisticated hydrodynamic behavior.

There are a lot of studies conducted on OWCs. A huge part of that is devoted to numerical studies which themselves can be classified into researches based on potential theory [1,2] or studies performed according to Navier-Stokes equation [3,4]. Experimental approach is another method which is undoubtedly crucial in order to reach commercializing stage of OWCs. Contrary to shore based or nearshore OWCs fixed at the sea bottom[5], [6], there are limited experimental tests for floating offshore OWCs. Offshore OWCs has the merit of being exposed to higher wave energy. Moreover, wave energy dissipation takes place more extremely at shallow water region so that 70% of energy may be dissipated through seabed friction and wave breaking [7]. Hence, in this paper efficiency of a fixed floating offshore OWC is investigated. As most of the previous studies focused on wave period and Power Take Off (PTO) damping, this paper is devoted to wave height effect on OWC efficiency.

2. Experimental Method

Experimental tests were performed at National Iranian Marine Laboratory (NIMALA), Tehran, Iran including a towing tank having 400 m length, 6 m width and 4 m depth. The piston type wavemaker generates both regular and irregular waves. The regular wave height can reach to 50 cm height and 3 s period while different types of irregular wave spectra with significant wave height of 40 cm and peak period of 3 s can be generated. Due to long length of the wave tank and existence of the dissipating beach at the end of the tank, interference of the reflected wave and incident wave is not an important problem. In this research a 1:15 scale of a stationary offshore OWC was built using plexiglass materials. To keep OWC in its position and to prevent any movement a holding frame was designed shown in Figure 1.

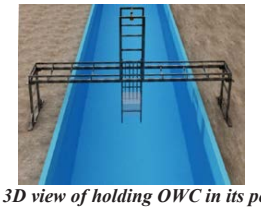

Figure 1. 3D view of holding OWC in its position

Dimensions of the OWC are shown in Figure 2. In this paper, as can be seen in Figure 2, slot shaped aperture is used to simulate PTO damping. Slot size was kept constant during these tests (S=0.5 cm). This value was selected according to previous results which showed that aperture ratio (the ratio of slot area to the chamber roof area) of 0.6 to 0.7% performs optimal. Water depth (d=4 m) and front wall draft (Dr=20 cm) were also remained unchanged during these tests. Figure 3 indicates the instruments such as Wave Gauges (WG) and pressure sensors (PS) installed in the chamber and along the wave tank. All data acquisition process was performed at 50 Hz. JONSWAP wave spectrum was introduced into the wave maker with 4 different wave height (H_{m0}) conditions and Tp between 1.5 up to 2.5 s.

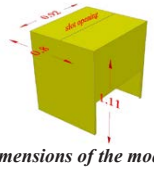

Figure 2. Dimensions of the model (meter)

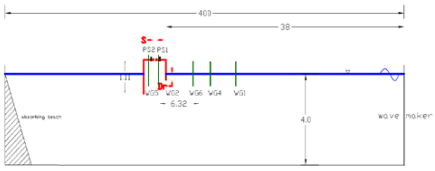

Figure 3. Wave gauges and pressure sensors location

3. Assessment of the OWC Performance

To evaluate OWC performance, efficiency of the device is defined as the ratio of the extracted power (P_{ext}) to the ratio of the incident power (P_{inc}).

$$\xi = \frac{P_{ext}}{P_{inc} \cdot w} \; [-] \tag{1}$$

where w is chamber width. It should be noted that P_{inc} is the wave power per unit width, therefore P_{ext} is divided by chamber width to have non dimensional value. P_{ext} is defined as follows;

$$P_{ext} = \frac{1}{t_{test}} \int_{t_1}^{t_n} P_{r\,air}(t) \cdot Q_{air}(t)\, dt \tag{2}$$

where t_{test} is test duration, t_1 and t_n are the arrival time instant of the first and the last wave. $P_{r\,air}$ is instantaneous air pressure, Q_{air} is instantaneous air flow rate passing from slot shaped aperture. P_{inc} can be defined as;

$$P_{inc} = \rho g \int_0^{\infty} C_g(f) S(f) df \tag{3}$$

where ρ is water density, g is gravitational acceleration, C_g is group velocity, f is wave frequency and $s(f)$ stands for wave spectrum after separation of incident and reflected waves.

4. Results

Prior to presenting results it is worth mentioning that in order to avoid wave breaking the peak wave steepness (H_{m0}/L_p) was limited to 0.062. The efficiency of the OWC against relative depth (kd) is shown in Figure 4 where k is wave number and d is water depth. The result shows that maximum efficiency of the device obtained at wave height H_{m0}=15 cm. For H_{m0} greater than 15 cm, even though more energy is extracted, the maximum efficiency of the device decreases. In other words, the maximum efficiency of the device was 0.35 at H_{m0}=15 while declined to 0.31 and 0.23 for H_{m0}=22 and 30 cm, respectively. The main reason for this behavior can be attributed to the different increasing rate of extracted energy and incident wave energy. For example, Figure 5 shows linear increasing rate of extracted energy versus squared increasing rate of incident energy for kd=4.03.

Looking carefully at Figure 4 shows that increasing wave height causes shifting the maximum efficiency to greater periods perhaps due to the decrease in their nonlinear effects as for H_{m0}=10 maximum ξ obtained at kd=4.97 while for H_{m0}=30 maximum ξ was correspondent to kd=3.3. This was not observed by [5] as they concluded for bottom standing OWCs, wave amplitude can be neglected.

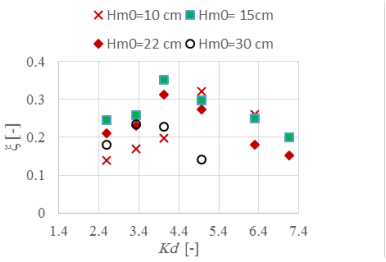

Figure 4. Efficiency of the model versus kd

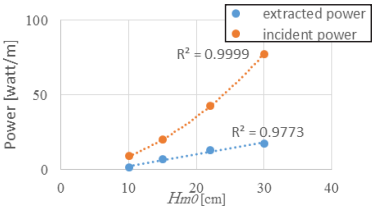

Figure 5. Extracted and incident power against H_{m0}

5. Conclusion

In this paper, wave height impact on OWC efficiency was studied through experiments. Although more energy extracted at higher waves the maximum efficiency of the device showed declining trend for wave height greater than 15 cm. Moreover, within the range of H_{m0} tested, H_{m0}=15 cm performed better as its efficiency was greater over a wider frequency range; i.e. whether in low frequency waves or high frequency waves.

6. References

[1] D. V Evans, "The oscillating water column wave energy device," J. Inst. Maths Applics, vol. 22, pp. 423–433, 1978.
[2] A. F. de O. Falcão and A. Sarmento, "Wave generation by a periodic surface pressure and its application in wave-energy extraction," in 15th international congress of theoritical and applied mechanics, 1980.
[3] I. Lopez, B. Pereiras, F. Castro, and G. Iglesias, "Optimisation of turbine-induced damping for an OWC wave energy converter using a RAS-VOF numerical model," Appl. Energy, 2014.
[4] A. Iturrioz, R. Guanche, J. L. Lara, C. Vidal, and I. J. Losada, "Validation of OpenFOAM® for Oscillating Water Column three-dimensional modeling," Ocean Eng., vol. 107, pp. 222–236, 2015.
[5] D.-Z. Ning, R.-Q. Wang, Q.-P. Zou, and B. Teng, "An experimental investigation of hydrodynamics of a fixed OWC Wave Energy Converter," Appl. Energy, vol. 168, pp. 636–648, Apr. 2016.
[6] T. Vyzikas, S. Deshoulières, O. Giroux, M. Barton, and D. Greaves, "Numerical study of fixed Oscillating Water Column with RANS-type two-phase CFD model," Renew. Energy, vol. 102, pp. 294–305, 2017.
[7] D. Stagonas, G. Muller, N. Maravelakis, D. Magagna, and D. Warbrick, "Composite seawalls for wave energy conversion: 2D experimental results," in 3rd International Conference on ocean energy, 2010.

ESTIMATION OF LONGSHORE SEDIMENT TRANSPORT RATE, A COMPARISION BETWEEN SEMI EMPIRICAL FORMULAS AND ARTIFICIAL NEURAL NETWORK MODEL (ANN)

Tayeb Sadeghifar[1], Amin Reza Zarifsanayei[2] and Reza Barati[1]

1) Department of physical oceanography, Faculty of marine science, Tarbiat Modares University, Iran, t.sadeghifar@modares.ac.ir& reza.barati@modares.ac.ir
2) Senior coastal engineer at Karan Sazeh Pasargad consulting engineers Co,Tehran, Iran, a.r.zarif@ut.ac.ir

1. Introduction

Measurement of the LSTR in the surf zone is one of the great challenges in coastal engineering and sciences. Several popular semi-empirical methods have been developed to estimate the alongshore sediment transport rate (LSTR), including CERC Shore Protection Manual (1984), Kraus et al. (1989), Walton and Bruno (1989), Kamphuis (1991), Bayram et al. (2001), and Kumar et al. (2003) methods [1, 2, 3, 4, 5, 6]. Moreover, to estimate LST some methods based on artificial Neural Network Model (ANN) have been developed recently by some researchers. ANNs is a fairly new nonlinear statistical technique that can be used to solve problems that are not suitable for conventional statistical methods. Bakhtyar et al., by Neural Fuzzy inference system estimate the sediment transport rate in Arge coast of India [7]. Also, Hashemi et al. stated that the ANN could predict the seasonal changes in Tremadoc Bay coast profiles. In another studies, In addition [8], Kabiri - samani et al., by using of Artificial Neural Network (ANN) and Fuzzy Logic (FL) evaluated the sediment transport rate methods in coastal zone of Iran and concluded that ANN, FL and Gradient descent method have better efficiencies from the others [9].

In this case study, the ANN model is developed for estimation of alongshore sediment transport rate in Noor coastal zone (Caspian Sea southern coasts) using wave parameters (wave breaking height (H), surf zone width (W) and alongshore current velocity (V)) as input and measured sediment transport rate as output. The prediction accuracy of the trained ANN model is compared with the top three popular existing semi-empirical formulas, including CERC (1984), Walton and Bruno (1989), and Kamphuis (1991) methods for estimation of the LSTR [1,3,4].

2. Field Measurement

A segment of beach by 2.4 km in length at Noor's coastal area, in the southern part of the Caspian Sea, in north of Iran, was selected for this study. In order to conduct the present study, through observation parameters from September to July 2012 including wave breaking height, wave period, wave breaking angle, surf zone width, were measured. Sediment samples collected at each trap location during September to the end of July 2012 were used for the sieve analysis and estimation of the median grain size. The frame holding the streamer was made of P.V.C. The streamer trap was used for measuring the sand transport rate in the surf zone. The name of the trap derives from the long rectangular bags of sieve cloth that stream out with the current and capture sediment, while letting water pass through. The streamer trap was originally designed to measure alongshore sand transport in the surf zone and the present discussion will mainly focus on that application.

3. Results and Discussions

The daily variations of breaking significant wave height, wave period, and breaker angle calculated from the wave measurements are shown in Figure 1.

Fig 1: Variation of (a) breaker height, beach slope, and alongshore current velocity, (b) breaker angle, period from September to June2012

The breaking wave height varied from 0.01 to 1.8 *m* with an average value of 0.47*m* during September 2011 to June 2012. The wave period mostly varied from 1.91 s to 7.4 s with an average value of 4.65 *s*, and the average wave-breaking angle was 27.8 *degree*. The breaking waves approached the coast predominantly from the south (positive values). The average surf zone width was about 84*m*.

3.1. Sediment Size Distribution

The variations of median size (d_{50}) and d_{90} of the sediment at each trap location are shown in Table 1. As expected, d_{50} increased from the water surface to the seabed at each trap location. In general, the sediments consist of fine sand (d_{50}= 0.12 to 0.2 mm) to medium sand (d_{50}= 0.2 to 0.25 mm).

Table 1. Sediment size article of the observation data in the study area

Deep (m)	$d_{10}(\mu m)$	$d_{50}(\mu m)$	$d_{90}(\mu m)$
0	154.3	219.2	590.3
5	92.15	173.7	283.6
10	60.02	117.0	577.0

3.2. ANN for Estimation of LSTR

To choose the best network for forecasting, different models were built with various nodes and middle layers. The ANN model (3-14-1) which was trained using three important parameters of sediment transport rate formulas has slightly more accurate results than other models with four inputs. The accuracy of the chosen ANN model (3-14-1) in comparison with other models of three inputs, especially those ones with more than one hidden layer, has insignificant difference. According to the intricacy and longer time needed for training of models with more than one hidden layer, the selection of ANN model (3-14-1) is reasonable. The comparison of the measured data and estimated total sediment load using ANN for training and testing procedures are shown in Figure 2.

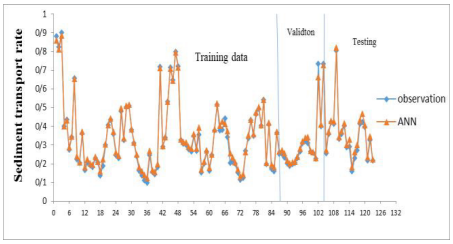

Figure 2. Comparison of observed and simulated sediment transport rate form ANN (3-14-1).

4. Conclusions

In the presented study, the accuracy of empirical formulas and ANN in prediction of daily sediment transport rate was evaluated. The LSTRs measured by the streamer sediment traps along the low-wave energy coast are lower than the rates predicted by the various empirical formulas.

The commonly used CERC, Kamphuisand W.B formulas' predictions are unrealistically high for the studied low-energy settings. The linear relationship between the energy flux factor and LSTR contained in CERC formula is supported by the streamer trap measurements. But, an order-of-extent lower empirical coefficient, 0.08 rather than 0.78 recommended by Shore Protection Manual (1984), is suggested by the trap data for low-energy coast.

The LSTR predicted by the Kamphuis (1991) formula was three times lower than the CERC prediction and closer to the measured values. The relationships between LSTR with the wave period, beach slope, and sediment grain size established in the Kamphuis (1991) formula are approved by the present study. It is essential to reconcile the different measurement techniques of sampling. Further studies on the comparability of the field techniques are recommended.

5. Reference

[1]. Shore Protection Manual, (1984)., U.S. Army Coastal Engineering Research Center, Department of the Army, Corps of Engineers, U.S. Govt. Printing Office, Washington, DC, USA, vols. 1 and 2.

[2]. Kraus, N. C., Gingerich, K. J and Rosati, J. D.., "DUCK85 Surf Zone Sand transport experiment. Technical report C.E.R.C 89-5". Department of the army waterways experiment station of engineer's PO Box 631, Vicksburg, Mississippi, 1989, 39181-0631.

[3]. Walton, Jr., T.L., Bruno, R.O., "Longshore transport at detached break water, phase II". Journal of Coastal Research 65 (9), 667– 668. Journal of Coastal Research. 1989, 5 (4), 679–691.

[4]. Kamphuis, J. W., "Alongshore sediment transport of sand, Journal of Waterway, Port, Coastal and Ocean Engineering", ASCE, 1991, Vol. 117 No.6, pp. 624-641.

[5]. Bayram, A., Larson, M., Miller, HC, Kraus, NC.,"Cross-shore distribution of longshore sediment transport: Comparison between predictive formulas and field measurements", Coastal Engineering. 2001, 44, 79–99.

[6]. Kumar, V. S., Anand, NM, Chandramohan, P, Naik, GN., "longshore sediment transport rate – Measurement and estimation, central west coast of India." Coastal Engineering; 2003, 48:95–109.

[7]. Bakhtyar.R, Ghaheri.A, Yeganeh-Bakhtiary.A, Baldock.T.E., "Longhshore Sediment Transport Estimation Using a Fuzzy Inference System." Applied Ocean Research. 2008, 30:273-286.

[8]. Hashemi,M.R., Ghadampour,Z., Neill, S.P., "Using an Artificial Neural Network to Model Seasonal Changes in Beach Profiles". Ocean Engineering; 2010, 37:1345-1356.

[9]. Kabiri-samani, A.R., Aghaee-Tarazjani, J., Borghei, S.M., Jeng, D.S.,"Application of Neural Network and Fuzzy Logic Models to Long-shore Sediment Transport". Applied Soft Computing; 2011, 11:2880-2887.

UPPER OCEAN RESPONSE TO THE HISTORICAL TROPICAL CYCLONE GONU IN THE GULF OF OMAN AND THE NORTHERN ARABIAN SEA

Kamran Koohestani[1] and Mohammad Nabi Allahdadi[2]

1) Civil Engineering Department, Iran University of Science and Technology, Tehran, Iran, kamrankoohestani@alumni.iust.ac.ir
2) North Carolina State University, Department of Marine, Earth, and Atmospheric Sciences, Raleigh, NC-USA mallahd@ncsu.edu

1. Introduction

Tropical Cyclone Gonu (Figure 1) that affected the northern Arabian Sea and Gulf of Oman in the early June 2007 was as intense as a category 5 hurricane and significantly affected ocean dynamics aspects of the region including waves [1], water level [2], sea surface temperature/salinity, and the oceanic mixed layer. In the present study, data of sea surface temperature from an optimally interpolated product are used along with the climatology data of water temperature vertical profiles and the cyclone wind filed to study and quantify the effect of Gonu on the upper water column dynamics including SST and the mixed layer depth (MLD).

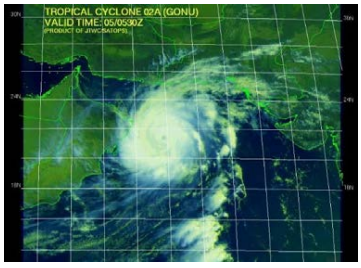

Figure 1. Satellite image of Cyclone Gonu at 5:30 on 5 June 2007 (image from the Joint Typhoon Warning Center (JTWC)).

2. Data and method

Spatial and temporal response of SST during Gonu and over the study region is studied using the satellite SST data provided by combination of SST from microwave sensors (cloud-transparent) and the infrared images obtained from the MODIS. The data are combined using an optimally interpolation (OI) approach to prepare high quality and cloud-free SST images that covers both coastal and offshore regions. SST data are used to calculate the MLD over the study area using the analytical methods suggested by Pan and Sun (2013) [4] and confirmed by Allahdadi and Li (2017)[3]. The equation of heat conservation for the mixed layer was modified by assuming negligible heat loss to the atmosphere and also small horizontal advection during the cyclone. This following integral relationship between the SST and MLD was obtained:

$$T = \frac{1}{D}\int_{-D}^{0} T_0(Z)dz \quad (1)$$

In this equation T is SST, D is the mixed-layer depth (MLD), $T_0(z)$ is the initial temperature profile, and z is the vertical coordinate within the water column. Due to lack of measured vertical temperature profile across the water column during Gonu and over the study area, the climatological temperature profiles for May were obtained from NOAA's long-term database and were used as the initial condition for calculating temporal and spatial variations of the MLD. This was identified as a good accuracy method by Pan and Sun (2013)[4] and Allahdadi and Li (2017)[3].

Following the single-vortex method of Holland (1980), the cyclone wind field was generated using the information of the track, central cyclone pressure, and the radius of maximum wind. The generated wind fields were used to study spatial and temporal variations of wind vectors during the cyclone and calculating rate of upwelling induced by the cyclone.

3. Results and Discussion

Examining the SST maps over the Gulf of Oman and northern Arabian Sea during Gonu showed high spatiotemporal variations of SST. The highest temperature cooling is observed off the Ras-Al_Hadd (off the Oman coast) on 6 June 2007 on the right side of the track with water temperatures as low as 22 ˚C (Figure2). This is corresponding to 6-8 ˚C cooling of the sea surface compared to the pre-cyclone time which is a significant amount compared to cyclones and hurricanes with similar categories [5] and was due to slower cyclone forward speed. Substantial mixed layer deepening occurred in the northern Arabian Sea that reached 100 m or larger in the right side of the track (Figure3).

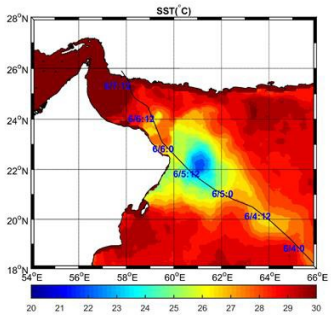

Figure2. SST map of the study area at 12:00 PM on 5 June 2005 when the eye is located off the Ras-al- Hadd (Oman). Cyclone track is shown with a solid line.

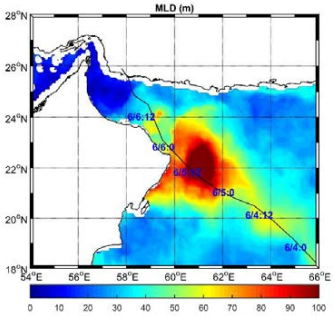

Figure3. MLD map of the study area at 12:00PM on 5 June 2005 when the eye is located off the Ras-al- Hadd (Oman).

Several reasons contribute to the larger temperature cooling and larger MLD deepening in the right side of the Gonu's track compared to the left side. The main reason could be the known phenomenon "rightward bias" that results in higher wind speeds and surface stress over the northeast quarter of the cyclone. This is due to the fact that over this zone the temporal variations of the wind vector is clockwise which is consistent with the direction of the Coriolis force vector, while for the left side two vectors rotate in opposite directions(Figure 4). Higher wind stress at this area caused more intense MLD deepening due to entrainment. The other important contributor is the shelf bathymetry in two sides of the track. While the right portion of the cyclone affects the deep areas, especially in the northern Arabian Sea, the left side translated over the shallow shelf and coastal waters. The upwelling induced by the anti-cyclonic wind stress transported colder water from deeper areas and caused more surface cooling.

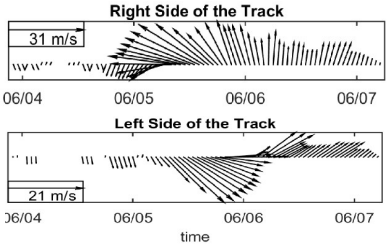

Figure 4. Time variations of the wind vector for locations in the left and right sided of the track

4. Summary and Conclusion

The relatively small forward speed of Gonu contributed to large amounts of the SST cooling and MLD deepening that along with specific translation direction and track, produced an asymmetric pattern of temperature cooling over the shallow and deep shelf. The intense upwelling and MLD deepening, especially on the right side of the track could significantly contribute to enhancing biological process over the area by transporting nutrient-rich deep water to the surface. Furthermore, it may substantially contribute to the water column re-oxygenation for several days to weeks over this oxygen-starved aquatic environment.

5. References

[1] Allahdadi MN, Chaichitehrani N, Allahyar M, McGee L., "*Wave Spectral Patterns during a Historical Cyclone: A Numerical Model for Cyclone Gonu in the Northern Oman Sea*", Open Journal of Fluid Dynamics. 2017 May 11,7(02):131.

[2] Allahdadi, M.N., Chaichitehrani, N., Jose, F., Nasrollahi, A., Afshar, A., Allahyar, M., "*Cyclone-generated Storm Surge in the Northern Gulf of Oman: A Field Data Analysis during Cyclone Gonu*". American Journal of Fluid Dynamics. 2018, 8(1), 10–18.

[3] Allahdadi, M.N., Li, C., "*Numerical Simulation of Louisiana Shelf Circulation under Hurricane Katrina*". Journal of Coastal Research. 2017, 34(1), pp.67-80.

[4] Pan, J., Sun, Y., "*Estimate of Ocean Mixed Layer Deepening after a Typhoon Passage over the South China Sea by Using Satellite Data*". Journal of Physical Oceanography. 2013, 43(3):498-506.

[5] Bender, M. A., Ginis, I. and Kurihara, Y., "*Numerical Simulations of Tropical Cyclone-Ocean Interaction with a High- Resolution Coupled Model*". Journal of Geophysical Research- Atmospheres. 1993, 98(D12), pp.23245-23263.

THE INVESTIGATION of WATERSPOUT STRUCTURE in a CASE STUDY OVER SOUTHERN COASTS of IRAN (BUSHEHR PROVINCE, DECEMBER, 15, 2017)

Rahele Ramezani[1], Sahar Tajbakhsh[2] and Parvin Ghafarian[3]

1) Master of Physics, Meteorological Research Center of Hormozgan Province, Iran,Rahilrm29@gmail.com
2) Assistant Professor, Atmospheric Science & Meteorological Research Center, Tehran, Iran,sahartajbakhsh@gmail.com
3) Assistant Professor ,Iranian national institute for oceanography and atmospheric science, Tehran, Iran,p.ghafarian@inio.ac.ir

1. Introduction

Tornados are rotating columns of cloud that can be in touch with the ground. These rotating clouds are formed under the cumulonimbus clouds and often can be seen as funnel clouds. If these tornadoes are formed on the surface of the water, they are called waterspout. The structure of this atmospheric hazard is very similar to the thunderstorms. The three conditions include static instability, lower surface humidity and lifting mechanisms near the earth surface are necessary for the creation of convection Figure 1)

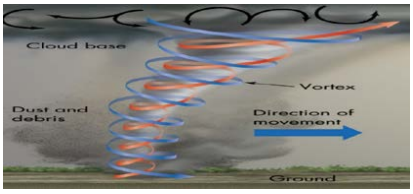

Figure 1. Three-dimensional structure of waterspouts. The blue and red rotating arrows show the rotational sinking of the cold air and rising of the warm air respectively. The solid blue arrow represents the horizontal motions of the waterspout.

There are few studies in Iran about the waterspout events, therefore the aim of this study is to investigate waterspout as a mesoscale phenomenon and analyzing the synoptic patterns at the time of the occurrence of this phenomenon. In order to study the most important indices related to the occurrence of this phenomenon in this section, we study the sea level pressure, wind, humidity vertical profile and LI, Helicity, CAPE and CIN indices.

2. The Study Background

Researchers such as Renko et al. (2013), Sioutas et al. (2012), Barrera et al. (2009), Beck et al. (2007) analyzed the waterspout occurrence. Also, a number of researchers, such as Tudor et al. (2011), Keul et al. (2008), studied on the prediction of this hazard.

The climatological study of tornadoes and waterspouts was carried out by Nunes et al. (2011) in Brazil and by Gaya et al. (2011) in Catalonia.

3. Materials and Methods

This study deals with the case of a waterspout on the Persian Gulf on December 15, 2017, over the area of Bandar Dayyer (Bushehr province). The data obtained from the synoptic station of Dayyer and Bushehr marine weather station. Also, GFS global data with a resolution of 0.5 degrees has been used to examine the synoptic patterns and associated instability indices. In meteorological operational predictions many indices are used to evaluate atmospheric instability. Such as lifted index (LI), which is an experimental parameter and is defined as:

$$LI = T(500\ mb) - Td(500\ mb) \quad (1)$$

Where T500 is the environmental temperature at 500 (hpa) and the Td500 is lifted parcel's temperature at 500(hpa). The different values of this index and the probability of thunderstorm are presented in Table1.

Table 1: LI values with the storm possibility

LI	Thunderstorm potential
-2 to 0	Showers probable
-5 to -3	Thunderstorms probable
-6	Severe Thunderstorms
< -7	Tornados possible

Cape (available energy potential) is effectively the positive buoyancy of an air parcel and is very valuable in predicting severe weather.

Table 2. Atmospheric stability and CAPE values

CAPE (j/kg)	conditions
0	Stable
0-1000	Slightly unstable
1000-2500	Fairly unstable
2500-3500	Very unstable
3500-4000	Extremely unstable

4. Results and Discussion

In order to study the most important indices related to the occurrence of this phenomenon in this section, we study the sea level pressure, wind, humidity vertical profile and LI, Helicity, CAPE and CIN indices.

4.1. Average Sea Level Pressure Analysis

The SLP map at 00 UTC on December 15th shows that a 1014 mb low pressure center is formed on the northwest of the Persian Gulf and two tongues of high pressure, one in the center of Iran with the pressure of 1044 mb and the other on the Saudi Arabia with the pressure of 1024 mb are weakening the low pressure center. At this hour, the study area also crossed the pressure 1016 mb (Figure 4a). at 06UTC, the pressure increased by about 2 mb (Fig. 4b). At 12UTC low pressure is amplified and again in the north of the Persian Gulf, a 2-mb pressure drop is observed (Figure 4c). For 6 hours later, increasing the pressure again occurs in the Persian Gulf region, which is visible in Figure 4d.

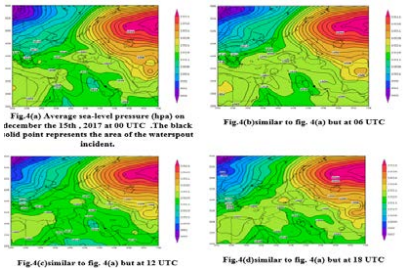

Fig.4(a) Average sea-level pressure (hpa) on december the 15th , 2017 at 00 UTC .The black solid point represents the area of the waterspout incident.

Fig.4(b)similar to fig. 4(a) but at 06 UTC

Fig.4(c)similar to fig. 4(a) but at 12 UTC

Fig.4(d)similar to fig. 4(a) but at 18 UTC

4.2. Lifted Index (LI) Analysis

At 00 UTC the lifted index is around zero (Figure 7a). After 6 hours, the value of this index is 2 and probability of occurrence of unstable and convective conditions in the western regions of the Persian Gulf and on the Saudi Arabia is provided (Figure 7b). At 12UTC, the value of this index increases to 4 that represents the creation of conditions for the storm. (Figure 7c). At 18 UTC, it can be seen that conditions are getting away from instability (Figure 7d)

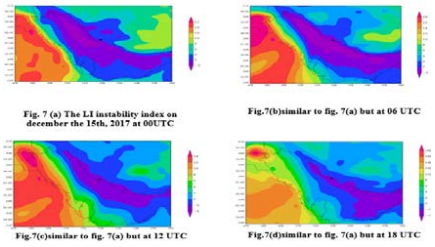

Fig. 7 (a) The LI instability index on december the 15th, 2017 at 00UTC

Fig.7(b)similar to fig. 7(a) but at 06 UTC

Fig.7(c)similar to fig. 7(a) but at 12 UTC

Fig.7(d)similar to fig. 7(a) but at 18 UTC

4.3. CAPE Index Analysis

By examining the CAPE index, it is determined that the amount of this quantity on the Persian Gulf is around 800 j / kg at 00 UTC, which is suitable for convection and the formation of a thunderstorm in this region (Figure 8a). At 06UTC, the amount of this energy in the northwest of the Persian Gulf has been reduced, but a few other cores with an average CAPE energy are formed in the southern regions of the Persian Gulf. The CAPE value for the study area approaches 400 j / kg (Fig. 8b). At 12UTC, the CAPE value approaches 700j / kg and conditions for instability are provided (Figure 8c). At 18UTC, the main core has weakened. (Figure 8d)

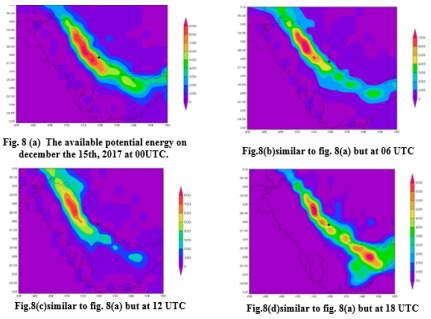

Fig. 8 (a) The available potential energy on december the 15th, 2017 at 00UTC.

Fig.8(b)similar to fig. 8(a) but at 06 UTC

Fig.8(c)similar to fig. 8(a) but at 12 UTC

Fig.8(d)similar to fig. 8(a) but at 18 UTC

5. Conclusions

The primary prerequisites for the formation of thunderous storms and tornadoes are high humidity, high temperatures, unstable atmosphere, and the proper structure of upper level winds and lifting mechanisms. The results of this study show that instability indices, especially LI and CAPE, and CIN and the numerical thresholds of these indicators are a good guide to predict the occurrence of a waterspout, although precise threshold values in each area for permanent applications require climatic research.

6. References

[1] Sioutas, M., Szilagyi, W., Keul, A., 2012. Waterspout outbreaks over areas of Europe and North America: Environment and predictability. Atmospheric Research 123 (2013) 167–179

[2] Renko,T., Kozaric,T., Tudor,M., An assessment of waterspout occurrence in the Eastern Adriatic basin in 2010: Synoptic and mesoscale environment and forecasting method, Atmospheric Research123(2013),71-81

[3] Keul, A., Sioutas, M., Szilagyi, W. Prognosis of Central-Eastern Mediterranean waterspouts. Atmospheric Research 93 (2009) 426–436

STORM SURGE MODELING OF NOSHAHR PORT IN SOUTHERN COAST OF THE CASPIAN SEA

Aliasghar Golshani [1,2], Atena Amiri[2,3] and Farhad Darabinia [2]

1) Lecturer, Dept. of Civil Eng., Tehran Azad Univ., Central Branch, Tehran, Iran, ali.golshani@iauctb.ac.ir
2) FDA Consultants, Tehran, Iran, f.darabi@faradarya.com
3) Ph.D. Student, Dept. of CivFil Eng., Tehran Univ., Tehran, Iran, amiri.atena.646@gmail.com

1. Introduction

Noshahr port is approximately located in the middle of southern coastline of the Caspian Sea (Lat.: 36.655 degree, Long.: 51.506 degree). The purpose of this paper is to investigate the surge levels in the vicinity of Noshahr Port. The contribution of different driving forces such as Mean Seal Level (MSL) pressure, wind components and wave radiation stresses in the total surge of this area is also estimated. There is almost no tide contribution to surge level in the Caspian Sea.

2. Storm Surge Modeling Procedure

The Storm surge model includes a regional hydraulic model covering the whole Caspian Sea and a local wave model covering Noshahr Port waters.

The local wave model was setup using Spectral Wave (SW) module of Mike21 package [1]. A new bathymetric survey data with scale of 1:1000 was input to mesh generator tool of Mike Zero and an unstructured mesh including 2698 nodes and 5146 elements was generated. The size of this mesh in Noshahr port is around 50m. The parametric wave boundary condition (extracted from Caspian Sea wave hindcast model) at northern model boundary and lateral boundary condition at western and eastern model boundaries were applied to transfer waves from deep water to nearshore. As there was not enough fetch for wind-wave generation, wind was not forced to this model.

Then, a regional hydraulic model of Caspian Sea (See Figures 1 and 2) was setup using Flow Model (FM) of Mike 21 package [2]. Large scale as well as small scale bathymetries covering the whole Caspian Sea with emphasize on Noshahr Port waters were input to mesh generator and a flexible mesh including 3955 nodes and 7325 elements was generated. The size of this mesh in Noshahr port is around 100m. Caspian Sea hourly wind and MSL pressure fields from WRF atmospheric model with spatial resolution of 0.3 degree, hourly wave radiation stresses from SW model output, 12-hourly evaporation and precipitation rates from ERA-Interim product of ECWMF, and monthly Volga river discharge times by 0.9 (It was assumed that 90 percent of this river discharge flows in the Caspian Sea and 10 percent is used for agricultural purposes) were input to FM model.

3. Model Calibration

The period of April to July 2013 was considered as the calibration period as the tidal gauge data was available in this period. Wave model was run initially for this period to provide radiation stresses as an input for FM model. Volga discharge was ignored in these modeling scenarios as river discharges have local influence on surge levels and is far away from Noshahr Port. Perception and evaporation rates are also phased out as their effects is relatively small.

Two important parameters namely wind friction factor (0.001255) and Manning number (32 m^(1/3)/s) were considered as calibration coefficients and their values were decided based on try and error procedure.

Figure 3 compares the model result with tidal gauge records which is located inside Noshahr Port basin. A very good agreement and correlation between these two datasets is seen depicting that the model results are reliable.

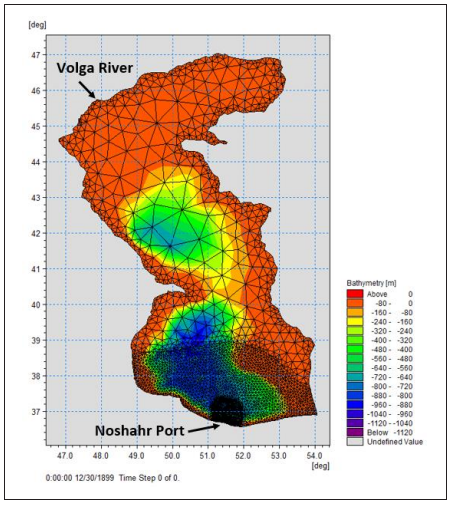

Figure 1. Caspian Sea FM model mesh

4. Results

To evaluate the contribution of each driving forces on the total surge level, the surge model was run for different scenarios. Three scenarios of firstly forcing wind, pressure and wave, secondly forcing wind and pressure and thirdly forcing wind to the FM model were implemented. The peaks of surge level during 7-month running FM model (January-July 2013) were studied and the contribution of each parameter were estimated. According to this study, MSL pressure and wind components are roughly responsible for 70 percent and 30 percent of total surge respectively in this area (See Figure 4 for instance at a point in depth of 5 m in front of the port). Waves also contribute to coastal sea levels during storms. The net effect of breaking waves at the cost produces wave setup and individual breaking waves produce wave run-up. Hubbert and McInns (1999) suggests that an allowance for wave setup can be made by increasing the storm surge levels by 10% [3]. Golshani et al (2012) showed that this suggestion is conservative based on a study done in South East Queensland coastlines of Australia [4]. The results of this study show that the above-mentioned allowance for Noshahr Port area is also conservative and an allowance for wave setup can be made by increasing the storm surge levels by 5%.

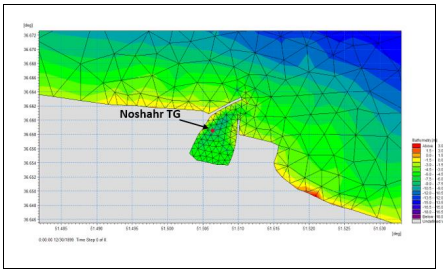

Figure 2. FM model mesh zoomed in Noshahr port

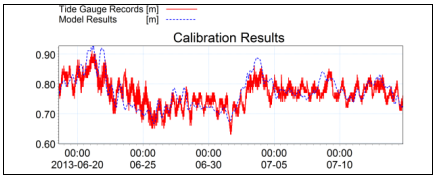

Figure 3. Calibration results at Noshahr tide gauge

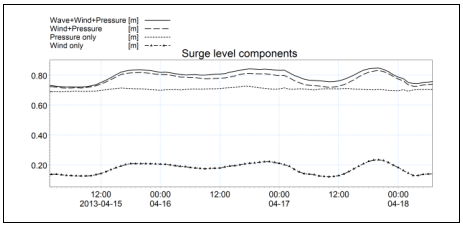

Figure 4. Storm surge components

5. References

[1] Mike21 Spectral Waves User Manual, DHI Water and Environment.

[2] Mike21 Flow Model User Manual, DHI Water and Environment.

[3] Hubbert, G.D. and McInnes, K.L. "A storm Surge Inundation Model for Coastal Planning and Impact Studies, J. Coastal Research,15, pp. 168-185,1999.

[4] Golshani, A, Stuart, G., and Tomlinson, R., "Storm Surge Modeling of Fraser East Coast Low Event in South East Queensland, Australia", Proceeding of COPEDEC 2012, 20-24 February 2012, pp.158-168.

WAVE CHARACTERISTICS IN THE MAKRAN COASTS

Mohammad Hosein Nemati[1], Ahmad Rezaee Mazyak[2], Mohammad Bagheri[3], Mahdi Shafieefar[4], Aghil Hajmomeni[2], Mohammad Reza Khosravi[2]

1) Ports & Maritime Organization, Tehran, Iran, mhn1382@gmail.com
2) Pars Geometry Consultants , Tehran, Iran, ahmadrezaee2010@gmail.com
3) Ports & Maritime Organization, Tehran, Iran,
4) Tarbiat Modares University, Tehran, Iran, shafiee@modares.ac.ir

1. Introduction

Waves have the most important role among the phenomena governing the marine environment and are the main cause of coastal morphological changes and the forces imposed on marine structures. Hence, determining the characteristics of a wave in each coastal region is of great importance.

So far, many studies have been done on specifying the waves in the Arabian Sea, Gulf of Oman, and the coast of Makran [1-5]. The results indicate that the waves of this area are most affected by the Monsoon winds. Monsoon Winds fall into two categories: Summer (SW) and Winter (NE) [6-8]. In general, the magnitude of the waves caused by the summer monsoon is higher.

In this paper, the results of wave hindcast in the Makran coastline are presented. For this purpose, after validation and verification the model with the measurement data, Wave hindcast has been performed for the period of 1980-2016. Finally, the study area is classified according to the maximum wave height in points at depths of 10 and 25 meters and wave height with a return period of 50 and 100 years.

2. Study Area

The current study area is located in the east of Guatr Bay (located on the border between Iran and Pakistan) and in the west to Rapch Estuary (located between Sistan and Baluchestan province and Hormozgan province). In Figure 1, the study area and the position of the measuring stations are shown.

Figure 1. Study area and measurement stations

3. Model Setup

In this study, the Mike21-SW spectral model was used to propagate waves to the coastal area.To set up the model, the study area was determined and then the bathymetry data were collected and analyzed. The eastern and western boundaries of the model were defined as the lateral and southern boundary of the model as wave parameters. The mesh of model has 3954 computational nodes and its resolution is 0.01 degrees in shallow water and 0.20 degrees in the other study area. The frequency resolution is logarithmically performed with 27 frequencies and directional resolution in 16 directions. In Figure 2, the boundaries and mesh are shown.

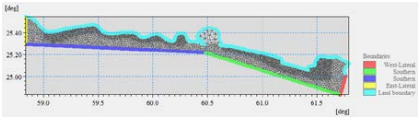

Figure 2. Boundary of simulation

Selection of validation coefficients is performed according to the model's behavior. Bed roughness and wave breaking, are the depreciable parameter of the energy of waves in the shallow water, which have been selected.

4. Validation and Verification

Based on the results obtained from the measurement stations, the results of the modeling are validated and verified. An example of the validation results at Tang station (depth is 25m) is shown in Figure 3. As can be seen, the model has been able to simulate wave characters as well. Also, the calculated error parameters (Bias, CC, RMSE, and SI) are within the range allowed in previous studies. The worst results of the error parameters are shown in Table 1.

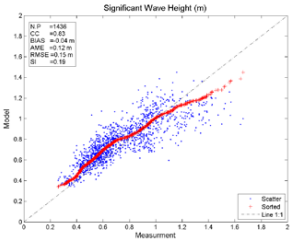

Figure 3. Scatter and Q-Q plot of significant wave height at the Tang station

Table1. The worst result of error parameters

	CC	Bias	RMSE	SI
H_s	0.62	-0.24	0.1	0.07
T_P	0.3	-2.07	1.15	0.09
MWD	-	-15.27	5.92	0.03

5. Analysis of Results

To carry out future marine projects in the Makran coast, having a comprehensive perspective on the climate of the waves of this region is important. Therefore, in this section, the results of modeling in all areas studied have been discussed. The maximum wave height at points of the depth of 10 and 25 meters is presented throughout the study area (Figures 5, 6).

Also, by using the Extreme Value Analysis, the wave characteristics for the return period of 50 and 100 years are presented (Figures 6) then the study area is classified based on wave height with the return period of 50 and 100 years (Figure 7, 8).

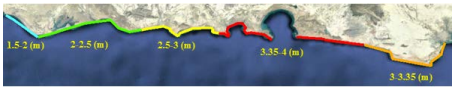

Figure4. Beach classification based on the maximum wave height at a point to a depth of 10 meters

Figure5. Beach classification based on the maximum wave height at a point to a depth of 25 meters

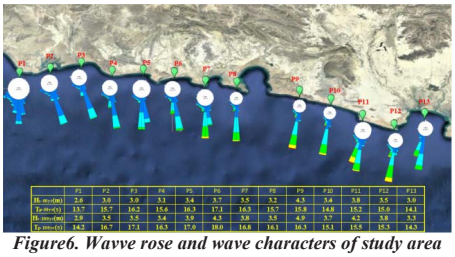

Figure6. Wavve rose and wave characters of study area

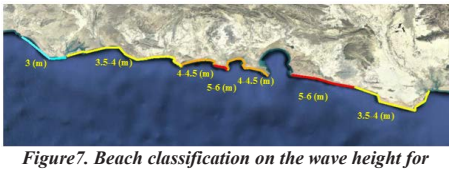

Figure7. Beach classification on the wave height for return period of 100 years

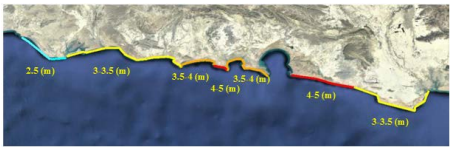

Figure8. Beach classification on the wave height for return period of 50 years

6. Conclusion

By studying the results of modeling, it can be said that the height of maximum waves in the coast of Makran decreases from west to east, and also for the dominant waves, changes from southwest to southeast.

In the study area, the height of waves with a 50-year return period varies from 2.6 to 3.8 m, and the wave period varies from 13.7 to 17.1 seconds. Also, the wavelengths vary with a return period of 100 years from 2.9 to 4.9 meters, and the period of waves varies from 14.2 to 18 seconds.

7. References

[1] Shanas, P.R., Sanil Kumar, V., (2014), Temporal variation in the wind and wave climate at a location in the eastern Arabian Sea based on ERA-Interim reanalysis data, Natural Hazards and Earth System Sciences.

[2] Shanas, P.R., Sanil Kumar, V., (2013), Comparison of ERA-Interim waves with bouy data in the eastern Arabian Sea during high waves, Indian Journal of Geo-Marine Sciences, Vol. 43(7), 1343-1346 .

[3] Semedo, A., Suselj, K., Rutgersson, A., Sterl, A., (2011), A Global View on the Wind Sea and Swell Climate and Variability from ERA-40, American Meteorological Society, Vol., No., 1461-1479.

[4] Caires, S. and Sterl, A., Comprative assessment of ERA-40 Ocean Wave Data.

[5] Anoop, T.R., Sanil Kumar, V., Shanas, P.R., Amrutha, M.M., (2016), Indian Ocean Dipole modulated wave climate of eastern Arabian Sea, Ocean Science, Vol. 12, No.,369-378.

[6] Baird & Associates Coastal Engineers Ltd., 2009, Development of a Wave climate for the Persian Gulf and the Strait of Hormuz. Ports and Maritime Organization.

[7] Danish Hydraulic Institute (2005). Summary of Iranian Seas Wave Modeling: Phase 3 (Persian Gulf and Gulf of Oman).

[8] Mohammadreza Khosravi, Mohammad Bagheri, Mohammadhosein Nemati, Mehdi Shafieefar, Aghil Hajmomeni, Ahmad Rezaee Mazyak, "The Wind-Wave Climate of the Makran Coastlines(A:appraising of ERA-Interim results),"*First International Conference on oceanoghraphy for West Asia*, Tehran, Iran, 2017.

A METHOD TO DETERMINE OF COASTAL SUBCELL IN THE MAKRAN COASTS

Mohammad Bagheri [1], Mohammad Reza Khosravi [2], Mohammad Hosein Nemati [3], Mahdi Shafieefar[4], Aghil Hajmomeni[2] and Ahmad Rezaee Mazyak [2]

1) Ports & Maritime Organization, Tehran, Iran,
2) Pars Geometry Consultants , Tehran, Iran, mohammad.r.khosravi@gmail.com
3) Ports & Maritime Organization, Tehran, Iran, mhn1382@gmail.com
4) Tarbiat Modares University, Tehran, Iran, shafiee@modares.ac.ir

1. Introduction

Coastal management needs to be organized on a scale that can provide a general overview of the dynamics of the coastal system. To create this general picture, beaches need to be explored from a variety of perspectives such as hydrodynamics, geology, and human activities. Coastal classification or selection of sample parcels is the first step in deciding on coastal management.

So far, many studies have been carried out on the determination of sedimentation of cells and sub-cells [1-4]. In these studies, based on the concept of Coastal Sediment Cell, attempts have been made to introduce broad concepts for the general identification of the coast and how its sediment budget is to be estimated. The concept of the sedimentary cell has been introduced in some studies with titles such as coastal management unit, sediment cell with smaller coastal process units or sub-cells, littoral cell, etc., all of which have almost the same framework and logic [5-7].

Considering the importance of determining the sedimentation of cells and sub-cells in the coastal assessment, in this study, we tried to categorize from two different perspectives. According to the available information, Makran beaches are examined and categorized in terms of bed slope and wave characteristics.

2. Study Area

The current study area is located in the east of Guatr Bay (located on the border between Iran and Pakistan) and in the west to Rapch Estuary (located between Sistan and Baluchestan province and Hormozgan province) (See Figure 1).

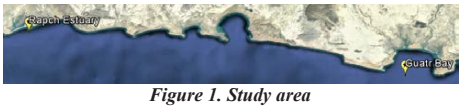

Figure 1. Study area

3. Material and Methods

Wave data and bathymetry have been used to classify the Makran coastlines. Wave data set has been extracted from the results of the Phase 6 of the Iranian Coastal Monitoring and Modeling Studies Hydrographic data with a scale of 1:20000 and 1:50000 are also used for slope classification.

To classify the beaches, the slope of the area is firstly extracted based on available hydrographic data and shores with almost identical slopes are considered as a type. In the second step, based on available wave information, the beaches are classified according to the characteristic storm wave ($H_{s,\ 12h/y}$) and wave direction. Finally, by aggregating both criteria, a general division of the region is presented.

4. Result Analysis

The Makran coast is classified according to the characteristics of the waves and the bed slope. According to the characteristics of the waves, the study area is divided into 3 groups and is classified according to the bed slope into 9 categories.

4.1. Coastal Classification Based On Wave Characteristic

A coastline classification for nearly straight coastline section is presented in this chapter. Only sedimentary coastlines, which are characterized by the presence of loose sediments on the shoreface and on the beach, will be included in the following classification. The coastline has been divided in five main types defined by the offshore angle of incidence of the prevailing waves such as Perpendicular, Nearly perpendicular, Moderate oblique, Very oblique, Nearly coast-parallel. Also the classification of coastline has been further subdivided according to wave exposure: Protected, Moderately, Exposed [8].

From Guatr bay to Chabahar bay, as well as from Pozm gulf to Tang, most beaches are exposed. But the angle of incidence of the prevailing wave of Guatr bay to Chabahar bay is below 10 degrees and at Pozm gulf to Tang is 50 degrees. From Tang to the Rappch estuary, almost all the coasts are moderate and the dominant angle of the wave is in the range of 10 to 45 degrees (See Figure 2).

4.2. Coastal Classification Based On The Bed Slope

By studying the bathymetry data, the study area can be classified into 9 categories based on the bed slope. The slope of Guatr bay is about 0.6 percent. From the Guatr to Chabahar, the slope of the bed increases and reaches about

3% in the Ramin. The bed slope in the Pozm Gulf has decreased and is about 0.1%. The slope of bed in the Gordim is 35 percent and it is reduced to around 0.2 percent as it moves toward the Rappch estuary. (See Figure 3)

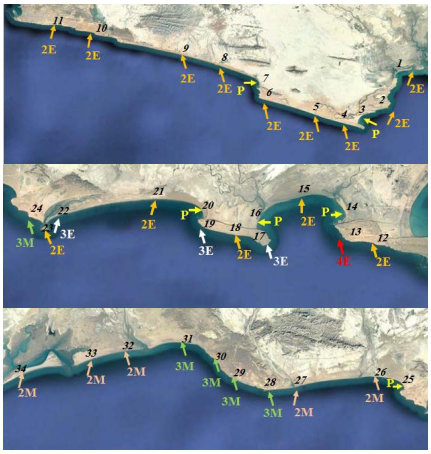

Figure 2. Classification of Makran beaches by waves parameter

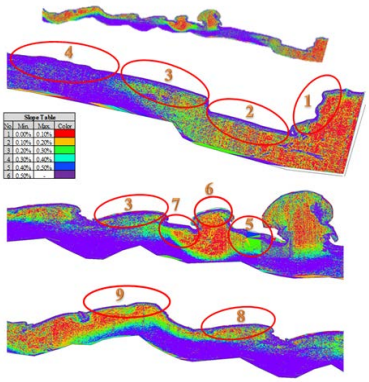

Figure 3. Classification of beaches by bed slope

5. Conclusion

After examining wave parameters and bed slopes, Makran beaches are classified into 16 categories (See Figure 4). It should be noted that in this category, protected beaches, without considering the slope of bed, are placed in a group. Group 4 and 5, are exposed and have the maximum slope. The main coastal characteristic of these groups is rocky beach. Based on the wave parameter, $H_{s,\ 12h/y}$ is at least 1.6 meters and a maximum of 3.1 meters. The lowest bed slope is 0.06% and the maximum bed slope is 3%.

Figure 4. Total calssification of beach

6. References

[1] HR Wallingford. (1997) *Coastal cells in Scotland.* Scottish Natural Heritage. Research, Survey and MonitoringReport 56.

[2] van Rijn LC. (1998) *Principles of Coastal Morphology*. Aqua Publications, NL.

[3] McGlashan DJ and Duck RW. (2002) The Evolution of Coastal Management Units: Towards the PDMU. *Littoral 2002, The Changing Coast.* 29-33.

[4] Cooper NJ & Pontee NI. (2006) Appraisal and evolution of the littoral 'sediment cell' concept in applied coastal management: Experiences from England and Wales. *Ocean and Coastal Management*, 49: 498-510.

[5] McGlashan DJ and Duck RW. (2000) Undeveloped Coasts: a protocol for the assessment of development potential. *Periodicum Biologorum*, 102(1):329-332. Cited within McGlashan & Duck (2002)

[6] Bowen AJ and Inman DL. (1966) *Budget of littoral sands in the vicinity of Point Arguello, California.* United States Army CERC Technical Memorandum No. 19.

[7] Motyka, JM; Brampton, AH. (1993) *Coastal Management: Mapping of Littoral Cells*. Wallingford UK: HR Wallingford. Hydraulics Research Report SR 328.

[8] Mangor, K and et al., (2017) *Shoreline Management Guidelines*, Published by DHI

NUMERICAL INVESTIGATION OF TSUNAMI WAVE GENERATION USING A PISTON-TYPE WAVEMAKER

Mohammad Javad Zareei[1], Morteza Anbarsooz[2] and Mohammad Passandideh-Fard[3]

1) Department of Mechanical Engineering, Ferdowsi of Mashhad University, Mashhad, Iran, mjzareei@mail.um.ac.ir
2) Department of Mechanical Engineering, Quchan University of Technology, Quchan, Iran, anbarsouz@qiet.ac.ir
3) Department of Mechanical Engineering, Ferdowsi of Mashhad University, Mashhad, Iran, mpfard@um.ac.ir

1. Introduction

A tsunami is a collection of water waves that is caused by the displacement of a significant volume of water due to unrestricted seas, and most of its damage is due to a large flood and a lot of forces that inflict on the coastal bodies. Since many important facilities such as nuclear power plants, oil and gas storage tanks, ports, customs, steel plants and ... are installed on the shores, a study on the tsunami is doubly important. [1]

In the past, the tsunami has been simulated as a "solitary wave"[2-4], however, recent research has shown that tsunami waves have a completely different behavior in spatial and temporal scales [5 ،6]. As a result, the tsunami profile generated using the solitary wave concept is different from reality. This difference is more apparent in coastal areas where the shoaling effect restrains the development of the tsunami wave. To overcome this problem, researchers used alternative methods such as "N-shaped waves" that combine multiple solitary waves. Chan and Liu[7], according to the recorded results from the Iwate Station in Japan Tsunami 2011, proposed a model of three sech^2(*) hyperbolic functions.

In this research, a new method has been used to integrate the three Sech^2(*) hyperbolic functions to regenerate Tokyo Tsunami Profiling with the help of a piston wavemaker. The wave generated by this method is called "tsunami-like".

2. Governing Equations and Boundary Conditions

The schematic of the wavemaker mechanism considered in this study is shown in Fig. 1 where the piston type is displayed. The domain of the computation is a rectangle (Lc×Hc) with two damping zones at both ends as shown in the figure. A solid object representing the wavemaker is positioned at x=Xp from the left and forced to move according to a specified function.

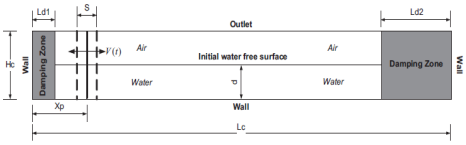

Figure 1. Computational domain and boundary conditions for piston-type wavemaker

2.1. Fluid Flow Governing Equations

The governing equations for fluid flow are the Navier–Stokes equations in 2D, Newtonian, incompressible and laminar flow:

$$\nabla \cdot \vec{V} = 0 \tag{1}$$

$$\frac{\partial \vec{V}}{\partial t} + \vec{V} \cdot \nabla \vec{V} = -\frac{1}{\rho}\nabla P + \frac{1}{\rho}\nabla \cdot \vec{\tau} + \vec{g} + \frac{1}{\rho}\vec{F}_{\mathrm{b}} \tag{2}$$

$$\vec{\tau} = \mu\left[(\nabla \vec{V}) + (\nabla \vec{V})^{T}\right] \tag{3}$$

where $\vec{V}$ is the velocity vector, ρ the density, μ the dynamic viscosity, p the pressure, $\vec{\tau}$ the stress tensor and $\vec{F}_{\mathrm{b}}$ represents body forces acting on the fluid. The interface is advected using the VOF method by means of a scalar field (F) that called liquid volume fraction, defined as:

$$F = \begin{cases} 0 & \text{in the gas phase} \\ 0 < , < 1 & \text{in the liquid-gas interface} \\ 1 & \text{in the liquid phase} \end{cases} \tag{4}$$

The discontinuity in F is a Lagrangian invariant, propagating according to:

$$\frac{dF}{dt} = \frac{\partial F}{\partial t} + \vec{V} \cdot \nabla F = 0 \tag{5}$$

2.2. Solid object treatment

In this study, the wavemaker's paddle is modeled as a solid object using the fast-fictitious-domain method [8] in which the solid is considered as a fluid with a high viscosity with a prescribed motion. The solid object in the computational domain is identified using a scalar parameter defined as:

$$\emptyset = \begin{cases} 0 & \text{Out of the solid} \\ 0 <, < 1 & \text{Solid boundary} \\ 1 & \text{Within the solid} \end{cases} \quad (6)$$

Then the fluid flow equations are solved in all over the computational domain including the solid zone. In the next step, the average translational and rotational velocities in the solid zones are calculated and the velocity distribution inside the solid zone is then updated accordingly. finally, the velocity in the computational domain is updated and the interface is advected using Eq. (5).

3. Results and Discussion

In order to generate the desired tsunami-like wave profile, the motion of the piston-type wavemaker in the water is modeled using a fast-fictitious domain method, and the VOF method is employed to detect the fluid's free surface. In order to remove recurring waves from the end of the solution domain, a high viscosity damping zone is set at the end of the computational domain. The governing equations are solved using a control-volume approach with a two-stage partial time step method to decouple the continuity and momentum equations.

First, the generation process of a solitary and a tsunami wave are simulated and the results are validated by comparing the numerical results with the existing analytics[9 ،10]. Figure 2 shows the comparison between the generated solitary wave profile with the analytics[10]. The generated tsunami profile which is the summation three $Sech^2(*)$ hyperbolic functions is compared with the analytical profile of Qu et al.[9] in Figure 3 where a conceiving agreement can be observed. Next, the run-up characteristics of a tsunami wave are compared with its corresponding solitary wave. The comparison shows the superior capability of the tsunami wave profile to run up the slope and penetrate more into the beach.

The use of the new method makes significant progress in simulating the tsunami wave motion.

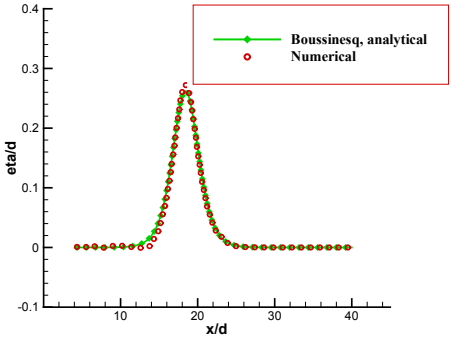

Figure 2. Comparing the numerical results for a solitary wave with the existing analytics.

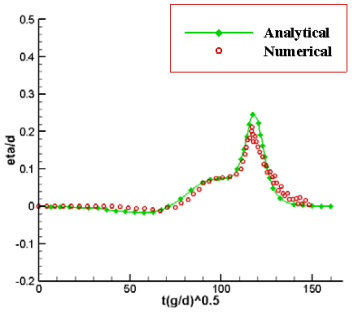

Figure 3. Comparing the numerical results for tsunami-like with the existing analytics.

4. References

[1] H. Yeh, A. Barbosa and B. H. Mason, Tsunamis effects in man-made environment, Encyclopedia of Complexity and Systems Science, pp. 1-27, 2014.

[2] Y.-S. Cho, K.-Y. Park and T.-H. Lin, Run-up heights of nearshore tsunamis based on quadtree grid system, Ocean Engineering, Vol. 31, No. 8, pp. 1093-1109, 2004, doi: https://doi.org/10.1016/j.oceaneng.2003.10.011.

[3] D. Liang, H. Gotoh, A. Khayyer and J. M. Chen, Boussinesq modelling of solitary wave and N-wave runup on coast, Applied Ocean Research, Vol. 42, No. Supplement C, pp. 144-154, 2013, doi: https://doi.org/10.1016/j.apor.2013.05.008.

[4] Z. Wei, R. A. Dalrymple, A. Hérault, G. Bilotta, E. Rustico and H. Yeh, SPH modeling of dynamic impact of tsunami bore on bridge piers, Coastal Engineering, Vol. 104, pp. 26-42, 2015, doi: https://doi.org/10.1016/j.coastaleng.2015.06.008.

[5] P. A. Madsen and H. A. Schaeffer, Analytical solutions for tsunami runup on a plane beach: single waves, N-waves and transient waves, Journal of Fluid Mechanics, Vol. 645, pp. 27-57, 2010.

[6] V. Sriram, I. Didenkulova, A. Sergeeva and S. Schimmels, Tsunami evolution and run-up in a large scale experimental facility, Coastal Engineering, Vol. 111, No. Supplement C, pp. 1-12, 2016, doi: https://doi.org/10.1016/j.coastaleng.2015.11.006.

[7] I. Chan and P. L. F. Liu, On the runup of long waves on a plane beach, Journal of Geophysical Research: Oceans, Vol. 117, No. C8, 2012.

[8] N. Sharma and N. A. Patankar, A fast computation technique for the direct numerical simulation of rigid particulate flows, Journal of Computational Physics, Vol. 205, No. 2, pp. 439-457, 2005.

[9] K. Qu, X. Y. Ren, S. Kraatz and E. J. Zhao, Numerical analysis of tsunami-like wave impact on horizontal cylinders, Ocean Engineering, Vol. 145, No. Supplement C, pp. 316-333, 2017, doi: https://doi.org/10.1016/j.oceaneng.2017.09.027.

[10] D. G. Goring, Tsunamis--the propagation of long waves onto a shelf, 1978.

ON ASSESSMENT OF LITTORAL DRIFT AND COASTLINE EVOLUTION MODELS CASE STUDY: THE PORT OF CHAMKHALEH

Ali Nasrollahi[1]

[1]Ph.D. Hydraulic Eng., Tehran, Iran, Nasrollahi_a@yahoo.com

1. Introduction

Along the southern coast of Caspian Sea, the port of Chamkhaleh is located east of Kiashahr port where coastline direction changes from relatively eastern-western to northern-southern direction. As seen in Figure 1, two rivers flow into the basin so that southern river has high concentration of suspended sediment while northern river discharge is much more than that. Building the port at the rivers' mouth leads to a calm area causes to settle much more sediment in the basin so that the basin becomes shallower. This is what currently happens in the port of Chamkhaleh.

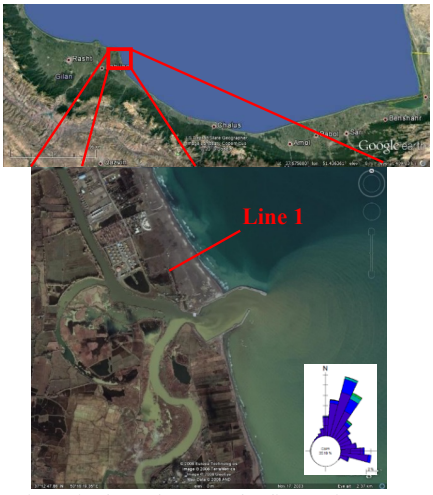

Figure 1. The study area and sedimentation upstream of breakwater in 2003

In the north-western of the port, alongshore sediment transport results in sedimentation so that sediments bypass the breakwater and affect port entrance. Thus, the greatest problem in this port is sedimentation. This sedimentation is because of alongshore sediment transport as well as sediment coming from rivers. However, in this paper considers littoral transport and coastline changes using mathematical models as well as assessing and comparing these models to each other and hydrographic surveys and evidence of coastline changes by satellite images as well.

2. Data

One of the most important data to study sediment transport as well as coastline changes is hydrography data. Two hydrographic surveys were performed in this area at 1999 and 2011. Depth changes between these hydrographic data are derived across line 1 as in Figure 1 and shown in figures 2. As they are depicted, there are substantially changes between two surveys especially at the beginning of lines. However, these changes are minimal at depth around 5 m. therefore, this depth was selected as closure depth.

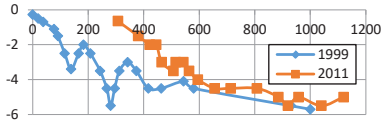

Figure 2. Depth variations along line 1

Sedimentation area behind the breakwater can be determined using satellite images and by comparing them to initial coastline. Hence, at first, coastline position was derived from 2003 satellite image and compared to the initial coastline derived form 1999 hydrographic survey. Comparison between these data shows there is about 400000 m^2 sedimentation behind the breakwater which occurred in around 5 years. Therefore, taking into account 5 m as closure depth, rate of sedimentation is calculated about 80000 m^3/year.

Furthermore, sediment characteristics such as mean diameter grain, critical shear stress as well as fall velocity are crucial to simulate sedimentation. Mean diameter grain is about d_{50}=0.15 mm based on measurements.

Wave data is a vital information in order to study sediment transport and coastline variations. In this study, the time series of wave in 13 m depth cover the period 1983-2013. The wave rose is shown in fig. 1. As seen in this figure, the dominant direction of offshore wave is north-northeast.

3. Mathematical Modeling

3.1. 1-D Modelling

The mathematical model, LITDRIFT, uses different theories to calculate littoral sediment transport. These theories are Stokes, Cnoidal, Vocoidal, Isobe & Horikawa and Doering & Bowen. After setting up the

model and defining various parameters, different theories was used as calibration parameter so that the results of the model was compared to the actual rate of littoral sediment transport calculated in previous section. The results of model showed that *Doering & Bowen theory* is the best theory in this area to calculate littoral sediment transport. The results of other theories are all underestimate.

Figure 3 displays accumulated net and gross sediment transport across the profile. It should be noted that coastline normal is about 60°. As illustrated in this figure, rates of net and gross sediment transport are about 80000 and 120000 m^3/year, respectively.

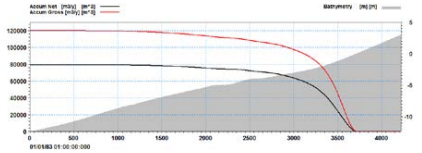

Figure 3. Accumulated net and gross sediment transport

In order to study coastline changes, LITLINE module is used. This module calculates coastline changes using continuous equation and considering the effects of waves and currents in a nearly uniform coast and non-cohesive sediment.

In this study, coastline changes are calculated by using one-line model and Figure 4 shows one of the results of such modelling. The results demonstrated that coastline progress on the breakwater and the volume of sedimentation after 5 years of development are about 140 m and 98000 m^3/year, respectively. As seen, although the rate of littoral sediment transport is more than actual value, the amount of coastline progress on the breakwater is less than actual one. The model was performed for various normal angles.

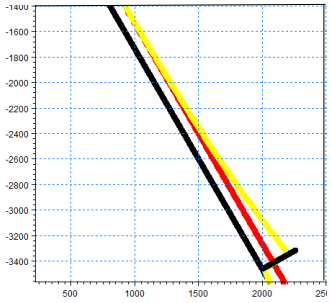

Figure 4. Coastline evolution, 5 years after start

3.2. 2-D Modelling

In order to study the patterns of sedimentation and erosion in the area, MIKE21 coupled model is used. One period covering 3 major storms was modelled in order to investigate the morphological evolution. This period covering 2 months from September to October 2001. These storms were really important for the alongshore sediment transport. Figure 5 shows selected time series of wave heights. These time series were used as boundary conditions. After introducing all parameters model was run for the selected period. Figure 5 indicates morphological changes 2 months after start.

Accretion and erosion patterns were analyzed based on morphological changes and the integrated net sediment transport was calculated across the profile as well. Alongshore and cross-shore sediment transport were calculated 33000 and 9000 m^3 in 2 months, respectively. Thus, in order to determine annual sediment transport in comparison with 1-D modelling, weight factor was found 3.0.

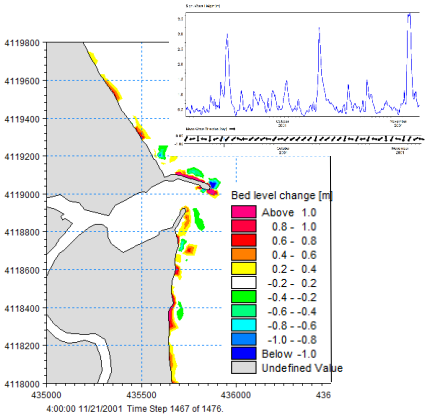

Figure 5. Sedimentation and erosion pattern and the time series of wave height

4. Conclusion

In this study, littoral sediment transport and coastline changes are modelled using 1-D and 2-D modelling and their results are compared to hydrographic surveys and satellite images. Some results of the study are:

- Direction of littoral sediment transport is northwest to southeastern.
- In this region, Doering & Bowen theory is the best option to calculate littoral sediment transport.
- Rate of littoral sediment transport is about 80000 to 100000 m^3/year.
- Deposition of sediment was occurred near the breakwater.
- In order to transform the results of 2-D morphological modeling to annual sediment transport in comparison with 1-D modelling, weight factor was given 3.0.

5. References

[1] DHI, 2011, "LITDRIFT and LITLINE, User Guide".
[2] DHI, 2011, "MIKE21/3 Coupled Model FM, User Guide".
[3]DHI, 2007, "Bakkafjara, Sediment transport and morphology, phase 2, final report".

EVALUATION SEDIMENT LOAD OF KOL AND MEHRAN RIVER AND ITS IMPACT ON EAST QESHM PORTS (CASE STUDY: ZAKERI PORT)

Amirhossein Parvin A. [1], Gholamreza Fazaee[2] and Hamed Mohammadnejead[3]

1) Coastal and marine engineer, Khakbaft consulting Engineers, ahparvin@yahoo.com
2) Project Manager, Khakbaft consulting Engineers, ghfazaeekhakbaft@gmail.com
3) Marine Structural Expert, Port and Maritime Organization, Tehran, Hamed.m.tce@gmail.com

1. Introduction

Kol and Mehran River considered as the two most important sediment sources in the Khouran strait. This study is aimed primarily at determination the impact of sediment loads of these watercourses on northern part of Hurmuz strait morphology and its influence on sedimentation process in port basins in east of Qeshm island. In Qeshm Island major of port centralized in east Island due its proximity to Bandar-e-abbas, which is the center of province in mainland.

2. Estimation annual Alluvial Discharge from Kol and Mehran River

Figure 1 illustrates the location of Kol and Mehran estuaries and three hydrometery stations -with almost 50 years record-, which we particularly benefited them for this project.

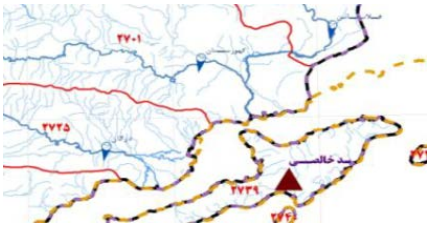

Figure 1- Location of Kol and Mehran mounts and three hydrometery stations

After scrutinizing all statics and considering all perspectives, we can propose below table to brief the water discharge and sediment concentration for kol and Mehran Rivers in one-year return-period flood condition.

Table 1. Characters of Kol and Mehran River during floods

River	Water Discharge (m^3/s)	sediment concentration (Kg/m^3)
Kol	400	60
Mehran	115	15

Plenty bed samples from north of Qeshm island reveals that we can consider sediments mainly with fine grading (fine sand or Silty sand).

3. Simulation

In first stage, a regional domain from Khouran strait and east of Qeshm Island established (Figure 2). The coupled mud sediment and hydrodynamic model performed for several days.

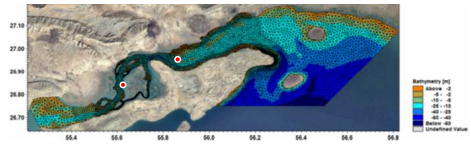

Figure 2. Regional domain and Kol and Mehran estuaries

The results are highly reliant upon factors in simulation. Most appropriate parameters should be determined with scrutinizing and comprehensive studies but one of most important parameters on driving suspending mud particles toward east of Island by tidal current is critical shear stress which related results illustrated for value of (0.07, 0.05 and 0.01 N/m^2).

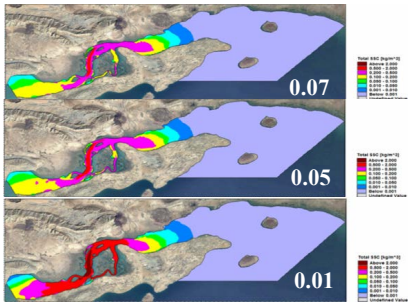

Figure 3. Suspended sed. Concentration based critical shear stress

The results reveal that due to flow tide is dominant a considerable share of flood sediments tends to concentrate on Khouran strait. Existence of Harrah ecosystem can prove the fact that most of suspended mud from rivers deposited in this zone.

Differences in critical shear stress was effective on mud density in area with high sediment concentration, nevertheless, it has a slight variation in suspended sediment concentration in east of Island and. It is expecting in long term a part of consolidated sediment gradually drifted to the east of Qeshm Island.

4. Zakeri Port's Basin Siltation Simulation

After assessing the sediment status in north of island, a local domain simulation also implemented around the east of the island in order to evaluate more specifically siltation situation in Zakeri port basin. This domain (consisted from 4439, 8212 nodes and elements, respectively) extended from Hamoon port in west to the Bahman Port in southeast of the Island and benefited from the most accurate available bathymetric (1/5000) and local bathymetry data (Figure 4).

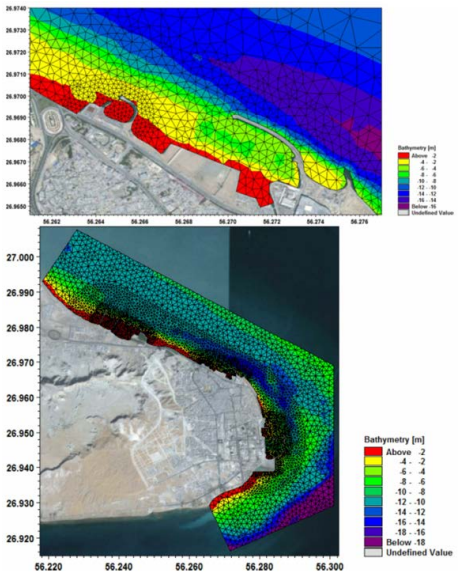

Figure 4. Local domain in east of island and around the Zakeri port

At this stage, the Zakeri port considered as case study. Because this passenger port has only eastern breakwater branch so its exposed basin can be vulnerable by ebb tidal flow and northwest wind. Chosen from below table.

Table 2. Model parameters

Parameter	Value
Manning N.	60
W_0 (for20µm)	120 m/s
τ_{cd}	0.07N/m^2
τ_{ce}	0.2N/m^2
n	1
E	0.00005 Kg/m^2
density	450 Kg/m^3
Bed roughness	0.001
S. Eddy V. for.	1

Based on samples, the deposited bed material mainly are fine grading (D_{50}=2 µm) and by passing the time it become denser than Soft Mud and can classified it as Partly Consolidate Mud. Model parameters.

Figure 5 shows the bed thickness change during one-month period of simulation. The results show that present basin can has more than 5000 m^3 deposition in a month.

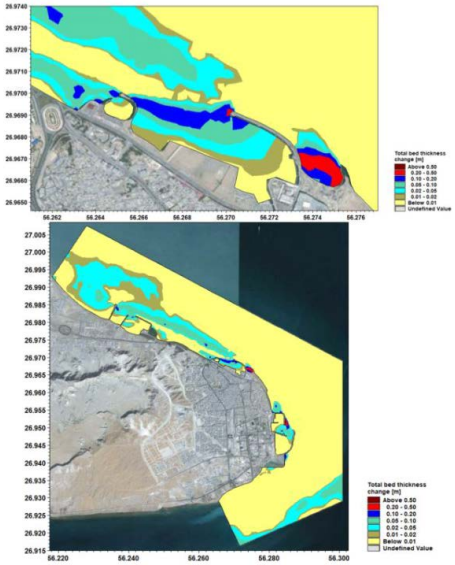

Figure 5. Total bed thickness change in area

5. Conclusion

In retrospect, this study provided a rough estimation about Kol and Mehran sediment load in flood condition and their alluvial impact on north of Qeshm islands morphologic status. Then we evaluate the siltation in ports basins located in east, results of these sources.

6. References

[1] Water deputy of Power Ministry, "Master Water Plan studies synchronizing for, Kol-Mehran catchment areas-Vol.1", Nov 2008, pp.50-250.

[2] DHI, "MIKE 21 Flow Model FM - Mud Transport", 2016

STUDY OF CURRENT BEHAVIOUR IN IRANIAN COASTLINE OF THE OMAN SEA, BASED ON FIELD MEASUREMENT DATA

Mohammad Bagheri[1], Aref Farhangmehr[2], Mehdi Ezzati[3], Abbas Haghshenas[4], Maryam Tabatabaee[5], and Mohammad Hossein Nemati[6]

1) Iran Ports & Maritime Organization (PMO) , Tehran, Iran, mbagheri@pmo.ir
2) Institute of Geophysics, Tehran University, Tehran, Iran, aref.farhangmehr@gmail.com
3) Faculty of Civil Engineering, Babol Noshirvani University of Technology, Babol, Iran, M.Ezzati@sina.kntu.ac.ir
4) Institute of Geophysics, Tehran University, Tehran, Iran, sahaghshenas@ut.ac.ir
5) Institute of Geophysics, Tehran University, Tehran, Iran, maryam.tabatabaee@ut.ac.ir
6) Iran Ports & Maritime Organization (PMO), Tehran, Iran, mhn1982@gmail.com

1. Introduction

The Gulf of Oman offers the only entrance from the Arabian Sea and the Indian Ocean into the Persian Gulf and is affected by the climate and hydrodynamic processes of this ocean. Makran Coast plays an important role in country's future navigation and trade due to its accessibility.

The Oman Sea is located in the northern margin of tropical climate systems, as the sea is exposed to monsoon rains. Seasonal changes in this sea are not long, since these changes do not generate currents. The surface flows of water in the Oman Sea are not similar everywhere, and depend on the wind direction.

In summers, when the southwest monsoon winds dominate the Oman Sea, water flows into the Oman Sea toward the northwest, and even there is a surface stream from the Oman Sea to the Persian Gulf. In winters, when northeast monsoons is dominant, water flows outside the Oman Sea. Strong winds blow in the spring and winter and are more intense in January and February than other months.

In 2015, Iranian Port and Maritime Organization (IRPMO) selected the Iranian Makran coastline to be studied as the 6th phase in the series of Monitoring and Modelling Studies of Iranian Coasts. A part of the field measurement was conducted by Darya Negar Pars (DNP) Consultant Engineers in 2016.

In this study, comprehensive field measurement studies have been done to investigate current behaviour of Iranian coastline of Oman seas.

2. Field Measurement Data

A total of 12 ACDP devices were used in this study, 11 of which were operational and one standby. Current parameters were measured at seven permanent and two temporary stations for a period of one year. During the measurement period, temporary devices were moved in the study area. The locations of the devices are shown in Figure 1 and Table 1. The deployment depths for fixed location were 25m and 30m.

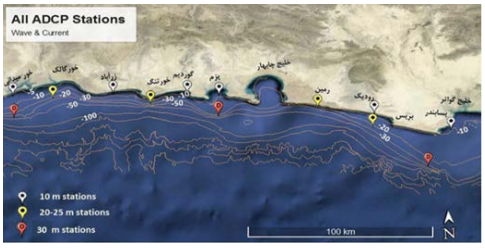

Figure 1. Locations of measurement devices.

Table 1. Location and depth of fixed measurement devices.

Num	Name	Lon.	Lat.	Depth
1	Meydani	59°11'45.97"	25°16'37.80"	30
2	Galak	59°24'0.53"	25°23'2.21"	25
3	Tang	59°52'57.34"	25°18'55.25"	25
4	Pozm	60°15'2.09"	25°13'36.09"	30
5	Ramin	60°43'4.56"	25°15'58.14"	25
6	Roodik	61°04'37.63"	25°07'18.74"	25
7	Pasabandar	61°18'36.71"	24°56'42.85"	30

3. Methodology (Data Analysis)

Prior to conducting the analysis, a quality control procedure was performed to eliminate deployment errors. Some items are to be controlled such as: Low Signal SNR threshold, Sidelobe rejection, tilt effects, compass and pressure offset and echo spikes [1].

The time series was filtered based on the frequency bands of the effective natural phenomena. Therefore, currents are separated into two categories, currents caused by tides and currents caused by other forces such as wind. In order to obtain currents produced by the non-tidal

forces, including wind driven and geostrophic current, all frequencies inside a band for periods of 3-18 hours were removed (Figure 2). The frequency domain analysis and band-pass filtering is based on the Fast Fourier Transform (FFT) [2].

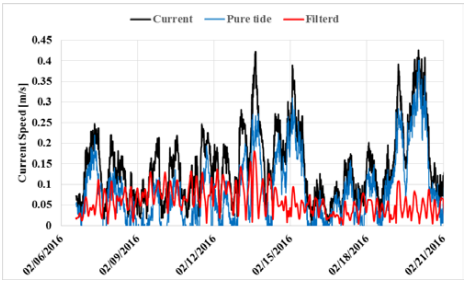

***Figure 2. Pure tide extraction by FFT filter* in Pasabandar station.**

4. Results and Discussion

Figure 3 shows currents roses in observation points. Dominant current direction is along the shoreline which corresponds to the West- East direction. Compared to wind rose plotted by wind data of Sham and Jod stations, there is a proper harmony between wind and surface current roses.

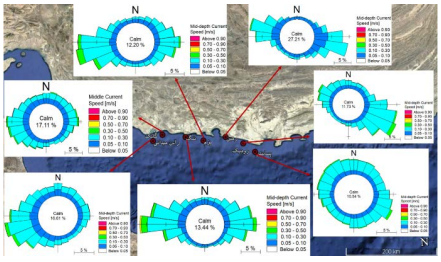

Figure 3. Current rose along Iranian coast of the Oman Sea in middle layer.

Measurements of currents show the presence of oscillating ocean currents along this coastline. The oscillation period of these currents varies approximately from 3 days to a week. They are typically strong through the water column with the near-bed current velocity reaching up to 0.5 m/s at 20~30 m depth in Pasabandar station.

In some cases, the surface current direction is not compatible with wind direction, especially in July and August. This phenomenon can occur for two reasons. Firstly, due to occurrence of the upwelling phenomenon which occurs in July and August in the study area. Secondly, the flow may not be generated by wind, but by geostrophic current.

As can be seen from current speed scatter tables, there are only 3 stations whose flow is exceeded 0.25 m/s for more than 60% of the time. Looking in more detail will help to identify the factor responsible for such an event. These stations are located down current or in bay mouth. This event is a proof of Bernoulli's principle which states that an increase in the speed of a fluid occurs simultaneously with a decrease in pressure or a decrease in the fluid's potential energy.

As can be seen in Figure 4, there is a similar tide phase even comparing the farthest stations. It shows that there is a cross-Gulf variability in tide phases.

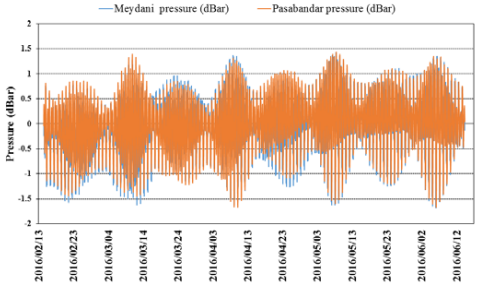

Figure 4. Water level of Stations Pasabandar and Meydani

5. Acknowledgment

The authors are grateful to the colleagues at Darya Negar Pars (DNP) and Pars Geometry Consultants (PGS) for their contributions in field measurements. Thanks are extended to Ports & Maritime Organization (PMO) for the support of the conducted research through the 6th phase of monitoring and modeling studies of Iranian coastline.

6. References

[1] Albertson, S. (2010), "Standard operating procedures for calibration, preparation, and deployment of Teledyne RD instruments acoustic Doppler current profilers (ADCPs)©(RDI)".

[2] Bendat, J. S., & Piersol, A. G. (2011). Random data: analysis and measurement procedures (Vol. 729). John Wiley & Sons.

[3] Beal L. M. , Hormann V. , Lumpkin R. , Foltz G. R (2013). The response of the surface circulation of the Arabian Sea to monsoonal forcing. J. Phys. Oceanogr. 43: 2008–2022.

[4] Johns, W. E.,Jacobs, G. A.,Kindle, J. C.,Murray, S. P.,Carron, M. (1999). Arabian Marginal Seas and Gulfs. Report of a workshop held at Stennis Space Center, Mississippi, May 11-13, 1999. RSMAS Technical Report#2000-01, University of Miami, 60pp.

WAVE CHARACTERISTICS OF IRANIAN COASTLINE OF THE OMAN SEA; BASED ON FIELD MEASUREMENT DATA

Mohammad Hossein Nemati[1], Maryam Tabatabaee[2], Mehdi Ezzati[3], Aref Farhangmehr[4], Abbas Haghshenas[5] and Mohammad Bagheri[6]

1) Iran Ports & Maritime Organization (PMO) , Tehran, Iran, mhn1982@gmail.com
2) Institute of Geophysics, Tehran University, Tehran, Iran, maryam.tabatabaee@ut.ac.ir
3) Faculty of Civil Engineering, Babol Noshirvani University of Technology, Babol, Iran, M.Ezzati@sina.kntu.ac.ir
4) Institute of Geophysics, Tehran University, Tehran, Iran, aref.farhangmehr@gmail.com
5) Institute of Geophysics, Tehran University, Tehran, Iran, sahaghshenas@ut.ac.ir
6) Iran Ports & Maritime Organization (PMO) , Tehran, Iran, mbagheri@pmo.ir

1. Introduction

The coasts of Makran or Oman are considered as the most critical geographical and economical regions in Iran. Makran is a semi-desert coastal strip in the southeastern province of Sistan and Baluchestan. It is known as Iran's golden gate to open seas and international waters such as Arabian seas and Indian Ocean. It has been considered as the most important region for importing and exporting in the global market during recent years. Furthermore, due to the presence of oil-producing area around the Persian Gulf, the petrochemical potential of this area and corresponding ports, it is a critical region in the middle-east. These coasts can be flourished economically, considering its tourism industry and construction of multi-purpose ports. Therefore, above discussion reveals that the Study of the Wave Behaviour in this area should be noticed more than previous [1].

Makran coastline is about 350 km stretching from Gwadar Bay at the border with Pakistan to Rapch Estuary at the border with Hormozgan Province.

The study area experiences three climatic seasons, including: prior to Monsoon, Summer Monsoon and Winter Monsoon. The southwest and northeast monsoons winds are dominant in summers and winters in the Oman Sea, respectively. Strong wind blows in the spring and winter. It is more intense in January and February than other months.

In 2015, Iranian Port and Maritime Organization (IRPMO) selected the Iranian Makran coastline to be studied as the 6th phase in the series of Monitoring and Modelling Studies of Iranian Coasts. Part of the field measurement was conducted by Darya Negar Pars (DNP) Consultant Engineers in 2016.

In this study, comprehensive field measurement studies have been done to investigate wave behaviour of Iranian coastline of Oman seas.

2. Field Measurement Data

In this study, two Nortek Acoustic Waves and Current (AWAC) instruments were deployed within the study area to record wave information. The instruments were placed at a depth of approx. 30m. The location and deployment depth of ADCP devices are shown in Figure 1 and Table 1. Pasabandar and Meydani stations are located in the eastern and western parts of the study area, respectively. The aim was to collect 9 months of data, which would require a service visit approximately every 2 months. This study summarises the data that covers the period from deployment on Feb. 2016 to Nov. 2016.

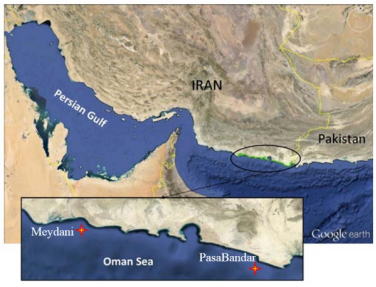

***Figure 1. Locations of* measurement devices.**

Table 1. Location and deployment depth of ADCP devices.

Name	Lon.	Lat.	Start Time	End Time	Depth
Meydani	59.1961°	25.27717°	2016- Feb	2016- Nov	30
Pasa Bandar	61.3102°	24.94524°	2016- Feb	2016- Nov	30

3. Methodology (Data Analysis)

High-quality marine observations require sustained quality assurance (QA) and QC practices to ensure reliability and validity of measured data. Required procedures to achieve this purpose include validation, processing, analysis and interpretation [2].

Prior to conducting the analysis, a quality control procedure was performed to eliminate deployment errors. Some items are to be controlled such as: Low Signal SNR threshold, Side-lobe rejection, tilt effects, compass and pressure offset and echo spikes [3].

Maximum Likelihood Method with Surface Tracking (MLMST) method was used for the directional wave processing. Moreover, for separating wave spectrum into wind sea and swell components, a separation frequency of 0.125 Hz was used. Waves having frequencies lower than the separation frequency are considered as swell and waves having a frequency exceeding this value, as wind sea.

4. Results and Discussion

Figure 2 shows wave characteristics in Pasabandar and Meydani stations. In general, the results represent 17% of calm sea state at Meydani station (western part of the Makran coastline), while this value equals 5% for Pasabandar station (eastern part of the Makran coastline). Furthermore, the direction of the prevailing mixed waves in the western station is from the south and south-east, but the dominant direction for the eastern station is from the south and southwest.

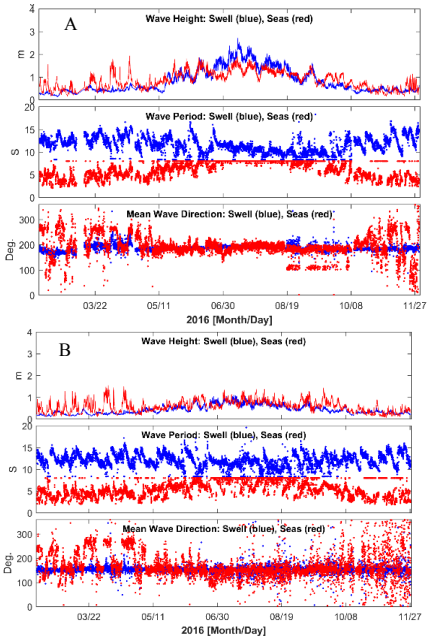

Figure 2. Time series of wave characteristics in PasaBandar (A) and Meydani (B) stations.

The direction of dominant swell waves gradually shifted from southwest to southeast and subsequently wave height reduced, moving from east to west. It indicates a trend of reduction in the summer effect of the monsoon and an increase in the effect of local winds from east to west. This suggests that, compared to the western part of the Makran coast, the eastern side is much more affected by waves produced hundreds of miles out to sea.

The study area experiences three climatic seasons, including: Monsoon, Southwest Monsoon (summer) and Northeast Monsoon (winter). According to the time series presented in Figure 2, at the beginning of May both swell and wind sea waves, began to grow and the trend of wave period became less scattered randomly. At the same time, as the wave height increased, the peak period of the mixed and swell waves decreased. Taking into account these indications, it is possible to estimate the beginning of the effects of summer monsoon in the area from the end of May. Moreover, local waves have less fluctuations in direction and height during the Summer Monsoon, due to more uniform wind direction. This trend continued until late September, after which the intensity of the waves reduced. In addition, wave period and direction became more scattered. Thus, the end time of the summer monsoon in this area is estimated in late September. However, due to the widespread influence of summer monsoon on the area, the swell waves formed during the summer monsoon continue to exist long after the end of this period.

From November to March, due to winter monsoon in the region as well as the winds of the north, the direction of both local and swell waves were scattered. This event is more tangible about local ones. Also, in proportion to the decrease in height and the average period of mixed waves, an increase in the peak period of these waves and swell waves is observed. In this period, the height of the mixed waves rarely reached 2m. But in the case of local waves we see an increase in wave height and a decrease in period.

5. Acknowledgment

The authors are grateful to the colleagues at Darya Negar Pars (DNP) and Pars Geometry Consultants (PGS) for their contributions in field measurements. Thanks are extended to Ports & Maritime Organization (PMO) for the support of the conducted research through the 6th phase of monitoring and modeling studies of Iranian coastline.

6. References

[1] Kiany, D. (2017). The Role of Makran in Political and Economical Horizon of Iran (Lost Treasure). International Journal of Economic Perspectives, 11(1), 1195-1205.

[2] Bushnell, M., Bouchard, R., & Worthington, H. Manual for real-time quality control of in-situ surface wave data: a guide to quality control and quality assurance of in-situ surface wave observations.

[3] Albertson, S. (2010), "Standard operating procedures for calibration, preparation, and deployment of Teledyne RD instruments acoustic Doppler current profilers (ADCPs)©(RDI)".

STUDY OF PHYSICAL PROPERTIES AND SURFACE CIRCULATION OF THE CASPIAN SEA USING HYCOM MODEL

Abdossamad Rahnemania [1*], Abbas Aliakbari Bidokhti [2] and Javad Babagolimatikolaei[2]

1) Faculty of Marine Science and Technology, Science and Research Branch, Islamic Azad University, Iran
2) Institute of Geophysics, University of Tehran, Iran
* abdossamad2003@gmail.com

1. Introduction

The Caspian Sea, the world's largest inland enclosed water body, consists of three basins namely northern, middle and southern (Aubrey et al., 1994). The enclosure and the growth of oil extraction from this lake in recent years have been an important issue in terms of biological contamination. The study of the Caspian Sea is significant for various aspects of research because of its oceanography specific characteristics. Due to the limitation of observation data in this area, numerical modelling is the best method to develop our physical insight into the principles of the phenomena which occur in the Caspian Sea. There are a number of numerical models that are used by researchers in the last 10 years to investigate physical oceanography properties in this basin. The seasonal circulation based on a coupled sea hydrodynamics, air-sea interaction and sea ice thermodynamics model of the Caspian Sea were investigated by Ibrayev et al (2010) and Gunduz and Özsoy, (2014). The effect of fresh water inflow to the Caspian Sea on seasonal variations of salinity and circulation and pattern of the Caspian Sea surface current has also been studied using HYCOM model (Kara et al, 2010). Shieh et al., (2016) used the COHERENS (Coupled Hydrodynamical Ecological model for Regional Shelf seas) to study the impact of wind and thermal forcing on the seasonal variation in this basin.

In this paper, we investigate the physical parameters of the water (temperature, salinity, and density) and circulation pattern in the Caspian Sea using the HYCOM ocean model. One the important feature of the model compared to other works (e.g. Shieh et al., 2016) is the inclusion of ice. The effects of ice on the distribution of temperature and salinity in the northern Caspian is very important due to its thermodynamic effects.

2. Model set-up

The HYCOM ocean model is used in this research, which is compatible with all three z-level, sigma, and isopycnal coordinate systems. This model can be used in shallow seas as well as the deep ocean. The horizontal resolution is set to 0.04 degree and the hybrid layers in the vertical are 50. The bathymetry of the region was extracted from GEBCO (General Bathymetric Chart of the Oceans) which contains the global Earth topography including land with 30" resolution. The model integration was started from rest on January 1, 2011, using WOA13 temperature and salinity, and integrated for five years for the period 2011–2016 using 0.2˚, with one-hourly NCEP-CFSV2 meteorological forcing. Due to the importance of the fresh water, the average monthly inflow of the three large rivers (Volga, Ural, and Kura) is considered. To validate the model, the results are compared to satellite data from sensor MODIS and also some works such as Kara et al., (2010) and Shieh et al., (2016). The results of the model will discuss in the last year of the run time (2016).

3. Results

To understand the physical properties of water under seasonal changes many fields are plotted. Figure 1 shows that the sea surface salinity in summer and also density anomaly in spring. The density anomaly is calculated relative to the mean value of the whole domain density (~1010 kg/m^3). The results indicate that the sea surface temperature changes are dramatically under seasonal changes. Mean value for temperature in autumn are recorded 18 and 4 °C in the southern and northern Caspian Sea respectively. The maximum temperature difference between the two domains is about 15 °C in winter. The results of surface temperature show that upwelling occurs the east coast in summer and the length of the coast where this phenomenon occurs is about 500 kilometers. However, the salinity change, particularly in the southern basin is negligible in different seasons. Typical value for salinity are about 12-13 and 5-6 PSU for southern and northern respectively. The results show that seasonal changes are interesting in the northern basin. It is observed that the fresh water front (relative to seawater) continually changes in different seasons. The salinity front has a drop of about 5 PSU and it covers most of northern basin particularly in autumn and winter. However, in spring and in summer this front is very small in terms of covered area. On the other hand, study of the surface current shows that the pattern of current is almost north-southerly (Figure 2). The range of velocity are different from 0.15 to 0.6 m/s in whole area. The surface flow pattern is in good agreement with the pattern provided by Lednev (1943). In the middle basin (between 42°-43° N), it is observed that the vorticity field is continuously changing in terms of intensity and location.

The maximum diameter of the eddy is about 300 km in the winter and it is counterclockwise (cyclone). In the southern basin, 1-3 eddy (es) formed, particularly near the Sepid Rud cape. Similar to the middle eddy, the length scale, shape, and intensity are different in various seasons. According to the results, in some seasons in the western part of the southern Caspian Sea, the flow moves from the middle to southern and rounds the whole southern region. The flows, clinging to shores of Iran, move along within the eastern coast, particularly in the summer.

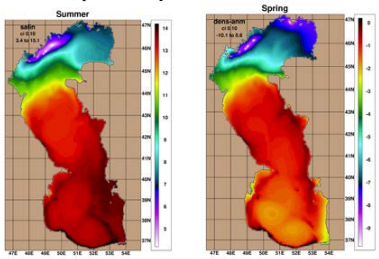

Figure 1. The sea surface salinity (left) in the summer and density anomaly (right) in the spring

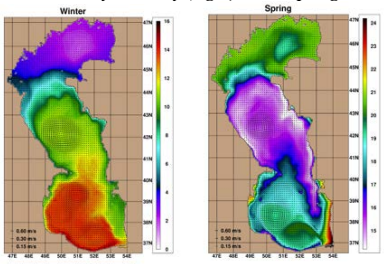

Figure 2. The sea surface temperature field overlay with the current vector in different seasons.

4. Discussion and Conclusion

Temperature plays a pivotal rule in the structure of water circulation in the Caspian Sea. As a result, pattern of pycnocline are very similar to thermocline (rather than halocline) in the whole area. Due to seasonal changes and also the depth of the basin, the thermocline gradient is very steep based on the depth. There are two factors affecting the distribution of surface salinity. The most important factor in salinity changes is the entrance of rivers. For this reason, salinity in the northern region is less than the southern one due to the presence of Volga, Ural, and Kura in this area. The evaporation is another factor that can affect the salinity of the Caspian Sea. This pattern of variation in temperature and salinity causes changes in density particularly in the northern basin due to the extreme cold weather in the winter. Hence, the density in surface increase and the water sink to the deep part. In the course of that, braian rejection can occur when the surface water begins to freeze. Due to this phenomenon, the water will sink to deeper parts. Regarding sinking water into deeper part of ocean basins, it can carry oxygen to living organisms at greater depths.

In terms of current, the results indicate that the surface patterns circulation are affected by wind and river influx. The effect of wind is more important than the river. These results are quite consistent with the Shiea., et al., 2015. They show that the approximate mean current created only by rivers was 1/10 of the circulation created by the wind driving force. In terms of upwelling, as the dominant wind pattern is from the north to south in the summer, especially on the eastern coast, it caused an upwelling on the eastern coast of the Caspian Sea during the summer. Apart from this, in this area the southward surface current move along the eastern coast. This phenomenon is very effective due to the pumping of water from the deeper parts. In the case of formation of eddies, they are formed by wind and surface circulation patterns, particularly in the middle basin. However, the eddies are formed in the southern basin as a result of separation of current from the Sepid Rud Delta cape. In the formation of these eddies, both factors surface and deep currents are effective (Babagoli et al., 2018). The results also indicate that these eddies also affect the bed which needs further investigation. Eddies have a great role in redistributing heat and salinity and pattern of surface currents in the Caspian Sea because they advect mass, and have the ability to propagate which is crucial to its contribution to the ocean mixing rates (Robinson, 2012).

5. References

[1]Aubrey, D.G., Glushko, T.A., Ivanov, V.A., (1994). North Caspian Basin: Environmental status and oil and gas operational issues, Report for Mobil-oil, 650 pages.

[2]Babagoli, J., Bidokhti, A.A. and Shieh, M., 2018. "Some aspects of the deep abyssal overflow between the middle and southern basins of the Caspian Sea". Ocean Sci. Discuss., doi.org/10.5194/os-2018-13.

[3] Gunduz, M., & Özsoy, E. (2014). Modelling seasonal circulation and thermohaline structure of the Caspian Sea. Ocean Science, 10(3), 459-471.

[4] Ibrayev, R. A., Özsoy, E., Schrum, C., & Sur, H. I. (2010). Seasonal variability of the Caspian Sea three-dimensional circulation, sea level and air-sea interaction. Ocean Science, 6(1).

[5] Kara, A. B., Wallcraft, A. J., Metzger, E. J., & Gunduz, M. (2010). Impacts of freshwater on the seasonal variations of surface salinity and circulation in the Caspian Sea. Continental Shelf Research, 30(10), 1211-1225.

[6] Lednev, V. A., (1943). Techeniya Severnogo i Srednego Kaspiya, Morskoy Transport, Moscow, USSR.

[6] Robinson, A. R. (Ed.). (2012). Eddies in marine science. Springer Science & Business Media.

[7] Shiea, M., Bidokhti, A.A. and Chegini (2015).study of the roles of important forcing mechanisms on the circulation of the Caspian Sea using numerical simulation. IJG, Volume 9, autumn 2015, Page 118-142.

[8] Shiea, M., Chegini, V., & Bidokhti, A. A. (2016). Impact of wind and thermal forcing on the seasonal variation of three-dimensional circulation in the Caspian Sea.

SIMULATION AND DESIGN OF SAND TRANSPORTATION SYSTEM IN KELARABAD FISH FARMING PORT USING LONG-TERM WAVE DATA

Amirhossein Parvin. A.[1], Peyman Badiei[2], Gholamreza Fazaee[3] and Hadi hosseinzadeh[4]

1) Khakbaft consulting Engineering, Ahparvin@yahoo.com
2) Assistant Professor of Tehran University, College of civil engineering, pbadiei@ut.ac.ir
3) Project Manager, Khakbaft consulting Engineering, ghfazaeekhakbaft@gmail.com
4) Marine Engineer, HSS Engineering, Malaysia, Hadi@hss.com.my

1. Introduction

The results of a case study on sand bypassing in a logistic fishing port at Kelarabad City at Caspian Sea described and discussed in this paper. The project location (51.2541E, 36.7025N) shown in Figure 1.

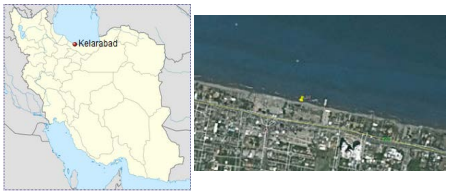

Figure 1. location of site project

The present study benefited from 31 years (from 1983 to 2012) wave data from Monitoring & Modeling Studies of Iranian Coasts project [1](Fig. 2). Offshore waves transmitted to nearshore area at a depth of 5 meters in front of the Port. The approved layout for the Port shown in Figure 2. It estimated that a distance of about 2.5 km at the east side of the breakwater would eroded as result of Port construction. Sand bypassing proposed as a measure to alleviate this problem.

2. A Worldwide Review on Sand Bypassing

Coastal erosion is a growing concern to the decision-makers, politicians. Where the erosive phenomena assume great importance, sand bypassing systems are often an available – if expensive – option to restore, partially or fully, the littoral drift at a given section of the coast [1]. Sand bypassing systems operate on simple principles, and consist of dredging, transporting and depositing sand [2]. There are many examples of utilization of sand bypassing system in all around the world; these systems cover a range of various types of systems in operation. Figure 3 illustrate the distribution location of 53 worldwide sand bypassing system [2]. Bypassing system consists of three major elements; dredging, transport and discharge sub-systems. The discharge location should be chosen so that the strength of the prevailing wave induced longshore currents is enough to transport and feed sand to the eroding down coasts and prevent the sand to be taken back to the breakwater location due to circulating and back flows.

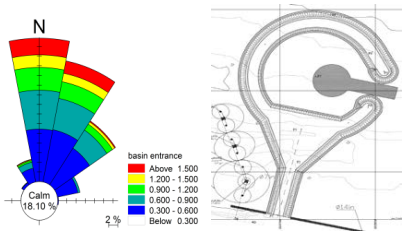

Figure 2. Layout of Kelarabad port and waverose

The discharge location should be chosen so that the strength of the prevailing wave induced longshore currents is enough to transport and feed sand to the eroding down coasts and prevent the sand to be taken back to the breakwater location due to circulating and back flows.

Evidences indicate that sediment bypassing system has a key important in preservation of coastal environment. Nowadays this system became more common in United states and Australia as a reliable solution for erosion of beaches and there are several successful examples such Tweed River in Queensland and Indian River in Delaware [2,3].

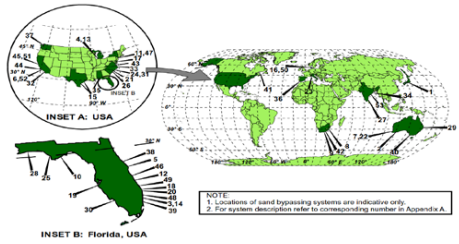

Figure 3. World-wide sand bypassing systems places [2].

[1] For further information: https://irancoasts.pmo.ir/en/home

3. Estimation of Littoral Drift

3.1. Numerical Simulation

For the estimation of littoral sediment transport in this area, LITDRIFT model in DHI-LITPACK coastal software package applied with below info [4]. (D50=0.18mm,Bed roughness and fall velocity of particle are 0.1m and 0.025 (m/s), respectively). More than 28 years data steps applied to calculate the sediment transport rate at the project site. Outputs demonstrated that there is 283000 (m3) net sediment transport potential during the 11.5-year period. In other words, annual transport rate is approximately 28400(m3) towards east and average of maximum weekly deposit amount is about 2600(m3).

Table 1. Accumulative amount of sediment transport.

Annual sediment transport	Amount
Accumulative Gross (m^3)	32770
Accumulative net (m^3)	28400

Figure 4 illustrates the predicted initial coastline changing patterns within 5, 10, 20 and 30 years.

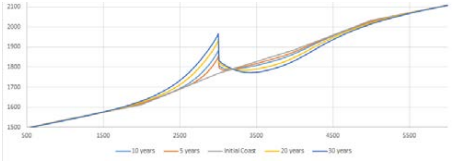

Figure 4. Predicted coastline change

3.2. Field Measurement Evaluation

The results of the three hydrographical surveying at April 2011, September 2013 and June 2016 provided an estimation about the volume of the sand trapped by partial construction of the breakwater. The annual sedimentation on west side of the port is about 18000(m3). However, anticipated that some sediments had bypassed from the tip of the breakwater during construction period. Also in Figure 5 you can see the bed level differences within 2011 and 2016 and the current pattern in breakwater adjacent.

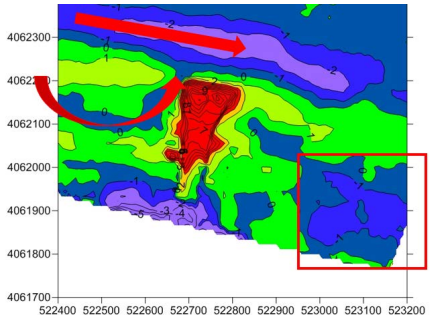

Figure 5. Bed level from 2011to2016

4. Determining the Sediment Discharge Location

The current pattern simulation based on the constructed length of the port access road shown in Figure 6. The circled zone in this Figure shows the location where the longshore current gains enough strength to carry sediment downstream.

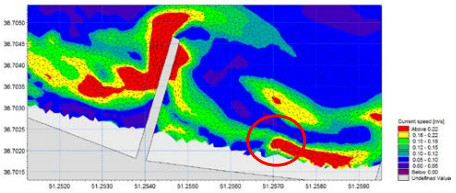

Figure 6. Current pattern around constructed access road

Based on the above simulation it concluded that the discharge location should be somewhere around 250 m at the east side of the breakwater. An estimated amount of 2500(m3) transmitted sediment would be enough. Figure 7 illustrates the simulated morphological impact on the deposited sand after 10 days. It is obvious that vortex current behind the port induced by longshore current plays a key role in beach nourishment in regions with high potential erosion risk in the beach.

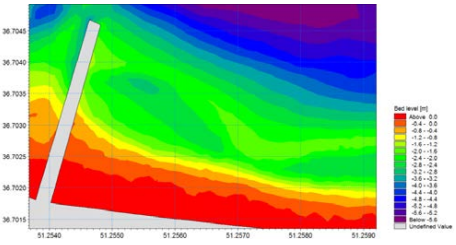

Figure 7. Effect of sediment deposition on beach morphology after 10 days

5. References

[1] Loza, P.,"Sand Bypassing systems- masters in environmental engineering", Revision0, June 2008,

[2] Boswood, P.K., Murray, R .J, " World-wide sand bypassing systems: data report ", *Conservation technical report No. 15*, *Coastal Services technical report R20*, August 2001, pp. 10-59.

[3] Keshtpoor, M., Puleo, J. A., Plant, N.G and Gebert, J., " Beach response to a fixed sand bypassing system ", Coastal Engineering, 73, 2013, pp. 28-42.

[4] DHI, Litdrift User Guide Manual, 2012

LONGITUDINAL VARIATIONS OF SALT FLUXES IN A SHALLOW ESTUARY WITH HYPERSALINE RUNOFF

Seyed Taleb Hosseini[1] and Seyed Mostafa Siadatmousavi[2*]

1) Iranian National Institute for Oceanography and Atmospheric Science, sthosseini@gmail.com
2) Iran University of Science &Technology, Tehran, Iran. siadatmousavi@iust.ac.ir

1. Introduction

As a result of high evaporation rate, a salinity maximum zone or salt plug [4] is likely to occur in a low-inflow estuary in which salinity is higher inside the salt plug than both its seaward and landward directions.

The freshwater lens estuary (FLE) which we describe here, as a unique phenomenon, might occur when a hypersaline runoff from the watershed follows an almost freshwater river discharge with a time lag of few hours/days. Such a condition is likely to occur when a source of salinity exists in the watershed. This condition is met for the Mond River Estuary (see Figure 1) in the northern coast of the Persian Gulf, and occurs occasionally during wet season in which precipitation over a saline soil area close to the river produces a rain-driven flood. This hypersaline water mass follows a freshwater river inflow and enters into the estuary.

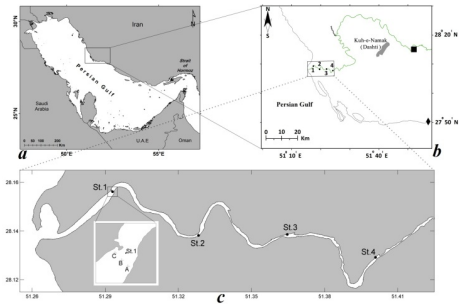

Figure 1. (a) The location of the Mond River Estuary in the Persian Gulf; (b) the locations of 4 CTD-Current meter stations 1 to 4, Kuh-e-Namak (Dashti) and the Qantareh rain and river discharge recorders (Black Square

Two at least 25-hour tidal cycles of velocity, water level, temperature, and salinity were recorded at 4 stations along the estuary (see Figure 1). One period was selected during spring tide from 2 to 3 February 2014 (denoted by Experiment-1 hereafter) which included intense rain, and another period was during neap tide from 22 to 23 February 2014 (denoted by Experiment-2 hereafter). The flood (18-21 February) was recorded in time series of the river inflow.

2. Methods

At each station, a CTD-current meter instrument (RCM9 KM- II; Aanderaa), was moored 1 m above the bottom to record data every 10 min.

The instantaneous u(z) and s(z) can be decomposed into depth-averaged mean values ($\bar{u}$ and $\bar{s}$) and deviations from the vertically mean values (ú and ś). The depth-averaged means may also be decomposed into time-averaged means ($\langle\bar{u}\rangle$ and $\langle\bar{s}\rangle$), and time-varying components (U, S) as follow [1]:

$$u = \langle\bar{u}\rangle + U + \acute{u} \quad (1)$$

$$s = \langle\bar{s}\rangle + S + \acute{s} \quad (2)$$

Note that $\langle\cdot\rangle$ represents the time-averaged quantity over one complete tidal cycle. The net salt flux per unit width, Q, can be calculated as follows [1]:

$$Q = \int_0^h us\,dz = \langle\overline{hus}\rangle \quad (3)$$

Using Equations (1) and (2), the Equation (3) can be rewritten as follows:

$$\langle\overline{hus}\rangle = \langle h\rangle\langle\bar{u}\rangle\langle\bar{s}\rangle + \langle hUS\rangle + \langle\bar{u}\rangle\langle HS\rangle + \langle\bar{s}\rangle\langle HU\rangle + \langle h\acute{u}\acute{s}\rangle \quad (4)$$

$$Q = Q_1 + Q_2 + Q_3 + Q_4 + Q_5 \quad (5)$$

The shear flux term, Q5, has negligible contribution in the net salt flux in a shallow micro-tidal estuary such as the Mond River Estuary, because this term is insignificant in a well-mixed embayment [1]. Water level fluctuations and longitudinal velocities were used for harmonic analysis [3].

The well-known logarithmic velocity profile at each station for an arbitrary time, [2], was used to calculate salt flux terms, as following:

$$u(z) = \frac{u_0}{\kappa}\ln\left(\frac{z}{z_0}\right) \quad (6)$$

in which $\kappa \approx 0.4$ is von-Karman's constant. In order to determine the friction velocity, u_0, in Equation (6), several measurements of horizontal velocity are required in the water column to perform regression analysis. Alternatively, one might use the following equation (Kjerfve, 1979):

$$C_d = \left(\frac{u_0}{u_1}\right)^2 \quad (7)$$

where C_d is the drag coefficient and u_1 is the velocity speed at 1 m above the sea bottom. The constant values of C_d=0.003 and z_0 = 0.068 cm [2] were used in this study, and velocity profiles at all four stations were calculated. The vertical profiles of salinity s(z) and the longitudinal velocity u(z) must be determined to calculate the net salt flux. Because of weakly stratified condition inside the

Mond River Estuary, s(z) is assumed vertically uniform for every 10-min time step.

3. Results and Discussion

3.1. Freshwater Lens Estuary

The gray zone represents the freshwater lens confined by two riverine and marine salt waters (see Figure 2).

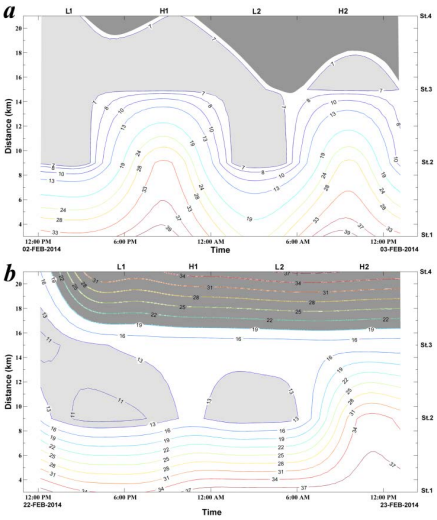

Figure 2. (a) Isohaline contours along the Mond River Estuary during 25 hour in Experiment-1 in wet season. The Persian Gulf waters intrude ~13 km along the estuary and dilute ~16; (b) The same as (a) but for Experiment-2. The Persian Gulf waters intrude 9 km along the estuary and dilute up to ~16 until L2. Thereafter, this salinity intrusion extent to a higher length than 14 km due to dissipation of freshwater lens during higher high tide. Freshwater lens and hypersaline runoff are specified with gray and dark zones respectively.

The salinity increase in the landward of this freshwater lens due to the riverine salt water (dark patch) induced by runoff of saline water from the watershed. Salt waters from the Persian Gulf close to the estuary mouth, also, surround the freshwater lens as the marine salt wedge.

3.2. Net Salt Flux

The advective flux, Q_1, determined the direction of the net salt flux, Q, at all stations except at St.2 during spring tide of weak FLE condition, in which the direction of Q was landward in contrast to the advective flux direction (see Table 1). Among salt dispersive fluxes, Q_2 (tidal sloshing term) played the most important role in the salt transport at St.2 during both FLE conditions. The term Q_3 (the cross-correlation between tide and salinity) was mostly the smallest term among the four salt flux components at all stations. The flux of the Stokes' drift dispersion (Q_4) was often directed upstream (see Table 1).

Table 1. Decomposed net fluxes of salt divided by the corresponding mean water depth,$\langle h \rangle$, (PSU cm/s), in the weak and strong FLEs. Positive and negative values indicate the seaward and the landward flux directions, respectively.

Station	St.1		St.2	
FLE	Weak	Strong	Weak	Strong
$Q/\langle h \rangle$	-291.95	680.18	-21.63	157.43
$Q_1/\langle h \rangle$	-272.97	667.24	85.20	190.47
$Q_2/\langle h \rangle$	3.31	4.06	-69.72	-54.23
$Q_3/\langle h \rangle$	-3.37	0.47	7.45	4.65
$Q_4/\langle h \rangle$	-18.92	8.42	-44.56	16.56
Station	**St.3**		**St.4**	
FLE	**Weak**	**Strong**	**Weak**	**Strong**
$Q/\langle h \rangle$	58.55	390.91	133.03	875.81
$Q_1/\langle h \rangle$	66.40	429.06	139.68	889.05
$Q_2/\langle h \rangle$	0.66	-14.84	0.07	5.19
$Q_3/\langle h \rangle$	-0.10	-2.28	-0.08	-3.93
$Q_4/\langle h \rangle$	-8.41	-21.02	-6.63	-14.51

4. Conclusion

A significant feature of the shallow micro-tidal Mond River Estuary in the Persian Gulf is the fact that hypersaline runoff from watershed enters into the positive estuary during reported measurements in wet season. This phenomenon is named as freshwater lens estuary (FLE). The net salt flux is dominated by advective salt flux during the strong FLE. It is only affected by the tidal signal during the spring tide of weak FLE at downstream stations (St.1 and St.2). The presence of strong hypersaline runoff induced noticeable seaward net salt fluxes at all stations in the strong FLE condition. The seaward advective fluxes at upstream stations (St.3 and St.4) were ~6 times more intense during the strong FLE condition when compared to the corresponding fluxes during the weak FLE condition.

5. References

[1] Ali, A., Lemckert, C. J., and Dunn, R. J. K., Salt fluxes within a very shallow subtropical estuary. Journal of Coastal Research, 26(3), 436–443, 2010.

[2] Kjerfve, B., Measurement and Analysis of Water Current, Temperature, Salinity, and Density. In K. R. Dyer, ed. Estuarine hydrography and sedimentation. Cambridge University Press, pp. 186-227, 1979.

[3] Pawlowicz, R., Beardsley, B., and Lentz, S., Classical Tidal Harmonic Analysis Including Error Estimates in MATLAB using T_TIDE, Computers and Geosciences, 28, 929-937, 2002.

[4] Valle-Levinson, A., Definition and classification of estuaries. In: A. Valle-Levinson, ed. Contemporary Issues in Estuarine Physics. Cambridge University Press. pp. 1-11, 2010.

AN INVESTIGATION ON THE FORMATION OF SUBMERGED BAR'S UNDER WAVES IN THE CASPIAN SEA COASTAL REGION

Fateme Ghanbari[1], Mehdi Adjami[2] and Soheil Ataei H.[3]

1) Faculty of Civil Engineering, Shahrood University of Technology, Shahrood, Iran; qanbari.ftm@gmail.com
2) Faculty of Civil Engineering, Shahrood University of Technology, Shahrood, Iran; adjami@shahroodut.ac.ir
3) Faculty of Civil Engineering, Shahrood University of Technology, Shahrood, Iran; ataei.h.s@gmail.com

1. Introduction

As a result of waves, cross-shore change, which will vary in stormy waves in compare to the sea normal waves. Profiles formed by stormy waves are called erosion profiles, and profiles formed by normal waves are called cumulative profiles. Hashemi *et al.* (2010) conducted studies of forecasting seasonal changes in coastal profiles; They collected data on the coast of the Gulf of Tremodoc by artificial neural network. The results show that the ANN method is more accurate than other expensive numerical models [1]. Demirci *et al.* (2011) studied the influence of parameters affecting sediment transport during 64 experiments in their studies. Regarding the proposed equation, the higher the wave steepness (H_0/L_0) increases, the amount of sediment transport increases, which will increase the size and volume of the bar. In addition, with increasing sediment transfer to the sea, the amount of erosion of sediments increases from the front of the beach (coastal forehead) and the distance between the coastline to the beginning and the end of the bar increases. They also discovered that the movement of sediments toward the sea leads to the movement of the bars and hence the place of wave break is also displaced [2]. Cheng *et al.* (2016) carried out studies on 165 beaches and used two Unibest-TC and S beach coastal profile software to estimate storm coastal changes. They argued that the unibest-TC model could be used to determine the direction of the motion of the sandy bars and the S Beach model can be efficient in determining the exact extent of coastal bars erosion as well as shore line changes [3].

2. Study Area

The Caspian Sea is the largest lake in the world; in recent decades, it has been connected to the Black Sea through the Volga River and the creation of the Volga Channel by Russia. The highest depth of the Caspian Sea is about 1025 meters, and in general the deepest areas of the sea are close to the coast of Iran; the average of the Caspian Sea water level is 27 meters below the free waters level.

3. Methods

Ataei *et al.* (2016) carried out studies on some parts of the southern coast of the Caspian Sea, based on measured data as well as the presented equations. The results of this study show that the Caspian Sea coasts are categorized as stormy type [4]. In addition to the relations found by Ataei *et al.* (2016), Sunamura and Horikawa (1974), carried out studies on the transfer of sediments and parameters affecting cross-shore profiles, provided the parameter C for the classification of coastal profiles.

$$C = \frac{H_0}{L_0}(\tan\beta)^{0.27}\left(\frac{d_{50}}{L_0}\right)^{-0.67} \quad (1)$$

Based on parameter C, the type of cross-shore profile can be determined such that if $C < 4$ is the cumulative profile, if $4 < C < 8$ is the equilibrium profile and if $C > 8$ is the erosional profile [5]. According to the relations provided by Short and Aagaard (1993), the number of bar in the coastal profiles can be found. Based on this, Eq. (2) presents the parameter B_0 for determining the number of bars. In such a way that if $B_0 < 20$ the profile does not have any bar and the profile is a balance one. If $20 < B_0 < 50$ the profile has one bar, $50 < B_0 < 100$ has two bars, $100 < B_0 < 400$ has a three-bar profile, and if $B_0 > 400$, then the profile will have four bars [6].

$$B_0 = \frac{X_s}{gT^2\tan\beta} \quad (2)$$

Beach slopes, sediment transport, sea bed, and sea level changes are among the factors affecting cross-shore profiles; In this study, the effects of effective parameters on cross-shore profile deformation has also been evaluated. Fig. 1 shows each of the geometric parameters of coastal profiles.

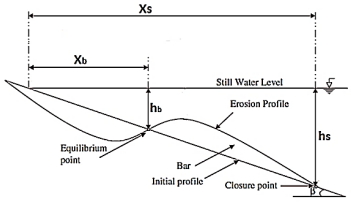

Figure 1. Geometric Parameters of Coastal Profiles.

4. Data Analyses

Due to the analysis and survey of the southern shores of the Caspian Sea and based on the Eq.'s (1) and (2), the performance of the coastal areas has been studied and analyzed based on the cumulative, equilibrium and coastal erosion categorize and the number of bars [7, 8]. The results are presented in Table 1.

Table 1. Calculating parameter C and determining the number of the Caspian Sea bars.

Parameters	Anzali	Dastak	Namakabrood	Mahmudabad	Larim	Miankaleh
C	19.22	19.89	18.32	21.64	20.15	16.71
Type of the cross shore profiles	erosion profile	erosion profile	erosion profile	erosion profile	erosion profile	erosion profile
B_0	177.6	176.3	141.7	111.2	208.2	810.5
Number of the bars	3	3	3	3	3	4

To facilitate the use of field data and reduce the error rate, X_b, X_s, h_b, h_s and H_0 parameters are converted to dimensionless numbers relative to the wave length, and the change in the water level. In Fig 2 the relation between the wave steepness and the geometric parameters of the profiles and in Fig. 3 the relation between H_0/s and the geometric parameters in a situation where the change in water level in all regions are the same is evaluated.

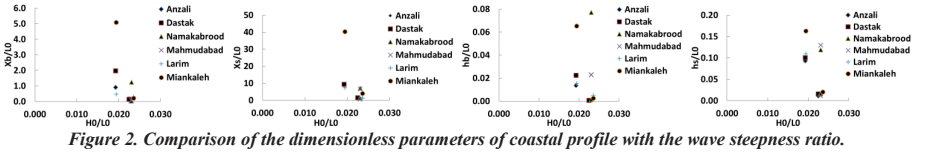

Figure 2. Comparison of the dimensionless parameters of coastal profile with the wave steepness ratio.

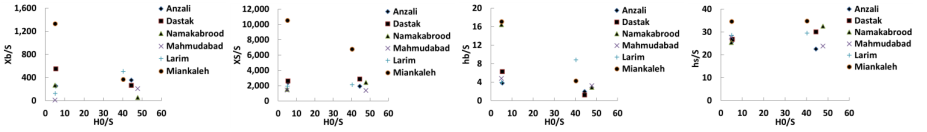

Figure 3. Comparison of the dimensionless parameters of the coastal profile with the H_0/s ratio.

5. Discussion and Conclusions

The purpose of this study is to investigate the southern shores of the Caspian Sea and determine the erosion or accumulation of coastal profiles, determine the number of bars, and also determine the relation between coastal parameters with the wave's steepness and water level changes. The C parameter in the areas determined is always greater than 8, so it can be stated that the Caspian Sea behavior has a stormy and erosional nature. The beach profiles for Anzali, Dastak, Namakabrood, Mahmudabad and Larim have three bars and the profile of the Miankaleh has four bars. With increase in the wave steepness, the ratios of X_b/L_0 and X_s/L_0 in all profiles are reduced, thus it can be stated that the coastal bars begin to form at a shorter distance from the coast line and the general displacement of the bars happens toward the coastline. The ratios of h_b/L_0 and h_s/L_0 are also reduced; as these ratios are reduced, the depth of water decreases at the beginning and the end of the bars, which indicates that the erosional beach will be created. With constant consideration of water level changes, it is observed that in the conditions of lowering in the water level, by the increase of the wave height, the location of the formation of coastal bars in all regions of the study is not approached to the coastline. Also, the process of water depth changes at the beginning and end of the bars is not uniform. This suggests the complexity of the sea's environmental conditions in the state of the water level change, since as water level decreases, the interactions of the wave particles with the bed change, and the type of wave break and its distance to the coast line will be affected.

The results show that the behavior of the coastal areas of the Caspian Sea is a stormy nature with a coastal erosion, which makes it possible to form multi bars profiles (three bars) very high. As the wave's steepness rises, the location of the formation of the bars moves toward the coast, and the depth of water decreases at the beginning and the ends of the bars; also, in terms of lowering in the water level with the change in the height of the waves, the position and the geometric shape of the bars will not follow a certain trend.

6. References

[1] Hashemi MR, Ghadampour Z, Neill SP. "Using an artificial neural network to model seasonal changes in beach profiles", *Ocean Engineering*. 2010 Oct 1;37(14-15):1345-56.

[2] Demirci M, Akoz MS, Unes F. "An Experimental Study on Cross-Shore Sediment Transport", *International Balkans Conference on Challenges of Civil Engineering*, 2011.

[3] Cheng J, Wang P, Smith ER. "Hydrodynamic conditions associated with an onshore migrating and stable sandbar", *Journal of Coastal Research*. 2015 Apr 8;32(1):153-63.

[4] Ataei H., S., Lashteh Neshaei, M., Adjami, M. "Classification Of Barred And Unbarred Beach Profiles In The Caspian Sea", *Journal of Coastal and Marine Engineering*, 2017

[5] Sunamura T, Horikawa K. "Two dimensional beach transformation due to waves", *Coastal Engineering*, 1974 (pp. 920-938).

[6] Short AD, Aagaard T. "Single and multi-bar beach change models", *Journal of Coastal Research*. 1993 Apr 1:141-57.

[7] Caspian Sea National Research Center report, *Caspian Sea Profiles*. Water Research Institute, Ministry of Energy of I.R. Iran, 2016. http://wri.ac.ir/csnrc

[8] Ports and Maritime Organization report, *Caspian Sea Level Changes*. Ministry of Roads & Urban development of I.R. Iran, 2016. http://www.pmo.ir/en/home.

A 37-YEAR WIND AND WAVE HINDCAST FOR THE OMAN SEA

Morteza Jedari Attari[1], Arash Bakhtiari[2], Mohammad Dibajnia[3], Aref Farhangmehr[4],S. Abbas Haghshenas[5], Mohammad Bagheri[6] and Homayoun Zaker[7]

1) Visiting Researcher, Inst. of Geophysics, Univ. of Tehran, Iran, mortezajedariattari@yahoo.com
2) Project engineer, Middle East Water and Environment Co., Tehran, Iran, arash.bakhtiary@gmail.com
3) Collaborating researcher, Inst. of Geophysics, Univ. of Tehran, Iran, dibajnia@gmail.com
4) Visiting Researcher, Inst. of Geophysics, Univ. of Tehran, Iran, aref.farhangmehr@gmail.com
5) Assistant Professor, Inst. of Geophysics, Univ. of Tehran, Iran, sahaghshenas@ut.ac.ir
6) Project manager, Iranian Ports and Maritime Organization, Tehran, Iran, mbagheri@pmo.ir
7) Project manager, Middle East Water and Environment Co., Tehran, Iran, zaker@mewe-ir.com

1. Introduction

The complex wave climate of the Sea of Oman (or Oman Sea) includes a mix of seasonal swells and wind waves from all directions across the Makran Coastline. With the increasing number of coastal and offshore projects, the need for a reliable hindcast wave climate has been recognized more than ever.

In Iran, study on wave characteristics of the Oman Sea started in 2009 as part of the ICZM project [1] which identified the need for more data collection in the region. Therefore, as part of the sixth phase of Monitoring and Modeling Study of Iranian Coasts, another attempt to hindcast wave climate along the Iranian coastline of the Oman Sea is presented here. The Phase 6 study coastline is about 350 km stretching from Gwadar Bay at the border with Pakistan to Rapch Estuary at the border with Hormozgan Province (Figure 1).

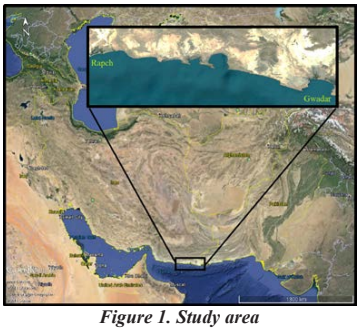

Figure 1. Study area

In general, the Oman Sea coast is subject to three distinct wave components:

i. waves generated during the summer monsoon season (June to September) off the southern coastline of Arabian Peninsula in the Indian Ocean and approach from a southerly direction,
ii. seas that are generated in the Oman Sea mainly during the winter season and arriving from a westerly to southwesterly directions; and
iii. swells that are generated in the southern hemisphere in the Indian Ocean and reach the study area from southerly to southeasterly directions.

The objective of this study is to develop a reliable hindcast wave climate that represents deepwater offshore wave conditions for engineering projects.

2. Data Gathering

Several instruments were deployed during the Phase Six study to measure waves at various times and locations. Figure 2 illustrates the study area and measurement stations. Measurements were conducted in 2015 and 2016. The collected data was used for model calibration and verifications.

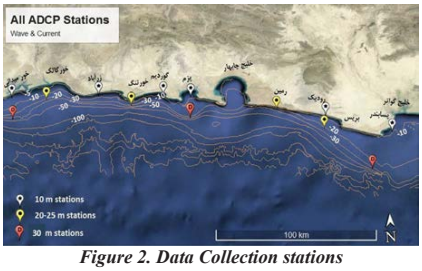

Figure 2. Data Collection stations

3. Methodology

Numerical hindcasting using surface winds provides essential space-time information to complement wave measurements and satellite observations for studies of the marine environment. In this study, the MIKE21 SW model is applied in an unstructured grid system to simulate the basin-wide processes as well as high-resolution wave conditions in the Oman Sea and along the study coastline from 1979 to 2018.

The wind forcing includes the European Centre for Medium-Range Weather Forecasts (ECMWF) for the region (from the South Pole) and downscaled regional winds from the Weather Research and Forecasting (WRF) model. Long-term wind data from synoptic stations and buoy measurements of wind speeds and wave characters allow thorough assessment of the modeling approach and the data products for this study. The high-resolution WRF winds were validated with satellite observations from 2000 to 2009.

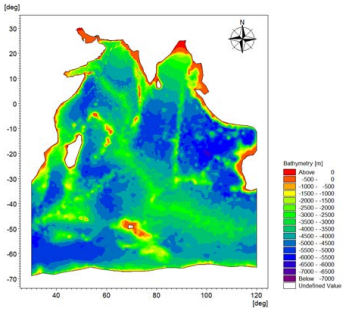

Figure 3. Hindcast model domain

4. Results and Discussion

Preliminary model runs indicated that proper simulation of the seasonal wave climate in the Oman Sea requires different settings of model parameters for each season. Therefore, the model was run separately for three seasons in each year.

Figure 4 illustrates comparisons between the data recorded at Roudik station from June to August 2018. Roudik is located on the east side of the Iranian Makran coastline where swells are generally predominant. In contrast, the geometrical shape of the Arabian Peninsula blocks southerly swells from reaching the western Makran coastline where seas become predominant.

Statistical analysis generally showed that the correlation coefficient of modeled significant wave height with measured data is above 80% while the root means square of errors was limited to 0.3 m on average.

Figure 5 presents a sample Tylor diagram at Meydani station located on the western side of the Makran coastline.

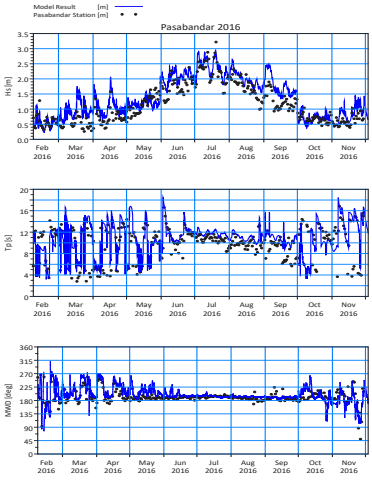

Figure 4. Comparisons between the data recorded at Roudik Station and results of hindcast model

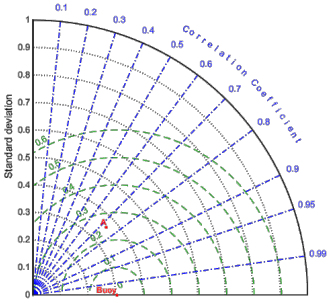

Figure 5. Taylor Diagram of measured data and model results Meydani station

5. References

[1] Ports and Maritime Organization (PMO): Integrated Coastal Zone Management (ICZM), 2009.

[2] Amante, & Eakins. (2009). ETOPO1 1 Arc-Minute Global Relief Model: Procedures, Data Sources and Analysis. NOAA Technical Memorandum NESDIS NGDC 24. National Geophysical Data Center, NOAA. doi:10.7289/V5C8276M

3D NUMERICAL SIMULATION OF MAKRAN INDUCED TSUNAMI GENERATION, PROPAGATION AND RUN-UP ON CHABAHAR BAY COASTLINE

Masih honarmand[1], Ahmad shanehsazzadeh[2*] and Mahdi zandi[3]

1) Department of Civil and Transportation Engineering, University of Isfahan, Isfahan, Iran, honarmand.masih@yahoo.com
2*) Department of Civil and Transportation Engineering, University of Isfahan, Isfahan, Iran, a.shanehsazzadeh@eng.ui.ac.ir
3) Department of Civil and Transportation Engineering, University of Isfahan, Isfahan, Iran, s.m.zandi@eng.ui.ac.ir

1. Introduction

Makran subduction at Oman Sea is the source of the most severe tsunamis in the region at 1945 which took more than 4000 lives in Pakistan, Iran and the Western India [1]. Makran subduction is located at 63.6° Longitude and 24.92° Latitude. The magnitude of the earthquake was 8.1 Richters with the focal depth of 15 kilometers. The generated tsunamis of Makran subduction are the potential of hazards for developing coastlines of northern Oman Sea and Chabahar bay. In this article, the generation and propagation of tsunami generated by Makran subduction is simulated and the run-up height on Chabahar bay coastlines is predicted. The algorithm of Okada is adopted for generation of tsunami and Flow 3D software is applied for wave propagation and prediction of run-up height.

2. 3D Simulation of Tsunami Generation through Okada Algorithm

Okada (1985) presented an algorithm for calculating the three dimensional deformation of the bottom of the sea bed, in the event of an earthquake with specified magnitude, M and focal depth, c [2]. The deformation of the sea bed due to Makran subduction is reproduced through Okada algorithm and the results are shown in Figure 1. Since the water is incompressible, it is assumed that the deformation of the sea bed is the initial tsunami profile.

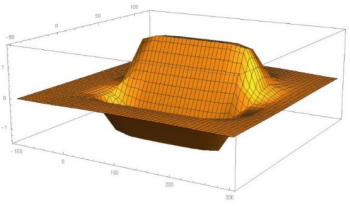

Figure 1. 3D Sea bed deformation due to Makran subduction

3. 3D simulation of wave propagation and run-up through Flow 3D software

The propagation of tsunami along Indian Ocean, Oman Sea and within Chabahar bay is numerically simulated. In this regard, Flow 3D software is applied. Flow 3D is an advanced CFD- based software for solving the continuity and Navier-Stokes equations [3]. The numerical simulation of the wave generation is adopted in two stages, in the regional and local scales. First, in order to simulate the propagation of tsunami wave in Indian Ocean, the initial tsunami profile of Okada algorithm is entered as an input into regional domain. 1000, 700 and 50 numerical meshes are considered for x, y and z directions, respectively. A number of sequential generation of tsunami propagation in regional scale is shown in Figure 2.

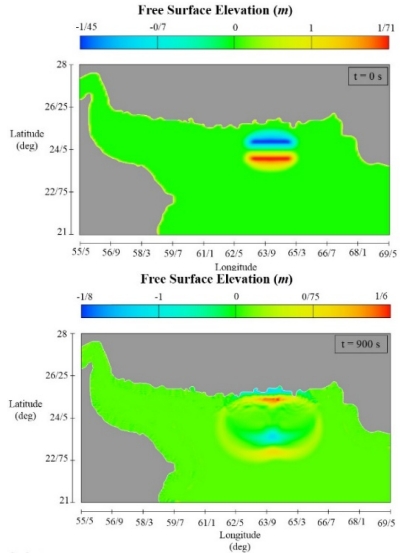

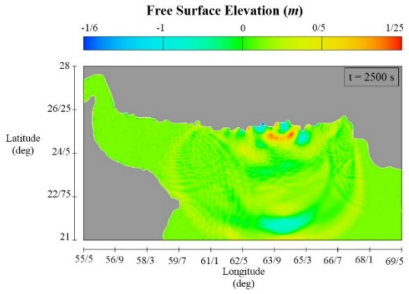

Figure 2. Tsunami propagation in Indian ocean

After the simulation of tsunami propagation in Indian Ocean, the water free surface elevation at the entrance of the Chabahar bay is extracted from the regional model, which is shown in Figure 3 and inserted as the input in the local model of Chabahar. 1200, 1200 and 150 numerical meshes are respectively considered in *x, y* and *z* directions, for local model of Chabahar.

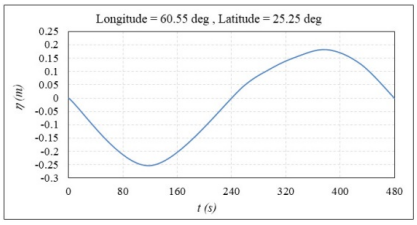

Figure 3. Free surface variations at the entrance of Chabahar bay

The results of tsunami propagation in Chabahar bay which produced by the local model is shown in Figure 4.

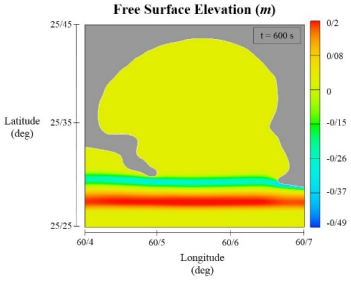

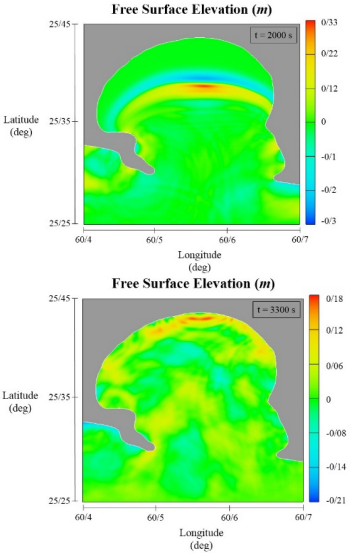

Figure 4. Tsunami propagation in Chabahar bay

The maximum run-up height alongside the Chabahar coastline is predicted from the local model. For Chabahar Port and Konarak the maximum run-up heights are 0.475 m and 0.1 m, respectively.

4. Conclusions

In this article, generation and propagation of the tsunami induced by Makran subduction in 1945 is simulated in three dimensional manner and by which run-up height at Chabahar coastline are predicted. The initial tsunami profile is calculated through Okada algorithm. The wave propagation is simulated in two stages of regional model of Indian Ocean and local model of Chabahar. The maximum run-up height of 0.475 m and 0.1 m are predicted for Chabahar Port and Konarak, respectively. Application of the advance algorithm of Okada for generated tsunami wave and two stages, three dimensional simulation of wave propagation and run-up are considered as the advantages of the present research.

5. References

[1] Heidarzadeh, M., Dolatshahi Pirooz, M., Hadjizadeh zaker, N. "Evaluating the potential for tsunami generation in southern Iran", Internatinal Journal of Civil Engineering, Vol. 5, No. 4, December 2007.

[2] Okada, M. "Surface deformation due to shear and tensile faults in a half-space", Bulletin of Seismological Society of America, Vol. 74, pp. 1135-1154, 1985.

[3] FLOW-3D user manual (Version 9.3), Flow Science Inc, 2008.

NUMERICAL SIMULATION OF THE WATER INTRUSION AND FLOW REGIME IN ARVAND RIVER

Majid Jandaghi Alaee[1], Mohammad Hadi Moeini[2], Ebrahim Jafari[3], Hamid Khalili[4], Mohamad Hossein Nemati[5] and Afshan Khaleghi[6]

1) PhD in Coastal Eng., Pouya Tarh Pars Cons. Eng. Company, Tehran, Iran, m.j.alaee@ptpco.com
2) PhD in Coastal Eng., Pouya Tarh Pars Cons. Eng. Company, Tehran, Iran, mhmoeini@gmail.com
3) PhD candidate in Coastal Eng., Pouya Tarh Pars Cons. Eng. Company, jafari.hydrostructure@gmail.com
4) Director General of Port and Coastal Eng., Iranian Ports and Maritime organization, Khalili@pmo.ir
5) Head of Coastal Eng. Department, Iranian Ports and Maritime organization, nemati@pmo.ir
6) Coastal Engineer, Iranian Ports and Maritime organization, afshan.khaleghi@yahoo.com

1. Introduction

Arvand is a narrow river-estuary in the south-west of Iran that forms a part of the border between Iran and Iraq (Figure 1). It is formed by merging the Tigris and Euphrates rivers in Iraq and Karun River in Iran. Three major cities, namely Abadan and Khoramshahr in Iran and Basra in Iraq, are located around it, with the river running mostly towards the south to reach the Persian Gulf [1]. The total length of this river is about 204 km.

Figure 1. Study area (Arvand River)

Since the upstream fresh water of Arvand river is used for agricultural purposes, the salinity intrusion and flow regime of the Arvand River has a great importance for the neighboring countries. The water quality of the river has serious implications for water security of neighboring regions of the river, with visible signs of ecosystem deterioration, and lack of adequate and good quality water for human consumption [2].

The tidal range in the Arvand River varies from up to 3 m in the southern part, at the river mouth, to about 1 m in the middle part, at Khoramshahr port and eventually to about 0.4 m at the upstream of the river (where Tigris and Euphrates connect).

Based on the tidal water level variation, Arvand estuary is classified as a Meso-tidal estuary [3].

The discharge of the Arvand River has experienced considerable variation over past decades. In the last century, the average annual discharge of the river was around 1000 m^3/sec [4]. However, in the recent decades, dozens of storage dams have been built and come into the operation. The dams are in Turkey, Syria and Iraq on Tigris and Euphrates Rivers and also in Iran on Karun River. On the other hand, the climate change has also led to the less precipitation and more evaporation in recent years which cause a less runoff into the rivers which is more sever in the Middle East region. Human activities and the consequent consumption has also increased along Arvand river in recent years. The combination of the above mentioned factors has led to significant decrease in the average of river annual discharge to a shocking value of about 50-70 m^3/sec [4].

The Iranian Port and Maritime Organization (PMO) initiated a project, carried out by Pouya Tarh Pars Consulting Engineers to study the hydrodynamics of Arvand River. In this paper the results of this study with regard to flow simulation are presented.

2. Study Area and Data

The study area covers the total length of the Arvand River from Tigris and Euphrates conjunction in al-Qurna to the end of the river at Persian Gulf (Figure 1).

For the calibration and verification of the model results, the water level data and current speed observations are used. Khuzestan Water and Power Authority (KWPA) recorded the surface level variation at Yademan station (~15 km upstream from the river mouth) in 2002 and 2003. These data were analyzed and tidal constituents were extracted in order to predict tidal levels for various times. On the other hand, in the global Admiralty charts there are tidal constituents for river mouth and Basra port which can be used as boundary condition for the numerical model. Some other data for water levels are also available that was used for the study that will be explained in full paper.

Concerning current speed data, the measurements in river mouth and also in Abadan station (~65 km upstream

of the river) that presented by Mohammadi et al. (2017) [5] were used. The locations of these measurement stations are shown in figure 1. The mentioned data were used for calibration and validation of the model.

3. Simulation and Results

In this study, a 2D simulation of fluid flow in the Arvand River is performed using MIKE21 flow model. MIKE21 is a well-known model for numerical simulation of fluid flow in water bodies. A combination of triangular and quadrangular mesh is used for the simulation, in which the river mouth and some irregular river bends spatially discretized using triangular meshes while for the main river body quadrangular mesh was used (figure 2).

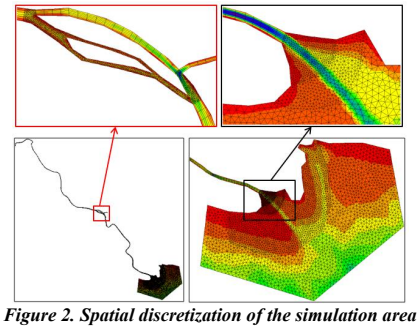

Figure 2. Spatial discretization of the simulation area

The boundary condition for the downstream of the river was forced with water level that predicted using Admiralty tidal constituents. For the upstream of the river, sensitivity analysis was performed on the effect of different discharges of the river on the water level and current speed . Figure 3 depicts the water level variation and current speed in river mouth and Basra for different upstream discharges (200, 500 and 1000 m^3/s). As seen, different discharges affect both water level and current speed and this effect increases by moving from downstream to upstream of the river.

The model was calibrated and verified by comparing the results with water level and current speed observations. Figure 4 shows the comparison between the model water level results and the observations, in Yademan and Basra stations. It can be seen that the model predicted the water level in Arvand River very well. The correlation coefficient corresponding the results, in both station, is 0.98. Figure 4 also shows the current speed comparison in the river mouth and Abadan station. It is also shown that the performance of the model for the simulation of current is also quite satisfactory.

Based on the numerical modeling results, the water intrusion from the Persian Gulf travels long into the most of the river length (more than 80% of the river length) and the tidal variation of the water level can be seen even in 200 km away from the river mouth. The salinity intrusion length was also estimated from the modeling results which is an important parameter for water quality management along the river.

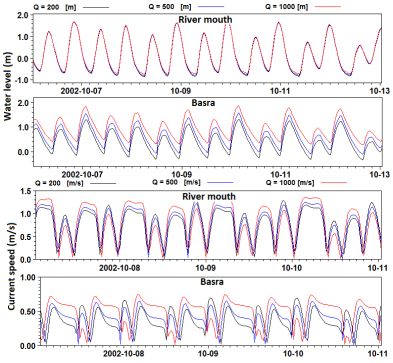

Figure 3. Water level variation and current speed at river mouth and Basra for different upstream discharges

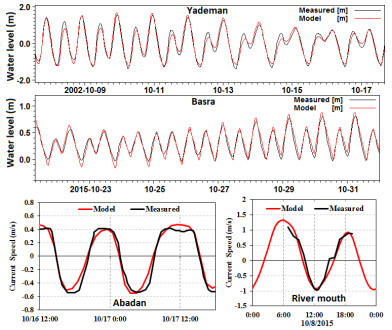

Figure 4. Comparison of the modeling results with the observations

4. References

[1] Etemad-Shahidi A, Pirnia M, Moshfeghi H, Lemckert C. Investigation of hydraulics transport time scales within the Arvand River estuary, Iran. Hydrological processes. 2014 Dec 15; 28 (25): 6006-6015.

[2] Abdullah AD, Karim UF, Masih I, Popescu I, Van der Zaag P. Anthropogenic and tidal influences on salinity levels of the Shatt al-Arab River, Basra, Iraq. International Journal of River Basin Management. 2016 Jul 2;14(3):357-66.

[3] Etemad Shahidi A, Saburi A.A, Parsa J. Control of salinity intrusion in arvand estuary under different hydrological conditions. Iran-Water Resources Research. Summer 2011; 7 (2), 50-60. (In Persian).

[4] Al-Taei S, Abdullah S, Lafta A. Longitudinal patterns of salinity in the mouth of Shatt Al-Arab River and causes. (U.O. Abdulaziz, Ed.). Journal of King Abdulaziz University. 2014; 25(2): 205-221.

[5] Mohammadi M.F, Sadrinasab M, Chegini V, Ashtari A. Comparison of flow control forces in Arvand River. *The 4th International Conference on Environmental Planning and Management (ICEPM)*, 23-24 May 2017 (In Persian).

TSUNAMI GENERATION AND ITS CHARACTERISTICS DUE TO LAND SLIDE IN CASPIAN SEA

Fariba Ghanbarpour[1], Seyyed Ahmad Neshaei[2] and Mehdi Veiskarami[3]

1) MS Graduate, Research Assistant, Civil Engineering Department, University of Guilan, Rasht, Iran, ghanbarpour.fariba@gmail.com
2) Associate Professor, Civil Engineering Department, University of Guilan, Rasht, Iran, maln@guilan.ac.ir
3) Associate Professor, School of Engineering, Shiraz University; Also, Faculty of Engineering, University of Guilan, Rasht, Iran, mveiskarami@gmail.com

1. Introduction

Tsunami waves can be generated in any coastal area, including inland seas and large lakes. Although there is enough information about the generation and propagation of tsunami in ocean environment, the assessment of such phenomenon in lakes with finite depth still suffers from the lack of theoretical work and sufficient measured data. The Caspian Sea is the largest lake in the world and has gone through different historical tsunami events. The reported tsunamis were generated due to earthquake and landslides particularly in the middle zone of the sea. It should be noted that the seismicity of the Caspian region has been studied in some detail, but the manifestation of a tsunami in the Caspian Sea and the degree of risk for the coast remain poorly understood. Similar to the other coastal regions around the world, the increase of the population along the coasts of Caspian Sea highlights the urgent need to assess tsunami hazards in the region [1, 2].

2. Theoretical Development

Tsunami wave has behavior like solitary wave as shown in figure 1. The equation of Boussinesq solitary wave is as follow:

$$\eta = asech^2\sqrt{\frac{3}{4}\frac{a}{h^3}}x \qquad (1)$$

Where: a: wave height, h: depth at infinity, η: wave profile.

The whole profile of solitary wave is positive and there is no negative η. So, a presents wave height and h is depth in infinite [3].

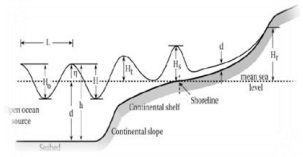

Figure 1. Tsunami wave height [4].

3. Modelling

In this study, some submarine landslides were assumed in 7 different points of Caspian Sea (Figure 2) with parameters mentioned in table1 and 2. GEOWAVE was used to simulate.

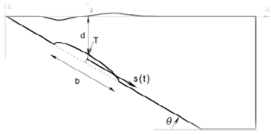

Figure 2. Definition sketch of the simulation domain for underwater slides [5].

Table1. Parameters of the Caspian Sea probable submarine landslide [2].

Estimated parameter	value
Slope (θ)	2°
Total Length (b)	5300 m
Maximum thickness (T)	1100 m
Total Width (w)	1500 m
Density	1880 kg/m^3
Initial submergence (d)	Table 2

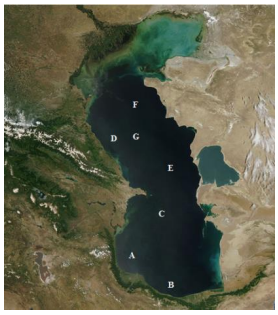

Figure 3. Locations of submarine landslide points

Table 2. Characteristics of submarine landslide points

	X_0	Y_0	d (m)	CCW [1](°)
A Point	49.12	37.71	167.60	310
B Point	50.81	36.61	209.51	20
C Point	50.19	39.40	302.94	190
D Point	48.40	41.43	138.15	260
E Point	50.10	40.80	306.45	75
F Point	49.65	42.67	218.51	180
G Point	48.68	41.56	415	270

4. Results and Discussions

Results of modelling listed in table 3 show that maximum wave heights and lengths of submarine landslide tsunamis are significant. Effect radiuses express large movement of water in Caspian Sea scale. Figures 4 to 6 reveal that the generated tsunamis can cause a considerable run-up along the coastlines of their adjacencies.

Table 3. Characteristics of generated tsunamis

Source	Depth (m)	Maximum Wave Height (m)	Wave Length (km)	Effect Radius (km)
A point	167.6	20.7	19.6	60
B point	209.5	12.4	21.9	65
C point	302.9	7.1	26.4	75
D Point	138.2	35.5	17.8	50
E Point	306.4	7	26.5	75
F Point	218.5	11.7	22.4	60
G point	415	8.8	30.8	90

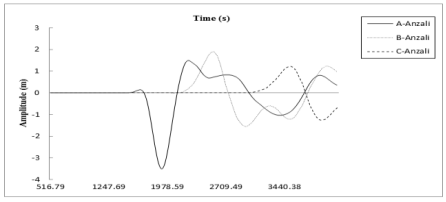

Figure 4. Wave height time series for Anzali Station

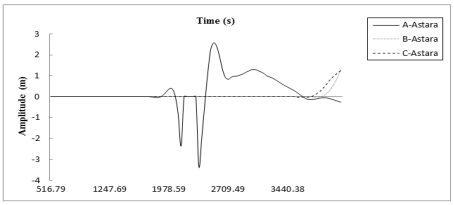

Figure 5. Wave height time series of Astara Station

[1] CounterClockWise

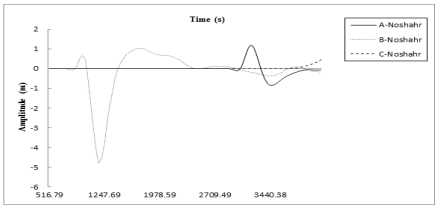

Figure 6. Wave height time series of Noshahr Station

5. Conclusions

Unlike tsunamis generated by earthquakes, submarine landslide tsunamis generated in shallow waters are more destructive compared to those generated in deep water. Based on numerical simulation results, it is inferred that a relatively high level of tsunami risk is characteristic for the Caspian coasts. Unfortunately, the incompleteness of the data prevents us from performing an adequate statistical analysis and assessing the probabilistic characteristics of the tsunami manifestation on the coast.

In accordance with visual observations, the heights of historical tsunamis have not exceeded 1-2 m, but it is possible to wait for tsunamis of high waves and considerable run-ups.

6. References

[1] Kulikov E. A., Kuzin I. P., and Yakovenko O. I., (2014), "Tsunamis in The Central Part of The Caspian Sea", Issn 0001_4370, Oceanology, Vol. 54, No. 4, Pp. 435–444. Pleiades Publishing, Inc.

[2] Soltanpour M. and Rastgoftar E., (2011), "Study of Tsunami Attacks on Neighboring Countries of Caspian Sea Caused by A Probable Submarine Landslide", Journal of Coastal Research, Special Issue 64, Si 64, 1195 – 1199, Ics (Proceedings), Poland, Issn 0749-0208.

[3] Dean R. G. and Dalrymple R. A., (2000), "Water Wave Mechanics for Engineers and Scientists". Advanced Series on Ocean Engineering- Volume 2, published by world scientific publishing Co. Pte. Ltd. ISBN 9810204205, 358p.

[4] Bryant E., (2008), "Tsunami, the Underrated Hazard", SPRINGER–PRAXIS BOOKS IN GEOPHYSICAL SCIENCES, ISBN 978-3-540-74273-9 Springer Berlin Heidelberg New York.

[5] Watts, P., Grilli, S.T., Kirby, J.T., Freyer, G.F., and Tappin, D.R., (2003), "Landslide Tsunami Case Studies Using A Boussinesq Model And A Fully Nonlinear Tsunami Generation Model", Hazards and Earth System Sciences Journal, 3(6), 391-402.

ENTRAINMENT IN AN OUTLOW GRAVITY CURRENT FROM A SEMI-ENCLOSED SEA (THE PERSIAN GULF)

Fatemeh Najafian[1], Abbasali Aliakbari Bidokhti [2] and Asghar Bohluly[3]

1)Student at Institute of Geophysics, Tehran University, Tehran, Iran, fatemeh.najafian@ut.ac.ir
2)Professor at Institute of Geophysics, Tehran University, Tehran, Iran, bidokhti@ut.ac.ir
3)Professor Assistant at Institute of Geophysics, Tehran University, Tehran, Iran, bohluly@ut.ac.ir

1. Introduction

Because of their consistent direction, density (gravity) currents are important in the distribution and removal of pollutants from the semi-enclosed seas such as the Persian Gulf. The extent of which a gravity current is diluted, through mixing of the current with surrounding ambient fluid, is of particular interest in ocean currents polluted by industrial effluents or pollutants. Such mixing also affects the dynamics of gravity currents propagating through the reduction of the density difference that drives the current. [1] The ultimate properties of the deep or intermediate waters are also determined not only by the direct processes of air-sea interaction that creates the initial overflowing water, but also by the mixing due to entrainment of surrounding fluid during the density current's descent [2, 3, 4]. The aim of the present study is to present a flow model for the gravity current exiting the Persian Gulf. In this model entrainment process is also included.

2. Field Measurement Data Used

In this study, CTD data that are obtained from ROMPE expedition of 1992 (Reynolds, 1993) is used in the model to extract desired results for the rate of entrainment in Persian Gulf outflow (Fgure 1). The data are available for summer and winter for specific points in the Persian Gulf, Strait of Hormuz and Oman Sea.

The average temperature, salinity and density of the Persian Gulf outflow clearly show that the outflow is diluting as it moves in to the Oman Sea, through the Strait of Hormuz [4]. This dilution rate is dependent on the entrainment of water into the outflow as it moves as a boundary trapped current through the Strait of Hormuz. Using these data we show transects of temperature, salinity and density of the current along its path.

3. Methodology (Model Used)

Persian Gulf Outflow (PGO) spills down the open mouth of the Strait of Hormuz, as it mixes with the Gulf of Oman water. This flow is very efficient in the recirculation of the Persian Gulf as a semi-enclosed sea.

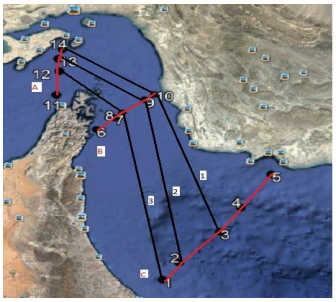

Figure 1. Study area including the data stations from which we have extracted the temperature, salinity and density fields of the Persian Gulf outflow.

The structure of PGO before and after the Strait of Hormuz is studied by its velocity, salinity and potential density profiles of this density current plume, while considering the entrainment rate at its boundaries which is a function of varying Richardson Number. "Recycling Box" model [3] is used to model the flow for study the changes in current width based on the salinity, temperature and density fields.

Some of relations in "Recycling Box" model for Richardson number and along-current velocity are as following:

$$Ri = \frac{g\,(\rho_p - \rho_e)}{\rho_r} B \sin\theta \qquad (1)$$

$$U_s^2 = c_1 \frac{g\,(\rho_p - \rho_e)}{\rho_r} B \qquad (2)$$

Where ρ_p is the density of the plume, ρ_e is the basin interior density, ρ_r is the reference density, B is the height of the current, θ is the slope that current makes with the horizontal, c_1 is the constant equals one.

For validation of model results, they are compared with the width resulted from considering the conservation of salt in 2 different areas using measured data.

4. Results and Discussion

Figure 3 shows along-current velocity from the model based on density profile of current used in "Recycling Box" model. The outflow is clearly shown as a bottom trapped current with a mean speed of about 0.5 m/s which is somehow higher that the observed value of about 0.3 m/s (Figures 2, 3). This is due to the fact that frictional effect at bottom is neglected in this bulk model.

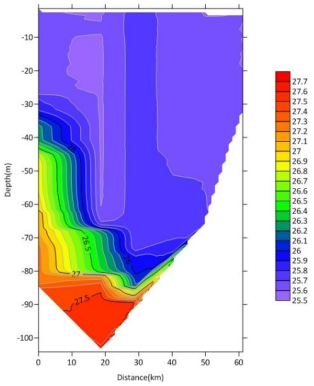

Figure 2. A transect of the density of the outflow in the Strait of Hormuz.

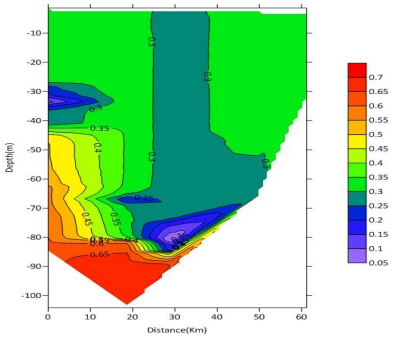

Figure 2. An example of transect of out flow speed obtained from the model, the outflow is near the bottom tended towards the southern coastal boundary due to the effect of earth rotation.

Results also show the presence of entrainment process between the plume and ambient waters (mainly water entering the Persian Gulf). The entrainment rate (coefficient) of this current varies and is approximately around 0.01 which is similar to the values reported by other research [e.g. 2]. This is based on the dilution of the outflow as it moves into the Oman Sea.

In some cases, due to lack of sufficient data in the area of study, the results are not as detailed as desired. This points to the need for more high resolution measurements in this important water ways.

5. References

[1] Johnson G. Ch., Hogg J. A., Entraining gravity currents, Journal of Fluid Mechanics, 2013, Volume 731, 477-508.

[2] Girton, J., B., Sanford, Th. B., Descent and modification of the overflow plume in the Denmark Strait, Journal of Physical Oceanography, 2003, Volume 33, 1351-1364.

[3] Hughes, G.O., Griffiths, R.W., A simple convective model of the global overturning circulation, including effects of entrainment into sinking regions, Ocean Modelling, 2005, Volume 12, 46-79

[4] Bidokhti, A. A., Ezam, M., the structure of the Persian Gulf outflow subjected to density variations. Ocean science, European Geosciences Union, 2008, Volume 5(2), 135-161.

CONTRIBUTION OF ATMOSPHERIC FORCES TO MEAN SEA LEVEL FLUCTUATIONS IN THE PERSIAN GULF AND OMAN SEA

Naghmeh Afshar-Kaveh[1] and Mostafa Nazarali[2]

1) Iran University of Science and Technology, Department of Civil Engineering, Tehran, afshar_n@alumni.iust.ac.ir
2) Pouya Tarh Pars consulting Engineers company, Tehran, Iran. mostafa.nazarali@gmail.com

1. Introduction

Sea level is an important oceanographic parameter which describes sea surface dynamics. The sea level data are necessary for a wide range of activities related to the marine environment such as safety of navigation, hydrographic survey, impact on the coastal infrastructures, scientific analyses of the sea level changes, etc. So, understanding the behavior of sea level fluctuations seems to be mandatory.

The Persian Gulf (PG) is the waterway located between Iran and Arabian Peninsula and joined to Oman Sea by Hormoz strait; so connected to the open seas. PG is considered as the third largest gulfs in the world after Gulf of Mexico and Hudson Bay. Length of PG is about 800 km from Hormoz strait to most western parts and the widest part is about 290 km, having maximum depth of more than 90 m. The weather of PG is (half) tropical so in summers the air temperature rises to 50°C and drops to 7°C in winters. Dominant wind in this area is called "Shamal" which is blowing from northwest and changes its direction in southern area in which tilts towards east.

The Oman Sea (OS) also divides Iran and Arabian Peninsula and forms the link between the PG and Arabian Sea. It is 560 km long and at its widest point is 320 km wide. The maximum depth of OS is 3500 m. During wintertime (November-March) the winds are not strong. However, during summertime (May-September) a very strong and continuous southwestern wind blows.

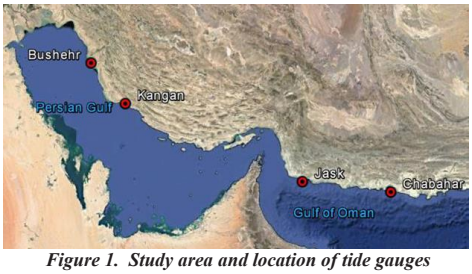

Figure 1. Study area and location of tide gauges

Although there were a lot of studies on tidal variation modeling in the PG, but only a few of them focused on non-tidal sea level variations [1,2]. In this paper the likely effect of atmospheric forces on mean sea level fluctuations will be investigated. Analysis of sea level records along PG and Oman Sea and extraction of non-tidal signals will be followed by evaluation of the correlation between atmospheric forces with sea level variations.

2. Data

The input data to carry out this research include sea level records and some meteorological parameters including wind velocity components and mean sea level pressure (MSLP).

Several tide gauge records were gathered in this research. Two stations were located in the Persian Gulf named Bushehr and Kangan which are handled by Iran National Cartographic Center of Iran. Sea level records of the other two stations including Jask and Chabahar were obtained from Permanent Service for Mean Sea Level [3] of UK. These data overlap each other in a period between 2008 and 2010 while they have some gaps in between.

MSLP parameter was obtained from ECMWF ERA Interim data set [4] while the wind velocity components were extracted from a novel product named Cross-Calibrated Multi-Platform (CCMP) gridded surface vector winds [5]. These data are produced using satellite, moored buoy, and model wind data, and as such, are considered to be a Level-3 ocean vector wind analysis product. The accuracy of the mentioned product is proved in other studies [1].

3. Analysis and Results

The first step to estimate residual sea level is to eliminate tide and other short-period oscillations from observations. A harmonic analysis was applied to the tide gauge records by UTide MATLAB code [6]. The computed tide by this code is subtracted from tide gauge observations. Tidal amplitude in the studies stations is between 2.5 and 3.5 m. In this way, the residual sea levels were obtained as shown in figure 2 at Kangan station (blue lines in the plot).

As shown in this figure, there are still some oscillations in the residuals which are due to short-period events and de-tiding errors. So a further analysis is needed to remove them from residuals. In this step, a low-pass filter was employed to remove any fluctuations shorter than tidal bands (i.e. less than 33 hours). The filtered time series is

also shown in figure 2 as red lines. The same filtering procedure was followed for MSLP and wind vector data sets at all stations. It must be mentioned that due to the inclination of coastline in different stations, cross-shore wind components were calculated and employed in this research.

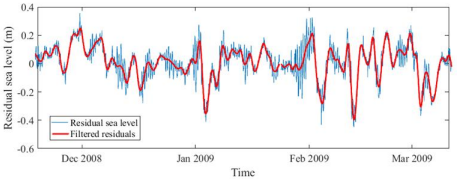

Figure 2. Residual sea level records at Kangan station

Theoretically, MSLP acts inversely with sea level as the higher pressure causes the sea level to drop and vice versa (eq. 1). The wind setup has direct correlation with power of cross-shore wind velocity and inverse correlation with water depth (eq. 2).

$$\Delta\zeta_P = \frac{\Delta P_A}{\rho g} \qquad \text{(eq. 1)}$$

$$\frac{\partial \zeta}{\partial x} = \frac{C_D \rho_A W|W|}{\rho g D} \qquad \text{(eq. 2)}$$

where ζ_P is pressure setup, P_A is atmospheric pressure, ζ is wind setup, x is cross-shore distance, C_D is drag coefficient, ρ_A is air density, D is water depth, and W is wind speed.

The response of sea level to the wind and MSLP changes can be seen in the following figures.

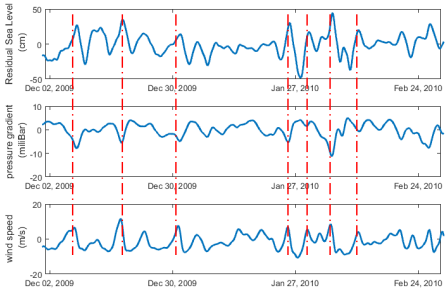

Figure 3. Time series of residual sea level MSLP and wind component (Bushehr station)

As shown in figure 3, almost in all instances of sea level rise/fall, there are peaks in the time series of wind velocity and inverse MSLP. But such correlation does not exist in the stations located in the Oman Sea (Fig. 4). The correlation between non-tidal sea level fluctuation and meteorological forces for all studies stations are shown in table 1.

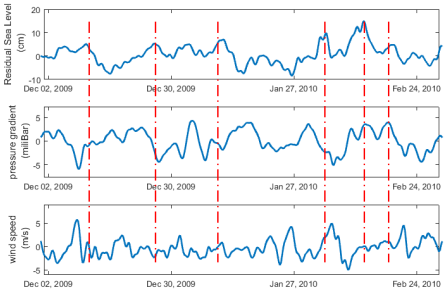

Figure 4. Time series of residual sea level against MSLP and wind component (Jask station)

Table 1. Correlation between sea level residuals and atmospheric forces

	Bushehr	Kangan	Jask	Chabahar
MSLP anomaly	0.21	0.18	0.00	-0.04
Cross-shore wind	0.44	0.36	0.04	0.00

According to table 1, mean sea level fluctuation in the Persian Gulf is correlated with wind and MSLP with the superiority of the later one. But sea level variation does not directly depend on the mentioned parameters in Oman Sea. So other phenomena such as upwelling [7], and long-period waves must be investigated in this regard.

4. References

[1] Afshar-Kaveh, N., Ghaheri, A., Chegini, V., Etemad-Shahidi, A. and Nazarali, M. "Evaluation of Different Wind Fields for Storm Surge Modeling in the Persian Gulf" *Journal of Coastal Research*. 33(3), 2017, pp. 596 – 606.

[2] Al-Subhi, A. M., "Tide and sea level characteristics at Juaymah, west coast of the Arabian Gulf", *JKAU: Marine Sciences* 21(1), 2010, pp. 133-149.

[3] Holgate, S.J., Matthews, A., Woodworth, P.L., Rickards, L.J., Tamisiea, M.E., Bradshaw, E., and Pugh, J., "New data systems and products at the permanent service for mean sea level" *Journal of Coastal Research* 29(3), 2013, pp. 493–504.

[4] European Centre for Medium-Range Weather Forecasts "ERA-Interim Project, Single Parameter 6-Hourly Surface Analysis and Surface Forecast Time Series," Accessed 1 Jun, 2018.

[5] Wentz, F.J., J. Scott, R. Hoffman, M. Leidner, R. Atlas, and J. Ardizzone, "Remote Sensing Systems Cross-Calibrated Multi-Platform (CCMP) 6-hourly ocean vector wind analysis product on 0.25 deg grid, Version 2.0". *Remote Sensing Systems*, Santa Rosa, CA. 2015. [Accessed 01 Jun 2018].

[6] Codiga, D.L., *"Unified Tidal Analysis and Prediction Using the UTide Matlab Functions. Technical Report 2011-01"*. Graduate School of Oceanography, University of Rhode Island, Narragansett, RI. 59pp, 2011.

[7] Shi, W., Morrison, J.M., Bohm, M., and Manghnani, V., "The Oman upwelling zone during 1993, 1994 and 1995" *Deep-Sea Research II* 47, 2000, pp. 1227-1247.

DEVELOPING IRANIAN SEAS WIND AND WAVE FORECAST SYSTEM

Edris delkhosh[1], Daniel Yazgi[2], Mahdi Kebriaee[3] , Mohamad Hossein Nemati[4], Hamid Khalili[5], Sarmad Ghader[6], S. Abbas Haghshenas[7], Morteza Jedari Attari[8] and Mohsen Soltanpour[9]

1) Institute of Geophysics, University of Tehran, Tehran, Iran, edrisdelkhosh@ut.ac.ir
2) Institute of Geophysics, University of Tehran, Tehran, Iran, daniel.yazgi@ut.ac.ir
3) Ports and Maritime Organization, Tehran, Iran, mehdy.kebriaee@gmail.com
4) Ports and Maritime Organization, Tehran, Iran, mhn1982@gmail.com
5) Ports and Maritime Organization, Tehran, Iran, khalili@pmo.ir
6) Institute of Geophysics, University of Tehran, Tehran, Iran, sghader@ut.ac.ir
7) Institute of Geophysics, University of Tehran, Tehran, Iran, sahaghshenas@ut.ac.ir
8) Institute of Geophysics, University of Tehran, Tehran, Iran, mortezajedariattari@yahoo.com
9) Khajeh Nasir Toosi University of Technology, Tehran, Iran, soltanpour@kntu.ac.ir

1. Introduction

Model applications serve two purposes: a practical one and a scientific one. In practical applications that is the aim of this study, the model is accepted as a reliable tool. As such it can be used either in real-time, to forecast sea conditions for ship routing, offshore operations and for coastal protection, or in a hindcasting model for computation of the sea state during a particular event and to determine wave climatology and extremal statistics [1].

The importance of the Iranian seas and the recognition of the ocean and atmospheric conditions in these regions created the scientific and operational cooperation between the Institute of Geophysics of the University of Tehran and the Ports and Maritime Organization. In this collaboration, the latest atmospheric models and wave-simulation third-generation numerical models that simulate oceanic waves with the least hypothesis have been used, which is a reliable system for wind-wave predictions.

This study reports on the performance of the Iranian wind-wave forecasting system, which has been promoted with the collaboration of the Institute of Geophysics of the University of Tehran and the Ports and Maritime Organization.

2. Study Area and Data Collection

As shown in Figure. 1, the Iranian Atmospheric and Oceanic forecasting System completely covers three important Iranian seas regions; including the Caspian Sea, the Persian Gulf and the Oman Sea.

Clearly, before using model results for practical purposes, we need to validate the model in extended comparisons with measured data under careful control of the input data, such as the wind, bathymetry and geometry of the basin. In Table 1, some events that have been used for this purpose in the present study are shown. These events are example of several executions that have been performed to validate the system in simulating surface wind field and wave parameters.

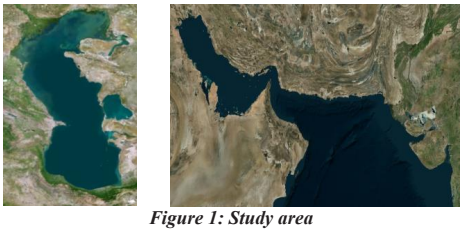

Figure 1: Study area

Table 1: Some information about selected events

EN	Location	Long	Lat	Start Time	End Time
1	Caspian Sea	51.190	38.385	2011/03/11	2011/03/17
2	Persian Gulf	53.094	26.868	2010/03/18	2010/04/07
3	Oman Sea	60.600	25.100	2007/02/16	2007/02/24

3. Wind Model Setup

Figure 2 shows the computational domain of the Weather Research and Forecasting model (WRF), which is used to construct a surface wind field for generating inputs of the wave model.

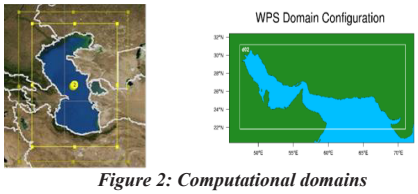

Figure 2: Computational domains

The WRF model is configured with two nests with 0.3 degree and 0.1 degree horizontal grid resolutions, respectively [2, 3]. It can be seen that the inner domain

covers the Caspian Sea, Persian Gulf and Oman Sea. WRF numerical model provides different physical configurations for different applications for the users and developed ensemble forecasting system [2] leads to a reliable wind field that makes the input of the wave model.

4. Wave Model Setup

Figure 4 illustrates the computational domain. The calibrated spatial grid resolution is 0.05 degree and time-step is set to be 720 s. The directional resolution is 10º and frequency is divided into 20 span ranging from 0.07 Hz to 0.5 Hz in logarithmic scale.

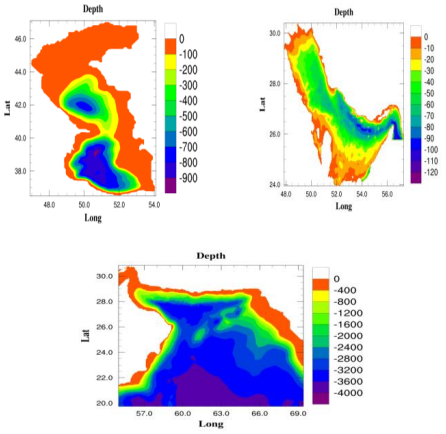

Figure 3: Bathymetry of the Iranian seas applied in the numerical model

5. Summary

As mentioned before, the model is run with the determined setup and the outputs were compared with the observations, as shown in Figure 5 and 6. To test the success of the model in the simulation of events in Table 1, statistical parameters are calculated and are shown in Table 2.

Table 2: Statistical parameters for Events in table 1

Events	R	MSE	RMSE
Event 01	0.98	0.03	0.19
Event 02	0.94	0.10	0.31
Event 03	0.92	0.13	0.36

As shown in Table 2 and illustrated in Figures 5 and 6, the high correlation coefficient of the model outputs (R) and the observation data indicates the model's success in simulating the selected events in Table 1. Also the small values of MSE and RMSE indicate that the Iranian Atmospheric-Oceanic forecasting System can be a reliable tool for atmospheric and Oceanic forecasting.

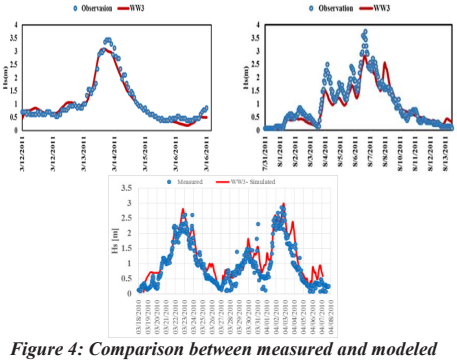

Figure 4: Comparison between measured and modeled Hs for Events in Table 1

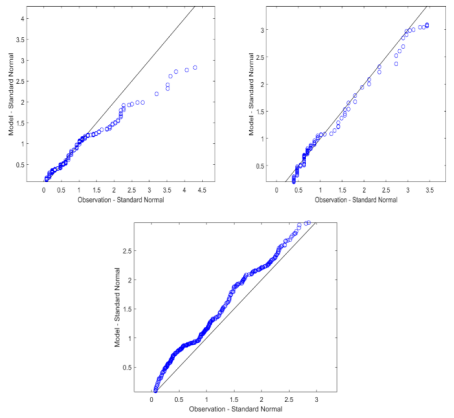

Figure 5: Q-Q plots for Events in Table 1

6. References

[1] Komen G.J., Cavaleri L., Donelan M., Hasselmann K., Hasselmann S., Janssen P.A.E.M., 1996: Dynamics and modeling of ocean waves, Cambridge University Press, 532pp.

[2] Ghader S., Yazgi D., Soltanpour M., Nemati M.H., "On the use of an ensemble forecasting system for prediction of surface wind over the Persian Gulf" in proceeding of the 12th International Conference on Coasts, Ports and Marine Structures (ICOPMAS 2016), Tehran, Iran, 31 Oct.- 2 Nov. 2016.

[3] Ghader S., Montazeri-Namin M., Chegini F., Bohlouly A., 2014: Hindcast of surface wind field over the Caspian Sea using WRF model, The 11th International Conference on Coasts, Ports and Marine Structures (ICOPMAS 2014), Tehran, Iran, 24-26 Nov. 2014.

AN UNUSUAL STORM ATTACK ON THE NORTHERN COASTLINE OF THE PERSIAN GULF

Alaleh Norouzi[1], Farhangh Ahmadi Givi[2] and S. Abbas Haghshenas[3]

1) Institute of Geophysics, University of Tehran, Tehran, Iran , alale.norozi@ut.ac.ir
2) Institute of Geophysics, University of Tehran, Tehran, Iran , ahmadig@ut.ac.ir
3) Institute of Geophysics, University of Tehran, Tehran, Iran , sahaghshenas@ut.ac.ir

1. Introduction

On March 19th 2017 an unusual storm hit a limited area on the Northern coastline of the Persian Gulf. The storm coincided with high tide condition at Dayyer Port and three long-crest waves hit the coastline of the port with an average period of 38 seconds with an average inundation level of 5 m with respect to the chart datum level. The storm damaged some part of the coastal strip of 2.5 km long and 0.5 km wide. The levels of inundation has measured through a field survey campaign on the day after. The focus of this event seems to be limited to this area. This study provides a collection of field observations after the storm, while trying to simulate the measured inundation levels through a multi-stages numerical modeling framework.

Figure 1. The inundation area of Dayyer port which has been plotted in GIS for the study area

Some researchers have studied meteotsunami or meteorological tsunami that is believed to be the phenomenon which occurred in Dayyer. Meteotsunais are unusual sea-level events, generated when the speed of an atmospheric pressure or wind disturbance is comparable to the phase speed of long waves in the ocean (Geist *et al.*, 2014). The understanding of meteotsunamis- significant atmospherically generated long ocean waves in the tsunami frequency band- has advanced considerably during the last two decades. In a study, modern approaches in meteotsunami research has been investigated and the drawbacks of existing early warning systems have been presented by Vilibić *et al.* (2016). In another study, Geist *et al*. (2014), presented a framework for the probabilistic analysis of meteotsunamis. In this study a general aggregation equation is proposed for the probabilistic analysis, based on previous frameworks established for both tsunamis and storm surges, incorporating different sources and source parameters of meteotsunamis. Another research which investigates the coast of Southern Britain- The English Channel, Bristol Channel, and the Severn estuary- for the occurance of tsunami-like waves that, in the absence of associated seismic activity, has been carried out by Haslett and Bryant (2009). Hibiya, T., and Kajiura, K., (1982), to study about Origin of the Abiki phenomenon (a kind of seiche) in Nagasaki Bay that relation to this study.

The study of various aspects of coastal cities for continuous attention. In this regard, ports and port late in this research investigated certain unorthodox event that in these areas the losses and damages (Figure2).

Figure 2. Photo of storm destruction

Current study provides a collection of field observations after the storm, while trying to simulate the

measured inundation levels through a multi-stages numerical modeling framework.

2. Case Study

The above incident has characteristics that make it unique from other conventional psychological phenomenon in the Gulf and how to distinguish ¬ occurrence it more important fitted. The basic and important thing associated with this phenomenon, a significant distance from the port of Assaluyeh is late so that water ¬ Eclipse specifically only in these two places and occurred in other coastal areas located.

Figure 3. Dayyer port a day after storm incident..

Using the analytical relations, the main source of waves in the middle of the Persian Gulf, tracking and identification of the causative. Citing data loaders, Earth Quake and the atmospheric and water map data, based on field fitted Eclipse area in the days after the storm, waves for effective simulation reproduces the terms recorded, is done.

Cities which are located along the coastlines all over the world are susceptible to storm damages. It goes without saying that according to great importance of cities and ports along the northern coastline of the Persian Gulf as a strategic semi-closed water body, every unusual (storm) events may lead to death of local residents and significant financial losses. For this reason, Dayyer and Asaluyeh ports have been come under scrutiny to investigate the unusual storm event on March 2017. What makes this event different from other common events in the Persian Gulf is entirely distinct features of this event. It is interesting that remarkable inundation has been occurred just in these two ports during the storm event. This bizarre situation would be more highlighted if we consider that Dayyer port is almost 80 km far from Asaluyeh and nothing special has been observed in the cities between. It is worth mentioning that three long-crest waves has been observed in the Persian Gulf which is a rare event.

Figure 4. The locations of inundation area and wave attacked

3. Summary

As there is an agreement between the applied numerical model (simulation) and field data, the inundation level or inundated area seems predictable. Hence, it is recommended to construct breakwaters and other barriers to dissipate the destructive force of storm waves for reaching to a better resource management and preventing financial losses and probable fatalities.

The location of the storm source is estimated adapting wave numerical models and then the inundation is simulated by using numerical modeling. In the next step, the inundation levels are compared with those data gathered after the storm and collected altogether through a GIS framework. The result of favorable agreement has been reached between observation data and the model output.

4. References

[1] Geist, E. L., Uri, S., and Gove, M., 2014: A framework for the probabilistic analysis of meteotsunamis. Natural hazards, 74(1), 123-142.

[2] Haslett, S. K., and Bryant, E. A., 2009: Meteorological tsunamis in southern Britain: an historical review. Geographical Review, 99(2), 146-163.

[3] Hibiya, T., and Kajiura, K., 1982: Origin of the Abiki phenomenon (a kind of seiche) in Nagasaki Bay. JO Society of Japan, 38(3), 172-182.

[4] Vilibić, I., Šepić, J., Rabinovich, A. B., and Monserrat, S., 2016: Modern approaches in meteotsunami research and early warning. Frontiers in Marine Science, 3(57).

THREE ALTERNATIVE COASTAL PROTECTION NEAR AMIR ABAD PORT

Abbas Yeganeh-Bakhtiary[1], Mahdi Ebrahimpur[2] and Fatemeh Hajivalie[3]

1) School of Civil Engineering, IUST, Tehran, Iran, yeganeh@iust.ac.ir
2) Graduate student, School of Civil Engineering, IUST, Tehran, Iran, mahdi_ebrahimpur70@yahoo.com
3) Ocean Engineering and Technology Research Center, Iranian National Institute for Oceanography and Atmospheric Science (INIOAS), Tehran, Iran, hajivalie@inio.ac.ir

1. Introduction

Changing the natural conditions of the coasts influenced by the port constructions and the longshore sediment transport is one of the main reasons for the erosion phenomena on Amir-Abad coast [1]. Due to the construction of Amir Abad port, the coast of this area has been out of balance and stability; the updrift port's breakwater interrupts the longshore sediment transport, which induced a massive erosion at the downdrift side of Port [2]. The main objective of this study is to propose three protection alternative to resolve the coastal erosion problem on the eastern part of Amir Abad port. Then, the performance of the proposed alternatives has been investigated numerical by using the MIKE 21.

2. Coastal Protection Alternatives

Three proposed alternatives are consisted of: (i) using group groins, (ii) employing groins and detached breakwaters namely the static equilibrium scheme, and (iii) combination of the two above-mentioned alternatives, namely the dynamic equilibrium scheme. Figures 1 to 3 show schematically the outline of the three alternatives. In designing the groin breakwater, the gap ratio to the effective length of the groins is set 1.5 [3]. Hence, by taking the distance between the groins as 200 m, the effective length of the groins is 150 m. For particle usage a 25 m artificial feeding nourishment was added [3]. Therefore, the groins are 175 m long and located at a distance of 75 m from each other. For the case of detached breakwaters, the distance of the wave refraction point is nearly 24 m, the ratio of the detached breakwater to the width of the refraction area is about 1.5 to 2 m. Thus, the distance between the detached breakwater and the coastline is set to 35m [4]. Also, the ratio of the breakwaters length to their distance from the coastline is 2.5, therefore the breakwaters length is 100 m [4]. In order to design the distance between the breakwaters, the ratio of the length of the breakwater to the distance between them is 0.75. According to this ratio, the distance between the breakwaters is 75 m [4].

The final outline of proposed alternatives is carried out as follows: in the static equilibrium scheme, the first groin is 175 m long, then their length are decreased by 6 degrees to the end of the sheltered area. The detached breakwaters is 100 m long each, and located at a distance of 75 m from the groins. In the third alternative, five groins are used at the beginning of the protecting area and then, the combination of breakwater and groin are used with a 6 degree angle to reduce the length of the groins.

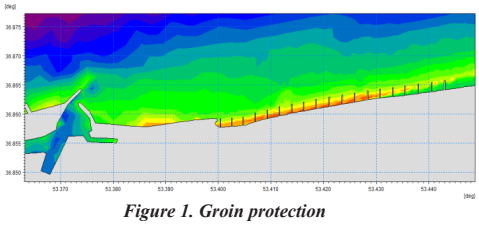

Figure 1. Groin protection

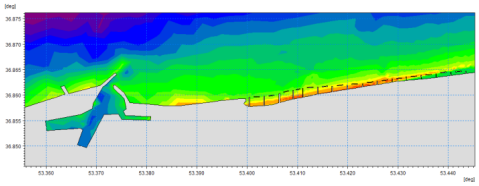

Figure 2. Groin and detached breakwaters

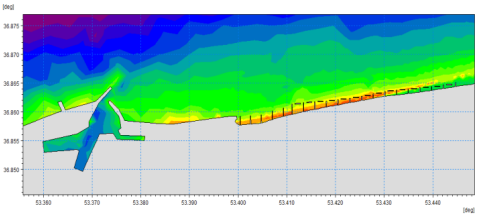

Figure 3. Combination of protections or dynamic equilibrium scheme

3. Results and Discussion

The total sediment transport rate is estimated according to Engelund and Fredose (1976) in different current-wave and wave-breaking conditions. The total load is calculated as the bed-material and suspended load, separately. The sediment transport rate of total load (q_t) is calculated as the sum of the bed-load transport (q_b) and suspended load transport (q_s):

$$q_T = q_b + q_s \quad (1)$$

$$q_b = 5p\left(\sqrt{\theta'} - 0.7\sqrt{\theta_c}\right)\sqrt{(s-1)gd} \quad (2)$$

P is the possibility of moving all particles in a single layer, θ' is the shear stress without the bed dimension, θ_c is critical shear stress for inception of the movement, s is relative density of the bed load, g is graviton acceleration and d is sediment diameter. The suspended load is calculated as follows

$$q_s = 1.83 q_B \left[I_1 \ln\left(\frac{h}{0.033 k_s}\right) + I_2 \right] \quad (3)$$

here I_1 and I_2 are the Einstein integral, k_s is the friction factor and h the local is water depth.

The wind data downloaded from ECMWF site, and the sediment budget as well as the Nekarud River data were introduced as the input data to MIKE 21. Figure 4 shows the bed level changes at the three different sections in the downdrift coast of Amir Abad port after one year of simulation time. As seen, the static equilibrium scheme, obtained the least amount of sediment accretion, while the groin protection scheme is collected more sediment than the static equilibrium scheme. On the other hand, the combination scheme of both alternatives, shows much better performance in terms of beach accretion than previous models. However, considering the cost effective scheme in resolving the erosion problem, the groin protection may provide a much less expensive solution alternatives.

4. Conclusion

Three protection alternative is proposed to resolve the coastal erosion problem on the downdrift of Amir Abad port. They are consisted of (i) using group groins, (ii) employing groins and detached breakwaters (static equilibrium scheme), and (iii) combination of the two above-mentioned alternatives (dynamic equilibrium scheme). Then, the performance of the proposed alternatives has been investigated numerical by using the MIKE 21. The obtained results indicated that the combination scheme of group groins with detached breakwaters (static equilibrium scheme), shows much better performance in terms of beach accretion. .

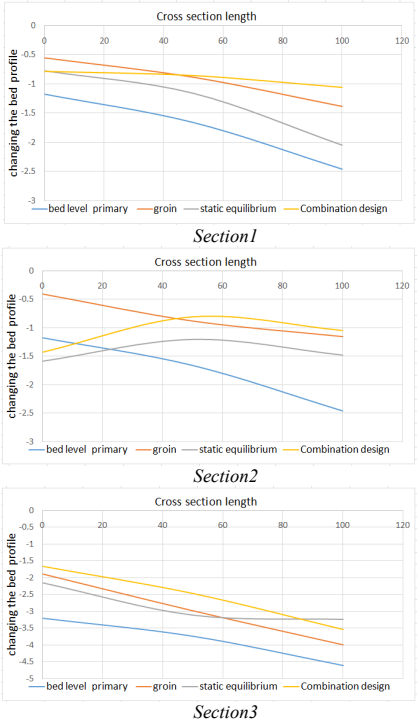

Figure 4. The results of changing the bed profile

5. References

[1] Malek, J., Bani Hashemi, M., Qolamnezhad, K. Investigating changes in Caspian Sea ine in the Amir Abad Range. International Conference on Coastal, Ports and Marine Structures November 2012, Tehran, Iran.

[2] Salargarna, M., and Ebrahimi, N., Mousavi, F., Hosseini, KH. The Impact of Human Interventions on the Coastline of the Sea (Case Study of Amir Abad Port), International Conference on Civil Engineering architecture and urban infrastructure July 2015,Tabriz, Iran.

[3] Basco, D.R., Pope, J., 2004. Groin functional design guidance from the Coastal Engineering Manual. *Journal of Coastal Research.*

[4] Ahrens, J. P., and Cox, J. 1990. Design and Performance of Reef Breakwaters, *Journal of Coastal Research*; 6 (1): 61-7.

[5] MIKE 21 and MIKE 3 current Model FM. 2012. Hydrodynamic and transport module, scientific documentation. DHI Software.

COASTAL UPWELLING ALONG THE SOUTHWEST COAST OF CASPIAN SEA BASED ON SATELLITE OBSERVATIONS AND NUMERICAL MODELING

Ehsan Shad[1], U. Reza Kamalian[2] and Amirpouya Bakhtiari[3]

1) PhD Candidate of Coastal, Port and Marine Engineering, Qom University, Qom, Iran, E.shad@stu.qom.ac.ir
2) Department of Technical Engineering, Qom University, Qom, Iran, ur.kamalian@qom.ac.ir
3) MSc of Coastal, Port and Marine Engineering, A.p.bakhtiary@gmail.com

1. Introduction

Coastal upwelling systems are major economic sources, which contribute to 20% of the global fish production from less than 3% of the world oceans' surface (Benazzouz et al., 2014). If the wind direction in the northern hemisphere is located on the left side of the beach, wind stress and the Coriolis force will cause the Ekman Transport along the beach and toward the sea. In this case, water the Ekman layer will replace the water surface from the coast during the vertical water transfer process. In this way, coastal upwelling will take place. Water that rises to the surface as a result of upwelling is typically more nutrient and colder. These nutrients fertilize water surface i.e. these water surfaces often have high biological productivity. Therefore, perfect fishing spots are typically found where upwelling is common. Upwelling phenomenon along the southern boundaries of Caspian Sea (CS) has received greater attention in the recent years due to its environmental and economic significance. The CS coasts can be divided into regions with the quite sustainable wind direction regimes. In this regard, there is a legal system so that in most times of the year the north winds (northwest, and northeast) and southeast winds are considered as the dominant winds of CS. In average, the frequency of northward winds is 41 percent, and their probability in summer is higher than other seasons (48.7 percent).The mean of eastern winds' annual blow is 35.9 percent (Mamedov and Khoshravan, 2012). The water surface of CS in the shallow coastal areas during summer is often warmer, reaching 30 degrees Celsius in some areas. The upwelling phenomenon in the warm seasons is almost constant in the CS. The extent of the upwelling lasted 5-20 kilometers from the coastline and tens of kilometers along the coast (Kosarev,1990)). Also the upwelling in warm seasons has been confirmed in atmospheric observations (Kosarev and Yablonskaya, 1994), and satellites Observations (Sur et al., 1998). In July, the prevailing wind in the middle of CS is mainly from the north, which has resulted in upwelling along the eastern coast (Knysh et al., 2008). The wind in the middle and the southern parts of CS draws water surface from the east coast to the west coast, causing an increase in water on the west coast, causing an upwelling on the eastern coast (Ibrayev et al., 2010). In this context, the available satellite data on sea surface winds, sea surface temperature (SST) between March and September 2013 are analyzed to identify the coastal upwelling pattern in the southern coast of CS. Also the three-dimensional hydrodynamic is used for modeling the CS circulation properties.

2. Numerical Model and Satellite Observations

The three-dimensional hydrodynamic Model of Mike 3 from DHI is used in this study. The atmospheric parameters i.e. wind speed, wind direction, and air pressure are provided from predictions of the Weather Research and Forecasting (WRF) model. Use of quadrilateral elements on the continental shelf of the southern part of the CS provides more accurate results while maintaining stable conditions for the numerical model. Moreover, comparing to a triangular grid with equal element lengths, employing quadrilateral meshes significantly reduces the cost of computational. The number of nodes and elements in the grid was 7742 and 12712, respectively. Twenty-one layers have been used for the vertical direction with a combination of sigma and Z-layer approaches.

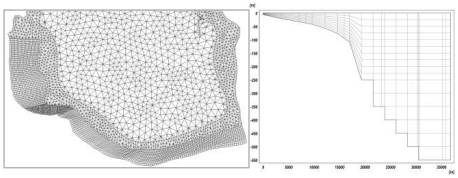

Figure 1: The computational grid used for the model.

An impermeable and zero normal velocity condition were used to define the coastline boundary condition. The model is validated based on measurement data. Table 1 summarizes statistical comparison between model's water level (WL), Alongshore current speed (ACS), and measurement data at five stations. The results demonstrate that the model relatively produces accurate results at all stations.

Table 1: Correlation Coefficient (CC) and Root Mean-Squared Error (RMSE) for all stations.

Station	Astara	Rodsar	Anzali	Nowshahr	Amirabad
WL CC	0.73	0.84	0.75	0.58	0.68
ACS CC	0.89	0.24	0.82	0.73	0.74
WL RMSE(m)	0.069	0.046	0.07	0.14	0.081
ACS RMSE(m/s)	0.062	0.057	0.093	0.019	0.13

MODIS/Aqua level 2 daily analyzed Sea Surface Temperature (SST) images at 4 km × 4 km scale from March to September of 2013 were downloaded from the website of National Oceanographic Data Center (https://nodc.noaa.gov). The sea surface winds data which are used for this study during the same period was obtained from scatterometer wind observations ASCAT. Sea surface winds were downloaded from the website of Physical Oceanography Distributed Active Archive Center (https://podaac.jpl.nasa.gov).

3. Results and discussion

Alongshore component of the southeast wind can make westward alongshore current which draws surface water from the coast to the offshore (due to Ekman Transport). It can cause upwelling in south of CS. As a result, cold water travels from deep water to surface layer. There are few upwelling events (15 events) in SST images during the study period because we had only one image per day while there are lots of them in numerical model result. As an example, figure 2 shows SST image on 1st to 3rd March with surface signature of the upwelling events (NW corner at [37.5°N, 50.7°E], SE corner at [36.8°N, 51.2°E]). The wind structure also plays an important role in determining upwelling. Figure 3 shows wind direction at the same time. As it can be seen the wind blows form southeast direction. This kind of wind can create westward alongshore current in the southern coasts of the CS.

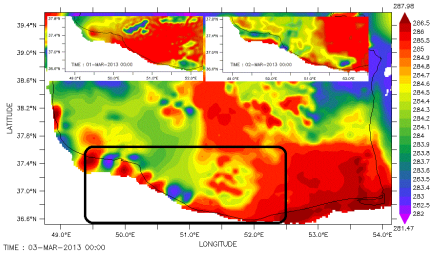

Figure 2: MODIS-SST image of area under study.

Numerical model result is also highly compatible with remote sensing. Figure 4 shows vertical component of water velocity (W) as well as vectors show current direction. Figure 5 shows cross section of the W at the same place and same time. As it can be seen, Ekman Transport happened in the coast. In fact, W is positive in coastal area and it is negative in the offshore i.e. deep water is transmitted to the surface in coast.

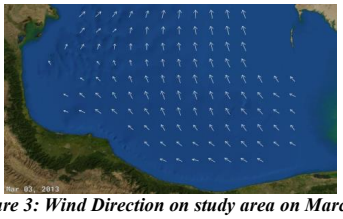

Figure 3: Wind Direction on study area on March 3.

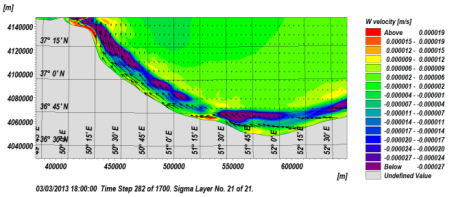

Figure 4: Vertical component of water velocity on March 3.

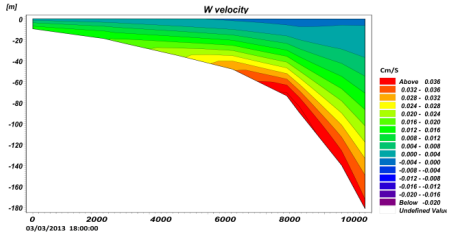

Figure 5: Cross section of Vertical component of water velocity on March 3.

4. References

Benazzouz, A., Mordane, S., Orbi, A., Chagdali, M., Hilmi, K., Atillah, A., Pelegri, J.L., Demarcq, H., 2014. An improved coastal upwelling index from sea surface temperature using satellite-based approach – the case study of the Canary Current upwelling system. Cont. Shelf Res. 81, 38–54.

Mamedov, R., & Khoshravan, H. 2012 . The Atlas of Caspian Sea Hydromorphology. (D. s. Smith, Sophia Publishing Group Inc.

Kosarev, A. N.,1990, The Caspian Sea,water structure and dynamics. Nauka, Moscow.

Kosarev, A. N. and Yablonskaya, E. A.,1994,The Caspian Sea, SPB Academic Publishing.

Sur, H. I., Ozsoy, E. and Ibrayev, R.,1998, Satellite – derived flow characteristics of the Caspian Sea, in: satellites, Oceanography and Society, edited by: Halpern, D. Elsevier Science B. V., 289-297.

Knysh, V.V., Ibrayev, R.A., Korotaev, G.K. and Inyushina, N.V., 2008, Seasonal variability of climate currents in the Caspian Sea reconstructed by assimilation of climatic temperature and salinity into the model of water circulation, Atmospheric and Oceanic Physics, 44(2), 236-249.

A THREE-DIMENSIONAL NON-HYDROSTATIC NUMERICAL MODEL FOR PREDICTION OF CURRENT CIRCULATION IN THE PERSIAN GULF

Saeideh Sami[1], Kourosh Hejazi[2] and Mohammad Reza Allahyar[3]

1) Civil Eng. Dept., K.N. Toosi University of Tech., Tehran, Iran, sami@dena.kntu.ac.ir
2) Civil Eng. Dept., K.N. Toosi University of Tech., Tehran, Iran, hejazik@kntu.ac.ir
3) Ports and Maritime Organization, Tehran, Iran, allahyar@pmo.ir

1. Introduction

The shallow water approach due to its low computational cost and simple formulation, has been extensively used in modeling of flow and transport in oceanic water bodies. However, over the past years, there has been a growing demand for three-dimensional hydrodynamic models in oceanic and estuarine studies, particularly where the ratio of the vertical to horizontal scale of motion is not small. This paper presents the development and application of a three-dimensional numerical model to simulate the hydrodynamics and scalar transport in oceanic water bodies. The hydrodynamic module is based on the three-dimensional Navier-Stokes equations, and is capable of solving the non-hydrostatic equations as well as giving a solution with the hydrostatic assumption. The transport module solves the transport equations of salinity and temperature.

2. Description of the Numerical Model

The three-dimensional numerical model employs a triangular unstructured-grid, and is based on the finite-volume method. The newly developed oceanic model deploys the σ-coordinate system giving an accurate representation of the moving free surface and bottom topographies. The scalar quantities, the pressure values for example, are defined at the vertexes, and the containment node-dual finite volumes are employed around a vertex. The horizontal velocities are located at the midpoint of each edge, and the vertical velocities are at the vertices, at the top and bottom of each polygon cell. The factional step method with a semi-implicit scheme was employed following the algorithm presented by Casulli and Cattani [1]. The method consists of two major steps. During the first step, the momentum equations are solved without pressure terms that yield an approximate velocity field. In the second step, a correction with the non-hydrostatic pressure is applied to the velocity field. Imposing the continuity constraint, yields to the pressure Poisson equation. The matrix of unknown pressures is then solved by the bi-conjugate gradient squared stabilized (BiCGSTAB) algorithm together with the modified incomplete lower upper pre-conditioner (MILU) [2]. The solution of the non-hydrostatic pressure updates the intermediate velocity field and then the water elevation.

3. Validation Results

To explore the role of non-hydrostatic pressure distribution, two test cases were simulated including a standing wave in a closed basin and a lock-exchange density flow. The modeling of the Persian Gulf is also presented and validated against the data reported from field measurements.

3.1. Hydrodynamic Tests

The first test involved studying the oscillations of a uni-nodal standing wave in a confined container. The numerical simulation results and the analytical solution for the velocity and hydrodynamic pressure distributions are shown in Figure 1. In the lock-exchange problem a rectangular basin was initially filled with two fluids with different densities, $\rho_1 = 1.03$ and $\rho_2 = 1.0$, separated by a vertical divider located centrally in the basin. Once the divider is removed the resulting solution shows the evolution of the fluid interface (Figure 2).

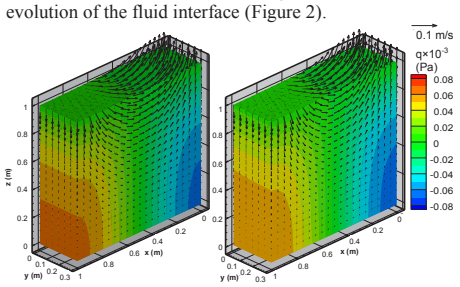

Figure 1. Velocity field and hydrodynamic pressure distribution, analytical solution (Left), model prediction (Right).

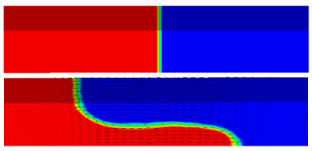

Figure 2. Initial configuration for the lock exchange (top), Lock exchange solution at t = 5 s (bottom).

3.2. Persian Gulf Modeling

The Persian Gulf is a shallow, semi-enclosed marginal sea with average depth of about 35 m, characterized by significant evaporation which is connected to the Gulf of Oman and the Arabian Sea through the Strait of Hormuz. The circulation in the Persian Gulf is primarily driven by the prevailing northwesterly winds and the associated momentum and buoyancy fluxes, secondarily by thermohaline forcing, and thirdly by the tides. A typical basin-scale circulation of the gulf is cyclonic and composed of a northwestward-flowing Iranian Coastal Current (ICC) from the Strait of Hormuz along the northern side of the basin and a southeastward flowing current in the southern portion of the gulf.

For the simulations, the domain was discretized into 10290 nodes (Figure 3) in the horizontal plane, and 10 sigma levels in the z-direction. The time step was set at 6 s. The bathymetry data was extracted from the ETOPO two-minute gridded dataset. Atmospheric parameters i.e. air temperature, relative humidity and sea level pressure were based on 12 hourly and daily data of NOAA [3]. WRF and WaveWatch III models provided wind speed and radiation stresses data respectively. The water level at open boundary was adopted from TPXO global tide model. The initial condition for sea surface level, velocity, temperature and salinity were extracted from HYCOM+NCODA Global 1/12° reanalysis. The simulation was set for August 2009. Model verification for water surface elevation was performed by comparing the model predictions with measured data at different stations along the Iranian coastline (Figure 3). Figure 4 presents the modeling results of free surface elevation at three sample stations, in comparison with the observations. Figure 5 compares the circulation patterns in the Persian Gulf produced by the newly developed model and the one reported by Thoppil and Hogan [4].

4. Conclusions

A three dimensional, non-hydrostatic, finite volume model has been developed and validated. The results of the hydrodynamic tests demonstrate the capability of the model to simulate non-hydrostatic effects. Also it can be seen that the model predictions for surface elevation of Persian Gulf are in close agreement with the on-site measurements. The circulations in the Persian Gulf are satisfactory modeled. According to the results of Thoppil and Hogan [4], the cyclonic circulations are being transformed into a series of mesoscale eddies, which are evident in the model predictions.

5. Acknowledgements

This work was supported by the Ports and Maritime Organization of Iran.

6. References

[1] Casulli, V., and Cattani, E., "Stability, accuracy and efficiency of a semi-implicit method for three-dimensional shallow water flow", *Computers and Mathematics with Applications*, 1994, 27 (4), pp. 99-112.

[2] Chan, T. F., and Van der Vorst, H. A., "Approximate and Incomplete Factorizations", *Parallel Numerical Algorithms*, 1997, 4, pp. 167-202.

[3] National Oceanic and Atmospheric Administration, U.S. Department of commerce, *http://www.noaa.gov/*.

[4] Thoppil, P. G., and Hogan, P. J., "A Modeling Study of Circulation and Eddies in the Persian Gulf", *Journal of Physical Oceanography*, 2010, 40, pp. 2122-2134.

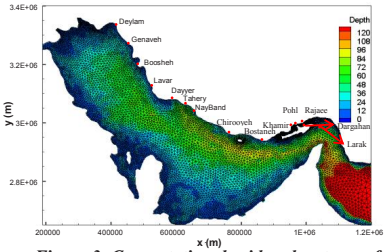

Figure 3. Computational grid and water surface elevation stations.

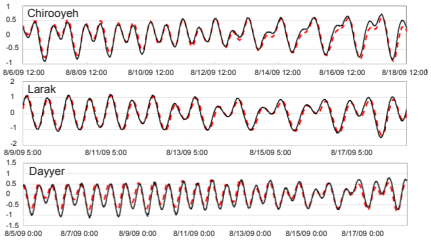

Figure 4. Comparison between the results of the model (black line) and observations (dashed red line) for time evolution of the free surface elevation.

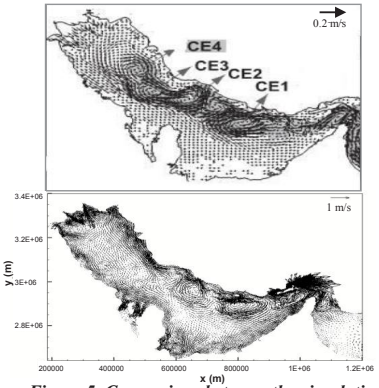

Figure 5. Comparison between the circulation structures simulated by Thoppil and Hogan [4] (top) and the model (bottom).

A CORRECTIVE METHOD FOR IMPROVING WIND-WAVE SIMULATIONS IN THE PERSIAN GULF

Nasibeh Rashidi[1], Sarmad Ghader[2], S. Abbas Haghshenas[3] and Edris Delkhosh[4]

1) Institute of Geophysics, University of Tehran, Tehran, Iran, Nasibeh.Rashidi@ut.ac.ir
2) Institute of Geophysics, University of Tehran, Tehran, Iran, sghader@ut.ac.ir
3) Institute of Geophysics, University of Tehran, Tehran, Iran, sahaghshenas@ut.ac
4) Institute of Geophysics, University of Tehran, Tehran, Iran, edrisdelkhosh@ut.ac.ir

1. Introduction

The wave climate either for a period of years in the past or the daily variations of wave parameters in the next couple of days are of great importance for structural design as well as for marine operations. Wave measurements data are essential for studying wave climate in a certain area; however, measurements are not usually available everywhere and on a long-term basis; thus reliability of wave simulation is a crucial issue in coastal, harbor and ocean engineering. Hence, numerical simulations are to be adopted to obtain such data in locations of interest. Due to the lack of wind/wave measured data, predicted wind waves are used to determine wave parameters in many regions.

Numerical wind wave modeling has been practiced since the mid 1950's for a variety of purposes, such as operational forecasting, coastal engineering design and coastal evolution studies, and general wind wave research. Moreover, this type of data is essential for environmental studies (Huang *et al.*, 2016). Traditionally, wind wave modeling has been most actively pursued by coastal engineers. Nowadays spectral wind waves model are the most practical tool for wave predictions. Since the outputs of these models generally contain some errors, their results should modify verifying against available measured data.

In this study, a new approach based on the error prediction of simulated wind/wave data at the observing stations and distributing the errors in the computational domain, was implemented for updating the model outputs. This aims to improve the accuracy of reproduced measured wind and wave data by adopting machine learning methods. To do so, wind wave simulation of meteorological model was carried out over the Persian Gulf and the results were compared with the measured data. A machine learning approach is used to find out the relationship between the output of numerical models and the measured data to be applied for improving model results.

2. Wind and Wave Simulations

Wind waves play a significant role in ocean and coastal activities. Hindcasting of wave parameters is necessary for many applications in coastal and offshore engineering and is generally made with the help of sophisticated numerical models (Mahjoobi, 2008). Wind and wave data are collected from buoys, voluntary observing ships, satellite altimetry and numerical models. The physical process of wind wave generation is extremely complex, uncertain and not yet fully understood. The forecasting of ocean wave heights and periods are conventionally conducted from the wind information on the basis of the wind–wave relationship.

Despite a variety of deterministic models presented to predict the heights and periods of waves from the characteristics of the generating wind, a large scope still exists to improve on the existing models or to provide alternatives to them. The error may become large due to uncertainty in the wave generation prediction, especially in the coastal zones.

For wind simulations in this study, the Advanced Research WRF (ARW) model, developed at US National Center for Atmospheric Research (NCAR) is applied in this study to simulate surface winds. This model is a fully compressible, Euler non-hydrostatic mesoscale numerical weather prediction model (Wang et al., 2010). Adopting the ARW dynamical core of the WRF model version 3.4.1, the model is configured with two nests with 0.3 degree and 0.1 degree horizontal grid resolutions in a Latitude-Longitude projection. To find the candidate configurations of the WRF model based on physical parametrizations, different choices are used to create a number of WRF model configurations. Then, to find the candidate WRF model configurations, the model is run with these different physics configurations. Finally, three of these configurations are selected to be more suitable for wind simulations over water based on statistical analysis against observational data. The Global Forecast System (GFS) data of the US National Center for Environmental Prediction are used to provide the initial and boundary data for WRF model control forecast. Assessing the performance of the system against observational data, one of the configurations are selected. The simulated wind field is modified by using machine learning methods.

The original and modified outputs of the wind model is introduced to the third generation WaveWatch III (WW3) model to simulate the wave characteristics over the simulation domain. Version 3.14 of the third generation WW3 model was implemented for the generation and

propagation of waves in the Persian Gulf (Tolman, 1991). A structured mesh is developed to resolve the bathymetry within the computational domain. The main parameters of the model were assigned based on a comprehensive sensitivity analysis study and the model performance was verified based on the available archive field data. Model runs were carried out for a one month period including the observational studies. The WW3 computations are compared with the observed wave parameters for original wind simulation results and modified results.

3. Outline of Machine Learnings Method

Machine learning is a subfield of artificial intelligence which gives computers the ability to learn without being explicitly programmed (Samuel, 1959). In other words, machine learning approaches and techniques are the ones which provide learning from data and make predictions according to potential governing patterns of data. Data classification, clustering and regression are just some applications of this broad field of study. A typical example in this field is how a robot can learn from previous experience (mistakes) in passing a barrier on its way. Decision tree learning, Association rule learning, artificial neural networks, support vector machine (SVM), genetic algorithms (GA) and Bayesian network are some well-known approaches of machine learning.

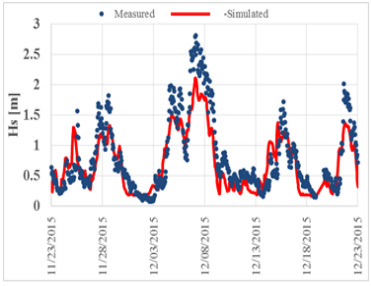

Figure 1. Simulated waves using the unmodified wind speed data at Assaluyeh Buoy Location.

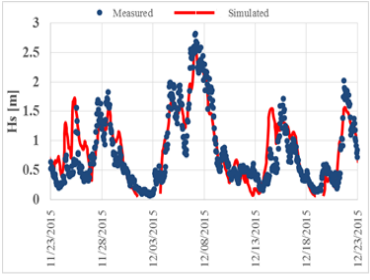

Figure 2. Simulated waves using the GP-Based modified wind speed data at Assaluyeh Buoy Location.

4. Summary

In summary, a combination of WRF-WWIII model simulations together with a machine learning corrective method are adopted to simulate wave generation at selected locations in the Persian Gulf. The modified wind field was introduced to WAVEWATCH III model to predict wave parameters over the Persian Gulf. The obtained results show that this approach has improved simulated wave parameters and a better agreement has been observed between simulated wave parameters and observation values.

5. References

[1] Agrawal JD, Deo MC, 2002: On-line wave prediction. Marine Structures 15 (1):57-74.

[2] Cheggaga, Nawal., 2013: New Neural Networks Strategy Used to Improve Wind Speed Forecasting, Wind Engineering, 37(4), 369-380.

[3] Demuth, Howard., 2002: Neural Network Toolbox, Networks, 24(1), 1-8.

[4] Makarynskyy O., 2004: Improving wave predictions with artificial neural networks, Ocean Engineering, 31(5-6), 709-724.

[5] Ching-PiaoTsaiChangLinJia-NShen., 2008: Neural network for wave forecasting among multi-stations, Ocean Modelling,Volume 25, Issues 1–2, Pp 35-47

[6] Ghader, S., Yazigi, D., Soltanpur, M., Nemati, M. H. 2016: Wind field forecasting over the Persian Gulf using an ensemble system developed for WRF, 3rd International Conference on the Persian Gulf Oceanography, Tehran, Iran.

[7] Hendrik L.Tolman, 2008 A mosaic approach to wind wave modeling, Ocean ModellingVolume 25, Issues 1–2, 2008, Pp 35-47

[8] Huang, Haosheng, Cui, Linlin, Sorourian, Soroush, and Justic, Dubravco. 2016. A coupled ocean-wave model for the Barataria Bay, Louisiana. Proceedings of *Gulf of Mexico Oil Spill & Ecosystem Science Conference 2016*.

[8] J.Mahjoobi, A.Etemad-Shahidi, M.H.Kazeminezhad 2008: Hindcasting of wave parameters using different soft computing methods, Applied Ocean ResearchVolume 30, Issue 1, February 2008, Pages 28-36

NUMERICAL MODELLING OF WAVE- MUD INTERACTION USING INCOMPRESSIBLE SMOOTHED PARTICLE HYDRODYNAMICS (ISPH) WITH A NEW KERNEL FUNCTION

Abolfazl Aslani Kordkandi[1], Kourosh Hejazi[2] and Mohsen Soltanpour[3]

1) K.N. Toosi University of Technology, Tehran, Iran, a.aslani@mail.kntu.ac.ir
2) K.N. Toosi University of Technology, Tehran, Iran, hejazik@kntu.ac.ir
3) K.N. Toosi University of Technology, Tehran, Iran, soltanpour@kntu.ac.ir

1. Introduction

A typical phenomenon of wave propagating over a muddy bed is the dissipation of the wave energy due to the wave-mud interaction. In this paper, due to some popular features of meshless method in simulation of fluid behaviour and particle tracing, incompressible smoothed particle hydrodynamics (ISPH) method has been deployed to simulate wave and non-Newtonian-mud interaction. A new hybrid kernel function and formulation of viscous term are presented, where different kernel functions for water and mud layer have been considered. The new hybrid kernel function and the spline kernel were used for mud and water layers, respectively. The combination of two kernel functions results in better simulation of the interface of the two layers as well as preventing particle clustering.

2. Governing Equations and the SPH Formulation

The two-dimensional governing equations of mass and momentum conservation, written in Lagrangian form are presented as follows [1]:

$$\frac{d\rho}{dt} = \sum_b m_b (\vec{u}_a - \vec{u}_b) \vec{\nabla}_a W_{ab} \tag{1}$$

$$\frac{\Delta(\vec{u}_* + \vec{u}_{**})}{\Delta t} = \left[\vec{g} + \left(\frac{1}{\rho} \nabla . \tau \right)_a \right] - \sum_b m_b \left(\frac{P_b}{\rho_b^2} + \frac{P_a}{\rho_a^2} \right) . \vec{\nabla}_d W_{ab} \tag{2}$$

where a and b indices indicate the reference and neighbouring particles respectively, m_b and ρ represent mass and density respectively, W is the interpolation kernel, $\vec{u}_*$ and $\vec{u}_{**}$ are the velocity in the prediction and correction steps respectively, t is the time, $\vec{u}$ the particle velocity, P the pressure and $\vec{g}$ the gravitational acceleration. Viscous term is written as:

$$\left(\frac{1}{\rho} \nabla . \tau \right)_a = \sum_b \frac{8 m_b \tau_b}{(\rho_a + \rho_b)^2} [\dot{\gamma}]_{a;b} \cdot \nabla_d W_{ab} \tag{3}$$

where τ_b is the stress of neighbouring particles. In this study water and mud are considered as Newtonian and non-Newtonian fluids, respectively. Bingham-Papanastasiou model was used for the rheology of mud layer [6].

$$\tau = \mu_B \dot{\gamma} + \tau_y \left(1 - \exp(-m \dot{\underline{\underline{\gamma}}}) \right) \tag{4}$$

where τ_y , μ_B , $\dot{\gamma}$ and $\dot{\underline{\underline{\gamma}}}$ are the Bingham yield stress, the Bingham viscosity, the shear rate and magnitude of shear rate, respectively. m controls the exponential growth of the stress. Noting that the neighbouring particles are involved in determining the shear stress of reference particle a, the effect of all neighbouring particles (b) on determining the magnitude of shear rate is involved. For example the longitudinal strain rates in the equation of total $\dot{\underline{\underline{\gamma}}}$ are calculated as follows:

$$\left. \frac{\partial u}{\partial x} \right|_a = \sum_b \left(\frac{\partial u_{ab}}{\partial r_{ab}} \frac{\partial r_{ab}}{\partial x_{ab}} \right) = \sum_b \left(\frac{u_a - u_b}{r_{ab}} \frac{x_a - x_b}{r_{ab}} \right) \tag{5}$$

A new hybrid kernel function composed of the combination of hyperbolic and spline kernels, has been used in this study (Figure1).

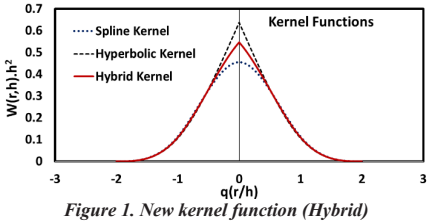

Figure 1. New kernel function (Hybrid)

Several tests showed that hybrid and spline kernels are appropriate for interface and free surface simulations, respectively. Therefore, two separate kernel functions are used for water and mud layers. The use of hybrid kernel in the mud layer prevents from penetration of mud particles into water layer. Furthermore, due to non-zero value of the derivative of the new kernel function, as the particle-spacing approaches to zero, non-zero force repels the particles, and subsequently this prevents particle clustering. Figure 2 shows the results of wave-mud interaction with double kernels: the hybrid kernel for mud layer and the spline for water (Figure 2a), and single kernel for both layers (Figure 2b). In Figure 2a, the position of the particles shows no clustering

occurrence and also the particles of each layer do not enter into other layer in comparison with the use of single kernel function (Figure 2b).

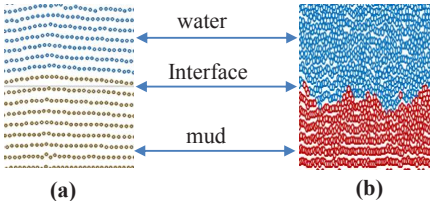

Figure 2. Simulation of wave-mud interaction: (a) use of double kernel functions, (b) single kernel function

3. Model Verification and Application

In order to validate the numerical scheme of the ISPH model, the propagation of a sinusoidal wave was simulated. Figure 3 shows the numerical results which are in a good agreement with the analytical solution. For the wave-mud interaction a two-dimensional simulation of wave and non-Newtonian-mud is presented. Figure 4 shows the attenuation of the wave height and the pressure contours for the wave-mud interaction. The number of particles employed in the computation was about 40000 and the initial spacing for the particles and the time step were set equal to 0.01 m and 0.001 s, respectively. The predicted wave attenuation is compared against the simulated results of Hejazi et al. [2], the experimental results of Sakakiyama and Bijker [3] and the theoretical solution of Dalrymple and Liu [4] and An [5].

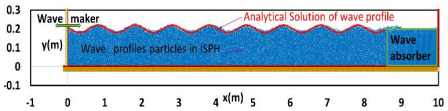

Figure 3. Comparison of the simulated (blue) and analytical (red) solutions of wave profiles

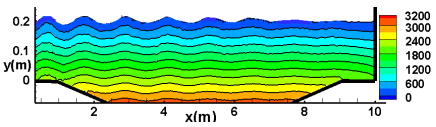

Figure 4. Total pressure (Pa) contours for the wave-mud simulation

4. Results and Discussion

The relation between the wave height (H), initial wave height (H_0) and wave damping coefficient (k_i) is presented as follows [4]:

$$H = H_0 e^{-k_i x} \quad (6)$$

As shown in Table 1, and consistent with the previous theoretical and experimental results, wave attenuation over a mud layer increases at larger densities (within the applied range). Both the laboratory data and numerical simulations reveal the decrease of wave attenuation rate with the increase of wave height. The results show that the predicted values of the present ISPH method using new hybrid kernel is much closer to the experimental results than the theoretical and other numerical simulations considering a linear approximation or the Newtonian mud behaviour in the governing equations. Comparisons with the experimental results reveal that the present model slightly overestimates the dissipation rate.

Table 1. Wave attenuation coefficient (k_i); comparison between the ISPH model, experimental, theoretical and other numerical results wave profiles

Wave and mud properties				K_i(1i/m)				
H_0 (cm)	T (s)	P (kg/m³)	υ (m²/s)	SB	DL	An	H.et al.	Present Model
4	1.0	1370	0.015	0.183				0.186
4	0.8	1300	0.01	0.068	0.058	0.073	0.041	0.071
3.2	0.8	1300	0.01	0.084	0.089	0.109	0.083	0.085
4	~0.8	1240	0.004	0.031	0.029	0.05	0.007	0.047
4	~0.7	1300	0.01	0.068	0.058	0.073	0.041	0.07
~2	0.7	1300	0.01	~0.1			0.085	0.108

5. References

[1] Shao, S. and Lo, E.Y., "Incompressible SPH method for simulating Newtonian and non-Newtonian flows with a free surface" Advances in water resources, 26,7, 2003, pp.787-800.

[2] Hejazi, K., Soltanpour, M., Sami, S., "Numerical modeling of wave-mud interaction using projection method" Ocean Dynamics, 63, 2013, pp. 1093-1111.

[3] Sakakiyama T., Bijker E.W., "Mass transport velocity in mud layer due to progressive waves" J Waterway Port Coast Ocean Eng ASCE, 115, 5, 1989, pp. 614–633.

[4] Dalrymple R.A., Liu PL-F., "Waves over soft muds, a two-layer fluid model" J Phys Oceanogr, 8, 1978, pp. 1121–1131.

[5] An N.N., "Mud mass transport under wave and current", Department of Civil Engineering, Yokohama National University, Yokohama Ph.D. dissertation, 1993.

[6] Papanastasiou, T.C., "Flow of materials with yield", J. Rheol., 31, 1987, pp. 385-404.

EXPERIMENTAL INVESTIGATION OF PARAMETERS AFFECTING THE WAVE-MUD INTERACTION USING A THIN PLASTIC COVER ON MUDDY SEABED

Reza Arefi[1], Kourosh Hejazi[2], Mohsen Soltanpour[3] and Faraz Jomehri[4]

1) Ph.D. Candidate, K.N. Toosi University of Technology, Tehran, Iran, rarefi@kntu.ac.ir
2) Assistant Professor, K.N. Toosi University of Technology, Tehran, Iran, hejazik@kntu.ac.ir
3) Professor, K.N. Toosi University of Technology, Tehran, Iran, soltanpour@kntu.ac.ir
4) Ph.D. Candidate, K.N. Toosi University of Technology, Tehran, Iran, fjomehri@kntu.ac.ir

1. Introduction

Typical muddy coasts can be found in many coastal areas of the world. In the presence of cohesive sediments, wave damping is enhanced; surface waves can be attenuated appreciably in a finite number of wave periods or wave lengths [1]. The damping of the surface waves can be considerable; in fact, Gade (1985) [2] noted that there was a location in the Gulf of Mexico, known as the Mud Hole, where the attenuation of waves due to the mud bottom was so great that fishing boats used it as an emergency harbor during storms.

The pressure gradient of water waves and the shear stress at the interface between the water layer and the mud layer are two main parameters in the wave-mud interaction. However, due to the interaction of wave and muddy bed, a zone with high suspended loads of cohesive sediments is formed. To investigate wave-mud interaction in laboratory, the suspended cohesive sediments will cause problems in the normal procedure of the experiments. Therefore, using a thin plastic cover which separates the mud from water body and facilitates the laboratory experiments, is also included in the investigations.

Although the plastic layer with very low bending strength over the muddy bed will transfer the pressure gradient from water body to mud, transmission of the shear stress will be negligible. However, the impact of the normal stress is much more than the shear stress at the water-mud interface for the wave attenuation and for the initiation of the movement of mud [3].

To investigate the impact of a thin plastic cover on wave attenuation on a muddy bed, a series of wave flume experiments for wave-mud system has been performed in this study on both flat and inclined muddy beds.

2. Experimental Set-up

The physical model was set up in the wave flume of the Hydraulic Model Laboratory, Department of Civil Engineering, K. N. Toosi University of Technology, Tehran. The flume had a length of 12.5m, width of 0.3m, and depth of 0.45m. The still water depth was 30cm on the top of the mud layer of 7cm with a water content of 100%. Regular waves were produced by a flap type wave maker.

Commercial kaolinite was used as bed sediment due to its close rheological behavior with natural mud and also due to its reproducible properties and easy handling. Mud samples were prepared by careful mixing of kaolinite with tap water. The wave height variation along the mud layer was recorded by using a series of HR Wallingford wave system including the conductive wave gauges and an eight-channel module. Wave gauges were placed at the center-line of the flume in order to reduce the effects of the friction of the sidewalls. During the experiments, an 18M camera was used for capturing images during the experiments. Figure 1 shows a sketch of the experimental setup for both flat and inclined muddy beds. A cellophane layer with a thickness of 0.02mm covered the muddy bed to prevent the mixture of water and mud.

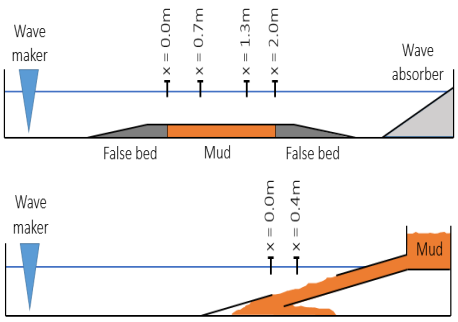

Figure 1. Sketch of the experimental setup for flat and inclined muddy beds

3. Results

As shown in Figure 1, wave height has been measured at 4 stations along 2m length flat muddy bed, where a number of wave conditions were considered. Figure 2 shows close rates of wave damping along 2m length flat muddy bed for wave heights of 6.4 and 9.8cm and wave periods of 0.8 and 1.1s, respectively, with and without the presence of the cellophane at the interface of the water and mud layers.. Water surface elevations at station 4 (x=2m) is depicted in Figure 3 which shows almost the same results for both conditions.

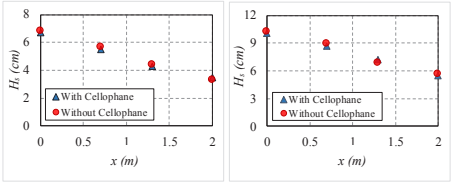

Figure 2. Wave damping over flat muddy bed for two different wave parameters, with and without cellophane

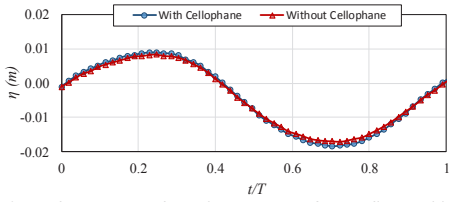

Figure 3. Water surface elevation at x=2m on flat muddy bed, with and without cellophane, with and without cellophane

For the second series of experiments, tests were conducted on inclined muddy bed with a slope of 1:10, to investigate the effects of cellophane layer on damping rate and wave breaking formation. Due to the gravity and wave-mud interaction, the fluid mud moves down on the sloped bed. The space underneath of the inclined bed was maintained to collect the mud (Figure 1). A reservoir at the top of the slope was embedded to feed the mud onto the slope.

Error! Reference source not found. shows the water surface elevation at x=0.4m, where x = 0 is the start point of the sloped muddy bed. Wave breaking over the inclined muddy bed has been depicted in Figure 5.

In these series of experiments, again it can be seen that the results of water surface elevation changes and wave breaking formation with and without the presence of cellophane are very close and the differences are negligible.

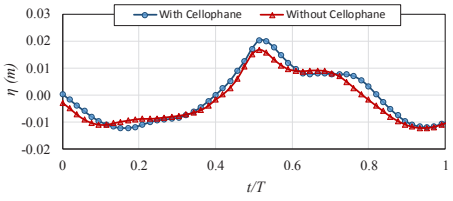

Figure 4. Water surface elevation at x=0.4m on the inclined muddy bed, with and without cellophane

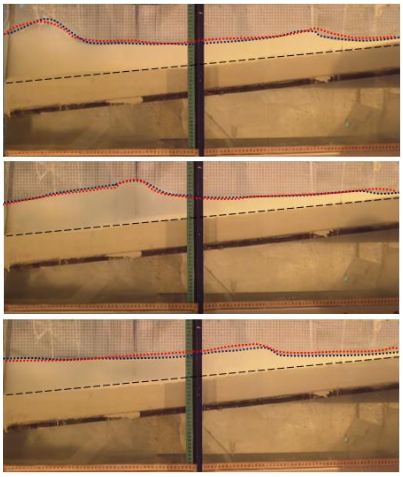

Figure 5. Wave propagation over inclined muddy bed with (blue dotted line) and without (red dotted line) cellophane layer

4. Conclusions

Normal and shear stresses between water and mud layer during wave propagation over muddy bed cause wave attenuation and mud transport. Although using cellophane layer on the muddy bed would accelerate the experiments and facilitate them, it removes transmission of the shear stresses at the water-mud interface to a high degree. To investigate the effect of a thin cellophane layer on the rate of wave damping over a muddy bed, a series of laboratory experiments were conducted on both flat and inclined muddy beds.

Wave height variation and wave deformation were analyzed along the muddy bed with and without the presence of cellophane layer. The observations showed very close results for two cases, suggesting that the effect of the presence of the cellophane layer between water body and muddy bed on wave-mud interaction and wave damping is negligible. This confirms the previous findings of the importance of the normal stress compared to the shear stress at the water-mud interface for the wave attenuation.

5. References

[1] Hejazi, K., Soltanpour, M. and Sami, S., "Numerical modeling of wave–mud interaction using projection method", *Ocean Dynamics*, 2013.

[2] Gade, H. G., "Effects of a non-rigid, impermeable bottom on plane surface waves in shallow water", *Ph.D. thesis, Texas A & M University*, 1957, 35 pp.

[3] An, N.N., and Shibayama, T., "Wave-Current Interaction with Mud Bed", *Coastal Engineering*, 1994, p. 2913-2927.

NUMERICAL STUDY OF SEDIMENTATION IN ANZALI HARBOR DUE TO NORTHWESTERN AND NORTHEASTERN WAVES WITH RESPECT TO THE EXTENDED BREAKWATERS

Hamed Mohammadnejad[1] and Habib Hakimzadeh[2]
1) Expert Ports and Maritime Organization, Tehran, Iran, Hamed.m.tce@gmail.com
2) Professor in Coastal Engineering, Faculty of Civil Engineering, Sahand University of Technology, Tabriz, Iran, Hakimzadeh@sut.ac.ir

1. Introduction

One of the most important aims of a port is to create favorable conditions for berthing, unloading and loading vessels. Because of the sedimentation and penetration problems of the waves in the basin and access channels are important issues that have a direct impact on the utilization and economics of the ports. Therefore, it is very important to study this issue in terms of heavy maintenance and dredging expenses.

As one of the important maritime terminals in Iran, Anzali harbor has a significant role in the Caspian Sea transportation. In this study, sedimentation and penetration of wave's problems in the pre and post breakwaters development of Anzali harbor has been investigated.

2. Boundary Conditions

The boundary conditions used in the wave model to the regional model with dimensions of 9 kilometers along the coast and 16 kilometers perpendicular to the coastline are shown in Figure 1 (a). Also deep water wave data received from the PMO was set for the northern boundary of the regional model in MIKE 21-Spectral Waves FM module, the eastern and western boundaries were defined as lateral boundaries and finally boundary conditions for the northern boundary of the local model were extracted from the numerical results of regional wave model [1]. The local wave model shows a wavelength of 3560 meters in the northern boundary and wavelength of 2000 meters in the western and eastern boundaries (Figure 1b).

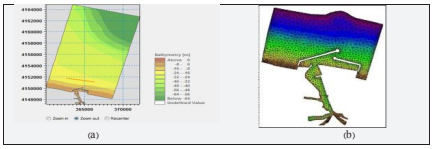

Figure 1. Study area of regional model and the local model

3. Utilized Software in Modeling

In this research, the wave transmission process from deep water to shallow water within Anzali Harbor (after construction of the new breakwaters) has been simulated using hydrodynamic model of MIKE21.

The FM module of MIKE21 software enables the user to use triangular grids with various areas within and outside of the basin and meshing is carried out based on the required accuracy of the numerical results for the study area.

Figure 2 shows an example of the triangular used mesh for two different models with and without breakwaters extension. Figure 3 shows the satellite/aerial photographs and the bathymetries of study area (before and after extension of breakwaters) that have been made using MIKE21 and hydrographic data for local model.

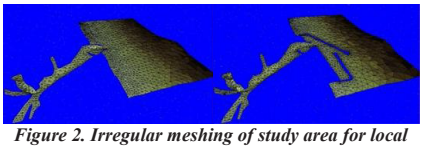

Figure 2. Irregular meshing of study area for local model

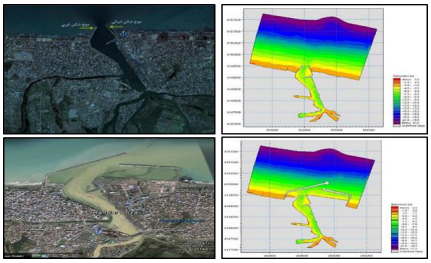

Figure 3. Aerial photographs and the bathymetries of study area used for the local model

4. Results

In this section, after the preparation of depth measurements, the Set up and calibration of the wave model for the local model and the extraction of boundary conditions from the regional model for extraction in the local model of numerical simulation were derived, which In the following, we study the results of this study with respect to the northeast and northwest waves in both cases before and after the development of Anzali harbor breakwaters.

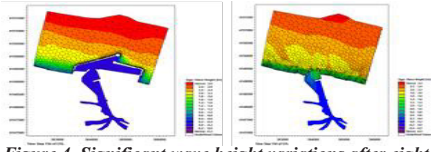

Figure 4. Significant wave height variations after eight days of the model running, the scenario in which wind is blowing from the North West at two states before and after extension of the breakwaters

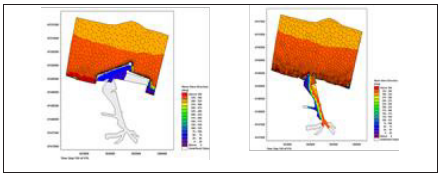

Figure 5. Variations of mean waves direction after eight days of the model running, the scenario in which wind is blowing from the North West at two states before and after extension of the breakwaters

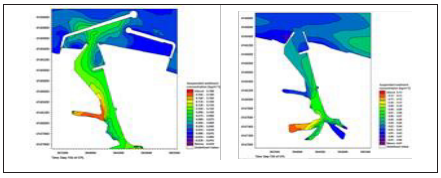

Figure 6. Variation of suspended sediment concentration after eight days of running the model, the scenario in which wind is blowing from the North West at two states before and after extension of the breakwaters

As may be observed from the results, the pattern of waves in the basin at two conditions before and after the development is such a way that height of waves after development plan is mainly lower than that before-development plan so that wave heights ranges between 0.6 -1.4 meters before development plan were reduced to 0.1 -1.0 meters after development plan. In other words, with extension of harbor breakwaters, the aim of development and rest ensuring of the harbor have relatively been achieved. These conditions show existence of the fairly good resting within the harbor after development plan which is also in good agreement with field observations.

Before the construction of new breakwaters, the large amounts of sediments that entered to the channel, discharged through two old breakwaters to the sea due to opening passage and the initial hydraulic gradient. During the rivers flooding, the effects of mud pollutant were visible to a distance of a few kilometers in the sea. But in practice with construction and development of the breakwaters in Anzali harbor, it can be seen that the movements of sediments from lagoon to the basin were controlled and deposited within the harbor and channel.

The above discussion can also be inferred from the sediment concentration output whereas the concentration after development was more than that before development, so that concentration range before development was between 0.030 – 0.055 kilograms per cubic meter and after development of the breakwaters the range was between 0.075 - 0.135 kilograms per cubic meter. Further, currently dragging activities tentatively confirm the results of this research study.

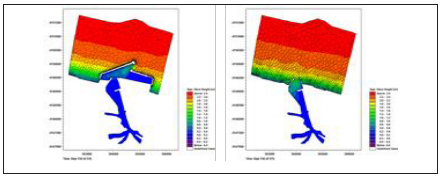

Figure 7. Significant wave height variations after eight days of the model running, the scenario in which wind is blowing from the North East at two states before and after extension of the breakwaters

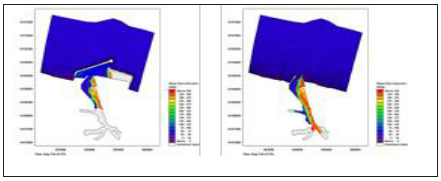

Figure 8. Variations of mean waves direction after eight days of the model running, the scenario in which wind is blowing from the North East at two states before and after extension of the breakwaters

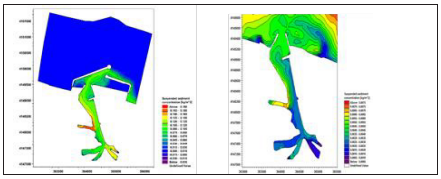

Figure 9. Variation of suspended sediment concentration after eight days of running the model, the scenario in which wind is blowing from the North East at two states before and after extension of the breakwaters

The overall essence of the results from this scenario is similar to the previous scenario, but the range of variations in wave and sediment parameters are different.

According to the modeling results for different scenarios, it can be concluded that Anzali harbor has a relatively acceptable condition for pond relaxation, but sedimentation in the pond and dredging with low time intervals is a problem for Anzali harbor. This problem appeared after the construction of new port breakwaters, which led to frequent dredging inside the pond.

Numerical simulation results indicate that breakwaters development, conditions are created where the pond ambience is calm and this pond relaxation provides conditions for sedimentation. With the construction of a new breakwaters, some of the sediments that were naturally entering the sea before the construction of the breakwaters were trapped, in other words, the developed part of the port acts as a sediment trap.

5. References

[1] DHI Software, complete package of MIKE ZERO & MIKE 21-Spectral Waves FM ,Hydrodynamic Module, User Guide, (2005,2007.2011)

A COUPLED FVM-DEM NUMERICAL MODEL FOR SIMULATION OF WATER WAVE INDUCED PORE PRESSURE IN POROUS SEABED

Mohammad Hadi Jabbari[1], Kourosh Hejazi[2] and Mohsen Soltanpour [3]

1) Department of Civil Engineering, K. N. Toosi University of Technology, Tehran, Iran, mrmhjabari@gmail.com
2) Department of Civil Engineering, K. N. Toosi University of Technology, Tehran, Iran, hejazik@kntu.ac.ir
3) Department of Civil Engineering, K. N. Toosi University of Technology, Tehran, Iran, soltanpour@kntu.ac.ir

1. Introduction

The interaction between water waves and porous seabed is one of the most attractive subjects in the field of coastal engineering. The evaluation of the wave-induced response of a porous seabed is a key factor in the study of sediment transport, because sea beds may be liquefied under the cyclic pressures induced by the incoming waves which provides potential nearshore sediment transport. In the last few decades, numerous models for the wave-induced seabed response have been developed with various assumptions. The examples for these models include [1]: uncoupled models, consolidation models, u–p approximation, dynamic models and poro-elastoplastic models. However, The seabed properties change by wave loadings, which in turn affect the wave propagation, a mechanism which has not been considered in the aforementioned models. The coupled FVM-DEM method has been successfully studied for modeling water seepage flow [2]. In this study a coupled FVM-DEM model is introduced which simulates the wave-porous medium interaction and includes the solution for the fluid and solid parts simultaneously.

2. Methodology

A two-dimensional coupled finite volume method (FVM) and discrete element method (DEM) model has been developed to simulate the pore water pressure buildup in the wave-induced seabed. The fluid motion was formulated by Navier-Stokes equations with the consideration of porosity and fluid-particle interaction terms [3]. The solution of the fluid flow is based on a 2DV model, (WISE; Width Integrated Stratified Environments) developed by Hejazi et al [4]. WISE uses finite volume method to discretize Reynolds-averaged Navier–Stokes equation on a structured non-orthogonal curvilinear staggered mesh. The model was further developed to include the wave-porous medium interaction using extended continuity and Navier-Stokes equations. The motion of the individual particles was numerically simulated using the DEM with the inclusion of the interaction with the fluid. DEM provided a solution of particle-particle collision problem by integration of Newton's second law equation based on a second order finite difference approach.

3. Discrete Element Simulation

The motion of discrete particles or solid phase was solved as follows:

$$m_i(du_i/dt) = f_c + f_{fp} + m_i g \quad (1)$$

$$I_i(d\omega_i/dt) = M_i \quad (2)$$

where u_i, ω_i , f_c, f_{fp} and M_i are particle velocity, angular velocity, particle contact forces, fluid particle interaction force and torque, respectively. The numerical code developed herein, solves equations (1) and (2) for a granular assembly. To evaluate the performance of the model, the experimental results [5] of the biaxial compression of 158 hexagonally packed disks were compared with the results of the numerical simulation and are presented in figure 1.

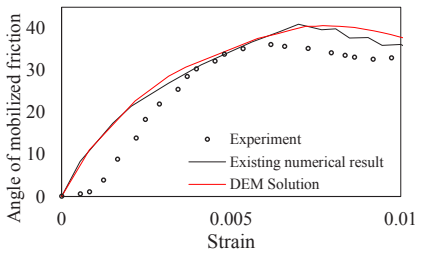

Figure 1. Biaxial compression of hexagonally packed disks, comparison of numerical and experimental results.

In these two dimensional systems, the angle of mobilized friction ($\emptyset_m$) was calculated and compared with existing numerical and experimental results.

4. 1D Upward Seepage Flow Simulation

The critical hydraulic gradient through saturated particles leads to failure of soil column. The coupled FVM-DEM model was used for the solution of the seepage flow failure problem. The physical and geometrical parameters are in accordance with Chen et al [2]. One hundred spherical particles were consolidated under gravitational and buoyant forces, and then the inflow was fed with a superficial velocity of 0.005 m/s , where the

pore water pressure exceeded and led to upward displacement of particles. Figures 2 and 3 show the comparison of the soil particles displacements and excess pore water pressures through the soil column with the simulated numerical results, respectively.

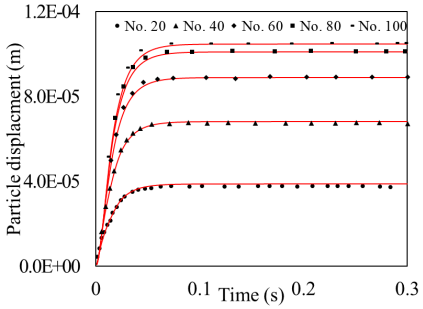

Figure 2. Displacements of soil particles (No. 100 is the index of the last particle located at the soil surface).

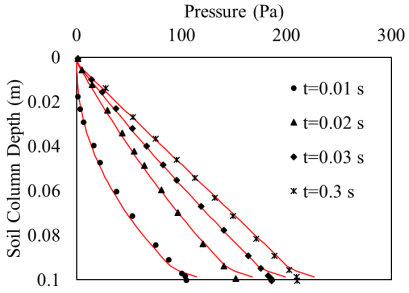

Figure 3. Excess pore water pressure at different times of seepage flow (t = 0.01, 0.02, 0.03 and 0.3 s).

In above figures solid lines represent results of the numerical model.

5. 2D Water Waves Induced Pressure in Porous Seabed

Pore pressure induced in seabed under the propagation of standing waves has been simulated by the FVM-DEM framework. The physical experiments used herein for the comparisons have been conducted in a wave flume [1]. The sketch of the experimental set-up is shown in figure 4. The generated wave height and period were 5.1 cm and 1.5 s, respectively. The length of the test section, filled by sand, was 2.0 m. A vertical wall was located at the flume downstream end to reflect induced waves and result in standing waves.

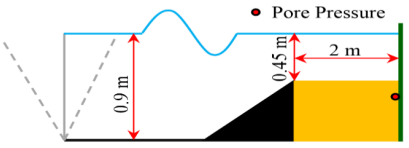

Figure 4. Sketch of the experimental set-up [1].

For the simulations, the spatial domain was divided by 200x10 control volume cells. The dimension of each cell along the horizontal axis was 0.24 m. The bed porosity was 0.4. Pore water pressure changes were recorded near the wall during the experiment. By comparing the simulated pore pressure results with the existing analytical and experimental data good agreement was achieved at 10 cm below the mud line (Figure 5).

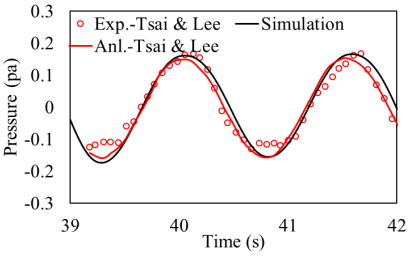

Figure 5. Pore water pressure time series.

6. Conclusions

A coupled FVM-DEM solver was developed for the simulation of induced pore water pressure in seabed under wave action. The simulated results showed the model is capable of simulating the interaction of the wave-porous medium.

7. References

[1] Jeng, D.S., *Book: Porous Models for Wave-seabed Interactions*, Shanghai Jiao Tong University Press,China , 2013.

[2] Chen, F., Drumm, E.C., "Coupled discrete element and finite volume solution of two classical soil mechanics problems", *Computers and Geotechnics*, 38, may 2011, pp. 638-647.

[3] Anderson, T. B., and Jackson, R., "A fluid mechanical description of fluidized beds", *Industrial & Engineering Chemistry Fundamentals*, 18, 2, September 1967, pp. 527-539.

[4] Hejazi, K., Soltanpour, M., and Sami, S., "Numerical modeling of wave–mud interaction using projection method", *Ocean Dynamics*, 63, 9, may 2013, pp. 1093-1111.

[5] O'Sullivan, C., and Bray, J. D., ''A comparative evaluation of two approaches to discrete element modelling of particulate media'', in *Proceedings 4th International Conference on Discontinuous Deformation*, Scotland, UK, June 5-8 2001, pp. 97–111.

A COMPREHENSIVE STUDY ON THE PERSIAN GULF HYDRODYNAMICS USING PMO DYNAMICS NUMERICAL MODEL

Zahra Ranji[1], Kourosh Hejazi[2], Mohsen Soltanpour[3], S.Mahya Hosseini[4] and Zohreh Hajisalimi[5]

1) Civil Engineering Dept., K. N. Toosi University of Technology, Tehran, Iran, zranji@mail.kntu.ac.ir
2) Civil Engineering Dept., K. N. Toosi University of Technology, Tehran, Iran, hejazik@kntu.ac.ir
3) Civil Engineering Dept., K. N. Toosi University of Technology, Tehran, Iran, soltanpour@kntu.ac.ir
4) Civil Engineering Dept., K. N. Toosi University of Technology, Tehran, Iran, sm.hoseini@mail.kntu.ac.ir
5) Port and Maritime Organization, Tehran, Iran, hajisalimi.zohreh@yahoo.com

1. Introduction

Tides, winds, wave radiation stresses and density and thermal gradients are the main factors that affect the circulation pattern in the Persian Gulf. In shallow waters, sharp gradients in bathymetry make the hydrodynamics more complicated. Since numerical modeling is highly dependent on the input parameters, i.e. coastline, bathymetry, and open boundaries, model calibration is also required to optimize unknown parameters i.e. bed roughness.

This study utilizes an Iranian numerical model (PMO Dynamics) for simulation of hydrodynamics in the Persian Gulf. For the wind field the model uses the simulated results of WRF model Ghader et al. (2016), and radiation stresses are imposed from WaveWatchIII modeling results Jedari Attari et al. (2016). A new approach for bed friction calibration is also presented.

2. Numerical Model Setup

A precise bathymetry which is a combination of GEBCO and local measurements was established (Figure 1) and assembled with GSHHG coastline to be employed for the grid generation.

Alternative locations for the open boundary were also considered (Fig. 2). These locations were examined upon the availability of the field observations and in conjunction with the best fitting global tide model to adopt the boundary condition. A previous study reveals that TPXO atlas Egbert and Erofeeva (2002) is the best candidate for supplying boundaries Ranji et al. (2017). A wide network of measurements along the Iranian coastline was employed for the calibration and validation processes (

Figure *3*). Mean measured velocities were used for comparisons with the depth-averaged simulated velocities.

An unstructured grid including 82598 cells and 42874 nodes (Figure 4) was generated by PMO Dynamics mesh generation tools. Wind fields and wave radiation stresses were also applied in the simulations. Grid sizes varied in a range between 200 to 5000 m for shallow to deep water zones, respectively.

Time step is a key factor for maintaining the model stability, which with the implementation of wind and wave radiation stresses need to be taken as small as 1 second.

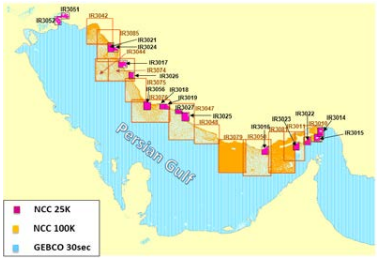

Figure 1. Available bathymetry data

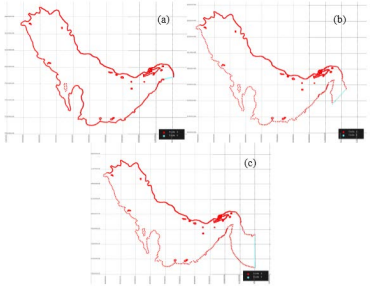

Figure 2. Different locations for the open boundary (a. Sirik, b. Koohmobarak, c. Jask)

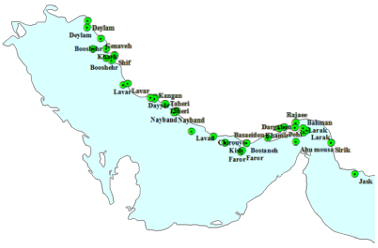

Figure 3. Measurement stations

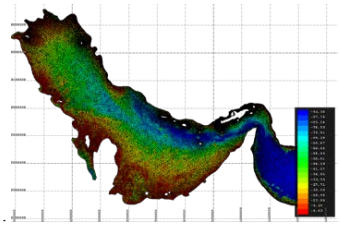

Figure 4. Final computational grid

Calibration was performed using an innovative and simple idea. For different Manning coefficients, error statistics, i.e. RMS, R^2 and correlation coefficients at different stations were computed. Then according to the statistics, the maximum error among the measurements was found. Next, the difference of the rest of stations with the maximum error was computed and another sorting according to the residuals was performed and the most accurate station was found, where the maximum weight of 1 was assigned to this station. For the rest of the stations, weights were computed by dividing their computed weight to the weight of the most accurate station (Table 1). The final Manning coefficient was then computed as follows:

$$M_f = \frac{\sum_{i=1}^{n} W_i M_i}{\sum_{i=1}^{n} W_i} \quad (1)$$

where W is attributed weight, M is examined Manning and M_f is the optimum Manning coefficient.

Table 1. Calibration procedure

1- Max($RMSE_i$) or Min(R^2_i) or Min(COR_i)
2- Max($RMSE_i$)- $RMSE_i$ or R^2_i -Min(R^2_i)
3- Max(Max($RMSE_i$)- $RMSE_i$) or Max(R^2_i -Min(R^2_i))
4- W_i=step(2)/step(3)
5- Equation (1)

3. Results and Discussion

Examining different locations for the open boundary, confirms that simulation results at the vicinity of the open boundaries, i.e. Larak and Sirik stations, are in a better agreement with the measurements. So Jask-Almasnaeh was selected as the best location for the open boundary.

Sensitivity analysis results revealed that the bed roughness was the most influential parameter, which required to be optimized. Smagorinsky coefficient was not a major factor, expect for the highly turbulent regions, e.g. around the islands, but still less significant compared with the bed roughness.

It was also found that the wind effect had a significant impact on water elevation, in shallow water zones, e.g. the area behind the Qeshm Island. Application of the wave radiation stress had lesser influence on the water level compared to the current speed, and may be neglected in 2D simulations. The reason is that the water body involved with the wave action is the surface layer, where the 2D models simulate the water column as a single depth averaged layer. Calibration results revealed that the optimized Manning coefficient should be taken equal to 0.0161 ($s/m^{1/3}$). Validation results are tabulated in Table 2 and shown in Figure 5.

The system was found reliable for further applications and may be utilized for three-day forecast of water levels and current speeds.

Table 2. Model validation statistics index

Station	RMSE	correlation
Bostaneh	0.139	0.97
Booshehr	0.10	0.97
Genaveh	0.10	0.98
Deylam	0.11	0.99
Lavar	0.07	0.99
Larak	0.23	0.95
Lavan	0.10	0.97
Lavan-u	0.12	0.67
Lavan-v	0.17	0.82
Larak-v	0.21	0.68
Larak-u	0.19	0.57

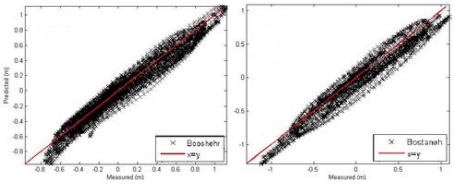

Figure 5. Validation results at Booshehr (left) and Bostaneh (right) stations

4. Acknowledgements

This study was conducted as part of "wind-wave-current forecast studies of the Persian Gulf" project and was supported by PMO, which is highly appreciated.

5. References

[1] Egbert, G. D. and Erofeeva, L., "Efficient inverse modeling of barotropic ocean tides.," *Journal of Atmospheric and Oceanic Technology,* vol. 19, pp. 183-204, February 2002.

[2] Ghader, S., Yazgi, D., Soltanpour, M., and Nemati, M. H., "Prediction of surface wind over persian gulf using an ensemble prediction system developed for the wrf model," in *12th International Conference on Coasts, Ports and Marine Structures*, Tehran, 2016, pp. 97-98.

[3] Jedari Attari, M., Haghshenas, S. A., Soltanpour, M., Razavi Arab, A., Hajisalimi, Z., Ahmadi, S. J., *et al.*, "Developing the persian gulf wave forecast system," in *12th International Conference on Coasts, Ports and Marine Structures*, Tehran, 2016, pp. 71-72.

[4] Ranji, Z., Hejazi, K., Soltanpour, M., and Allahyar, M. R., "Inter-comparison of recent tide models for the persian gulf and oman sea," in *International Conference on Coastal Engineering (ICCE)*, Antalya, Turkey, 2017.

TWO-WAY COUPLING OF 2D AND 3D MODELS FOR THE FORECAST OF HYDRODYNAMICS IN THE PERSIAN GULF

Ehsan Sarhadizadeh[1], Kourosh Hejazi[2], Mohsen Soltanpour[3] and Mohammad Hossein Nemati[4]

1) Department of Civil Engineering, K. N. Toosi University of Technology, Tehran, Iran, sarhadi@gmail.com
2) Department of Civil Engineering, K. N. Toosi University of Technology, Tehran, Iran, hejazik@kntu.ac.ir
3) Department of Civil Engineering, K. N. Toosi University of Technology, Tehran, Iran, soltanpour@yahoo.com
4) Ports and Maritime Organization, Tehran, Iran, mhn@gmail.com

1. Introduction

Over the past few decades, numerical modeling of ocean circulation with complex geometries became prevalent with rapid growth of computing power. As a result, researchers have been able to develop multiscale models for accurate and efficient simulation of oceans in large scale.

1D models are applicable for predicting scouring and sedimentation while 2D and 3D models with hydrostatic pressure assumption can be used for shallow waters where secondary flows and vertical gradients are negligible. However, in cases such as lakes, rivers with flood plains, intertidal zones and continental shelves, due to high-pressure depression changes and presence of strong secondary currents, shallow water assumption cannot be applied. Accurate perdition of velocity field and the water surface in these cases requires non-hydrostatic 3D models. Generating a high quality mesh and imposing suitable surface and bottom boundary conditions are two of the most challenging aspects of such 3D models which makes them computationally demanding. An effective way to address this issue is to couple numerical models.

In the present study, numerical domain is comprised of two independent 2D and 3D unstructured triangular grids. A two-way coupling was employed by mapping the solution of one mesh onto another in overlapping regions at each time step. Therefore, performance and accuracy of each model was maintained while the total accuracy was improved due to more accurate imposition of initial and boundary conditions.

2. The Coupled Model Structure

In the present model, the simulation is carried out by employing the PMO Dynamics (Persian Model for Ocean Dynamics) 2D model using the finite volume method on the entire computational domain at the first time step. After the simulated 2D values, such as horizontal velocities and the water surface elevations are obtained, the values for the 3D model [5] at desired locations are interpolated using an advanced algorithm developed by Beluga branch of the TELEMAC [4]. In order to increase the computational efficiency, these values are used as a preliminary estimation (initial conditions) for the 3D model. Again, these calculated values update the corresponding previous values obtained from the 2D model, such that the values at the 2D model nodes are averaged from the 3D simulated results. In the two-way coupled model, not only the 2D model provides the boundary values for the 3D model, but also the 3D simulated values are used to correct the corresponding 2D values. This structure greatly facilitates rapid convergence and increases the accuracy of the model in calculating the flow parameters, indicating the interaction of 2D and 3D models on each other. This method gives more accurate results in the coupled area for the 2D model.

3. Verification of the Coupled Model

In order to evaluate the performance of the model on a real scale and under real conditions, the model was setup for the Persian Gulf region, whereas the Persian Gulf and part of the Oman Sea were considered as the computational domain.

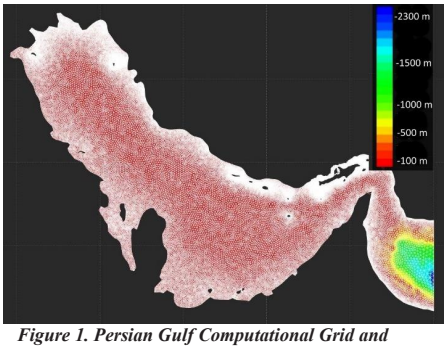

Figure 1. Persian Gulf Computational Grid and Bathymetry.

A high-resolution shoreline data set was implemented using a Global Self-consistent, Hierarchical, High-resolution Geography Database (GSHHG); the bathymetry was extracted from Two-minute gridded Earth

Topographic (ETOPO 2) database and Iranian National Cartographic Center data (Figure 2).

A 2D unstructured triangular mesh was created on the domain with 42874 nodes. The results of Hybrid Coordinate Ocean Model (HYCOM) were used as initial and boundary conditions for the 2D model. Tidal data, based on the series of fully global models of ocean tides (TPXO), were used on the open boundaries. To get realistic results, weather conditions were implemented from the simulations of the Weather Research and Forecasting (WRF) model.

Also, in order to account for the effect of waves on the hydrodynamics, wave radiation stresses were applied to the model using the full-spectral 3rd generation wave model WAVEWATCH III.

Validation of the simulations in the present modeling strategy was based on the detailed field measurements using Acoustic Doppler Current Profiler (ADCP) in Bushehr port. A 3D unstructured triangular mesh with 10 layers in the sigma coordinate was created with 9345 nodes (Figure 3).

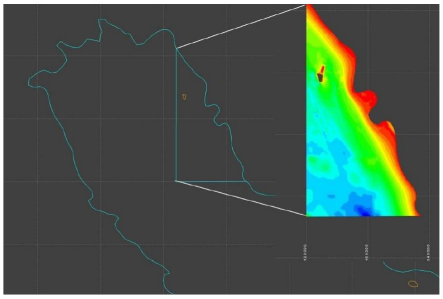

Figure 4. Bathymetry of Bushehr Port

4. Results and Conclusions

Figure 5 shows the comparison of water level elevations of 2D, 3D and the coupled model.

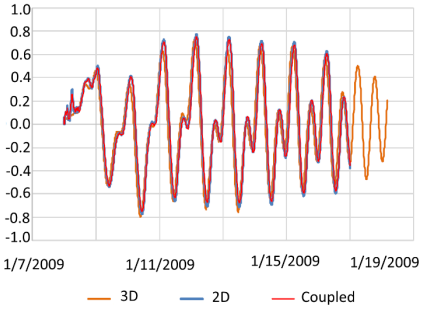

Figure 6. Model Comparison.

The figure demonstrates a reasonable agreement between the computed results of the coupled model, 2D and 3D models individually.

It can be concluded that the presented coupling system is efficient in terms of computational time and accuracy. The proposed approach effectively combines advantages of a 2D model, where shallow water assumption can be applied, and a 3D model, where vertical effects e.g. salinity, temperature and density gradients are important. The developed model improves the convergence rate at each time step as well as the overall accuracy.

5. Acknowledgments

This study was funded by the Ports and Maritime Organization.

6. References

[1] Dallimore C.J., Hodges B.R., Imberger J., "Coupling an underflow model to a three dimensional hydrodynamic model". *J. Hydraulic Eng* 2003.

[2] Namin M.M., Falconer R.A., "An efficient coupled 2-dh and 3-d hydrodynamic model for river and coastal applications" *Proceedings of 6th International Conference on Hydroinformatics*, Singapore, Singapore, World Scientifc, pp. 374-382. 2004.

[3] Zounemat-Kermani M., Sabbagh-Yazdi S.R., "Coupling of two- and three-dimensional hydrodynamic numerical models for simulating wind-induced currents in deep basins". *J. Computers & Fluids*, 2010.

[4] Gourgue O., Chen M., Delgado R., Sarhadi E., Schramkowski G. and Vanlede J., "An unstructured grid model for the Belgian continental shelf and the Scheldt estuary", *JONSMOD 2014, Joint Numerical Sea Modelling Group Conference*, Brussels, Belgium, 2014.

[5] Sami S., Hejazi K., "A Three-dimensional Non-hydrostatic Numerical Model for Prediction of Ocean Currents", *12th International Conference on Coasts, Ports and Marine Structures, ICOPMAS* 2016.

SHORT-TERM ANALYSIS OF RANDOM SEA WAVES IN THE PERSIAN GULF

Sepehr Samiee Nasrabadi[1] and Mohsen Soltanpour[2]

1) Civil Engineering, K. N. Toosi University of Technology, Tehran, Iran, sepehr.samiee@email.kntu.ac.ir
2) Civil Engineering, K. N. Toosi University of Technology, Tehran, Iran, soltanpour@kntu.ac.ir

1. Introduction

Waves are the most important phenomenon to be considered among the environmental conditions affecting maritime and coastal structures, because they exercise the greatest influence. There is a great amount of randomness in the sea, and statistical techniques need to be used in order to analyze ocean waves. Long-term wave analysis aims to the derivation of statistical distributions that cover many years. However, short-term analysis refers to the analysis of waves that occur within one wave train or within one wave storm [1].

Persian Gulf is a shallow, semi-enclosed marginal sea, nearly 1000 km long water body located in the south of Iran with an average depth of 40 meter and a maximum depth of 170 m at its entrance, the Strait of Hormuz. Literature shows few studies conducted on the tide behavior and general circulation and currents of the Persian Gulf but the analysis of its wave characteristics are limited. Employing the offshore measured field data at different locations of the north coast of the Persian Gulf and the Strait of Hormuz, the present study offers some findings of the short-term characteristics of the irregular waves in these water bodies as well as the analysis of the field data. The representative waves at measuring stations are also calculated and compared with the general statistically derived relations at other seas.

2. Field Measurements

Starting from 2005, a number of large projects were defined by the Iranian Ports and Maritime Organization (PMO) along Iranain coastlines. In these projects, comprehensive field measurements including continuous data of currents, offshore and nearshore waves at different locations of the Persian Gulf and Strait of Hormuz were recorded. Figure 1 shows the study area and the locations of deployed instruments. Four Nortek AWAC instruments, namely Khark, Taheri, Lavan and Faror, all deployed at 25 m water depths were chosen among wave stations to represent the variety of wave characteristics at the north, center and east parts of the Persian Gulf. The selected stations are not affected by islands or other geomorphological features and there are no fetch limitations through major wind directions [2].

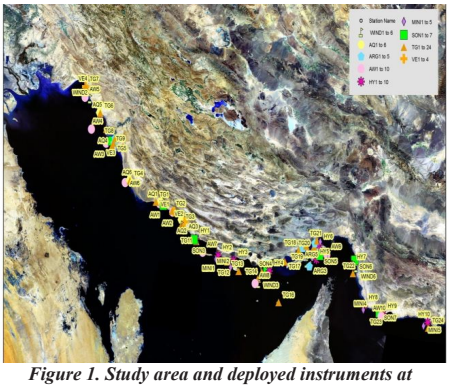

Figure 1. Study area and deployed instruments at monitoring and modelling studies (phases 2, 3 and 4)

3. Data Analysis and Discussion

One-year Acoustic Doppler Current Profiler (ADCP) data from four stations were employed in this study. Nortek AWAC instruments were equipped with AST (Acoustic Surface Tracking) system that also allows detection of short period surface waves. This vertically oriented transducer in the center of the AWAC allows direct measurements of the bottom distance to the sea surface by using a simple echo sounder. The AST measurements enable both time series, which result to direct estimation of representative wave heights such as H_{10} and H_{max}, and spectral analyses.

AWAC measurements were extracted using Storm Software (v1.17.05) of Nortek. The data was carefully examined to observe the storm events, storm directions and frequency of occurrences. Figure 2 shows a sample storm at Khark Station [2].

Rayleigh distribution is normally adopted as an approximation to the distribution of individual wave heights. This distribution was originally derived by Lord Rayleigh in the late 19th century to describe the distribution of the intensity of sounds estimated from an infinite number of sources. Longuet-Higgins (1952) demonstrated that Rayleigh distribution is also applicable to the wave heights in the sea [3]. Following the Rayleigh distribution, the representative wave heights can be estimated as

H_{10}=1.277H_{mo} (1)

H_{max}=1.6-2.0H_{mo} (2)

in which H_{mo} , H_{10} and $H_{\max}$ represent significant wave height, one-tenth highest wave height, and highest wave height, respectively.

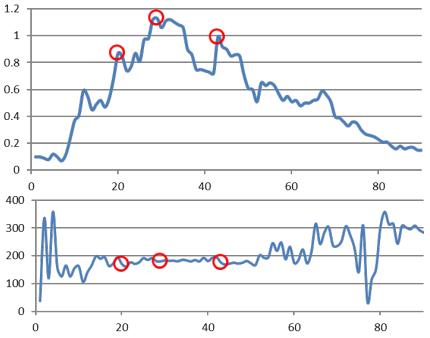

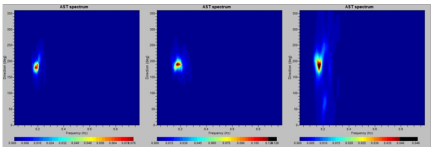

Figure 2. A sample storm at Khark due to north wind

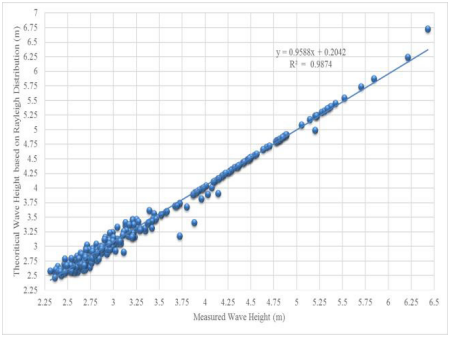

Figure 3. Comparison between measured and estimated one-tenth highest wave heights (H_{10}).

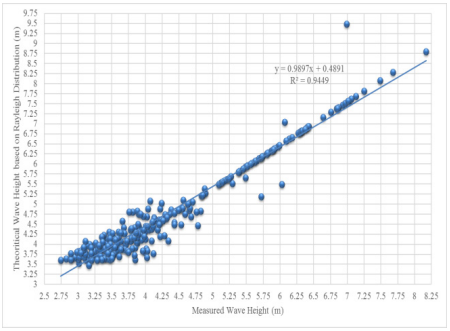

Figure 4. Comparison between measured and estimated highest wave heights (H_{max}).

Figures 3 and 4 show sample comparisons between the measured representative wave heights of H_{10} and H_{max} with Eqs. (1) and (2) at Lavan Station, respectively. A favorable agreement is observed between the data and theoretical equations.

4. Summary and Conclusion

The large valuable data set of Monitoring Projects at the north coastline of the Persian Gulf were analyzed to study the characteristics of storm waves and common representative waves in the area. It was concluded that Rayleigh distribution provides a good approximation to the distribution of individual wave heights, which are defined by the zero-upcrossing and zero-downcrossing methods.

5. References

[1] Goda Y., "Random seas and design of maritime structures", *Advanced Series on Ocean Engineering–Volume 15*, *World Scientific Publishing Co.*, 2000, 443 p.

[2] Niroomand B., Kamalian R., Soltanpour M., Allahyar M. R. "Study of the Wave Spectra in the Persian Gulf", *34th International Conference on Coastal Engineering, ASCE, 2014 (poster).*

[3] Longuet-Higgins, M. S. (1952). "On the statistical distribution of the heights of the sea waves", *Journal of Marine Research, 11(3),* 1952, 245–266.

PORT FACILITY MANAGEMENT USING AUGMENTED REALITY IN GIS

Seyyed Esmail Mousavi[1] and Jalal Karimi[2]

1) Department of Coast and Port Management, Imam Khomeini (MBUH) Port, iran, smlmousavi26@gmail.com
2) Ports and Maritime Organization (PMO), Tehran, Iran, Jkarimi@pmo.ir

1. Introduction

Because of the numerous problems and financial - Life losses caused by mistakes in the location of port facilities, such as the location of water pipes, firefighting, oil, sewage, etc., it is necessary to investigate and prepare the exact geographic information systems (GIS) of Infrastructures. Managers and decision-makers in this field try to get better solutions to their goals by taking advantage of different aspects of the scientific environment. Advances in the information technology and over-the-web-related technologies [3], such as Ubiquitous computing, Internet of Things, and the Extreme Sensor Network, have driven GIS towards the Ubiquitous GIS, enabling this new generation of GIS to enter the field works. Monitoring the status of this infrastructure gives policy makers, planners and decision makers the required information about their current state of affairs, and GIS is the essential tool for analyzing this situation [4]. Therefore, GIS is used to store and organize information related to Infrastructure [5].

Underground infrastructure departments in the port, including electricity, gas, water and sewage, telecommunications, and energy infrastructure, are dependent on GIS to manage their infrastructures [6]. With the advent of science and technology, the management of this infrastructure has led to more automation. When an incident occurs in installation systems, the entire port facility is affected and may cause secondary accidents. These systems are also destroyed by natural disasters such as floods, earthquakes, storms and tsunamis.

2. Augmented Reality

Virtual reality is a direct or indirect, real-time visualization of the physical world that is composed of Augmented Reality by adding virtual information generated by the computer to reality. The augmented reality is an interactive environment, and it is documented in a three-dimensional fashion while combining true and virtual objects together. The augmented reality is defined as follows: Augmented Reality is the background of computer studies that leads to the combination of real world and computer-generated data. AR can include the use of moving tracking data, identifying the fiducial mark using the visual machine, and creating controlled environments with any number of sensors and activators [3]. The Millgram chain in Figure 1 relates virtual reality to the real world, and between them there is an augmented reality and added virtual reality.

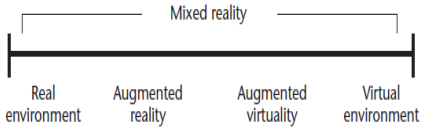

Figure 1. The Millgram chain.

In the past, the augmented reality was lower than the lab, but today, with smart phones, it is possible to implement this technology on mobile phones, and this itself provides the most advanced components of any location, anytime, every service, every user and each network. The increased processing power and the availability of tools such as gyroscopes, accelerometers, compasses, mobile camera and other sensors, along with a display on the device, have created the proper capabilities for producing AR programs. In fact, the main advantage of these systems is that they have all the necessary equipment and that they need to purchase devices such as expensive HMDs and not add them on these devices. Figure 2 shows an overview of these infrastructures that have been visualized using AR.

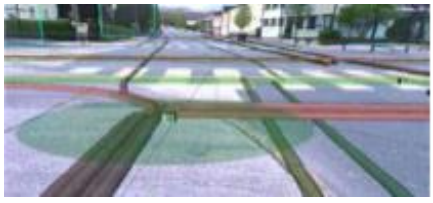

Figure 2. Display the infrastructure on an AR device

In Figure 3, system architecture is proposed to retrieve ground-based information in an augmented reality application. In order to visualize the pipes, it is necessary to convert the data from the database into a simple GML format. With the help of the GPS, the current position of the user is detected in the field, with this information is asked from a WFS to retrieve relevant data online and in real time for visualization of the AR. Data modified in the field can be matched in the database.

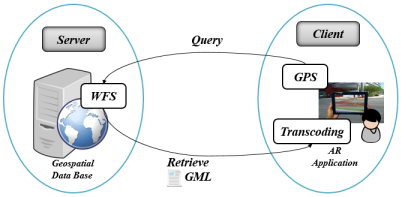

Figure 3. Proposed system architecture to retrieve and display facility information.

3. Mobile GIS

One of the major tools for organizing GIS information is Mobile GIS. The Mobile GIS is the development of GIS technology from the office that is capable of receiving, storing, updating, manipulating, analyzing and displaying Provides spatial information for fieldworkers; and provides the possibility of exchanging data between field data sets and GIS. This technology combines one or more technologies, such as mobile devices, GPS, and wireless information to access GIS information. This portable instrument can be used locally and provides information about the facility and sends it to the relevant office. Since in the normal state, visual inspection of underground infrastructure is impossible, it is difficult to identify or estimate their position for reconstruction or replacement.

Some companies use Mobile GIS systems for local inspections , in Table 1, a comparison between Mobile GIS and AR was performed in local site inspections of underground facilities. This comparison shows that since AR has a more intuitive user interface, it has more precision and speed, and it works more automatically, which means that the user has less dependency, making it faster and faster.

4. Conclusion

The purpose of this paper was to manage port facilities using augmented reality in GIS. In this paper, a comparison was made between different visualization techniques and on-site visits, including Augmented Reality and Mobile GIS. This comparison shows that the augmented reality method is much more suitable for this application than Mobile GIS. Another comparison was made between existing technologies for determining the location of underground utilities. This article showed that Ubiquitous GIS can have many applications in the field of infrastructure. For example, the use of this technology in monitoring and control of infrastructures, maintaining the security of infrastructures, their three-dimensional visualization, integration of information with the use of spatial data infrastructure between departments and many other applications is mentioned. It is recommended to use this technology in the future development of the Ports GIS.

Table 1. Comparison between Mobile GIS and AR in Local Inspection.

	AR	Mobile GIS
Visualization techniques	Display the link between GIS data and the real environment	Hide the link between GIS data and the real environment
Infrastructure addressing	True addressing	Problem in addressing
Interpreting data	By machine (auto)	By user (manual)
Access to data in place	Access to complex data	Unable to access
System development	Possibility of development	limited
Fieldwork operations and maintenance	More effectively	limited
Unwanted Damage	Low	High
Overall safety at the site	High	Low
Breakdown management, leakage detection and failure	Easy and useful	Hard
Tracking and positioning	Fast and accurate	Slow and low accuracy
Precision	High	Low
Display of Overlay	Better and faster	Inappropriate
Interactive tools	Real-time and direct without post-processing	Indirect and need post processing
Battery life of the device	Low	High
Cost	High	Low

5. References

[1] Difallah, D. E., Cudre-Mauroux, P., & McKenna, S., "Scalable anomaly detection for smart city infrastructure networks", Internet Computing, IEEE, 17(6), 39-47, 2013.

[2] Heydari, N., Mansourian, A., Taleai, M., & Fallahi, G. R.,"Ontology-based GIS web service for increasing semantic interoperability among organizations involving drilling in city of Tehran", In 11th GSDI World Conference (GSDI 11), Spatial Data Infrastructure Convergence: Building SDI Bridges to Address Global Challenges, POSTER FORUM, Rotterdam, The Netherlands, 2009, June.

[3] Ho Lee, S., Hoon Han, J., Yigitcanlar, T., & Taik Leem, Y., "Ubiquitous infrastructure: urban infrastructure planning and management experience of Korea", 2008.

[4] Wang, H., Zhang, Y., & Cao, J., "Ubiquitous computing environments and its usage access control", In Proceedings of the 1st international conference on Scalable information systems (p. 6). ACM. 2006, May.

[5] Tulloch, M., & Hu, W., "A proposed solution for mapping underground utilities for buried asset management." Ryerson Graduate Student Research Article, 2005.

[6] Schall, G., "Handheld Augmented Reality in Civil Engineering", proceedings of Rosus09, 19-25, 2009.

NUMERICAL MODELING OF UNDERTOW CURRENT BY INCOMPRESSIBLE SMOOTHED PARTICLE HYDRODYNAMICS (ISPH) METHOD IN THE SURF ZONE

Mohammad Ahmadi[1] and Kourosh Hejazi[2]

1) Dept. of Civil Eng., K. N. Toosi University of Technology, Tehran, Iran, m.ahmadi8733@gmail.com
2) Dept. of Civil Eng., K. N. Toosi University of Technology, Tehran, Iran, hejazik@kntu.ac.ir

1. Introduction

The undertow current is a near-bed and sea-level current that compensates for the mass transfer of water to the shore. In this paper, the Lagrangian method of incompressible smoothed particle hydrodynamics has been deployed to simulate the undertow current. To account for the surface roughness a wall function is implemented in the model. The sub-particle scale turbulence has also been included in the model. The capability and accuracy of the new model for free surface simulations, and modeling the undertow current was examined and confirmed.

2. Lagrangian Governing Equations

The governing equations read as follows:

$$\frac{1}{\rho}\frac{d\rho}{dt} + \nabla \boldsymbol{V} = 0 \qquad (1)$$

$$\frac{D\vec{V}}{Dt} = -\frac{1}{\rho}\vec{\nabla}P + \vec{g} + \nu_0\nabla^2\vec{V} + \frac{1}{\rho}\vec{\nabla}\tau \qquad (2)$$

where ρ is the fluid density, t is the time, $\vec{V}$ the velocity vector, P pressure, g the gravity acceleration, v_0 is the physical viscosity, and τ is the shear stress of sub-particle scale (SPS) turbulence.

3. Implementation of Surface Roughness in ISPH

According to Svensson and Hansen [4], the study of undertow current includes two perspectives: to select the appropriate boundary conditions for the undertow current, and to determine the shear stress of the bed.

Wall roughness increases the wall shear stress and breaks up the viscous sub layer in turbulent flows. The wall boundary conditions are implemented by the following equations [5]:

$$u^+ = \frac{U}{u_\tau} \qquad (3)$$

$$y^+ = \frac{\rho u_\tau y}{\mu} \qquad (4)$$

where y is the distance of near wall particle to the solid surface, y^+ is the dimensionless distance from wall and $u^+$is the dimensionless near wall velocity. If the near wall particle is taken to be in the linear or turbulent zone, then equations (5) and (6) apply, respectively:

$$u^+ = y^+ \qquad (5)$$

$$u^+ = \frac{1}{k}ln^{y^+} + B - \Delta B \qquad (6)$$

where B = 5.2. The shift ΔB is a function of the dimensionless roughness height. Figure 1 shows the downward shift in the logarithmic velocity profile.

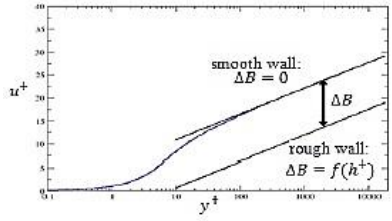

Figure 1: Downward shift of the logarithmic velocity profile

By solving equation(6), u_τ is obtained and $\tau_w$can then be calculated as follows:

$$\tau_w = \rho u_\tau^2 \qquad (5)$$

where τ_w is the shear stress on the wall and u_τ is the friction velocity.

4.Implementation of Turbulence Model

Turbulence is an effective factor in the calculation of turbulent flows with high Reynolds numbers. In this study, the relations introduced by Lo and Shao [2] have been used to model turbulence stresses in the equation of momentum.

4-1. Sub-Particle Scale (SPS) Turbulence

The eddy viscosity assumption (Boussinesq's hypothesis) is often used to model the SPS stress tensor using Favre-averaging as follows:

$$\vec{\tau}_{ij} = \rho\left(2\upsilon_t S_{ij} - \frac{2}{3}k_{sps}\delta_{ij}\right) \qquad (6)$$

where $\vec{\tau}_{ij}$ is the sub-particle stress tensor, $\upsilon_t = (C_s\Delta x)^2|S|$, the turbulence eddy viscosity, k the SPS turbulence kinetic energy, C_s the Smagorinsky constant (0.12), Δx the particle-particle spacing and $|S| = \sqrt{|2S_{ij}S_{ij}|}$, the element of SPS strain tensor.

Following [1], Equation (2) can be written in SPH notation as Eq. (9). The quantic kernels have been used in the present simulations (Wendland 1995) [6].

$$\frac{d\rho_a}{dt} = \sum_b m_b\vec{\boldsymbol{v}}_{\boldsymbol{ab}}\vec{\nabla}_a w_{ab} \qquad (7)$$

$$\frac{d\vec{v}_a}{dt} = -\sum_b m_b\left(\frac{P_b}{\rho_b^2}+\frac{P_a}{\rho_a^2}\right)\vec{\nabla}_a w_{ab} + \vec{g} + \sum_b m_b\left(\frac{4v_0\vec{r}_{ab}\vec{v}_{ab}}{|\vec{r}_{ab}|^2(\rho_a+\rho_b)}\right)\vec{\nabla}_a w_{ab} + \sum_b m_b\left(\frac{\tau_b}{\rho_b^2}+\frac{\tau_a}{\rho_a^2}\right)\vec{\nabla}_a w_{ab}$$

$$\begin{cases} w(r.h) = \frac{7}{4\pi h^2}\begin{cases}\left(1-\frac{q}{2}\right)^4(2q+1) & .\ 0\le q\le 2\\ 0 & .\quad q>2\end{cases} \\ q = r/h \end{cases}$$

$$h = cr\sqrt{L_x^2+L_y^2} \qquad (8)$$

where a is the reference particle and b is its neighboring particle. m_a, ρ_a, P_a, and $\boldsymbol{v_a}$are mass, density, pressure and velocity of particle a, respectively. $\vec{r}_{ab}$ is the distance between particles a and b, w_{ab} is the kernel function, and h is the smoothing length.

5. Model Verification

The model was verified against the experimental measurements of Okayasu etal. [3]. In the experiments the still water depth was d = 40cm, the slope of the beach 1:20 and the incident wave height H=8.5cm. The initial particle spacing was considered to be L_0 = 1cm, and 19690 particles were used in the simulations.

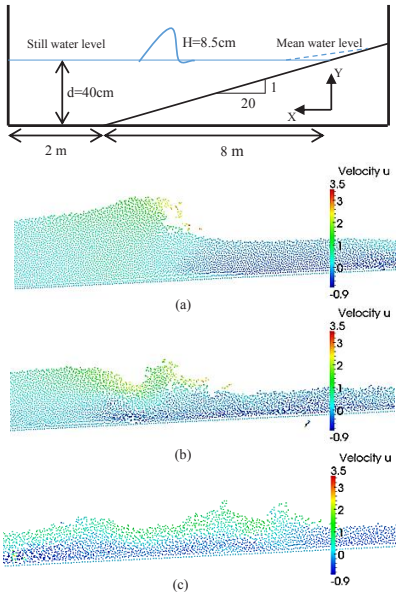

Figure 2 The results of the numerical simulation of model setup of Okayasu et al. (1988) In different sections at a) t = 8.5s, b) t = 9.5s, c) t = 10.5s

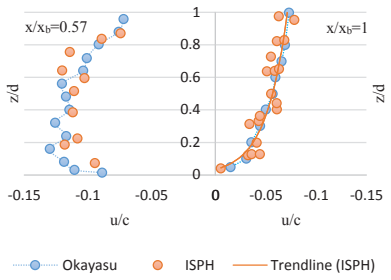

Figure 3 Comparison of numerical simulation results and laboratory measurements by Okayasu et al (1988)

According to Fig.2, after wave breaking, a backflow stream is formed which is the same as the undertow current. The velocity of undertow current near the bed has been reduced due to the presence of friction, which is less effective with the increase of depth. Figure 3 shows the good agreement of the ISPH simulations with the experimental measurements.

6. Conclusions

In this paper, the undertow current was modeled using the ISPH method, where the focus was made on the importance of shear stresses. The existing numerical model was further developed to include the friction and SPS turbulence model. The results of the comparisons of the numerical model simulations with the experimental data showed the accuracy of the ISPH method for undertow current modeling. The results also showed that the shear stress and friction have a significant effect on the calculation of undertow current velocity. Also, by comparing the calculated velocity of the undertow current, it can be concluded that the sediment transport rate is reduced relative to the depth of the coast with the distance from the coastline.

7. References

[1] Darlymple, R.A., and Rogers, B.D., Numerical modeling of water waves with the SPH method, *Coastal Engineering*, 2006, 53(2), pp.141-147.
[2] Lo, E.Y.M. and Shao, S. Simulation of near-shore solitary wave mechanics by an incompressible SPH method, *Applied Ocean Research*, 2002, Vol. 24, No. 5, pp. 275-286.
[3] Okayasu, A., Shibayama, T. and Horikawa, K. 1988, Vertical variation of undertow in the surf zone, Proc. 21st *Coastal Eng. Conf., ASCE*, pp. 478{491.
[4] Svendsen, I. B. and Buhr Hansen, J.,"Cross-shore currents in surfzone modeling",1988, *Coastal Engineering* , 12:23-42.
[5] Versteeg, H.K., and Malalasekera, W., An introduction to computational fluid dynamics: The finite volume method, John Wiley and Sons Inc., New York, 2007, 272 pp.
[6] Wendland, H. Piecewiese polynomial, positive definite and compactly supported radial functions of minimal degree. *Advances in computational Mathematics*,1995, 4(1):389-396.

2

PORT AND COASTAL MANAGEMENT

EVALUATION OF THE AIDS TO NAVIGATION MARKS MONITORING SYSTEM PERFORMANCE ON SAFE NAVIGATION (CASE STUDY IN BOUSHER PORT)

Soudabeh Khabazsabet[1]

1) MS in Electrical engineering telecommunications, Ports and Maritime Administration of the Bushehr province; soudabeh.khabazsabet@yahoo.com

1. Introduction

This system of buoy monitoring is a kind of advanced sea monitoring in recent years. It includes main processing unit and local station. It can obtain warming alarm, level of voltage and current light in the less time. It don't need, anybody goes to the sea to know the situation of the light. The advantage of buoy monitoring for sea navigation is Forecasting and warning marine hazards and helping the response organizations for best Crisis Management of Marine Hazards. It helps ships to find maritime channel and to navigate in safe area.

The objective of this paper presents operation of buoy monitoring that how it shows warning and helping the response organizations for the best crisis management of marine hazards. The buoy monitoring system operates in the VHF maritime mobile band. The optimum method for buoy monitoring system based on AIS network. The monitoring data will be transmitted between the buoy and base station. The transmission data presents the status of the lights and batteries, voltage, current, alarm of systems.

This system has some advantages such as: lees of human being, remote control system and observation important parameter of this system at any time of the day[1].

2. Buoy Monitoring System In Boushehr Port

ATONIS Pro is a unique, state-of-the-art, modular, Aids to Navigation Information System designed to operate seamlessly in an AIS VDL environment using FATDMA or optional RATDMA protocols. ATONIS Pro is designed to be fully compliant with the governing directives for AIS ATON transponders[1].

The customer should select a VHF-FM antenna suitable for the location where the unit is installed and designed to operate on the AIS frequencies. The ATONIS Pro VHF-FM antenna connection is DC isolated.to ensure proper protection from nearby lightning strikes, the antenna should have an in-line surge protector installed at the antenna, or as close to the antenna, as possible

User must configure this system and they set name, MMSI number and position for every buoys.

Buoy sends data in the VHF channel. Monitoring data will be transmitted to radio station and user can see information in base station that shows in figures 1, 2.

ATONIS Pro is configured using ATONISCfg program. The program is designed with built-in explanations for all parameter settings.

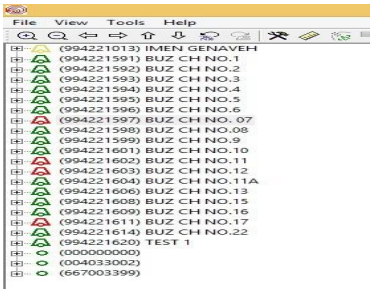

Figure 1. Boushehr PMO Monitoring system with MMSI number and name

Figure 2. Graphic view of Bushehr Port Buoy

Clicking on any buoy in display window will show some information about buoy such as MMSI number, latitude, longitude, name, AtoN type, off-position, position accuracy, flag, AIS class, last update.

Figure 3. display MMSI, name of the buoy

Figure 3. display MMSI, name of the buoy

3. Massages of buoy monitoring system

ATONIS Pro is designed to transmit selected AIS messages over the AIS VHF-FM Data Link (VDL). The

Following messages are supported per IALA Guideline No. 1062

Table 1: AIS Message

AIS Message	Description
21	Aids to Navigation Report
6	Binary addressed message for Aton Monitoring
8	Binary broadcast message for Met/Hydro information
12	Safety related addressed message
14	Safety related broadcast text message

Right clicking on any target in the Info Panel will open a Menu to allow access to several features of iNAV such as show on chart, safety related Text, weather, AtoN status Msg6, custom Binary and other things.

The important message of this system is massage 6. Clicking on AtoN status Msg6 will open the page. It shows battery voltage, current, lamp status, light status, solar charge, battery status, position status.

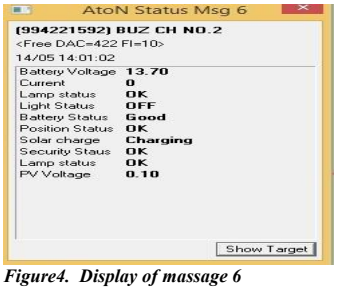

Figure4. Display of massage 6

4. Output display in buoy monitoring system

User can select parameter to plot from drop down window. Data can be displayed in Real Time (as data is received) or past data using period selected from database. The data can be printed using the print options such as pdf or excel format.

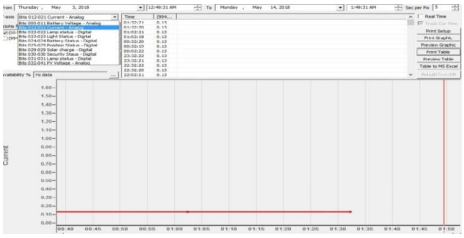

Figure5. Graphic and Table Report for ATON Window

Table 2: display of output condition buoy (Buz CH No.3) at different times

time	Name and MMSI number	current	voltage	Battery status	Light status	Solar charge
01:32	(9942211593) Buz CH No.3	0.13	12.5	ok	on	charging
01:02	(9942211593) Buz CH No.3	0.13	12.5	ok	on	charging
00:32	(9942211593) Buz CH No.3	0.13	12.6	ok	on	charging
00:02	(9942211593) Buz CH No.3	0.13	12.6	ok	on	charging

5. Result

One of the important responsibilities in ports is to prepare safety channel for ships. It is necessary to help navigation with modern equipment. Buoy monitoring system provides that information about buoy receive in radio station in AIS network. Users can monitor buoy every time in day. All of alarms will be received on mobile or Email.

An AIS AtoN can be fitted to any remote maritime structure and operate for years on solar power without maintenance. It sends important data about buoy such as: battery voltage, current, lamp status, light status, solar charge, battery status, position status and weather.

6.References

[1] International Association of Marine Aids to Navigation and Lighthouse Authorities (IALA), "Recommendation A-126 – the use of the Automatic Identification Systems (AIS) in Marine Aids to Navigation Services June 2004 – Revised June 2011" ,10, rue des Gaudines 78100 Saint Germain en Laye, France, Edition 1.5, June 2011.

ESTIMATION OF HIGHEST AND LOWEST ASTRONOMICAL TIDE ALONGSIDE THE COAST OF THE HORMOZGAN PROVINCE, IRAN

Reza Arabsheibani[1], Bahman Tajfirooz[2] and Hamid Khalili[3]

1) GIS division, School of Surveying and Geospatial Information Engineering, University of Tehran, Tehran, Iran, rasheibani@ut.ac.ir
2) Faculty of Marine Science and Technology (FMST), Ocean Physics Department, Science and Research Branch of Islamic Azad University, bahman.tajfirooz@srbia.ac.ir
3) Ports & Maritime Organization Tehran, Iran (the Islamic Republic of), hkhalili@pmo.ir

1. Introduction

Boundary delimitation is a complicated subject because of both the number of real and potential boundary situations throughout the world, and the complexities of the delimitation process [1]. The highest high tide (also referred to as Highest Astronomical Tide or HAT) is defined by Marine Science Australia and International Hydrographic Organization as the highest level which can be predicted to occur under average meteorological conditions and any combination of astronomical conditions. Estimation of HAT is vital in order to delimitate the coastlines and shorelines. HAT is essentially a geometrical line which is introduced to enable the coastal management and systems such as ICZM (integrated coastal zone management).

In the present study, we addressed the estimation of HAT in the Hormozgan province of Iran by integrated use of different data sources. Basically, the specific 19-year period of tide observations must be taken and reduced to obtain the astronomical constituents for tide prediction. So, considering the fact that HAT can be derived from astronomical tide predictions [2], to enhance the reliability of the tide analysis and predictions, we have used and compared data sources such as long-term and short-term observations, tidal models, national cartographic center predictions, Admiralty sources, hydrodynamic model [3], and available tidal constituents. HAT may not occur every year [4] and it depends on the mean sea level [5]. Mean tide level is not the same as mean sea-level because of the influence of the shallow-water tidal harmonics, although variations in the two values are highly correlated [6].

2. Methodology

The highest elevation reached the sea as recorded by a water level gauge during a given period. Most of the national organizations which are responsible for tide, routinely documents monthly and yearly extreme low water for its control stations [7]. In this study, NCC tide gauges' long-term information of the significant ports of Iran including Chabahar, Jask, Shahid Rajayi, Kangan, and Bushehr. Moreover, short-term information of some other ports are investigated such as Sirik, Ras-e Maidani, Shahid Haghani, Persian Gulf Shipyard Company (PGSC), Hasineh, Kong, Teben, Berkehseflin, and Pol.

Along with the real observations of tide, global and regional tide models are evaluated in our study. Tidal Model Driver (TMD) which is developed by Oregon State University is a remarkable example of tidal constituents' extraction in regional meso scale [8]. The resolution of this model is one minute which include north of the Indian Ocean, Oman Sea, and Persian Gulf. This model is able to predict the tide and tidal currents. Besides, it is possible to extract 7 tidal constituents from the model database including M2, S2, N2, K2, K1, O1, P1, and K1.

In order to verify the validity of the TMD outputs, we have compared the results of the TMD with real observations in a variety of locations. Some results are provided in Figure 1.

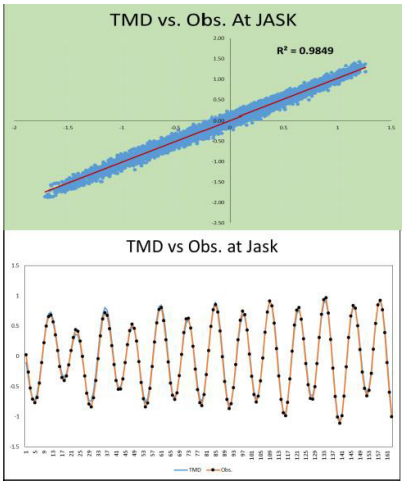

Figure 1. Comparison of TMD and observations in Chabahar

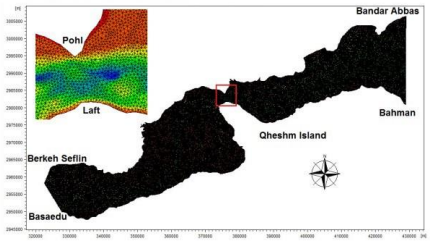

Figure 2. Comparison of TMD and observations in Chabahar

As illustrated in Table 1 the results of the comparison is acceptable in the selected ports. The TMD evaluation procedure proves that in a 95% confidence interval the TMD model functionality and effectiveness is appropriate. However, our experience shows to us that TMD does not function appropriately at some regions. In order to calibrate TMD and have more reliable calculations, two sources are used:

- Constituents derived from observation analysis
- Hydrodynamic Model

A hydrodynamic model is provided in the region of Khuran Strait to enhance the accuracy of the HAT calculations. Depicted in the picture 3 is the selected points are spread alongside the border of the Hormozgan province in each 20 km.

Figure 3. Sample points of the Hormozgan coastline

For each point, the tide prediction is made from the beginning of 2010 to the end of the 2030. So, the duration of the prediction for every selected point contains at least Saros (A period of 223 synodic months corresponding approximately to 19 eclipse years or 18.03 Julian years, and is a cycle in which solar and lunar eclipses repeat themselves under approximately the same conditions. [7])

By finding the minimum and maximum of the predicted values, HAT and LAT could be derived. The results based on the point numbers are shown in the figure 4 and 5.

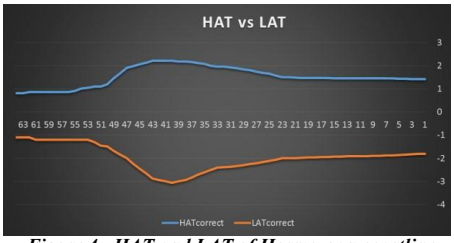

Figure 4. HAT and LAT of Hormozgan coastline

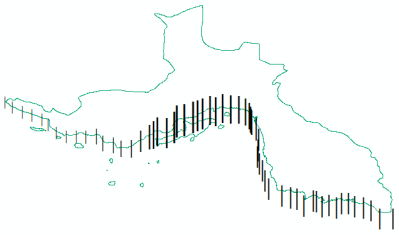

Figure 5. Hormozgan HAT values (not to scale)

3. References

[1] Alexander, L.M., *The delimitation of maritime boundaries*. Political geography quarterly, 1986. **5**(1): p. 19-24.

[2] Foreman, M.G.G., *Manual for tidal heights analysis and prediction*. 1979: Institute of Ocean Sciences, Patricia Bay.

[3] Warren, I. and H.K. Bach, *MIKE 21: a modelling system for estuaries, coastal waters and seas*. Environmental Software, 1992. **7**(4): p. 229-240.

[4] Boon, J.D., *Secrets of the tide: tide and tidal current analysis and predictions, storm surges and sea level trends*. 2013: Elsevier.

[5] Parker, B.B., *Tidal analysis and prediction*. 2007: US Department of Commerce, National Oceanic and Atmospheric Administration, National Ocean Service, Center for Operational Oceanographic Products and Services.

[6] Pugh, D.T., *Tides, surges and mean sea-level (reprinted with corrections)*. 1996: John Wiley & Sons Ltd.

[7] Hicks, S.D. and P. Schureman, *Tide and current glossary*. 1984: US Department of Commerce, National Oceanic and Atmospheric Administration, National Ocean Service.

[8] Padman, L. and S. Erofeeva, *Tide Model Driver (TMD) Manual*. Earth and Space Research, 2005.

INSTRUCTIONS FOR RESPONDING TO PORTS SECURITY PLAN

Zhila Hosseininezhad[1], Mohammadreza Fallah[2], Akram Barzegar[3], Hanieh Noorollahi[4] and Mahdi Nouri[5]

1) Disaster Management Research Group, Passive Defense Complex, Malek Ashtar University of Technology, Tehran, Iran, zhila.hosseini.n@gmail.com
2) Disaster Management Research Group, Passive Defense Complex, Malek Ashtar University of Technology, Tehran, Iran, m.fallah.teh@gmail.com
3) Disaster Management Research Group, Passive Defense Complex, Malek Ashtar University of Technology, Tehran, Iran, ak.Barzegar@gmail.com
4) Disaster Management Research Group, Passive Defense Complex, Malek Ashtar University of Technology, Tehran, Iran, h_nurollahi@yahoo.com
5) Disaster Management Research Group, Passive Defense Complex, Malek Ashtar University of Technology, Tehran, Iran, Nouri4285@gmail.com

1. Introduction

The important role of ports for the support of economic activities in the hinterland since they act as a crucial connection between seas and lands transport, the total volume of goods handled in ports, and the large share of passenger transportation, indicate the position of seaports all over the world. Ports constitute an important economic activity in coastal areas. The higher the throughput of goods and passenger's year-on-year, the more infrastructures, provisions and associated services are required. One of these provisions and services, which every single port, as a kind of an infrastructure or complex, needs, is a security plan.

The experiences about seas conflicts, specially during the first and the second world wars, the battle between Iran and Iraq and lots of other examples happened during the past century beside the unstable political situation in middle-east which leads to army and terrorist attacks, show why every single infrastructure or complex such as ports which could be attacked by an adversary, should be ready to be resistant. In other word, a security plan is a compulsory option, which is added to other management protocols. Security is complicated and is the result of several factors. Some must always be present while the others will be added at specific moments and together they constitute the security plan. This paper will discuss about how to develop a security plan for ports in general. Then by using content analysis methodology in literature review of security risk assessment it will identify the factors influencing the risk. These factors will be formed in a structure based on two validated and well-known methodologies for assessing security risk. Then, based on this structure, the level of risk for the various components of a fictitious port will be determined. In this regard, according to the security experts familiar with the port equipment, the vulnerabilities of various port facilities will be identified. Validated checklists commensurate with what are common about components of the ports will be used. The reliability of the results of these surveys is measured and at the end of the paper, instructions or guidelines will be recommended to reduce vulnerabilities and to respond to ports security management plan.

2. What Is a Security Plan

In general, a security plan has to decrease vulnerabilities of a complex and increase its capabilities. So that, the threats are being reduced or made less feasible and therefore the risk is reduced. A security plan must fit the actual needs and work space.

There are some words and concepts mentioned above, which are necessary to be explained. The word "risk" is one of those concepts, which is the combination of some others. In several security related contexts, risk is a conjunction of some basic factors. Figure1, depicts the risk assessment process presented in this paper to help identify the best and most cost-effective responses and mitigation instructions for any complex's own unique security needs.

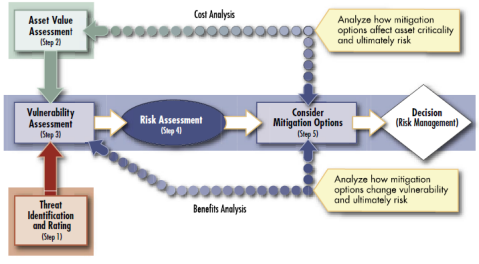

Figure 1. Risk assessment process in a security plan model [1].

Based on the process shown above, the concept of risk, asset, vulnerability, criticality and threat should be clarified. However, Because of the limited number of pages in this article, risk, is the only concept of the paper,

which is introduced briefly here, while the others will be declared in the full paper.

3. WHAT IS A RISK ASSESSMENT?

A very brief definition of risk is [2]:

"Risk is an expression of the likelihood that a defined threat will target and successfully exploit a specific vulnerability of an asset and cause a given set of consequences."

A Qualitative Risk assessment is based on an expert's estimate, both the probability of activation of the source of hazard/threat and consequences of undesirable event [3]. The basis for risk estimation of a complex is the equation (1):

$$R(t) = p(t) \times N(t) \quad (1)$$

Where R(t) represents the risk, p(t) the probability of activating the source of hazard/threat, and N(t) impacts (consequences) of undesirable event depending on time. Nevertheless, the impacts of undesirable event reflect the vulnerability of the assets of relevant hazards [3].

The third factor on which the risk level is dependant is time (t).

If there is for each *j-th* hazards assembled, all pairs Threat / vulnerability against each *i-th* asset of the complex, it is possible by using equation (2) derived from the equation (1) to calculate for the investigated complex in its details (persons, wharfs, jetties, terminals, warehouses, oil tanks, sheds, silos, buildings, etc.) risk *Rj (τ)* that results from j-th hazards/threats in a given time *τ* [3].

$$R_j(\tau) = \sum_{i=1}^{q} p_j(\tau) \times C_{j,i}(\tau) \quad (2)$$

3.1. WHAT IS THE RISK ASSESSMENT METHODOLOGY?

Every concept shown in Figure 1 is like a step in the risk assessment process, and it helps to identifies port assets, analyzing their vulnerabilities, their corresponding threats and their level of importance among the others. Identification of the factors affecting risk and their indices is carried out by using the content analysis methodology in literature review on security risk. Then each factor has a definition and evaluation process includes the following tasks (see Figure 2):

- Identifying the factor (asset importance, asset vulnerability, threats).
- Collecting information
- Determine rankings for threats, vulnerabilities, and attractiveness of assets by using experts' opinion and ensuring the reliability of their opinion.
- Determining the consequence rating [1].

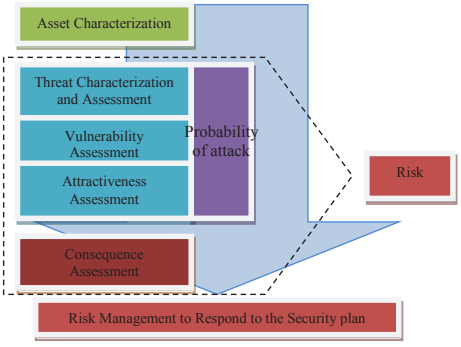

Figure 2. The steps in risk assessment methodology

There are a lot of risk assessment methods for different kind of infrastructure, but the one will be used in this research for analyzing the threats and the consequences for seaports is the combination two methods represented by two research group working on security risk. API[1] and FEMA[2] represent these Methods.

This method will be implemented in a fictitious seaport layout to be more tangible and understandable but it has been proportionate in terms of threats and vulnerabilities in Iranian seaports. Therefore it could be easy to use by Iranian experts for ports.

4. THE RESULTS

Compliance with the port security plan and reducing the level of risk through the provision of instructions is possible, and this can only be achieved by reducing the level of each component affecting risk, especially the vulnerabilities in the group of buildings, wharfs, jetties, terminals, warehouses, oil tanks, sheds, silos, buildings, etc base on corresponding threats.

5. REFERENCES

[1] FEMA452. "Risk Assessment, A How-To Guide to Mitigate Potential Terrorist Attacks, Providing Protection to People and Buildings". Federal Emergency Management Agency, 2005.

[2] American Petroleum Institute (API). "Security Vulnerability Assessment and Security Guidelines for the Petroleum Industry". Washington, D.C.: API Publishing Services, 2005.

[3] Božek, F., Urban, R. "Management rizika" Obecná část. 1. vyd. Brno: Univerzita obrany, 2008, s. 67. ISBN 978-80-7231-259-7., 2008.

[1] American Petroleum Institute

[2] Federal Emergency Management Agency

DEVELOPING OF MARINE TOURISM IN NORTH OF IRAN, CASE STUDY: COASTS OF MAZANDARAN PROVINCE

Alireza Vaselali[1] and Samira Ghafourian[2]

1) Project Manager, BEhin Tarh Apadana (BETA Group), Tehran, Iran, a_vaselali@yahoo.com,
2) Landscape Architect, BEhin Tarh Apadana, Tehran, Iran, ghafouriansamira@gmail.com.

1. Introduction

Today marine tourism as one of the subcategories of the extensive tourism industry, can play a significant role in economic flourishing and entrepreneurship along with suitable usage of natural and cultural resources. Decrease of destructive effect of tourism on natural, social, cultural and other resources depends on the need for accurate and academic studies and planning.

Caspian coastlines, especially the coasts of Mazandaran province, have a great potential for development of the marine tourism industry due to its exclusive natural and socio-cultural attractions. The first step in this direction is the recognition and assessment of prone areas with comprehensive consideration on aspects of tourism development. In this regard, the Integrated Coastal Zone Management (ICZM) program, on purpose of sustainable development, prepared to promote the proper allocation of land use on shoreline, have especial consideration on tourism sector.

Unfortunately, due to the lack of knowledge and citation on academic methods for site selection, the weakness in implementation of existing plans and the lack of clarification of the high-level documents in grand scale, action taken to the growth of this industry, failed to provide the required quality and caused great damages to the environment.

BEhin Tarh Apadana (BETA Group) was retained by the Iranian Port and Maritime Organization (PMO) to analyze and select the appropriate sites for marine tourism development on the coasts of Mazandaran province.

2. The Study Process

In the first step, some basic characteristics such as appropriate zoning and in conformance with public plans for the area, have sufficient water depth (without dredging), have adequate upland area (no fill required), have adequate water frontage, locate outside of resource protection area, locate outside of designed port area, locate outside of restricted historic preservation area, locate away from military centers, have access to utilities, have adequate transportation infrastructure, locate near a metropolitan area have been chosen to determine appropriate locations. Afterward, by holding expert opinion polls through AHP method, 10 superior parameters were selected and each parameter was weighted in terms of priority. The entire shoreline of Mazandaran province has been assessed based on these effective parameters and those have been analyzed via data management system of the "GIS software" used to determine areas and rank them in order of development priority according to marine tourism potentials.

Table 1. Parameters studied in the location of tourism-prone areas

Environmental situation	Marine hazards	wind	**Hydrodynamic conditions**
Important ecosystems	Geological hazards	Drought and mildew	Caspian Sea level
Environmental pollutants	Environmental hazards	**Geology and morphology**	Coastline changes
Zoning plant and animal species	Areas vulnerable to sea level fluctuations	Stratigraphy	currents
Rules and requirements	**Infrastructure status**	Seismic state	sediment
Areas under the management of the environmental organization	water	Coastal zone zoning status	Erosion
Others	soil	Stability and instability	storm
Fisheries	Sewage and waste	mine	waves
Boundary	Electricity	Geomorphology of coastal areas	**Climate**
Coastal Management Plan	Gas	**Hazards**	Annual precipitation
Tourist attractions	Transportation network	Storm water level	Temperatures

Table 2. The main 10 parameters affecting the location of tourism-sensitive areas

No.	Parameter	Priority
1	Environmental Protected Area	5
2	Marine Parameters (Water Depth, Waves, Currents and so on)	5
3	Upland Area	4
4	Tourist Attractions	3
5	Access Roads	3
6	Accommodation Facilities	3
7	Private Financial Sectors	2
8	Fisheries Attractions/Facilities	2
9	Marine Structures	2
10	Water Supply	1

Table 2. The main 10 parameters affecting the location of tourism-sensitive areas

No.	Parameter	Priority
1	Environmental Protected Area	**5**
2	Marine Parameters (Water Depth, Waves, Currents and so on)	**5**
3	Upland Area	**4**
4	Tourist Attractions	**3**
5	Access Roads	**3**
6	Accommodation Facilities	**3**
7	Private Financial Sectors	**2**
8	Fisheries Attractions/Facilities	**2**
9	Marine Structures	**2**
10	Water Supply	**1**

3. Results

Based on GIS maps results, the coastal cities of the Mazandaran province have been ranked, which after normalizing their weights, their priority is shown in the figure below.

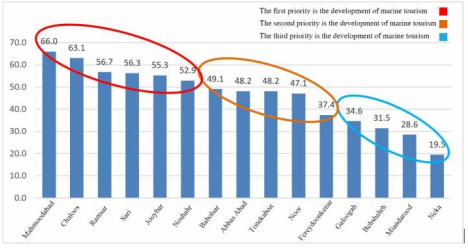

Figure 1. Prioritization of coastal cities of Mazandaran province for the development of maritime tourism

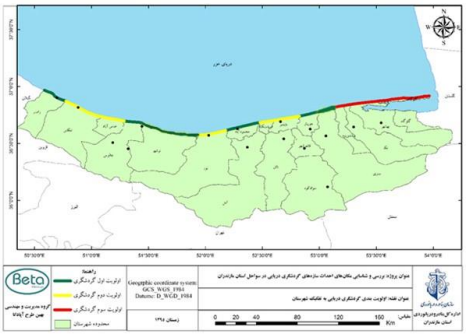

Figure 2. map of Prioritization of coastal cities of Mazandaran province for the development of maritime tourism (green: the first, yellow: the second and the red the third priority)

4. References

[1] Ports and Maritime Organization of IRAN (PMO), "Integrated Coastal Zone Management Plan", *2008.*

[2] Sabzandish Payesh consultant company, " Development plan of tourism industry in the coastal zone of Mazandaran Sea", *2008.*

[3] Pouya Tarh Pars consultant company, "Planning and simulation studies of the northern coast of the country", *2012.*

[4] Khak Baft consultant company, "studies of comprehensive passenger ports of the Caspian Sea ", *2008.*

[5] Sharif University of Technology, "Road Map for Passenger Sea Freight in 1404 solar year ", *2008.*

[6] Khak Baft consultant company, "Logistics of Mazandaran Province", *2012.*

[7] Clark, J. R, coastal seas, the conservation challenge. blackwell science,1998.

[8] Kastianoy, A. G., & Kosarev, A. N, The Caspian sea environment. science & business media, 5,2005.

[9] Thompson, I. H, The Ethics OF Sustainability. In J. F. Benson, & M. H. Roe, Landscape and Sustainability. Spon Press,2000.

[10] www.ostan-mz.ir.

[11] www.mazandaran.doe.ir.

[12] www.ichto.ir.

[13] www.amar.org.ir.

INTELLIGENT PORTS BASED ON INTERNET OF THINGS AND GIS

Hamed Sartipi[1] and Behzad Alvand[2]

1) Fara Omran Negar Co., Tehran, Iran, hamedsartipi@yahoo.com
2) Ports Engineering Department, PMO, Tehran, Iran, hamedsartipi@yahoo.com

1. Introduction

Major ports in the world have gone through three development stages: informationalized ports, digital ports, and intelligent ports [1]. In recent years, many coastal countries begin actively to construct intelligent ports [2, 3].

With the popularization and application of the Internet of Things (IoT) and using Geographic Information systems (GIS), many new Intelligent Ports has been started [4].

Intelligent Ports are urgently needed to be closely integrated with IoT and GIS in order to achieve efficient data spatially location based data sharing and stability of port services. It other words, Intelligent Ports are new generation of ports, which has a new, intelligent port infrastructure and integrated and smart management and service [5].

In this article, the informatization developments of main international ports are summarized. Then, the detail requirements of next generation Intelligent Ports are collected and analyzed. Later, the corresponding key technologies of Internet of Things and GIS are summarized. And, a kind of Intelligent Ports solution is proposed, and its main functions are designed in detail. Finally, the future development trend of Intelligent Ports is predicted.

2. The key technologies of IoT and GIS to construct intelligent ports

Many key technologies and products of IoT and GIS are needed in the construction of Intelligent Ports, whose performance requirements such as high security, high reliability, high recognition rate, high stability are put forward.

A. Sensor
B. RFID
C. Wireless Sensor Network (WSN)
D. Network Communication Technology
E. Machine to Machine (M2M) F. Vehicle terminal
F. Handheld mobile terminal H. GIS web services (WMS, WFS)

3. The Overall Framework of Intelligent Ports

It can online real-time monitor the vehicle, the container, the cargo, the ship, and clearance process, ultimately to form a whole-process, intelligently, and visually visualization monitoring system. Firstly, the unified data standardization system and data exchange system are built to do business carding and data needs analysis. Then, taking IoT technology as basic infrastructure, using such technologies as RFID, sensors, WSN, wireless communications, cloud computing, 3D virtual reality, the fast automatic supervision, acquisition and tracking of containers, transport vehicles and goods can be achieved, to achieve information networking and real-time data exchange of ports, yards, warehousing, customs, freights, to form the intelligent management of traffic flow, logistics, and information flow.

3.1. Intelligent Production Scheduling Management System

Using such technologies as GPS, WiFi wireless terminal, 3D virtual reality technology, many functions, including 3D scene management, smart jobs, intelligent scheduling management, set card scheduling in dock container yards can be realized, to achieve visualization, intellectualization, real time dynamic management and monitoring of the whole process, to achieve high scheduling optimization, to improve operational efficiency, and to save operating and maintenance costs, to increase safety and traceability.

Figure 1. Intelligent production scheduling management system

shut/closed or other smart devices, can be identified by RFID readers.

3.4. Smart Ship Management System

Using the Automatic Identification System (AIS) technology, GIS technology, GPS, as well as Electronic Data Interchange (EDI) technology, Smart Ship Management System can be formed.

3.5. Intelligent Warehouse Management System

As shown in Figure 2, by means of RFID technology, data acquisition and processing can be fast, accurate, achieved, and warehouse business processes can be optimized. Then, the customs supervision warehouse goods out of warehouses are intelligent real-time monitored, to improve the speed and efficiency of supervision customs clearance, and to reduce the cost of warehousing. enterprises to understand the situation of the goods in a warehouse, and greatly improve work efficiency, reduce operating costs.

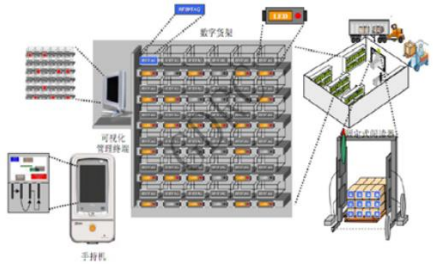

Figure 2. Intelligent Warehouse Management System

3.6. Electronic monitoring channel

Using RFID, short-range wireless communication, automatic detection, intelligent control and many other technologies, equipped together with RFID electronic seals, cargo regulatory base station, the transmission of information can be completed through the equipment and control center, to constitute electronic monitoring channel, to achieve real-time visual monitor and manage of transport vehicles and cargo of the customs regulatory sites during transit, to improve the supervision of vehicles and goods and operation efficiency.

3.7. Unified platform for monitoring command center

The logistics data of transport and cargo and video information of all docks, yards, bayonets and special supervision areas can be integrated into a unified logistics information exchange platform, to achieve real-time, efficient and safe intelligent monitoring of cargo, containers, cars, boats, trains etc.

3.8. Regional data center

Regional data center is services data source of Intelligent Ports and its aggregators and switching center.

4. Future prospects

The changing of development patterns of ports is a strategic task, whose restructuring target is modern service industry. IoT technology-based intelligent ports by using GIS can achieve information sharing and dynamic collaboration between deferent things, to improve the efficiency, accuracy, visualization, safety and environmental protection of port operations. In the future, IoT technology and GIS will penetrate into the development and construction of the Intelligent Ports, which has an important economic value and significance.

5. References

[1] Xisong, Dong, Gang, Xiong, Lv, Yisheng, Intelligent Ports Based on Internet of Things, Chinese Academy of Sciences, 2013

[2] Wang B., Liu S. F. Port Process Reengineering Based on Information Technology, Proceedings of International Conference on Engineering and Business Management, 2012.

3] Mohammadi S., Ardast S. A new model for evaluation of RFID utilization in various ports of the world, IEEE International Conference on Communications Technology and Applications, 2009: 36- 39

[4] Chlomoudis C. I., Pallis A.A. Port Governance and the Smart Port Authority: Key issues for the Reinforcement of Quality Services in European Ports. 10th World Conference on Transport Research, Istanbul, 2004

[5] Chen Y. Q., Guo J. L., Hu X. N. The Research of Internet of Things' Supporting Technologies Which Face the Logistics Industry, International Conference on Computational Intelligence and Security, 2010: 659- 663

[6] Yoo Y. H., Kim J. H., Gou H. S., Hu Y. J. RFID reader and tag multichip communication for port logistics, IEEE International Symposium on a World of Wireless, Mobile and Multimedia Networks & Workshops, 2009: 1- 8 [7] Siror J. K., Sheng H. Y. Dong W. RFID based model for an intelligent port, Computers in Industry, 2011, 62(8-9):795-810

CLASSIFICATION OF SATELLITE IMAGERY WITH TWO APPROACHES OF SPATIAL ATTRACTION (CASE STUDY: PARTS OF HORMOZGAN SHORES)

Alireza Tilkoo[1], Seyed Mostafa Siadatmousavi[2] and Barat Mojaradi[3]

1) Civil engineering Department, Iran University of Science and Technology, , alitili92@gmail.com
2) Civil engineering Department, Iran University of Science and Technology, Siadatmousavi@iust.ac.ir
3) Civil engineering Department, Iran University of Science and Technology, mojaradi@iust.ac.ir

1. Introduction

A wide range of methods have been evaluated for analyzing aerial and satellite images. Remote sensing data are used in many applications. Typically, the process of image classification is started to convert data into meaningful information [1]. In this article, two approaches based on the theory of spatial dependence are described. Spatial dependency is known as attracting the near observations more than the distant observations. The first theory of spatial dependence was presented by Atkinson in 1997 [2]. In spatial attraction models, this spatial dependence is interpreted by attraction between neighboring pixels or subpixels [3]. The results show that the modified subpixel/spatial attraction model (MSPSAM) with an overall accuracy of 99.83% and kappa of 0.99 has a good performance for classification. The results confirm the quality of both methods for the classification of satellite imagery.

2. SPSAM Classification

In a subpixel/spatial attraction model (SPSAM), the attraction between each subpixel in pixels of coarse resolution and its neighboring pixels is calculated to determine the subpixel spatial distribution of each class [4]. Assumptions of this approach is as follows: The model acts on the basis of fraction values in neighboring pixels relative to subpixels in a central pixel. A subpixel can only be attract by pixels around the center pixel (which includes the subpixel); as a result, the maximum of eight neighboring pixels can be considered for attraction, the rest of pixels are too far to be attracted [5]. The formulas of this method are:

$$SD_{cf} = \sum_{k=1}^{N_A} \omega_k F_c(P_k) \qquad (1)$$

$$D_{c.ij} = \sum_{k=1}^{N_A} \omega_k F_c(P_k) = \sum_{k=1}^{N_A} \frac{F_c(P_k)}{d_k} \qquad (2)$$

where SD_{cf} is the measure of spatial dependence of class c to subpixel pf, N_A is the number of neighboring pixels, ω_k is the weight of spatial dependence, $F_c(P_k)$ is the proportion of the kth neighbor pixel P_k to class c, and d_k is the Euclidean distance between geometric centers of subpixel p_{ij} and its neighbor pixel P_k.

3. MSPSAM Classification

In the SPSAM method, the subpixels of each neighbor of the central pixel were considered to be the central points of the neighboring pixel. Then the spatial attraction caused the class c to be calculated for the subpixel p_{ij} from each neighboring pixel as the attractor between the p_{ij} center and its neighbor center. Clearly, this description of attraction is not correct because the subpixels of the internal pixel may not be entirely close to the central point. Instead, they may locate at a corner or near to a boundary of that pixel so that each pixel cannot be considered as a point [4].

In MSPSAM method, the spatial attraction of each neighboring pixel is the sum of the attraction between the center p_{ij} and the center of each subpixel in the neighboring pixel. Suppose p_m is a subpixel within P_k, and d_m is the Euclidean distance between geometric centers of subpixels p_{ij} and p_m; then the SD_{cf} can be modified as [3,4]:

$$SD_{cf} = \sum_{k=1}^{N_A} \omega_k F_c(P_k) = \sum_{k=1}^{N_A} \omega_k \frac{F_c(P_k)S^2}{S^2} =$$

$$\frac{1}{S^2} \sum_{m=1}^{N_A S^2} \omega_k x_{cm} = \frac{1}{S^2} \sum_{m=1}^{N_A S^2} \frac{x_{cm}}{d_m} \qquad (3)$$

Mixed pixel P_{ab} in the coarse low resolution image (i.e. fraction image) is selected in order. Attractions for subpixels within P_{ab} caused by each class from neighbors are calculated according to equation (3). The $F(P_{ab})S^2$ subpixels with highest attraction values are allocated to class c [3].

attraction models. Aerial image at approximately the same acquisition time was used for validation.

5. Results

According to the results obtained from the error matrix (Table 1,2), the modified MSPSAM model with an overall accuracy of 99.83% and kappa of 0.99 has a better performance for classification. Figure 1 and 2 show the implementation of both spatial attraction methods on two selected coastal areas. The location of the areas selected is close to the Teban beach in the Hormozgan province. The size of the Landsat pixels is 15 meters after implementing the fusion technique. The pixel size of the classified images is selected as 7.5 meters.

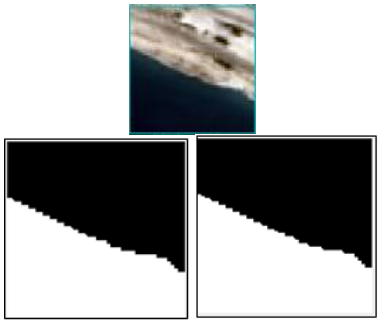

Figure 1. Top center image is selected coast from Landsat satellite. Classified images from left to right relative to SPSAM and MSPSAM with scale factor of 2.

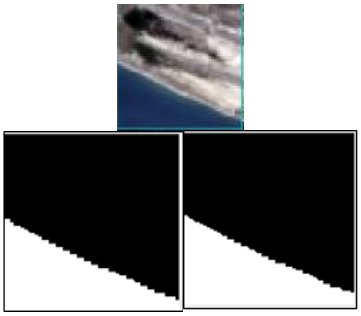

Figure 2. Top center image is another selected coast from Landsat archive. Classified images from left to right relative to SPSAM and MSPSAM with scale factor of 2.

Table 1. Error matrix of the first coastline shown in Figure 1

Validation	SPSAM	MSPSAM
Overall Accuracy	97.87%	99.32%
Kappa Coefficient	0.97	0.99

Table 2. Error matrix of the second coastline shown in Figure 2

Validation	SPSAM	MSPSAM
Overall Accuracy	98.54%	99.83%
Kappa Coefficient	0.98	0.99

6. Conclusions

In this research, both employed methods to classify images are of highly accuracy. Therefore, the methods can be used to monitor sedimentation and erosion, extraction of coastlines and other coastal management programs. As a suggestion for future research, it is possible to improve the results by targeting combined research along with new algorithms and spectral water indexing.

7. References

[1] G. Mountrakis, J. Im, and C. Ogole, "Support vector machines in remote sensing: A review," *ISPRS Journal of Photogrammetry and Remote Sensing,* vol. 66, pp. 247-259, 2011.

[2] P. M. Atkinson, "Mapping sub-pixel boundaries from remotely sensed images," *Innovations in GIS,* vol. 4, pp. 166-180, 1997.

[3] L. Wang, Q. Wang, and D. Liu, "Sub-pixel mapping based on sub-pixel to sub-pixel spatial attraction model," in *Geoscience and Remote Sensing Symposium (IGARSS), 2011 IEEE International*, 2011, pp. 593-596.

[4] Q. Wang, L. Wang, and D. Liu, "Integration of spatial attractions between and within pixels for sub-pixel mapping," *Journal of Systems Engineering and Electronics,* vol. 23, pp. 293-303, 2012.

[5] K. C. Mertens, B. De Baets, L. P. Verbeke, and R. R. De Wulf, "A sub-pixel mapping algorithm based on sub-pixel/pixel spatial attraction models," *International Journal of Remote Sensing,* vol. 27, pp. 3293-3310, 2006.

DEVELOPING A LAND USE MONITORING MODEL TO ACHIEVE SUITABLE LAND USES IN COASTAL ZONES

Sharareh Pourebrahim[1], Fateme Nikooy[2], Hamid Khalili[3], Rasoul Ghanbari[4] and Mani Moghadam[5]

1) Environment Department, University of Tehran, Karaj, Iran, sh_pourebrahim@ut.ac.ir
2) Environment Department, University of Tehran, Karaj, Iran, fatemenikooy@yahoo.com
3) Port & Maritime Organization of Iran (PMO), Tehran, Iran, hkhalili@pmo.ir
4) Port & Maritime Organization of Iran (PMO), Tehran, Iran, rghanbari@pmo.ir
5) Port & Maritime Organization of Iran (PMO), Tehran, Iran, mani.moghadamm@gmail.com

1. Introduction

The LUP land use monitoring program has been designed according to a couple of purposes such as achieving the sustainable development goals, identify development goals based on sustainable potential of land resources in long-term, land compatibility, avoiding the subjective goals in planning, and finally, identify the land resources: stocks, capabilities and potentials via a scientific approach. Therefore, the indicators used in this evaluation should indicate the proximity or distance of performance with the suitable criteria at a specific, scientific and measurable time. Based on the conceptual model of national plan, determining the suitable land uses in coastal zones needs three main information layers:

1. Current status; which displays the current land situation without any cassette
2. Constraint (planned lands); areas separated by one or more approved programs from the others.
3. Land Capability (capable lands); includes ecological and agricultural capabilities

Regarding to existing layers, the ecological Capability model has been selected as the base model of combination. Adaptation of ecological Capability to planetary landscapes and agricultural potential, a plan has been made which finally provided the ultimate model that includes six main land uses: conservation, agriculture, industrial, tourism, urban and aquaculture.

2. Methodology

According to ICZM goals and approaches, three approaches including conservation, development and integration, have been selected. Their indicators have been collected, then the actions, approaches, plans have been evaluated based on the main objectives mentioned above. Figure 1 illustrates a framework for evaluation of suitable land uses in a particular territory.

Identification of stakeholders and their participation in the first step of evaluation is an important factor, because they play a decisive role in defining the land use goals, requirements, as well as the collection of output indicators. Both output and impact indicators point out the outcomes and effects occurring in the land. Comparison of input and output indices shows the efficiency.

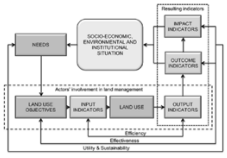

Figure 1. Evaluation Model for Suitable Land Use [1]

Comparison of land use goals and results shows the effectiveness, and finally, to what extent the results can meet the needs of a community, demonstrates the utility and sustainability of land use management systems. Two matrices are used as the decision-making model in land planning program (table 1 and table 2). In table 1, the current status of land use is compared with the ecological potential of it. In the current land use column, if it is based on the ecological potential of it, there is a balanced development; if there is the possibility of deployment of land use based on the ecological potential, it is the possible land use. Otherwise, if the land does not have the ecological capability, it is unbalanced development, and, if it is not possible to deploy, the development of the suitable development is impossible. The comparison of two land use maps in the year of the ICZM establishment and the current land use measures the effectiveness and efficiency. There are two situations: 1) The situation that the land is in use currently; 2) The situation that the land without any land uses currently.

Table 1. Decision Making Matrix in LUP Monitoring [2]

Situation Analysis		Current status	
		has the suitable land use Currently	Without any suitable land use
Ecological capability Outcomes	has the ecological capability for the intended land use	Balanced development	There is the possibility of developing the intended land use
	Without the capability for the intended land use	Unbalanced development	There is not the possibility of developing the intended land use

Table 2. Capability Matrix of Existing Land Uses and Applications for the Year of the Establishment of ICZM

		The Year of the Establishment of ICZM	Existing land uses	Adaptation
Results of Capability	Have current land use	Balanced	Balanced	+
		Unbalanced	Unbalanced	-
		Balanced	Unbalanced	-
		Unbalanced	Balanced	+
	Without land use	Possible	Possible	+
		Impossible	Impossible	+
		Impossible	Unbalanced	-
		Possible	Unbalanced	-

1. The situation that the land is in use currently: If the land use of deployment time was balanced, and the same land use has been preserved, indicates the input and output fit. However, in cases where A: the land use of deployment time was unbalanced, and the same land use has been preserved, B: The land use of deployment time was unbalanced, but was created in the current state of the balanced land use, and C: The cases where the previous land use was balanced and is unbalanced in the current situation; indicates the lack a alignment between the expected goals and results and the effectiveness of national plan.

2. In cases where: 1) The land has not been in use at the time of ICZM establishment, but it is possible to develop in the present situation; 2) The land has been impossible to use at the time of the ICZM establishment, and it is impossible to develop in current situation; 3) The cases where the land use of deployment time is known to be unbalanced; 4) Issues that the land use deployed may be known and unbalanced in the present situation indicates that the goals or expected results and the effectiveness of the national plan are not aligned. The capability matrix is presented in Table 2. Indicators of evaluation and monitoring of the suitable land use plan are two parts:1- The first category of indicators is similar to the managerial, ecological, and socio-economic indicators. Since the goal of suitable land use is sustainable development, the three main aspects are economic and social, environmental and governance and policy making. [2]. 2. The second category of suitable land use indicators should monitor the compliance of outputs with ICZM goals and programs spatially. Regarding to the main outputs of ICZM, that is the zoning of the land use consistent with the capability land, planned land uses and agricultural capability, in this section, the indicators that are allowed to be monitoring spatially should be considered.

3. Results

The results include: 1) The monitoring and evaluating indicators for suitable land use, and 2) The tree of goals and indicators according to the suitable land use action plan.

1) All the management indicators, and sub-indices used in suitable land use, which are not sometimes listed in the IOC, are listed in table 3.

2) The tree of indicators has been developed based on the action plan related to coastal management and environmental hazards in the National ICZM Plan. In this tree, the indicators are presented for the three main approaches: conservation, development and integration (Figure 2).

Table 3. Indicators and Sub-Indices Used in Monitoring the Suitable Land Use

Indicator		Sub-Indices	
E9	Habitat quality	E9.2	Habitat changes
		E9.4	Landscape Integrity (Integrity of Coastal Habitats)
SE5	Human pressures on habitats	SE5.1	Land cover/land use
		SE5.5	Coast changes (in the terms of land use)
G3	EIA, SEA and CCA approaches for the plans, programs and projects affecting on coastal zones	G3.1	Status of EIA in the projects with legal obligations
		G3.2	Status of SEA in the projects with legal obligations
		G3.3	Level of activity or loading outside the boundary capacity in the land
G4	Existence of a mechanism to solve the conflicts and its function	G4.1	If there is a land use planning document to solve the land use conflicts or not?
G5	Existence of the comprehensive coastal management plans	G5.1	Status of the programmed and changed land uses, including conserving, Developing and Integrating
		G5.2	The status of licenses issued for the deployment of activities in accordance with ICZM programs
G6	Active management in the ICZM zones	G6.1	Status of the land uses changed to conserving land use due to the land destruction
		G6.2	Geographical variation features of existing and changed uses compared to the time of ICZM deployment

Figure 2. Tree of Goals and Indicators in the Conservation Approach for Suitable Land Use Monitoring

References

[1] Handbook on Monitoring and Evaluating for Results. 2002. UNDP, Evaluation Office, United Nations Development Program, One United Nations Plaza, New York, NY 10017, USA

[2] Evaluation of Integrated Coastal Zone Management (ICZM) in Europe – Final Report. 2006. Rupprecht Consult, Forschung and Beratung GmbH Waltherstrasse 49-51. 51069 Cologne, Germany.

EVALUATION OF ERA5 REANALYSIS SURFACE WIND DATASET USING SATELLITE MEASUREMENTS IN THE SOUTHERN PART OF THE CASPIAN SEA

Hossein Farjami[1], Parvin Ghafarian[2] and Nafiseh Pegahfar[3]

1) Iranian National Institute for Oceanography and Atmospheric Science, Tehran, Iran, h.farjami@inio.ac.ir
2) Iranian National Institute for Oceanography and Atmospheric Science, Tehran, Iran, p.ghafarian@inio.ac.ir
3) Iranian National Institute for Oceanography and Atmospheric Science, Tehran, Iran, pegahfar@inio.ac.ir

1. Introduction

Wind forcing plays an important role in various oceanic processes such as wind-waves, ocean circulation, surface currents and etc. [3]. Since the field-measured wind data are limited in spatial-temporal resolution, therefore it is unavoidable necessary to use reanalysis data in numerical models, especially ocean models, to forecast local weather conditions.

Various applicabilities, such as wide usage in different models, motivated many scientists to improve reanalysis datasets. To evaluate them as an input for the ocean models, the first step is to check these datasets in peripheral seas. For example, Mazaheri et al (2016) modified ECMWF (European Centre for Medium-Range Weather Forecasts) wind data by using QuikSCAT data for wave hindcasting in Iranian peripheral Sea [4].

ERA5 is the latest reanalysis dataset of atmospheric, oceanic and land parameters that produced by ECMWF on a global grid [1].

In this research, sea-surface wind data from ERA5 reanalysis dataset have been evaluated to illustrate their accuracy as an input for ocean models. This test has been done over the Caspian Sea. For this aim, sea-surface wind data measured by scattrometer satellite and also in-situ measurements have been used. The results can be used in ocean models for coastal applications and offshore operations.

2. Materials and Methods

Sea-surface wind data of ERA5 reanalysis dataset is evaluated by comparing in-situ and satellite measurements over the Caspian Sea basin. ERA5 data, available from 2008 to present in http://apps.ecmwf.int/datasets/, has 30-km spatial resolution [6].

In-situ data include ones measured by buoy in Bandar-e-Anzali, Kiahsahr, Nowshahr and Amiraband and also by automatic weather station in the Amirkabir oil platform (Table 1.) and the satellite data measured by scatterometer. The Advanced Scatterometer (ASCAT) instrument is on MetOp-B platform, which was launched on 17 sep. 2012. ASCAT operates in the C-band frequency (5.255 GHz) at 25 km sampling resolution [5] (http://satin.rshu.ru/).

The wind data from buoys and automatic weather stations have been measured in different altitudes. To acheve wind velocity at 10m height, we used power law formula of $u(z_1) = u(z_2)\ln(z_1/z_0)/\ln(z_2/z_0)$ [2], where, $u(z_1)$ and $u(z_2)$ are wind velocity at the heights of z_1 and z_2 respectively, and z_0 is constant coefficient. To interpolate satellite data, the nearest grid point method has been used.

Table 1. Information of buoys and auto-station

Buoy or Sta. Name	Location	Period of observation	Time Duration (day)
Bandar-e-Kiashahr	37.48E 49.86N	01 Jan. 2015 – 30 Sept. 2015	143
Oil platform	38.45E 51.25N	01 Jun. 2014- 08 Jul. 2014	38
Bandar-e-Anzali	36.95E 53.31N	28 Oct. 2012- 14 Jul. 2013	333
Bandar-e-Nushahr	37.52E 49.44N	14 Mar. 2013- 24 Jun. 2013	76

3. Results and Discussion

The statistics comparing of ERA5 data to scatterometer and in-situ measured data during 2013-2015 was done over deep water and in shallow water of the Caspian Sea. For example, the ERA5 wind speed on January 04, 2015 at 18:00:00, ASCAT measurements of 10-m wind vector on January 04, 2015 at 18:06:00 and oil platform position are shown in Figure 1. The quantile-quantile (Q-Q) plot (Figure 2) shows a remarkable agreement between ERA5 wind speed and scatterometer measurements for wind velocity values in the range of 6 - 8 m/s. The ERA5 measured data underestimate wind velocity between zero and 6 m/s, comparing with ASCAT data. Time series analysis of wind speed from ERA5, ERA-Interim reanalysis data and in-situ measurements are shown in Figure 3 from June 01, 2014 to July 09, 2014 at 12:00 over the deep water of the Caspian Sea.

Generally, the results of this study indicate that it is necessary to modify ERA5 reanalysis wind velocity data over the coastal areas of the Caspian (Figures not shown here).

In some cases, the statistical analysis of ERA5 wind speed in deep water area shows the mean bias of -0.4m/s and the correlation coefficient of 0.96.

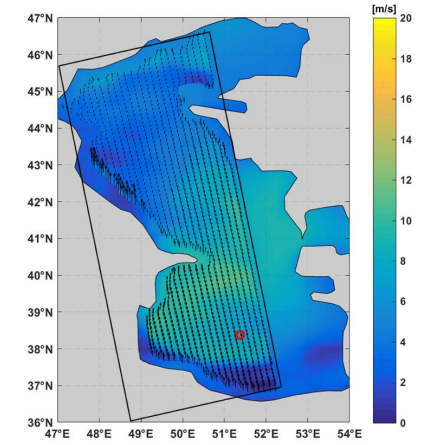

Figure 1. The ERA5 wind speed, ASCAT wind vector and oil platform position (red circle).

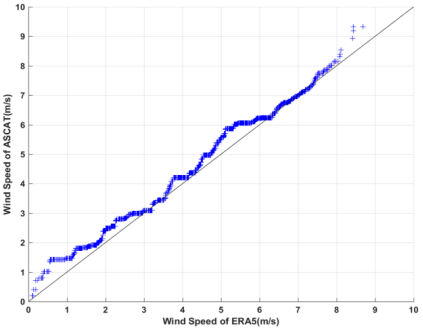

Figure 2. The Q-Q plot of ERA5 comparing ASCAT measurements on January 04, 2015.

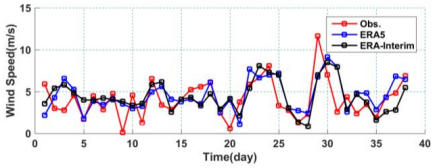

Figure 3. Wind speed comparison of in-situ measurements and ECMWF dataset in the oil platform position.

In this paper the sea-surface wind velocity of ERA5 reanalysis data were evaluated over the Caspian Sea using satellite scatterometer data and in-situ measurements.

The results show that the wind speed of ERA5 has good correlation with satellite and in-situ measurements in the offshore of the Caspian Sea. However, in the coastal area need an algorithm to modify that and decrease wind speed error to increase its accuracy for using in local weather forecasting and also ocean models.

4. References

[1] ERA5 data documentation, {*Available online at: https://software.ecmwf.int/wiki/display/CKB/ERA5+data+documentation*}.

[2] Garratt, J., "The Atmospheric Boundary Layer", Cambridge University Press, 1992, 316 pp.

[3] Grifoll, M., Navarro, J., Pallares, E., Ràfols, R., Espino, M. and Palomares, A., " Ocean–atmosphere–wave characterisation of a wind jet (Ebro shelf, NW Mediterranean Sea)". *Nonlin. Processes Geophys*., 2016, No. 23, pp. 143-158.

[4] Mazaheri, S., Kamranzad, B. and Hajivalie, F., "Modification of 32 years ECMWF wind field using QuikSCAT data for wave hindcasting in Iranian Seas", *Journal of Coastal Research*, Jan 2013, pp. 344-349.

[5] Ocean and Sea Ice SAF EUMETSAT Advanced Retransmission Service, "ASCAT Wind Product User Manual", Version 1.14, March 2016.

[6] Uppala S, Ka¨llberg P, Simmons A, Andrae U, daCosta Bechtold V, Fiorino M, Gibson J, Haseler J, Hernandez A, Kelly G, Li OK X, Saarinen S, Sokka N, Allan R, Andersson E, Arpe K, MA B, Beljaars A, van de Berg L, Bidlot J, Bormann N, Caires S, Chevallier F, Dethof A, Dragosavac M, Fisher M, Fuentes M, Hagemann S, Hlm E, Hoskins B, Isaksen L, Janssen P, Jenne MA R, Mahfouf JF, Morcrette JJ, Rayner N, Saunders R, Simon P, Sterl A, Trenberth K, Untch A, Vasiljevic D, Viterbo P, Woollen J., "The ERA-40 re-analysis". *Q J R Meteorol Soc* 131, pp. 2961–3012.

STRATEGIC AND OPERATION PLANNING FORREDUCING PORTS VULNERABILITY FACING THREATS

Mohammad Reza Fallah Ghanbari[1], Hoda Fasihi Karami[2], Morteza Mansour Dehghan[3] and Mona Moghaddam[4]

1) Faculty of Special Planning and Passive Defense, Poly technique university of Malek Ashtar, Tehran, Iran, m.fallah.teh@gmail.com
2) Road, Housing & Urban Development Research Center, Tehran, Iran, hoda.fasihi@gmail.com
3) Port & Maritime Organization, Tehran, Iran, mortezadeh@gmail.com
4) Road, Housing & Urban Development Research Center, Tehran, Iran, mona.moghaddam@yahoo.com

1. Introduction

Due to the type of imported and exported commodities, Iran has a significant dependency on import some commodities, including cereals and some basic commodities. The inappropriate distribution of imports through the ports and importing essential goods from one or two ports will lead to high vulnerability in the case of threat occurrence and have national adverse consequence. In addition, in recent years, some of the Iranian ports have been moved towards the development and creation of third-generation ports, which has led to the build of warehouses, conversion facilities, specialized warehouses in the port and hinterland. However, it should be noted that the aggregation of infrastructures in one location will increase the overall vulnerability of complex and causes significant adverse effects for the country as a result of the threats occurrence [1].

Currently, more than 90% of the country's commodity exchanges are transported through sea routes and ports, and among the 17 ports belong to the Iranian Ports and Maritime Organization, nearly 85% of the volume of goods exchanges is performed only through two ports, and 15% of exchanges goods are delivered through the remaining 15 ports [2]. Other issues in this area are the import of essential goods and its relation to the ports. While the country has a high dependence on some of the essential commodities, such as oilseeds and edible oils as well as cereals, the import of these items from one or two ports leads to vulnerability in the case of threat occurrence. At present, a large amount of the Iran's essential goods are imported only from one port and if this route stopped will result in adverse consequences in the supply chain and various sections and rise in prices for basic goods [3]. Moreover, the development of third generation ports and the creation of warehouses and conversion industries in the hinterland will lead to the accumulation of installations and goods and increases the stand time of goods in the port. On the other hand, in the absence of appropriate strategies at the national level, the accumulation of certain industries in an area, make vulnerable target facing the threats. Sanctions are one of the other issues that have always affected various parts of the country's economy in recent years [4]. The Sanctions is one of the threats of ports and shipping lines, which have had various impacts on ports and maritime in recent years. Considering these issues, adopting appropriate strategies for port development could lead to a general reduction in vulnerability of ports [4]. In Figure 1, the subject of the vulnerability of ports is summarized.

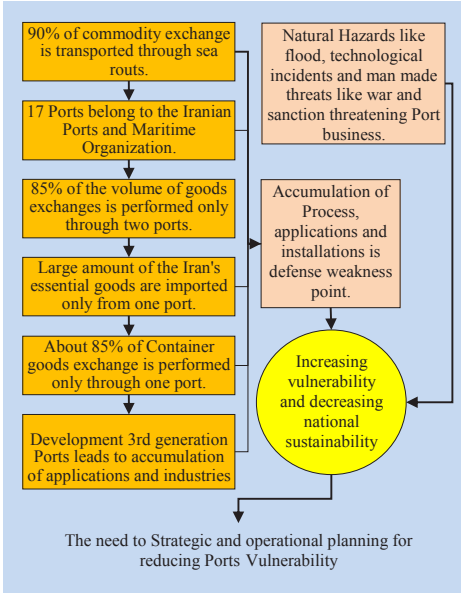

Figure 1.Vulnerability of Iranian Ports

2. Methodology

This study was conducted to strategic and operational planning activities in the ports and maritime domain. This article is part of the research project of the Passive Defense and Emergency Management of two key ports of Iran. The

SWOT matrix was used to extract strategic planning approaches, and the strengths, weaknesses, opportunities and threats in the ports and maritime domain were determined using this matrix [6]. For operational planning, the FEMA452 risk assessment method was used with some changes for port zone studies. This method is used to assess the vulnerability of buildings to terrorist attack, which was developed for this study to cover all threats such as military, terrorist, sabotage, cybercrime and etc. It is intended to extract vulnerabilities in this regard in order to determine operational planning approaches [7].The FEMA452 method was implemented as a case study in a port. In this research, statistical resources and documents study, field study, case study, interview with experts and use of evaluation method and 10 experts in the form of a focused group were conducted. In the focus group meetings, the initial results from documents study, interviews and field studies were presented to experts and, using their comments, final results were extracted.

3. Results

In the strategic level, 5significant weaknesses, 3-strengths, 5 threats and 3opportunities were identified. Identified threats include: economic sanctions, threats of military attack, cyber threats, terrorist threats and the presence of regional and international rivals. The identified strategic weaknesses include:

- Import and Export large volume of goods through two ports in the country
- Import large volumes of essential goods from a port in the country.
- Import and export large volume of container goods through a port
- Lack of 100% of resiliency and business continuity of the vital ports of the country in the event of threats.
- Limited use of foreign investors in the ports of the country

In the operational level and case study, four high risks and eight average risks were extracted in a port. The high risks that are extracted for a key port include:

- Uniqueness of access road to the port and its high vulnerability to air strikes and other threats.
- Exclusive development in one or two areas in the hinterland and accumulation of one or two specific Application.
- contiguity with hazardous installations
- The vulnerability of electricity infrastructure
- Specific import Pier for some of the essential goods.

4. Discussion and Conclusion

Port planning to reduce vulnerability can be considered in strategic and operational level. At strategic level, the issue of development of the ports, use of dry ports, distribution of volume of commodity exchanges among existing ports, development of linear shipment and building of hub ports for servicing other countries (subsequently reduces the level of threats), the use of foreign investors in the development of ports, especially in the development of hinterland, as well as use of alternative ports in emergency situations, and so on should be considered. These approaches are those that use in strategic level that can reduce vulnerability and increase National Sustainability. At the operational level, dispersion of activities, multipurpose use of installations and applications, increasing the capability of replacing processes and activities in ports should be considered. For example, while 50% of the country's edible oil imports from one port, the use of the dedicated pier with the transmission pipeline to this purpose which, if damaged, will require a great deal of time to recovery, will have dimensions beyond the boundaries of the port and will have significant consequences for the country, hence planning in the operational level should be used to correct and reduce vulnerabilities in the design of the Port elements. It should be known that enemies seeks to identify such weaknesses in the country in order to exploit these weaknesses in military attacks or other threats in order to inflict the most damage. In contrast, planning to reduce the vulnerability at strategic and operational level will increase the stability of ports and country in the face of threats, and it is deterrent factor against the implementation of threats [8].

5. References

[1] Passive defense and emergency Management Plan for Iranian Port, Research Project, Road, Housing and Development Research Center, Ministry of Roads & Urban Development, 2017-2018

[2] Statistical Yearbook of Iranian Maritime organization, in access at website: pmo.ir

[3] Statistical Yearbook of Islamic Republic of Iran Customs Administration, in access at website: www.irica.gov.ir

[4]A.K.C. Beresford and, B.M Gardner, the UNCTAD and workout model of Port Development: evolution or Revolution, Cardiff University, 2011

[5] https://www.westpandi.com/Special/Sanctions/iran/

[6] http://www.quickmba.com/strategy/swot/

[7] FEMA 452 - Risk Assessment: A How-To Guide to Mitigate Potential Terrorist Attacks against Buildings

[8] jalali, Gholamreza, 4speech in passive defense, Iranian Passive Defense organization, Publisher, Mohades, 1391

MARINE SPATIAL PLANNING, A NEW MARINE MANAGEMENT POLICY IN IRAN

Saeed Lotfikhah[1], Monir Haghighat[2], Marjan Mirhosseini[3] and Ali Pak[4]

1) Sazeh Pardazi Iran (SPI) Consulting Eng. Co, Tehran, Iran, s.lotfikhah@sazehpardazi.com
2) Ports and Maritime Organization (PMO), Tehran, Iran, mhaghighat@pmo.ir
3) Sazeh Pardazi Iran (SPI) Consulting Eng. Co, Tehran, Iran, mirhosseini.marjan@gmail.com
4) Civil Engineering Department, Sharif University of Technology, Tehran, Iran, pak@sharif.edu

1. Introduction*

Marine Spatial Planning (MSP) has been increasingly recognized as an efficient tool for sustainable management of marine environment all around the globe. Based on UNESCO (2009) Marine Spatial Planning is the process of analyzing various human activities in the marine areas and zoning them with the aim of achieving ecological, economic, and social goals based on a specific political will. In the course of this analysis, different spatial and temporal variables of human activities are distinguished and used in the planning process.

Marine Spatial Planning (MSP) has certain characteristics as mentioned below:

- MSP is an ecosystem-based plan. MSP has specific socioeconomic and environmental goals for sustainable development.
- MSP is an integrated plan. This means that MSP strives to create integration among all stakeholders such as governmental and private sectors at all levels.
- MSP is a spatial plan and is bounded with certain boundaries.
- MSP is adaptive. This means that MSP learns from previous experiences and modifies the plan accordingly.
- MSP is a strategic plan and is based on long-term goals.
- MSP is a participatory plan and tries to involve all the stakeholders in the management process.

Marine ecosystem due to the multitude services and resources that provides for human being exploitation, has always been attractive. However, its capacity is less than the ever-growing expected demand. Seas from the management viewpoint are considered "Common Property Resources" and access to them should be open and remain open for all people. The rate of exploitation of coastal and territorial waters has caused problems such as fish stock reduction, threat to biodiversity, sea water pollution, conflicts among stakeholders, etc. Following a sustainable development process, coordinating human activities, and creating integration among various types of uses in the marine area requires establishment of an ecosystem-based management for wise exploitation of the marine resources. Different types of human activities in marine environment are summarized in Table (1).

* This article is retrieved from Marine Spatial Plan for Hormozgan Province

Table 1. Human activities in Sea Area

No.	Activity
1	Commercial Fishing
2	Mari culture
3	Recreational Fishing
4	Sea Tourism
5	Sea Transportation
6	Berthing and Mooring
7	Waste disposal
8	Offshore Industries
9	Offshore Airports
10	Offshore LNG terminals
11	Offshore oil/gas extraction
12	Sea bottom pipelines
13	Sand/gravel extraction
14	Offshore renewable energy extraction
15	Water desalination plants
16	Water desalination plants
17	Co_2 sequestration
18	Cultural/historical heritage
19	Sea protected areas
20	aqua parks
21	Military zone
22	Research and Monitoring

The major outcome of Marine Spatial Planning can be summarized as follows:

- Conflicts among the stakeholders are diminished by establishing a prioritization scheme.
- Non-governmental sector is involved in the plans and related budget allocations in marine area
- Efficient use of space and resources of the sea is exercised
- Ecosystem-based management is employed for new activities
- Mutual understanding between the stakeholders grows by exercising the participatory measures

2. Previous MSP Cases

By mid-2017, 65 countries around the world have initiated MSP endeavors. Six countries including Belgium, Holland, Germany, Norway, Australia, and China and three states of the U.S.A have already implemented their Marine Spatial Plans in their territories. Almost 140 MSP cases are currently under way at three different borders; Territorial Waters, Contiguous Zone, and Exclusive Economic Zone (EEZ). Figure (1) illustrates the countries that have maritime policies.

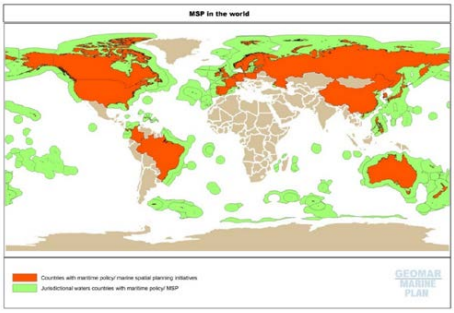

Figure 1. Countries that have Maritime policy or MSP

Most of the countries that have started their efforts for spatial planning of their marine territories, consider MSP as part of their Integrated Coastal Zone Management (ICZM) plan. Although MSP should not necessarily become part of ICZM, since both plans try to regularize the human activities and aim to create equalization with respect to the environmental capacities and sensitivities, integrating the ICZM plans with MSP is expected to yield positive outcome.

3. MSP Procedure and Outcome

Marine Spatial Planning (MSP) can be carried out through the followings steps:

1) Pre-planning: In this stage the authority, stakeholders, financial resources, work plan draft, existing problems, long-term objectives, boundaries, SMART objectives and vision will be explained.

2) Plan Analysis: In this stage data gathering, data structuring, analysis of existing situation, analysis of future circumstances is carried out and a data Atlas/data portal is provided.

3) Plan development: In this stage primary management actions, efficiency indices, performance monitoring will be introduced.

4) Plan Completion: In this stage all the issues will be completed in the project framework.

5) Plan Approval: In this stage, the prepared plan will be endorsed by the governmental authorities.

6) Plan Implementation: In this stage, the approved plan will be implemented while the monitoring and evaluation of the performance will be considered.

7) Management Plan Revision: Based on the implementation outcome, the plan will be modified/ revised.

4. Main MSP in Iran

Marine Spatial Planning pilot project is initiated by Ports and Maritime Organization (PMO) of Iran as a complementary project for Hormozgan ICZM plan. The project will follow the steps that mentioned above considering the sensitivities of the Persian Gulf, Hormuz Strait, and Oman Sea from ecological, economical, and political viewpoints. The boundaries of Iran's Marine Spatial Plan are depicted in Figure 2.

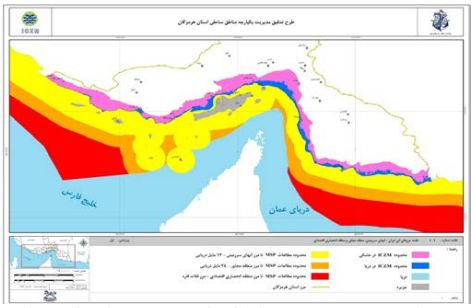

Figure 2. Three zones of MSP in Hormozgan Province

5. References

[1] Collie, J.S., Beck, M.W., Craig, B., Essington, T.E., Fluharty, D., Rice, J. and Sanchirico, J.N., 2013. Marine spatial planning in practice. Estuarine, Coastal and Shelf Science, 117, pp.1-11.

[2] Douvere, F., 2008. The importance of marine spatial planning in advancing ecosystem-based sea use management. Marine policy, 32(5), pp.762-771.

[3] Douvere, F. and Ehler, C.N., 2011. The importance of monitoring and evaluation in adaptive maritime spatial planning. Journal of Coastal Conservation, 15(2), pp.305-311.

[4] Ehler, C. and Douvere, F., 2009. Marine spatial planning: a step-by-step approach toward ecosystem based management. UNESCO/IOC.

[5] Flannery, W 2015, Review of Marine Spatial Planning Best Practice of Relevance to Ireland. Marine Institute.

[6] Flannery, W., O'Hagan, A.M., O'Mahony, C., Ritchie, H. & Twomey, S. 2015. Evaluating conditions for transboundary marine spatial planning: challenges and opportunities on the island of Ireland. Marine Policy, 51: 86–95.

[7] Lund, Nicholas. J.D., 2011. What Is Coastal and Marine Spatial Planning conference presented at National Sea Grant Law Center

[8] Maes, F . 2008. Legal perspectives in coastal zone management. A future for fisheries? Towards effective strategies for sustainability. Symposium conducted at Maritime Institute, Ghent University, Belgium.

ASSESSING COASTAL FLOODING EXPOSURE TO SEA LEVEL RISE- A CASE STUDY OF BANDAR ABBAS CITY

Vahid Hadipour[1], Freydoon Vafaie[2] and Abouzar Hadipour[3]

1) Civil Engineering Faculty, K.N. Toosi University of Technology, Tehran, Iran, vahid.hadipour85@gmail.com
2) Civil Engineering Faculty, K.N. Toosi University of Technology, Tehran, Iran, fvafai@kntu.ac.ir
3) Civil Engineering Faculty, K.N. Toosi University of Technology, Tehran, Iran, abha571@yahoo.com

1. Introduction

Coastal population has been increasing since the last century, approximately three times more than global average [1]. Coastal cities also play an important role on national and global economy.

On the one hand, Intergovernmental panel on climate change (IPCC) anticipates that sea level rises due to climate change and greenhouse gases emission. On the other hand, storms with more frequency and intensity will take place in the future years. Generally, coastal zones always are exposed to sea level rise (SLR) and other types of coastal hazards like storm surge, current, etc. [2].

Exposure analysis as a vulnerability component is employed to determine to some extent people, assets, and ecosystems: wetlands, aquifers, and estuaries are affected during coastal hazards. As a significant factor it can be also used by decision makers to reduce disaster risks.

In this regard, the main objective of this paper is to assess the coastal exposed zones due to SLR and extreme flooding in Bandar Abbas City, Iran.

2. Case Study

This study is applied to Bandar Abbas city as a case study area. Bandar Abbas, the largest port city in Iran, has been located in Iranian southern coastal areas and in the north of Persian Gulf (see Figure 1). It plays an important role in national economy. In addition, its population has been estimated around 520000 based on Iranian Statistical Center, 2012 [3].

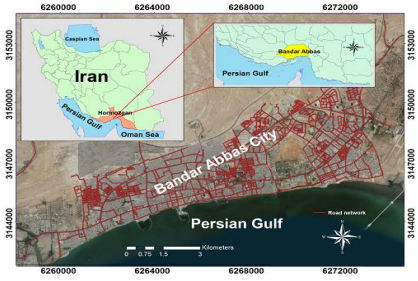

Figure 1. Geographical location of case study area

3. Material and Methods

3.1. Permanente and Temporary Sea Level Rise

In this study, extreme sea levels are categorized into two main factors: permanent and temporary sea levels. The former caused by climate change while the latter is related to hydrodynamic phenomenon including wave setup, wind setup, tidal range and storm surge.

To estimate SLR caused by climate change, some global models have been employed [2]. However, these models are based on global scale and in reality would not be able to predict SLR at local area. In this regard, these global models can be downscaled into local scale to be more precise and logical. In this study, we follow a downscaled model, based on Representative Concentration Pathways (RCPs): IPCC 2013, in Hormozgan province [4]. According to RCPs, SLR caused by climate change will have been predicted until the future years.

Determining temporary sea lever rise is regarded as one of the most important factor for coastal zone management since it assists decision makers to calculated hazard line: the extent of water moving to inland. For the temporary sea level rise in the case study area, wave setup, wind setup, tidal range and storm surge were considered according to Integrated Coastal Zone Management project provided by Iranian maritime and port organization [5]. Concerning temporary sea levels, wave setup, wind setup and storm surge took into account with emphasize on return periods while tidal range was determined based on Mean Higher High Water (MHHW) in the study area.

3.2. Scenario Definition

Temporary and permanent sea levels are accompanied with some uncertainties. To overcome this, scenarios were applied to calculate future floods. Finally, the flooded area can be estimated under different scenarios: present time without considering SLR caused by climate change to the worst case scenario considering: wave setup, wind setup and storm surge (50 and 100 years return periods); MHHW and SLR (RCP2.6 and RCP 8.5).

4. Results

Permanent and temporary sea levels are combined to each other under different scenarios (see Figure 2). As we can see, under S_0 scenario there is no SLR due to climate

change and by considering temporary sea level: wave setup and wind setup (50 years return periods) along with MHHW (144 cm), the total expected sea level rise is around 233cm. However, in the worst case scenario (S_1) SLR caused by climate change in 2100 along with wind setup and wave setup (100 years return periods), MHHW and storm surge were regarded. In this case, a significant difference in sea level was seen (501 cm). Considering Digital Elevation Model (DEM) of Bandar Abbas, a remarkable southern area of this city has elevation around five meters higher than mean sea level. So, using GIS the total coastal flooded areas of Bandar Abbas city in S_0 and S_1 was approximately estimated 70 and 200 hectares, respectively. This means that coastal exposed areas in S_1 scenario will be increasing around three times compared to S_0 scenario by 2100. In addition, residential areas were affected more than the other land uses in S_1 scenario. Results showed that, by taking into account the SLR caused by climate change, Bandar Abbas city will be more at flood risk in the future.

5. Conclusions

The main purpose of this study is to assess coastal flooding of Bandar Abbas city under different scenarios. The exposure analysis in this study predicts the flooded areas by considering different land uses. Some southern districts of Bandar Abbas are more affected due to coastal flooding under S_1 scenarios since these districts are low-laying area (around five meters above mean sea level). In addition, in S_1 scenario a large number of residential areas are exposed to inundation compared to S_0 scenario. Therefore, some adaptation strategies including engineering and non-engineering approaches are strongly needed to reduce a disaster risk in this area. Though, there are some seawalls and breakwaters in Bandar Abbas city but decision makers should be aware for future disasters. Furthermore, other triggers like socio-economic developments and population growth should be taken into account for the future along with SLR and coastal extreme flooding.

6. References

[1] Small, C. and Nicholls, R.J., "A global analysis of human settlement in coastal zones", *Journal of coastal research*, 2003, pp.584-599.

[2] IPCC, "Climate Change 2013: The Physical Science Basis. Contribution of Working Group I to the Fifth Assessment Report of the Intergovernmental Panel on Climate Change", *Cambridge University Press, Cambridge, United Kingdom and New York, NY, USA*, 2013.

[3] ISC, "Iranian Statistic Center, Census data", Tehran, Iran, 2012.

[4] Irani, M., Massah, A., Mashal, M., Bohloli, A. and Alizadeh, H., "Coastal inundation assessment under sea level rise". *1st International Conference on Climate Change, Tehran, Iran*, 2017.

[5] ICZM, "Integrated Coastal Zone Management project", *Iranian port and maritime organization*, 2014.

Table 1. Constructing SLR scenarios for case study area

Scenarios	Permanent sea level rise (cm)		Temporary sea level rise			Total expected sea level rise (cm)
			MHHW (cm)	Parameters	Level (cm)	
S0 (present time)	-		144	Wave setup+ Wind setup (50 years return periods)	89	233
S1 (2100)	Average (RCP2.6 and RCP 8.5)	57	144	Wave and Wind setup (100 return periods)+ Storm surge	300	501

LONG-TERM SHORELINE DETECTION AND MEASUREMENT IN BOUSHEHR PROVINCE, IRAN

Saeed Zeinali[1], Maryam Dehghani[2] and Naser Talebbeydokhti[3]

1) Civil & Environmental Engineering, Shiraz University, Shiraz, Iran, E-mail: zeinali.saeed@shirazu.ac.ir
2) Civil & Environmental Engineering, Shiraz University, Shiraz, Iran, dehghani_rsgsi@yahoo.com
3) Professor, Civil & Environmental Engineering, Shiraz University, Shiraz, Iran, naser@shirazu.ac.ir

1. Introduction

There has been so many methods in studying coastal and shoreline evolution. Each has been used in so many studies and their performances have been reported in literature. Some of these methods could pointed out as numerical models based on historical data, Mote-Carlo, mathematical models, models based on regime equations and models using data assimilation [7, 8, 9, 10, 11 & 12]. Although, these methods are very reliable, but they might have some defects. The need for huge amount of input data, which are mostly field data, increases the computational cost and effort for modeling. The fact that field data for shoreline modeling usually must be obtained in the same time of each year, makes useless some of the historically recorded data. Fairly most of these models are site-specific and could be used for a particular area. Due to complexity of coastal and the significance of affecting parameters, these models may exclude some parameters for the sake of simplification.

Improvements in coastal studies suggests that remote sensing (RS) and geographical information system (GIS) are very useful tools and make the studies easier [13]. Application of satellite images simply provides images of study area for the desired time period and acquisition date [14]. Also, these images have recorded the effect of all dominant parameters on the coastal area and shoreline. Therefore, no unnecessary simplifying assumption is needed. Furthermore, the fact the satellite images are available for any area that the study might be, makes it globally applicable.

2. Study Area

In order to carry out this work, a part of southern shoreline of Iran is selected. This region is located in south of Bushehr province and is part of the Persian Gulf shores (Figure 1).

3. Methodology

There are several methods to extract shoreline in a satellite image such as visual interpretation, classification, band ratio and thresholding [15, 16, 3, 17 & 18]. The accuracy of visual interpretation is very dependent on the accuracy of interpreter. It is fast but can have high approximation that leads into low accuracy. The classification method also is based on the sample point chosen for each class. So, the accuracy of classification is highly related to the accuracy of chosen sample points.

Since we are dealing with shoreline which is the boundary between water and land, a specific band ratio could be used that is Normalized Difference Water Index (NDWI). This criteria highly differentiates the digital numbers of water and land in an image. The equation for NDWI is [19]:

$$NDWI = \frac{X_{green} - X_{nir}}{X_{green} + X_{nir}} \quad (1)$$

in which X_{green} and X_{nir} are the digital numbers for green and near infrared bands, respectively. This equation is applied to every single pixel in the image. The resulted images will be then applied by a thresholding equation. In thresholding if an image $I(x,y)$ contains light objects on a dark background, then these objects may be extracted by a simple thresholding:

$$I(x,y) = \begin{cases} 1 & I(x,y) > T \\ 0 & I(x,y) \le T \end{cases} \quad (2)$$

where T is the threshold value supplied empirically or statistically by the analyst. All the pixels which belong to the object are coded 1, and the background is coded 0 [20]. The resulted images will be used to calculate the changes in time.

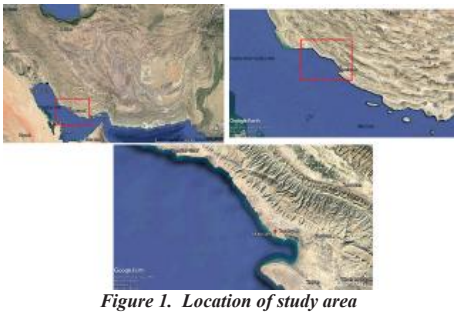

Figure 1. Location of study area

4. Results and Discussions

In the resulting images, the red and blue colours represent shoreline advance and retreat, respectively. In other words, pixels from water that are changed into land, are marked in red and pixels changed from land to water, are marked in blue. In order to have a better understanding of changes, different cross sections are defined to extract the magnitudes of shoreline change between years 1987-2017. Cross sections are defined in places with high changes, both sides of dikes and both sides of river mouths. Overlay of changes on the study area and location of cross sections are shown in Figure 2.

5. Conclusions

The most unpleasant event in coastal areas with commercial and trading activities, is the accretion and recession near the dikes and ports. This may put them out of service that will be huge loss of money spent on construction and large damage because of shut down commercial activities. This chain of events, at the end, will affect the community that profits from the coast and the sea. No need to remind that sedimentation and erosion is act of nature and cannot be stopped. So, the only solution is to control this phenomenon in the favour of the environment. In order to control it, its attribute and characteristics through time must be studied. In this study we have tried a simple yet efficient and accurate method to extract shoreline changes in time. This scheme can simply be implemented in any coastal area.

Understanding the behaviour of shoreline and the pattern that it is changing itself, is a key element in coastal zone management. Carefully studied the shoreline changes, one can separate the changes caused by natural forces and those that are human induced. Each of these changes needs separate methods to care. A low budget for coastal protection in potential parts of a shoreline may prevent to spend of a large budget for recovering a port filled with sediments.

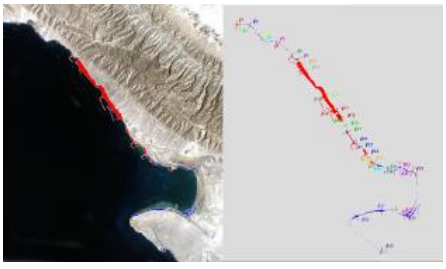

Figure 2. Location of study area

6. References

[1] Santra, A., Mitra, D., and Mitra, S., "Future shoreline prediction along Junput coast, west Bangal, India", *Geo-Spatial Information Science,* 14, 3, 2011, pp. 157-163.

[2] Scott, D. B., *Encyclopaedia of Coastal Sciences,* Springer, Netherlands, 2005, pp. 253-255.

[3] Chalabi, A., Mohd-Lokman, H., Mohd-Suffian, I., Karamali, M., Karthigeyan, V., and Masita, M., "Monitoring shoreline change using IKONOS image and aerial photographs: A case study of Kuala Terengganu area, Malaysia", *ISPRS Commission VII Mid-term Symposium*, Netherlands, 2006.

[4] Mani, J. S., Murali, K., and Chitra, K., "Prediction of shoreline behavior for Madras, India-A numerical approach", *Ocean Engineering*, 24, 10, 1997, pp. 967-984.

[5] Kaminsky, G. M., Buijsman, M. C., and Ruggeiro, P., "Predicting shoreline change at decadal scale in the Pacific northwest, USA", *Proc. 27th Int. Coast Engrg. Conf ASCE*, 2006, pp. 2400-2413.

[6] Adamo, F., De Capua, C., Filianoti, P., Lanzolla, A. M. L., and Morello, R., "A coastal erosion model to predict shoreline changes", *Measurement*, 47, 2006, pp. 734-740.

[7] Banno, M., and Kuriyama, Y., "Prediction of future shoreline change with sea-level rise and wave climate change at Hasaki, Japan", *Coastal Engineering*, 34, 2006, pp. 1-10.

[8] Davidson, M. A., Lewis, R. P., and Turner, I. L., "Forecasting seasonal to multi-year shoreline change", *Coastal Engineering*, 57, 2006, pp. 620-629.

[9] Kaewpoo, N., Nakhapakorn, K., Pumijunong, N., and Silapathong, C., "The integration of GIS and mathematical model for shoreline prediction", *The 33rd Asian Conference on Remote Sensing*, Thailand, 2012.

[10] Leont'yev, I. O., "Predicting shoreline evolution on a centennial scale using the example of the Vistula (Baltic) spit", *Marine Geology*, 52, 5, 2012, pp. 757-767.

[11] Vitousek, S., Barnard, P. L., Limber. P., Erikson, L., and Cole, B., "A model integrating longshore and cross-shore processes for predicting long-term shoreline response to climate change", *Journal of Geophysical Research*, 122, 2012, 782-806.

[12] Yamano, H., Shimazaki, H., Matsunaga, T., Ishoda, A., McClennen, C., Yokoki, H., Fujita, K., Osawa, Y., and Kayanne, H., "Evaluation of various satellite sensors for waterline extraction in a Coral Reef environment: Majuro Atoll, Marshall Islands", *Geomorphology*, 82, 2012, pp. 398-411.

[13] Chen, L. C., and Rau, J. Y., "Detection of shoreline changes for tideland area using multi-temporal satellite images ", Int. J. Remote Sensing 19(17), 1998, pp. 3383-3397.

[14] Winareso, G., and Budhiman, S., "The potential application of remote sensing data for coastal study", *Proc. 22nd Asian Conference on Remote Sensing Singapore*, 2001.

[15] Yamani, M., Rahimi Harabadi, S., and Goudarzi Mehr, S., "Periodic changes of the east strait of Hormuz shoreline by remote sensing*", Environmental Erosion Researches Hormozgan University,* 2011.

[16] Zeinali, S., Dehghani, M., Rastegar, M. A., and Mojarrad, M., "Detecting shoreline changes in Chabahar bay by processing satellite images", *Scientia Iranica*, 24, 4, 2017, pp. 1802-1809.

[17] Guariglia, A., Buonamassa, A., Losurdo, A., Saladino, R., Trivigno, M. L., Zaccagnino, A., and Colangelo, A., "A multisource approach for coastline mapping and identification of shoreline changes", *Annals of Geophysics*, 49, 1, 2006, 295-304.

[18] McFeeters, S. K., "The use of the normalized difference water index (NDWI) in the delineation of open water features", *Int. J. of Remote Sensing*, 17, 7, 1996, pp. 1425-1432.

[19] Singh, A., "Digital change detection techniques using remotely-sensed data", *Int. J. Remote Sensing*, 10, 6, 1989, pp. 989-1003.

REVIEW ON UNDER SENSOR NETWORK APPLICATIONS FOR PORT AND HARBOR SECURITY

Mohammad Akhundy[1] and Rohollah Goudarzi[1]

1) Malek Ashtar university of technology, Tehran, Iran, rohadi@mail.com

1. Introduction

Nowadays, there are many methods for protecting offshore platforms and ports. Underwater sensor network is the newest way which is recently occupied in developed countries for port security.

Sensors are utilized to determine various parameters in terrestrial, air and marine environments. Underwater sensor applications are still rarely used and comparatively expensive which express the request for long range communication and improve sensors' power usage. Such applications are working on marine environmental in-situ monitoring issue, port and harbor security, surveillance, tsunami early detection and autonomous underwater vehicle navigation [1].

Recent improvements in technologies have made the possibilities to investigate underwater by sensors at all levels. Consequently, underwater sensor network (UWSN) is rising as an enabling technology for underwater investigations. UWSN is a combination of wireless technology with small micromechanical sensor technology having smart sensing, intelligent computing, and communication abilities. UWSN is a network of sensor nodes [2] which are distributed underwater to sense the water-related features like quality, temperature, and pressure. The sensed data can be occupied using different applications. The stationary or mobile sensor nodes are connected wirelessly by communication modules to convey many different events of interest [3]. Underwater communication is mainly done with a set of nodes transmitting their data to buoyant gateway nodes that relay the data to nearest coastal monitoring and control station also called remote station [4]. In UWSN acoustic transceivers are utilized for communication. The acoustic waves are low frequency waves which give small bandwidth but have long wavelengths. So, acoustic waves can travel long distances and are occupied for relaying information over kilometers [5].

UWSNs are used for a wide range of applications like monitoring the marine environment for scientific exploration to commercial exploitation and coastline protection to underwater pollution monitoring, from water-based disaster preventions to water-based sports facilitation. UWSN presents a promising solution to ever demanding applications. In this paper, we investigate underwater acoustic sensor network for protecting offshore platforms and port security. This new method enhances security and protection. First, we introduce underwater acoustic network and we familiar with these kinds of networks and their benefits and disadvantageous. In the next section underwater sensor network architecture is described. Then some applications of UWSNs are investigated and also major technical aspects of a proper UWSN for domestic application will be explored at the end. These networks can be used for protection of port and harbor because these networks assist us to gather more information from underwater environment.

2. Underwater Acoustic Network

Underwater Acoustic Network (UAN) [6] is a public expression depicting a network of various units communicating with acoustic transmission in marine environments. Basic underwater networks are emerged by producing two way acoustic links between the many different units making up the network. Based on the given architecture these links could search over longer ranges or one might have short range links like terrestrial local area networks (LAN). Occupying underwater networks provides an efficient and cost effective method for ocean bottom and ocean column monitoring.

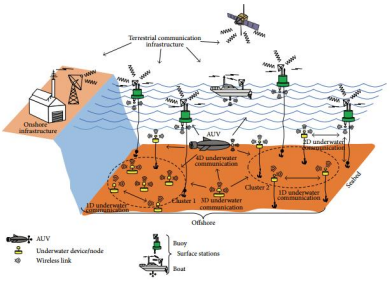

Figure 1. Underwater sensor network architecture

3. Underwater Acoustic Sensor Network Architecture (UW-ASN)

Because of the high cost involved in underwater devices, underwater monitoring missions are usually very expensive, it is essential that the deployed network be enough reliable, so as to prevent failure of monitoring missions due to failure of single or multiple devices. [7].The network capacity is also affected by the network topology.

There are various architectures for Underwater Acoustic Sensor Networks, depending on the application:

Two-dimensional UW-ASNs for ocean bottom monitoring. These are constructed by sensor nodes that are attached firmly to the bottom of the ocean. These applications may be environmental monitoring, or monitoring of underwater plates in tectonics .

Three-dimensional UW-ASNs for ocean column monitoring. These consist of networks of sensors whose depth can be controlled, and may be occupied for surveillance applications or investigating of ocean phenomena

Three-dimensional networks of Autonomous Underwater Vehicles (AUVs). These networks involve fixed portions included anchored sensors and mobile portions constructed by autonomous vehicles.

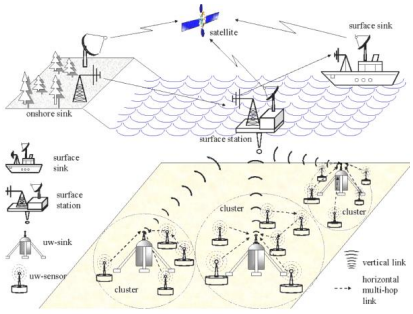

Figure 2. Two dimensional underwater sensor networks

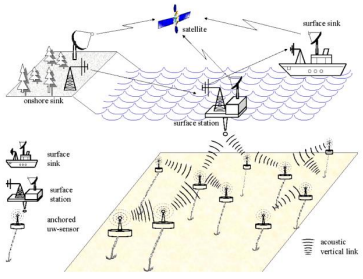

Figure 3.Three dimensional underwater sensor networks

4. UASN applications

Many applications of underwater networks are mentioned in this paper [8].

Ocean Sampling Networks. Consists of both ocean bottom sensors and AUVs. Have the ability to do synoptic, cooperative adaptive sampling of the target area, Long range and full 3D coverage.

Environmental Monitoring. By using environmental sensors in a UAN may enhance the monitoring of pollution, weather changes, ocean currents and marine ecosystems.

Disaster prevention. Ocean bottom sensors can save seismic activity and give essential information about earthquake and tsunami probabilities in a given zone.

Seismic exploration. Ocean bottom sensors can be utilized as receivers within 4D seismic and one can prevent the time consuming and expensive process of installing permanent streamers on the seabed.

Tactical surveillance. UAN alone or in connection with AUVs can present an effective monitoring of unwanted activity within a given zone both for military and civilian goals.

Equipment monitoring. For short term monitoring of underwater equipment. Complicated underwater installation could be equipped with sensors to guarantee correct deployment and failure detection.

5. Conclusions

The sensor networks use are common in recent years because of different applications. The requirement for harbor security applications causes the development of underwater sensors networks. We have mentioned practical problems. The Underwater network protocols will have to adapt to different optimization measures for application. They have the ability to ease the deployment and provide online access remote resources. In this paper, we have presented a literature review of UWSN applications. It was observed that new approaches for harbor security could be based on UWSNs applications.

6. References

[1].Mohd Rizal Arshad "Recent advancement in sensortechnology for underwater application", *Indian Journal of marine sciences*, 2009, 267-273.

[2] I. F. Akyildiz, D. Pompili, and T. Melodia, "Underwater acoustic sensor networks: research challenges" *Ad Hoc Networks*, vol.3, no.3, 2005, 257–279.

[3] S. Iyer and D. V. Rao, "Genetic algorithm based optimization technique for underwater sensor network positioning and deployment," *in Proceedings of the IEEE Underwater Technology* (UT '15), , IEEE, Chennai, India, Feburary 2015, 1–6.

THE STUDY OF THE SPATIAL-PHYSICAL INDICATOR OF PASSIVE DEFENSE IN INTEGRATED COASTAL ZONE MANAGEMENT (CASE STUDY OF BANDAR-E-ABBAS TO BANDAR-E-JASK)

Seyed Ahmad Fersati[1], Fereydoun Vafaie[2] and Pedram Shokri[3]

1) Department of civil engineering , khaje nasir university of technology, tehran, Iran, seyed_a.f@yahoo.com
2) Department of civil engineering , khaje nasir university of technology, tehran, Iran, fvafai@kntu.ac.ir
3) Department of civil engineering , khaje nasir university of technology, tehran, Iran,pedramshokri1993@gmail.com

1. Introduction

Today, regarding the new science of passive defense and necessity and requirement of its use in all vital and sensitive projects of the country including coastal zone, so far integrated coastal zone management (ICZM) has not been studied in this perspective and its threats and vulnerability and some approaches for reducing them have not been studied yet. On one hand, since the coasts have many vital, sensitive and significant centers, it is possible to make a sustainable development by determining and expressing the factors of passive defense in the integrated coastal zone management in order to protect the infrastructures and also to localize the proper, secure and non-vulnerable regions and to reduce vulnerability and to increase inhibition and continuity of crucial functions and to improve national sustainability and to facilitate critical management and to reduce contradictions and conflicts in coastal zones. Also using these factors will enable the decision makers to perform decisively in the future by having enough knowledge in the terms of effective elements of passive defense aiming sustainable development.

2. Methods

In this study, passive defense indicators have been derived using library and filed studies and the experts' views and then they were delivered to research population who were reports and employed managers who were familiar with the issues of coasts and passive defense by using questionnaire. Afterward, the derived indicators were classified and graded, and in the next stage each factor was weighted according to its significance using AHP method and the weighted factors were integrated and combined in the form of informational layers by applying the model of layer superposition method in GIS environment and the proper regions were determined regarding non-executive defense in the coasts (case study in the coasts of Bandar -Abbas to Bandar -Jask).

3. Determination of Indicators

As you see in the table (1) , according to the opinions of experts and specialist, 21 indices were studied in 3 general group including:

1. Demographic, poitical and military
2. Geographical, natural and environmental
3. Spatial-physical

Table 1. Determining the indices of passive defence in ICZM

Goal	Determining the indices of non-executive defense in integrated coastal zone management (ICZM)		
criteria	Spatial-physical	Geographica, natural and environmental	Criteria demographic, political and military
Sub-criteria (indices)	Existence of road communication arteries	Landfill distance	Population density in the cities and their distribution
	Rail communication arteries	Seismology	
	Existing ports in the coasts	Topography (height in m)	
	Airports	Rivers	Population density in the villages and their distribution
	Zoning and land use	Height of stormy waves	
	Power lines	Forests	
	Observing the privacy of oil and gas refineries	Climate (arid and supra-arid)	Existence of military centers
	Observing the privacy of gas and oil lines	Danger line	
	Observing the privacy of industrial areas	Sensitive regions	
Integrating the indicators and determining the proper regions	Determining the proper regions with low vulnerability from Bandar-e-Abbas to Bandar-e-Jask		

Table 2. summary of indices of spatial-physical criteria

Indices of spatial-physical criteria	Situation
Existence of road communication arteries	Dirt road
	The way
	The paved way
	4 highway
Existence of rail communication arteries	other zone
	Existing railroad
Existing ports in the coasts	The ports of Shahid Rajaie and Shahid Bahonar
	Bandar-e-Jask
	Other coastal zones
Airports	Other zones
	The airports of Baheragn and Jask
	Qeshm airport
	International airport of Bandar-e-Abbas
Zoning and land use	Other zones
	The zone of farming and agriculture
	Tourism zone and environmental and industrial sensitivity
	Residential area
Observing the privacy of gas and oil refineries	Observing the privacy of 2 km distance from refinery
	Observing the privacy of 2-5 km distance from refinery
	Observing the privacy of 5-10 km distance from refinery
Observing the privacy of gas and oil plump lines	Observing the privacy of 500 m distance
	Observing the privacy of 500m-1km
Power lines	400 kw lines
	230 kw lines
	63 kw lines
Observing the privacy of industrial areas	Observing the privacy of 2 km
	Observing the privacy of 5 km
	Observing the privacy of 7 km

4. Conclusions

1. according to the obtained results, the significance of spatial-physical indicators is 0.421 by impact factor and considering that the obtain factors for those two criteria has been less than 0.421, so it is revealed that the effect of spatial-physical indicators are more than the others which is also observed in the final integration role which its cause is the existence of properties and dependence of the country to these infrastructures such as gas and oil refineries and their attraction to the providers.

2. the obtained results from the final integration by the model of superposition of the indicators suggest that the proper place in the terms of passive defense as a secure place and with low vulnerability in the studied zone is as following: regarding the existence of vital and sensitive centers and high population, Bandar-e-Abbas is quite vulnerable and this vulnerability is reduced by proceeding towards the coasts of Bandar-e-Jask and these regions are proper places according to the indicators of passive defense.

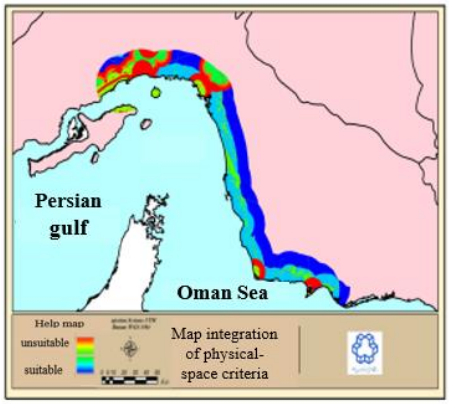

Figure 1. Integration of spatial-physical criteria

5. References

1. Ferasati, S. A. , *Determination of indicators of passive defense in the integrated coastal zone management* , Industrial university of Khaje Nasiraldin Tousi, Tehran, Iran, Thesis of M.A. , 1359 .

2. Sanad Golnezami, M., *Expression of localization indices of new ports in Oman sea coasts with passive defense approach* , Industrial university of Malek Ashtar, Tehran, Iran, Thesis of M.A., 1391 .

IMPLEMENTATION OF MONITORING AND EVALUATION ON IRANIAN ICZM-SMP MODULE BASED ON PROGRESS AND OUTCOME MEASURES

Reza Parsa[1], Peyman Badiei[2], Rasoul Ghanbari[3] and Mani Moghadam[4]

1) Khakbaft Consulting Engineers, Tehran, Iran, rparsa@aut.ac.ir
2) Department of Civil Engineering, Tehran University, Tehran, Iran, p.badiei@ut.ac.ir
3) Port & Maritime Organization of Iran (PMO), rghanbari@pmo.ir
4) Port & Maritime Organization of Iran (PMO), mani.moghadamm@gmail.com

1. Introduction

Integrated Coastal Zone Management (ICZM) is a process which ensures a balance between coastal socioeconomical demands and environmental aspects. An ICZM plan is regarded as a management plan to improve the quality of communities' life dependent on coastal resources and maintain the existing biodiversity and ecosystems. It is also a guide to concert future stakeholders' actions to attain the desired goals [1]. The coastal projects and actions should be monitored and evaluated to ensure compliance with the ICZM. Monitoring and Evaluation Plan (MEP) provides a codified method to measure the progress and outcome of the plan to be sure about the programs implantation and effectiveness. In this study, the MEP was developed to monitor and evaluate Shoreline Management Plan of Iranian ICZM (I-ICZM-SMP) based on Progress and Outcome assessment. I-ICZM-SMP was performed by Iranian Port and Maritime Organization (PMO) and signified in 2012 A.D. (1391 S.H.).

2. Materials and Methods

Achievement of a specific goal is followed by a series of programs in a management plan (see Figure 1); therefore, determination of relation between goals and programs is an important part of developing the plan. These relations are basis of assessment of goal achievement in the Monitoring and Evaluation Plan, too.

The programs' tree of management plan in Figure 1 shows that goals are defined to pursue the problems' solution. Moreover, goals are followed by objectives and targets, respectively. A series of programs are designed to achieve target which necessitate specific inputs and requirements to provide particular outputs. To monitor and evaluate all part of the programs' tree; completely, it is important to consider both Progress and Outcome of the proposed programs. The Progress Assessment checks the performance of program and measure its progress. As shown in Figure 1, to appraise the progress of the programs, their inputs, requirements and outputs are assessed. Complete progress of a program leads to achievement of the connected target. Furthermore, the Outcome Assessment evaluates effectiveness of the program to achieve the related goal. According to the tree (see Figure 1), an objective is accomplished if all related targets are attained. Similarly, a goal is reached when the linked objectives are fulfilled. Ultimately, goal achievement means that the connected problem is solved.

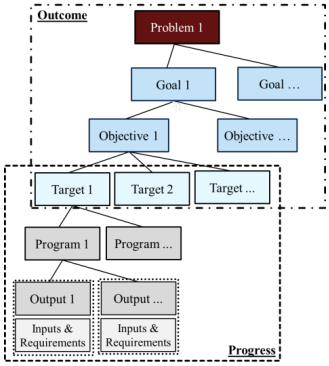

Figure 1. Programs' Tree of Management Plan

For evaluating the progress and outcome of the programs, two independent indicators' groups are necessary. Indicators are quantitative/qualitative statements or measured/observed parameters used to describe existing situations and measure changes or trends over time. Three main functions of indicators are simplification, quantification and communication [2]. In this study, indicators were selected from Intergovernmental Oceanographic Commission's (IOC) proposed indicators. The IOCs' approach is based on DPSIR method which considers Drivers, Pressures, State, Impact, Responses in the planning. IOCs' indicators are classified in three categories (see Figure 2) [2]:

- Governance Performance Indicators
- Ecological Indicators
- Socioeconomic Indicators

Indicators were selected considering their application in MEP of Iranian ICZM-SMP. These indicators extended by sub-indicators regarding to pursued goals, objectives and targets of the I-ICZM-SMP. Application of the indicators measured the progress and outcome of I-SMP.

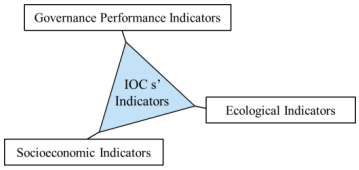

Figure 2. IOC s' Indicators Categories [2]

ICZM is a dynamic, multidisciplinary, iterative and continuous process to promote sustainable management of coastal zones [3]. It covers the full cycle of problem identification, development and modification of plan, implementation, monitoring and evaluation (see Figure 3) [4]. MEP identifies problems; then, ICZM is modified considering problems' solutions. The planning cycle leads to intelligent dynamic plan in a longtime.

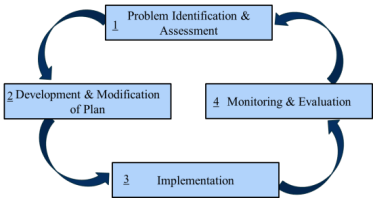

Figure 3. Planning Cycle [4]

3. Application

The relations between proposed programs and pursued goals are not determined in I-SMP; therefore, detection of the relations was the first main part of MEP of Iranian ICZM-SMP. Figure 4 shows two examples of the SMP's programs tree which illustrates the relation of goal, objective, targets and programs in Shoreline Management Plan. The tree indicates that solution of the problem of Disasters/Hazards Damages is pursued by the goal of Improving Safety and Declining Damages of Natural Disaster and Human Caused Hazard. This goal is followed up by objective of Risk Management and Protection Against Disasters and Hazards including protection against coastal erosion and coastal flooding and etc.. In the following, targets of Establishment of Protection System for Coastal Erosion and Establishment of Warning System for Coastal Flooding and etc. are defined to provide the objective achievement. Targets, objectives and goals achievement are evaluated as outcome assessment in different levels.

According to the Figure 4, appropriate programs are designed to reach the targets. As an instance, two programs of system specification studies; and implementation of the protection projects are designed to establish protection system against coastal erosion. These programs have specific outputs of locating map, design plan; and implementation of the protection projects in identified locations and time. Moreover, the programs require budget, legislation, manpower, technology, data, hardware, institutional coordination and public participation. Assessment of the programs' implementation is carried out as Progress measurement of the plan. Measuring both the progress and outcome of the plan give an overall view of the plan implementation and evaluate its' success.

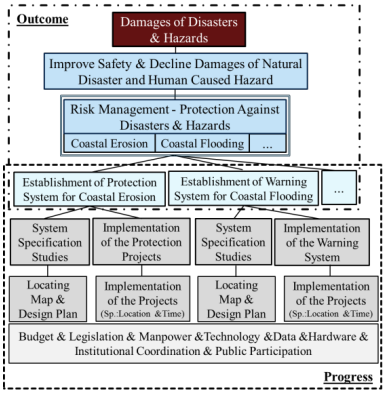

Figure 4. Examples of SMP's Programs Tree

4. Conclusion

The most important item for developing a plan and consequently, for monitoring and evaluation of it is developing a comprehensive explicit method to consider all aspects of the planning subjects. In this study, Monitoring and Evaluation Plan was proposed based on the Progress and Outcome measurement and was applied on the I-SMP. The relation between SMP's programs and goals was determined as one of the main part of management plan and MEP. Indicators were selected considering their application in I-MEP. These indicators extended by sub-indicators regarding to pursued goals, objectives and targets of the I-SMP. ICZM is followed by a dynamic process to be re-planned considering updated problems.

5. References

[1] Beeharry, Y; Makoondlall-Chadee, T. and Bokhoree C., "Policy Analysis for Performance Assessment of Integrated Coastal Zone Management Initiatives for Coastal Sustainability", Elsevier, APCBEE Procedia, V 9, 2014, p 30-35.

[2] IOC (Intergovernmental Oceanographic Commission), "A Handbook for Measuring the Progress and Outcomes of Integrated Coastal and Ocean Management", UNESCO, 2006.

[3] Basraouia, Y.; Chafia, A.; Zarhloulea, Y. and Demnati, S., "An Integrated Coastal Zone Management Initiative for Sensitive Coastal Wetland on either Sides of the Moulouya Estuary in Morocco", Elsevier, Procedia Social and Behavioral Sciences, V 19, 2011, p 520–525.

[4] GESAMP (Group of Experts on the Scientific Aspects of Marine Environmental Protection), "The Contributions of Science to Integrated Coastal Management", UNESCO-IOC, Reports and Studies No. 61, 1996.

FINE URBAN SYMBOLS: AXIS OF MARINE AND COASTAL TOURISM COMPLEX

Mohammad Moonesun [1] and Mehdi Kamyab Roudsari [2]

1) Member of the faculty of Malek Ashtar University of Technology. Tehran, Iran
2) PhD Research Scaller, Project Manager for Maritime Tourism Infrastructures Development .PMO

1. Abstract

Almost all of big coastal cities in the world have an urban symbol that travelers and tourists take photos in front of them, actually these symbols are the kind of identity certificate for a city and the subject of memorable photos. As well several hectares of land are allocated to tourism purposes and numerous facilities are integrated as various tourism complexes around these urban symbols. So that travelers and tourists can have leisure time for a week. Tourist facilities such as marine museums, seasonal and non-seasonal exhibitions, swimming pools, aquariums, dolphinariums, movie theaters, amphitheaters, conference halls, sport fields, cafes, restaurants, wide green space, modern amusement parks, play grounds, department stores, shopping centers, etc. moreover, there is the possibility for the individuals to be inside and on top of urban symbols in such a way that they can get picturesque views of the sea and the city from a high elevation. In fact, another major advantage of an urban symbol, in addition to introducing an identity certificate for a city, is that it turns in to a tourist attraction. For example, Eiffel tower in Paris and Milad tower in Iran. In Arab states of the Persian Gulf there are well-known and magnificent symbols such as Arab tower, Khalifa tower and many other symbols. Of course the meaning of an urban symbol is not just a tower, it can have different shapes and forms such as Opera House in Australia, Atomium structure in Belgium, Jesus statue in Brazil, Statue of Liberty in the United states. Unfortunately, there is not any fine urban symbol in dozens of big and populated cities and towns on the 5800 km coast line of Iran. Not only is not fine or high rise urban symbol, but you will not find a typical building over fifty meters in any coastal city.

The most important characteristics of an urban symbol can be summarized as follows:

1) It is high and huge so that it can be seen within a few kilometers
2) It has a unique shape and form in Iran and the world
3) It is adjacent to the sea or in a high place which overlooks the sea or the city
4) It has enough space to collect tourism facilities.

In this case, the following advantages can be considered as the advantages of the placement of urban symbols in a city:

1) To create a certain and unique identity certificate for a city.
2) To create tourist attraction.
3) To have significant increase of city income by constructing tourist complexes and various service centers and department stores.
4) To create the subject of photography, advertising of a city or country.
5) To establish open tourism area around an urban symbol and to create a tourism center.
6) To provide tourism facilities on top of urban symbols and to have a great view.
7) The possibility of having telecommunication facilities on the top an urban symbol.
8) To create self-esteem and engineering ability and knowledge.
9) To have a place to hold local, national and international events.

Unfortunately, none of coastal cities of northern and southern Iran have an urban symbol as a tourist attraction. What urban symbol should be shot to differentiate between travelling to the southern and northern cities (such as Babol, Khoramshahr, Chabahar, Bandar Abbas, …)? The lack of attention to the construction of fine structures in coastal cities especially in south of country has caused most of these cities to look poor and deprived. Even Kish Island, which has the bulk of coastal tourism investment, does not have a modern urban symbol but an old sunken ship is a symbol of the city.

2. Conclusion

Construction of a magnificent, luxurious urban symbol, for example, 100 meters height symbols in each of the coastal cities of northern and southern Iran, can be converted to the center of a large coastal tourism complex and will change the whole face of the city.

A definite objection to tourism managers' attitude toward tourism especially coastal tourism is emphasizing just two items to flourish marine tourism and to develop coastal areas: 1-Old and ancient monuments. 2-Beautiful nature. This imperfect and defective view has led to the waste of rich resources of gas and petroleum in our country instead of using them to build fine engineering structures which can be a symbol of engineering knowledge and national proud.

A coherent and national effort should be launched to build high rise structures as urban symbols in all coastal cities in Iran. In this article, more details are provided on the characteristics of urban symbols and tourism facilities

3. References

[1] Mason, Peter (2003).Tourism impacts , planning and management (pdf) .Burlington MA: Buterworth – Heinemann (Elsevier) .ISBN 0 7506 5970X Retrieved 22 August 2017 .

[2] Pearce,D.G.& Butler,R.W.(1993)Tourism Research :Critiques and Challenges .Routledge.

[3]Rollins,R,Dearden p and Fennell,D.(2016)"Tourism,Ecotourism and protected Areas".in p. Dearden R. Rollins and M . Needham (ed).Parks and Protected Areas in canada: Planning and Management(4th ed)(P.391-425) Toronto : Oxford University Press.

[4] Muchapondwa , E, & Stage , j.(2013)."The Economic impacts of Tourism in Botswana , Nimibia and South Africa : is poverty subsiding ?".Natural Resources Forum.37(2): 80-89.doi10.1111/1477-8947.12007.

[5] Moghimehfar , F, & Halpenny , E .A.(2016)." How do people negotiate through their constrants to engage in pro – environmental behavior ? a study of front – country campers in Alberta , Canada " . Tourism Management ,57,362-372.

[6] Butler , R.M.(1980).The cocept of a tourist area cycle of evolution ." implications for management of resources ".The Canadian geographer / Le Geographe Canadian, 24 (1) ,5-12.

REVIEW AND ANALYZE CHALLENGES OF KHUZESTAN PORTS IN MARINE TOURIST BY SWOT

Mahmoud Hoseinzadeh

Supervisor of Special terminals, Imam Khomeini Port, Mahshahr, Iran, m.hoseinzadeh59@yahoo.com

1. Introduction

Despite increased awareness of the economic and environmental significance of marine and coastal tourism in the world but attention it in Iran and coastal province is very low. The Khuzestan marine tourism industry is currently facing a serious downturn due to a combination of unfavorable factors. These factors are frequently found both inside and outside the country, and they are linked to each other. This study will review and analyse factors that influence the competitiveness of the Khuzestan marine tourism industry.

1.1. Marine Tourist

Tourism has emerged as an important economic activity in worldwide. Coastal and maritime tourism can be a major source of growth and jobs, especially for the young population. For example, Coastal and maritime tourism is the largest maritime activity in Europe and employs almost 3.2 million people, generating a total of € 183 billion in gross value added and representing over one third of the maritime economy [1].

Many researcher study of factors impact on marine tourist. Dwyer (2015) study on fostering competitiveness of coastal and marine tourism in Europe. Result of research show environmental and heritage features of the area, social and cultural characteristics of residents, stage of economic development of area and carrying capacity (physical, social) known as the characteristics of the destination which impact on marine tourist [2]. Ramli (2014) study Factors influencing tourist visitation in marine tourism in Malaysia. This study demonstrates that Seasonality, Size and intrusiveness of tourist facilities, Degree of local involvement in ownership and operation of tourism facilities and public-private sector cooperation effect of this industry [3]. Thitthongkam and Walsh (2011) Analysis of Factors Influencing the Competitiveness of the Thai Tourism Industry. Findings of research show political turmoil and military, epidemic diseases, the economic situation, media, disaster, crime and war, technology, marketing plan, culture, education, environment, demographic change and other factors for example, language and cultural issues influence on attract marine tourist [4].

2. Research Methodology

This research has applicable nature and in terms of methodology is a descriptive-survey research. After studying literature and history of the research, a questionnaire containing 13 special questions developed. In this research 50 of expertise of Khuzestan port are questioned. To analyses of data use T test and SWOT model. By T test, condition of identified factor determined (good or inappropriate). Then base of T test result and nature of factor (internal or external) defined tit in SWOT model.

3. Data Analyses

13 factors defined in base of literature review. 46 questionnaire respond. In this section use of T test to analyses of questions (see Table 1).

Table 1. T test result

No	Factor	T
1	Norouz days	13.8
2	Climate	12.3
3	Coast	15.1
4	Recreational berth	-2.1
5	Hotel	7.5
6	Introduction of Marine tourist capacities	-8.8
7	Public transport vehicle	-5.9
8	Professional tour	-11.4
9	Planning for establishment of village tourist	12.4
10	Attention superior mangers to Marine tourist	9.7
11	Security and safety	10.2
12	Passenger vessel	15.9
13	Development of marine tourist in countries of Persian Gulf	12.5

After analyses of factors, in this part define them in SWOT model (see Table 2).

Table 2. T test result

S	W	O	T
Climate	Recreational berth	Norouz days	Development of marine tourist in countries of Persian Gulf
Coast	Introduction of Marine tourist capacities	Hotel	
Security and safety	Public transport vehicle	Planning for establishment of village tourist	
Passenger vessel	Professional tour	Attention superior mangers to Marine tourist	

4. Conclusion

Many factors that influence the Khuzestan marine tourism industry competitiveness have been mentioned and highlighted in this paper. It is up to the decision makers to take actions and prepare to deal with situations that might occur and create change leading to better outcomes for the industry, which is can convert to one of the country most important.

Result of research show good climate, beautiful coast, high safety and security and existence passenger vessel are strengths؛ shortage of Recreational berth, Introduction of Marine tourist capacities, Public transport vehicle for carrying passengers and professional marine tour are weaknesses؛ Norouz days, existence of hotel, Planning for establishment of village tourist and Attention superior mangers to Marine tourist are opportunities and Development of marine tourist in countries of Persian Gulf is threat confront to Marine Tourist in Khuzestan Ports.

To increase Marine Tourist share in Khuzestan Ports following solutions submit:

- Establishment Recreational berth include of marine exercises.
- Use of marketing for introducing Marine tourist capacities of provinces and ports capabilities.
- Prepare Public transport vehicle to carrying passengers between ports and main places of city.
- Training of tour leaders and issue professional marine tour certificate to improvement services.
- Speed up establishment village tourist by use of public-private investment.

5. Acknowledgment

For implementation of the comprehensive scientific plan of the country, Port and Maritime Organization support of this research in terms of scientific and financial due to done its role in subjects of port, maritime, shipping and commercial matters.

6. References

[1] European Commission., "A European Strategy for more Growth and Jobs in Coastal and Maritime Tourism", 2013.

[2] Dwyer, L., "Fostering Competitiveness of Coastal and Marine Tourism in Europes", *International Academy for the Study of Tourism*. New South Wales, Australia, Jan 2012015, pp 1-12.

[3] Ramli, S., " Factors influencing tourist visitation in marine tourism: Lessons learned from FRI Aquarium Penang, Malaysia", *International Journal of Culture Tourism and Hospitality Research,* February 2014, Vol. 8 Iss 1 pp. 103 – 117.

[4] Thitthongkam, T., and Walsh, J., "An Analysis of Factors Influencing the Competitiveness of the Thai Tourism Industry", *2010 International Conference on Business and Economics Research,* IACSIT Press*, Kuala Lumpur,* Malaysia, 2011, pp 138-141.

3

PORT ENGINEERING AND COASTAL STRUCTURES

A REVIEW OF THE INFLUENCES OF THE DREDGED MARINE SAND EXTRACTED FROM PERSIAN GULF (SHAHID RAJAI PORT) ON DURABILITY AND RESISTANCE PARAMETERS OF THE ROLLER COMPACTED CONCRETE PAVEMENT

Saeed Moradi[1], Shohre Shahnoori[2] and Seyed Taha Tabatabai Aghda[3]

1) Department of Civil Engineering, University of Hormozgan, Bandar Abbas, Iran, saeed.moradi69@yahoo.com
2) Department of Civil Engineering, University of Hormozgan, Bandar Abbas, Iran, s.shahnoori@gmail.com
3) Road , Housing & Urban Development, Bandar Abbas, Iran, taha.taba@gmail.com

1. Introduction and Background

Overusing the natural resources leaves the future generations only with waste and pollutions [1]. In order to avoid such impacts serious efforts are required in various industries. Construction industry is a major counterparts of the World's activities [2]. Although it is the main source of income for about 30% of population [3], it plays a significant role in the environmental issues, such as excavation and landscape deterioration, etc. As the most used material, concrete has a significant effect on the environment [4, 5, 6].

In a standard concrete about 0.75 % of the mix is filled with sand and gravel. Due to the growing increase of usage, the extraction of natural resources and mines will cause considerable impacts. Nevertheless, in some areas (e.g. islands and Persian Gulf marginal lands) these resources are rare, involving transportation cost and pollutions as well. Therefore, finding other sources of aggregates is very effective. From transportation point of view dredging the sediment from the coastal areas is a sensitive matter as it is conditional in order to provide passages with appropriate depth for loading or/and unloading the ships. However, these deposed and left open dredges cause air and land pollution.

Combining the latest with the former shows that using the dredging materials, as a replacement for the whole or a percentage of the aggregates is a perfect solution. Regarding various aspects related to this new source of materials several studies have contributed. Examples of which are being followed as: Limeira et al. (2012); Moradi et al. (2018); Etxeberria et al. (2016); Liu et al. (2016); [7, 8, 9,10].

2. Experiments and the Tests Setup

The experimental works are categorized in three main sets. First is the mix design and programming, in addition to the required tests on the ingredients and the basic materials. The second category is providing the specimens, (mixing, casting, curing etc.). The final is the mechanical and permeability tests on the specimens.

Figure 1& 2. Dry and wet processes of test and curing specimens

3. Outcomes of the Laboratory Tests

The experiments are excluded from this text but the final ones. As shown in figure 3. and 4. In the last stage of these tests, the data of each mixing plan (sulfate and non-sulfate) is the average of three 10*10*10 cm sample cubes. In the obtained graphs, the average compressive strength of sulfate samples has a slight difference with non-sulfate samples. In fact, in the middle (six months) and long-term (one year), despite the change in strength, there was no significant effect on the compressive strength of the test specimens Also, in all three types of Portland cement, the mixing plan of the 15% dredged sand has the highest strength to the control concrete, and in special Pozzolona Portland cement and Portland cement type 5, the mixing plan containing 25% dredged sand has also shown more strength than the control concrete and after that, the strength such as the test of strength of the 15 * 15 * 15 cm specimens were on a downward path.

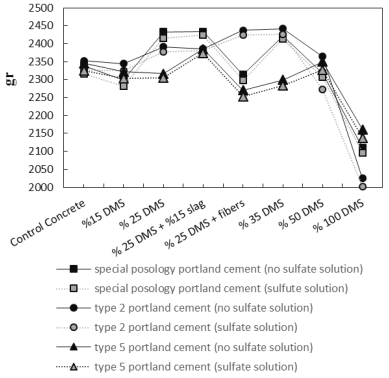

Figure 3: Weight variation of six months' sodium sulfate test specimens containing special Pozzolona Portland cavities, Portland cement type 2 and Portland cement type 5

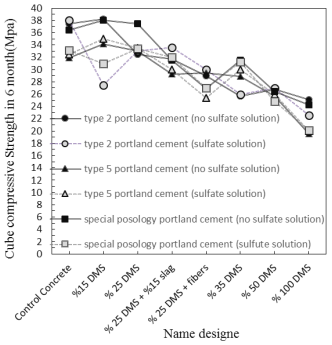

Figure 4: compressive strength variations of six months' sodium sulfate test specimens containing special Pozzolona Portland cavities, Portland cement type 2 and Portland cement type 5

4. Discussion and Conclusions

In the present study, we have tried to due to lack of mines to extract the materials in addition to using existing materials in the region and also high costs and long-term non-performance of flexible asphaltic pavements compared with rigid pavements due to reduction of air pollution and environmental hazards of Sea dredged sand, use this material to produce a useful product. In this regard, the research results are as follows:

- According to the existing conditions, the replacement of 15% DMS instead of mine sand has the maximum strength and durability of test specimens in all three types of Portland cement.
- Adding higher percentages of DMS from 50 to 100 percent has disturbed the proportional distribution of fine and coarse aggregates in concrete, due to the uniformity of aggregates and the non-overlapping and interlocking between aggregate, lead to reducing the strength
- Reducing trend of strength by using high percentages of up to 100% of DMS, although apparent, is a good idea if used in less-favored structures in remote areas of the islands and Persian Gulf ports, which have the potential to convey and supply mineral materials.
- The results of the sulfate test indicate that there is no effect on the compressive strength of the sulfate specimens in the medium (six months), and the test has only a slight weight loss of 10 grams, which can be due to the dissolution of some salt in the dredged sand in sulfate solution or human precision and measuring device.

5. References

[1] Langston, C. & Ding, G.K.C. (2001). Sustainable practices in the built environment, 2nd Edn., Butterworth Heinemann, Oxford.

[2] Bentivegna, V., Curwell, S., Deakin, M., Lombardi, P., Mitchell, G. & Nijkamp, P. (2002). 'A vision andMethodology for integrated sustainable urban development: BEQUEST', in Building Research and Information,Vol. 30, No. 2, pp. 83–94.

[3] (Jain, et al. 2016) Gagnesh Jain; Vaishant Gupta; Mukesh Pandey Case Study of Construction Pollution Impact on Environment International Journal of Emerging Technologies in Engineering Research (IJETER) Volume 4, Issue 6, June (2016) www.ijeter.everscience.org.

[4] Ayarkwa, Acheampong, Hackman, J. and Agyekum,. Environment impact of Construction site Activities in Ghana, ADDRI JOURNAL: VOL.9, NO9 (2). June, 2014.

[5] Chrisna du Plessis (2002). Agenda 21 for Sustainable Construction in Developing Countries. A discussion document. The International Council for Research and Information in Building and Construction (ICRIBC), CIB, and UNEP International Environmental Technology Center. CSIR Building and Construction Technology, Pretoria, S.A.

[6] Zolfagharian Samaneh, Mehdi NOURBAKHSH, Javier Irizarry, Aziruddin Ressang, Masoud Gheisari Environmental Impacts Assessment on Construction Sites Construction Research Congress 2012 ASCE 2012.

[7]. Limeira, J., Agullo, L., Etxeberria, M.;"Dredged marine sand as a new source for construction materials"; Materiales de Construccion, 2012, Vol. 62, No. 305, pp. 7-24

[8] Moradi, S., Shahnoori, Sh.; " The use of Dredged Marine Sand in Roller Compacted Concrete Pavements; an experimental study on the Persian Gulf Dredged Marine Sediments"; The Rilem week 2018 & The 4th International Conference on Service Life Design for Infrastructures (SLD4) and Concrete Modelling (ConMOD), 2018.

[9] Etxeberria, M., Femandez, J,M., Limeira, J.; "Secondary aggregates and seawater employment for sustainable concrete dyke blocks production: Case study"; Construction and Building Materials, 2016, Vol. 113, pp. 586-595.

[10] Liu, W., Cui, H., Dong, Z., Xing, F., Zhang, H., Y.Lo, T.; "Carbonation of concrete made with dredged marine sand and its effect on chloride binding"; Construction and Building Materials, 2016, Vol. 120, pp. 1-9.

INVESTIGATION OF THE PERFORMANCE OF GEOTEXTILES AS THE FILTER LAYER IN RUBBLE-MOUND BREAKWATERS

Mahvin Ebadi[1] and Mir Ahmad Lashteh Neshaei[2]

1) MSc Student, Department of Civil Engineering, University of Guilan, Rasht, Iran, Mahvinebadi1993@gmail.com
2) Associate Professor, Department of Civil Engineering, University of Guilan, Rasht, Iran, Maln@guilan.ac.ir

1. Introduction

Today, using geotextile in engineering has become prevalent, owing to some of their features such as: durability, resistance, permeability and incorruptibility against destructive factors within soil. Whereof geotextiles work simultaneously as a water drainage and a soil conservator against being washed up, it is allowed to use them as a filtering material. Geotextiles are also very easy to carry, simple to use and reasonable in a matter of price [1].

The most common types of breakwaters are the rubble-mound breakwaters with a long lifespan which can moderate wave energy very well. For a better and more efficient use of these types of breakwaters, some important properties must be optimized, for example reducing the amount of pore water pressure in core layer [2].

Since pore water pressure is related to permeability, it can be reduced by a better replacement of filtering materials in breakwaters. To improve the efficiency of this process, the material of the filter layer can be changed. In this study, it has been tried to use a number of geotextiles as the filter layer to find out their effect on the reduction of the pore water pressure of the core layer of breakwaters.

2. The Replacement of the Granular Filter Layer by Geotextile

In this study, the cross sections of a constructed breakwater (located in Anzali free zone) are used and GeoStudio 2012 is employed for modeling. First, the main as-built section is modeled. Then, it is modeled by removing half of the thickness of filter layer and inserting a layer of geotextile instead, removing the entire filter layer and inserting one, three and five layers of geotextile in a row, respectively. Figure 1 shows the models.

At the end, by comparing the entire results, it is concluded that by using five layers of geotextile, the pore water pressure has been efficiently dropped. The geotextile which is used in this research is a type of GMH300 with a permeability of 0.0023 m/s and a thickness of 2.8 mm.

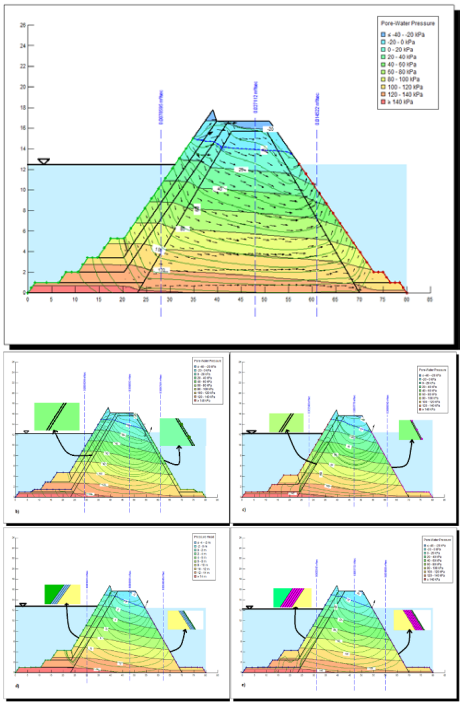

Figure 1. The section of models in GeoStudio 2012: a) Main section, b) One layer geotextile instead of half of the thickness of filter layer, c) One layer of geotextile, d) Three layers of geotextile and e) Five layers of geotextile instead of the entire filter layer

3. Calibration of the Coefficient in the Wave Height Equation in a Porous Layer

The theoretical wave height in each point of a breakwater (which is known as a porous layer) can be normally calculated by the following equation [4].

$$H = \frac{H_0}{\sqrt{1 + \frac{K.X.{H_0}^2}{2D_{50}.d^2}}} \quad (1)$$

Where H is the wave height in a porous layer, H_0 is the input wave height, K is a coefficient which is assumed to be 2 for granular materials, X is the distance from the start point, D_{50} is the medium nominal diameter of grains and d is the water depth.

At first step, to calculate the wave height in each point, D_{50} for every layer of breakwater must be calculated by equations 2 to 5.

$$r = \frac{1}{2}D_{50} \quad (2)$$

$$V = \frac{4}{3}\pi r^3 \quad (3)$$

$$\rho = \frac{M}{V} \quad (4)$$

$$D_{50} = \sqrt[3]{\frac{6M}{\rho\pi}} \quad (5)$$

Where V is the nominal volume, ρ is the density and M is the mass of grains.

Finally, by inserting the data in equation 1, calculating the theoretical pressure heads and comparing them with the estimated pressure heads from GeoSudio, it is figured out that the differences between them are noticeable as it is shown in table 1.

Table 1. Comparison of the theoretical and the estimated wave pressure

H_t	H_G	Δ
3.6066	11.49	7.8834
3	10.49	7.49
2.5812	8.0384	5.4572
1.4061	11.4607	10.0546
2.4377	6.6696	4.2319
2.3355	4.0569	1.7214
2.2065	1.1175	1.089
1.4549	-4.0073	5.4622
1.0024	-4.7467	5.7491
1.31	-3.0694	4.3794
1.2414	2.9611	1.7197
1.1788	4.2857	3.1069
0.7683	7.0011	6.2328

Since the differences are extremely considerable, the equation 1 has a major deficiency which might be solved by calibrating the coefficient. To overcome the problem, the equation 1 should be used recessively. Figure 2 shows the K fluctuations.

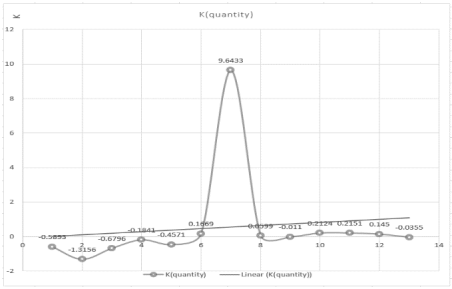

Figure 2. Diagram of K fluctuations

Therefore, the K coefficient is calibrated around 0.25. In such case we can expect to have a better result.

4. Results and Discussion

In this paper the pore water pressure parameter has been studied and it is comprehended that changing the material of the filter layer helps reducing the amount of pore water pressure in the core layer. This purpose can be successfully achieved by using five layers of geotextile (GMH300) instead of traditional filter layers.

The coefficient in the wave height equation was not good-defined to overcome the differences between the theoretical answers and the estimated ones. This study has reached a new coefficient by comparing the answers and using the equation 1 recessively. Considering the boundary conditions, the coefficient is calibrated around 0.25. Thus, the conclusions are satisfying up to here.

5. References

[1] Chu, s., Yan, S.W. (2011), "Geosynthetic Tubes and Geosynthetic Mats: Analyses and Applications" Geotechnical Engineering Journal of the SEAGS and ASSGEA vol. 42, no.1. 1-2.

[2] Shakeri, M. (2017), "Investigation of the Intrusion of Waves into Riprap Structures (Breakwaters and Groyne) by GeoStudio SEEP/W" Master Thesis. Civil Engineering Department. Lahijan Azad University. 7-10.

[3] Adeli, A., Lashteneshaei, M.A., Rastgar, S. (2014), "The Usage of Sand Cores made by GeoTube to Control of Shorelines" The 8th National Congress in Civil Engineering, Civil Engineering Department, Babol University. 1-2.

[4] Ports and Marine Structures Design Manual of Iran, (2004), "Breakwaters and Coastal Protection Structures" no.300-5.

IDENTIFICATION AND RANKING OF THE CLAIM CAUSES IN THE CONSTRUCTION PROJECTS OF BUSHEHR PORTS AND MARINE ORGANIZATION

Seyyed Abdossalam Hosseini[1] and Nahmat Khodaie[2]

1) Islamic Azad University, Estahban branch, Estahban, Iran, Nahmat.khodaie@uma.ac.ir
2) Islamic Azad University, Khormouj branch, Khormouj, Iran, Sahosseini1344@gmail.com

1. Introduction

Generally, a claim is defined as the seeking of change by one of the parties involved in the construction process [1]. Also, claims are described as the assertion of the right to money, property or remedy [2]. Construction claims are considered by many project participants to be one of the most disruptive and unpleasant events of a project [3]. Once a claim has been presented, the owner and contractor can come to an agreement concerning the claim and, thereby, create a change order or a modification, or they may disagree and create a construction contract dispute. Analyzing the various types and causes of claims is an important task to resolving these claims [4, 5, and 6]. Claims may result in cost overruns, schedule delays and may jeopardize the working relationships amongst the contracting parties [7]. Due to conflicts and differences over claims, the construction industry is plagued by an adversarial atmosphere between clients and contractors [8]. The claim management process in the construction industry has to be clear and be understood by all parties especially the contractor in order to know how to manage them [9].

Several attempts were made in the literature to study the types of construction claims and determine their main causes and ways of avoiding them. Al-Khalil and Al-Ghafly determined the most important causes of delay claims in public utility projects in Saudi Arabia based on the frequency and severity of these causes [10]. Scott conducted a survey to investigate the causes and mechanisms that are used to prepare and evaluate delay claims in United Kingdom [11].

2. Research methodology

The first step in this study was to identify the causes for claims in construction projects of Bushehr port and marine organization. The primary list, containing 142 reasons of the claims, was produced using the ideas of the invited representatives of client, contractors and consultants, in a brainstorming meeting. The identified reasons were ranked based on the weighted average of the responses collected at the meeting. A questionnaire was then developed containing the first 40 root causes. The questionnaires were sent to the construction professionals, who frequently deal with the studied construction projects. The responded questionnaires were analyzed using SPSS software, and the identified main causes of claims were ranked according to their relative importance. Finally, new recommendations are suggested to minimize claims and improve the performance of the construction projects.

Table 1. Identified causes presented in the questionnairy

Index	Cause Description
X1	Lack of documentation at the right time
X2	Change orders during construction issued by the client
X3	Price Fluctuation and inflation
X4	Not to use the consultant's expert price
X5	Client tendency to the lowest suggested price
X6	Increase of the volume of works more than the limits of general conditions of contracts
X7	Lack of specific list price for repair works
X8	Nonexistence of claim management methodologies
X9	Variations in the work qualities
X10	Mistakes in the project time schedule
X11	Time-limits on preparing tender documents
X12	Insufficient knowledge about law and circulars
X13	Disagreement over price of the new works
X14	Lack of Funding proportional to cash flow
X15	Not to follow the required steps to confirm the project estimation
X16	Quantitative variations in drawings and materials
X17	Insufficient information on relationship management
X18	Inaccuracy of the project study and design phases
X19	Lack of timely decisions on new prices
X20	Increase of the project cost more than the limit of 25 of the primary cost
X21	Mistakes in project estimation
X22	Change in client's needs and decisions
X23	Payment delays
X24	Requiring the additional works to be done based on the basic price list
X21	Mistakes in project estimation
X22	Change in client's needs and decisions
X23	Payment delays
X24	Requiring the additional works to be done based on the basic price list
X25	Project extension due to the delays
X26	Change in roles of client authorities
X27	The limitation of new prices during project estimation

X28	Lack of claim management knowledge of contractors
X29	Changes relative to the primary conditions
X30	Entrance of inspection organization in tender process
X31	Impropriety of existing contracts for repair works
X32	Orders of provincial and local governments
X33	Client nonobligatory to the contract contents
X34	Inaccuracy in examination of contractors documents during bidding
X35	Poor consideration of site condition and ignoring bidders comments on this subject
X36	Changes in client view points during construction phase
X37	Lack of specific price list for marine structures
X38	Lack of appropriate procedures for contractor selection
X39	Unacceptable delays at project completion stage
X40	Weakness of general conditions of contracts to analyze contractor delays

3. Results

In the designed questionary, each cause of claim is evaluated from three viewpoints: occurrence possibility, time effect and cost effect. For every condition of cause and the stated viewpoint, five probable levels of importance are defined as follow: 1) very low, 2) low, 3) medium, 4) high, 5) very high. Table 1 presents the identified causes presented in the questionary which are obtained with narrowing the primary list produced in the brainstorming meeting. Figure 1 shows the average importance level of the causes for the three indexes of occurrence factor, time and cost effects based on the analysis of the completed questionnaires. According to the ranking results, the following causes are respectively ranked as the first five important causes of claims in the construction projects of Bushehr ports and marine organization:

(X25) Project extension due to the delays, (X39) Unacceptable delays at project completion stage, (X5) Client tendency to the lowest suggested price, (X2) Change orders during construction issued by the client and (X34) Inaccuracy in examination of contractors' documents during bidding.

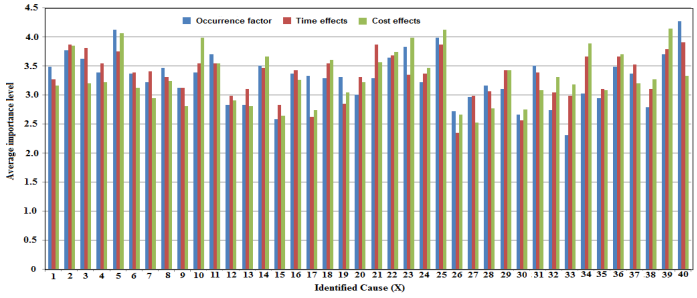

Figure 1. The average importance level of the causes for the three indexes of occurrence factor, time and cost effects

4. References

[1] Arditi, D. and Patel, K., "Expert system for claim management in construction projects", *International Journal of Projects Management*, 1989, 7(3), 141-146.

[2] Powell, S. V. and Stephenson, D., *Civil Engineering Claims*. Blackwell Science, Oxford, 2000.

[3] Ho SP, Liu LY., "Analytical model for analyzing construction claims and opportunistic bidding", *Journal of Construction Engineering and Management*, 130(1), 2004, 94–104.

[4] Zaneldin K., "Construction claims in United Arab Emirates: Types, causes, and frequency", *International Journal of Project Management*, 24, 2006, 453–459.

[5] Ren, Z., Anumba, C., and Ugwu, O., "Multiagent system for construction claims negotiation", *Journal of Computing in Civil Engineering*, 17(3), 2003, 180–188.

[6] Janney, JR., Vince, CR., Madsen, JD., "Claims analysis from risk-retention professional liability group", *Journal of Performance of Constructed Facilities*, 10(3), 1996; 115–22.

[7] Mishmish, M. and El-Sayegh, S., "Causes of claims in road construction projects in the UAE", *International Journal of construction Management*, 18(1), 2018, 26–33.

[8] Harmon K. M. J., "Conflicts between Owners and Contractors: Proposed Intervention Process", *Journal of Management in Engineering*, 19 (3), 2003,121 – 125.

[9] Enshassi A., Choudhry, R., El-Ghandour S., "Contractors'perception towards causes of claims in construction proj-ects", *Int J Constr Manage*. 9, 2009, 79–92.

[10] Al-Khalil, M., Al-Ghafly, M., "Important causes of delay in the public utility projects in Saudi Arabia", *Construction Management and Economics*, 17(5), 1999, 647–655.

[11] Scott, S., "Delay claims in UK contracts", *Journal of Construction Engineering and Management,* 123(3), 1997, 238–244.

PLANNING FOR SPACE & SPATIAL DEVELOPMENT OF PORTS CASE STUDY: ANZALI PORT

Jafar Sayareh[1] and Nariman Mehrgan[2]

1) Faculty of Navigation and Marine Engineering, Chabahar Maritime University, Chabahar, Iran, j.sayareh@cmu.ac.ir
2) Faculty of Navigation and Marine Engineering, Chabahar Maritime University, Chabahar, Iran, narimanmehrgans@gmail.com

1. Introduction

Threats come from sea shipping to ports, the process of moving towards larger ships, ship specialization and ultimately, the threat of community-based ports. A well-known theory that describes how to progress the port infrastructure in terms of time and place is the Anyport model. This modela Pattern the port development process, indicates Which side will they go to?

Then Rodrigue and Notteboom (2005) added Development-Regionalization to these steps. In this research, the process of growth and development of Anzali Port clause with Anyport model is examined, In the next step, the analysis of the growth and progress of this port from the past to the present has been done according to the Anyport model And then it refers to the differences and similarities that this port has been developing with the model, Then there are two types of development, concentrated and de concentrate will be examined. Considering port constraints based on the Anyport model, a framework for decision making is proposed with consideration of the basic constraints. These constraints include Geographical, economic and supportive. The decision framework for Location development of the port includes port planning, Location, study and decision making. In this research, Bandar Anzali has been studied and in the end it becomes clear that this port needs a centralized or decentralized development.

2. Anyport Model

The Anyport model is a well-known theory that developed by Bird in 1963, This Model is an initial attempt to categorize port development, which is still used as a reference. The steps Bird used for his model include: primitive, marginal quay extension, elaboration dock, marginal quay elaboration, simple lineal quayage and specialized quayage. Bird also recognized the various parts of the port that could be some writer believe that the six phases proposed by Bird can be categorized into three broad categories: Setting, Expansion, Specialization (Rodrigue et al, 2009).
Three major steps can be identified in the port development process identified by ANYPORT:

2.1. Setting

The initial setting of a port is strongly dependent on geographical considerations. A standard evolution of a port starts from the original port, most of the time a fishing port with trading and shipbuilding activities, which includes several quays (1). For many centuries until the industrial revolution, ports remained rather rudimentary in terms of their terminal facilities. Port-related activities were mainly focused on warehousing and wholesaling, located on sites directly adjacent to the port. The port district was a key element of urban centrality.

2.2. Expansion

The industrial revolution triggered several changes that impacted on port activities. Quays were expanded and jetties were constructed to handle the growing amounts of freight and passengers as well as larger ships (2). As the size of ships expanded, shipbuilding became an activity that required the construction of docks (3). Further, the integration of rail lines with port terminals enabled access to vast hinterlands with a proportional growth in maritime traffic. Port-related activities also expanded to include industrial activities. This expansion mainly occurred downstream towards deeper draft areas.

2.3. Specialization

The next phase involved the construction of specialized piers to handle freight such as containers, ores, grain, petroleum and coal (4), which expanded warehousing needs significantly. Larger high-capacity ships often required dredging or the construction of long jetties granting access to greater depths. This evolution implied for several ports a migration of their activities away from their original setting and an increase of their handling capacities. In turn, original port sites, commonly located adjacent to downtown areas, became obsolete and were abandoned (Rimmer, 1967).

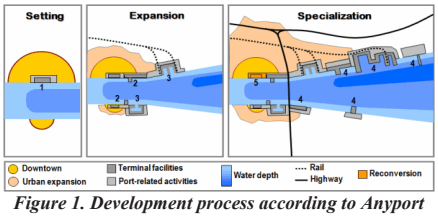

Figure 1. Development process according to Anyport Model

3. Location Development of the Port

Seaport development is divided into two categories:

- Concentrated: That is the development and expansion of the port at original site or near the place
- De concentrate: Here the development and expansion of the port moves towards a new position, while the original site of port is preserved (Chan et al, 2010).

Four stages of decision-making have been taken to help develop the port's space:

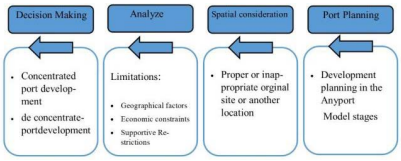

Figure 2. Framework of decision for location development of the port (Chan et al, 2010)

4. Toc Analysis for Port Development

In this study, following the conformity of Anzali port with the stages of the Anyport model, Theory of Constraints has been used to determine the decision framework. In this study TOC has been used to determine the decision framework and whether port development should be separate from the original site or not.

Therefore, it is necessary to first identify the effective constraints on port development decision-making, as shown in Table 1 of these constraints.

Table 1. Development Constraints of the port's spatial

Elements	Secondary Constraints	Main Constraints
Earthquake Areas	Shore	Geographical Constraints
Ability To Progress		
Inappropriate Weather	Air	
Depth Of Water	Sea	
Hinterland	Freight Resources	Economical Constraints
Cargo Transfer		
Tendency	Volume Of Freight	
Transportation	Supportive Options	Supportive Constraints
Human Resources		
Environmental Effects	Green Production	
Control Power	Government Planning	
Terminal Operators	Port Operations	

5. Results

By combining the idea of the anyport model and TOC, a port development space was formed. It was shown to be a concentrate development for Anzali port to achieve more goals is more suitable in terms of geographical, supportive, economic constraints**.**

The Anyport model examines the port infrastructure's evolution in terms of time and position, It can also be considered as the basis for comparing the true development of ports. The process of formation and expansion of the Anzali port was the same in any of the three stages of the Anyport model but because of the weakness in hinterland infrastructures, such as railways, it makes it difficult to enter the port of Anzali to the regional development stage (regionalization).

Table 2. Spatial & space development of Anzali port

De Concentrate Development	Concentrated Development	Objectives	Development Constraints of The Port's Location
1	3	Allow Access To Large Vessels	Geographical Constraints
1	1	Enough Space To Build The Terminal	
1	2	Lower Risk In Navigation And Port Operations	
1	2	Proximity To Cargo Resources	Economical Constraint
1	1	Cargo Growth	
1	2	Maket Access	Supportive Constraints
1	2	Minimum Environmental Impact	
2	2	Workforce For Daily Operations	
2	2	Flexibility In Decision Making	
11	17		Results

6. References

[1] Rodrigue, J , Comtois, C, and Slack, B., The Geography of Transport Systems. Abingdon, Routledge. 2009.

[2] Tracy Chan,W. Leung Yip, T., Port Spatial Development and Theory of Constraints, 2010.

[3] Rimmer, P. J., The search for spatial regularities in the development of Australian seaports. Geograkiska Annaler,. 1967, 49, 42-54.

[4] Notteboom, T. E. and Rodrigue, J. P., Port regionalization: Powards a New Phase in Port Development, Maritime Policy & Management., 2005.

[5] Chan, W & Yip, T. Port Spatial Development and Theory of Constraints. Department of Logistics and Maritime Studies., 2010.

A NOVEL DESIGN OF CAISSON QUAY WALL BASED ON PILES AND INVESTIGATING THE SEISMIC PERFORMANCE USING FINITE DIFFERENCE TIME HISTORY ANALYSIS

Roohollah Abbasi Shanbehbazari[1]

1) School of civil engineering, University of Tehran, Tehran, Iran, Rh.abbasi@ut.ac.ir

1. Introduction

Quay walls, which are an important part of maritime transportation system, function as a protective structure for the soil behind and all port facilities built on it, including cargo and passenger shipping equipment; Thus optimal and innovative design of these structures is a high-priority issue in coastal engineering and important to the national interest. Caissons are among the largest berthing structures which are used for the construction of quays, breakwaters, coastal walls, bridges, etc. caisson type quay wall, is one of the most widely used kinds of quays, specially due to its structural and economic advantages, including working as a breakwater, relatively easy and quick implementation, and also much less need for repair and maintenance compared to traditional pile-supported wharves which are highly vulnerable to corrosion, deformation of the piles due to chemical factors and dynamic loading. On the other hand, caisson walls demand a rigid and firm foundation to resist their significant weight and consequently cannot be built everywhere. The present study suggests a novel design in order to make it possible to use the advantages of caisson quay walls even in lands with inappropriate soils [1-2].

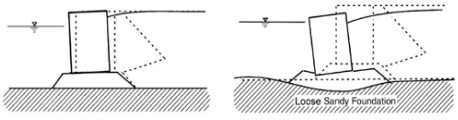

Figure 1. Caisson quay wall on loose foundation.

2. Damage of Caisson-type Quay Walls

After the 1995 Kobe earthquake, Japan PHRI[1] conducted an extensive survey on the seismic performance of 24 ports. It had been observed that the peak ground accelerations (PGA) recorded at the Kobe port were 0.54 g and 0.45 g in the horizontal and vertical directions, respectively. The field investigation reports showed that the characteristic damage patterns of a caisson-type quay wall are large lateral movements, tilting, and settlements of caissons and ground movements of the backfill in the form of lateral movements and settlements of the apron.

[1] Port and Harbor Research Institute

3. Proposed Method

In the proposed method, which can be used both for construction of new quay walls and repair and rehabilitation of damaged pile-supported wharves, a number of piles would be driven almost at the seabed elevation and then prefabricated concrete caissons will be placed on them by proper procedures, and be filled with sand and gravels. In case of repairing the existing damaged pile-supported wharves, old piles may be cut at seabed elevation and used to build a new quay wall on. Gravity load of caissons are transferred to the lower layers this way and lateral loads caused by earthquakes would be better resisted. The caisson quay wall of Kobe has been selected as the basic model to simulate the proposed method on.

4. Seismic Analysis

The need to assess the seismic behavior of these structures is obvious considering the high risk of earthquake in Iran and most coastal sites. Results of dynamic analyses performed by FLAC software, was validated using reliable data and the role of piles in improving the seismic performance of the wharf is well demonstrated by comparing the seismic performance of the wall with piles and without them. Live and dead loads, soil pressure, and earthquake forces were determined and considered in the simulated model which was firstly designed statically and then analyzed dynamically with 5 real earthquake acceleration records in vertical and horizontal directions.

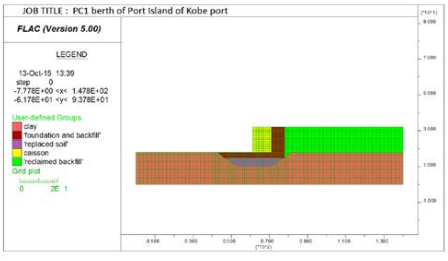

Figure 2. Simulated caisson and soil model in FLAC.

FLAC 2D is an explicit finite difference computational software for performing soil–structure interaction analyses under static and seismic loading conditions. The reason behind selecting this program is that it has various constitutive models for soil and structural elements, and thus, can be used for analyzing and simulating the behavior of structure on the ground or located in the soil. In addition, FLAC 2D offers the free-field boundary condition and damping properties for the seismic analysis [3-4].

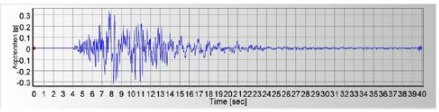

Figure 3. One of the excreted earthquake records.

The main parameters that were utilized to verify the model and evaluate the proposed method were horizontal and vertical displacements, a sample of which is shown in Figure 4.

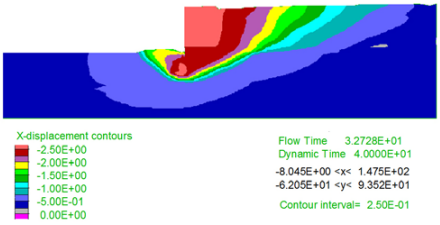

Figure 4. Horizontal displacement contour.

The soil beneath the caisson was replaced with inappropriate soft sand and the model was analyzed again. After modeling three piles below the caisson the model was investigated by performing seismic analyses (Figure 5).

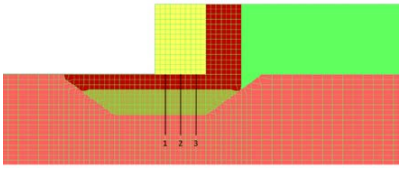

Figure 5. Caisson quay wall placed on 3 piles.

It was observed that horizontal and vertical displacements of the caisson were reduced 53% and 61%, respectively with the aid of added piles.

5. Further Sensitivity Analyses

Some sensitivity analyses were also performed on various parameters such as diameter of the piles, shear modulus and internal friction angle of the soil, to evaluate their impact on structural responses and horizontal and vertical displacements to provide optimized design criteria for the proposed quay. Results of one of these sensitivity analyses can be seen in Figure 6.

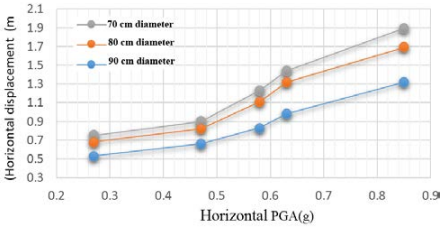

Figure 6. Displacement- PGA diagram for different pile diameters.

6. Liquefaction Evaluation

Finn and Byrne model [5] has been used to carry out coupled dynamic groundwater flow calculations to investigate the effects of seismically induced pore water pressures and estimate the degree and extent of liquefaction that can occur in the foundation and reclaimed soil during an earthquake excitation and ensure the seismic safety of the structures. The pore water pressure contour during earthquake can be observed in Figure 7.

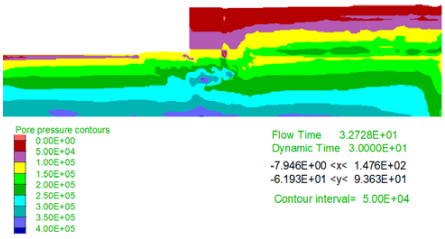

Figure 7. Pour water pressure contour during earthquake.

7. References

[1] Na, U.J., S.R. Chaudhuri, and M. Shinozuka, *Probabilistic assessment for seismic performance of port structures.* Soil dynamics and earthquake engineering, 2008.

[2] Inatomi, T., et al., *Damage to port and port-related facilities by the 1995 Hyogoken-Nanbu earthquake.* Technical note of the Port and Harbour Research Institute, 1997.

[3] McCullough, N.J., *The seismic performance of a pile supported wharf, PhD Dissertation*, Oregon state University. 2001.

[4] Iai, S. and K. Ichii. *Excess Pore Water Pressures behind Quay Walls. Observation and Modeling in Numerical Analysis and Model Tests in Dynamic Soil-Structure Interaction Problems*. ASCE. 1997.

[5] Byrne, P.M. *A cyclic shear-volume coupling and pore pressure model for sand. 2nd International Conference on Recent Advances in Geo. Earthquake Eng. and Soil Dynamics.* 1991.

CONSTRUCTION OF BREAKWATER BY GEOTEXTILE SANDBAGS: TECHNICAL SPECIFICATIONS

Mohammad Hadi Moeini[1], Mahmood Pourali[2], Majid Jandaghi Alaee[3] and Mohammad Rahim Ravan-Bakhsh

1) PhD in Coastal Eng., Pouya Tarh Pars Cons. Eng. Company, Tehran, Iran, mhmoeini@gmail.com
2) PhD St. in Hydraulic Structures Eng., K. N. Toosi Uni. of Tech., Tehran, Iran, mahmoud.pourali@gmail.com
3) PhD in Coastal Eng., Pouya Tarh Pars Cons. Eng. Company, m.j.alaee@ptpco.com
4) Omran-Sahel Insitute, Tehran, Iran, m.ravanbakhsh@omransahel.ir

1. Introduction

Although rock is the most popular material for construction of the coastal structures, such as breakwaters and various types of shore protections, there are difficulties in providing appropriate rock materials in some areas based on the economic and environmental conditions. In these cases, substitute materials such as concrete blocks and sandbags could be the alternatives of rock materials. In the plentitude of sand, for example when a project includes dredging, the sandbag is one of the best options from economic and environmental viewpoints.

Due to development of various types of the geotextiles, these materials have become one of the best selections to be used in making sandbags. In such cases, determination of the type of geotextile, technical specification of it and dimensions of the sandbags are very important.

Specification of the final product mostly depends on the bag size and texture quality. In this study some experimental tests have been designed and conducted to examine effective parameters. On this basis some recommendations have been proposed for the geotextile properties and size of sandbags for using in breakwater and shore protection structures.

2. Historical Usage of Sandbags

Geotextile Sandbags have been considered and used in different branches of civil engineering. In the coastal engineering, sandbags have been used mostly in construction shore protection structures. Building a temporary dam for blocking one of Pluimpot estuary's channels in Netherlands in 1957 is one of the earliest usage of sandbags in coastal zone [1]. Clifton Springs port in Australia is an example of sandbag usage in breakwaters. In 2004, the second breakwater of this port comprised of 100 meters length and 2 meters height has been made of 2.5 m^3 sandbags [2]. Sediment trap in Maroochydore-Queensland of Australia is an example of sandbag usage in shore protection structures [3]. Sandbags have been rarely used for construction of breakwaters. Thus, there is not specific recommendation for determination of their technical specification in breakwaters.

3. Recommended Specifications

Sewing, sand-filling, delivery and positioning the sand bags needs various equipment and facilities. Based on the available construction equipment and materials in Iran, it is recommended to use 1 m^3 sandbag for breakwater core, which has had good results for one of the actual cases. To make this size of sandbag, a piece of 6.7 m^2 geotextile is needed. When the sandbags are not exposed to sunshine radiation, Polypropylene geotextile is better than Polyester because it better keeps its strength in water. As it will be explained in full paper non-woven geotextiles have better behavior during construction rather than woven ones. However, the woven geotextile must be considered for suitable positions too because it is cheaper than non-woven with the same strength.

The bags are under several forces in different phases such as filling, lifting, dumping and load due to the traffic of trucks on the core. After construction obviously the main force is just the weight of the upper sandbags and surcharges and of course the waves' load.

Based on the theoretical computations and historical studies, the technical specifications of the recommended geotextile for 1 m^3 sandbag is described in Table 1.

Table 1. Technical specifications of geotextile for 1 m^3 sandbag

Parameter	Value	Description
Type	Non-woven or Woven	Non-woven is recommended
Material	Polypropylene	-
Mass (gr/m^2)	600	ASTM D5261
Tensile Strength (KN/m)	30	ASTM D4595
Punching Strength (N)	4000	ASTM D6241
Sewing Strength (KN/m)	24	ASTM D4595

Sandbags often are sewed and filled at the beach. During loading, unloading and installation, it is necessary to keep sandbags safe. Using inappropriate equipment may

tear the geotextile or sewn strings. There should not be sharp materials such as shell pieces and woods in the sand. Generally, any touch by sharp objects should be avoided in the site. In case of using dump trucks for sandbags transportation, it is necessary to remove or cover any sharp edge of trucks and other instruments. The dumping bed can be covered by appropriate type of geo-textile. In case of using excavators, it is necessary to use proper hoe to avoid damaging of the sandbags (Figure 1).

Figure 1. Special hoe for carrying sandbags

4. Experimental Tests and Results

Different sizes and different types of geotextile were tested. Figure 2 shows some of tested sandbags. Evaluation of the size, specification of the used geotextile and quality of stitches were the main issues in these tests.

There are some parameters for optimizing the size of bags including price, operational equipment and speed of operation. Bigger bags contain more sands resulting in heavier bags that need stronger geo-textiles. In case of using inappropriate geotextile, it is most likely to face tearing of bags during drop or even transportation. Figure 3 shows an example of inappropriate used geotextile related to the size of the bag. Cost of bags strongly depends on the quality of the used geotextile. It worth to mention that small bags also cannot be good economic choice because of more needed amount of geotextile per 1 m^3 of sand.

Figure 2. In-situ test bags.

Considering all effective parameters, 1 m^3 bag was recommended in this work as mentioned before.

The in-situ tests consisted of a series of drop tests, tension and drag tests. Figure 4 depicts how a dropping test was conducted. In this test every bag has been dropped several times starting from 2 meters up to a maximum of 7 meters. Some of bags failed in drop tests. The most effective reason of drop failure was inappropriate texture

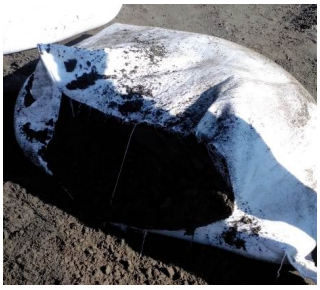

Figure 3. Tearing of bag due to weakness of geotextile

Figure 4. Drop test

5. Conclusion

In this study, technical specifications of sandbags for using in construction of breakwaters were presented. 1 m^3 sandbags with Polypropylene geotextile was found to be the appropriate selection. Some strength parameters were also proposed based on the theoretical and experimental findings. The designed sandbags were also rechecked by some in-situ tests that were in agreement with the presented criteria.

6. References

[1] Zimmermann, C., Dean, R., Penchev, V., Verhagen, H. J., "Environmentally Friendly Coastal Protection", Springer, 2004, pp 63-64.

[2] Hornsey, W.P., Carley J.T., Coghlsn I.R., Cox R.J., "Geotextile sand container shoreline protection systems: Design and application", *Geotextiles and Geomembranes*, 29, 4, 2011, pp. 425-439.

[3] Oyegbile B. O., Oyegbile B. A., "Applications of Geosythetic membranes in soil stabilization and costal defence structures", *International Journal of Sustainable Built Environment*, 6, 2, 2017, pp. 636-662.

EXPERIMENTAL INVESTIGATION OF THE EFFECT OF HYDRAULIC PARAMETERS ON THE WAVE REFLECTION FROM THE ICELANDIC BERM BREAKWATER

Majid Ehsani[1], Mohammad Navid Moghim[2] and Mehdi Shafieefar[3]

1) Department of Civil Engineering, Isfahan University of Technology, Isfahan, Iran, saeed.ehsaninoori@gmail.com
2) Department of Civil Engineering, Isfahan University of Technology, Isfahan, Iran, moghim@cc.iut.ac.ir
3) Civil and Environmental Engineering, Tarbiat Modares University, Tehran, Iran, shafiee@modares.ac.ir

1. Introduction

In terms of design and operation, the berm breakwaters are divided into two types of homogeneous and multi-layered berm breakwaters. In the homogeneous berm breakwater, the armor layer consists of only one grading, but in the multi layer berm breakwater, the armor layer consists of several stone classes. A multi berm breakwater (IBB) is a statically stable breakwater that only a small amount of reshape is permitted, also stones are divided into classes depending on their sizes. The philosophy of choosing different classes of stone is the best usage of dedicated quarry. The largest class of rock is called class I is located in front of the berm and in some cases in the upper slope of the berm which has the greatest impact wave. Also Smaller stone classes are placed in the lower parts of the slope and inner layers where the effective of the wave is less.

Hydraulic parameters are one of the most important factors in choosing the type and geometric characteristics of coastal structures. Among the hydraulic parameters, wave reflection is one of the most important parameters. Coastal structures can reflect part of the incident wave energy. The interaction of incident and reflection waves creates a turbulent environment in front of the structure and it makes difficult to navigate the vessels in this area. In addition, turbulent flows created around the structure can cause erosion and scour on the toe of the structure. The reflection of the wave is expressed by the reflection coefficient C_r as following:

$$C_r = H_r / H_i \quad (1)$$

Where, H_i is the incident wave height and H_r is the reflected wave height.

A number of researchers have worked on conventional rubble mound breakwater and proposed some experimental formulae for estimating reflection coefficient, e.g., Postma, Hughes, Muttray, Zanuttigh and Siguradarson [1-5]. However, the investigation of the wave reflection in IBB has been rarely done.

2. Experimental Set up and Structure Design

Experimental model have been carried out on an IBB in a wave flume at the hydraulic laboratory of Tarbiat Modarres University. The wave flume is 16 m long, 1 m wide and 1 m deep. In all tests, an irregular waves with a JONSWAP spectrum were used with a peak enhancement factor γ=3.3. Along the flume, four wave gauges have been used to record water level fluctuations. Three wave gauges were installed in front of the breakwater to separate the incident and reflected waves by using Mansard and Funke method [6]. Figure 1 shows the initial cross section of the IBB that situated at the end of the flume. The material properties in different layers for all tests are as following: Nominal stone diameter D_{n50} (m) for classes I, II and III is respectively (0.027, 0.02 and 0.012), stone gradation factor f_g for classes I, II and III is respectively (1.2, 1.5 and 1.5) and mass density for all classes is equal 2650 kg/m^3. The range of dimensionless parameters covered in the present study is as following: stability number H_o=1.3-2.3, stability index H_oT_o=23.7-67.4, wave steepness S_o=0.016-0.067 and breaker parameter ξ=3.4-5.3. To minimize the scale effect, Van der Meer proposed that Reynolds number as following [7]:

$$R_e = D_{n50}\sqrt{gH_s} / \upsilon > (1-4)\times 10^4 \quad (2)$$

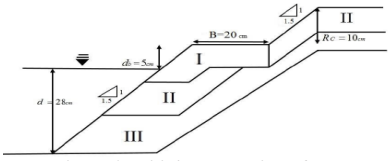

Figure 1. Initial cross section of IBB.

3. Results

In this research, the effects of environmental parameters such as wave height and wave period are investigated on the wave reflection from an IBB. The results are illustrated as dimensional and non-dimensional graphs. Finally, a relationship is proposed based on the non-dimensional parameter. It is noticeable that the IBB was designed in all tests as non-overtopped structure. The effect of wave height on wave reflection is shown in Fig. 2. According to Figure 2 wave height does not have a considerable effect on wave reflection. Muttray et al. express that the effect of wave breaking and the effect of permeability are approximately balanced. Therefore, the reflection coefficient is almost independent of the effect of wave height [3].

Figure 3 is shown the influence of wave period on the reflection coefficient. According to Fig. 3, it is observed that the wave period has a significant influence on the reflection coefficient. If the wave period with same wave height increases, the reflection coefficient will increase.

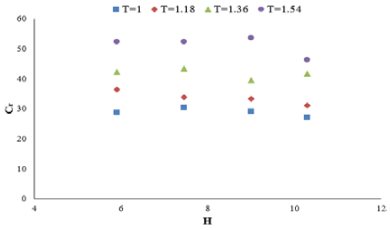

Figure 2. Influence of wave height on reflection coefficient.

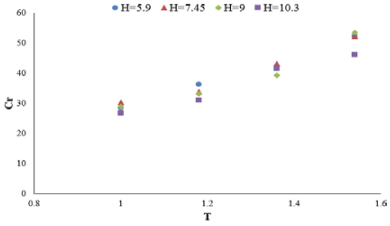

Figure 3. Influence of wave period on reflection coefficient.

Most relationships to the wave reflection are defined as a function of the breaker parameter ($\xi = \tan(\alpha)/\sqrt{S_0}$). Where ξ = breaker parameter, S_0 = wave steepness and α = front slope angle. In the figure 4, the effect of wave steepness on wave reflection is investigated.

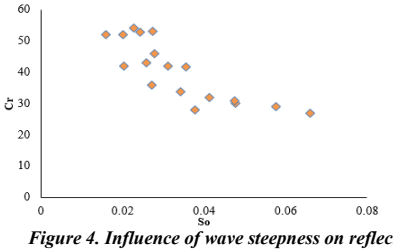

Figure 4. Influence of wave steepness on reflection coefficient.

As shown in Figure 4, with increasing wave steepness, wave reflection is reduced. But, there is a lot of scatter between data, which is mainly due to the dependence of the wave steepness to the wave height. Therefore, it should be used an approach independent of wave height in related to wave reflection. Muttray et al. is assumed that wave reflection is a function of T^2/d or dimensionless parameter L_0/d. According to assuming Muttray et al., Ffigure 5 is plotted.

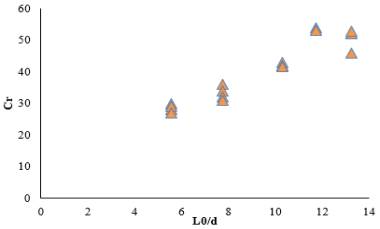

Figure 5. Dimensionless parameter L_0/d versus reflection coefficient.

Now, the wave reflection for an IBB can be calculated according to the following formula:

$$C_r = 7.6 \times (L_0/d)^{0.744} \quad (3)$$

The square of the correlation factor between experimental and predicted formula (Eq. (3)) is about 92%, while the E error is about 5.2%. These statistical quantities represent very good compliance. The results of this study indicate that the wave steepness in the breaker parameter (due to wave height) is not a suitable parameter for the wave reflection coefficient analysis.

4. Acknowledgments

The authors wish to express their sincere thanks to Iran National Science Foundation (INSF), who contributed financially to the project.

5. References

[1] Postma, G. M., *Wave reflection from rock slopes under random wave attack*, Delft University of Technology, Delft, Netherlands, M.Sc. thesis, 1989.

[2] Hughes, S. A. and Fowler, J. E., "Estimating wave-induced kinematics at sloping structures", *Journal of Waterway*, Vol. 121, No. 4, pp. 209-215, 1995.

[3] Muttray, M., Oumeraci, H., and Oever, E. T., "Wave reflection and wave run-up at rubble mound breakwaters", In *Coastal Engineering*, 2006, In 5 Volumes, pp. 4314-4324.

[4] Zanuttigh, B. and Van der Meer, J. W., "Wave reflection from coastal structures in design conditions", *Coastal engineering*, 55.10, pp.771-779, 2008.

[5] Sigurdarson, S. and Van der Meer, J. W., "Design of berm breakwaters, recession, overtopping and reflection", *Proceedings of Coasts, Marine Structures and Breakwaters*, September 18-20, 2013.

[6] Mansard, E. P. D. and Funke, E. R., "The measurement of incident and reflected spectra using a least squares method", *Coastal Engineering*, pp.154-172, 1980.

[7] Van der Meer, J. W., *Rock Slopes and Gravel Beaches under Wave Attack*, Delft University of Technology, Delft, Netherlands, Doctoral Thesis, 1988.

USE MARINE DREDGED SAND FOR PORT AREA CONSTRUCTION: A CASE STUDY OF SHAHID RAJEE PORT, IRAN

Seyed Taha Tabatabaei Aghda[1], Ali Ghanbari[2] and Gholamhosein Tavakoli Mehrjardi[3]

1) Department of Civil Engineering, Kharazmi University, Tehran, Iran, taha.taba@gmail.com
2) Department of Civil Engineering, Kharazmi University, Tehran, Iran, ghanbari@khu.ac.ir
3) Department of Civil Engineering, Kharazmi University, Tehran, Iran, ghtavakoli@khu.ac.ir

1. Introduction

Nowadays, mismanagement of dredged materials and its consequent accumulation at the shore results in both environmental and economic drawbacks. The annual worldwide estimations of dredging operations are between 15 and 20 billion tons [1]. Dredged marine sands (DMS) are generally very soft soils with low shear strength, usually treated as waste [2]. The sustainable development, environmental issues and shortage of the construction materials lead to finding a beneficial solution for reusing dredged material. Currently, one of the largest dredging projects in northern coast of Persian Gulf is the developing project of Shahid Rajaee port. In total, 11.5 million cubic meter of natural coastal sediment were carried out by cutter suction dredger, and disposed in foreshore area next to western part of the calmness basin.

The geocell-reinforcement technique is one of suggested method in terms of its soil confinement and increases the strength and stiffness property of the soft soil [3].

In this paper application of geocell reinforcement has been examined. Also, the effect of cover soil layers over geocell was studied, using sand and gravel. In order to evaluate the possibility of constructing low volume roads with marine sediments, plate loading tests were conducted.

2. Materials and Methods

2.1. Geocell

The geocell used in this study were made of heat-bonded non-woven (HBNW) polypropylene geotextiles with 21.3 kN/m Tensile strength. Single cells were 110 mm long, 100 mm wide and 100 mm height (Figure 1).

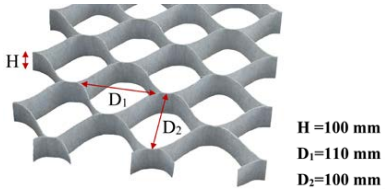

Figure 1. Geometric characteristics of geocell

2.2. Soils

Two types of soils were used in this study. The first type, which formed the higher volume of material used, was the sand derived from the dredging process of Shahid Rajaee port which has been used in different layers of the models. The second type of soil was well-graded gravel which was obtained from a mine near Bandar Abbas city and was used only in the cover layer. Particle size distributing of both materials is presented in Figure 2.

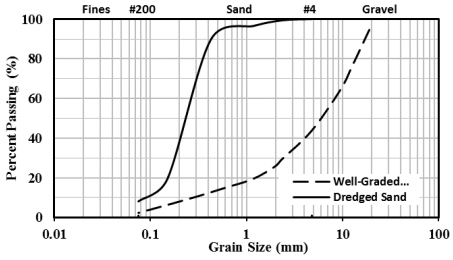

Figure 2. Dredged sand and well-graded gravel grain size distribution

2.3. Plate Load Test

In order to determine the bearing capacity of test backfills was used plate load test. Figure 3 illustrates the schematic of testing box.

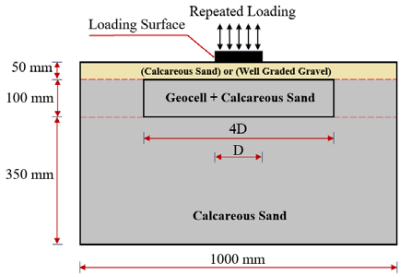

Figure 3. Plate load test setup

Backfills was made by manually compacting the dredged sand, with tamper in 50 mm lifts up to 350 mm in reinforced cases and 450 mm in unreinforced cases. Then geocells placed and dredged sand filled with accuracy in cells. Finally, a 50 mm thick sand or gravel cover layer, placed and compacted. All lifts were compacted to 70% of relative density with 4% moisture content. The specifications of the four prepared backfills are shown in Table 1.

Table 1. Lab tests specifications

Test No.	Notation	Geocell height (mm)	50-mm cover layer type
1	UR-S	--	Dredged sand
2	GR-S	100	
3	UR-W	--	Well graded soil
4	GR-W	100	

Loading process included four stress levels (250, 500, 750 and 1000 kPa) consisting of 10 cycles each. A circular plate with a diameter of 150 mm was used in this study.

3. Results and Discussion

Figure 4 plots the total settlement at the end of each repeated stress level and Figure 5 plots the plastic settlement at each loading cycles.

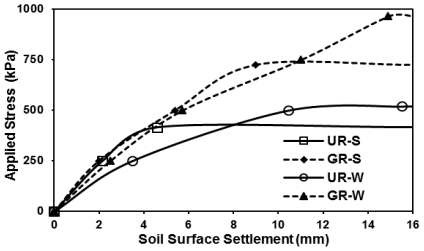

Figure 4. Stress –Settlement at the end of each load cycle

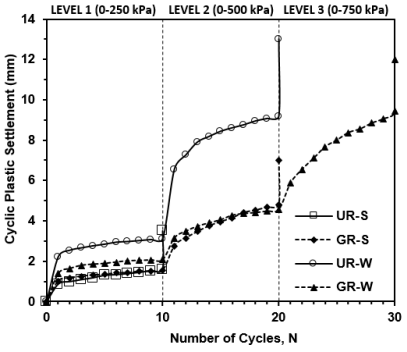

Figure 5. Plastic settlement

For a better comparison of results, the maximum force, total and plastic settlement at failure and the number of loading cycles are summarized in Table 2.

Table 2. Results of PLT and performance ratings.

Backfill name	UR-S	GR-S	UR-W	GR-W
Maximum stress (kPa)	416	725	520	960
Settlement at failure (mm)	4.6	9.0	15.5	14.9
Plastic settlement (mm)	3.5	7.0	12.5	12.0
Number of load cycles	10	20	20	30
Tolerable stress level	1	2	2	3
Bearing capacity ratio (BCR)	1	1.74	1.25	2.32
Performance rating	4	2	3	1

According to the results, only geocell reinforcement backfills can carry standard truck wheel load (550 kPa). Geocell can increases ultimate strength of backfills with a sand cover layer by 70% (from 416 kPa to 725 kPa) while in backfill with a gravel cover layer showed 80% increase (from 520 kPa to 960 kPa) in ultimate strength. The gravel cover layer in unreinforced backfills increases the ultimate strength by 25 percent (from 416 kPa to 520 kPa).

Reinforcement endured 10 more load cycles before failure compared to un-reinforcement backfill. Base on Table 2, bearing capacity ratio (BCR) increased up to 2.3 and have best when geocell reinforcement and gravel cover layer were used together. Using geocell as reinforcement for sand backfills, improved the stress-settlement behavior. Dredged sand can be used as backfill material for yards and access roads when reinforced with geocell and covered with a layer of well-graded gravel.

4. Acknowledgement

The authors gratefully acknowledge the support provided by Shahid Rajaee Port and Persian Gulf branch of Road, Housing & Urban Development Research Center (BHRC).

5. References

[1] Maher, A., Douglas, W.S., Jafari, F. and Pecchioli, J. "*The Processing and Beneficial Use of Fine-Grained Dredged Material, A Manual for Engineers*". New Jersey, Washington: RUTGERS Centre for Advanced Infrastructure and Transportation, 2013.

[2] Wang, D., Abriak, N.E. and Zentar, R. "Dredged marine sediments used as novel supply of filling materials for road construction". *Marine Georesources and Geotechnology*. 35, 4 2017, 472–480.

[3] Tavakoli Mehrjardi, G., Moghaddas Tafreshi, S.N. and Dawson, A.R. "Combined use of geocell reinforcement and rubber–soil mixtures to improve performance of buried pipes". *Geotextiles and Geomembranes*. 34, 2012, 116–130.

PREDICTION OF WAVE OVERTOPPING AT VERTICAL BREAKWATER

Zahra Heidari Tavasani[1] and Hadi Fadavi Hosseini

1) Civil engineering Department, Islamic Azad University, Tonekabon, Iran, zheidari93@yahoo.com
2) Civil engineering Department, Islamic Azad University, Tonekabon, Iran, drhadifadavi@yahoo.com

1. Introduction

Coastal structures are designed and constructed to protect coastal regions against storm waves and high water levels during storm surges. Reliable prediction of wave overtopping plays a significant role in the design and safety assessment of these structures. Excessive wave overtopping can harm people, damage vehicles, and damage properties on or close to the breakwaters. Commonly, the mean wave overtopping rate should be below an acceptable rate under the design conditions. Construction of a higher structure produces more protection than a lower one, but it would be costly and greatly impair the harbor aesthetics [1]

For the design, safety assessment and rehabilitation of coastal structures, reliable predictions of wave overtopping are required. Several design formulae exist for simplified types of dikes, rubble-mound breakwaters and vertical breakwaters [2]. The prediction of wave overtopping has been studied by various researchers like Franco et al., (1994) [3], EurOtop (2007) [4], Goda (2009) [5].

in this study we use the method of decision tree for developing the previous and predicting the wave overtopping rate for vertical breakwaters. The proposed were trained and validated using the selected small scale data from the CLASH database [6]. The results were also compared to those of previous empirical formulae.

2. Decision Tree

A decision tree is a decision support tool that uses a tree-like graph or model of decisions and their possible consequences, including chance event outcomes, resource costs, and utility. It is one way to display an algorithm that only contains conditional control statements. Decision tree has two algorithms: MARS [8] and M5 [9,10]. The new writing for M5 algorithm presented by Wang and Witten, (1997) [11] that called M5' algorithm. In this study M5' algorithm is used.

3. Description of the Parameters Affecting the Overtopping Rate:

Overtopping discharge is mostly related to the wave run-up. When the rising water caused by incident waves reaches the crest of the structure and pass over it, overtopping occurs [7]. Several structures and hydraulic parameters affect the overtopping rate on vertical breakwaters such as crest freeboard (R_c), Significant wave height ($H_{m0,\ toe}$) and The mean period ($T_{m,\ toe}$).

4. CLASH Database:

The international CLASH project of the European Union (Crest Level Assessment of coastal Structures by full scale monitoring, neural network prediction and Hazard analysis on permissible wave overtopping, www.clash-eu.org) [12] focuses on the modelling and predictions of wave overtopping for a wide variety of coastal structures, both in prototype and laboratory conditions.

5. Modeling:

In this study M5' model tree is used for wave overtopping modeling. First, Multiple models were built by CLASH datasets for vertical breakwaters that eventually, more accurate model selected. Then, the function of presented formula has been compared with previous with the help of the statistical charts and tables.

The formula is presented in this study by M5' model tree:

$$\text{If } \frac{R_c}{H_s} \le 1.092 \text{ ; } \frac{q}{\sqrt{g.H_s^3}} = \exp((-0.0897\frac{h_c}{H_s}) - (2.0977\frac{R_c}{H_s}) - (13.9577 S_{om}) - 2.88) \quad (1)$$

and

$$\text{If } \frac{R_c}{H_s} > 1.092 \text{ ; } \frac{q}{\sqrt{g.H_s^3}} = \exp((-1.2833\frac{h_c}{H_s}) - (0.8947\frac{R_c}{H_s}) - (23.8144 S_{om}) - 5.0644) \quad (2)$$

$$S_{om} = \frac{2\pi H_{m0}}{gT_m^2} \quad (3)$$

The statistical indices such as X_G (Geometric mean), δ_{XG} (Geometric deviation), BIAS (Deviation index) and RMSE (root mean square error) have been used to evaluate the accuracy of the models.

Table 1. Calculated errors for estimated values by different models for vertical breakwaters.

Error index	Franco	EurOtop	Goda	M5'
XG	3.627	3.23	3.83	2.82
δXG	15.9	13.46	15.27	11.38
BIAS	0.00011	0.000035	-0.00017	-0.00018
RMSE	0.00086	0.00095	0.00069	0.00067

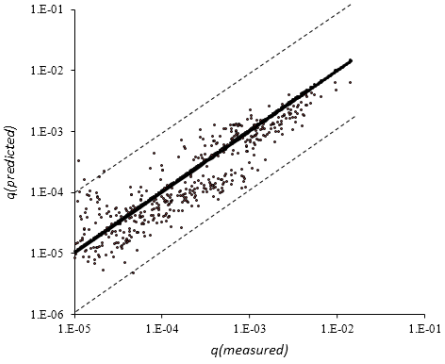

Figure1. Comparison of the measured and predicted overtopping rates by the M5' model tree.

This chart shows three inclined lines demonstrate conditions that the predicted rates are 10 times, equal, and 0.1 times of the measured rate.

6. Result

The obtained results were also compared with those of previous models. The accuracy of the model was evaluated by statistical measures, and it was shown that the developed model (M5') is more accurate than previous models.

7. References

[1] Shankar, N. J., and Jayaratne, M. P. R. "Wave run-up and overtopping on smooth and rough slopes of coastal structures", *Ocean Eng*, 2003, 30(2): 221–238.

[2] Van Gent, M. R. A., Van den Boogaard, H. F. P., Pozueta, B and Medina, J. R., " Neural network modelling of wave overtopping at coastal structures", *Coastal Engineering*, 2007, 54(8): 586-593.

[3] Franco, L., de Gerloni, M and van der Meer, J.W., "Wave overtopping on vertical and composite Breakwaters". *ASCE, Proc. ICCE*, Kobe, Japan, 1994.

[4] EurOtop, "Wave Overtopping of sea defences and relate structures – assessment manual", 2007

[5] Goda, Y.,"Derivation of unified wave overtopping for seawalls with smooth, impermeable surfaces based on selected CLASH datasets" *Coastal Eng*, 2009 56(4): 385–399.

[6] Van der Meer, J. W., Verhaeghe, H and Steendam, G. J., "The new wave overtopping database for coastal structures", *Coastal Engineering*, 2009, 56(2): 108-120

[7] Verhaeghe, H., "Neural network prediction of wave overtopping at coastal structure", *Dept. civil Eng, Ghent University, Doctorate Dissertation*, 2005.

[8] Friedman, H., "Multivariate adaptive regression splines", *ANN, Statist*, 1991, 19(1): 1-67.

[9] Quinlan, J. R., "Induction of Decision Trees", *Machine Learning*, 1986, 1(1): 81-106.

[10] Quinlan, J. R., "Learning with continuous classes", *Proceedings of AI'92 (Adams and Sterling Eds), World Scientific*, 1992, 343-348.

[11] Wang, Y. and Witten, I. H., "Induction of model trees for predicting continuous lasses", *Proceedings of the Poster Papers of the European Conference on Machine Learning, Prague, University of Economics, Faculty of Informatics and Statistics*, 1997.

[12] CLASH, Crest level assessment of coastal structures by full scale monitoring, neural network prediction and hazard analysis on permissible wave overtopping, *Fifth Framework Program of the EU, Contract no. EVK3-CT-2001-00058*, www.clash-eu.org.

FINITE ELEMENT ANALYSIS OF DEZHPOD® ARMOUR UNIT UNDER STATIC LOADING AND COMPARING WITH XBLOC®

Alireza Sadat Hosseini[1] and Abbas Mousavi[2]

1) Sazeh Pardazi Iran (SPI) Consulting Eng. Co., Tehran, Iran, a.sadat@sazehpardazi.com
2) Sazeh Pardazi Iran (SPI) Consulting Eng. Co., Tehran, Iran, a.mousavi@sazehpardazi.com

1. Introduction

Concrete armour units specially the Third generation armour units, the units are placed randomly in a single layer, are more cost efficient for rubble mound breakwaters. Often the lack of indigenous technical knowledge and implementation of this type of armor is unnoticed. Dezhpod® armour unit has been launched by Sazeh Pardazi Iran Consulting Engineers [1] as the first Iranian concrete armour, based on processing experiences in recent years of design, construction and operation of onshore and offshore structures formed in Iran. The development studies of this armour began about seven years ago. Dezhpod® is used in a single layer and its stability is based on the interlocking between adjacent blocks. The high interlocking quality of Dezhpod® has been proven in laboratory tests, and its suitable geometry showed satisfying hydraulic and structural stability. The ease of fabrication and placement are the other advantages of this armour unit. As Dezhpod® is randomly placed in a single layer, it is comparable to the other single layer armour units such as Xbloc® [2].

The breakwater armour unit Xbloc® has been launched by Delta Marine Consultants and is used in some Iranian projects. Unfortunately, some examples of this armour failure has been observed that were attributed by breakage of the armour units. For instance Figure 1 shows examples of Xbloc® Armour units in Anzali port, Iran, which is broken due to wave impact.

Figure 1. Breakage of Xbloc® armour units

The observed armour breakage for Xbloc® in above mentioned project, made the Dezhpod® developers to investigate the structural resistance of this armour unit.

In this study a set of structural analysis was performed to investigate the tensile stress distribution in Dezhpod® armour unit comparing to its well-known competitor Xbloc®. To this aim, three-dimensional (3D) Finite Element (FE) model of both armour units are built. Results of the numerical analysis showed that Dezhpod® armour unit has better performance in distributing the tensile stresses and higher resistance to cracking.

2. Finite Element Modeling and Results

The static structural response of Dezhpod® as well as Xbloc® unit through investigating the tensile stress distribution has been investigated with a three-dimensional (3D) Finite Element (FE) model using the computer program ABAQUS 6.14. The 3D FE models of both armour units have the same properties: unit volume 4m^3, solid density 2400 kg/m^3, Young's Modulus 30 kN/mm^2, Poisson ratio 0.20. These particulars are comparable to those used by Hakenberg et al. [3] and Muttray et al. [4]. The armour units have been exposed to flexure, torsion and combined flexure and torsion. The load cases are the same as the ones used by Muttray et al. [4] to study the Xbloc®. These static load cases are outlined in Figure 2.

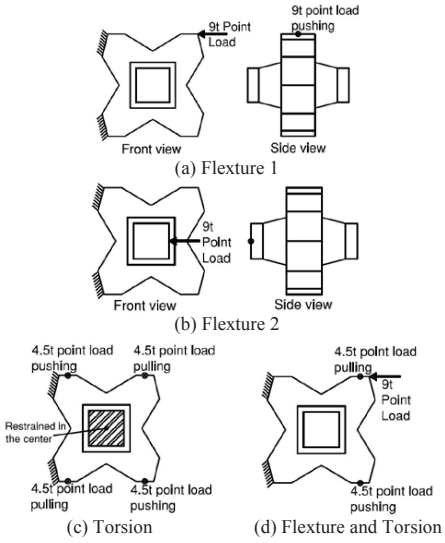

Figure 2. Static load cases for FE analysis

The numerical analysis in this study focused on the assessment of the tensile tresses in the FE models, because these stresses are the governing factors for initial damage and cracking in concrete armour units. The stresses and strains that are computed in each of the elements are linearly related to the displacement of the corresponding nodes of the elements. The graphical presentation of the FE models used in this study along with the critical paths corresponding to the load cases are given in Figure 3.

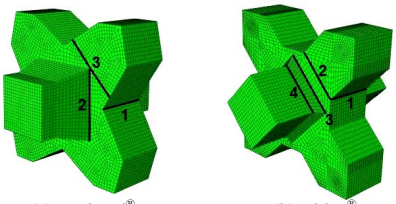

(a) Dezhpod® (b) Xbloc®

Figure 3. The FE models used in the numerical study

Both finite element models were analyzed under the action of the four load cases and results are presented in Figure 4. This figure presents the tensile stresses along the critical paths shown in Figure 3. As depicted from Figure 4, in all load cases Dezhpod® gives lower values of stresses along the critical paths. Although in Figure 4(c) and 4(e), for Dezhpod®, stresses are raised locally due to the armour geometry, the overall stress values are lower than Xbloc®.

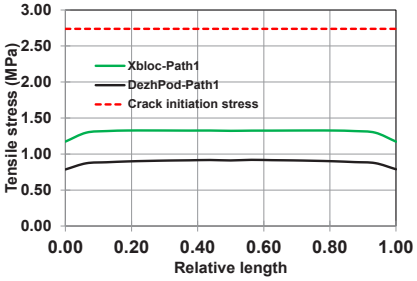

(a) Flexture 1

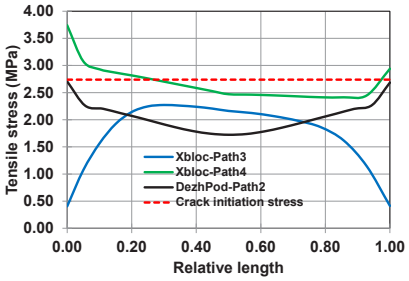

(b) Flexture 2

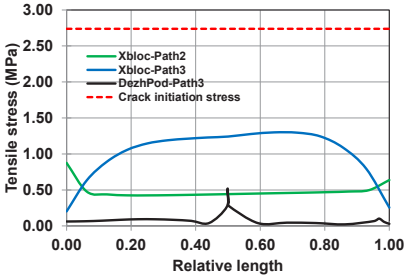

(c) Torsion

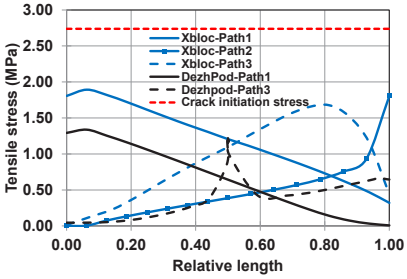

(d) Flexture and Torsion

Figure 4. Results of the numerical analysis. The red dash line represents the stress corresponds to the armour crack for f'_c=30MPa

3. Conclusion

A set of numerical analysis is performed to investigate the tensile stress distribution along the critical paths on a 4m^3 Dezhpod® armour unit and comparing the state of stresses with Xbloc® armour unit with the same volume and material properties. Results show smoother stress distribution in Dezhpod® armour unit, and lower values of stresses in comparison with Xbloc®. It can be concluded that Dezhpod® unit has higher resistance under static loads and cracking.

4. References

[1] Mousavi, A., Hajmomeni, A., "Hydraulic and Structural Performance of Dezhpod® Iranian Armour", The 11th International Conference on Coasts, Ports and Marine Structures (ICOPMAS 2014), Tehran, Iran, 24-26 Nov. 2014.

[2] Reedijk, B., Bakker, C., and Klabbers, M., "Introduction of the Xbloc Breakwater Armour Unit", Terra et Aqua – Number 94 – March 2004.

[3] Hakenberg, R., Vos-rovers, I., Reedijk, B., and Muttray, M., "Structural Integrity of Xbloc® Breakwater Armour Units Prototype and Numerical Drop Tests", International Conference on Coastal Engineering, 2004, Lisbon.

[4] Muttray, M., Reedijk, J., Vos-Rovers, I., and Bakker, P., "Placement and Structural Strength of Xbloc® and other Single Layer Armour Units", International Conference on Coastlines, structures and breakwaters, 2005.

SOME SOLUTIONS FOR SOIL ESCAPING PROBLEM IN CONTIGUOUS PILED QUAY WALLS

Ali Varesvazirian[1] and Abolfazl Aliasgari[2]

1) Sazehpardazi Consulting Eng., Tehran, Iran, vazirian@sazehpardazi.com
2) Sazehpardazi Consulting Eng., Tehran, Iran, aliasgari@sazehpardazi.com

1. Introduction

Where executive and geotechnical conditions allow, one of the most common quay structures is concrete bored pile wall. Two techniques are used for this purpose: Secant piles and contiguous piles [1-4].

Contiguous piled walls process involves the construction of a run of piles with pre-calculated gaps dependent on soils structure and surrounding ground conditions. In contrast, in secant piled walls, primary piles which are composed of plain concrete or even plastic concrete are constructed initially and the main secondary reinforced pile will be executed between them while cutting a portion of the primary ones. As a result, no gap will remain between piles.

Construction of secant-pile wall is more complicated than the other method and required especial equipment. Consequently, Iranian contractors as well as consulting engineers used to prefer contiguous-pile wall. This, nowadays, leads to a significant problem in some of Iranian ports like Anzali and Amirabad: crown settlement and/or creating extended hole under pavement due to soil escaping from pile gaps. This issue will intensify when the adjacent piles have tolerances of pile position and vertical alignment.

In this paper some solutions are proposed to limit material escaping from pile gaps in existing quaywall based on project condition. In addition, some techniques which can be employed for new berth construction is presented.

2. Description of the Problem

Although backfill and subsoil escaping is also common in steel–pile wall, its rate is significantly less than those cases observed in bored concrete-pile wall. This is because steel piles in quaywalls are usually equipped with interlock which can tighten the gaps appropriately. Even with no interlock element, steel piles drive particularly close enough to each other to limit material escaping. But cast-in-situ concrete piles have more executive tolerance and therefore open gaps between them are more probable than steel-pile walls (see Figure 1).

These gaps result in backfill escaping and gradually form large cavities behind the wall. One of these huge holes which have been formed under utility trench behind the main wall of old Anzali quaywall is shown in Figure 2. These cavities should be filled as soon as possible with non-shrinkage material to prevent future damage of trench, pavement, etc.

Figure 1. Open spaces between concrete piles, Anzali old quaywall.

Figure 2. A large cavity formed under utility trench due to material escaping, Anzali Old quaywall.

3. Material Escaping Remediation

3.1. New Berths

Although contiguous piled walls are common in urban excavation, the best recommendation is using secant-pile wall for new maritime structures. Available experiences show that even perfect construction could not prevent material escaping completely in contiguous pile walls.

If contiguous piled wall is unavoidable, gap tightening should be carried out perfectly. A traditional method is employing tightening pile, a small diameter plain concrete pile cast in situ between two main piles behind their gap. However as they are executed as the same manner, there are some spaces between tightening and main piles. In this condition a modification is using a wedge added to steel casing to occupy the space between piles (see Figure 3).

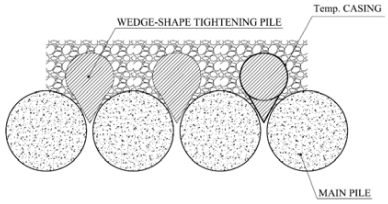

Figure 3. Using wedge added to tightening pile casing.

Injection grouting or even jet grouting behind the gaps are other methods which are appropriate when the soil in front of the piles is not excavated/dredged yet. Injection grouting is useful for granular soil such as sand and sand-gravel mixture. Jet grouting may be applicable in extended rage of soil grading. However jet grouting should be used with caution because it may damage concrete piles. Moreover, the quality control for these method is usually with some difficulties.

Another tightening method which used successfully is driving a large H/U Pile behind the pile gap, drilling the space between main piles and the H/U steel pile and finally concreting it. It is obvious that the soil around the piles should not be removed until tightening is completed. More explanation will be presented in the next section.

3.2. Existing Quaywalls

For existing contiguous-piled walls which are subjected to material escaping, remediation methods are so complicated because:

- The soil in front of piles which act as a barrier does not exist.
- The space behind the piles is hardly accessible to setup and handle required equipment.
- Unpredicted obstruction may be occurred during executive processes.
- Remediation methods are not usually under control.

Where backside of the wall is accessible from the top, the following method may be used:

- Driving a U-shape sheetpile or H-shape steel profile (see Figure 4)
- Drilling the space between two adjacent piles and the profile by conventional method like air-lifting.
- backfilling the hole by concrete or filter material

The main executive challenge for this method is the pile gaps where the concrete may escape from them. Therefore, temporary tightening is necessary. Manual placement of bags filled by dry concrete, between piles may be a fast solution.

However, the perfect method is tightening the gap by an under-water comprehensive concrete work (see Figure 5):

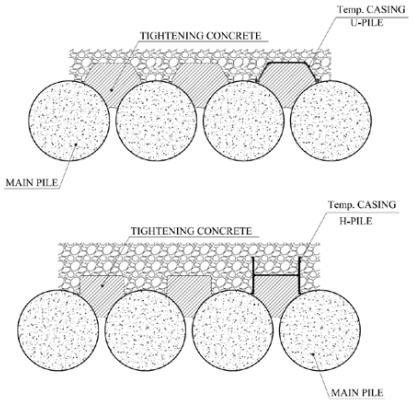

Figure 4. Using temporary H or U-shape casing to drilling and concreting between piles.

- Placement permanent forms alongside the gap;
- Pouring grouting mortar from the bottom until it overflow from the top of the form.

Grouting mortar is a fine-grain concrete mixed with additives such as Superplasticizers etc.

The latter method is going to be used for the old Anzali Berth. In spite of several difficulty encountered during execution, this method seems to be more reliable than the other method and its quality can be controlled during construction.

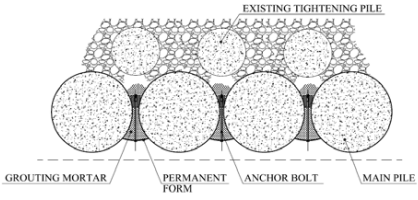

Figure 5. Tightening with grouting mortar via permanent anchored forms

4. References

[1] British Standard Institute, BS 6349-Part 2-"Design of quay walls, jetties and Dolphins", 2009.

[2] Centre for Civil Engineering Research and Codes, CUR, "Handbook Quay wall, 1st ed. Taylor and Francis, 2005.

[3] Recommendations of the Committee for Waterfront Structures Harbours and Waterways- EAU, 11th ed. 2012.

[4] Godvarthi, V. & Mallavalli, R., "Contiguous Pile Wall as a Deep Excavation Supporting System", Leonardo Electronic Journal of Practices and Technologies, 2011, p. 144-160

DESIGN OF AN OFFSHORE PORT BASED ON COASTAL SEDIMENT AND ENVIRONMENTAL ASPECTS

Reza Arefi[1] and Aghil Hajmomeni[2]

1) Senior Engineer, Sazeh Pardazi Iran (SPI) Consulting Eng. Co., Tehran, Iran, r.arefi@sazehpardazi.com
2) Head of Coastal Process and Hydraulic Discipline, SPI, Tehran, Iran, a.hajmomeni@sazehpardazi.com

1. Introduction

Sand deposition at the port entrance and erosion along the down-drift side of the port are the most important points to be taken into consideration for designing the layout of small fishing ports constructed on sandy beaches [1]. Breakwaters trap sediment moving along the coast, and at least in the first year after construction of the port, no (or hardly any) sediment will pass the breakwater and serious erosion may occurs at this side of the fishing port. On the other hand, sediment will deposit just after the construction of the port at the up-drift side and sand deposition at the approach channel and at the entrance of the port will occur [2].

Cage culture is one the most commonly used methods which recently has been considered for fish farming in many countries. In this regard, Iran Fisheries Organization has a plan to develop fish cage cultures at some locations in the Caspian Sea. Larim site which is located at the 30km east of the Babolsar port is one of these selected locations. Marine section of each site is going to have two main parts: 1- An offshore part including cage, feeding barge, … and 2- An onshore port which supports the service and feeding vessels.

Many small ports constructed along the southern coasts of the Caspian Sea suffer from different modes of sediment problems. An offshore port connected to the shore by an open bridge which doesn't block the littoral drift and so could be proposed as an alternative for connected small nearshore ports and a solution for relative sediment problems.

The purpose of this study is to propose an offshore port layout to reduce the sedimentation problems for the Larim service port located in Mazandaran province, north of Iran. To achieve this goal, a series of numerical modeling of waves, currents, sediment transport and coastline evolution have been conducted by LITPACK and Mike21 for 1D and 2D simulation respectively. Also the functional design and dimensional ratios of main parts have been controlled by the relative design references advice.

2. Project Site Conditions

The Project site is located in south-eastern of the Caspian Sea almost 30 km east of the Babolsar port. The hydrography counter lines are parallel to the coastline. As shown in Figure 1, predominant wave direction is NW, the calm period (H_s<0.5m) is 32.7% and the maximum wave height is 5.5m at the depth of 20m. Bed slope is uniform and about 0.6%. Based on the local sediment sampling at the depth of -5m, mean grain diameter of bed sediments (D_{n50}) is about 0.2mm. Site project hydrography shows a shoreline parallel sandbar formed at the depth of around -4m. This bar is a clear sign of cross-shore sand transport and should be considered in port layout design (Figure 2).

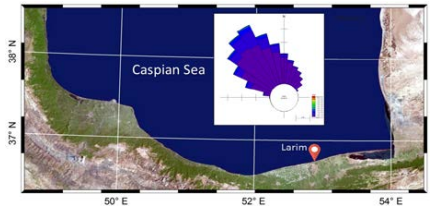

Figure 1. Wave rose at the project site location

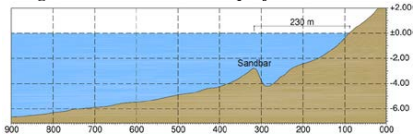

Figure 2. Bed level changes at project site

3. 1D Sediment Transport Modeling

Based on 1D numerical modeling executed by LITPACK, the net and gross longshore sediment transport rate is estimated approximately 110,000 (from west to east) and 160,000 m^3/year respectively. Also surf-zone width is calculated 350m (depth -4.5m) and 450m (depth -5m) corresponding to 80% and 90% of littoral drift rate respectively. Sediment transport model calibration has been done by using historical shoreline evolution behind the Fereydounkenar and Neka breakwaters.

4. Different Scenarios of the Port Layout

To design a small service port at the Larim site, three scenarios have been considered from view point of the port function on littoral sediment transport blockage (see Figure 3). The first scenario is based on partially blockage of littoral drift. The proposed layout is a conventional short port which several years after evolution of the up-drift shoreline will be located in the surfzone. On the other hand the breakwaters have to be extended beyond the sandbar. Then in this layout the basin entrance is located at -5m depth and the length of main and secondary arm is 575 and 360m respectively. The entrance shoaling is expected after a few years but can be decreased by mechanically bypassing of up-drift sediments.

Completely blockage of longshore sediment transport by a long rubble mound jetty is the second scenario. Based on the Litline results, extending the port to -6m depth by a 650m long breakwater will guarantee the sand not to be deposed at the port entrance within a period of 20 years after construction. The up-drift sedimentation and down-drift serious erosion and consequently morphological and environmental problems are the most important defects of this alternative. An offshore port is proposed as the third scenario to reduce the morphological and environmental effects of the hard-blocking coastal structures. Although the offshore port function is similar to 1D offshore detached breakwaters, the two dimensional effects of the basin should be considered on the future shoreline changes.

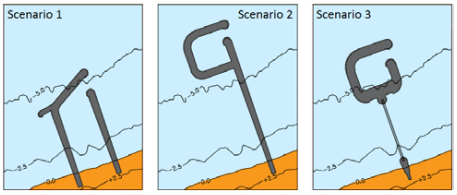

Figure 3. Different scenarios of port layout design

Attention to the high importance of sedimentation, coastal erosion and environmental problems and the result of economically-technically comparison of the proposed layouts, the offshore port scenario is selected as the best effective alternative for the Larim service port.

One of the main concerns about the selected layout is high construction costs of the pile and deck system comparing with the rubble mound breakwater. To compare the construction cost, detail design is performed for both structural systems. Calculation of the cost for pile and deck system and rubble mound breakwater shows that the costs of the two mentioned structural systems are almost the same. The long distance of borrow materials to the project site (which is common problem in all coastal projects in the north of Iran) is the most important factor that increases the cost of rubble mound breakwater system.

5. Determination of Offshore Port Geometry

The function of an offshore port with a 2D offshore basin is similar to a 1D offshore breakwater. The most important concept to design an offshore breakwater is to prevent development of tombolo behind the offshore port during the service life. Breakwater length relative to breakwater distance to shoreline ($L^*_B=L_B/x$) is the main parameter which determines accumulation form behind the breakwaters [3]. When $L^*_B<0.6$ to 0.7, a bell-shaped salient will form in the shoreline in the lee side of the breakwater. Also it is better to construct the breakwater out of surf-zone to have small impact on littoral transport [4]. The offshore port can be considered equivalent to a detached breakwater if the shadow zone, wave, current and sediment transport pattern as well as the bed level changes are the same behind both of them (see Figure 4). To achieve this purpose, 2D numerical modeling (Mike21) has been performed and finally, offshore port geometry has been determined as depicted in Figure 4.

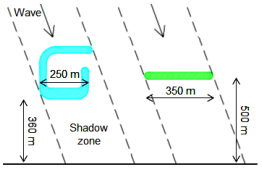

Figure 4. Offshore port and equivalent detached breakwater

6. Similar Examples of Existing Offshore Port

Two samples of offshore ports are shown in Figure 5. Kunnuy fishing port is located in Japan as an offshore fishing port to prevent coastal erosion at down-drift of the port by allowing longshore sediment transport. For Kudankulam power plant in west of India, an offshore breakwater has been constructed as a surface water intake.

Figure 5. Offshore port in Japan and India

7. Conclusion

Different scenarios have been proposed as the port layout alternatives for the Larim service port. Sedimentary, morphological and environmentally concerns of the small-short ports especially in the Caspian Sea, guide the layout to an offshore port connected to the shore by a 360m length pile and deck access road. The detail design of the project components and exact cost estimation showed that the pile and deck structural system could be considered as an effective alternative for rubble mound breakwaters in the Caspian sea with almost the same (or not very higher) construction cost. Rock mines excavation and transportation problems, long distance of the borrow materials to the project site for rubble mound structures, besides the morphological and environmental advantage of the offshore port, make the offshore port to be introduced as an economically-technically layout for small ports in the Caspian Sea in Iran. Finally, the sediment monitoring is strongly recommended for offshore ports.

8. References

[1] Kawaguchi, T., "Construction of Offshore Fishing Port for Prevention of Coastal Erosion", *Coastal Engineering,* 1994, pp. 1197-1211.

[2] Aagaard, T., Hughes, M.G., " Equilibrium shoreface profiles: A sediment transport approach ", *Marine Geology,* Vol. 390, pp. 321-330, 2017

[3] United States, "Coastal engineering manual", *Washington, D.C., U.S. Army Corps of Engineers*, 2006.

[4] Mangor, K., "Shoreline Management Guidelines", *DHI Water & Environment*, 2004.

STRATEGIC PLANNING IN SMALL PORTS (CASE STUDY OF SAJAFI PORT)

Seyede Masoome Sadaghi[1], Mohammad Ghazaie [2] and Saeed Lotfikhah[3]

1) Road, Housing & Urban Development Research Center, Tehran, Iran, sonasadaghi@gmail.com
2) Tarbiat Modares University, Tehran, Iran, mohammad.ghazaie@yahoo.com
3) Sazeh Pardazi Iran (SPI) Consulting Eng. Co, Tehran, Iran, s.lotfikhah@gmail.com

1. Introduction

Unlike large global ports which play a key role in many supply chains, small regional ports are usually more stagnant and have not reached the same level of development as the larger ports. Port development is mostly focused on large ports and small ports have gradually lost their national or regional roles. However, these ports have many potentials and can serve as a part of the whole to help the Port and Maritime Organization (PMO) to achieve the desired long-term goals. Investigation and study of strategic orientations of small ports along Persian Gulf, Oman Sea and Caspian Sea is under consideration by PMO. The present paper focuses on the strategic plans for development of Sajafi Port in Khuzestan Province as a case study [1, 2].

Sajafi port is one of the small ports situated near Hendijan city in Khuzestan Province. The aerial view of the port is shown in Figure 1.

Figure 1. Aerial view of Sajafi Port

2. Methodology

In order to determine the strategic orientation of the small port, first the basic information is gathered by desk studies, site visits and interviews with the stakeholders. According to the available data, the relative advantages (the advantages that depend on the nature of the port itself or are achieved in comparison to other small ports), structural bottlenecks (obstacles that affect and prevent the development and operation of the port) and the prevailing tendencies (affairs that affect the future function of the port in some way) are studied. The mentioned issues are investigated in four categories of physical, operational, managerial, and socio-economic considerations. Based on the analysis of the existing situation and considering the perspective of the PMO [3], the objective will be to determine the strategic orientation of the desired port. The SWOT matrix is used for this purpose [2].

3. Analyses of the Current Status of Sajafi Port

The division of port related issues of Sajafi port in comparison with other small ports of Khuzestan Province (Arvand Kenar, Chebdeh and Shadegan ports), are presented in Table 1.

Table 1. Division of port related issues

Physical	
Relative Advantages	-Longer Wharf (compared to other small ports of Khuzestan) -Fairly suitable port area -Enough space in hinterland for future development -Neighboring with the fishery wharf -Proximity to the vessel repair yard
Structural Bottlenecks	-Maximum distance to the nearest transportation infrastructures -Maximum distance to the nearest industrial/commercial centers -Low quality of access road
Operational	
Relative Advantages	-Relatively high annual revenue -The fairly high flow of vessels -Placing along Zohreh river, No need for breakwater and basin construction
Structural Bottlenecks	-Maximum distance to main marine navigation routs -Low depth in front of the wharf and sedimentation problems -Proximity to rival small ports (Deylam, Genaveh and Shadegan) -Limitation of port infrastructures -Environmental restrictions in Zohreh River
Prevailing Tendencies	-Tendency to import general tax free products (products transferred by small vessels without paying any tax to the customs duty) -Tendency of vessel owners to use neighbor small ports

Managerial	
Relative Advantages	-Most non-state employees compared to other ports -Most employees of relevant organizations
Structural Bottlenecks	-Inadequate official space -Failure to observe the laws related to import of goods
Socio-economic Considerations	
Structural Bottlenecks	-Lack of manufacturing and service jobs in the city -Weakening of farming and fishery
Prevailing Tendencies	-Dependency of people of Hendijan on Sajafi port -Tendency to provide tax free and cheaper goods from Sajafi port -Tendency to use indigenous labor forces -Due to the drought and decline of agriculture, residents tend to engage in port-related activities

4. Strategic Position of Sajafi Port

The scores derived from the internal and external factor evaluation matrices (IFE and EFE) should be imported to the vertical and horizontal dimensions of the SWOT matrix. The SWOT method, analyzes the strengths, weaknesses, opportunities and threats associated with the port in a systematic way and reflects the appropriate strategies for the port. Four categories of ST (Strength-Threat), WT (Weakness-Threat), WO (Weakness-Opportunity), and SO (Strength-Opportunity) strategies are achieved according to the results.

In order to provide a more precise analysis, the strategic orientation of the port is once investigated separately for physical, operational, managerial and socio-economic factors and eventually the integration of all influential factors are considered. The results are summarized as follows.

Assessing the physical factors led to ST position. The most important physical factors that threaten the port are the large distance from the transportation systems and the shortages in the infrastructures, such as storage areas and marine navigation equipment. These threats can be controlled with the help of strengths such as the relatively high annual income and high vessel traffic in the port.

Assessing the operational factors led to ineffective zone of WT in the SWOT matrix. This important result have several reasons including inadequate port equipment, high sedimentation and low depth of Zohreh River, environmental restrictions in dredging of the river mouth, the uncertainty about the rate of loading and unloading and the tendency to import tax free goods.

In the managerial viewpoint, the port is in the ST position. Inadequate office space, many employees and lack of compliance with the laws related to the import of goods have led to such a situation for Sajafi port. Increasing the office space and the establishment of commercial rules in the port can lead the port management position to the SO zone.

From the socio-economic point of view, the port is situated in SO zone. The droughts and agricultural decline has expanded the resident's tendency to port-related activities and has led to the dependence of the people of the city of Hendijan to Sajafi port. Radar charts of SWOT matrix for different factors are shown in Figure 2.

5. Conclusion

The strategic orientation of Sajafi port considering the integration of all influential factors is in the ST position (Figure 2). Considering the total strengths, weaknesses, opportunities and threats of Sajafi port, it can be concluded that the development of the port is not cost-effective due to the natural status of the river and the possibility of competitiveness of the port is low compared to other nearby small ports. The strategy of this port is to preserve and organize the existing commercial activities and to revitalize light fishing activities. Some of the short-term actions in this port could be organizing the legal system of import and export, upgrading navigational and berthing equipment, as well as improving the quality of the access road to the port.

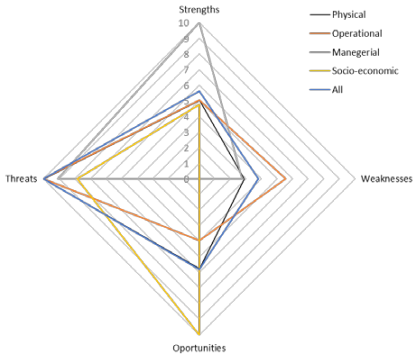

Figure 2. Radar chart of SWOT matrix

6. References

[1] Olesen, P. B., Popovska, I. D., Hvolby, H. H., Jensen, K. S., "Strategic port development: identifying a development approach for small and medium-sized ports", Proceedings from the Annual Transport Conference at Aalborg University, 2014.

[2] Road, Housing & Urban Development Research Center, "Investigation and study of strategic orientations of the small ports of Bushehr, Khuzestan and Golestan provinces, focusing on usage and management patterns", (In Persian), 2018.

[3] The perspective of the Ports and Maritime Organization (In Persian), 2018.

DESIGN CONSIDERATION OF PILES AGAINST LATERAL SPREADING CAUSED BY LIQUEFACTION

Hamid Bayesteh[1,2] and Farshid Jandaghi Alaee[3]

1) High Performance Computing Lab, School of Civil Engineering, University of Tehran, Tehran, Iran. hbayesteh@ut.ac.ir
2) Pouya Tarh Pars Consultant Engineers, Tehran, Iran.
3) Civil Engineering Department, Shahrood University of Technology, Shahrood, Iran, fjalaee@shahroodut.ac.ir

1. Introduction

The liquefaction is response of loose saturated sand to cyclic loading of earthquake in which the sand loses its strength as a result of excess pore water pressure and tends to liquefy. Accordingly, there is a high potential for lateral movement of soil on slop and severe damage to structures in coastal ports during earthquake as reported around the world [1].

Generally, excessive pore water pressure in vulnerable soils during earthquake has twofold unwanted effects on structures as:

- lateral and vertical strength reduction of soil
- additional lateral load due to the lateral spreading/movement of soils on slope

In this study, the flexural mode of failure in marine piled-structure, as one of the most important cases of maritime structures is investigate and local strengthening of vertical piles in a real case is examined. Upper and lower band of lateral strength of soil is considered to adopt strengthening length of piles.

2. Soil Strength Reduction

Strength reduction of liquefied and its adjacent non-liquefied soil due to the excess of pore water pressure should be considered in evaluation of inertia force on structures. This phenomena is mostly taken into account via p-multiplier reduction factor of P-Y curves or developing a new P-Y curves like soft cohesive soils [2]. In the present study, strength reduction factor according to the JRA in terms of factor of safety against liquefaction and dynamic shear strength ratios for liquefied soils has been used [1]. Additionally, reduction factor for adjacent non-liquefied soils with approach presented in [3] has been considered.

3. Lateral Spreading

Lateral spreading is lateral movement of liquefiable soil during earthquake that can exert a massive extra kinematic load on piles. Nevertheless, according to the JRA (Japan Road Association), the peak ground inertia force and kinematic loading due to the lateral spreading does not occur at the same time, and, consequently, they are not considered simultaneously on structures [1]. Two main approaches of kinematic lateral spreading load, as demonstrated schematically in Figure 1, are applying appropriate displacement to fixed point of P-Y springs or equivalent static load [1]. In this study, the latter one is considered based on JRA 2002.

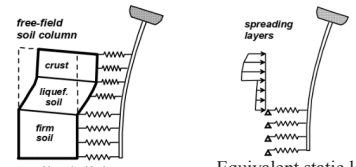

Figure 1. Lateral spreading kinematic load [1].

The lateral pressure of liquefied layers (q_L) and non-liquefied (q_{NL}) above liquefiable layers are considered as:

$$q_{NL} = C_S C_{NL} K_p \gamma_{NL} z \quad (0 \le z \le H_{NL}) \tag{1}$$

$$q_L = 0.3 C_S \sigma_v \quad (H_{NL} \le z \le H_{NL} + H_L) \tag{2}$$

where

$$C_S = \begin{cases} 1.0 & S \le 50\text{m} \\ 0.5 & 50\text{m} < S \le 100\text{m} \\ 0.0 & 100\text{m} < S \end{cases}, \quad C_{NL} = \begin{cases} 0 & I_L \le 5 \\ \dfrac{0.2\, I_L - 1}{3} & 5 < I_L \le 20 \\ 1 & 20 < I_L \end{cases}$$

$$I_L = \int_0^{20} (1 - F_L)(10 - 0.5z)\,dz \tag{3}$$

where H_L is the height of liquefiable soil and H_{NL} is the height of non-liquefiable soil above liquefiable layer. Furthermore, K_P and σ_v are passive earth pressure coefficient and total overburden stress, respectively.

4. Local Strengthening of Piles: a Real Case Study

A real case study of an operational oil platform in south of Iran (Qeshm island)[1] in 8 meters of water depth, located at the end of a jetty access bridge (Figure 2), is investigated in this study.

[1] Owner: National Iranian Oil Products Distribution Company (NIOPDC).

Figure 2. Oil terminal platform.

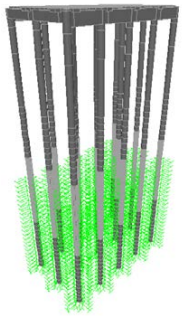

Figure 3. P-Y spring model of operational oil platform.

The structure (Figure 3) consists of 15 vertical piles (St52) with 40in diameter and 0.625in thickness, with concrete slab-beam top deck. All cyclic P-Y curves have been generated based on API [4] and p-multiplier reduction factors have been used based on Section 2. The modified SPT values of soil, obtained from in-field geotechnical investigations, are demonstrated in Figure 4. Lateral spreading load is applied from seabed to -13m in liquefiable and its above non-liquefiable layers based on Section 3.

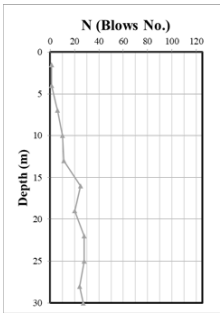

Figure 4. Variation of SPT versus depth.

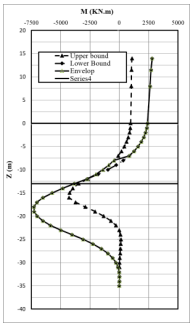

Figure 5. Upper and lower limits and envelop of bending moment.

The stress in embedded part of pile is so high that increasing neither pile diameter nor thickness can solve the problem. Additionally, increasing pile diameter absorbs more kinematic lateral spreading load and is inappropriate herein. On the other hand, available soil improvement choices in seabed were not economical due to the size of project and depth of liquefiable soil. Furthermore, filling pile with concrete in total length was not considered due to the increasing of seismic mass of the structure and cost. Accordingly, local strengthening of pile using reinforced concrete is employed in this project. Two upper and lower band of soil strength were considered based on PLOA [5], and the envelop of bending diagram, as depicted in Figure 5, was regarded to find the length to be strengthened by reinforced concrete.

Finally, the composite section is designed based on the maximum bending values of envelop as depicted in Figure 6. This figure clearly shows that the maximum axial force-bending demand is lower than the capacity of the composite sections. Furthermore, composite section will be applied in the model between 9 and 23 below seabed beyond which the steel pile capacity is sufficient. It should be noted that, while in the present study the flexural failure mechanism in the embedded part of piles was investigated, the global buckling of the long pile in the presence of the lateral spreading has been also taken into account for free span of pile columns.

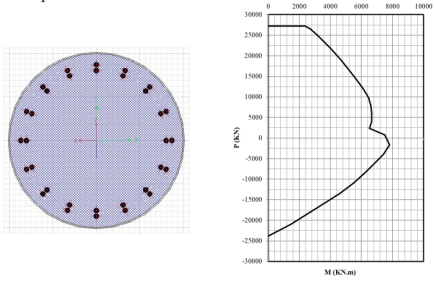

Figure 6. Interaction moment-compression diagram of concrete-filled-steel pile.

5. References

[1] Boulanger, R. W., Kutter, B. L., Brandenberg, S. J., Singh, P. and Chang, D., "Pile foundations in liquefied and laterally spreading ground during earthquakes: centrifuge experiments & analyses", Center for geotechnical modeling, Report no. Ucd/cgm-03/01, 2003.

[2] NHI Course No. 130093 and 130093A, "LRFD Seismic analysis and design of bridges reference manual", U.S. department of transportation federal highway administration, 2014.

[3] Shantz, T. "Guidelines on foundation loading and deformation due to liquefaction induced lateral spreading." California Department of Transportation, Sacramento, CA, 2013.

[4] API RP 2A-WSD, "Recommended Practice for Planning, Designing and Constructing Fixed Offshore Platforms—Working Stress Design", American Petroleum Institute, 2002.

[5] POLA, "The Port of Los Angeles Code for Seismic Design, Upgrade and Repair of Container Wharves", Pola Seismic Code, 2010.

COMPARISON OF STRUCTURAL DESIGN PROCEDURES OF RCC PAVEMENTS DUE TO HEAVY LOADED APRONS (CONTAINER TERMINALS)

Mohammad Reza Shakeri[1], Abolfazl Aliasgari[2] and Ali Vares Vazirian[3]

1) Senior Geotechnical Engineer, Sazehpardazi Iran Consulting Engineering Company, Department of Ports, Coasts and Marine Structures, Tehran, Iran, shakeri@sazehpardazi.com
Assistant Professor, Faculty of Technology and Engineering, Islamic Azad University, Central Tehran Branch, Tehran, Iran, m.shakeri@iauctb.ac.ir
2) Engineering Manager, Sazehpardazi Iran Consulting Engineering Company, Department of Ports, Coasts and Marine Structures, Tehran, Iran, aliasgari@sazehpardazi.com
3) Senior Geotechnical Engineer, Sazehpardazi Iran Consulting Engineering Company, Department of Ports, Coasts and Marine Structures, Tehran, Iran, vazirian@sazehpardazi.com

1. Introduction

Roller-compacted concrete (RCC) or cement bound granular mixtures (CBGM or CBM) is an ultra-tough, zero-slump concrete pavements. It is placed with asphalt pavers to form a nonreinforced, concrete pavement. RCC successfully and economically combines strength and durability with ease of construction especially in heavy-duty industrial pavements (e.g. ports and multimodal terminals). Ports and heavy industrial facilities are large, open areas with few obstructions that may delay the construction process, making them ideal candidates for RCC. Pavements for port and other heavy industrial facilities must be strong and durable because container handling equipment can have wheel loads of 14 to 28 tons or more per tire with traffic speeds typically less than 48 km/hr which are uncommon.

The selection of the pavement course materials and thicknesses is a major part of the pavement design process. There are already several manuals providing guidance on this aspect of container terminal pavement design such as BPA, OCDI, USACE and RCC-PAVE computer program that are the most common pavement design methods used for this application [1-7]. This paper compares the pavements designed by each manual in view of technical and construction procedures and reveals the differences in each procedure.

2. Design Basis

To gain the abovementioned aims, a heavy loaded pavement is analyzed with various procedures. An 8 wheel Rubber Tired Gantry (RTG) crane has been selected to transmit full container as block layout (6 containers with truck lane) in 1 over 5 high stacking. The travel speed of RTG without load is about 8 km/hr. The distances between axles are 2.5, 6.7 and 2.5 m and the gantry span is 23.6 m. The self-weight and capacity of RTG are approximated to 131.5 and 41 tons, respectively. It means that the maximum wheel load is about 28 tons. Number of passes of RTG is assumed 365,000 throughout design life. The contact area of a tire of handling plant is assumed to be circular with a contact pressure equal to that of the tire pressure. Container handling equipment such as RTG with pneumatic tires is normally operated at a tire pressure of approximately 1.0 MPa.

To compare the results, subgrade is sand or sand-gravel mixtures relatively free of plastic fines. The California Bearing Ratio (CBR) is considered 10% which is equivalent to subgrade reaction modulus of about 54 MN/m^3.

The concrete pavement a mixture of coarse and fine stones, cement and water, similar to common concrete but with approximately 40% as much cement and water as normal concrete. It has an average 28-days characteristic compressive cylinder strength of 12 MPa and flexural strength or modulus of rupture of about 2.5 MPa and tensile strength of about 1.5 MPa. The elastic modulus and Poisson's ration of concrete is about 30,000 MPa and 0.15, respectively. This type of concrete is equal to Cement Bound Material 4 (CBM4).

It is important to note that CBM4 comprises all inclusive elements of RCC but with a reduced strength. For example the compressive strength of RCC can be more than 32 MPa.

On the other hand in RCC, surface appearance and texture are generally not of great importance and the surface smoothness typically has a 9.5 mm maximum variance for a 3 m straight edge. Therefore unsurfaced RCC pavement can be allowed in low traffic speeds areas such as ports. Nevertheless concrete block paving is a preferred container terminal surfacing material in many regions especially Europe because it combines the benefits of the durability of concrete with the flexibility of asphalt. The driving factor was the anticipated settlements and the ability to remove and relay areas of pavers from time to time to maintain the required terminal surface level. Thickness of pavers is usually 80 mm and even roles directly in pavement structure design by Material Equivalent Factor (equals to 0.87*80=70 mm CBM4) [6].

3. Design Procedures

The existing design manuals are based upon computing stresses and/or strains at critical locations within and directly below concrete pavements, comparing those computed stresses/strains with values which the pavement construction materials are known to be able to sustain successfully, sometimes referred to as permissible stresses/strains and thereby providing pavements of sufficient structural capacity. The permissible stresses/ strains are established by using a Transfer Function, which is a relationship between the number of repetitions of a loading event and the corresponding permissible stress/strain. Transfer functions are entirely empirical relationships which have been derived by observing the way in which pavements have performed historically and are usually informed by scientific fatigue relationships. Each design procedure has particular formulations to calculate the concrete pavement thickness.

In PBA [4], the geometry configuration of all wheels should be determined for each vehicle. Based on effective depth, proximity factor and dynamic load factors, single equivalent wheel load (SEWL) is calculated and thereafter regarding load repetition proportional to damaging effect of wheel loads, CBM4 thickness is approximated. If abovementioned RTG specifications and subgrade condition are considered, this procedure results in SEWL 32.2 ton, about 1,400,000 repetitions and consequently a 330 mm CBM4.

OCDI and RCC-PAVE computer program have a similar technique to design the pavement. In this method, the fatigue characteristics of concrete pavements are calculated based on the wheel load stresses imposed on concrete and their numbers of load repetition during design working life. The relation between the above mentioned characteristics and the degree of fatigue as a failure criterion is proposed to set the thickness of RCC. Allowable numbers of wheel load have been shown in Figure 1 depending on stress ratio (ratio of critical applied flexural stress to flexural strength). The degree of fatigue of a concrete slab is calculated from $F_D = \sum \frac{n}{N}$ (n = wheel load repetition, N = Allowable numbers of wheel load).

Using the degree of fatigue as the failure criterion of a concrete slab, concrete thickness is set so that the degree of fatigue is equal to 1.0 or less. Each procedure uses a method to calculate the flexural stress due to wheel loading. A 28 ton wheel load of RTG causes a 560 mm and and 540 mm respectively for OCDI and RCC-Pave methods which are almost the same.

The USACE procedure for RCC pavement design is similar to the procedure for conventional concrete pavements. The vehicle loading is expressed as an equivalent number of repetitions of an 8.2 ton single-axle loading, and, as a further simplification, the range of equivalent repetitions of the basic loading (i.e., traffic) is designated by a numerical scale defined as the pavement design index. USACE applies only a chart to determine the pavement thickness regarding to subgrade reaction, flexural strength and pavement design index. This method consequences in a RCC pavement with a thickness not more than 250 mm.

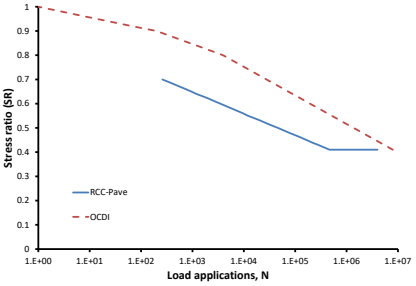

Figure 1. Fatigue relationship for RCC.

4. Conclusion

The following important conclusions can be drawn:

- Tensile and flexural strengths are the key characteristics factors of RCC respectively for BPA and OCDI design procedures.
- For a specific vehicle loading and subgrade condition together with a determined concrete pavement, The BPA and USACE lead to a near range of pavement thickness and two other methods show a notable increase about 90 percent in concrete thickness.

Although the examined codes introduced to design of heavy duty pavements, the results show noticeable deviation to each other and the design procedure can directly affect on pavement design and consequently the design economy. Therefore especially in national ports it is needed to codify a unique standard to design heavy duty pavements.

5. References

[1] ACI 327R-14, 2014, Guide to Roller-Compacted Concrete Pavements, American Concrete Institute.

[2] Department of the Army and the Air Force, 1992, Pavement Design for Roads, Street, Walks, and Open Storage Areas, Technical Manual No. 5-822-5, Air Force Manual (AFM) 88-7, Chapter 1, Washington, DC.

[3] Harrington, D; Abdo, F; Adaska, and W; Hazaree, C, 2010, Guide for Roller-Compacted Concrete Pavements, National Concrete Pavement Technology Center, Portland Cement Association.

[4] Knapton, J., 2008, Heavy Duty Pavements, The Structural Design of Heavy Duty Pavements for Ports and Other Industries, Edition 4, Interpave.

[5] OCDI, 2009, Technical Standards for Port and Harbour Facilities in Japan, The Overseas Coastal Area Development Institute of Japan.

[6]. PIANC, 2015, Design and Maintenance of Container Terminal Pavements, MarCom Report No. 165.

[7] Portland Cement Association, 2002, RCC-PAVE Computer Program, Item Code MC043, Skokie, IL: Portland Cement Association.

DESIGN OF BREAKWATER FOR A NEW MULTI-CARGO PORT IN BLACK SEA

Merih Ozcan[1] and Mehmet Sag [2]

1) ARTI Proje, Dubai, UAE, merih@artiproje.com
2) Ministry of Transport, Maritime Affairs and Communications, Ankara, Turkey

1. Introduction

Filyos Port is planned as Turkey's third largest port for multi-cargo handling including containers, dry bulk and break bulk. It is located at central Black Sea coastline of the country, presently a greenfield area with long sandy beach. When completed, it will have total container throughput capacity of 1.5 million TEU's and 20 million ton bulk cargo.

Figure 1. Project location.

The Port will have a 2,700 meters long main breakwater placed mostly at 10 meters water depth and 1,500 meters long secondary breakwater protecting the berths from harsh Black Sea wave climate. Various armor layer design options with tetrapod, accropode and xbloc units were investigated in the project and the final design was developed with xblocs, which is also a first application with these units in the country.

Construction of the port is presently ongoing and in the first stage breakwater construction is progressing ahead of other activities to provide a sheltered work area for the berth constructions to start.

In this paper, basic design criteria employed and main issues addressed in developing the design of the breakwaters will be discussed.

2. Geotechnical Conditions

The seabed in the project area is mostly sand in the region close to the shore however soft clay layers at sea bottom starts to appear as one goes towards offshore. At the location of the main breakwater which is approximately at 10 meters water depth, thickness of the soft silty-clay layer reaches to 5 meters in average. The cohesion of the soft clay layers are determined to be less than 20 kPa.

Geotechnical investigations showed that thick and hard to medium hard sand layers exist under the soft clay layer. Slope stability, bearing capacity and settlement analysis carried out for the breakwater showed that a safe and stable breakwater cannot be built without improving the parameters of the soft clay layer underneath the breakwater. After assessing various alternatives of improvement, replacement method was selected as the most economical approach. It was decided to dredge all soft material under the breakwater and replace with quarried rocks to create a stable foundation for the structure.

3. Design Wave Height

The design wave parameters for the breakwater were based on the offshore wave parameters as described in the Turkish Wave Atlas for the Black Sea [1]. Numerical modelling studies were conducted for transformation of waves as propagate from deep water to the breakwater location. The main breakwater was designed for Hs= 7.0 m. at deepest sections.

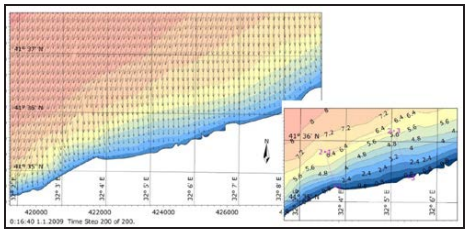

Figure 2. Sample output from wave modelling studies.

4. Comparison of Concrete Armour Units

Many breakwaters with concrete armour units have been constructed in the Black Sea coastline of Turkey in the past. In those projects initially cubes and tetrapods have been used. In 1990's various projects with antifer cubes were realized however tetrapods stayed as the most favored units both in public and private sector projects.

Filyos Port's breakwater was initially planned and tendered with tetrapod units however EPC Contractor decided to assess the overall construction economy (cost + time) by comparing design alternatives with tetrapods, accropodes and xblocs. The final decision was made in favor of xblocs and breakwater design was prepared by using 10 m^3, 8 m^3 and 4 m^3 units at different depths.

In the design of the breakwater protection with xblocs, the guidelines issued by the product licensor Delta Marine Consultants were used [2] together with various study results published on the subject [3-5].

Figure 3. Photo of the xblocs on the filter layer from the project site

5. Hydraulic Design and Tests

Stability tests for the designed breakwater sections were done in the laboratory facilities of Ministry of Transportation. A series of wave conditions were used in the tests along with design water levels including sea level rise due to climate change. The designed breakwater sections were verified by the tests against allowable damage levels and provided input the final design of the structure.

6. Seismic Design

Being located in an earthquake prone area with relatively weak soil conditions, the seismic design of the breakwater was a challenging issue. The local codes required the breakwater to be designed against the Contingency Level Earthquake with a return period of 475 years and only controlled damage is allowed. This design earthquake corresponded to an equivalent seismic coefficient, kh of 0.16.

Extensive pseudo-static and full dynamic geotechnical analysis were conducted to determine the behavior of the breakwater under seismic events. Dynamic analysis included Finite Element Modeling of the breakwater with time domain analysis.

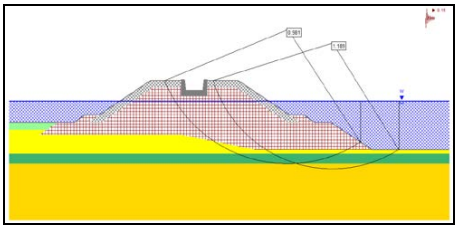

Figure 4. Sample output from pseudo-static slope stability analysis.

7. Conclusions

Design studies for the breakwaters of Filyos Port involved extensive comparative analysis of different concrete armour units with regard to material, labour, formwork, handling and placement costs. In this very first application in Turkey of single layer armour design with semi-random placement, construction speed and less dependency on heavy-lift equipment were the main factors effective on the final decision.

Wave and geotechnical modelling studies conducted during the study set examples for the similar project in the area to cope with the wave and seismic design conditions in weak soil conditions. Following the finalization of design works of Filyos Port, two another major port projects with xbloc units were initiated in the region.

8. References

[1] NATO TU WAVES, Turkish Wave Atlas

[2] Delta Marine Consultants, "Guidelines for Xbloc Concept Designs", 2014

[3] Bakker, P., Klabbers, M., Muttray, M., van den Berge, A., "Hydraulic Performance of Xbloc Armour Units", 2005

[4] Pearson, J., van der Meer, J.W., Bruce, T. and Franco, L., "Overtopping performance of different armour units for rubble mound breakwaters"

[5] Muttray, M., Reedijk, B., de Rover, R., van Zwicht, B., "Investigations on quarry stone to berm stability", *Coastal Engineering*.2015

THE EFFECT OF SEA SAND DEREDGER ON THE RESISTANCE OF CONCRETE PIECES REINFORCED WITH METAL FIBERS

Saeed Moradi[1], Seyed Taha Tabatabai aghda[2] and Shohre Shahnoori[3]

1) Department of Civil Engineering, University of Hormozgan, Bandar Abbas, Iran, saeed.moradi69@yahoo.com
2) Road , Housing & Urban Development, Bandar Abbas, Iran, taha.taba@gmail.com
3) Department of Civil Engineering, University of Hormozgan, Bandar Abbas, Iran, s.shahnoori@gmail.com

1. Introduction and Background

The unique properties of concrete, especially reinforced concrete, and economic costs make it the most suitable material for most infrastructures of the world.

The aggregate is known as cost reduction factor of concrete production which is now a challenging topic for sustainable development. The most urgent issue in this regard is the environmental impacts of aggregate production. Many areas in the world including Persian Gulf are suffering from excessive deterioration and even inaccessibility to appropriate rock and minerals. The unconventional use of aggregate mines in the country and the limited source of these mines and their accessibility cost made us to consider a solution for this issue concerning the demolition of dredging materials on the coast and the shortage of materials in far distances of south Iran and margins of Persian Gulf. In this paper, it is tried to use metal fibers for reinforcing this concrete with various percentages of 4%- 6% and 8% in addition to using sea dredging sand (prepared from Shahid Rajaee Port Complex of Bandar Abbas) as 25% substitute for fine aggregates in concrete. In so far as mostly in making reinforced concrete armatures, fabric is used instead of bar, therefore, the impact of sea sand on metal fibers for reinforcing this type of concrete will be studied in this application.

In most parts of the world, there is a legal restriction on utilization of pits and mines. For example, in parts of the southwest of England, the supply of aggregates is very low, so that in order to meet the demand, it is inevitable to import it from the Midlands, Ireland and Manche Channel. In a study in Spain, three different concrete treatments have been used for construction of the pavement and the impact of dredger sand as a sandstone in production of concrete has been analyzed. In Barcelona, another study has been conducted on making a cement mortar from three types of sand. The purpose of this research was to determine the effect of adding dredge sand on bonding and consistency of concrete and the effect of modified fine grains on compressive strength in the different mixing scenarios of concrete. In their study, Chapman et al concluded that the dredged material of the sea could be used in the manufacturing of concrete [1, 2, 3, 4].

using the dredging materials, as a replacement for the whole or a percentage of the aggregates is a perfect solution. Regarding various aspects related to this new source of materials several studies have contributed. Examples of which are being followed as: Limeira et al. (2010); Limeira et al. (2012); Moradi et al. (2018); Etxeberria et al. (2016); Liu et al. (2016) [5, 6, 7].

2. Experiments and the Tests Setup

The experimental works are categorized in three main sets. First is the mix design and programming, in addition to the required tests on the ingredients and the basic materials. The second category is providing the specimens, (mixing, casting, curing etc.). The final is the mechanical and permeability tests on the specimens.

Figure 1. Dry and wet processes of test and curing specimens

3. Outcomes of the Laboratory Tests

In this section, the laboratory program, the specifications of concrete materials used in concrete and also the results of compressive strength test on the concrete tests made from sand of sea and reinforced with metal fabrics will be presented. The Persian Gulf dredged sand is consisted of various materials, a percentage of metals and different kinds of marine sediments that have been passed from sieve number 4 as replacement for fine-grained concrete. These materials with a density of 2.7 have high water absorption rate. In Figure 1, the optimum moisture content of dredge sand of sea that in this moisture content reaches its maximum density is shown.

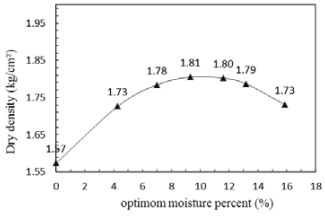

Figure 2. Optimum moisture curve of sea dredged sand

The mixture patterns used in this type of concrete are presented in Table 1.

Table 1: Specifications of the number specimens, materials used and the percentage of substitutes for sea dredged sand

cement type	control concrete	25 %DMS	25%DMS & 4 %Fiber	25%DMS & 6 %Fiber	25%DMS & 8 %Fiber
2	C0	C25	C25 – 0.4	C25 – 0.6	C25 – 0.8

In this test, end hook steel fiber of diameter 0.8 and length of 50 mm of 4%-6% and 8% as replacement for cement has been used. The used fiber is shown in Figure 3.

Figure 3. End hook steel fiber

The cube test pieces of 15*15*15 cm have been tested in five mixture pattern for compressive strength. The fresh concrete temperature has been measured in range of 28 to 33 degrees Celsius and controlled 12 cm-concrete slump which increased by 15 cm by adding sea sand to concrete. It means that the concrete will be more consistent and easily condensed with increase of sea sand which is rounded and fine-grained and filling the space between coarse grains It is worth noting that by adding metal fibers, the concrete's consistency is reduced and its slump decreases by about 7 cm. The results obtained from mean of data related to three cubic samples are the same. In this project, the compressive strength of the test specimens has been measured according to standard C39 ASTM [8] in 28 days whose results are depicted in Figure 4.

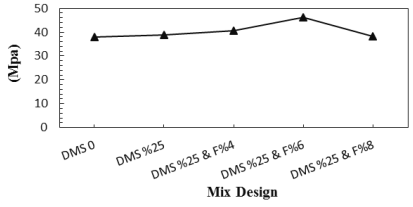

Figure 4. Compressive strength

4. Discussion and Conclusions

As shown in the diagram, adding 25% dredging sand to concrete leads to its increased resistance compared to control concrete and by adding metal fibers up to 6 weight percent of cement, the compressive strength reaches its maximum and adding more fibers leads to decreased strength of concrete due to lack of compression and cohesion of materials and lack of uniform dispersion of fibers in concrete. One of the challenges of adding these fibers is their lack of flexibility and length and lack of uniform dispersion in concrete that leads to shrinkage of fiber and materials in a limited area and reduces the slump and concrete performance. Therefore, in order to reinforce concrete with this type of fiber, a special method and instrument should be used for mixing that does not lead to their entanglement.

5. References

[1]. Alexander, M., Sidney, M.; "Aggregates in Concrete"; Talyor & Francis, London, 2010.

[2]. Limeira, J., Agullo, L., Etxeberria, M.; "Dredged marine sand in concrete: An experimental section of a harbor pavement"; Construction and Building Materials, 2010, Vol. 24, No. 6, pp. 863-870.

[3]. Limeira, J., Agullo, L., Etxeberria, M.;"Dredged marine sand as a new source for construction materials"; Materiales de Construccion, 2012, Vol. 62, No. 305, pp. 7-24

[4]. Chapman, G.P., Roeder, A.R.; "The Effect of Sea Shells in Concrete Aggregates"; London, Vol. 4, No. 2, pp. 71-79, 2008.

[5] Moradi, S., Shahnoori, Sh.; " The use of Dredged Marine Sand in Roller Compacted Concrete Pavements; an experimental study on the Persian Gulf Dredged Marine Sediments"; The Rilem week 2018 & The 4th International Conference on Service Life Design for Infrastructures (SLD4) and Concrete Modelling (ConMOD), 2018.

[6] Etxeberria, M., Femandez, J,M., Limeira, J.; "Secondary aggregates and seawater employment for sustainable concrete dyke blocks production: Case study"; Construction and Building Materials, 2016, Vol. 113, pp. 586-595.

[7] Liu, W., Cui, H., Dong, Z., Xing, F., Zhang, H., Y.Lo, T.; "Carbonation of concrete made with dredged marine sand and its effect on chloride binding"; Construction and Building Materials, 2016, Vol. 120, pp. 1-9.

[8]. ASTM (American society for Testing and Materials), "Standard Test Method for Compressive Strength of Cylindrical Concrete Specimens", ASTM C39/C39M-15a, 2015.

PRE-FEASIBILITY STUDY OF USING SANDBYPASSING SYSTEM AND INITIAL DESIGN CRITERIA, A CASE STUDY IN CASPIAN SEA

Amin Reza Zarifsanayei[1] and Shahin Maghsoudi Zand[2]

1) Senior coastal engineer at Karan Sazeh Pasargad consulting engineers Co,Tehran, Iran, a.r.zarif@ut.ac.ir
2) CEO at Karan Sazeh Pasargad consulting engineers Co,Tehran, Iran, shahinzand@ksp-eng.com

1. Introduction

Generally, coastal structures could be impediments to natural flow of sand. Sedimentation and erosion close to small ports are acute problems and there is no general consensus on appropriate measures to mitigate their adverse effects. Some mitigating approaches include beach nourishment and sediment bypassing. Sand transfer systems are a means of transporting sand around an impediment in an attempt to reinstate the flows of sand that would occur naturally [1]. Sand bypassing systems operate on simple principles, and consist of dredging, transporting and depositing sand. Mechanical bypassing is an approach to transport sediment from the updrift to the downdrift side of ports or inlets. Bypassing can be achieved through dredging or excavator and truck delivery. Many sand bypassing systems have been being designed and operated in the last decades. Boswood and Murray [2] list 53 different bypassing stations from around the world and document their environmental and system parameters. A pump or eductor is used for dredging operations with bypassing systems which could be a water-based mobile system: where the dredge pump is operated from a floating, mobile platform, or a land-based mobile system: where the dredge pump is generally operated by a crane, or a fixed system: where the dredge remains in a single location ([1], [2], [3]).

Since construction of Chamkhaleh port (the former port located in Guilan, The Caspian Sea), heavy sedimentation behind the west breakwater and rapid shoreline advance have been observed. Also the port basin was located at river mouth which itself was at the influence of two rivers discharge. Inaccurate layout of the breakwaters has caused a calm region for siltation and accumulation of fine sediments in the port basin and eventually led to disruption in the port operations in recent years (see Figure 1). The required offshore data providing important information for the detailed 2D morphological assessment and 1D littoral drift study of Chamkhaleh coastal area has been extracted from two wave hindcasting projects of ISWM I (covered 1992 to 2003 at 6-hour intervals), and monitoring and modeling study of northern coasts of Iran (covered 1983 to 2013 at 1-hour intervals). Comparison of hydrographic surveys (years: 1998, 2010, 2012, 2014, 2017), satellite images and aerial photos has shown the average annual net long shore sediment transport (LST) rate is about 100,000 m^3 from west to east ([4]). This paper presents some results of Chamkhaleh's port development plan proposed by Karan Sazeh Pasargad consulting engineers Co.

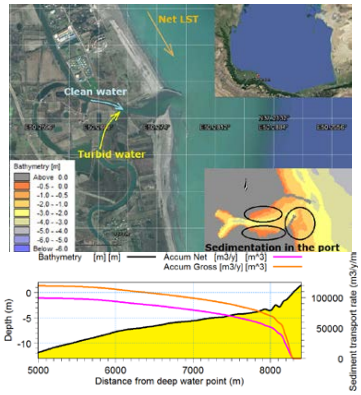

Figure 1. Top: study area, Bottom: upstream coastal profile

2. Outline of the Project

The location of former port (at river mouth) has not been recognized appropriate for further development. Hence, different port layouts along the coast have been studied in detail [4]. With regard to special conditions in The Caspian Sea and uncertainties in prediction of long-term fluctuation of water level, any new project in this region should be adaptable enough to any probable changes. Finally, by considering different scenarios, it became clear that construction of a-single-main-breakwater port with sand bypassing system would be a viable solution for future development plan of Chamkhaleh coastal area. At the development plan, effect of breakwaters layout on the port basin tranquility and sedimentation pattern has been studied numerically using DHI model. Change in orientation of the main breakwater near the port mouth along with the effect of reflected waves from the secondary breakwater could mitigate adverse influence of eddy formation and sedimentation close to the port entrance. Additionally, at the development plan a calm area close to the port has been considered in order to trap the littoral drift coming from upcoast. Figure 2 illustrates different

parts of the project. Also the breakwaters construction would be implemented by means of geotubes (filled up with pumping sands from the bed of upcoast and river mouth) protected by a layer of geotextile, armor and tetrapod.

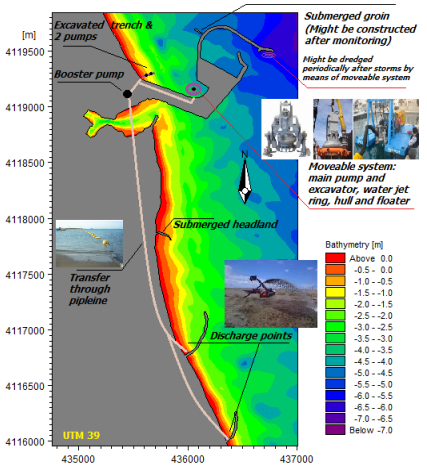

Figure 2. The proposed port and sand by-pass system

3. Finding Design Capacities, Technical Specifications and Costs of the System

As previously mentioned offshore waves data (from 1983 to 2013) have been used to investigate the variation of longshore sediment transport rate and its distribution along coastal profiles. The results after calibration, have been stored in time series format indicating critical situations of LST during storms, seasonal variations and average annual rate of LST. Afterwards sediment transport along the coastal profile for each storm has been studied in detail using LITPACK model. Besides, the time spans between strong storms have been considered as criteria for finding the required time for operating the system in most critical situation. The system was designed to bypass a target rate of 100,000 – 210,000 m^3 of sand per year, but it has sufficient capacity to bypass up to 340,000 m^3 per year. During extreme events, such as a storm, the system was also designed to be able to bypass a capacity of 20,000 m^3 (sand) in seven days. The bypassing system would only require working in a few months of year, and even in some months the system could be completely turned off. It should be also noted that in practice, normally the slurry (mixture of sand and water) is pumped on a 1/3 ration, so capacity of pumps in the aggregate should be larger than three times of the rates mentioned above.

The main equipment of the system encompasses three submersible pumps (capacity: two pumps 44 kW-140 m^3/hour and one pump 60 kW-350 m^3/ hour), a booster pump and control panel, an excavator along with water jet ring and its pump, pipes and valves, a floater and two diesel generators. The initial costs of the system amounts to 1.2 million Euros.

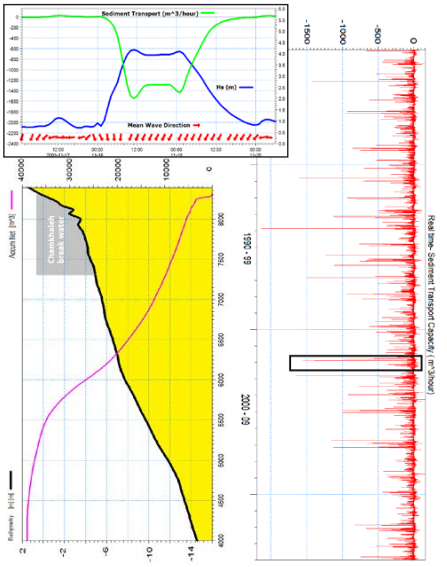

Figure 3. LST rate and behavior of LST along a coastal profile during one of severe storms (negative values are corresponding to direction of LST from left to right)

4. Conclusion

The results of this pre-feasibility study show that the proposed sand bypassing system adaptable to the port layout, the sand trap and Caspian sea level fluctuation is a viable alternative for Chamkhaleh coastal development plan. The study, provided vigorous data needed for designing specifications of the systems and estimating its initial costs, however, some robust studies should be conducted in order to see all aspects of the project.

5. References

[1] Dean, R. G., (2002). "Beach Nourishment, Theory and Practice"

[2] Boswood, P.K., Murray, R.J., (2001). "World-wide sand bypassing systems: data report". Queensland, Australia. (60 pp.).

[3] Dyson, A., Lawson, S., Victory, S., Boswood, P., Mahon, B., Trucchi, L., Cummings, P., (2002). "Tweed River entrance sand bypassing project post commissioning coastal behavior". Proceedings of the 28th International Conference on Coastal Engineering. American Society of Civil Engineers, Cardiff, Wales, UK.

[4] Zarifsanayei.A.R, Maghsoudi Zand. S, (2012-2017). "Hydrodynamic and Sedimentation Study Report of Chamkhaleh Port", Karan Sazeh Pasargad Co, Iran

GEOTECHNICAL VARIATION IN MARITIME WORKS AND NECESSITY OF PERFORMING GEOTECHNICAL INVESTIGATION FOR EACH SITE SEPARATELY

Ali Varesvazirian[1] and Majid Beigi[2]

1) Sazehpardazi Consulting Eng., Tehran, Iran, vazirian@sazehpardazi.com
2) Sazehpardazi Consulting Eng., Tehran, Iran, m.beigi@sazehpardazi.com

1. Introduction

Gathering sufficient geotechnical information from a project area is one of the most important parts of the design phase of marine structures. Since significant variation in both layering and geotechnical parameters alongside of shore area is expected, lack of comprehensive information about subsoil usually leads to unforeseen problems during construction phase and sometimes causes great change in the project layout and/or structural system. Moreover, marine structures construction and maintenance is more complicated than the other ones and usually required more time and money. Therefore, appropriate planning for geotechnical investigation proportional to the project cost, is of crucial importance to save money as well as the safety.

In this paper, in order to show how much the subsurface can be variable in a shoreline area and to show the importance of adequate site investigation, the results of some geotechnical studies performed for a part of Persian Gulf coastal area in Hormozgan province, Iran, are assessed here. As a result, necessity of new geotechnical investigation for a new project near the ones that have field investigation is obvious. In the following, some recommendations for geotechnical investigation derived from international maritime codes are presented.

2. Problem Description

In order to construct marine structures including protection dikes and breakwaters and also some berths, four sites which are close to each other were explored separately. Figure 1 shows these sites location, case 1 to 4. They are located alongside the shoreline with 3.5km long and extended to the sea up to 1km.

The first case includes 10 boreholes with lengths of 20-30 meters [1], and the second one comprises 7 boreholes with lengths of 10-30 meters [2]. The third and fourth cases include 6 boreholes with a length of 20 meters [3] and 5 boreholes with lengths of 25 meters respectively [4]. A variety of in-situ and laboratory tests have been carried out during the investigation (e.g. S.P.T, Relative Humidity, Atterberg Limits, Soil Specific Gravity, Direct Shear, Triaxial, Consolidation and Uniaxial).

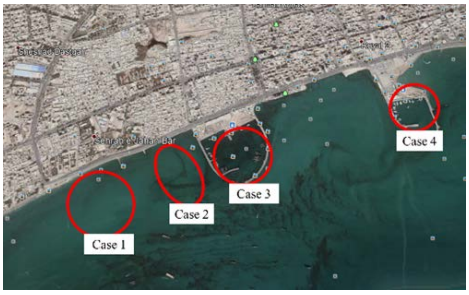

Figure 1. Sites Location, Bandar Abbas.

3. Subsurface Variability

Based on 4 series geotechnical investigation carried out at the project location, soil layering profile alongside the shoreline is illustrated in Figure 2. As shown in this figure, in the case 1, the surface layer is composed of medium dense silty sand (SM). Thereafter, there is a fine-grained layer of CL and ML, with increasing consistency with depth. The last layer is a sandy soil (SM) with moderate to high density. In the case 2, subsoil consists of fine-grained (clay and silt) layers that their consistency increases with depth. In addition, medium to dense Silty and clayey Sand (SM / SC) is also observed in the middle layers. In the case 3, a soft clay surface layer underlain by a dense silty Sand (SM) layer which is observed up to the end of the boreholes. A smooth clay layer (CL) layer is also observed in the case 4. Below this layer, thin lens of Coral followed by a SM soil with moderate density is observed.

In addition to the variability alongside the shoreline, the cross-section profiles also revealed that as the distance from the coast increases, the thickness and density of layers changes. For example, the cross-section profile of the case 1 is shown in Figure 3. The result shows reduction in SPT numbers and increase in the thickness of loose layers with increasing the distance to the coast.

Results show that altough geotechnical trend is predictable for the site near the mentioned cases (for example the area between case 3 and 4), some details may not be predicted exactly without performing special

geotechnical investigation for that site. For example, the thickness of shallow soft layer which affect the breakwater settlement and the amount of material penetration varies significantly from case to case. Moreover, soil relative density in second layer changes rapidly and can affect, for one, on the penetrating length of deep foundation which are common for berths in soft soils. Both of these cases may have great influence, at least on the project cost because breakwater and the berths are the main structures in a marine projects.

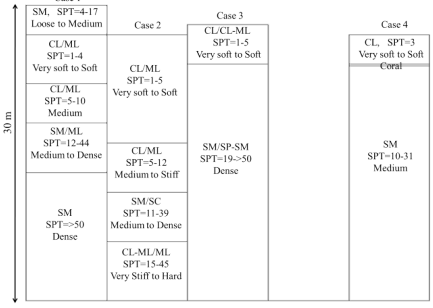

Figure 2. Soil profile variation in 4 close project.

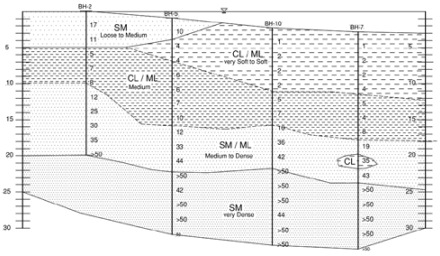

Figure 3. Case 1 cross section perpendicular to the shoreline

4. Some Recommendations for Field Investigation

Exploratory borings and in-situ investigation are the most common methods for recognizing geotechnical conditions of a project site. Worldwide design marine codes, have provided a number of suggestions on the location and number of explorations, some of which are summarized in Table 1. Also, taking advantage of studies in adjacent projects leads to an initial estimation of the existing conditions and hence a more appropriate selection of the location and depth of the exploratory boreholes.

Some important parameters that can affect the site investigation are:

- Design phase (Preliminary / Detail);
- Soil stratification (Simple / Complicated);
- Project Scale;
- Type of Marine Structures;

Table 1. Borehole layout & spacing [5-6]

Code	Design Phase	Soil Condition	Type of Required Structures	BH SPACING (m)		
				Along the Face Line of Structures	PERP. to Face Line of Structure	Max dist. From the Face Line of Structure
OCDI 2002	PRELIMINERY	HOR. AND VER. UNIFORM STRAT.	Large scale area (MARINE ST.)	300 ~ 500	50	50 ~ 100
			Small scale area (MARINE ST.)	50 ~ 100	50	50 ~ 100
		Complicated stratification	(MARINE ST.)	50	20 ~ 30	50 ~ 100
	DETAILED	HOR. AND VER. Uniform start		50 ~ 100	20 ~ 30	50 ~ 100
		Compification stratification		10 ~ 30	10 ~ 20	50 ~ 100
EAU, 1990	NO SPEC.	NO SPEC.	Waterfront Structures	50	Contingent on Results of Principal BH, 1.5H at Shoreside & 0.75H at seaside; H:Total Height of str. From Top Level To Dredge Level	

5. Conclusion

Based on the results of exploratory boreholes presented in this study, it is observed that the thickness and density of different layers of soil vary at different points in the soil layering profile and cross sections. Therefore, depending on the importance of the project, geotechnical studies and full understanding of the in-situ geotechnical conditions are of crucial importance.

Recently, because of high price of maritime geotechnical investigation, clients' trend is to omit these investigation and used available data from the investigation carried out near the project area. Although it can be useful for preliminary design, it cannot predict all of the geotechnical challenges of a maritime project. It should be noted that projects costs also rise as well as site investigation price rise. Therefore geotechnical investigation is still a little portion of a project cost either marine project or other ones.

6. References

[1] Sahel Consulting Engineers "Geotechnical investigation report for Sayyadi port (case1)", 2000.

[2] Omran Rahvar Consulting Engineers, "Geotechnical investigation report for MARZBANI port", 2014.

[3] Sahel Consulting Engineers, "Geotechnical investigation report for SAYYADI port (case2)", 2000.

[4] Iran Khak Consulting Engineers, "Geotechnical investigation report for Haghani port (case2)", 2008.

[5] Technical Standards for Port and Harbour Facilities in Japan, OCDI 2002.

[6] Recommendations of the Committee for Waterfront Structures Harbours and Waterways, EAU 1990.

DEVELOPING FRAGILITY CURVES AS AN EFFICIENT METHOD FOR ASSESSING COMMON RETROFIT METHODS OF PILE-SUPPORTED WHARVES

Mohsen Soltani[1] and Rouhollah Amirabadi[2]

1) Department of Civil Engineering, University of Qom, Qom, Iran, M.Soltani1@stu.qom.ac.ir
2) Department of Civil Engineering, University of Qom, Qom, Iran, r.amirabadi@qom.ac.ir

1. Introduction

The aim of this study is proposing fragility analysis as an efficient method to evaluate common retrofit methods (FRP and batter pile) for pile-supported wharves damaged by aging effect in harsh environment of sea. In this study, fragility curves are developed for the concrete pile-supported wharf located in Persian Gulf by Capacity Spectrum Method (CSM) [1]. To compare retrofit methods, the wharf is modeled in ABAQUS 6.12. Then, results are shown in four different conditions i.e. before aging effect (initial condition), after aging effect (damaged condition), and retrofitted conditions (FRP without batter pile and FRP with batter pile). The damaged condition is considered for the splash zone having the highest corrosion rate among the other zones. In this zone, the behavior of damaged concrete is modeled according to the physical modeling carried out for concrete material in Persian Gulf environment [2], and for rebar, the corrosion rate proposed by OCDI is considered [5]. To retrofit the damaged model, at first, FRP layer is wrapped around damaged areas. Then, the batter pile with the degree of 43° is attached by rubber isolator (Figure 1).

CSM is a Pushover (SPO) based method which measures performance points of structures under scaled selected spectrum. Here, this method is performed by choosing 8 records (Table 2), and the probability of the responses exceeding from the damage states, defined by PIANC [6], is obtained. The cross section of the wharf and property of soil layers are respectively displayed in Figure 1 and Table 1 [3]. The soil layer is modeled by Mohr-Coulomb theory.

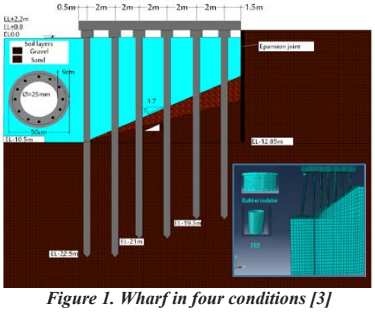

Figure 1. Wharf in four conditions [3]

Table 1. Soil layers

Soil layer	Density (kg/m^3)	E (kg/m^2)	Φ°
Gravel	2000	17×107	30
Sand	1835.65	173×105	40

Table 2. Ground motion used for seismic analysis [4]

Event	year	M	R (Km)	PGA (g)
Chi-chi-1118	1999	7.6	26.8	0.147
Chi-chi-1132	1999	7.6	18.7	0.165
Chi-chi-1143	1999	7.6	25.9	0.639
Imperial-0200	1979	5.2	17.9	0.179
Kobe-1041	1995	6.9	26.4	0.345
Hills-0728	1987	6.6	27.1	0.167
Cape Mendocino1	1992	7.0	16.5	0.116
Manjil	1990	7.3	39.0	0.350

2. Developing Fragility Curves

In order to develop fragility curves for all the models in the predefined damage states, SPO curves, base sheer (V_i) versus deck displacement Δ_{deck} (Figure 2), are converted to capacity curves, spectral acceleration (S_{ai}) and spectral displacement (S_{di}) (1-2). Then, the performance points (x) are driven by intersection of capacity curves under scaled demand spectra i.e. the spectra of chosen recordings. The scaling should cover the whole range of structural responses from elastic to global instability. Furthermore, fragility curves are developed by lognormal distribution with the probability density function (PDF) in the predefined damage states (x_i) i.e. serviceability (I), repairable (II), and near collapse (III) (Table 3) (3-6) [1].

$$S_{ai} = \frac{V_i}{W \times \alpha_i} \quad , \quad S_{di} = \frac{\Delta_{deck}}{PF_i \times \emptyset_{deck}} \qquad (1),(2)$$

where α and PF_i are respectively the modal mass coefficient and participation factors for the first natural mode of the structure and $\emptyset_{roof}$ the roof level amplitude of the first mode.

$$f_x(X) = \frac{1}{\sqrt{2\pi}\zeta x} \exp\left[\frac{-1}{2}\left(\frac{\ln(x-\lambda)}{\zeta}\right)^2\right] \quad 0 \le x < \infty \qquad (3)$$

Where ζ and λ are the parameters of lognormal distribution of random displacement variable X. Tthese two parameters can be calculated by mean value (μ) and

[1] Recorded in Fortuna station

standard deviation (σ) of sample population (x) in each scaled level: (4-5)

$$\lambda = \ln\mu - \frac{1}{2}\xi^2 \ , \ \zeta^2 = \ln[1+\delta^2] \qquad (4, 5)$$

Where $\delta = \frac{\sigma}{\mu}$

Fragility curves for damage states of s_i is the conditional probability of wharf responses exceeding damage states of s_i at a specific PGA level (6) [3].

$$P[S > s|PGA] = P[X > x_i|PGA] = 1 - \Phi[\frac{ln\, x_i - \lambda}{\zeta}] \qquad (6)$$

Where ϕ is normal cumulative distribution function, x_i is the upper bound for s_i (i=I, II, III), and λ *and* ζ are the parameters mentioned above and dependent on PGA level (Figure 3-5).

3. Results

In this study, fragility analysis is suggested to assess the efficacy of two common retrofit approaches, and fragility curves are developed to show how much these methods improve the performance of structure in each damage states. It is shown that using the batter pile could almost alleviate the conditional probability of wharf responses exceeding serviceability state. For the other damage states, however, there are no discernible changes. Therefore, in this wharf, it might not be economical to apply batter pile.

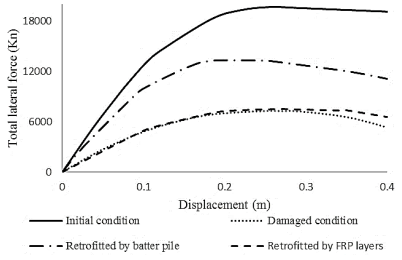

Figure 2. SPO analysis for each condition

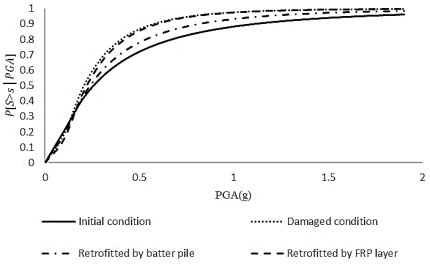

Figure 3. Fragility curves for serviceability state

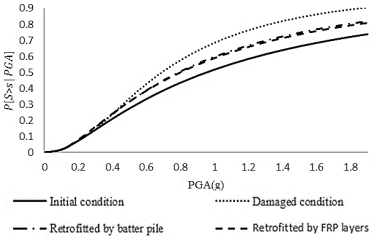

Figure 4. Fragility curves for repairable state

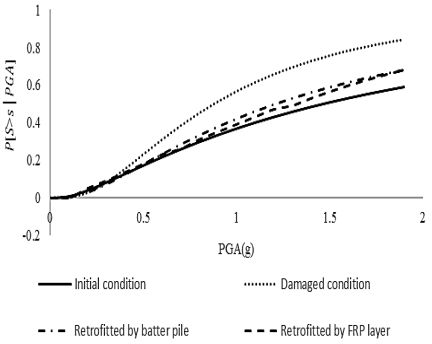

Figure 5. Fragility curves for near collapse state

Table 3. Ground motion used for seismic analysis

Damage states / Types	I	II	III
Initial condition	0.048	0.150	0.250
Damaged condition	0.021	0.120	0.200
Retrofitted by FRP layer	0.030	0.125	0.220
Retrofitted by batter pile	0.040	0.133	0.217

4. References

[1] ATC-40 Seismic Evaluation and Retrofit of Concrete Buildings,Volume 1 by APPLIED TECHNOLOGY COUNCIL 555 Twin Dolphin Drive, Suite 550 Redwood City, California 94065.

[2] A., Gharachorlu, Ramezanianpour," Durability of concrete cylinder specimens strengthened with FRP laminate under penetration of chloride ions'', International Journal of Civil Engineerng, Vol. 8, No. 4, 2010.

[3] Jiunn-Shyang Chiou, Chiou, Chi-Han, Chiang, Yang, Ho-Hsiung, Hsu, Shang-Yi, ''developing fragility curves for a pile-supported wharf'', Soil Dynamics and Earthquake Engineering, 2011.

[4] http://ngawest2.berkeley.edu/users/sign_in

[5] OCDI Tehcnical Standards and Commentaries for Port and Harbour Facilities in Japan, 2000.

[6] PIANC, Seismic Design Guidelines for Port Structures, 2001.

DUCTILITY ENHANCEMENT OF CEMENT BASED SECTIONS REINFORCED WITH FRP BARS

Masoud A.Rahimi[1] and Farshid J.Alaee[2]

1) Civil Engineering Department, Shahrood University of Technology, Shahrood, Iran, Masoud.Arabrahimi@gmail.com
2) Civil Engineering Department, Shahrood University of Technology, Shahrood, Iran, fjalaee@shahroodut.ac.ir

1. Introduction

The major cause of deterioration on steel-reinforced concrete structures exposed to marine environments, is corrosion of the reinforcing steel. This deterioration is most evident on substructure components (e.g., foundations, footers, pilings, etc.); however, reinforcing steel corrosion can also be present on superstructure components (e.g., bridge decks, beams, pile caps, etc.). Fiber-reinforced polymer (FRP) materials have emerged as an alternative for producing reinforcing bars for concrete structures. Fiber-reinforced polymer reinforcing bars offer advantages over steel reinforcement because they are noncorrosive [1]. The primary motivation of this paper is to investigate the ductility of concrete beams reinforced with brittle FRP composite.

2. Ductility

As concrete and FRP rebars are both brittle materials, ductility becomes a great concern [1]. Unless ductility requirements are satisfied, FRP materials cannot be used reliably in structural engineering applications. The term ductility describes the ability of a member to undergo large deformation without rupture before failure occurs. The ductility index is often defined as the ratio between the ultimate deflections (or curvature) over the deflection at yielding [2].

In some cases, the traditional definition of ductility cannot be directly applied to concrete structures reinforced with FRP reinforcement, it is necessary to develop a new approach as well as a set of ductility indices for evaluating the ductility performance of FRP reinforced members. Accordingly, two main approaches have been widely used. One of them is deformation-based approach. This approach was first introduced by Jaeger et al. [3]. According to this approach, the ductility index is equal to:

$$J-index: \frac{M_u \phi_u}{M_{0.001} \phi_{0.001}} \quad (1)$$

where M and φ are the beam moment and curvature and the subscripts u refer to the ultimate state, and 0.001 to the service state that corresponds to a concrete maximum compressive strain of 0.001[3]. This factor must be greater than 4 for rectangular sections and greater than 6 for T-sections.

3. Numerical Model

The load-deflection behavior of reinforced concrete beams is calculated by a program in FORTRAN. The beams are discretized into multi-layered short elements. The moment-curvature diagram of each element is calculated by applying the assumptions that plane sections remain plane and that the strain in the reinforcement is the same as that in the surrounding concrete. Any stress–strain diagram can be used for concrete and steel.

3.1. Validation

This methodology was validated with an experimental data from Meda et al. for conventional RC beam [4]. All samples were 4m long with a span of 3.6m.The height, depth and the width of the section were 300mm, 260mm and 200mm, respectively. For tension reinforcement 2φ16 and 4φ16 and for the compression ones 2φ10 were used. In the studied experimental study the yield stress of reinforcing steel and compressive strength of concrete were 500Mpa and 49.7Mpa, respectively. It should be noted that the post-peak behaviour of concrete in tension has been neglected. Figure 1 compares the experimental records with the results of the numerical study. It can be seen that the test results are in good agreement with the numerical results.

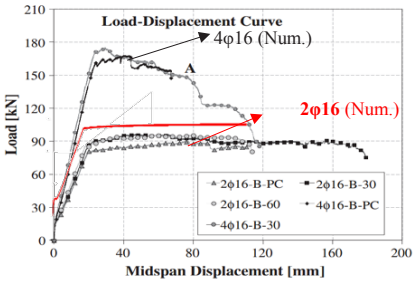

Figure 1. Load-Deflection curve for experimental [4] and numerical (green and red) model.

4. Results and Discussion

In this paper, to overcome the lack of ductility of concrete sections reinforced with FRP bars, two approaches were considered; replacing conventional concrete with Polymer-Modified-Concrete (PMC) and using ECC.

Figure 2 and Figure 3 show compressive stress-strain curve for PMC (modified with SBR polymer) [5] and tensile stress-strain curve for ECC (used PVA fibers) [6], respectively.

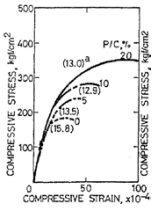

Figure 2. Compressive stress-strain curve for PMC [5]

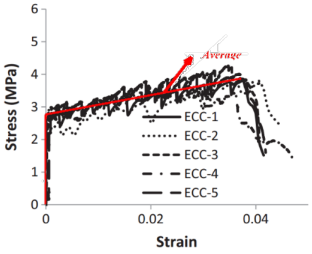

Figure 3. Tensile stress-strain curve for ECC [6]

The modulus of elasticity and ultimate strain of GFRP are 46GPa and 1.42%, respectively. Table 1 shows the results for the combination of PMC and GFRP. The cross-section of all models were considered to be 400mm×400mm. The J-index for all models were calculated and it was found that all values are greater than the minimum requirement, i.e. 4. Therefore, the mentioned beams are acceptable by codes from ductility point of view.

Table 1. Results of PMC and GFRP models.

I-D	GFRP Area (mm^2)	J-index	Failure mode
SBR-GFRP900	900	5.92	FRP rupture
SBR-GFRP2000	2000	15	FRP rupture
SBR-GFRP3000	3000	25.28	FRP rupture
SBR-GFRP7000	7000	27.84	Concrete crush
SBR-GFRP15000	15000	29.66	Concrete crush

Table 2 shows the details of models for considering ECC as a replacement for concrete and GFRP as a tensile rebar. All sections were 400mm×450mm with 10mm cover. Figure 4 shows the moment-curvature diagrams of these models.

To calculate ductility index (μ), a bilinear transformation method, based on ATC-40[7], was used. Figure 5 shows a bilinear graph using the mentioned approach. The graph shows that μ equals to 23.96. Therefore, to improve ductility of concrete sections reinforced by FRP bars ECC can also replace the conventional concrete.

Table 2. Details of ECC and GFRP models.

Num.	Af (mm^2)	Fc (Mpa)	Failure mode
1	1φ20	40	FRP rupture
2	2φ20	40	FRP rupture
3	5φ20	40	Con. crush
4	7φ20	40	Con. crush
5	9φ20	40	Con. crush
6	11φ20	40	Con. crush
7	1φ12	40	FRP rupture

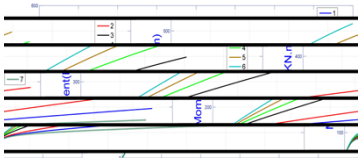

Figure 4: Moment-curvature diagrams for ECC-GFRP models

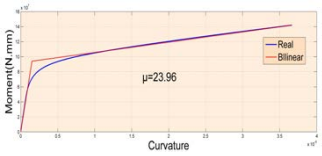

Figure 5: Bilinear graph for case num.7

5. References

[1] American concrete institute (ACI): committee 440, Guide for the Design and Construction of Structural Concrete Reinforced with Fiber-Reinforced Polymer (FRP) Bars, 2015.

[2] Paulay T., Priestly M. J. N.: "Seismic Design of Reinforced Concrete and Masonry Buildings", A Wiley Interscience Publication. 1923.

[3] Jaeger GL, Tadros G, Mufti AA.: "The concept of the overall performance factor in rectangular-section reinforced concrete beams". In: Proc of 3rd int symp on non-metallic (FRP) reinforcement for concrete structures, vol. 2, Sapporo, Japan; 1997. p. 551–8.

[4] A. Meda, F. Minelli and G. A. Plizzari, "Flexural behavior of RC beams in fiber reinforced concrete," Compos. Part B, no. 43, pp. 2930-2937, 2012.

[5] Yoshihiko Ohama-Handbook of Polymer-Modified Concrete and Mortars-Noyes, Building Materials Science, 1995.

[6] Pourfalah S.: "Behaviour of engineered cementitious composites and hybrid engineered Cementitious composites at high temperatures", DOI 0.1016/ j.conbuildmat. 2017.10.077, 2018.

[7] Applied Technology Council (ATC-40), Seismic evaluation and retrofit of concrete buildings, 1996.

ANALYTICAL APPROACH FOR ESTIMATION OF WAVE TRANSMISSION COEFFICIENT FOR π-SHAPE FLOATING BREAKWATER

Abubaker Alamailes[1] and Umut Türker[2]

1) Ph.D. candidate. Civil Engineering Department, Eastern Mediterranean University, Famagusta, 99450 North Cyprus Mersin 10, Turkey. abubaker.alamailes@students.emu.edu.tr (Corresponding author)
2) Ph.D. Associate Professor, Civil Engineering Department, Eastern Mediterranean University, Famagusta, 99450 North Cyprus Mersin 10, Turkey. umut.turker@emu.edu.tr

1. Introduction

This study presents a simplified analytical approach, based on power transmission theory [9], to estimate the transmission coefficient of a π-shape floating breakwater (FB) with finite width. In evaluating the transmitted wave power, this approach considers both the incident wave kinetic power and the heave oscillation of the FB. Additional power due to the acceleration of the floating body and the hydrodynamic mass increases the transmitted wave power behind the FB and consequently increases the transmission coefficient. The proposed theoretical approach is validated using laboratory-scale experimental data obtained from the literature for π-shape FB. The results of the proposed approach are in good to excellent agreement with those of experimental studies. In addition, the reliability of the proposed approach is assessed by comparing its results with those of other theoretical models. The effects of sea depth, relative draft, and incident wave height on the magnitude of the transmission coefficient are examined. It is found out that effect of the incident wave height distinguishes the proposed model from others in the existing literature.

2. Methodology

Wave decay on FB can be related to the ratio between incoming wave height H_i and transmitted wave height H_t. As a wave passes a FB, it decays and attains new height, *Ht*. [1, 6, 8]. Such wave attenuation can be expressed by the wave transmission coefficient K_t as

$$K_t = \frac{H_t}{H_i} \quad (1)$$

The incident wave energy includes potential, kinetic, and wave-induced pressure energy. Under the assumptions of linear wave theory, the energy transport (wave power) in the wave propagation direction is estimated by considering only the power resulting from the work done by the wave-induced pressure ignoring the transport of kinetic energy (wave kinetic power), owing to approximation to a certain order of [2]. However, in the presence of FB, wave kinetic power should be considered because their heaving behavior significantly affects the total transmitted kinetic power. Wave kinetic power accumulates with the kinetic power generated from the heaving oscillation of the FBs. Both kinetic powers increase the total transmitted power and hence, the transmission coefficient. Therefore, the total incident wave power $P_{I.tot}$ comprises incident wave kinetic power $P_{I.1}$ in addition to wave-induced pressure power $P_{I.2}$.

Part of these two wave powers is transmitted from beneath the FB draft D to the lee side (see Figure 1). The transmitted part includes the transmitted wave kinetic power $P_{T.1}$ and wave-induced pressure power ($P_{T.2}$). In addition to these two transmitted powers, $P_{T.3}$ (kinetic power per unit FB width resulting from the heaving motion of the FB) is transmitted in the x direction to the lee side. This power consists of two parts: the kinetic power of the heaving body of the FB and the kinetic power of the hydrodynamic mass that accelerates simultaneously with the floating body.

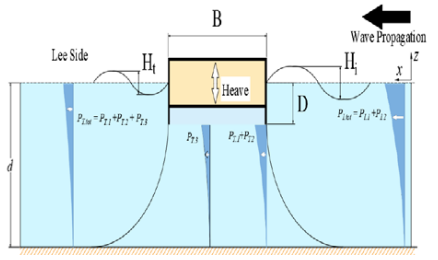

Figure 1. Process of power transmission theory.

The transmitted wave (at the lee side of the FB) carries a total power that equals the total transmitted power ($P_{T.tot} = P_{T.1} + P_{T.2} + P_{T.3}$). The transmitted wave becomes the incident wave toward the coastline with a height of H_t, which is attained after attenuation of the seaside incident wave. The leeside incident wave carries a total power $P_{L.S}$ that comprises the wave-induced pressure power and wave kinetic power. $P_{L.S}$ is a function of H_t, and once the value of $P_{L.S}$ is found (i.e., $P_{L.S} = P_{T.tot}$), the value of H_t can be obtained and transmission coefficient K_t can be calculated using Eq. (1).

3. Model Validation

The proposed approach was evaluated using laboratory data that was obtained from an experimental study on the

hydrodynamic performance of π-shape FBs conducted by Koutandos et al. (2005) [4]. The experimental date is shown in Table 1.

Table 1. Full-Scale Properties and Wave Conditions for Experimental Study.

Draft D (m)	Width B (m)	Wave Height Hi (m)	Wave Period T (s)	Water depth d (m)
2.5	10	1.5	14.9, 12.4, 9.5, 7.5, 6.4, 5.4	10

In addition, earlier theoretical approaches from Macagno (1954), Kriebel and Bollmann (1996), and Ruol et al. (2013) [3, 5, 7] were evaluated using the same laboratory data; the results were compared with those of the approach proposed in this study.

Figure 2 compares the experimental and theoretical transmission coefficients. The curves show the relationship between relative FB width *B/L* and transmission coefficient K_t.

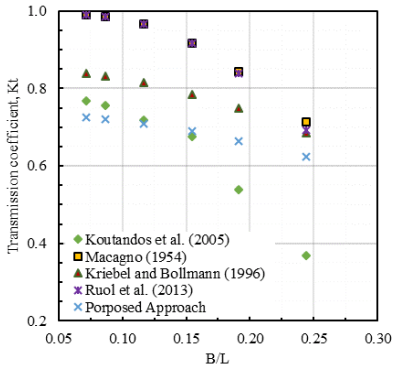

Figure 2. Change in the transmission coefficient with respect to the FB width B/L.

4. Discussion

4.1. Effect of Draft and Water Depth

The results show that as the draft increases (a higher value of D/d), the transmission coefficient decreases, indicating better blocking wave power transfer and successful additional attenuation of the transferred wave height. For a constant relative draft value, another important finding is the reduction of the transmission coefficient with respect to increasing sea depth. Thus, the FB's wave reduction performance is better in deep water owing to the change in wave orbital velocity with respect to changes in water depth.

4.2. Effect Incident Wave Height

Based on the proposed approach, as the incident wave height increases, so does the transmission coefficient of the FB under the same wave period condition. This result is expected, as incident wave height *Hi* is a factor that affects the calculation of transmission coefficient K_t. The kinetic power resulting from the heaving movement of the FB and its hydrodynamic mass is a function of *Hi*, and the kinetic power increases with wave height, leading to additional power transmission.

5. Conclusion

The results obtained using the proposed approach agreed with the small-scale results in the literature for waves with long periods and low steepness, in accordance with linear wave theory. Some scatter is to be expected, because it is difficult to adequately consider the effect of mooring stiffness in a simple approach. Part of the scatter is also attributed to scale effects that are likely to influence the transmission behavior, especially for very high waves, ignoring overtopping. Therefore, this approach may be inaccurate when applied to waves higher than the freeboard of the FB, especially in the case of full-scale structures.

6. References

[1] Hales, L. Z. "Floating breakwaters: State-of-the-art literature review." *Technical Rep. TR81-1*. United States Army Corps of Engineers, Springfield, VA, 1981

[2] Holthuijsen, L. H. *Waves in oceanic and coastal waters.* Cambridge University Press, Cambridge, U.K, 2010.

[3] Kriebel, D. L., and Bollmann, C. A. "Wave transmission past vertical wave barriers." *Proc., 25th Int. Conf. on Coastal Eng. (ICCE),* ASCE, Reston, Va., 1996, pp. 2470–2483.

[4] Koutandos, E., Prinos, P., and Gironella, X. "Floating breakwaters under regular and irregular wave forcing: Reflection and transmission characteristics." *J. Hydraulic Res.*, 2005, 43(2), pp. 174–188.

[5] Macagno, E. O. "Houle dans un canal présentant un passage en charge." *La Houille Blanche,* 1(1), 10–37 (in French).

layouts." *Appl. Ocean Res.,* 1954, 30(3), pp. 199–207.

[6] McCartney, B. L. "Floating breakwater design." *J. Waterway Port Coastal Ocean Eng.,* 1985, 111(2), pp. 304–318.

[7] Ruol, P., Martinelli, L., and Pezzutto, P. "Formula to predict transmission for π-type floating breakwaters." *J. Waterway Port Coastal Ocean Eng.,* 10.1061/(ASCE)WW.1943-5460.0000153, 2013, pp. 1–8.

[8] Türker, U. "Excess energy approach for wave energy dissipation at submerged structures." Ocean Eng., 88, 2014, pp.194–203.

[9] Wiegel, R. L. "Transmission of waves past a rigid vertical thin barrier." J. Waterways Harbors Div., 1960, 86(1), pp. 1–12.

CONDITION ASSESMENT OF HARBOR AND OFFSHORE PLATFORMS USING FIBER OPTIC SENSORS

Mohammad Reza Hedayati[1], Mehdi Kamyab Roudsari[2], Mohammad Hossein Amiri[3], Fatemeh Khodadadi[4]

1) Assistant professor Scientific-Applied Faculty of Post &Comm. Tehran, Iran
2) PhD Research Scaller, Chemical Engineering, Islamic Azad University–Tehran North Branch, Iran
3) MSc student, Islamic Azad University–Tehran North Branch, Iran
4) MSc student, Software Engineering, University of Hertfordshire, Hatfield Hertfordshire, UK

In this research work FBG has been used as a new kind of sensing element for health monitoring in the large composite and concrete civil infrastructures. The core problems focus on the novel proposed expert system using FBG sensors application. As a new kind of sensor for structural health monitoring system, Popularization and generalization of FBG is still a challenge for researchers.

This research work shows that FBG sensors have become one of the key sensors in structural health monitoring (SHM) and will take the place of some conventional electrical sensors.

In this work, the performances of a proposed solution, based on expert fiber Bragg-grating were tested and directly compared both in laboratory and in field conditions. The results are presented and discussed, aiming at the assessment of generalization the main characteristics of this technology for quay wall and other similar type, structural health monitoring applications, and also taking into account the principal requirements in-field of civil engineering applications.

Figure 1. FBG sensors incorporated in the laboratory indoor test setup

The efficiency of a monitoring method based on long-gauge sensors is illustrated through an application at the Shahid Rajaee port in Iran. For developing the present expert system the knowledge domain is organized so that the information can be structured in the computer program for effective use and originated from source of knowledge should be the domain expert. To design and develop knowledge based expert system, the specific knowledge domain or the subject domain is acquired. In the proposed scheme the change of reference FBGs signal with expert system, implies that something within the subsea concrete structure has altered and diagnosis is made.

A distributed on-line temperature and strain fiber sensing system based on the fiber Bragg grating (FBG) technology is presented and investigated experimentally for expert monitoring of the Harbour and Getty Structures.

The implementation of fiber optic sensing (FOS_ technology is the solution to incapability of traditional electrical stain gauges in a large sensing network for structural health monitoring of different building and civil engineering structures. It is Difficult and sometimes not possible to measure a fault or crack in the offshore or onshore construction for various reasons, including climate and environmental conditions.

The present work survey the principles and a criterion of the diagnosis signal processing and introduces these achievements to an expert system technique using Fiber Bragg Grating (FBG) sensors to monitor the dynamic strain and temperature of Shahid Rajaee harbour.

This article aims to ensure the protection, safety and health monitoring of the concrete structure quay wall in the Shahid Rajaee harbour using proposed method of measuring defected parts, incorporating the Fiber Bragg Grating sensors and extracting knowledge from expert system.

Figure 2. ROV Inspection of quay wall after receiving FBGs notification in Shahid Rajaee harbour

References

[1] M. Hedayati, M. Kamyab and All "Health Survey and monitoring Components in the propulsion system for use in a storage vessel of propellants," in The 13th conference on coast, post and marin structures (MIC 2011), Kish island, 2011.

[2] H. Mohammad reza and S. Seid.Attaollah, "ROV Based Condition Monitoring of Quay Wall Bottom and Maneuverability effect of vessels with large draft and thruster in Shahid Rajaee harbour," in 9th International Conference on Coasts, Ports and Marine Structures, 1391.

[3] R.-J. Sun, Z. Sun, D.-H. Dan and L.-M. Sun, "An integrated FBG sensing system for bridge health monitoring," in SPIE 6174, Smart Structures and Materials 2006: Sensors and Smart Structures Technologies for Civil, Mechanical, and Aerospace Systems, 61742Q, 2006.

[4] R. Valilou and E. Hadi, "Usage of optical fibre in construction structures," in 1th conference, extended and estimate the age of aviation structures and old rusty industry, Tehran, 1390.

[5] M. VELDHUIS, "Monitoring of Harbour Structures in The Netherlands," in European Conference on Structural Control , 2015.

[6] Tavner, P.J, Gaydon and B.G., "Monitoring Generators and Large Motors," 1986.

[7] A. Obaton, "Tilted Fiber Bragg Gratings And phase sensitive-Optical Low Coherence Interferometry for refractometry and liquid level sensing," 2012.

[8] S. Javadpour and M. Hedayati, "traffic monitoring system parameters and external road in remote areas using radio frequency (RFID) And sensor Network Bragg grating (FBG)," in The First Congress on Intelligent Transportation Systems (ITS), 2013

[9] M. R. Hedayati, A. A. Amidian, S. A. Sadr and A. Razazan, "Intelligent Ship Hull Inspection and NDT Using ROV Based Flux Leakage Expert System," 2010 Second International Conference on Computational Intelligence, Modelling and Simulation, Bali, 2010, pp. 412-415. doi: 10.1109/CIMSiM.2010.68

THE EFFECT OF EXPOSURE CONDITIONS AND CONSTRUCTION METHODS ON THE CHLORIDE DIFFUSION INTO CONCRETE IN THE PERSIAN GULF REGION

Majid Safehian[1] and Shapur Tahouni[2]

1) Assistant Professor, Department of Civil Engineering, Architecture and Art, Science and Research Branch, Islamic Azad University, Tehran, Iran, safehian@srbiau.ac.ir
2) Assistant Professor, Department of Civil and Environmental Engineering, Amirkabir University of Technology, Tehran, Iran, stahouni@aut.ac.ir (Engineering Manager of Tadbir Sahel Pars Consultant)

1. Introduction

The reinforced concrete structures present in marine environment are susceptible to reinforcement corrosion due to the presence of chlorides. The chlorides disposed in marine environment come mainly from seawater. Its contact with concrete structures can happen directly by seawater or through the marine aerosol. After contact, the chlorides are deposited on the surface of concrete and can penetrate on it through different mechanisms, depending on the characteristics of materials, construction methods and the exposure conditions in which it operates [1,3].

Due to different characteristics of attack, resulting mainly from different accesses of oxygen and humidity, the marine environment is divided in different zones of aggressiveness. These zones are segmented having the sea level as reference, and are defined as follows [2]:

Atmospheric zone: Concrete suffers the action from marine aerosol, however the structure is not affected directly by water splashes. The winds can carry the salts in the form of solid particles or as droplets of saline solution. The quantity of salt present decreases as a function of the distance from the sea, suffering influence of speed and prevailing wind directions.

Splash zone: Zone immediately above the maximum level of intertidal variation and concrete is directly affected by water splash. The height of the splash zone is a function of the wave height and speed/direction of wind. The most significant damage is produced by reinforcement corrosion by chlorides. The splash zone is subjected to cycles of wetting and drying and this fact becomes more significant as water evaporates and the salt remains into the concrete.

Tidal zone: It is the concrete zone between the min/max levels of tide. This region is also subjected to the wetting and drying cycles action. Degradation occurs due to the action of aggressive salts (chemical attack), reinforcement corrosion, waves' abrasive action and other substances in suspension, and attack of microorganisms.

Ghods et al. [4] consider that exposure zones play an important role in the service life design of concrete structures that should be concerned as a main input parameter in models. This means that in many cases, a model that is related to only one type of exposure zone relative to the chloride attack, should not be generally used. Thus, the expected life of a structure in a marine environment needs to be considerable different depending on the 4 exposure zones previously mentioned.

The aim of this study is assessment of the basic parameters in long term chloride penetration in the Persian Gulf region. So, five year-old concrete jetties located in Imam Khomeini Port Complex were investigated depending on two parameters, a) construction method: in-situ and precast, b) exposure conditions: atmospheric, splash and tidal zones. Also some accelerated durability tests were carried out on standard samples with same concrete mixture in laboratory. Finally, corrosion initiation time was estimated by five service life prediction models.

2. Description of Structures and Materials

With a history of more than 80 years, Imam Khomeini Port is considered as one of the largest and the most important commercial port of Iran which handles about half of all non-oil trades of the country. Bandar Imam Khomeini (BIK) is located on the tidal lands of the northern parts of Khure Musa which provides a safe and protected and approach channel for vessels up to 150000 ton.The under investigated structures are located in southern part of BIK zone and are called Eastern and Western jetties. These on-shore structures were built in 1927-41 and were totally rehabilitated in 2004-07 (fig. 1).

Figure 1. Eastern and Western jetties in BIK zone

Based on the official documentary information, investigated parts of structures have the same concrete mixture and were repaired five years ago. The concrete mixtures containing type I(PM) blended cement from

Bushehr company and silica fume (SF) with 89% SiO_2 and pozzolanic activity index 103%. A mix ratio of 1:2.1:2.6 by mass was used with water to binder ratios of 0.35. Because of low w/b ratio in mixture, polymer-based superplasticizer was used to achieve desired workability.

3. Experimental Program and Results

In order to analyze long term chloride penetration into concrete and predict corrosion initiation time, two series of experiments were performed. The first series were on standard samples with similar concrete mixture of field structures in laboratory that is presented in table 1.

Table 1. Durability tests on concrete mixture in laboratory

Compressive strength (28-day) (MPa)	Surface Resistivity (kΩ.cm)	Rapid Chloride Migration Test (mm^2/year)	Rapid Chloride Penetration Test (Coulomb)
BS-1881 part116	Wenner test	NT Build-492	ASTM C1202
55	36	169	1365

The field surveys are applied on three exposure conditions of precast (P) and In-situ (I) structural members included: atmospheric (A), splash (S) and tidal (T) zones. Also, each measurement is repeated at two point (1, 2) in specified structural members. Additionally, abbreviations PTB, ITS and PTC is related to previous study on samples with w/c ratio of 0.50 in Bandarabbas (B) [2], extracted core with plastic spacer (S) and special core from cracked concrete (C), respectively.

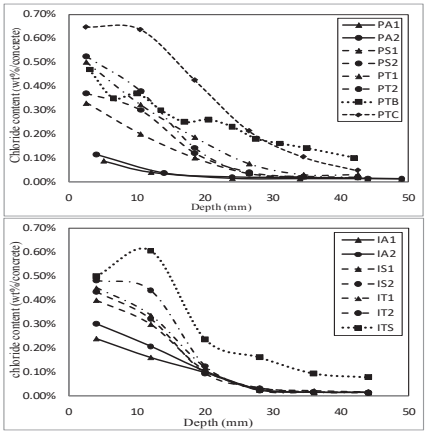

Figure 2. Chloride profiles in various exposure conditions

4. Discussion

Equations governing the diffusion are based on Fick's laws in the form of differential equation and can be solved in various forms. Some consider this equation as constant diffusion coefficient (crank solution) [3] that is called apparent diffusion coefficient used for estimations. It is generally noted from figure 3.top, D_{app} parameter is more or less the same at the majority of samples and the exposure conditions didn't indicate considerable effect on it after five years of exposure.

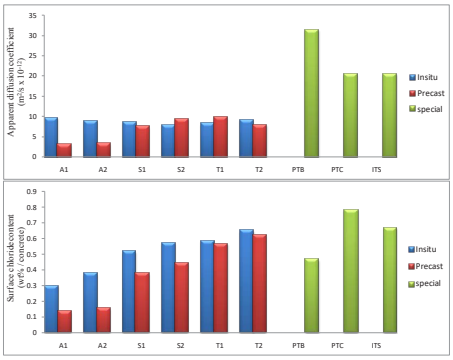

Figure 3. Calculated apparent diffusion coefficients (top) and surface chloride content (bot) in various conditions

Surface chloride content is another parameter that is obtained after fitting of the equation of the Fick's second law. Surface chloride outlined in figure 4.bot, show that the order of C_s with regard to the level from seawater is tidal > splash > atmospheric zone. Also, the differences of C_s, generally indicates how concrete quality and exposure conditions can significantly affect the chloride penetration. As it well known in previous studies, in tidal zone near high water level due to wet/dry cycles, resulting in a successive supply of chlorides by wetting with sea water, and salt crystallization by drying.

5. Conclusions

As a main conclusion, the ingress of chlorides in concrete is different in each exposure zone and influenced by microclimatic factors such as temperature, relative humidity, wind and solar radiation. However, it is noteworthy that most of the mathematical models of service life prediction available in literature do not consider all these variations in their formulations. The difficulty of monitoring these variations in the locals of the concrete structure exposure is recognized, but this effect should be considered in models and technical standards related to the life of these structures.

6. References

[1] Medeiros-Junior, R., Lima, M, "Chloride penetration into concrete in an offshore platform - analysis of exposure conditions", *Ocean Engineering,* Vol.103, 2015, pp.78-87.

[2] Safehian, M., Ramezanianpour, A.A. "Assessment of the long term chloride penetration and prediction of RC structure service life in the Persian Gulf region", *4th international conference on concrete and development*, Iran, Tehran, 2013.

[3] Safehian, M., Ramezanianpour, A.A. "Assessment of Service Life Models for Determination of Chloride Penetration into Silica Fume Concrete in the Severe Marine Environmental Condition", *Construction and Building Materials*, Vol.50, 2013, pp.1-10.

PHYSICAL MODELING OF RUBBLE MOUND BREAKWATER DEFORMATION ON SOFT SEABED

Hamed Ghazi[1], Hadi Shahir[2], Masoud Haghparast[3] and Seddigheh Masoudi[4]

1) Civil Engineering Department, Kharazmi University, Tehran, Iran, std_ghazi@khu.ac.ir
2) Civil Engineering Department, Kharazmi University, Tehran, Iran, shahir@khu.ac.ir
3) Civil Engineering Department, Kharazmi University, Tehran, Iran, std_m.haghparast@khu.ac.ir
4) Civil Engineering Department, Kharazmi University, Tehran, Iran, std_s.masudi@khu.ac.ir

1. Introduction

Soft seabed in some coastal areas causes noticeable problems in the course of construction of marine structures such as rubble mound breakwaters. Pouring rubbles for constructing this type of breakwaters, rock particles sink into the soft soil and a foundation for the breakwater cannot be developed [1] causing excessive settlement, instability of breakwater and waste of materials. Except that the individual penetration of rock particles into the soft soil, other phenomena such as immediate deformation and consolidation of the seabed, flow of soft material into pores of rock fill and erosion of the seabed effect the total waste of rock material [2].

Before choosing the best technique to encounter the problem, it is essential to make an accurate estimation of breakwater deformation and volume loss. There are numerous projects that underestimating the rock material volume required for construction lead to lack of resources, contracting problems, funding difficulties and at least delay in construction process because of need for redesign and change the approach. On the other hand, overestimating the volume loss can lead the project to an expensive improvement technique.

In this paper at the first step, data gathering from several projects with considerable waste of rock material was carried out and as case histories took into account. Then, a 1g physical modeling test procedure was suggested for a more detailed study on the subject.

2. Case Histories

Many coastal projects in the south and north of Iran have encountered with soft beds problem. Here the available records of 7 breakwaters and/or access roads have been presented: Hendijan, Mohammad Ameri, Nakhl-e-Nakhoda, Shenas, Shah-Abdullah, Bandar-Abbas, and Deylam [3-9]. The thickness of the very soft layer was variable from 3 to 12 m in various projects and the maximum settlement reported was about 8 m.

There are often some shortcomings and ambiguities in the reported information:

- The breakwater section that settlement is recorded usually is not specified precisely.
- Time dependent data for deformation records during construction and afterward usually is not available.
- The geotechnical characteristics of the seabed which have been documented in the geotechnical report of the project, usually has been carried out before construction and in a wide area, and the soil parameters at the exact recording position of settlements are not available. Even sometimes enough studies have not been performed in the project area.
- Generally, reported data is related to the settlement and the amount of sinking stones in seabed and total volume loss of the materials have not been presented.

Considering the above, some physical modeling tests were proposed.

3. Proposed 1g Physical Modeling Tests

The amount of stone material required to construct a breakwater can be obtained from multiplication of the designed section volume to the specific gravity measured for the rock material ($W_{Initial}$). But during construction, the pre-designed section changes and consuming material becomes much higher than the initial estimation (W_{Total}). The deformed cross-section can be divided into the following areas (see Figure 1):

$W_{Settled}$: Material placed in the deformed bed.
$W_{Penetrated}$: Material sinked into bed.
W_{Uplift}: Uplift area in the pre-designed body.
W_{Over}: Extra material due to the toe deformation.
W_{Extra}: Extra material added to the initial estimation to reach the design surface.

Between the above areas, the following relationships can be written:

$$W_{Total} = W_{Initial} + W_{Extra} \quad (1)$$

$$W_{Total} = W_{Initial} + W_{Over} + W_{Settled} + W_{Penetrated} - W_{Uplift} \quad (2)$$

Then:

$$W_{Extra} = W_{Over} + W_{Settled} + W_{Penetrated} - W_{Uplift} \quad (3)$$

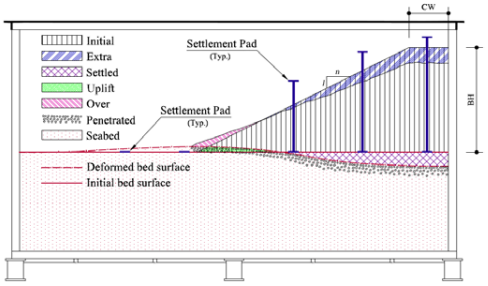

Figure 1. Different area definitions of deformed breakwater modeled in 1g physical modeling box.

W_{Extra} is known during construction. Also, by integrating from the deformed surface of the soft seabed, $W_{Settled}$, W_{Uplift} and W_{Over} can be obtained and, according to Equation 3, sinking stoned into the bed ($W_{Penetrated}$) can be calculated, too. In this way, all areas of Figure 1 will be known.

A sample of the tests performed inside the physical modeling chamber of Kharazmi University is shown in Figure 2. Time dependent vertical deformation of bed surface for the test is presented in Figure 3 and the deformed shape and consuming material for each sector have been presented in Figure 4 and Table 1, respectively.

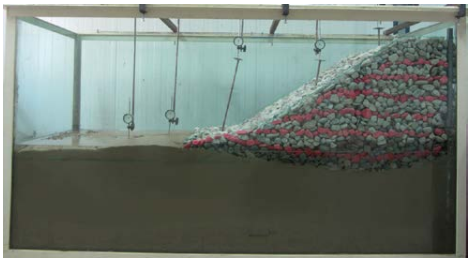

Figure 2. 1g physical modeling test performed inside the physical modeling chamber of Kharazmi University.

Table 1. Consuming relative to design material for two average undrained shear strengths of bed ($C_{u.ave}$).

$C_{u.ave}$ (kPa)	$W_{Settled}$	W_{Uplift}	W_{Over}	W_{Extra}	$W_{Penetrated}$
1.25	5.9	2.2	1.1	**11.6**	6.7
1.10	6.2	0.4	0.9	**15.7**	9.0

In the proposed 1g physical modeling tests, by measuring and calculating each of the above quantities, the role of each sector in the total amount of consuming stone materials can be studied. Also, their relationship with design parameters such as undrained shear strength of clay, geometric dimensions of the breakwater and the type of rock materials used in the construction can be investigated.

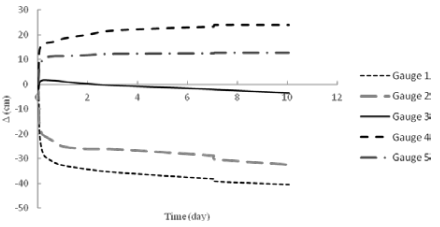

Figure 3. Time dependent vertical deformation of bed surface (Gauge numbering is done from the right).

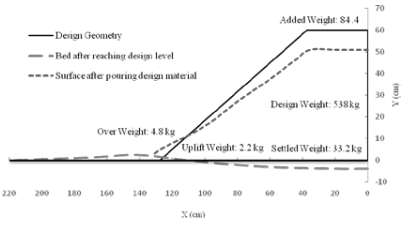

Figure 4. Deformed shape diagram used for integration and calculation of areas.

4. Acknowledgements

The authors acknowledge financial support from the Port and Maritime Organization under contract 35757.

5. References

[1] Mobarrez, R., Ahmadi-Tatfi, h. and Fakher, A. "An Essential Foundation Control for the Design of Rubble Mound Breakwaters on Soft Soil." *International Conference on Geotechnical Engineering*, October 3-6, 2004.

[2] Beemsterboer, T. N. "Modelling the immediate penetration of rock particles in soft clay during subsea rock installation, using a flexible fallpipe vessel". Diss. TU Delft, Delft University of Technology, 2013.

[3] Nikghalbpour, M. "Common methods evaluation of the gravitational marine structures settlements during construction" M.S. Thesis, Guilan University, 2010.

[4] Sahel consulting engineers, "Studies and design report of Shah-Abdullah breakwater", 2012.

[5] Sahel consulting engineers, "Studies and design report of Shenas breakwater", 2010.

[6] SES Co., "Geotechnical report of Deylam breakwater", 2009

[7] Pouya Tarh Pars consulting engineers, "Phase 1 & 2 studies report of Nakhl-e-Nakhoda port", 2011

[8] Sazeh Pardazi Iran consulting engineers,"Studies and design report of Bandar-Abbas breakwater", 2012

[9] Kazemi, M.A., Bardideh, A. and Jandaghi, M. "Studies on Nakhl-e-Nakhoda breakwater settlement and suggested solution". ICOPMAS, 2014.

4

OFFSHORE AND PIPELINE ENGINEERING

AN INSIGHT INTO THE SETTLEMENT MECHANISMS OF RUBBLE MOUND BREAKWATER ON MUDFLAT USING DEM

Hamed Bayesteh[1] and Roham Mansouri Boroujeni [2]

1) Ph.D, Department of Civil Engineering, University of Qom, Qom, Iran, h.bayesteh@qom.ac.ir
2) M.sc, Department of Civil Engineering, University of Qom, Qom, Iran, rohammb71@gmail.com

1. Introduction

Because mudflats are compressible, substantial settlement will occur during construction of a rubble mound breakwater at such a site. The use of geosynthetics as reinforcement is common during breakwater construction [1]. A suitable numerical model should be selected to provide insight to the mechanisms of settlement of such a reinforced rubble mound breakwater. Although numerical methods based on continuum mechanics have been used to model the behavior of embankment systems, they cannot provide insight into settlement because they cannot approximate the individual movement of the particles. Rubble mound breakwaters consist of rockfill, which is naturally discontinuous (Figure 1). Moreover, basing the numerical method on discontinuum mechanics to simulate the behavior of rockfill has not been achieved. The aim of the current study was to evaluate the control mechanisms of settlement of rubble mound breakwaters and the effect of geosynthetics on their performance. A full-scale case study of a rubble mound breakwater constructed on soft soil is considered for which the effect of the pattern, size and number of layers of the geogrid on performance was monitored. A series of numerical simulations using the discrete element method were done to evaluate settlement caused by submersion of the particles into the seabed. The effects of geosynthetic parameters such as stiffness, number of layers and length of geosynthetic material were analyzed. The results showed that the submersion of the individual particles of rockfill into the seabed is the main mechanism of settlement in an unreinforced breakwater (Fig. 1). This value is higher than for classic settlement (elastic or consolidation) [2]. However a reinforced geogrid acts as a separator and prepares a continuous base for the rockfill to prevent individual movement. Classic settlement is main mechanism of settlement which controls the behavior. It was shown that the length and number of geogrid layers had greater influence over decreasing settlement than the tensile strength of the geogrid.

2. Geometry of the Model

In order to model the geometry of the breakwater, a trapezoid with a 7 m height, 7 m crest width and side slopes 1:1 was considered (Figure 2). As the rockfill materials usually are rough, they are resistance to rolling. The particles used in this study were circular so the rolling resistance linear contact law was used to simulate the rubble mound particles [2]. The parameters of a model are usually calibrated using known macro-mechanical responses. For calibration the rubble mound parameter, the particles deposited from a hopper above the base wall (Figure 3).

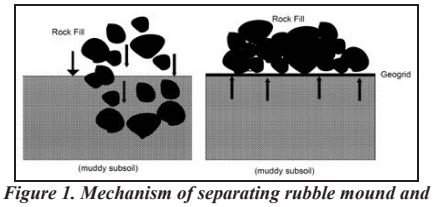

Figure 1. Mechanism of separating rubble mound and soft soil by geosynthetic

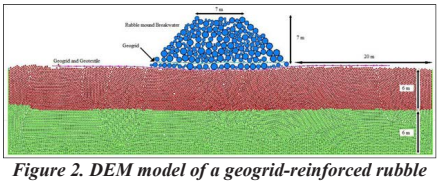

Figure 2. DEM model of a geogrid-reinforced rubble mound breakwater

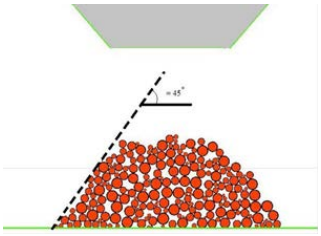

Figure 3. Calibration micromechanical parameters of the breakwater particles to reach an angle of response

3. Settlement Due to Submerging Mechanism

The total settlement was 4.2 m which is compatible with the monitored data in an Iran projects. This finding shows that a large deformations and large strain can be simulated

with DEM [4]. As described in the theoretical background section, this large value of the settlement was induced due to the individual submerging of the rockfill, because the breakwater media is naturally discontinuum. Fig. 4 plots a part of the displacement vectors of the particles after settlement of the breakwater. It can be seen that displacement vectors for rockfill are towards the seabed while for seabed particles, the displacement vectors are laterally or upward due to the soil heaving. Submerging of the rubble mound into seabed leads to lateral movement of the seabed particles and inducing shear band.

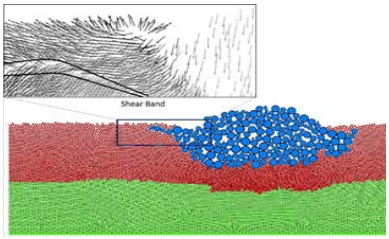

Figure 4. Settlement due to the submerging of the breakwater particles

4. Settlement Due to Continuum Mechanism

In order to have an insight to the continuum settlement of a rubble mound breakwater, it is necessary to prevent individual settlement of the rockfill. As described in Figure 1, using geosynthetic below a rubble mound section, cause uniformity between rockfill and can acts as a continuum media. The results show that using the geosynthetic reinforcement leads to the decrease of the breakwater settlements at the seabed. This function leads to prepare a continuum media which is prevent separate submerging of the rockfill into seabed. Thus, the induced settlement in this situation (0.65 m), was due to the continuum settlement according to the subsoil geotechnical parameters. Figure 5 shows the force chains for the reinforced rubble mound breakwater. It is clear that the vertical force due to the self-weight of the rubble mound creates a tensile force in geogrid reinforcement which leads to transfer vertical load to horizontal load. Figure 6 shows the settlement of the breakwater with various geogrid length. By decreasing the length of the geogrid, the settlement increases. The results shows that although there is not deference between the 45 m and 30 m length of the geogrid, but the value of the seabed heaving increase by reducing in the geogrid length.

5. Conclusions

In this paper, in order to have an insight to mechanism of settlement a rubble mound breakwater, a discrete element simulation was performed. According to the discontinuum based of DEM. the results indicated that this method can simulate the submerging particle into seabed. The induced force chains in the model show that the local large forces on the seabed particles, lead to push away the subsoil particle so the individually large settlement of the rockfill occurs. A series of simulations were conducted to evaluate the effect of the geogrid length, the reinforcement layers and the geogrid tensile strength on the performance of reinforced breakwater. The results shows that by increasing the length of the geogrid, the settlement decrease. Whereas the vertical load (due to the self-weight of the breakwater) transferred to a horizontal load through a longer length of the geogrid, the settlement reduces. Also, by increasing the geogrid layers, the settlement decreases. Indeed the more geogrid layers lead to reduce the tensile force in one geogrid. Redistribution of the contact force in the geogrid, causes suitable local interaction between seabed and lower geogrid layer and causes reduction in the settlement. By the way, the overall tendency is the reduction of the breakwater settlement with the increase of tensile strength can be concluded. But there is an upper bond for the geogrid tensile strength for preventing over reinforcement.

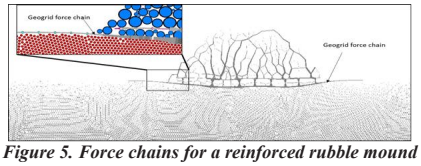

Figure 5. Force chains for a reinforced rubble mound breakwater

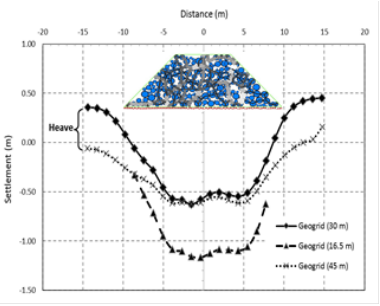

Figure 6. Effect of the geogrid length on the breakwater settlement

6. References

[1] Mobarrez, R., Ahmadi-Tafri, H Fakher, A., 2004. *"An essential foundation control for design of rubble mound breakwaters Engineering",* October 3-6– United Arab Emirates, 347-350.*on soft soil. International Conference on Geotechnical*

[2] Verhaeghe, H., De Vos, L., Boone, X., Goemaere, J., 2014. Using Field Data to Improve the Settlement Prediction Model of a Breakwater on Soft Soil. J. Waterway, Port, Coastal, Ocean Eng., 140,173-187.

[3] Cundall, P.A. and Strack, O.D.L., 1979. *"A discrete numerical model for granular assemblies",* Geotechnique, 29 (1), 47-65.

[4] Chen, C., McDowell, G.R., Thom, N.H., 2012. *"Discrete element modelling of cyclic loads of geogrid-reinforced ballast under confined and unconfined conditions".* Geotextiles and Geomembranes 35, 76-86.

EXPERIMENTS ON SCOUR AROUND SUBMARINE PIPES AND STUDY OF KC NUMBER UNDER SOLITARY WAVES

Hassan Vosoughi[1] and Hooman Hajikandi[2]

1. M.Sc. Department of Civil Engineering, Islamic Azad University, Central Tehran Branch, Tehran, Iran.
qalan_vosoughi@yahoo.com
2. Assistant Prof., Department of Civil Engineering, Islamic Azad University, Central Tehran Branch, Tehran, Iran.
h_hajikandi@iauctb.ac.ir

1. Introduction

Pipelines are a very opportune means to transport oil, gas, water, waste water or other hydrocarbons from the sea bed or river crossing is current in water environments. Pipelines are widely used coastal structures, and scour around them can influence their stability. Pipelines installed on sandy sea beds in coastal areas are exposed to wave and current action.

Sumer and Fredsøe [3] demonstrated that the relative scour depth, S/D, is remarkably well correlated with the Keulegan–Carpenter (KC) number. The scour increases with increasing KC number. S/D can be expressed in terms of the KC number as follows:

$$\frac{S}{D} = 0.1\sqrt{KC} \tag{1}$$

Çevik and Yüksel [1] studied scour below submarine pipelines in shoaling regions for normal-incidence regular waves using four different rigid pipes. They conducted tests of both horizontal beds and 1/5 and 1/10 sloping beds in shoaling regions. They investigated the effects of several parameters on the non-dimensional scour depth. They identified the wave height, wave period and pipe diameter as the dominant parameters in the development of scour. As each of these parameters increases, the non-dimensional scour depth increases.
They proposed an expression for the equilibrium scour depth in terms of the KC number for both sloping (1/5 and 1/10) beds and horizontal bottoms.

$$\frac{S}{D} = 0.11KC^{0.45} \tag{2}$$

Kızılöz et al. [2] studied scour around rigid submarine pipelines under irregular wave attack on horizontal and (1/10) sloping beaches and relative scour in regular and irregular wave attack. Sumer and Fredsøe [4] studied the influence of irregular waves on scour using the JONSWAP wave spectrum. They proposed the following equation for the scour depth in the case of irregular waves:

$$\frac{S}{D} = 0.1\sqrt{KC} = 0.1\sqrt{\frac{U_m T_p}{D}} \tag{3}$$

Most of the experimental studies of scour around submarine pipelines to date have been conducted under conditions of regular and irregular wave attack. The purpose of this study is to model the local scour depth around a fixed submarine pipeline under solitary wave attack on horizontal and sloping conditions.

2. Experimental Setup and Procedure

Figure 1 shows a schematic of the experimental setup. As it is shown in Figure 1, a sluice gate is installed in the middle of the flume, approximately 5 meters from the inlet pipe. Prior to each experiment, water is reserved upstream the gate. The opening velocity of the gate is controlled by means of a rotary-motor. Total 40 experimental runs are performed for two conditions of horizontal flume and 0.6% longitudinally slope flume. All the experiments are conducted for two identical sediment layers the mean sediment size of which are 3.1 mm and 5.8 mm respectively. The Thickness of the sediment layer is 15 cm before the beginning of the experiments. Rigid PVC model pipe with diameter *dp*=4cm were placed 1 mm from the channel sides. To avoid wall effects, all measurements were made in the middle of the cylinder axis. At the end of the flume a tailgate with adjustable height was used to create desired depth in the flume.

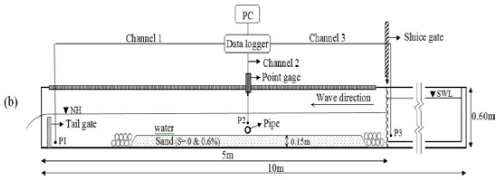

Figure 1. Experimental setup-Sectional

At the beginning of each experiment the inlet flow rate was controlled and adjusted to provide the desired normal depth above the sediment recess. The sediment recess was located 0.5 m from the sluice gate. In order to provide a flat bed, artificial bed was made in the flume before and after the sediment recess. By closing the sluice gate, water is stored upstream the gate and when the water head reaches the desired head it is released by sudden opening of the gate.

3. Results

The results of extensive experimental runs on scour around submarine pipes under solitary waves generated by suddenly releasing of flow from an upstream sluice gate. The effect of relevant parameters including depth of flow before the sluice gate, channel slope, wave Froude number and sediment gradation on the scour hole is investigated. In this study, 40 random wave tests were conducted to study the scour depth below submarine pipelines and exposed to normal incident solitary wave attack. In this study proposed an expression for the equilibrium scour depth in terms of the KC number for both sloping beds and horizontal bottoms.

Relative scour depth increases with increasing wave height, wave period, and pipe diameter and scour depth can be expressed by the KC number for a horizontal and sloping bed. The following expression is proposed for a fixed pipe in contact with a live bed under solitary wave attack.

Figure 2 shows the variation of relative scour depth with KC number. This figure includes regular wave data of Sumer and Fredsøe [3] and irregular wave data of Kızılöz et al. [2] and those of this study which are the results of solitary wave data. The present data are located above KC numbers very different from the regular and irregular wave data Sumer and Fredsøe [3] and Kızılöz et al. [2].

Founded on the present experimental data, a new equation (Eq. 4) is suggested for dependence of S/D on KC, relating the maximum equilibrium scour depth for the live bed condition for a rigid pipe fixed initially in contact with the bed under solitary wave attack.

$$\frac{S}{D} = 0.15KC^{0.83} \quad (4)$$

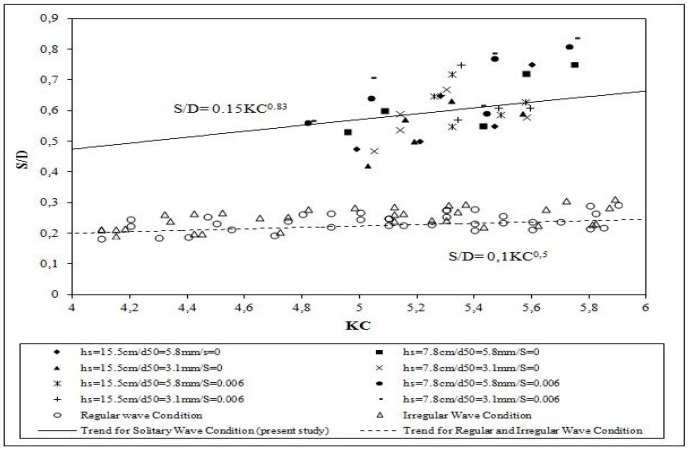

Figure 2. Variation of maximum scour depth with the Kleugan-Carpenter number. Experiment: Present solitary wave data. Regular data from Sumer and Fredsøe (1990). Irregular wave data from Kızılöz et al. (2013).

4. Reference

[1] Çevik, E.Ö., Yüksel, Y., "Scour under submarine pipelines in waves in shoaling Conditions", *Journal of Waterway, Port, Coastal and Ocean Engineering*, ASCE 125, 1999, pp. 9–19

[2] Kızılöz, B., Çevik, E., Yüksel, Y., "Scour below submarine pipelines under irregular wave attack", *Coastal Engineering*. 2013, pp. 79, 1-8.

[3] Sumer, B.M., Fredsøe, J., "Scour below pipelines in waves", Journal of Waterway, *Port, Coastal and Ocean Engineering*, ASCE 116 (3), May/June 1990, pp. 307–323.

[4] Sumer, B.M., Fredsøe, J., "Scour around pipelines in combined waves and current", *Proc. 7th International Conference on Off-shore Mechanics and Arctic Engineering Conference: Pipeline Technology*, vol. V. ASME, Florence, Italy, 1996, pp. 595–602.

IMPLEMENTING THE "SELF-UPENDING CONCEPT" FOR THE JACKETS IN PERSIAN GULF WITH THE NEW ARRANGEMENT OF BUOYANCY TANKS

Seyed Ali Amid[1], Majid Sohrabpour, PhD[2] and Sara Allahyaribeik[3]

1) Marine Systems Technologists Limited, Tehran, Iran, ali.amid@yahoo.com
2) Marine Systems Technologists Limited, Tehran, Iran, sohrabpr@gmail.com
3) Science and Research Branch, Islamic Azad University, Tehran, Iran

1. Introduction

The Crane-assisted upending procedure for installation of jacket platforms requires heavy floating cranes. The alternative way to install jacket platforms is the "self-upending'' procedure, in which belt-shaped Buoyancy tanks are deployed to self-upend the jackets. This belt-shaped buoyancy tanks comprise different tanks welded together. Hence, they cannot be deployed to self- upend other jackets which have different dimensions. The new positioning of buoyancy tanks on Jackets has been presented in this paper which makes the self-upending procedure much more cost-effective thanks to the Modularization of Buoyancy Tanks. By virtue of this method, buoyancy thanks are no longer welded together; therefore, they can be used to self-upend the other jackets with different dimensions. Furthermore, before positioning jackets on the seabed, the stability of floating jackets increases due to the new arrangement of Buoyancy tanks on jacket. Parametric study demonstrated that, with this new arrangement of buoyancy tanks, self-upended jacket has a considerable stability. This new arrangement has been applied on two different existing jackets in Persian Gulf, located in 40 and 70 meters of water depth.

2. Example A: Jacket in 37.6m Water Depth

Self-upending concept has been implemented for 662 tons Jacket in Persian Gulf; the Software Sacs is implemented to perform 3-D Time-domain Launch and Self-upending Analysis [1]. Figure 1 shows the 662-ton jacket with its modular buoyancy tanks designed according to DNV-RP-C202 [2] as stiffened circular cylindrical shells. It has been concluded that, In order for the jacket to assume its vertical position soon after launching, center of gravity of jacket must be located 1.92 meter below the center of buoyancy. Considering the jacket located horizontally on launching barge, two buoyancy tanks with dimensions of 2 m outside diameter and wall thickness of 1.5 cm control the transverse stability of jacket during self upending. One, with the same dimensions, perpendicular to the longitudinal axes of launching barge, assists jacket reaches its vertical position- pitch angle of 82 degrees. Four buoyancy tanks are deployed to comply the minimum bottom clearance criteria. Table 1 shows the jacket launch results.

Table 1. Launch results- jacket example A

Jacket Example A				
Time(sec)	Pitch	Roll	Yaw	Mudline clearance(m)
148	-56.9	-7	0	5.45
156	-75	-6.4	0	6
164	-86	2.6	1.8	7.57
189	-82	1.3	2	7.18

Four phases are considered in the launch analysis, tipping position occurs at time 114, separation occurs at 124 sec, and the final position of jacket occurs at 189 sec. Therefore, it takes 65 sec for the jacket to be self-upended. The minimum bottom clearance during the launching process is 5.45 meters occurring 148 seconds after the launch is commenced. Table 2 shows jacket's final orientation with its metacentric properties.

Table 2. Jacket's final position- jacket example A

Jacket final orientation				Metacentric properties			
Pitch	Roll	Yaw	MC	LGM	TGM	BG	RB
-82 deg	1.3 deg	0 deg	4.35 m	6.34 m	4.17 m	2.46 m	24%

Transverse as well as longitudinal metacentric heights are 4.17 and 6.34 m correspondingly, which are well above the minimum criteria of 0.5 and 0 m [3].

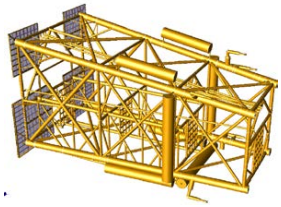

Figure 1. Jacket model example A

3. Example B: Jacket in 70m Water Depth

Launch and Self-Upending analyses have been implemented for a larger jacket of 1828 tons dry weight in Persian Gulf. Buoyancy tanks with outer diameters of 2.5 and 2 m and wall thickness of 1.5 cm with a total weight of 176 Tons are implemented in the design. As it could be observed in figure 2, the arrangement of buoyancy tanks is the same as the 662-ton jacket. Table 3 shows the jacket launch results.

Table 3. Launch results- jacket example B

Jacket Example B				
Time(sec)	Pitch	Roll	Yaw	Mudline clearance(m)
279	-3	-2	0.2	44
291	-41.5	-7.4	-0.4	21
325	-79	-12	-2.8	5.4
348	-82	3.5	0	7.39

Table 4 shows the jacket's final orientation with its metacentric properties.

Table 4. Jacket's final position- jacket example B

Jacket final orientation				Metacentric properties			
Pitch	Roll	Yaw	MC	LGM	TGM	BG	RB
-82 deg	3.5 deg	0 deg	7.39 m	4.26 m	3.22 m	2.64 m	21%

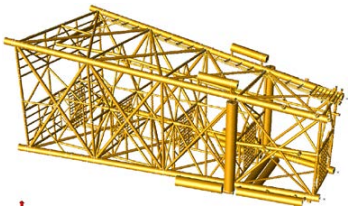

Figure 2. Jacket model example B

4. Conclusion

Implementing the self-upending concept with the new arrangement of buoyancy tanks is quite attractive due to the following reasons:

1) The amount of time it takes both jackets to be self-upended is 69 seconds.

2) Several more launch simulations were performed to investigate the sensitivity of varying jackets parameters—that is—weight and CG sensitivity. Some of which are depicted in table 5.

3) Damaged cases are also considered, in which three buoyancy tanks of the jacket example A were allowed to free flood at the point of submersion. In this case of failure, the Pitch angle of Jacket A would be 79.7 degrees and longitudinal and transverse metacentric heights would be 4.74 and 1.48 meters correspondingly. It shows the considerable stability of the self-upended floating Jacket even with the failure of 3 compartments thanks to the new arrangement of buoyancy tanks.

4) This new arrangement of buoyancy tanks presents and suggests Cost-effective [4] and Secure Installation of jacket platforms through self-upending concept. Buoyancy tanks are selected and designed in an optimal as well as modular manners with the same dimensions, so that they could be used for other projects.

5) Before the positioning of self-upended floating jacket on the sea bed, Current with the velocity of 1.4 m/s has been applied to investigate the behavior of the floating jacket example A. In this case the velocity of floating jacket in x direction would be 0.7 m/s, which can be completely kept in the position by tug boats.

6) In order for the jackets to assume their nearly-vertical positions, there is no need to flood any compartment of the jackets because of the new arrangement; however, before positioning the jackets on the sea bed, two legs of the jacket example A and two legs of the jacket example B must be flooded with the ratio of 60 and 30% correspondingly without any assistance of the floating cranes.

Table 5. Weight tolerance for jacket example A

	Shift jacket XCG -0.9 meters	%5 increasing in weight	%5 decreasing in weight
Pitch Angle	83 deg	83.45 deg	79.6 deg
Reserve Buoyancy	24 %	20.2%	27.8%
Mudline clearance	4.63 m	4.35 m	4.63 m
Longitudinal GM	7.53 m	5.40 m	5.81 m
Transverse GM	4.75 m	4.38 m	2.85 m

5. References

[1] Bentley Systems Incorporated, "SACS® Launch, Flotation and Upending Analysis Manual, version 5.6.2.3", 2014;

[2] DNV Recommended Practice "DNV-RP-C202, Buckling Strength of Shells", January 2013.

[3] Noble Denton Marine Services (DNV GL Group), Report No: 0028/ND Rev 6 - 14 December 2015 – "*Guidelines for steel jacket transportation & installation*".

[4] Amid, Seyed Ali & Majid Sohrabpour PhD, 1395, New Method of Jackets Installation in Persian Gulf, 18th Marine Industries Conference, Kish Island, Iran

RELIABILITY ANALYSIS OF M5-GP PREDICTION MODELS FOR UPLIFT CAPACITY OF SUCTION CAISSONS

Ali Derakhshani [1]

1) Department of Civil Engineering, Faculty of Engineering, Shahed University, Tehran, Iran
adera@shahed.ac.ir

1. Introduction

Different models for predicting the uplift capacity are available in the technical literature. The recommended models for uplift capacity prediction do not account for the input uncertainties affecting the results.

Generally, uncertainty in the inputs, is effective on the reliability of the system responses. Suction caisson is among the widely used engineering systems that its uplift capacity is influenced by uncertainties.

To improve the reliability of the designs, the input uncertainties need to be considered directly [1]. For this purpose, various approaches have been used for analyzing the engineering systems ranging from engineering judgments to the complicated statistical and intelligent methods.

The fuzzy sets theory can be considered as the most general method to be used for uncertainty analysis in engineering [2]. Examples of successful civil engineering studies that utilized the fuzzy sets theory include the uncertainty analyses in water pipeline networks [3, 4], structural engineering [5, 6] and geotechnical engineering [7].

2. Methodology

The uncertainties in the inputs can influence the estimated suction caisson uplift capacity. For the reliable design, analysis of the possible uncertainties and their influence on the uplift capacity is necessary. In this paper, the uncertainty analysis of the suction caisson uplift capacity is done based on the Fuzzy sets theory using fuzzy numbers.

First, the uplift capacity of the suction caisson is estimated using the various approaches without consideration of uncertainty of input parameters. Then the suction caisson uplift capacity is evaluated considering the input uncertainties using the suggested fuzzy approach. Comparison of the results of different models shows that how the input uncertainties are spread out over their relationships.

3. Data

The governing parameters with considerable influence on the uplift capacity of suction caissons (Q) are shown in Figure 1. The database used in this study consists of the experimental test results reported by Rahman, Wang [8]. This database has been employed in different researches conducted to develop models for predicting the uplift capacity of suction caissons. One recent approach is to employ M5 model tree together with GP (M5-GP) as used by Derakhshani [9] to propose two robust methods (Table 1).

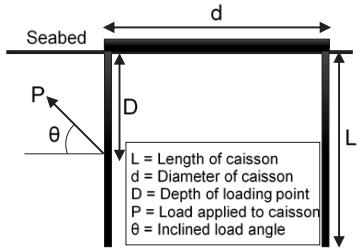

Figure 1. Suction caisson geometry.

Table 1. M5GP models [9].

M5GP1
$for\ S_u \le 12.28 : Q = 1.105 \dfrac{\left(\frac{D}{L}+1\right)\left(\frac{\pi}{2}+\theta\right)^{0.8} S_u^{0.9}}{T_k^{0.1}}$
$for\ S_u > 12.28 : Q = 0.083 \dfrac{\left(\frac{D}{L}+1\right)^{3.7}\left(\frac{\pi}{2}+\theta\right)^{2.9} S_u^{1.6}}{\left(\frac{L}{d}\right)^{0.2}(10^5 T_k)^{13.1}}$
M5GP2
$for\ S_u \le 12.28 :$ $Q = 0.272 \dfrac{\left(\frac{\pi}{2}+\theta\right)^{1.2} S_u}{T_k^{0.1}} \exp\left[1.2\left(\frac{D}{L}+1\right) + 2.23T_k - 0.0004S_u^2 \exp\left(\frac{L}{d}\right)\right.$
$for\ S_u > 12.28 :$ $Q = 11.964 \dfrac{\left(\frac{D}{L}+1\right)^{0.2}\left(\frac{\pi}{2}+\theta\right)^{4.1}(10^5 T_k)^{1.4}}{\left(\frac{L}{d}\right)^{1.6} S_u^{2.8}} \exp\left[0.36\left(\frac{L}{d}\right) + 0.18S_u + 1.69\exp\left(\left(\frac{L}{d}\right)\Big/\left(\frac{\pi}{2}+\theta\right)\right)\right.$

4. Results and Discussion

Membership functions of M5GP models for CC and RMSE statistical measures are provided in Figure 2. Based on the results given in this Figure, it can be found that although the performance of the two M5GP models is good regarding the crisp (most likely) values, the responses are vulnerable to the input uncertainties.

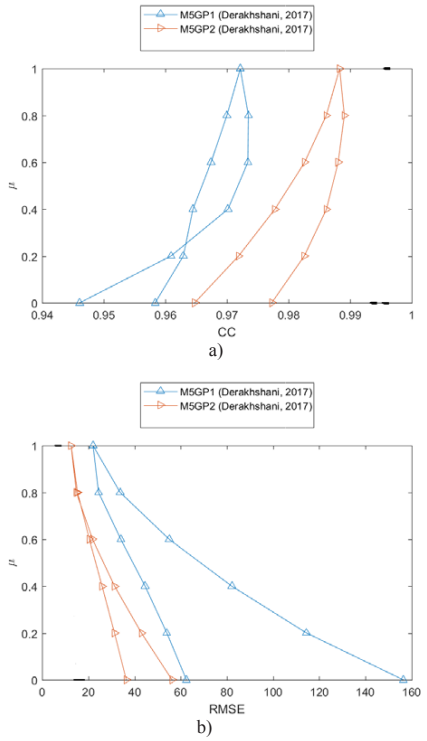

Figure 2. Membership functions of M5GP models: a) CC, b) RMSE.

5. Conclusions

Among different prediction models recommended for the uplift capacity of suction caissons, the recent hybrid M5GP models were investigated regarding the influence of input uncertainties. Reliability of the predictions made by these two methods was evaluated and compared by the fuzzy statistical indices including correlation coefficient (CC) and root mean squared error (RMSE). It is inferred that, although these models are remarkably accurate, they may be vulnerable to uncertainties of predictors.

6. References

[1] Verhoosel CV, Scholcz TP, Hulshoff SJ, Gutiérrez MA. Uncertainty and reliability analysis of fluid-structure stability boundaries. AIAA Journal. 2009;47:91-104.

[2] Liu Q, Rao SS. Fuzzy finite element approach for analysis of fiber-reinforced laminated composite beams. AIAA journal. 2005;43:651-61.

[3] Haghighi A, Asl AZ. Uncertainty analysis of water supply networks using the fuzzy set theory and NSGA-II. Engineering Applications of Artificial Intelligence. 2014;32:270-82.

[4] Sabzkouhi AM, Haghighi A. Uncertainty Analysis of Pipe-Network Hydraulics Using a Many-Objective Particle Swarm Optimization. Journal of Hydraulic Engineering. 2016;142:04016030.

[5] Valdebenito M, Jensen H, Beer M, Pérez C. Approximation concepts for fuzzy structural analysis. Vulnerability, Uncertainty, and Risk: Quantification, Mitigation, and Management2014. p. 135-44.

[6] Haghighi A, Ayati AH. Stability analysis of gravity dams under uncertainty using the fuzzy sets theory and a many-objective GA. Journal of Intelligent & Fuzzy Systems. 2016;30:1857-68.

[7] Cheng M-Y, Tsai H-C, Ko C-H, Chang W-T. Evolutionary fuzzy neural inference system for decision making in geotechnical engineering. Journal of Computing in Civil Engineering. 2008;22:272-80.

[8] Rahman MS, Wang J, Deng W, Carter JP. A neural network model for the uplift capacity of suction caissons. Computers and Geotechnics. 2001;28:269-87.

[9] Derakhshani A. Estimating uplift capacity of suction caissons in soft clay: A hybrid computational approach based on model tree and GP. Ocean Engineering. 2017;146:1-8.

CHALLENGES OF GAS EXPORT PIPELINE PROJECTS

Maryam Sarajian[1] and Mohammad Reza Bahaari[2]

1) School of Civil Engineering, University of Tehran, Tehran, Iran, maryam.sarajian@ut.ac.ir
2) School of Civil Engineering, University of Tehran, Tehran, Iran, mbahari@ut.ac.ir

1. Introduction

In the following research, gas challenges and solutions adopted for gas export pipelines will be studied . In recent decades, many successful projects such as Nord Stream, South Stream, Langeled and Trans-Mediterranean pipelines have been constructed, include lots of creative ideas. Many of those can be implemented in similar projects.

Gas exports to Oman and India are expected to be implemented in coming years. So it would be beneficial to become familiar with experiences of similar projects because future projects may encounter these obstacles too. For instance, in the Nord Stream pipeline, which transports the natural gas from Russia to Germany, existing cables and pipelines, munitions dump, cultural heritage, fishing activities, logistic and shipwreck sites were constraints which have been solved with creative ideas and solutions.

At the present time, more than 50 percent of world's energy consumption is oil and gas (Figure 1). Disparity between consumption and domestic production, makes oil and gas trading more important, for example, about 60 percent of proven gas reserves are in Russia and the Middle East while the European Union's share is just 0.7 percent [1].

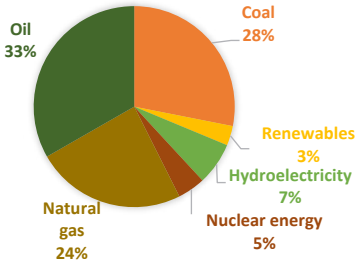

Figure 1. Distribution of world's energy consumption in 2016 [1].

A continuing increase in the demand for natural gas within the EU is expected, coupled with a decline in the EU's own productive capacity and reserves. As a consequence, imports will supply a greater share of total EU consumption. Natural gas import requirements are expected to rise from 314 bcm (billion cubic meters) per annum, corresponding to 58 percent of total demand, in 2005 to 509 bcm, corresponding to 81 percent of total demand, in 2025 [2].

On the other hand, a country like Iran has 18 percent of world's natural gas reserves, as Figure 2 illustrates only small amount of these reserves have been consumed. With the big advantage of being located close the EU and having the large natural gas reserves, Iran can provide a significant proportion of the EU's gas imports. Also due to Iran's geographical location, proximity to markets and the dependency of Iran's budget on oil and gas export earnings, a further increase in exporting is expected.

Usually, the natural gas is transported in a form of gas (NG) through pipelines or in a form of liquefied natural gas (LNG) by specially designed ships. Small amounts of natural gas are also exported on trucks as LNG and as compressed natural gas (CNG) [3], see Figure 3.

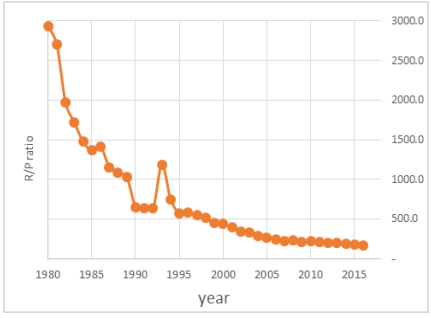

Figure 2. Iran's reserves to production (R/P) ratios [1].

So far, Iran does not have the infrastructure to export or import liquefied natural gas (LNG) [4]. The most natural gas transported via pipeline is sweet and less corrosive.

Exports or imports through transmission pipelines have distinct advantages in terms of carbon dioxide emissions, traffic and energy efficiency compared to LNG transports [2]. Also LNG transports need infrastructures such as LNG ports and regasification terminals. From an economical

point of view, transmission pipeline systems could be more efficient than LNG transports. There are many factors in the choice of the exporting medium and methods. These factors are specified at the conceptual design stage.

If the pipelines pass through the seas or oceans, special methods and economic considerations must be taken.

Investment, type of contracts, political conflicts, route and diameter selection, environmental concerns, seabed conditions, national and international legislation etc., are some issues that can cause difficulties.

Generally, the aforementioned challenges can be divided into four groups: management, engineering, installation and operation.

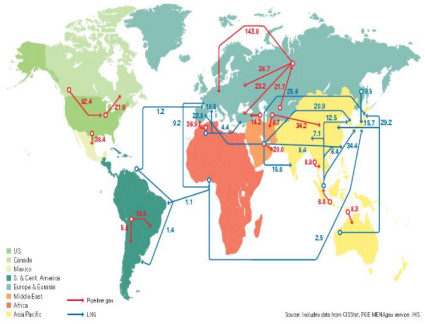

Figure 3. Major trade movements in 2016 (billion cubic meters) [1].

1.1. Iran-Oman Gas Pipeline Project

Based on an agreement signed in 2013, Iran will export 28 million cubic meters of gas to Oman per day via a subsea pipeline through Persian Gulf for 15 year period.

The length of the subsea pipeline will be approximately 200 kilometers with 36 inches diameter. It can be expected that the aforementioned project will be commissioned by 2020 [5]. Some of the Iranian gas volumes will be exported as LNG from Oman and the remaining gas will be used for Oman's domestically demand [4, 5].

The pipeline route will establish a direct link between Iran and Oman besides it will not pass through another country's waters. By achieving this purpose, the length will be shorter, although the pipeline should be laid in deeper sector [5].

Type of contracts, financing and procurement, owner and operator of the pipeline system, maintenance and repair systems are main challenges of this project. For instance, is it possible for the other gas purchasers to rent this pipeline for transporting gas?

1.2. Iran-India Gas Pipeline Project

The aim of the project is to supply gas from Iran to India. Indirect route from Iran to Oman then from Oman to India instead of the direct route from Iran to India is an alternative option [Figure 4]. The estimated length of pipeline is around 1300-1400 km. Maximum water depth will be 3600 meters [6].

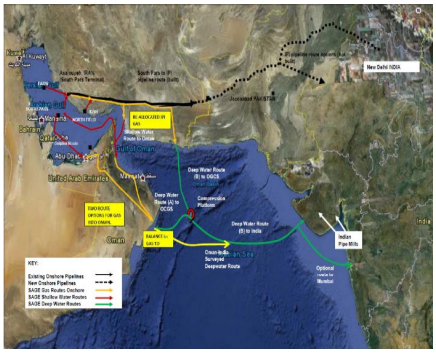

Figure 4. Potential pipeline routes to supply gas to India [6].

2. Conclusions

Megaprojects face immense technical, legal, political, economic, and social challenges and sometimes require innovative solutions to mitigate environmental risk. For instance, lack of technology, expertise or facilities is one of the limitation. To overcome this challenge, indigenous infrastructure must be upgraded or borrowed. The shareholders, foreign investors or bank loans can finance project cost. An extensive and transparent communication strategy must be adopted to achieve agreement on political and legal issues. Finally, the potential impact of the project must be evaluated to avoid possible negative effects on the environment.

3. References

[1] British Petroleum, "Statistical Review of World Energy", June 2017.

[2] Nord Stream AG, "Information about Nord Stream", Espoo Report, February 2009, pp. 21-54.

[3] U.S. Energy Information Administration, 2017, "Natural gas imports and exports", https://www.eia.gov/energyexplained/index.php?page=natural_gas_imports, May 22, 2018.

[4] U.S. Energy Information Administration, 2017, "Country analysis brief: Iran", https://www.eia.gov/beta/international/analysis.cfm?iso=IRN, May 22, 2018.

[5] PetroEnergy Information Network (shana), 2017, "Iran, Oman gas pipeline project operational by 2020", https://www.shana.ir/en/newsagency/275624/Iran-Oman-Gas Pipeline-Project-Operational-by-2020-Official, May 22, 2018.

[6] Nash, I. F. J., Roberts, P. M., "MEIDP - the Deep Sea Gas Route to India", *Offshore Technology Conference,* Texas, USA, May 2-5 2011.

PIPE/SOIL INTERACTION EFFECT ON THERMO-MECHANICAL RESPONSE OF SUBSEA PIPELINES

Iman Seyfipour[1] and Mohammad Reza Bahaari[2]

1) PhD candidate, School of Civil Engineering, College of Engineering, University of Tehran, Tehran, Iran
(Currently Sabbatical Researcher, Centre for Offshore Foundation Systems (COFS), UWA, Australia)
2) Professor, School of Civil Engineering, College of Engineering, University of Tehran, Tehran, Iran
Iman_seyfipour@ut.ac.ir

1. Introduction

Offshore pipelines are typically designed to operate in high pressure and high temperature loading conditions. Operational loads potentially lead to pipe expansion, whereas seabed resistance force act to resist pipeline movement. Lateral deflection of exposed pipelines subject to high axial loads is known as "lateral buckling" phenomena. Well-ordered deformation can be a challenge during the design phase and uncontrolled movements may result in structural integrity problems and catastrophic failure [1]. Thermo-mechanical behavior strongly depends on pipe-soil interaction [2].

Influence of various assumptions for pipe-soil interaction models on lateral buckling performance is investigated in this paper.

2. FEM

A series of FE analyses in ABAQUS software is utilized for investigating pipeline response in different conditions. Deformable pipe element (PIPE1H) is used for modeling the pipe over an analytical rigid seabed. Gravity load and internal pressure loads are applied to the pipeline. Consequently, cyclic thermal loads are added for seven shut-down and start-up conditions. The project characteristics is presented in Table 1.

Table 1. Case study information.

Modeling Parameters	Unit	Value
Pipeline Outer Diameter (OD)	in	14
Pipeline Wall Thickness (WT)	mm	19.8
Pipeline Total Length	km	4.881
Maximum Operating Temperature	oC	120
Seabed Ambient Temperature	oC	12
Maximum Operating Pressure	bar	200
Pipeline Material Modulus	MPa	205,000
Coefficient of Thermal Expansion	1/°C	1.3 ×105
Pipe-Soil Axial Friction	-	0.5
Pipe-Soil Lateral Friction	-	0.5

A practical initial curvature patented by Statoil [3] is utilized in this paper for creating three initial imperfections with equal intervals along the pipe. Initial strain equal to 0.2% is considered at each imperfection location as result of residual curvature from reel-laying installation operation [4].

3. Pipe-soil Interaction Models

Uncoupled axial and lateral friction model besides coulombic friction are used in this paper for pipe-soil interaction response. Considered PSI models represent a lightweight pipeline response. Failure surface illustrated in Figure 1 based on lateral and axial friction and normal force on the pipe-soil interface. "Friction model" shows a rectangular face which means distinct values of fiction in axial and lateral directions are specified during the simulation. This "Friction model" model is defined via a friction subroutine in ABAQUS software [5,6]. On the other hand, "Coulomb model" shows the situation that resultant vector of friction is calculated based on two lateral and axial forces and friction coefficient is considered the resultant slip of the pipe on seabed [5]. Coulomb friction assumption has been used widely for lateral buckling analyses [6]. Failure surface for "coulomb model" is presented in an oval shape that is the default response in ABAQUS software [7].

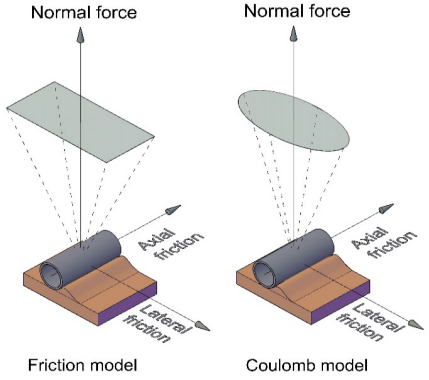

Figure 1. Failure surface of pipe-soil interaction.

Figure 2 shows four typical models for seabed resistance force. The elasto-plastic interaction model is

considered for axial friction (Friction model 2). Nonetheless, lateral restriction force can be different. Soil berms during the lateral deformation may generate different brittle breakout. So, all four possible behaviors are assumed for lateral response. Besides, one model with coulombic friction (Figure 1) is provided. Lateral buckling response is compared for these five situations in following parts of this paper.

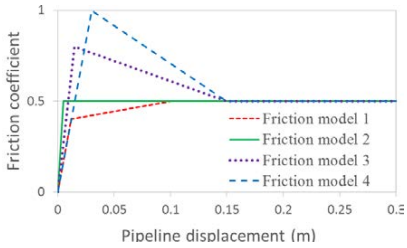

Figure 2. Friction coefficient versus displacement.

4. Results

Effect of different models of lateral buckling response was investigated in diverse analyses. Lateral deflection of the pipeline at the middle point is shown in Figure 3 as an example for comparing friction models. These lateral deflections demonstrate the situation that the buckle occurred at the middle section of the pipeline. Buckled pipe in "Friction model" represents sharper configuration which is a more realistic model [8]. The maximum stress value occurred at the crown of the buckled zone. Lateral displacement value governs final curvature and induced stress on the pipeline section.

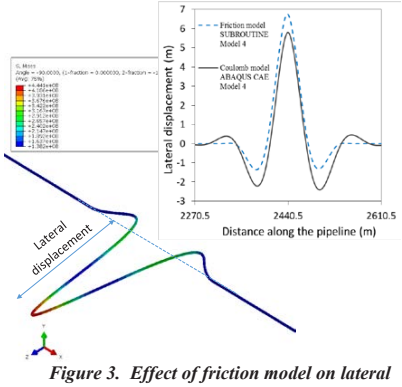

Figure 3. Effect of friction model on lateral buckling response.

A number of shut-down and start-up cycles may happen through the system lifetime for repair purposes. Lateral deflection at the midline section is presented in Figure 4 during seven cycles of start-ups and shut-downs. Lateral displacement increases during each heat-up and decrease in each cool-down. Maximum displacement in each cycle occurred at full heat-up condition (operation phase). The growth of maximum lateral deflection is observed in subsequent cycles because of changes in initial curvature after each cycle. Almost equivalent response is detected for four friction models. However, coulomb friction model represent lower range of lateral displacements.

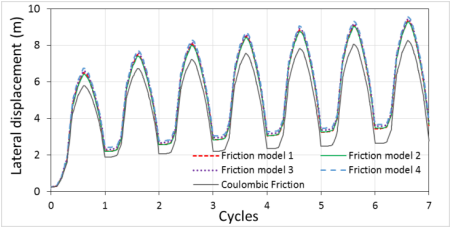

Figure 4. Effect of friction during 7 loading cycles.

5. Conclusion

The extreme lateral deflection of "Friction model" option is about 1.16 times larger than "Coulomb model" for the case study presented in this paper.

The buckle shape for "Friction model" option is happened in mode 3; however, it is occurred in mode 5 for "Coulomb model" case.

Nearly 49% buckle dimension development is observed after seven cycles of start-up and shut-down cycles.

Based on presented results for "Friction model" 1 to 4, it can be grasped that brittle breakout and elastic slip values have a minor influence on the final size and configuration of the buckled pipe (about 5.3%).

6. References

[1] Palmer AC, King RA. Subsea Pipeline Engineering: PennWell Corporation; 2008.
[2] RANDOLPH MF, WHITE DJ, YAN Y. Modelling the axial soil resistance on deep-water pipelines. Géotechnique. 2012;62:837-46.
[3] Endal G. Method for pipelaying from a coil to the sea bed, controlling thermal expansion. Google Patents; 2005.
[4] Cooper P, Zhao T, Kortekaas F. Residual Curvature Method for Lateral Buckling of Deepwater Flowlines. OPT, March. 2017;1.
[5] White DJ, Cheuk CY. Modelling the soil resistance on seabed pipelines during large cycles of lateral movement. Marine Structures. 2008;21:59-79.
[6] Bruton D, White D, Cheuk C, Bolton M, Carr M. Pipe/Soil Interaction Behavior During Lateral Buckling, Including Large-Amplitude Cyclic Displacement Tests by the Safebuck JIP. Offshore Technology Conference. Houston, Texas, USA: Offshore Technology Conference; 2006.
[7] Abaqus V. 6.14 Documentation. Dassault Systemes Simulia Corporation. 2014.
[8] Chee J, Walker A, White D. Controlling lateral buckling of subsea pipeline with sinusoidal shape pre-deformation. Ocean Engineering. 2018;151:170-90.

INSTALLATION ANALYSIS OF PIPELINES IN SAKO DESALINATION PLANT

Atena Amiri[1,2], Farhad Darabinia[2] and Aliasghar Golshani[2,3]

1) Ph.D. Student, Dept. of Civil Eng., Tehran Univ., Tehran, Iran, amiri.atena.646@gmail.com
2) FDA Consultants, Tehran, Iran, f.darabi@faradarya.com
3) Lecturer, Dept. of Civil Eng., Tehran Azad Univ., Central Branch, Tehran, Iran, ali.golshani@iauctb.ac.ir

1. Introduction

Desalination plants create drinkable freshwater from ocean water in areas where there are not sufficient supplies of freshwater.

Subsea pipelines are considered to be the most efficient and economical way to transport liquids from offshore to land or other areas. Loads on a marine pipelines can be divided into the categories: functional, environmental, accidental and installation loads [1]. A marine pipeline is exposed to different loads during installation such as tension, bending, and high external hydrostatic pressures which are becoming greater problems in increasing water depths. Pipeline installation process of SAKO desalination plant is numerically analyzed in this paper using OrcaFlex software.

2. SAKO Project Overview

SAKO plant is a power and desalination complex located in the Northern coast of Persian Gulf, Bandar Abbas, Iran. The project consists of desalination units with total capacity of 1,000,000 m3/day freshwater and a power plant rated at 1000MW. Approximate location of the project is shown in Figure 1.

Figure 1. Approximate location of SAKO project.

This project is consists of 6 intake pipelines and 3 outfall pipelines. The internal diameter of pipeline is 2.5 meter. Other characteristics of the pipeline are introduced in Table 1.

Table 1. Pipeline characteristics.

Material type	High Density Polyethylene
Grade	PE100
Profile No.	SM530, SM550, SM515
Wall Thickness	78, 87, 126 mm

3. Pipeline Installation Method

Pipeline installation is one of the important stages of offshore field development. The choice of installation method is influenced by the water depth, pipeline type and material, time and cost among other things. There are four major pipeline installation methods: S-Lay, J-Lay, Reel Lay, Towing [2].

Here the surface towing method is used (Figure 2). In towing lay, the pipe is made up at some remote location onshore, transported to the offshore installation site by towing, and layed down. The buoyancy of the pipe is selected and designed to verify that a controlled-depth towing can be performed [3].

Figure 2. General View of Pipe String Towing Route.

In the present project, guide piles are employed to anchor pipe strings against environmental loads during positioning and installation procedure as well as providing a directional route; then by gradual penetration of seawater inside the pipes, pipes become immersed and finally lay on the sea bed.

4. Numerical Modelling

Numerical modeling was performed using OrcaFlex software. OrcaFlex is a fully 3D non-linear time domain finite element. A lumped mass element is used which greatly simplifies the mathematical formulation and allows quick and efficient development of the program to include additional force terms and constraints on the system in response to new engineering requirements [4].

According to the met-ocean study of the area, significant wave height of 0.5 m, wave period of 4 sec and current speed of 1.2 m/s were considered for pipeline's installation period. The maximum modelling depth was assumed to be 19.14 m relative to MSL.

Model includes a string with length of 300 m which is linked to a tugboat. Several airbags are installed on the pipe to control the stresses occurring during installation process and Guide piles are used with spacing of 45m (Figure 3).

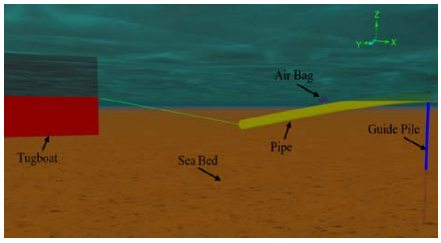

Figure 3. Modeling items

This procedure is modeled for all three types of cross-section and results are mentioned in Table 2.

Table 2. Results of three types of cross-section.

Profile type	Length (m)	Max depth (m)	Max von mises stress (MPa)
SM515	130	9.05	7.4
SM550	300	17.23	8.38
SM530	300	19.14	9.4

The installation process is presented in the Figure 4 in several time steps during installation.

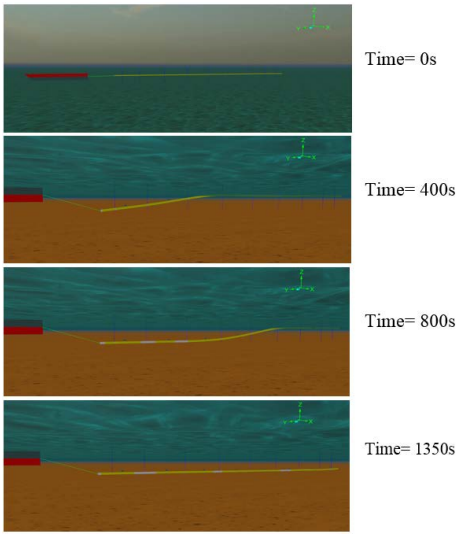

Figure 4. Modeling results in different time steps

5. Conclusions

1- OrcaFlex software is capable of modeling of marine environmental conditions such as wave and current loads.
2- In this study, sea water gradually flows inside the pipelines causing them to move from sea surface to sea bed which is similar to what happens in reality during installation process.
3- Pipeline's structural specifications are also reasonably modeled.
4- The bed slope is also modeled.
5- Modeling results showed that there will be maximum stress of 9.4 MPa in the pipelines.
6- Airbags and guide piles were modeled as well to control the installation process.

6. References

[1] Mikael, W. B., Andersen, J B., Andersen, L W., Bryndum, M., Christensen, C J., Nielsen, N J R., "Design and Installation of Marine Pipelines ", Blackwell Science, 2005.

[2] Subramanian, S., *Analysis and Optimization of Rigid Pipeline Installation with Inline Structure*, Stavanger University, Master Thesis, 2013.

[3] Bai, Q., Bai, Y., "Subsea Pipeline Design, Analysis, and Installation ", Elsevier, 2014.

[4] OrcaFlex User Manual, Version 9.4a. Cumbria, UK. Orcina, 2011.

REDUCING HEAVE RESPONSE AMPLITUDE OPERATOR OF A SEMI-SUBMERSIBLE PLATFORM USING PORO-ELASTIC PLATES

Arefe Emami[1] and Ahmad Reza Mostafa Gharabaghi[2]

1) Faculty of Civil Engineering, Sahand University of Technology, Tabriz, Iran, a_emami@sut.ac.ir
2) Faculty of Civil Engineering, Sahand University of Technology, Tabriz, Iran, mgharabaghi@sut.ac.ir

1. Introduction

In this paper, the attempt has been made to analytically solve the coupling problem of a monochromatic linear wave with a semi-submersible platform which is modified by attaching Poro-Elastic Plates (PEPs) at the bottom of its pontoons. The PEP is considered to be homogenous, isotropic and saturated. The region around the semi-sub is divided into different parts and their related governing equations with appropriate boundary conditions (BC's) are developed. By applying Eigenfunction Expansion Method (EEM), these equations with their related BC's for each region are solved numerically. In order to verify the developed model, it is applied to a typical GVA4000 semi-submersible drilling rig and its heave Response Amplitude Operator (RAO) is extracted and compared with available experimental data. Furthermore, the PEP is attached to the rig and its heave RAO is estimated and compared with the original case. It is concluded that using PEP reduces the peak value of the heave motion response as well as the resonance frequency. Therefore, it can be a suitable method in order to improve the performance of a semi-submersible platform particularly its heave motion response.

2. Semi-Submersible Platform with Poro-Elastic Plate

A Semi-submersible drilling platform is a floating mobile offshore drilling unit (MODU) which is designed for drilling in water depths beyond the capacity of jack up drilling rigs. They are typically made from two submerged pontoons with four or more columns connecting the pontoons to the hull. One of the main problems of semi-submersible drilling rigs is their heave motion response which can often restrict their operability range or even lead to damage to their risers and mooring systems. There are several attempts in order to reduce the heave motion response of these platforms which can be categorized to the modification of their geometry, increasing their draft, installing heave plates or using truss type columns. As a new concept, in this study, the PEPs are attached to the lower part of rig's pontoons in order to reduce its heave motion response. The PEP is a type of flexible material which can deform due to the fluid flow through its porous structure. The interaction between fluid flow and linear porous material deformation was originally proposed by Biot (1941) [1]. In literature, such material was used for some type of submerged structures. Lan and Lee (2010), Lan et al. (2011, 2012, 2014), and Lan and Hsu (2014) analytically studied the interaction of waves with submerged breakwaters made from poro-elastic material [2-6].

3. Mathematical Equations

In this study, a typical GVA4000 drilling semi-submersible rig was modified by a layer of PEP at the bottom of its pontoons. The rig is assumed to be located at water depth of h_1 under a monochromatic small amplitude wave train propagating in the +x direction (Figure 1). It is assumed that the fluid is incompressible, homogeneous, inviscid and poro-elastic martial is homogeneous, isotropic and saturated. It is necessary to calculate the exciting forces, added mass, damping coefficient and stiffness in order to determine the modified rig's heave motion RAO. The exciting force can be determined by using incident and radiated wave potentials. The added mass and damping coefficient are calculated by radiated wave potential. The incident wave potential is obtained with assuming the harmonic wave in the absence of platform and with the aid of the Laplace equation (Eq. 1) [7]:

$$\Phi_I = -i\frac{Ag}{\omega}\frac{\cosh\left(k(z+h_1)\right)}{\cosh(kh_1)}\exp(ikx) \qquad (1)$$

The radiation potential is obtained by assuming the oscillation of the structure in the absence of waves [7]. As shown in Figure 1, the domain around the rig is divided into five separate regions. Each region has its own governing equations with appropriate BC's. The governing equation for Regions I, II-1, III and IV is Laplace equation which can be solved by satisfying the relative dynamic and kinematic boundary conditions which are consisted of the free surface, sea bed and the normal velocity over the structure BC's. The governing equations for Region II-2 are the continuity and momentum equations for the PEP. The continuity equation can be written based on Verruijt's equation [8] and the momentum equations for PEP can be obtained by Biot's theory [9]. These equations should be solved simultaneously in order to satisfy the interface boundary conditions between two adjacent regions. The unknown coefficients are derived by using EEM and with the aid of the continuity conditions for pressure, normal velocity and other boundary conditions that are illustrated in Figure 1. Finally, they are solved by the LU decomposition method.

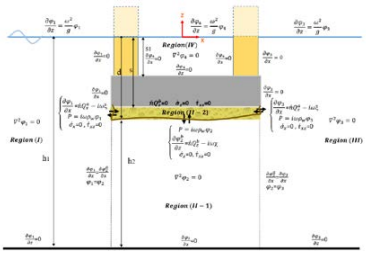

Figure 1. Definition sketch of the semi-submersible platform modified by PEP with its surrounded regions and related governing equations and boundary conditions.

4. Verification of the Developed Model

In order to verify the developed analytical model, the results obtained for the RAO of heave motion of a GVA4000 drilling semi-submersible platform without PEP is compared with the experimental data [10]. The input parameters are a=40.28m, s=20.5m, s_1=13m, l=20.91m and h_1=1000m. As shown in Figure 2, the results of experimental data and analytical method are close enough to be considered acceptable.

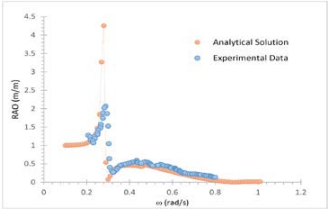

Figure 2. The comparison of the experimental results obtained for the RAO of heave motion of a GVA4000 drilling semi-submersible platform with analytical solution.

5. Results

In the next step, the PEPs are attached at the bottom of GVA4000's pontoons in order to study its effect on the heave motion response. The input parameters of PEPs are the PEP's porosity=0.4, PEP's Poisson ration=0.333, fluid kinematic viscosity=1.12×10^{-9} (m^2/s), fluid pore compression=4.35×10^{-10}, turbulent drag coefficient=0.2, added mass coefficient=0.015, elastic solid density=2650 (kg/m^3), fluid density=1000 (kg/m^3), PEP's thickness= 0.5 (m), shear module=5×10^6 (N/m^2), and intrinsic permeability= 2.28×10^{-6} (m^2).

The convergence is satisfied by applying 20 modes in EEM. Then, the heave RAO is calculated and compared with the original case in Figure 3. It is noticed that the heave motion response of the modified semi- submersible platform reduced significantly after installing the PEPs.

6. Conclusion

The main objective of the present study was to investigate an approach for reducing the heave motion response of the semi-submersible platform. Therefore, the PEPs are installed at the bottom of its pontoons. The EEM was used to solve the governing equations with related BC's. Results showed that the heave motion response of the modified semi-submersible decreased significantly compared to its original case. Indeed, the PEPs not only reduced the resonance amplitude but also the resonant frequency displaced to the lower frequency. This research offers an applicable way for reducing heave motion response of a semi-submersible platform with easy installation on the all semi-submersible platforms even in operation.

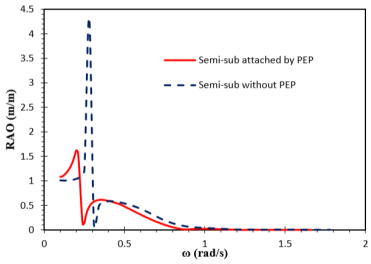

Figure 3. The comparison of the heave RAO of semi-submersible platform with / without PEPs.

7. References

[1]Biot, M. A., "General Theory of Three-Dimensional Consolidation". Journal of Applied Physics. **12** (2). 1941, pp. 155–164.

[2] Lan, Y.J., and Lee, J.F., "On waves propagating over a submerged poro-elastic structure", Ocean Engineering, No (37), 2010, pp. 705-717.

[3] Lan, Y.J., Hsu, T.W., Lai, J.W., Chang, C.C., and Ting, C.H., "Bragg scattering of waves propagating over a series of poro-elastic submerged breakwaters", Wave Motion, No (48), 2011, pp. 1-12.

[4] Lan, Y. J., Hsu, T. W., and Ching, Y. Ch., "Analysis of wave interaction with submerged adjacent poro-elastic breakwaters", Coastal Engineering, No (33), 2012, pp. 2156-1028.

[5] Lan, Y. J., Hsu, T. W., and Liu, Y. R., "Mathematical study on wave interaction with a composite poroelastic submerged breakwater", Wave motion, 8, 2014, pp. 1799-1816.

[6] Lan, Y. J., and Hsu, T. W., "Analytical solution for Wave Interaction with Stack-type Double-layer Composite Poroelastic", Applied Mathematical Sciences, 51, pp. 2014, 1055-1070.

[7]Linton, C. M. and McIver, P., "Handbook of mathematical techniques for wave/structure interactions", CRC Press, 2001.

[8] Verruijt, A., "Elastic Storage of Aquifers. Flow through Porous Media", edited by De Wiest, R.J.M., Academic, New York, 1969, pp. 331-376.

[9] Biot, M.A., "Theory of propagation elastic waves in a fluid saturated porous solid. I. low frequency range", The Journal of the Acoustical Society of America, 28(2), 1956, pp.168-178.

[10] Clauss, G. F., Schmittner, C., and Stutz, K., "Time-domain investigation of a semisubmersible in rogue waves" ASME 2002 21st International Conference on Offshore Mechanics and Arctic Engineering, American Society of Mechanical Engineers, 2002.

INTERACTION JACKED AND RISER IN THE FATIGUE DAMAGE OF THE RISER USING TIME HISTORY ANALYSIS METHOD

Hamid Anbarestani[1] and Naser Shabakhty[2]

1) MSc, Department of Marine industry, Science and research branch, Islamic Azad University; Tehran, Iran, hamid.anbarestani70@gmail.com
2) Assistant professor, School of Civil Engineering, Iran University of Science and Technology; shabakhty@iust.ac.ir

1. Introduction

The life of the offshore platform under fatigue damage is estimated using the time history of the structural stress [1]. This research was conducted on the basis of the API code for one of the platforms installed in the South Pars region. The result shows, fatigue damage is an important failure mode for riser and it may effect on the lifetime of riser.

2. Sea State Scatter Diagram

Fatigue damages in riser are combination of damage arise from several sea states and incorporating all these sea states are time consuming task in the time history analysis. Therefore, sea state scatter diagram should be divided into several blocks which each one is concentrated in the center of block to reduce the fatigue analysis time... To calculate the wave height and period for center of this block, the weighted average method is used. Therefore, for wave height the following equation,

$$H_S = \frac{\sum H_{si} \times N_i}{\sum N_i}$$

and the following expression can be used for wave period.

$$T_P = \frac{\sum Tp_i * N_i}{\sum N_i}$$

Where in these equations N_i is the number of occurrence of sea state considered in each block. The scatter diagram is divided to four block and wave heights and periods are estimated and shown in Table 1.

Table 1. Sea state in fatigue analysis

sea-state	Hs	Tp	Pi
Block1	0.67	2.7	0.315
Block2	1.1	4.56	0.49
Block3	1.25	6.25	0.114
Block4	2.7	8.6	0.079

According to the centeral sea states, we obtained the hydrodynamic forces on the riser for 20 minutes and axial and flexural stresses for in-plane and out-off plane (σ_{ipb} and σ_{opb}) are estimate for eight points around intersection of the riser. Hot Spot stress is estimated by incorporating the stress concentration factor (SCF) for each component by the following expression.

$$\sigma_{HS} = \sigma_a * SCF_a + \sigma_{ipb} * SCF_{ipb} + \sigma_{opb} * SCF_{opb}$$

This hot spot stress should be considered for at least 8 points around intersection of riser, to determine the highest point that fatigue damage may occurs.

1) $\sigma_1 = SCF_A \sigma_X + SCF_{MIP} \sigma_{My}$
2) $\sigma_2 = 0.5\ SCF_A \sigma_X + 0.5\sqrt{2}\ SCF_{MIP} \sigma_{My} - 0.5\sqrt{2}\ SCF_{MOP} \sigma_{Mz}$
3) $\sigma_3 = SCF_A \sigma_X - SCF_{MOP} \sigma_{Mz}$
4) $\sigma_4 = 0.5\ SCF_A \sigma_X - 0.5\sqrt{2}\ SCF_{MIP} \sigma_{My} - 0.5\sqrt{2}\ SCF_{MOP} \sigma_{Mz}$
5) $\sigma_5 = SCF_A \sigma_X - SCF_{MIP} \sigma_{My}$
6) $\sigma_6 = 0.5\ SCF_A \sigma_X - 0.5\sqrt{2}\ SCF_{MIP} \sigma_{My} + 0.5\sqrt{2}\ SCF_{MOP} \sigma_{Mz}$
7) $\sigma_7 = SCF_A \sigma_X + SCF_{MOP} \sigma_{Mz}$
8) $\sigma_8 = 0.5\ SCF_A \sigma_X + 0.5\sqrt{2}\ SCF_{MIP} \sigma_{My} + 0.5\sqrt{2}\ SCF_{MOP} \sigma_{Mz}$

3. Riser Fatigue Estimation

To estimate the fatigue damage, we should determine the number of stress cycle. We used rain-flow counting method and the final fatigue damage is calculated by the Palmgren-Miner method by the following equation,

$$D_{FAT} = \sum_{i=1}^{Mc} \frac{ni}{Ni} * Pi \leq 1$$

Where, n_i is the number of stress cycle in riser, N_i is the number of stress cycles to failure which is derived from API Regulations. The total damage should be less than one to prevent fatigue failure. Howerever, this damge should be divided to the safety factor recommended in this regulation. Figure 1 shows the recommended stress number to failure N_i in API [2]. This stress number to failure can be shown by the following equation:

$$N(s) = 2\times10^6 \times \left(\frac{\Delta\sigma}{\Delta\sigma ref}\right)^{-m}$$

$\Delta\sigma$ is existing stress range in riser and $\Delta_{\sigma ref}$ shows the reference stress range given by codes and, m is the slope of S-N curve given in API code.

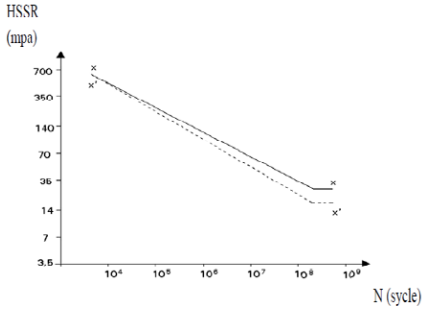

Figure 1. S-N curve given in API code [2]

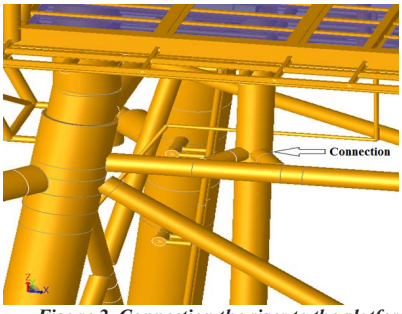

Figure 2. Connection the riser to the platform

Table 2. Three initial period of the structure in the first model without riser-platform interaction

MODE	1	2	3
FREQ	0.546961	0.586158	0.801797
PERIOD	1.828285	1.706024	1.247198

Table 3. Three initial period of the structure in the second model with riser-platform interaction

MODE	1	2	3
FREQ	3.957124	4.956002	5.230491
PERIOD	0.252709	0.201776	0.191187

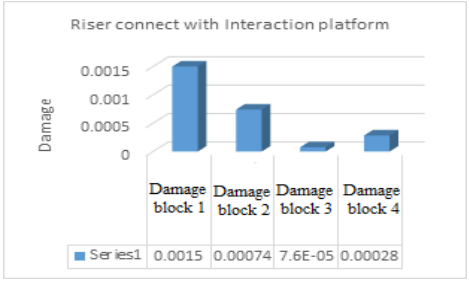

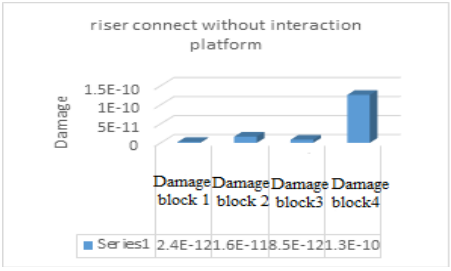

Figure 4. Fatigue damage in riser without riser-platform interaction

4. Conclusion Summary

Comparing and examining of two riser and platform interaction models, it shows when the stiffness of platform increase to ignore the riser-platform interaction, the period of the structure decreases, By reducing the period of the structure, the vibration impacts on riser reduced, so the fatigue life of the riser increases. Therefore, for fatigue riser evaluation, interaction of platform and riser is an important issue and should be taken into account.

5. References

[1] Hamid Anbarestani, "Fatigue Damage Analysis of Fixed Platforms Risers",MSc thesis, Faculty of Marine Science and Technology, Department of Marine Industries, Science and Research branch, Islamic Azad University, Autumn, 2017.

[2] API (2007). API RP 2A-WSD, *Recommended Practice for Planning, Designing and Constructing Fixed Offshore Platforms*. 22nd Edition.

COMPARISON BETWEEN CONDITIONAL AND UN-CONDITIONAL FAILURE PROBABILITY OF CORRODED GAS TRANSMISSION PIPELINES CONSIDERING STOCHASTIC PROCESS FOR INTERNAL PROSSURE AND CRACK GROWTH RATE

Mohammad Mahdi Shabani[1], Mohammad Daghigh[2] and Reza Taravati[3]

1) Offshore Structural Engineering, Petroleum University of Technology, Isfahan, Iran, m.shabani@mnc.put.ac.ir
2) Assistant Professor and Ph.D. in Offshore Engineering, Pars Oil and Gas Company (POGC), mdaghigh@gmail.com & daghigh@pogc.ir
3) Technical Inspector, Iran, Iran, reza_taravati@yahoo.com

1. Introduction

Pipelines are the safest and most economical form of natural gas transmission which are remarkable for their efficiency and low cost [1]. Generally, subsea pipelines carry oil and gas products from wellhead to the riser base [2].

According to study of Shabani [3], corrosion is the most deteriorative factor on pipeline health and safety. So identifying and recognizing corrosion and it's resultant are essential and necessary for pipeline integrity management [4]. Shabani et. al present a Stochastic-Based Approach for determining risk of corroded pipelines considering un-conditional form of corrosion attacks.

This paper deals with RA of corroded gas transmission pipelines considering all probable failure modes of corrosion attacks. Reliability level of pipeline is evaluated in three different modes. All pipeline geometrical parameters are modeled as inherent uncertain parameters. Relationship between crack dimension is modeled using correlations. Crack growth rate and internal pressure are modeled using Poisson Square Wave Process and Ferry Borges- Castanheta, respectively, using In-Line Inspection (ILI) and pipe pressure data. Distribution of holes is assessed through pipeline using ILI data. Also, both conditional and un-conditional form of failure modes of corrosion attacks are discussed. Finally, Probability of Failure (POF) for both conditional and un-conditional is determined using importance sampling technique.

2. Reliability Assessment

Non-deterministic approaches are used to evaluate uncertainties in both load and resistance parameters. Reliability of a component can be defined as probability that component meets some specified demands under specific environmental conditions[6]. There are too many methods (techniques) for determining POF. Zhou et. al [5] recommends to use IS technique for reliability assessment of corroded pipelines. IS technique is a modified form of Monte-Carlo sampling method by FORM.

Based on study of Zhou et. al[5], three different failure modes are taken into account in this study which are:

- Small leak
- Large Leak
- Rupture

According to study of Shabani et. al, ASME B31.8 presents the best model for estimating burst capacity of corroded pipelines that is:

$$P_{burst} = 1.1\frac{2*t*SMYS}{D}\left(1-\left(d/t\right)\right) \quad (1)$$

$$for\ \sqrt{0.8\left(\frac{L}{D}\right)^2\left(\frac{D}{t}\right)} \le 4$$

$$P_{burst} = 1.1\frac{2*t*SMYS}{D}\left(\frac{1-\left(2/3\right)\left(d/t\right)}{1-\left(2/3\right)\left(d/t\right)/Q}\right) \quad (2)$$

$$for\ \sqrt{0.8\left(\frac{L}{D}\right)^2\left(\frac{D}{t}\right)} > 4$$

Where d is depth of corroded region and Q is Fulias factor.

3. Methodology

All pipeline parameters are modeled using recommended distribution by Shabani et. al [7]. Based on the ILI data, correlation coefficients and coefficient of variation is determined. As there is no clear pattern for variating pressure and crack growth rate using stochastic processes, and also internal pressure is the most effective factor on reliability level of corroded pipelines. Therefore, internal pressure and crack growth rate are modeled by Ferry Borges and Poisson Square Wave Process, respectively (see Figure 1).

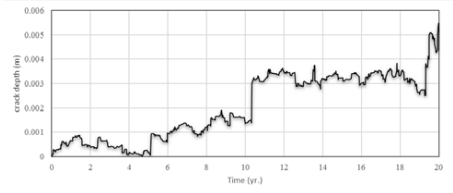

Figure 1. Poisson Square Wave Process model of internal pressure

For figuring out that results are trustable, a criterion should be applied to control failure probability which is converging of results. This paper uses coefficient of variation of calculated failure probabilities. Normally, it set up five percent and for harsh condition it set up two percent; this paper use harsh condition.

Based on studies of Zhou et. al [5] and Shabani et. al [7] definition of conditional and un-conditional form of corrosion attack is such below:

- **Conditional:**

- Small leak: when small leak occurs pipeline doesn't fall in large leak and rupture:

$$g_{SL} \le 0 \bigcap g_{LL} > 0 \bigcap g_{rupture} > 0 \quad (9)$$

- Large leak: pipeline falls in large leak, however pipeline doesn't suffer from rupture and small leak:

$$(g_{SL} > 0 \bigcap g_{LL} \le 0 \bigcap g_{rupture} > 0) \quad (10)$$

- Rupture: pipeline bursting happens while large leak occurred:

$$(g_{SL} > 0 \bigcap g_{LL} \le 0 \bigcap g_{rupture} \le 0) \quad (11)$$

- **Un-Conditional:**

$$P_{rupture\_total} = P_{rupture} + P_{rupture|LL} + P_{rupture|SL} \quad (12)$$

Let assume priority of each failure mode such below:

Figure 2. Procedure of corrosion defect growth

If we neglect interaction between each failure mode (i.e. consider each failure mode independently), then un-conditional form of corrosion attack formula changes to following form:

$$P_{rupture\_total} = P_{rutpure}(\tau) + P_{rupture}(\tau).P_{LL}(\tau) + P_{rupture}(\tau).P_{LL}(\tau)^2.P_{SL}(\tau) \quad (13)$$

4. Results

Using described method, un-conditional POF of the pipeline for different service times is determined and discussed as follows:

Figure 3.a indicates that small leak has no significant impact on pipeline integrity in first ten years, but due to larger POF than target POF its affect should be considered in RBI plan.

Also, Figure 3.b indicates that ASME considers larger in service time in comparison to initial reliability index for the pipeline.

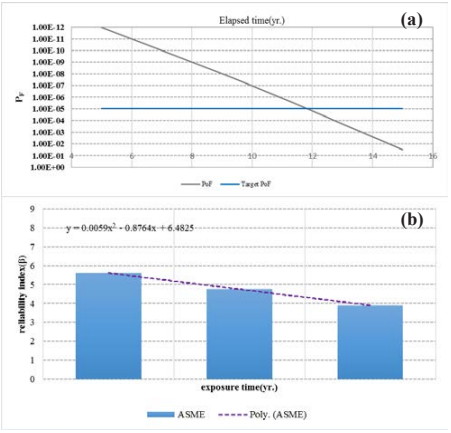

Figure 3: Variation POF of pipeline vs. exposure time. a: small leak, b: large leak

5. Conclusion

An attempt was made to determine better form of corrosion attacks failure modes for reliability based design (inspection). According to numerical results, SL has no significant impact on pipeline safety, but POF of SL reaches to three percent in 15 years. Furthermore, results indicated that ASME considers larger POF for servicing time in comparison to initial POF at design step. Also, using un-conditional form for pipeline rupture could cause larger POF. In other words, higher degree of safety could be planned in detailed design stage and in RBI plan.

6. References

[1] Shabani, H., Goudarzi, N. and Shabani, M. (2017) Failure analysis of a natural gas pipeline. Engineering Failure Analysis,. https://doi.org/10.1016/j.engfailanal.2017.11.003

[2] Shabani, M.M., Taheri, A. and Daghigh, M. (2017) Reliability assessment of free spanning subsea pipeline. Thin-Walled Structures, 120, 116–23.

[3] Shabani, M.M. (2017) Reliability Assessment of Existing Subsea Pipelines in Persian Gulf. Petroleum University of Technology(PUT).

[4] Shabani, H., Goudarzi, N. and Shabani, M. (2018) Failure analysis of a natural gas pipeline. Engineering Failure Analysis, Elsevier. 84, 167–84.

[5] Gong, C. and Zhou, W. (2018) Importance sampling-based system reliability analysis of corroding pipelines considering multiple failure modes. Reliability Engineering and System Safety, Elsevier Ltd. 169, 199–208.

[6] Shabani, H., Shaban, M.M. and Goudarzi, N. (2018) Probabilistic Assessment of Corroded Offshore Pipelines: pitting. 5th International Reliability and Safety Conference, University of Shiraz, Iran. p. 1–10.

[7] Shabani, H., Shabani, M.M., Goudarzi, N. and Taravati, R. (2018) Stochastic-Based Quantitative Risk Assessment of Corroded Gas Transmission Pipelines Considering Multiple Failure Modes. Thin-Walled Structures, 131.

SEISMIC BEHAVIOR OF HUNCHBACKED BLOCK-TYPE GRAVITY QUAY WALLS

Babak Ebrahimian[1], Amir R. Zarnousheh Farahani[2] and Ali Noorzad[3]

1) Faculty of Civil, Water and Environmental Engineering, Shahid Beheshti University, Tehran, Iran, b_ebrahimian@sbu.ac.ir, ebrahimian.babak@gmail.com
2) Faculty of Civil, Water and Environmental Engineering, Shahid Beheshti University, Tehran, Iran, a.zarnoosheh@sbu.ac.ir
3) Faculty of Civil, Water and Environmental Engineering, Shahid Beheshti University, Tehran, Iran, a_noorzad@sbu.ac.ir

1. Introduction

Herein, the seismic behavior of hunchbacked block-type gravity quay walls is investigated using 2D fully non-linear dynamic time-history analyses. They take into account material and geometric non-linearities. Both static and seismic conditions are considered. The obtained numerical results are compared with those of 1g shaking table tests [1]. Comparisons are proposed in terms of acceleration, displacement, and total lateral earth pressure time histories across the height of two types of quay walls with different configurations, as shown in Figure 1. Quay wall Type *I* has a larger hunch than that of Type *II*.

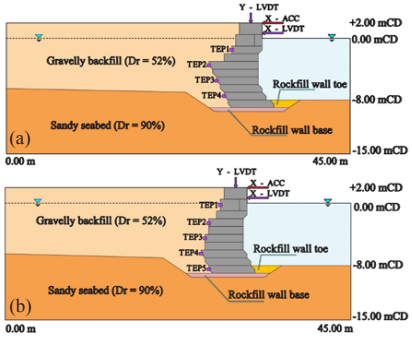

Figure 1. Schematic cross section of quay wall: (a) Type I, (b) Type II in prototype scale and location of instrumentations (TEP: Total Earth Pressure; ACC: Acceleration; LVDT: Displacement).

2. Numerical Modeling Procedure

Numerical simulations are conducted by an explicit finite difference code incorporating hysteretic Mohr-Coulomb constitutive model to describe the stress-strain response of soil and the Rayleigh damping to increase the level of hysteretic damping in the model [2]. The Seed modulus reduction curve is employed to consider the soil non-linear behavior before yielding [2]. Contact conditions between wall and adjacent soil are modeled via special interface elements allowing for slipping and gapping through the Coulomb frictional law. Element size is selected small enough to allow the seismic wave propagation throughout the numerical model. The sea water is simulated through the hydrostatic pressures applied to the front side of the wall. Correspondingly, the hydrodynamic effects are exerted by the Westergaard's added masses on the seaward face of the wall. In dynamic analyses, the free-field condition is applied to the lateral boundaries eliminating the wave reflection into the model [2]. To avoid spurious oscillations at very small deformations and high frequency components of motions, 5% of Rayleigh damping, centered at a frequency of around 2.5 *Hz* (close to the fundamental frequency of the system), is considered in the dynamic analyses. It is noted that liquefaction cannot be triggered during shaking and the developed excess pore water pressures are negligible due to the presence of coarse grained backfill soil and very dense seabed sand foundation.

3. Results and Discussion

For the applied input motions demonstrated in Figure 2, the predicted and measured responses are illustrated in Figures 3-7. According to Figure 3, overall agreement is achieved between the predicted and measured horizontal accelerations, with the predicted values giving somewhat higher amplitudes. Figure 4 shows that the displacement of quay wall head increases incrementally during seismic loading. Quay wall Type *I* moves seaward about 30 *cm* and has very small amount of vertical settlement, showing wall translational sliding on its base, whereas the backfill settle up to about 55 *cm* behind the wall. Quay wall Type *II* moves extensively toward the sea by amount of about 100 *cm*, accompanied by a maximum settlement of about 4.5 *cm*. For the latter wall, the backfill has maximum settlement of 100 *cm*. The very small differences between the predicted and measured vertical displacement of quay wall head are likely attributed to the minor rocking motion of the walls, Figure 4. Figure 5 shows the wall movement and backfill deformation patterns in wall Type II. Particularly, the wall on the very dense sandy soil foundation significantly slides and slightly rotates seaward. Apron settlement immediately behind the broken-back

quay wall is large. The deformation patterns obtained from numerical simulations are in proper agreements with those of model experiments [1]. Lateral earth pressures on walls are calculated in Figure 6 and compared with the measured ones. It is seen that, in general, both the magnitude and the trend of all time histories are in reasonable agreement. It is confirmed that quay walls with steeper broken-back angle have better seismic performance and are preferred to the vertical-back block quay walls in high seismicity regions.

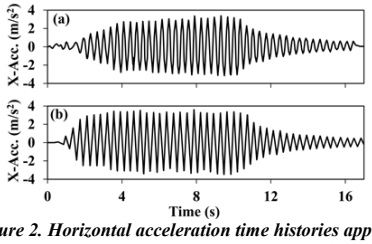

Figure 2. Horizontal acceleration time histories applied at the base of numerical model for quay wall: (a) Type I, (b) Type II.

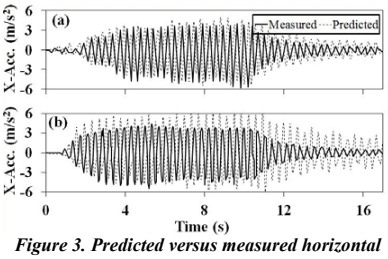

Figure 3. Predicted versus measured horizontal acceleration time histories at head of quay wall: (a) Type I, (b) Type II.

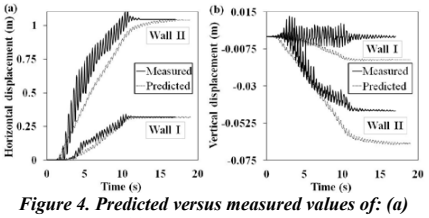

Figure 4. Predicted versus measured values of: (a) horizontal, and (b) vertical displacements time histories at head of quay walls Types I and II.

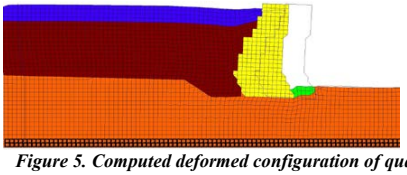

Figure 5. Computed deformed configuration of quay wall type II at the end shaking

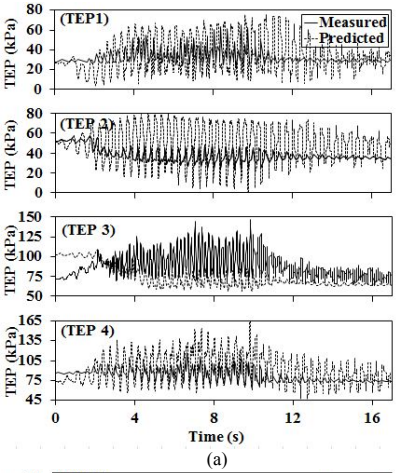

(a)

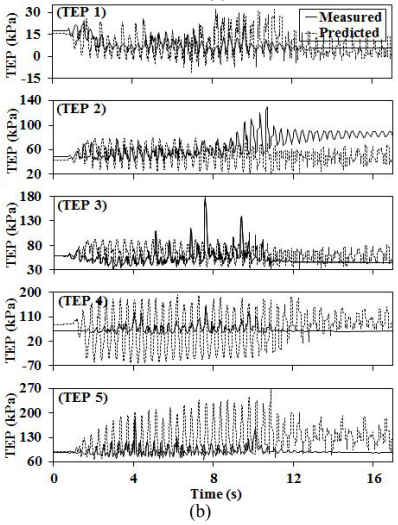

(b)

Figure 7. Predicted versus measured total earth pressure time histories across the height of quay wall: (a) Type I, (b) Type II.

4. References

[1] Sadrekarimi, A., Ghalandarzadeh, A., and Sadrekarimi, J., "Static and dynamic behavior of hunchbacked gravity quay walls", *Soil Dynamics and Earthquake Engineering*, 28, 2008, pp. 99 – 117.

[2] Itasca, *FLAC Version 7.0: Fast Lagrangian Analysis of Continua-User's Guide*, Itasca Consulting Group Inc., Minneapolis, Minnesota, 2014.

EFFECT OF THE WATER SALINITY ON THE CONSOLIDATION AND MECHANICAL BEHAVIOR OF THE PERSIAN GULF MARINE CLAYS: A CASE STUDY

Ali Bayat [1] and Hamed Bayesteh[2]

1) M.sc, Department of Civil Engineering, University of Qom, Qom, Iran, a.bayat@stu.qom.ac.ir
2) PhD, Department of Civil Engineering, University of Qom, Qom, Iran, h.bayesteh@qom.ac.ir

1. Introduction

One of the most important indicators of the development of countries is the development of the marine infrastructure and the expansion of development activities in coastal strips, which has become popular in Iran in recent years. On the other hand, the soils of coastal areas have unique characteristics due to their formation and their structural nature. High water content, high porosity, low resistance and high corrosive salt content are the most important engineering properties in marine soft soils. One of the soils that is always considered is clay that is scattered in many coastal regions of the country, such as Khuzestan and Bushehr. The behavior of clay is the function of minerals and pore water. The chemical status of pore water may be significantly altered by the exchange of exchangeable cations in clays that in most cases affect its engineering characteristics. Most engineering problems in clay take place due to the physical-chemical changes of the pore water. On the other hand, the environmental conditions and climate change are such that changes in the pore water salinity in the adjacent clay, therefore it is necessary to recognize this interaction in the soil of each region. The effect of change in the water salinity on the marine clay behavior in the Persian Gulf area has not been well investigated yet. Therefore, it is necessary to study the effect of water salinity on the above-sea and the compressibility and the parameters of the consolidation of marine clay as well as parameters such as horizontal and vertical permeability coefficients in geotechnical terms. This issue should be investigated in southern soils of the country that are in opposition to salt changes to make. In this research, the clay-water approach in natural conditions has been selected from the southern coast of the country and the effects of salinity changes on different levels of stress have been investigated on the consolidation behavior marine clay, by considering the soft clay located in the Bushehr city.

2. Materials and Methods

The clays were collected from the coasts of Bushehr province, as indicated in Figure1.

Figure 1. Sampling site in Bushehr province

In order to know the mechanical and microstructural properties of this soil, XRD analysis and Field Emission scanning electron microscopy (FESEM) were prepared from this clay and related experiments were performed. In Figure 2, the results of the XRD test as FESEM images are shown, which states that the nature of the sample is carbonate and given that 50% of the soil is formed by calcium carbonate. According to previous studies this soil is in the category of calcium Silicate [1]. The FESEM image states that carbonate soil has a needle-like structure [2].

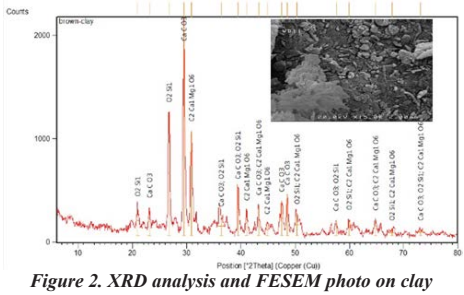

Figure 2. XRD analysis and FESEM photo on clay samples

A test program was developed with two methods of water leakage with different salinity in soil, as well as intrinsic salinity changes in soil. In Table 1, the types of soil and water are summarized. Soil electrical conductivity has been used to express the amount of water salinity. To prepare the sweet and semi-sweet soil according to the number of times listed in Table 1, add distilled water to the

soil site with a ratio of 1 to 10 and mix it for 2 hours, each time for a period of 10 minutes at a rotational speed of 2000 rpm centrifuges. Seawater was used to create salt water and in order to carry out the test in real conditions, it was used as seawater. The salt water used is the same as seawater. To investigate changes in the characteristic of the clay due to the water change as well as the nature of the soil (sweetening), the Atterberg limits have been tested according to the standard ASTM D4318[3] and the results of variations with regard to the different conditions of water and soil are reported in Figures 3.

Table 1. Different types of soil and water

Soil	Electric conductivity of soil (mmohs/cm)	Times of washing soil with centrifuges	Water	Electric conductivity of water (mmohs/cm)
In situ soil	4	0	Distilled water	0.18
Intermediate soil salinity	1.53	2	Intermediate water salinity	22.5
Sweet soil	0.3	5	Sea water	44.65

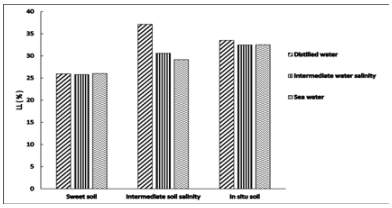

Figure 3. Effect of Salinity on the liquid limits

The results show that water changes do not have a significant effect on the nature of plastic behavior of soil in the short time. In all different states of soil with distilled water, there is an increase in the liquid limit, which in fact indicates a tendency to absorb more water in this state. [4] To investigate the changes in soil consolidation behavior, the specimens were prepared in a very loose wet weight at the place of 1.8 gr/cm^3 in an extension ring with a diameter of 51 mm and a height of 20 mm. For this purpose, firstly mix the tested soil with suitable water (for example, the soil with sea water) with excessive water of liquid limit and in the pipe and the ring we are looking for and allow to be grainy in the ring. Then the consolidation test has done. Some Results changes in soil consolidation behavior in different conditions of water and soil, which are normalized with the normalized e/e_L are plotted in Figure 4.

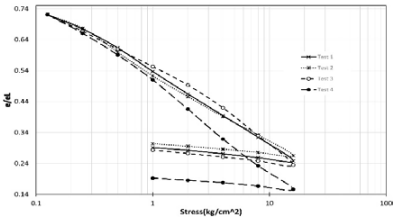

Figure 4. Effect of salinity on the consolidation of clay

The soil and water profiles of each test are: 1) in situ soil with intermediate water salinity, 2) in situ soil with sea water salinity, 3) washed soil to E1.53 mmohs/cm with distilled water and 4) washed soil to E0.3 mmohs/cm with sea water. The results show that according to the osmotic theory, the water moves from a lower concentration medium to a higher concentration environment, so that when seawater is added to the soil, since all 2 concentrations are the same, they do not significantly change the particle arrangement. The strong bonds of the present are not broken down and cause a lower settlement than when the semisweet and distilled water enters the environment, because the semisweet water changes the structure of the soil from the complex to the dispersed state, weakening the vanadium bonds between the particles he does. The results of unconfined compressive strength (UCS) test on samples with the change of water conditions of the project are shown in Figure 6. The results show that formation of a stronger bonds between clay particles lead to increase strength.

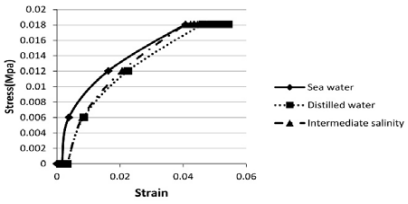

Fig5: Effect of salinity on UCS

3. Conclusions

Change in water salinity has major effect in volume change behavior of marine clays. The amount of water salinity, in the short time, has little effect on the Atterberg limits except in distilled water. The presence of distilled water in the environment increases the Atterberg limits of soil types because the tendency to absorb water due to unbalanced negative loads in the soil environment increases. Changes in the amount of water salinity cause tangible changes in the soil liquid limit. At a constant stress level about 16 kg /cm^2, the lowest level of seagrass is due to the presence of strong seawater seams due to strong bonds and the highest sewage in soils with sea water because during the sweetening process the breaks have broken down and the soil structure has changed from the complex to the dispersed.

4. Reference

[1] Sterianos, Benjamin, 1988, Geotechnical properties of carbonate soils with reference to an improved engineering classification, University of Cape Town.

[2] Tucker, Maurice E & Wright, V Paul, 2009, Carbonate sedimentology, John Wiley & Sons.

[3] Standard Test Methods for Liquid Limit, Plastic Limit, and Plasticity Index of Soils, 2017, West Conshohocken, No. 10.1520/D4318-17E01

[4] Collins, K t & McGown, A. 1974, The form and function of microfabric features in a variety of natural soils, Geotechnique,

DEVELOPING A MULTI-OBJECTIVE OPTIMIZATION ALGORITHM FOR PREDICTING HULL DIMENSIONS OF SEMI-SUBMERSIBLE PLATFORM

Arefe Emami[1] and Ahmad Reza Mostafa Gharabaghi[2]

1) Faculty of Civil Engineering, Sahand University of Technology, Tabriz, Iran, a_emami@sut.ac.ir
2) Faculty of Civil Engineering Faculty, Sahand University of Technology, Tabriz, Iran, mgharabaghi@sut.ac.ir

1. Introduction

One of the main approaches in order to improve the performance of semi-submersible drilling platform is its hull geometry optimization. Developing a method for optimal design of this type of platform that achieves the best answer in a short time according to certain objectives, is incredibly significant. In this paper, by developing Grid Search (GS) algorithm as multi-objective optimization, the hull dimensions of a typical semi-submersible platform was estimated. The objectives were minimizing hull weight and its heave motion response. In this algorithm, design constraints of semi-submersible platform such as stability, air gap, draught, geometrical limitations, hull weight, and heave motion response were considered. Then, by implementing GS' algorithm, the optimal hull dimensions of the studied platform were estimated. It achieved valid and reliable results with low computational time. Moreover, it is a more easy method to use for multi-objective functions in the floating or semi-floating structures.

2. Semi-Submersible Platform

Increasing need to the energy sources such as oil and gas, has encouraged its production from deep waters. Floating platforms are the most favorable units used for gas and oil production in deep waters. They are massive structures which usually are classified based on their objective such as drilling rigs, production platforms, storage platforms and drilling/storage/offloading platforms [1]. Semi-submersible drilling platforms are a type of floating mobile offshore drilling units (MODUs) designed for drilling in deep waters. They are typically made from two submerged pontoons with four or more columns connecting the pontoons to the hull. One of the main problems of this type of platform is its heave motion response which is much larger than the other types of deep water platforms. One of the major methods in order to reduce these motions is the optimal design of its hull-dimensions. There are different methods in order to find the optimal dimensions of its hull such as applying the optimization algorithms. In literature, there are several investigations to find the optimal form or dimensions of its hull such as Akagi and Ito (1984), Birk and Clauss (2001, 2008), Gallala (2013) [2-5]. In this paper a simple and logical multi objective optimization algorithm is applied for prediction of the hull dimensions of a typical semisubmersible platform. Indeed, the goal of this article is to provide a method that enables solving multi-objective problems using a simple way and achieving valid results with devoting less time and energy.

3. Grid Search Algorithm

The Grid Search algorithm (GS) is one of the multi-dimensional grid methods that has a centroid where the optimum point has been located on there. Indeed, GS' algorithm searches a multi variable function on a computational grid and after finding the optimum point, it saves the information in its memory (Figure 1) [6]. This algorithm is a simple and reliable method which has been used extensively in Biomedical Engineering for single objective optimization. In this paper, GS' algorithm is implemented for multi-objective functions for prediction of the hull dimensions of the semisubmersible platform for the first time.

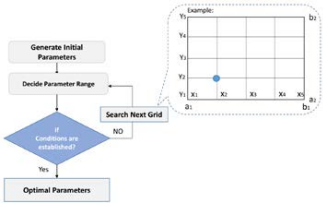

Figure 1. Flowchart of Grid search method

4. Optimization of Semi-submersible

For prediction of the dimensions of the semi-submersible platforms' hull, a certain shape of the main parts of the platform is required. Since the main goal of this paper is prediction of optimum hull dimensions of semisubmersible platform using GS' algorithm, two geometrical panels are taken into account: the first geometrical shape is similar to the case related to the Gallala's work (2013) and it is used to confirm the efficiency of the GS' algorithm [5], another panel is related to the Iran Amirkabir semi-submersible drilling platform that the GS' algorithm was applied to find its optimal geometry. Iran Amirkabir platform is a GVA4000 type platform which was designed and manufactured for drilling of oil and gas at water depth of 1000 m in Caspian Sea, north of Iran [7]. The GS' algorithm is defined according to some constraints. The most important constraints for the

semi-submersible platform includes: hull weight, stability constraints, air gap constraints that must be considered because of the risk of wave slamming, geometrical constraints which due to the logical output must be considered, and heave response constraints. It should be noted that in this algorithm, the main parameters are the hull weight and buoyancy of the semi-submersible platform's hull form and its heave motion which is calculated by Morrison equation and Froude-krylove relation.

5. Validation of Grid Search Algorithm

To prove the accuracy and efficiency of the developed GS' algorithm for optimal design of floating platform's hull, a proposed semi-submersible platform by Gallala (2013) is considered. Then GS' algorithm is implemented as a single objective algorithm with the goal of minimizing hull weight of semi-submersible platform. Finally, its results are compared by Gallala' work (Table. 1). The results show that both of optimization algorithms have a very close answers. So, GS' algorithm is suitable and has enough efficiency for optimizing the geometry of semisubmersible platform's hull.

Table 1. The comparison of optimization methods for semisubmersible platform

Parameters (m)	Optimization with Grid Search algorithm	Optimization with GRG Method
Pontoon Length	87	87
Pontoon Height	8	8.04
Pontoon breadth	12.6	12.06
Column Length	9	9.11
Column breadth	11	9.92
Column height	28.7	27.96
Distance between Columns	74	74

6. Development of GS' algorithm

In the next step, the GS' algorithm was developed as multi-objective optimization method for minimizing the hull weight, and heave motion response (Figure 2). Initial parameters are based on the Iran Amirkabir drilling platform's data. By applying design variables and criteria, optimization algorithm is implemented. It is noteworthy to mention that calculations have been done by a personal computer device SONY with Core i5.

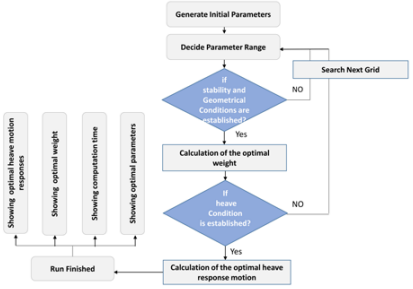

Figure 2. Development of multi-objective Grid Search algorithm

7. Results

The results obtained from GS' algorithm have been compared by hull dimensions of Iran-Amirkabir drilling platform (Table 2). It has given close answers to Iran-Amirkabir platform's hull dimensions. Also, the short computational time to calculate optimal hull dimensions of semisubmersible platform is observed.

Table 2. Optimal dimensions of Iran-Amirkabir platform

Parameters	Optimization	Reference (Amirkabir drilling platform)
Length of pontoons (m)	80.392	80.56
Width of pontoons (m)	18.124	18.68
Height of pontoons (m)	7. 25	7.5
Radius of columns (m)	7	6.45
Height of columns (m)	20.55	21
The longitudinal GM value (GML) (m)	2.4232	2.48
The transversal GM value (GMT) (m)	2.4232	2.48
Min. Weight (ton)	8846.7	8825
Min. Heave Motion Response (m)	2.0371	1.8
Computational Time (sec)	2.8111e+4	Unknown

8. Conclusion

One of the methods to increase the efficiency of semisubmersible platforms is to minimize their motions and achieve more stability. Therefore, the hull dimensions of these platforms are usually optimized. In the present paper, the Grid search algorithm has developed as two-objective optimization for the prediction of the hull dimensions of semi-submersible platform including: minimizing the hull weight, and its heave motion response. The results obtained for the most suitable optimal dimensions for its hull with low computational time. The most significant advantages of this algorithm are simple expression, logical function and easier to use for multi objective functions. So it is suggested for optimization of other floating platforms such as spar and tension leg platforms (TLP).

9. Reference

[1] Sharma, R., Kim, T.W., Sha, O, P and Misra, S. C., "Issues in offshore platform Research-Part 1: Semi-submersibles." Inter J Nav Archit Oc Engng. 2, 2010, pp. 155-170.

[2] Akagi, S., and Ito, K., "Optimal design of semisubmersible form by minimizing its motion in random seas." Journal of Mechanisms, Transmissions, and Automation in Design, 106(1), 1984, pp. 23-30.

[3] Birk, L., and Clauss, G., "Automated Hull Optimization of Offshore Structures Based on Rational Sea keeping Criteria" International Offshore and Polar Engineering Conference, Stavanger, Norway, 2001. pp. 382-389.

[4] Birk, L., Clauss, G.F., "Optimization of offshore structures based on linear analysis of wave-body interaction" In: Proceedings of the 27th International Conference on Offshore Mechanics and Arctic Engineering. OMAE 2008–57631, Estoril, Portugal, June 2008, pp. 15–20.

[5] Gallala, J.R., "Hull Dimensions of a Semi-Submersible Rig, A Parametric Optimization Approach," Master thesis, NTNU-Trondheim, Marine Technology, 2013.

[6] Singiresu, S. R., "Engineering Optimization: Theory and Practice," School of Mechanical Engineering, Purdue University, West Lafayette, India, 1996.

APPLICATION OF TUNED LIQUID COLUMN DAMPER FOR PITCH MOTION REDUCTION OF SEMISUBMERSIBLE FLOATING PLATFORMS

Hamidreza Feizian[1] and Roozbeh Panahi[2]

1) PHD Candidate, Civil Engineering Department, Tarbiat Modares, Tehran, Iran, h.feizian@modares.ac.ir
2) Assistant Professor, Civil Engineering Department, Tarbiat Modares, Tehran, Iran, rpanahi@modares.ac.ir

1. Introduction

Offshore floating platforms have been employed worldwide in many applications for decades. For the sake of safety, human comfort and increasing productivity it is suitable to reduce motions and vibrations of platforms as much as possible. Many researches have been conducted on different methods to reduce the motions of floating platforms. Recently, utilizing passive methods such as Tuned Mass Dampers (TMD) and Tuned Liquid Column Dampers (TLCD) are being considered increasingly [1]. Among all passive methods, using TLCD is the most attractive one, because of its low cost, easy handling and few maintenance requirements [2, 3].

TLCD is a U-shaped tube, containing a liquid (commonly water). Usually, there is at least one orifice at the middle part of the tube causing a head loss when the liquid oscillates in the tube, resulting in energy dissipation.

Application of TLCD in floating platforms is mostly studied on Tension-Leg Platforms (TLPs), so far.

Lee et al. incorporated a TLP with a huge TLCD for the first time on the topside in order to reduce the wave-induced vibration of the floating platform [4]. In order to calculate the response spectrum of the structure-TLCD system, they derived a transfer function for each DOF and multiplied it by the wave spectrum.

A TLP, equipped with an underwater TLCD; known as UWTLCD; was later studied experimentally by Lee and Juang [5]. The pontoons of the platform were used as the vertical parts of the TLCD while connected with a horizontal small diameter tube. This scheme was used to equip the platform with a TLCD without any space occupation on the topside. As mentioned, both of the studies are concerning TLPs and application of TLCD is not studied on semisubmersibles. In this study application of TLCD on a semisubmersible drilling rig is surveyed and especially the pitch motion of the platform is concerned. Because of slackness of semisubmersible catenary mooring lines, it is free to rotate and reducing the pitch motion is of importance.

2. Equations of Fluid Motions in TLCD and Generated Forces

A conventional U-shaped TLCD is shown in Figure 1. The damper is assumed to be attached to the main structure and they move in the X, Y and θ directions.

Using a general form of the Bernoulli's equation for a moving reference frame as done by Hochrainer the complete form of the equation of the water surface in the TLCD tube can be derived [6]:

$$L_{eq}\ddot{w} + \frac{1}{2}\xi\dot{w}|\dot{w}| + 2gw = -B.\ddot{X} - (2w)\ddot{Y} - B\left(\ddot{\theta}\left(\frac{L-B}{2} + D\right) + g\theta\right) \quad (1)$$

where L_{eq} is defined as $L_{eq} = L - B(1 - A_v/A_h)$ and L and B are the total length of internal fluid and width of the TLCD respectively as shown in Figure 1. A_v and A_h are the cross section area of vertical and horizontal tubes. w, $\dot{w}$ and $\ddot{w}$ are denoting the fluid displacement, velocity and acceleration in the vertical part of the tube. g is the gravity acceleration and ξ is head loss coefficient depending on the blocking ratio of the damper orifice. D is the distance of the rotation center from the center of the TLCD.

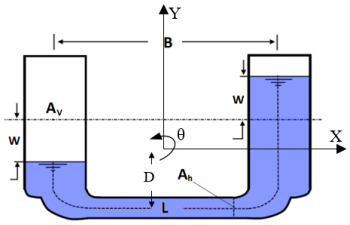

Figure 1. TLCD definitions and dimensions

The forces generated by damper as produced by the fluid fluctuations within the TLCD can be calculated as described by Hochrainer and Xue et al. as below [6, 7]:

$$F_X = -\rho A_h B\ddot{w} \quad (2)$$

$$F_Y = -\rho(2A_v w\ddot{w}) \quad (3)$$

$$M_\theta = -\rho A_v B(H + D)\ddot{w} - \rho g A_v\left(\left(2\frac{L-B}{2} + B\frac{A_h}{A_v}\right)D\theta + Bw\right) \quad (4)$$

3. Numerical Modelling of Semisubmersible-TLCD System

The drilling rig, GVA4000 is selected to investigate the effect of utilizing TLCD on response mitigation of semisubmersibles.

Numerical modelling is carried out in two stages. The first stage is done in frequency-domain to provide hydrodynamic specifications of the floating structure. In the second stage, the position of the semisubmersible with and without a TLCD is calculated at each time-step under irregular waves. TLCD forces and moments are calculated and exerted to the structure at such steps using the aforementioned equations.

Simulation of the floating platform motions is performed by Ansys®AqwaTM (17.0) and TLCD forces and moments are calculated in the time-domain stage by means of a fortran code. The fortran code is coupled with Ansys®AqwaTM via an external dynamic library link file. It is good to remember that the software is based on boundary element method which simplifies calculations when compared with other methods e.g. the one proposed by Panahi et al.[8]

Numerical model of the floating platform (without TLCD) is verified by frequency-domain results of numerical and experimental simulations of Clauss et al. as shown in Figure 2 [9]. Comparison shows that the current numerical results are well matched with the experimental and numerical data of the mentioned study.

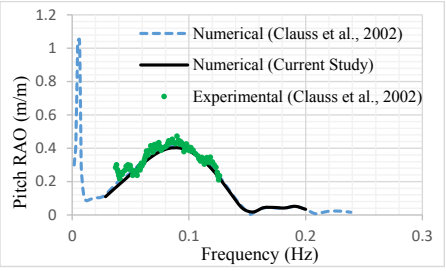

Figure 2. GVA4000 pitch RAO – comparison of current numerical results with Clauss et al. [9]

Time domain analysis of the floating platform has been done with active and inactive TLCD on the structure. Also, the effect of head loss coefficient (ξ) variation on damper efficiency is studied. The frequency of the applied TLCD is about 0.1 Hz and the ratio of $TLCD_{Mass}/Structure_{Mass}$ is approximately 4.5 percent. Irregular wave time series, based on JONSWAP spectrum are applied with a significant wave height of 5 meters and pick period of 11 seconds.

In order to better study the phenomenon, time domain results are transformed into response spectrum. Figure 3 shows the response spectrum in the range of natural frequency of the structure, without and with TLCD for different values of head loss coefficient. It can be concluded that application of TLCD has a significant mitigation effect on pitch response of the semisubmersible platform and greater values of ξ would result in more efficiency of damper. It means that bigger blocking area of the damper orifice will cause more energy dissipation. It is noteworthy that the greatest value of head loss coefficient (ξ=55) is related to about 80 percent orifice blocking ratio, according to Wu et al. calibration tests [10]. It is also concluded that there is not a linear relation between head loss coefficient and mitigation effect of the damper. As it can be observed in Figure 3, by increasing the value of ξ from 35 to 55, a small reduction in pitch response is achieved.

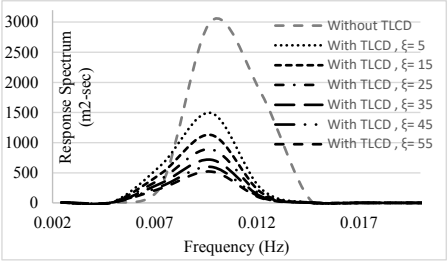

Figure 3. GVA4000 pitch response spectrum without and with TLCD

4. References

[1] Kandasamy R, Cui F, Townsend N, et al. A review of vibration control methods for marine offshore structures. Ocean Eng. 2016;127(October):279-297.

[2] Gao, H., Kwok, K. C. S., & Samali, B. (1997). Optimization of tuned liquid column dampers. Engineering Structures, 19(6), 476–486.

[3] Di Matteo, A., Lo Iacono, F., Navarra, G., & Pirrotta, A. (2014). Experimental validation of a direct pre-design formula for TLCD. Engineering Structures, 75, 528–538.

[4] Lee, H. H., Wong, S. H., & Lee, R. S. (2006). Response mitigation on the offshore floating platform system with tuned liquid column damper. Ocean Engineering, 33(8–9), 1118–1142.

[5] Lee, H. H., & Juang, H. H. (2012). Experimental study on the vibration mitigation of offshore tension leg platform system with UWTLCD. Smart Structures and Systems, 9(1), 71–104.

[6] Hochrainer, M. J. (2005). Tuned liquid column damper for structural control. Acta Mechanica, 175(1–4), 57–76.

[7] Xue, S. D., Ko, J. M., & Xu, Y. L. (2000). Tuned liquid column damper for suppressing pitching motion of structures. Engineering Structures, 22(11), 1538–1551.

[8] Panahi, R., Jahanbakhsh, E., Seif, M. S., Step, F., & Motion, S. (2006). Developement of a Numerical Hydrodynamic Tank for Ship Motion Simulation. In European Conference on Computational Fluid Dynamics.

[9] Clauss GF, Schmittner CE, Stutz K. Time-domain investigation of a semisubmersible in rogue waves. 21st IntConf Offshore MechArct Eng. 2002;(January 2002).

[10] Wu, J. C., Shih, M. H., Lin, Y. Y., & Shen, Y. C. (2005). Design guidelines for tuned liquid column damper for structures responding to wind. Engineering Structures, 27(13), 1893–1905.

NUMERICAL MODELING OF LOCAL SCOUR BELOW A PIGGYBACK PIPELINE IN CURRENTS

Sahar Asrari[1], Habib Hakimzadeh[2] and Nazila Kardan[3]

1) Faculty of Civil Engineering, Sahand University of Technology, Tabriz, Iran, S_asrari@sut.ac.ir
2) Faculty of Civil Engineering, Sahand University of Technology, Tabriz, Iran, Hakimzadeh@sut.ac.ir
3) Department of Civil Engineering, Azerbaijan Shahid Madani University, Tabriz, Iran, n.kardan@azaruniv.edu

1. Introduction

Investigating Local scour around an offshore pipeline has received most attention both experimentally and numerically in the last few years. So far, most of the studies on scour below the pipeline are related with a single pipeline. Offshore pipelines of different diameters are sometimes laid together as a bundle due to technical or economical attentions. A pipeline bundle comprises a large pipe and a few of small pipes. The pipelines in the bundle could either be in direct contact with each or be separated by small gaps. The most popular configuration of pipelines bundles consists one large pipeline with a small one installed exactly above the large one, as shown in Figure 1. It is supposed that the existence of a small pipeline and a gap between the two pipes will affect local scour below the piggyback pipelines. In this study the effects of the gap between the two pipelines in piggyback configuration on local scour profiles are investigated numerically.

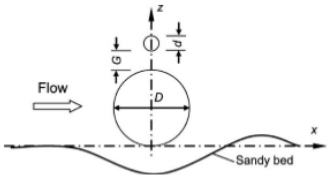

Figure 1. Sketch of flow past two pipelines in piggyback configuration

2. Hydrodynamic Observation below a Single Pipeline

The numerical model developed in this study is validated against hydrodynamic model results available by Figan Htipoglu (2003-Ocean Engineering) on Flow around a cylinder in a steady current. Figure 2 Shows the streamlines near the pipeline. This agrees with the experimental observation reported by Hatipoglu (2003). The length of separation region was observed in the downstream of cylinder in the case of surface mounted cylinder (G/D=0) was 0.54 m.

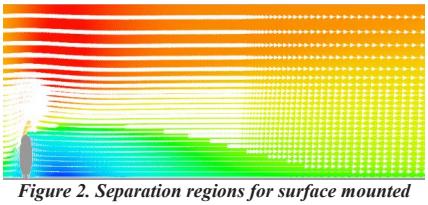

Figure 2. Separation regions for surface mounted cylinder, G/D=0

3. Scour below a Single Pipeline

The water flume experiment reported by Mohammadi (2014) is simulated for this purpose in this study. In order to allow for a direct comparison with the experimental results, the computation is carried out under the conditions as close as possible to those specified in the physical experiment by Mohammadi (2014) by FLOW 3D. In Mohammadi's experiments, the water depth was 0.15 m. the pipeline diameter was 0.4 m. the grain size was 0.00078 mm. the shields parameter was 0.03. the pipeline diameter and sediment particle size used in the computations are the same as those in the experiment.

Figure 3 Shows the scour under the cylinder at 10 s. In the continue Figure 4 shows the scour ta 600 s.

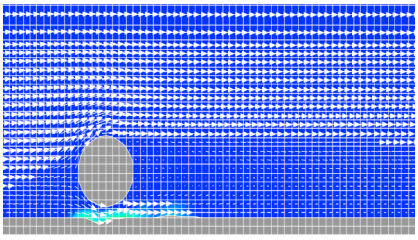

Figure 3. Scour at 10 s

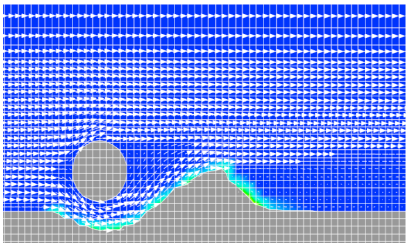

Figure 4. Scour at 600 s

4. Scour below a Piggyback Pipeline

Local scour below a piggyback pipeline is investigated using the validated numerical model by FLOW 3D. the configuration of the piggyback pipeline is shown in Figure 1. The large pipeline diameter (D) is 60mm, the small pipeline diameter (d) is 15mm, the flow velocity is 0.262 m/s and the sand size and computational domain are set the same as those in the single pipeline case studied before. The diameter ratio of the small pipeline to the large one is d/D= 0.25. computations are carried out for the gap ratio of G/D= 0.0, 0.25.

Figure 5 shows the final result for scouring of these modes at 600 s.

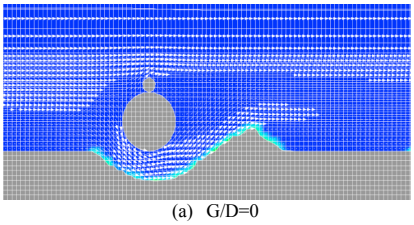

(a) G/D=0

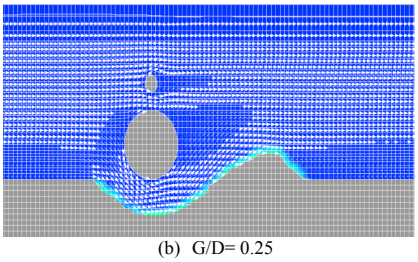

(b) G/D= 0.25

Figure 5. G/D= 0.0, 0.25

5. Conclusion

It can be seen that local scour below piggyback pipelines with different diameters has been affected noticeably with the existence of the small pipeline. The scour depth below the piggyback pipeline is greater than single pipeline. It is assumed that the scour profile should reach to the scour profile for the single pipe case when G/D is very large. It can also see that the scour depth in front of the pipelines decreases with the increase of G/D.

6. References

[1] Figen hatipoglu, I. Avci, (2003), "Flow around a partly buried cylinder in steady current", J, Ocean Engineering, 30. Pp 239-249

[2] Summer, B.M. and Fredsoe, J. (1999), "Scour around marine structures". Advanced in coastal and ocean Eng. 4, pp200-245

[3] Ming Zhao and Liang Cheng, (2008), "Numerical modeling of loacal scour below a piggyback pipeline in currents", ASCE, 0733-9429

[4] B. Arshad Shabkhaneh, H. Hakimzadeh, "Investigation of flow pettern around parallel pipelines due to steady currents using numerical and phisycal models, July 2011, Sahand university of technology

[5] Hakimzadeh H, Mohammadi A. Protection of Offshore Pipelines with Adding a Longitudinal Blade beneath the Pipe. Journal Of Marine Engineering. 2016; 11 (22) :25-38

[6] Hakimzadeh H, Mosahebi Mohammadi M. Experimental Investigation on Impact of Reynolds Number, Fitting Distance and Relative Diameter on Flow Separation around Piggyback Pipelines. Journal Of Marine Engineering. 2016; 11 (22) :109-117

CONSTRUCTION OF ARTIFICIAL ISLANDS BY USING STEEL CYLINDERS (CASE STUDY: HONG KONG-ZHOU-MACAO BRIDGE)

Khaled Pourali[1], Mohammad Javad Ketabdari[2*] and Arno Petrosian[3]

1,2,3) Faculty of Marine Technology, AmirKabir University of Technology, Tehran, Iran,
*ketabdar @aut.ac.ir

1. Introduction

Artificial islands refer to islands that are created by humans in aquatic environments without the involvement of natural agents. Construction of artificial islands may perform with goals such as extracting oil and natural resources, military, development of ports and coastal towns and for entertainment purposes. In this research, a new method for constructing an artificial island has been investigated. In this method, the large diameter steel pipes create a temporary dam against the water and wave forces. Building the island inside the enclosed area is the next step Therefore the issue that has been addressed in this leading research is human advancement in coastal areas and near coastal areas by construction of artificial islands. It is possible to encourage governments and countries into the construction of such structures. For example, the countries of the southern margin of the Persian Gulf, such as Bahrain, Qatar, Oman and the United Arab Emirates, have been brought to the construction of artificial islands, due to the shortage of coasts and withdrawals from the single-product economy [1]. Because of the increase in the population of China to facilitate the flow of citizens and the link between the two cities of Hong Kong and Zhou Macau, two artificial islands as two spans of the submarine tunnel have been used [2].

2. Design and Implementation Consideration

In design of artificial islands, factors such as depth of water, wave height, ice conditions, tidal range, sea floor conditions, earthquake risk, borrowing resources, and environmental conditions are influential [3].

3. Construction Steps

3.1. Geometric Shape and Island Location

Figure 1 shows the submarine tunnel route in China. There are two openings of a submarine tunnel that longitudinally is 6.7 km. The project began in mid-December 2010 with the construction of a Western artificial island. The goal is to complete the island in 20 months or less. The arrangement of the western island is shown in Figure 2. As shown in this figure the construction of the island is divided into two phases. Each of these islands are made by 67 cylindrical steel that their thickness and weight are 16 mm and 450 tons respectively [4].

3.2. Manufacturing and Carrying Cylindrical Tubes

Cylindrical tubes made of corrosion-resistant and ant-abrasion steel in shipyard and offshore industries near the shore (Figure 3). The steel cylinders are designed to penetrate 15 meters in a permeable layer of alluvial layers with SPT N> 8. The length of each of these cylinders is more than 45 meters. These cylinders are shipped to special vessels carrying large industrial shipments. Each vessel has a capacity of more than 10,000 tons.

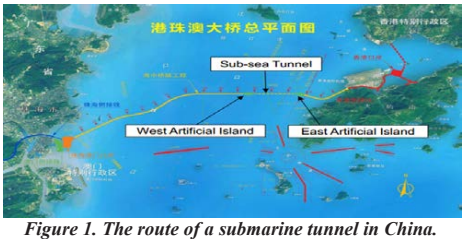

Figure 1. The route of a submarine tunnel in China.

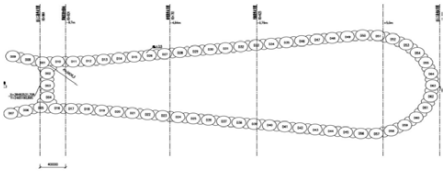

Figure 2. The shape of the island and the location of each of the cylinders.

3.3. Installing the Cylindrical Tubes

After being transferred the cylindrical tubes with special vessels from the workshops to the desired location (Figure 4), they are installed using marine cranes and other specially designed vibrating equipment at the desired location (Figure 5). On each of these cylinders, the guide lines are laid out to ensure that they are not removed from the installation line. After the installation process, the cylinders are filled with dredging ships that sucks the sea bed so that they fill the cylinders 2 meters above sea level from the bedding (Figure 6).

Figure 3. Cylinders under construction in shipbuilding and offshore industries.

Figure 4. Carry the steel cylinders from the workshop to the construction site of the island.

Figure 5. Guiding lines and vibration equipment for installing cylinders in the sea bed.

Figure 6. Filling the cylinders interior with sea bed sediments by using dredging ships.

3.4. Preparing The Inside Of The Island

After the above steps, with the help of suction equipment, the water inside the enclosed area by steel cylinders is drained. Approximately the discharge of this water last for 90 days, Then the soft soil layer is removed to depth of approximately 20 meters. After that, the area is filled with sand dunes to a height of about 5 m (Figure 7).

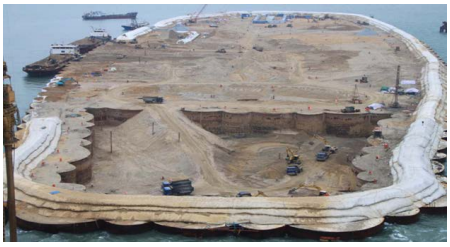

Figure 7. The final stages of building the island and the embankment within it.

4. Conclusions

Steel cylinders method can be used to construct artificial islands in deep water. One of the advantages of this method is the speed of its implementation. But this method is very expensive due to the need for special equipment. Furthermore the risks for using such a method include:

• Possibility of tilting cylinders during installation.

• Instability during construction, since each cylinder is connected with large parts by welding, so the likelihood of instability in these cylinders increases.

By creating additional reinforcing elements in each cylinder, it is possible to reduce the chance of their tilting.

5. References

[1] Ghaderi, D., Taqinejad, R., "The study of artificial islands with regard to the development of the seas and its problems," Third International Conference on Oceanographic Oceanography in the Persian Gulf, Tehran, Meteorological Organization, 2014.

[2] https://www.arup.com/projects/hong-kong-zhuhai-macau-bridge

[3] Pour Zafarani, M., "An overview on the methods of designing and constructing artificial islands", Tenth International Conference on Marine Structures, Tehran, Ports and Maritime Organization, 2012.

[4] Li, B., and Zhao, Y., "Research on simulation of soft foundation treatment'', 3rd International Conference on Advances in Energy, Environment and Chemical Engineering, 2017.

A NOVEL MODELLING APPROACH FOR EARTHQUAKE-INDUCED SEABED LIQUEFACTION

V.S. Ozgur Kirca[1,2], Giray Civak[3] and B. Mutlu Sumer[2]

1) Faculty of Civil Engineering, Istanbul Technical University, Istanbul, Turkey, kircave@itu.edu.tr
2) BM Sumer Consultancy & Research, Istanbul, Turkey
3) Graduate School of Science, Engineering and Technology, Istanbul Technical University, Istanbul, Turkey, civakg@itu.edu.tr

1. Introduction

Under cyclic loading conditions, shear deformations gradually rearrange soil grains and the pore water pressure increases in saturated, undrained soils at the expense of pore volume. In case of the presence of sufficient time and room, the pore water pressure reaches such a level that exceeds initial effective stresses and because of disappearing stresses between individual grains, the soil acts like a fluid, loses the ability to bear any load thus it fails. The term "liquefaction" is used to define this phenomenon in engineering terminology. It has been recognized that soils that can be liquefied under cyclic conditions are basically limited to fine soils or composite soils such as silty or clayey sands. As it was mentioned in the definition, liquefaction susceptibility is closely related with sort of soil parameters and cyclic loading conditions as expected. Through the years many soil failures caused by earthquake induced liquefaction has been reported by engineers and scientists. For example; in 1999 Kocaeli earthquake, an extensive liquefaction caused sinking of breakwaters, large displacements of quay walls and huge settlements of backfills which were resulted in serious damages to coastal structures (Figure 1).

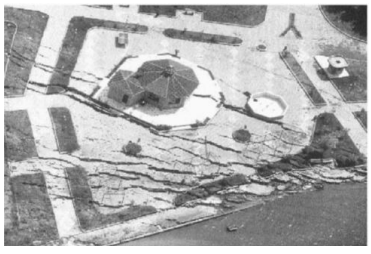

Figure 1. Liquefaction induced lateral spreading case after 1999 Kocaeli Earthquake.

There are limited comprehensive analysis methods for earthquake induced seabed liquefaction and ordinarily, specially prepared charts where the dimensionless parameter Cyclic Stress Ratio (CSR) is plotted versus corrected SPT blow counts gathered from Standard Penetration Tests to define relative density of the soil have been used by practitioners to assess liquefaction susceptibility, albeit as a first approximation [1].

In this study; an experimentally-validated mathematical model [2], which was originally developed for wave induced liquefaction, was modified and adapted to predict earthquake-induced seabed liquefaction. While earthquakes and waves both produce cyclic shear stresses (and accordingly cyclic shear deformations) in the seabed, the ones induced by earthquakes are more severe compared to that caused by waves. The early results obtained from this modified mathematical model were compared to the widely used CSR-SPT assessments to investigate liquefaction susceptibility.

2. Methodology

The method used in this study basically covers the comparison of the results obtained from a series of parametric model runs with the estimated ones from recent CSR-SPT liquefaction susceptibility assessment procedures. Primarily, earthquake-soil interaction was analyzed, then the shear stresses caused by cyclic loadings during an earthquake were used as the model input. Below equation (1) where; g is gravitational acceleration and γ_t is the total specific weight of the soil, was used with soil depth (z) dependent proper reduction coefficients (r_d) to translate maximum cyclic ground acceleration during an earthquake ,a_{max}, into average equivalent cyclic shear stresses, τ_a, in the seabed [3].

$$\tau_a = 0.65 \frac{\gamma_t z}{g} a_{max} r_d \qquad (1)$$

The modified one-dimensional mathematical model basically simulates the pore pressure build-up under cyclic loading conditions depending on the intensity of shear stresses/deformations. More than a hundred parametric runs containing different cyclic loading conditions were done for various relative densities (D_r) and pore water pressure levels where liquefaction occurs defined to calculate Cyclic Stress Ratio's by using Equation 2 shown below [3].

$$CSR = \left(\frac{\tau_a}{\sigma'_0}\right) = 0.65 \frac{a_{max}}{g} \frac{\sigma_0}{\sigma'_0} r_d \qquad (2)$$

Because of the incapability of obtaining undisturbed specimens to be analysed in the laboratory, empirical approach based in-situ penetration test results gained more popularity among engineers, and therefore, SPT

based assessments were referred to in this study. Table below summarizes the approximated relation between density indexes and numbers of corrected SPT blow counts [4].

Table 1. SPT with corrected blow counts.

Corrected SPT blow count	Relative Density (Dr)
3	0.15
8	0.35
15	0.50
25	0.65
42	0.85
58	1.00

Furthermore, a sensitivity analysis was conducted by changing the values of related soil parameters. As an addition exercise, the results obtained from the adapted mathematical model for pore pressure levels were compared to the ones measured during a centrifugal shaking table test set up to investigate earthquake induced liquefaction.

3. Results and Discussions

In this study, pore pressure build-up in the seabed under cyclic loading conditions was modelled via one dimensional experimentally validated mathematical model and then, results were compared to recent and widely used Cyclic Stress Ratio (CSR) and Cyclic Resistance Ratio (CRR) approaches to investigate liquefaction susceptibility. Figure 2 below briefly compares both model and traditionally used SPT based earthquake induced liquefaction potential assessment results.

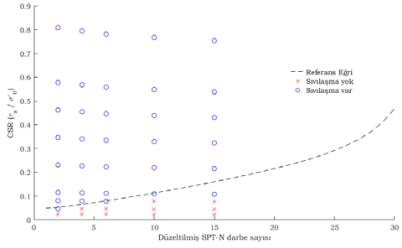

Figure 2. Simplified base curve of CRR from SPT data together with modelled liquefaction results.

In conclusion, early results showed that the adapted model has a potential to estimate earthquake-induced pore pressure buildup and seabed liquefaction, especially for soils with 30 or less SPT blow counts.

4. References

[1] Sumer, B.M. (2014). Liquefaction around marine structures, Advanced series on ocean engineering, volume 39, Singapore, New Jersey, World Scientific, 2014.

[2] Sumer, B.M., Kirca, V.S.O. and Fredsøe, J. (2011): Experimental validation of a mathematical mode for seabed liquefaction in waves. Proceedings of the 21st International Offshore and polar Engineering Conference, Maui, Hawai, USA, June 19-24, 2011,1010-1018.

[3] Youd, T.L. and Idriss, I.M. (2001). Liquefaction Resistance of Soils: Summary Report from the 1996 NCEER and 1998 NCEER/NSF Workshops on Evaluation of Liquefaction Resistance of Soils, Journal of Geotechnical and Geoenvironmental Engineering, 127(4), 297–313.

[4] Powrie, W. (2004): Soil Mechanics. 2nd edition. Spon Press, Taylor and Francis Group, London.

AXIAL COMPRESSION BEARING CAPACITY OF DRIVEN OFFSHORE PILES IN THE PERSIAN GULF – A CASE STUDY

Babak Ebrahimian [1] and Amir Hossein Shamshirgaran [2]

1) Faculty of Civil, Water and Environmental Engineering, Shahid Beheshti University, Tehran, Iran, Email: b_ebrahimian@sbu.ac.ir, ebrahimian.babak@gmail.com
2) Faculty of Civil, Water and Environmental Engineering, Shahid Beheshti University, Tehran, Iran, Email: shamshirgaran.amir@gmail.com

1. Introduction

Cone penetration test (CPT) is broadly employed in the design of offshore piles. The reliability, high-quality results and continuous recording of soil resistance in depth are the CPT advantages which result in excellent performance of CPT rather than the other in situ tests. Moreover, the shapes of CPT and pile as well as the failure mechanisms developed during penetration are similar. These significant characteristics have motivated many researchers to propose direct estimation methods of pile bearing capacity using CPT data. Herein, the axial compression bearing capacity of an offshore steel-pipe pile driven in marine clay deposits of the Persian Gulf-South Pars field is estimated using three property-based static analysis methods including API (2011), FBV (Fugro, 1996) and NGI (2005) as well as ten popular direct CPT-based methods including Aoki & Velloso (1975), Penpile (1975), Shmertmann (1978), de Ruiter & Beringen (European/Dutch, 1979), Tumay & Fakhroo (Cone-m, 1981), Bustamanate & Gianeseli (LCPC/LCP, 1982), Price & Wardle (1982), Eslami & Fellenius (Unicone, 1997), Jardine et al. (ICP, 2005), and Niazi & Mayne (Enhanced Unicone, 2015). The question is why these methods have been selected? A majority of offshore piles worldwide has been designed based on API standard as the most common design code for offshore structures. In addition, the selected CPT-based methods in this study can be classified in two groups. The first group contains the more commonly used CPT-based methods which were mainly developed before the year 2000 and the second consists of the more recently developed CPT-based methods which were included in the commentary of the new 22nd Edition of the API RP 2A Recommendation. It is mentioned that the direct CPT methods developed based on older types of mechanical CPT equipment with no pore pressure measurement, apply total stress values. The total stress approaches govern the short-term behavior of piles capacity, whereas property-based static analysis methods apply effective stress values, and govern the long-term behavior of piles capacity. Determining the pile capacity in clay necessitates using CPTu sounding with pore pressure measurements. Details of the above CPT-based methods have been given in [2] and hence not reproduced here due to space constraints. For verification purposes, the results of the aforementioned methods are compared against the PDA records obtained from dynamic load tests conducted at various pile depths during jacket installation. The paper presents the predictive performance of the above thirteen methods. The considered pile is a tubular steel pile with around 90 *m* length, 1.52 *m* diameter, and 50.88 *mm* wall thickness. Water depth at the location of jacket structure is nearly 75 *m*. Soil and CPT data relevant to the location of corresponding offshore structure are shown in Figure 1. The profiles have a general trend of increasing linearly with depth; however, the values fluctuate in some occasional cohesionless granular lenses. In the South Pars field, the clayey soil is very soft to soft at above 20 *m* depth, stiff at 20–70 *m* depth, and very stiff to hard beyond 70 *m* depth. This layering pattern is dominant; it means that no considerable variation is seen in the entire field [1].

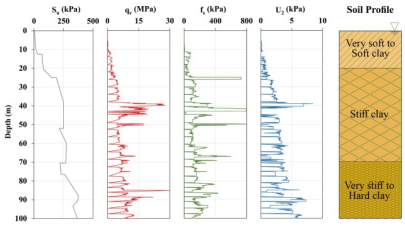

Figure 1. Soil profile and field and laboratory results in the location of considered pile.

2. Results and Discussion

The calculated curves of skin friction, end and ultimate compression bearing capacities obtained from different methods are presented in Figure 2. The results have been generated through a series of Spreadsheets which were developed and precisely verified by the authors. It is seen that the results demonstrate a very wide range of variation in the predicted capacities. The methods yield skin friction, end and ultimate bearing capacities between 13400-72600 *MN*, 4100-16200 *MN* and 19600-78600 *MN*, respectively. The calculations confirm that the end bearing contributes very little to the total ultimate bearing capacity.

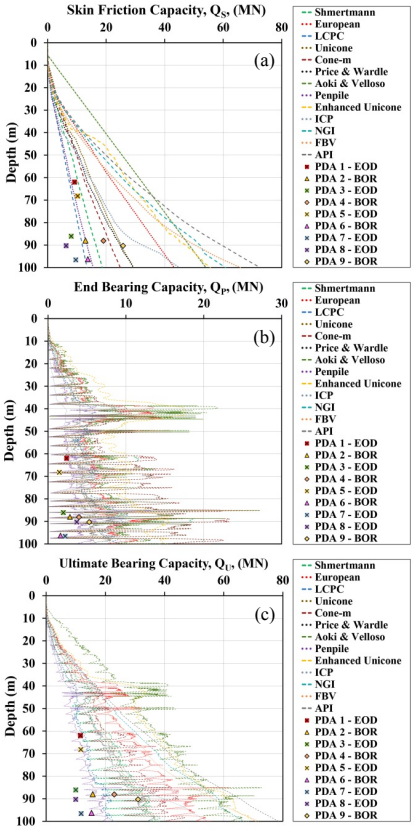

Figure 2. Axial compression capacity curves obtained from different methods and PDA results for: (a) skin friction, (b) end bearing, and (c) ultimate bearing

In order to evaluate the performance and applicability of different methods in predicting the axial compression capacity of piles in clay, PDA data and CAPWAP analysis results in EOD (End Of Driving) and BOR (Beginning Of Restrike) conditions are employed and depicted on Figure 2. It is observed that the EOD PDA data are mainly settled on the lower bound of bearing capacity curves. BOR results have been gained after 21 hours, 9 days, 29 hours and 263 days in PDA 2-BOR, PDA 4-BOR, PDA 6-BOR and PDA 9-BOR, respectively, to study the time and set-up effects on the long term behavior of soil-pile system. PDA 9-BOR has been chosen as a reference of measured pile capacity (Q_m) in long term and shown in Figure 3. As illustrated, the methods with green and red columns are close to and far from the PDA result, respectively. According to Figure 3, Eslami & Fellenius (Unicone, 1997), Price & Wardle (1982), Shmertmann (1978) and Jardine et al. (ICP, 2005) methods propose the best predictions among all methods. In contrary, API (2011), Aoki & Velloso (1975), NGI (2005), Fugro (1996), Penpile (1975) and Bustamanate & Gianeseli (LCPC/LCP, 1982) present the worse consistency with PDA result. Figure 3 confirms that API method shows the poorest performance and CPT-based methods generally provide more reliable estimates of pile capacity in clay than the API method.

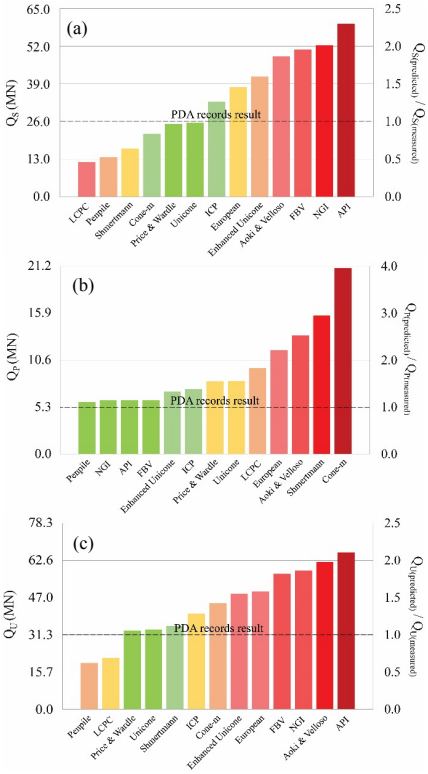

Figure 3. Comparison between different design methods and PDA 9-BOR result for: (a) skin friction, (b) end bearing, and (c) ultimate bearing

3. References

[1] Ebrahimian, B., Movahed, V., and Nazari, A., "Soil characterisation of South Pars field, Persian Gulf". *Environmental Geotechnics*, 1(2), 2014, pp. 96-107.

[2] Niazi, F. S., and Mayne, P. W., "Cone penetration test based direct methods for evaluating static axial capacity of single piles". *Geotechnical and Geological Engineering*, 31(4), 2013, pp. 979-1009.

A COMPARISON BETWEEN THE LATERAL RESPONSE OF MONOPILE IN CALCAREOUS AND SILICA SANDS BY CENTRIFUGE MODELING

Farzad Memari[1], Mohammad Reza Rasouli[2] and Majid Moradi[3]

1) M.Sc. Student, University of Tehran, Tehran, Iran, fmemari@ut.ac.ir
2) Ph.D. Candidate, University of Tehran, Tehran, Iran, rezarasouli@ut.ac.ir
3) Associate Professor, University of Tehran, Tehran, Iran, mmoradi@ut.ac.ir

1. Introduction

By increasing the demand for renewable, sustainable and greener energy resources, the offshore wind farm industry is experiencing quick growth in many countries, such as the UK and Germany. It is expected for near-term (2020), and long-term (2050) offshore wind turbines (OWTs) play an important, paramount role in reducing greenhouse gas emission. The most common foundation type for offshore wind turbines is a single large diameter pile, termed a mono-pile, which the turbine is located on. Furthermore, they are used as breasting and mooring dolphins in port structures. As the diameter of such piles is envisaged to increase in future installations, there are concerns that current design methods are not applicable. Although many types of research have done on the lateral response of mono-piles, still a paucity of comprehensive data exists to make general rules. Such piles are always subjected to significant lateral loads due to the wind, mooring force and wave actions (Figure 1). This paper describes the results of a centrifuge modeling study of the response of mono-piles embedded in calcareous and silica sands subjected to monotonic lateral loading. The experimental program involved a comprehensive set of centrifuge modeling tests on reconstituted samples of calcareous and silica sands with a similar grain size distribution tested by utilizing the Geotechnical Centrifuge of the University of Tehran at similar conditions for comparison purposes. In this study, the main characteristics of mono-pile static lateral behavior are investigated.

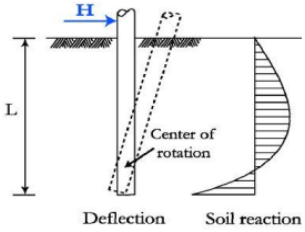

Figure 1. The response of a pile to lateral load.

2. Location of the Soil Materials

A comparison is made between the lateral response of mono-piles embedded in calcareous sand retrieved from northern coastal of Hormuz Island in the Persian Gulf and silica sand obtained from Firuzkuh, north of Iran (Figure 2). The Firuzkuh silica sand was selected to compare with Hormuz calcareous sand because it is sand widely used in Iranian geotechnical researches.

Figure 2. Location of Hormuz Island and Firuzkuh

3. Soil Characteristics

The properties of the soil materials which were tested are shown in Table 1.

Table 1. Physical Properties of the soil materials.

Sand	C_u	C_C	e_{min}	e_{max}	G_s	$CaCO_3$
F161	1.54	1.13	0.58	0.865	2.65	1.03%
Hormuz	1.49	1.11	0.64	0.92	2.78	95.3%

Details of the soil fabric can be observed through a scanning electronic microscope (SEM) on a sample or a thin of the sample. To determine the shape of soil grains, the SEM images of the soil materials were prepared as well. Images of soil samples are shown in Figures 3.a and 3.b. These figures are showing clearly the difference in particle shape. The calcareous sand has fragile, angular and hollow particles as opposed to the hard, rounded silica grains.

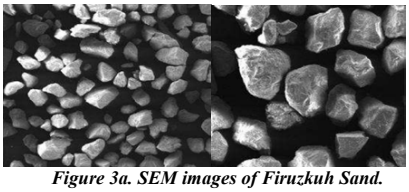

Figure 3a. SEM images of Firuzkuh Sand.

Figure 3b. SEM images of Hormuz Sand.

4. Centrifuge Modeling

As geotechnical and marine issues often have great dimensions and their modeling involves applying small exponential coefficients, there are a considerable amount of modeling-caused errors (scale effect) in them. If it is possible to equalize stress conditions at corresponding points of the model and real situations, the problem caused by scale effect errors will be largely negligible. The geotechnical centrifuge is a device that compensates the reduction of the stress caused by model shrinkage and reduces modeling errors through the local increase of gravitational acceleration by revolution. Soil models are placed on a swinging platform at the end of the centrifuge arm and then accelerated so that they are subjected to an inertial radial acceleration field of N times earth's gravity g acting normal to the surface of the platform. In centrifuges, linear dimensions of a model are reduced (1/N) based on the ratio of gravitational acceleration to acceleration of gravity (N). General scaling factors for different quantities in Ng space may be derived and summarized in Table 2.

Table 2. Scaling factors for centrifuge modeling.

Quantity	Scale Factor (Model / Prototype)
Acceleration	N
Stress and Strain	1
Length	1/N
Area	$1/N^2$
Volume	$1/N^3$
Mass	$1/N^3$
Force	$1/N^2$
Energy	$1/N^3$

4.1. Geotechnical Centrifuge at the University of Tehran

The Geotechnical Centrifuge at the University of Tehran has components such as A) floating basket, B) centrifuge beam, C) counterweights, D) hydraulic rotary connections and electronic sliding connections, E) driving system (driver), F) aerodynamic hood, G) automatic control system of balance in rotation and other minor components. It is shown in Figure 4.

Figure 4. Geotechnical Centrifuge Facility at the University of Tehran.

5. Experimental Testing

Concerning the limited space in a centrifuge, driving system and its components should occupy minimum volume. As there is no appropriate loading system in a centrifuge, it was decided to consider a lateral loading setup with a mechanical stepper motor for imposing static loading in proportion to soil chamber. Performance mechanism of the system is in a way that the rotation of the stepper motor is transferred to two pulleys and a belt round them. This motion is imposed to the end of a ball screw. The ball screw converts the rotational movement created in the motor into a translational movement.

Here, a stainless steel pipe with a 51 mm diameter was considered for modeling mono-pile to examine and compare the response of mono-piles embedded in calcareous and silica sands subjected to monotonic lateral loading. Lateral loads were applied on piles with similar embedded depth and load eccentricity. They were tested by the geotechnical centrifuge facility, and all the experiments were performed under the same acceleration.

6. References

[1] McClelland, B., "*Calcareous sediments: an engineering enigma*", Proceeding, Int. Cong. On Calcareous Sediments, Perth, Australia, 1988, pp. 777-784.

[2] Hassanlourad, M., Rasouli, M. R., Salehzadeh, H., "*A comparison between the undrained shear behavior of carbonate and quartz sands*", Int. J. Civ. Eng. 12, 4, 2014, pp. 338–350.

[3] Randolph, M. F., Gourvenec, S., "*Offshore Geotechnical Engineering*", CRC Press, 2011.

[4] Dyson, G. J., Randolph, M. F., "*Monotonic Lateral Loading of Piles in Calcareous Sand*", J. Geotechnical and Geoenvironmental Eng, 127, 4, 2001, pp. 346-352.

[5] Hassanlourad, M., Rasouli, M. R., "*Triaxial shear behavior of carbonate and silica sands*", 10th ICOPMAS, Tehran, Iran, 2012.

[6] Moradi, M., Ghalandarzadeh, A., "*A new geotechnical centrifuge at the University of Tehran, I.R. Iran*", Proceeding of the 7th ICOMG, Zurich, Switzerland, 2010, pp. 251-254.

DAMAGE DETECTION IN JOINTS LOCATION OF OFFSHORE JACKET PLATFORMS

Amin Rahimzadeh[1], Ahmad Reza Mustafa Gharabaghi[2] and Mohammad Reza Chenaghlou[3]

1) Faculty of Civil Engineering, Sahand University of Technology, Tabriz, Iran, a_rahimzadeh@sut.ac.ir
2) Faculty of Civil Engineering, Sahand University of Technology, Tabriz, Iran, mgharabaghi@sut.ac.ir
3) Faculty of Civil Engineering, Sahand University of Technology, Tabriz, Iran, mrchenaghlou@sut.ac.ir

1. Introduction

The fixed offshore jacket platforms are always at exposure of the sever environment condition of sea. Because of the high importance of these structures, early detection of damages, when they are minor, and their repair can prevent from further serious dangers. According to a report from the damages caused to the jacket platforms in the NFS[1] from 1974 to 2016, mostly damages are of crack type at the joints [1]. The purpose of the paper is to detect damages in jacket platforms with respect to minor damages at the joints. Among different methods of damage detection, signal processing methods have better performance in health monitoring of complex structures with nonlinear behavior. By studying the researches of Kim and Melhem, Byissa et al., Rakowski, Zhu and Huang et al. [2-6], it is found that the wavelet transform method has a high ability to detect minor damages. In this paper, the wavelet packet transform is used to extract the wavelet packet energy rate to damage detection at the joints. However, these detects have errors. Therefore, a target function formulated based on the wavelet packet energy rate index (WPERI). Then, the LSE[2] optimization optimizes target function to obtain a new index (WPTLSE) to reduce the errors and improve the results.

2. Modeling and Verification

For modeling, the SPD16 platform of the South Pars Gas Field Development Phase 12 in the Persian Gulf was simulated in Abaqus. According to Figure 1, for substructure modeling, the Wire element based on the cross section characteristics, and for deck modeling, Shell element based on its loading characteristics is used. For the pile-soil interaction the equivalent length of pile with fixity point at the end was used. Water effect is considered as an added mass and hydrodynamic damping.

To verify the structure modeling, the natural frequencies of the first three modes were compared to the original designed structure frequency that has acceptable difference below 8%.

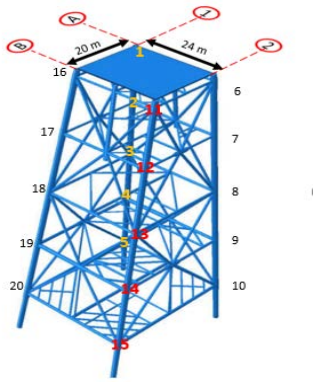

Figure 1. The modeled jacket platform

3. Identification Method

The principles of damage detection methods are often based on the comparison of a structural system in two different states (damaged and undamaged). Accordingly, structure signals must be available in the two phases, and then processed. Wavelet packet transform is one of the signal processing approaches provides level by level decomposition of signal. However, processed signal properties should be extracted to be comparable in two different states.

Wavelet packet energy, E_{f_j}, at the level j of signal decomposition is the extracted property calculated according to the following equation:

$$E_{f_j} = \int_{-\infty}^{\infty} f^2(t)dt = \sum_{m=1}^{2^j}\sum_{n=1}^{2^j}\int_{-\infty}^{\infty} f_j^m(t) f_j^n(t)dt \quad (1)$$

And the wavelet packet energy rate (WPERI) at the level j is calculated according to Equation 2:

$$WPERI = \sum_{i=1}^{2^j} \frac{\left|\left(E_{f_j^i}\right)_{sd} - \left(E_{f_j^i}\right)_{wd}\right|}{\left(E_{f_j^i}\right)_{wd}} \quad (2)$$

In this equation, *sd* and *wd* refer to damaged and undamaged states respectively. f^i_j is the i th component of the j th level of decomposition. Lotfollahi Yaghin et al.

[1] Norwegian continental Shelf
[2] Least Squares Estimator

used wavelet packet energy rate as a damage index by applying a damage threshold (WPERI-UL WPERI) [7]. In this paper, this index is used as WPERI and is compared to the proposed index.

In this research, a two-step method for damage detection is designed. At first, by shaking an undamaged structure under an impact load, the displacement-time signals are taken in 20 seconds for 20 points of the structure at the joints location, where cross platform floor elements with leg elements as shown in Figure 1. Then, by causing damage to each joints, while other joints are undamaged, and re-shacking the structure under the same load, displacement-time outputs are obtained again at the same previous points. Here, all damages are considered as 5% decrease in cross-section along 2mm of the member connected to the joints. At this step, WPERI is calculated according to equation (2). In this paper, based on the signal frequencies and trial and error method, the db5 mother wavelet is used at the fifth decomposition level. Therefore, each joint will then have a WPERI index for different damages.

At the second, a data-based optimization, in which the information extracted from the system used as training data for target function is applied. In this step, the WPERI is used to train the target function and LSE optimization method is used to optimize target function. By considering the WPERI obtained from each joint in each damage as a component of a vector, each damage will be a vector [Xi]:

$[X_i] \rightarrow$ *Damage in* i_{th} *node*

Now, any other damage in the structure will create a unique vector by WPERI as *Y*. By weighing the vector [Xi] with A[i], a target function is formed based on these vectors according to equation (5). To minimize this target function, the LSE algorithm is used to find the weight combination of *Ai* that is more similar to *Y*. This combination of *Ai* is introduced as WPTLSE index by using the threshold of damage and it is used to identify the location of the damage.

$$A_i \rightarrow [X_i]$$

$$\left(\sum_{n=1}^{20} A_i X_i\right) - Y \qquad if \quad 0 \le A_i \le 1 \tag{3}$$

4. Results

In this section, the performance of the proposed WPTLSE index is evaluated to detect the damage location by applying several damage scenarios. The scenarios were considered while two damages exist in the structure and the results are compared between WPTLSE and WPERI. In this paper, merely the combination of damage in No.1 joint with other joints has been investigated.

It is determined that in 38 possible cases of damage, the WPERI index detected 24 damages successfully and 71 errors. Where, WPTLSE detected 28 damages successfully and 14 errors. The following graph shows the improvement in the results of the WPTLSE index.

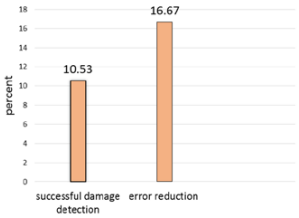

Figure 2. The improvement in the results of the WPTLSE

5. Conclusion

The purpose of this research was minor damage detection at the joints of fixed offshore jacket platform. With this aim, the method of wavelet packet transform was used as an appropriate tool for minor damage detection. Then, the wavelet packet energy rate was calculated and the WPERI index obtained by applying a threshold of damage. However, due to the number of errors identified in this method, the new index, WPTLSE, was introduced by creating a target function based on the wavelet packet energy rate and using the LSE algorithm. Several damage scenarios were applied to the structure in existing of two damages at the same time and then WPERI and WPTLSE indices were compared. The results indicate an increment in successful detection of damages, reduction in errors, and improvement in the accuracy of using the WPTLSE index.

6. References

[1] Vestli, H., (2016), "*Structural Health Monitoring of Offshore Jackets",* Master's thesis, University of Stavanger, Norway.

[2] Kim, H., & Melhem, H., (2004), "Damage detection of structures by wavelet analysis", *Engineering Structures*, *26*(3), 347-362.

[3] Bayissa, W. L., Haritos, N., & Thelandersson, S., (2008), "*Vibration-based structural damage identification using wavelet transform*", Mechanical Systems and Signal Processing, *22*(5), 1194-1215.

[4] Rakowski, W. J. (2017). "*Wavelet approach to damage detection of mechanical systems and structures*". Procedia Engineering, *182*, 594-601.

[5] Zhu, X. Q., Law, S. S., & Jayawardhan, M. (2011). "*Experimental study on statistical damage detection of RC structures based on wavelet packet analysis*". In Journal of Physics: Conference Series (Vol. 305, No. 1, p. 012107). IOP Publishing.

[6] Huang, Y., Yang, Y., & Li, H. (2010, April). "Fractal theory and wavelet packet transform based damage detection method for beam structures". In *Health Monitoring of Structural and Biological Systems 2010* (Vol. 7650, p. 76503I). International Society for Optics and Photonics.

[7] Lotfollahi-Yaghin, M. A., Shahverdi, S., Tarinejad, R., & Asgarian, B. (2011, January). "*Structural Health Monitoring (SHM) of Offshore Jacket Platforms*". In ASME 2011 30th International Conference on Ocean, Offshore and Arctic Engineering (pp. 579-588). American Society of Mechanical Engineers.

LONG TERM STRESS RANGE DISTRIBUTION OF THE RISER OF AMIRKABIR SEMISUBMERSIBLE PLATFORM UNDER THE EFFECT OF WAVES

Zohreh Sadat Haghayeghi[1] and Mohammd Javad Ketabdari[2]

1) Marine Engineering Department, Amirkabir University of Technology, Tehran, Iran. z.haghayeghi@aut.ac.ir
2) Marine Engineering Department, Amirkabir University of Technology, Tehran, Iran. ketabdar@aut.ac.ir

1. Introduction

Top-tensioned risers, are prone to high amplitude vibrations under the effect of waves, vortex shedding, vessel motion and internal flow. Due to the oscillating nature of forces acting on the riser, it experiences varying stress ranges which leads to fatigue damage. In this research the riser of Amirkabir semisubmersible rig was modeled to estimate the long-term stress range distribution over its length. For this purpose a FEM model of a tensioned Euler-Bernoulli beam was developed for simulation of riser's motions. The vibration of riser under the effect of waves in the long-term was calculated in the time domain for different sea states from the wave scatter diagram. The riser has been analyzed in each sea state of the wave scatter diagram by 50 times to reduce the sampling error. Then a rainflow cycle counting method was applied to find the stress ranges and the number of their occurrences. Finally a Weibull distribution was fit to the stress ranges to find the distribution of stress ranges in the lifetime of riser

2. Riser Analysis Methodology

The equation of motion of a riser connected to a semisubmersible rig as shown in Figure 1 can be written as [1]:

$$EI\frac{\partial^4 u(z,t)}{\partial z^4}-\frac{\partial}{\partial z}T(z)\frac{\partial u(z,t)}{\partial z}+m\frac{\partial^2 u(z,t)}{\partial t^2}=f(z,t) \quad (1)$$

where EI denotes the flexural rigidity, m mass, $T(z)$ the variable tension along riser defined by:

$$T(z)=T_t-W_s(L-z) \quad (2)$$

W_s is the submerged weight of riser, $f(z,t)$ is the transverse force on the riser calculated via the following relation [2]:

$$f_X(z,t)=\frac{1}{2}\rho C_d\left|U_C+U_W-\dot{u}\right|(U_C+U_W-\dot{u})+\rho\frac{\pi D^2}{4}(C_m-1)\ddot{u} \quad (3)$$

In this equation U_C is the marine current velocity along the riser:

$$U_c=U_C\left(1-\frac{z}{h}\right) \quad (4)$$

and U_w is the wave particle velocity, $\dot{u}$ and $\ddot{u}$ are riser velocity and acceleration respectively while C_d and C_m denote the drag and added mass coefficients.

The pinned-pinned boundary conditions has been applied to the FEM model of riser and the stress in the cross section of riser due to bending moment and top tension can be written as [3]:

$$\sigma_x(z)=\frac{T_t}{A_c}+E\frac{D_0}{2}\frac{\partial^2 u}{\partial z^2} \quad (5)$$

where A_c is the riser's cross-sectional area. The model dimensions and parameters used in this study are listed in Table 1.

Table 1. Riser properties.

Property	Value
Outer diameter (D_o)	0.53 m
Inner diameter (D_i)	0.48 m
Riser length	800 m
Modulus of elasticity	2.07 GPa
Water density	1025 Kg/m^3
Steel density	7850 Kg/m^3
Inner flow density	998 Kg/m^3
Added mass coefficient (C_a)	2
Drag coefficient (C_d)	0.7
Current velocity at surface (U_C)	0.5 m/s
Top tension (T_t)	3000 KN
Water depth (h)	800 m

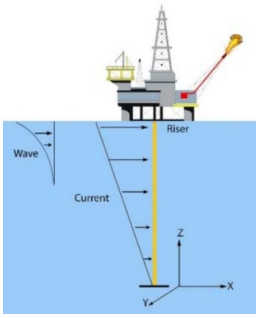

Figure 1. Schematic of riser in the marine environment.

3. Long-term Wave Data

Wave data used in this research was provided by KEPCO (Khazar Exploration and Production Company). The wave scatter table contains the characteristics of 87 possible sea states. Figure 2 shows the contour plot of probabilities of occurrence of sea states of the wave scatter table.

For each combination of H_s and T_p, an irregular wave is produced from a Pierson-Moskowitz spectrum as [4]:

$$S_\eta(\omega)=\pi^3\left(\frac{2H_s}{T_p^2}\right)\frac{1}{\omega^5}\left[\exp\left(-\pi^3\left(\frac{2}{T_p\omega}\right)^4\right)\right] \quad (6)$$

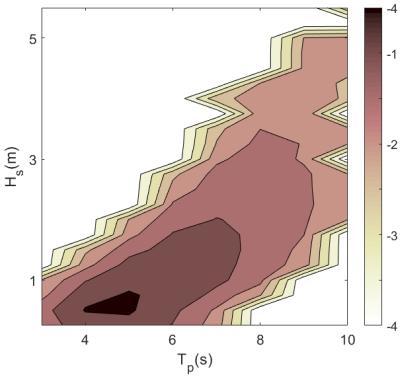

Figure 2. The logarithmic contour plot of probability of occurrence of wave height and period.

4. Stress Time History Statistics

As previously stated, the riser was analyzed in each sea state 50 times to reduce the modelling error. The stress time histories in 200 points along the riser were selected to find the stress ranges and their numbers. Finally a Weibull distribution was fit to these stress ranges to find their long-term distribution. The distribution is as follows [5]:

$$F_S(s)=1-\left[\exp\left(-\left(\frac{s}{A}\right)^B\right)\right] \quad (7)$$

The result of this analysis can be directly applied in the prediction of the lifetime of the structure. The Weibull distribution for the long-term stress distribution of midpoint of riser is displayed in Figure 3.

This distributions can be used to acquire the probable hotspots. A more refined analysis may be required for places where the Weibull distribution has higher amounts of shape and scale parameters (A and B).

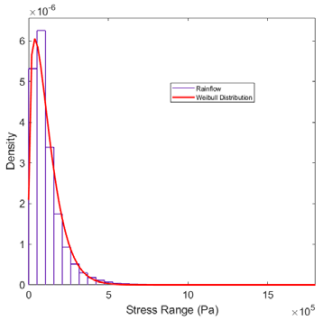

Figure 3. Weibull distribution fit to the stress ranges of midpoint of riser.

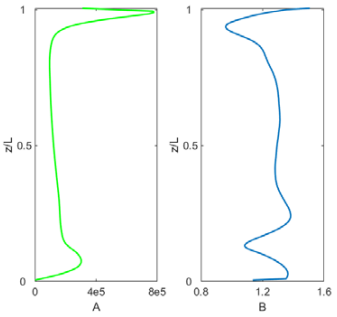

Figure 4. The parameters of Weibull distribution fit to stress ranges along the riser vertical axis.

The results of the analysis for 200 sections over the length of riser have been finally plotted in Figure. 4.

5. References

[1] Huera-Huarte, F. J., Bearman, P. W., and Chaplin, J. R., "On the force distribution along the axis of a flexible circular cylinder undergoing multi-mode vortex-induced vibrations," *J. Fluids Struct.*, vol. 22, 2006, pp. 897–903.

[2] Xiaomin L.I., Haiyan G.U.O., Meng F., "Stress analysis of top tensioned riser under random waves and vessel motions", *J. Ocean Univ. China.* Vol. 9, 2010, p.251–256.

[3] DNV, "DNV-OSS-302 Offshore Riser Systems",October 2010.

[4] Patel, M. H., "Dynamics *of Offshore Structures*", Butterworth-Heinemann, 1989

[5] Naess, A., Moan, T., "Stochastic *dynamics of marine structures*", Cambridge University Press, 2013

PARAMETRIC STUDY ON STRUCTURAL GEOMETRY OF WIND TURBINE IN PERSIAN GULF CONDITIONS

AmirAli Safaralizade[1] and Mohammad Javad Ketabdari[2]

1) MSc Graduated, Faculty of Marine Technology, Amirkabir University of technology, aa.safaralizadeh@ aut.ac.ir
2) Associate Professor, Faculty of Marine Technology, Amirkabir University of technology, ketabdar@aut.ac.ir

1. Introduction

In recent years, various methods have been innovated and developed for attaining clean and renewable energies. In this regard different types of wind turbine at land and sea have been used for transforming kinetic energy to electrical energy. By considering cumulative power of wind at marine environment and also increasing cost of construction, implementation and operation in the environment, it is necessary to perform serious researches to optimize design costs. Among this, analysis of geometry parameters effects on applied forces on mooring and establishment of foundation in floating wind turbines and stability maintenance and optimization of mooring cost is very important. According to global statistics up to 2050, 12% of electricity generation in world will be obtained from renewable resources. The length of Iran shoreline is 5800 Km and the area of sea is 1900 Km^2 that cause a good availability to high potential of renewable energy of wind [1].

A few studies had been performed by researchers on stability and establishment of offshore platforms and wind turbines. Among them Larsen analyzed spar platform and optimization its geometry [2]. Jain and Agarwal studied mooring behavior at spar platform affected by waves [3]. Raeis Zade and Motahar stated that use of turbine with horizontal axis is optimal on Persian Gulf [4]. Ketabdari and Mirzaee Sefat studied interactions of linear waves with behavior of spar platform and modeled structural behavior against linear waves [5]. In present study, effect of geometry changes of different parts of wind turbines on applied forces and platform stability modeled and simulated by ANSYS AQUA Software and its effect on applied forces on mooring by considering JONSWAP wave spectrum are evaluated.

2. Force Estimation

Diffraction-dispersion theory was used for estimating applied forces on floating turbine structure. ANSYS AQWA Software uses 3D panel model for object with arbitrary shape and the mean of progress rate for estimating hydrodynamic forces and movements of floating turbine in waves. Panel method is a numerical method for estimating potential around object based on Green Integral theory [5]. In this method there is no limitation for form and shape of the body and it is assumed that oscillation amplitude of fluid respect to dimensions of object is small. Since every panel meet principles of potential theory, flow separation is ignored.

Here, the fluid is incompressible and non-rotational type and fluid field is defined as total potential function obtained by sum of functions:

$$\phi(x,y,z)e^{-i\omega t} = \left[(\phi_I + \phi_d) + \sum_{j=1}^{6} \phi_j x_j \right] e^{-i\omega t} \quad (1)$$

This potential function should be applied on following Laplace equation:

$$\nabla^2\Phi = \frac{\partial^2\Phi}{\partial x^2} + \frac{\partial^2\Phi}{\partial y^2} + \frac{\partial^2\Phi}{\partial z^2} \quad (2)$$

In this study proportional to 25 m depth, for JONSWAP spectrum the Gamma spectrum factor of 3.3 and peak frequency of 0.125 Hz are considered to model real condition of Persian Gulf. It leads to a significant wave height (Hs) of 4 m for such a condition. In the present study a mini spar wind turbine with four catenary type mooring cables were used (See Figure 1). Results of these modeling for maximum tension in cables were presented. Findings show that tension in mooring cable is increased with increase of spar diameter which has exponential relation. In the case of analysis of effect of draft depth of spar on mooring force of floating wind turbine, several model with different depth including 7.5, 10, 12.5 and 15m were generated and studied (see Figure 2). Figure 3 shows the cables tension against spar draft. This shows the rate of increase in maximum mooring forces. On the other hand, induced forces on moorings with 100, 150 and 200 mm diameter were calculated in order to study applied forces from floating wind turbine with 2m diameter and 10m draft depth. This shows that average mooring forces increased up to 30% by increasing the mooring diameter (see Figure 4).

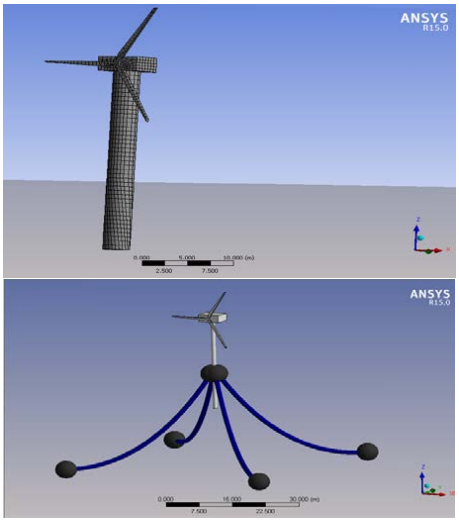

Figure 1 Modeled wind turbine in software

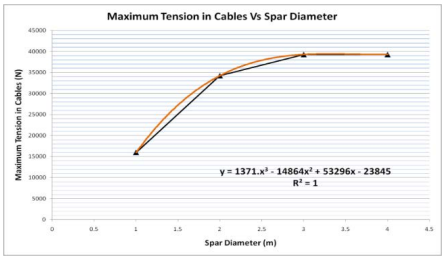

Figuer 2. Maximum Tension in Cables Vs Spar diameter

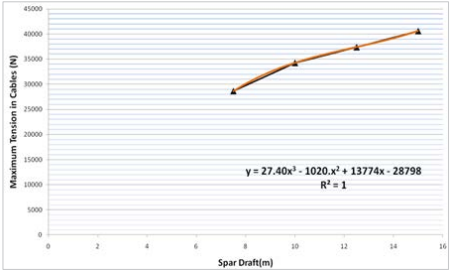

Figuer 3. Maximum Tension in Cables Vs Spar Draft

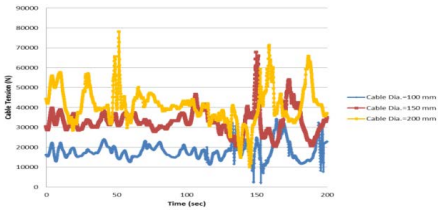

Figuer 4. Mooring force changes versus diameter

3. Conclusion

In this paper a mini spar wind turbine with four catenary type mooring cables were modeled in sea state of Persian Gulf by Ansys Aqwa software. The most important results are as follows:

- Mooring forces of floating turbine increased by increasing diameter of spar, while the rate of this increase decrease by increasing the diameter of spar.
- Relation between spar diameter and maximum tension is an exponential relation
- Maximum value of mooring force increases by increasing the draft diameter of spar.
- The average value of mooring force which is generated in different models with different diameter of mooring is increased up to 30 % by increasing the mooring diameter.
- By increasing the moorings diameter, their applied forces increase.

4. Reference

[1] Arapogianni. A, Moccia. J and Wilkes. J "The European Offshore Wind Industry – Key Trends and Statistics" *European Wind Energy Association*, Brussels, 2013, p 31.

[2] Larsen, T. J(2002). "Modeling of Wave Induced Motions of a SPAR Buoy", M.Sc. Thesis, Norwegian University of Science and Technology, 2002.

[3]Agarwal, A. and A. Jain "Nonlinear coupled dynamic response of offshore Spar platforms under regular sea waves." Ocean engineering 30(4), 2003. pp. 517-551.

[4] Reiszadeh, M. and Motahar, S., "The wind energy potential in the coasts of Persian Gulf used in design and analysis of a horizontal axis wind turbine." In: World Renewable Energy Congress, 8-13 May, 2011, pp. 4058-4065

[5] Ketabdari, M and Mirzaee Sefat ,S, "Dynamic analysis of interaction of linear waves with spar floating platform", civil engineering and planning Journal 45(1), 2011, pp. 45-52.

BEHAVIOUR OF SEASTAR TLP IN CASPIAN SEA WAVE CONDITION USING NUMERICAL MODELING

Ali Firoozpur[1], Mohammad Javad Ketabdari[2] and Farhood Azarsina[3]

1) Science and Research Branch of the Islamic Azad University, Tehran Iran, ali.firoozpur@gmail.com
2) Faculty of Marine Technology, Amirkabir University of Technology.Tehran-Iran, ketabdar@aut.ac.ir
3) Science and Research Branch of the Islamic Azad University, Tehran Iran, f.azarsina@srbiau.ac.ir

1. Introduction

SeaStar platform is a new generation of tension-leg platform, somewhat similar to Spar platform, which in addition to the benefits of Spar, benefits from the positive properties of tension-leg platform. SeaStar platform uses a cylindrical main body with three completely submerged appendages and provides the required Buoyancy for load-bearing deck and equipment. Pre-stretched cables are connected to these three appendages [1]. Due to this remarkable buoyancy a SeaStar platform can handle up to about 1.8 times its own weight while for a Spar platform this is equal to 0.6. Also, less use of steel in this platform has made it very economical [2]. The movement of SeaStar platform to three degrees of freedom (Surge, Sway, Yaw) is comparative and the natural period is large while it is less in the other three degrees of freedom (Heave, roll, pitch) which are known as the hard movements of the platform [3]. The process results from initial stretching exercise sufficient to control the platform. Sreekumar et al. (2001) using linear diffraction radiation theory studied the behavior of a mini seastar TLP [4]. In 2006, Tabeshpour and his colleagues analyzed the hydrodynamics of a TLP under the influence of waves [5]. Abaiee et al. conducted numerical and laboratory studies on the seastar TLP platform in 2015 and presented and discussed the results [6]. Substantial benefits of the SeaStar platform as well as proving the existence of huge oil resources in deep waters of the Caspian Sea forced us to analyze this kind of platform and establish a positive step towards enhancing the countrys capacity in the field of oil extraction drilling. In this paper, the behavior of a mini SeaStar platform in deep water of Caspian Sea due to regular waves was investigated using Moses software. The RAO charts of the hard and soft movements of the platform are then estimated in different collision angles.

2. Numerical Modeling

To analyze the model, the SeaStar platform was implemented in the current environmental conditions of Amirkabir Semi-Submersible platform in a water depth of 700 m, wave height of 7 m and wave period of 9.4 sec using INCO wave modeling data in Figure 1 [7]. Figure 2 shows the SeaStar TLP geometry used in this research and its modeling in software.

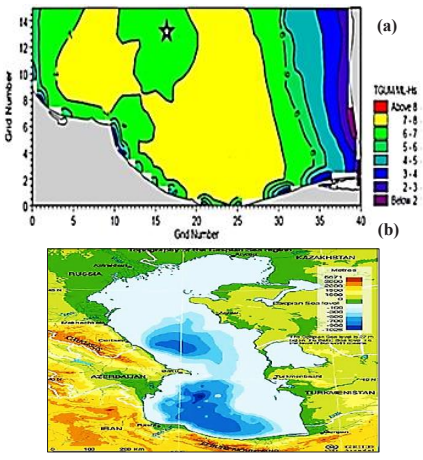

Figure 1. a) Waves characteristics b) Bathymetry on the south coast of the Caspian Sea [7]

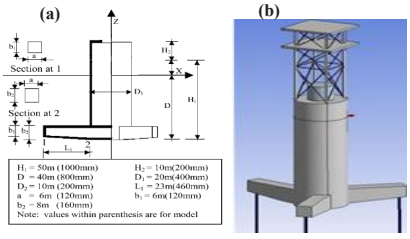

Figure 2. a) SeaStar platform geometry b) Its numerical modeling

3. Results

The RAO values of the modeled SeaStar TLP platform for 0, 45 and 90 degrees angles of the collision of waves are shown in Figures 3 and 4. As shown in these Figures, the RAO values for the Heave movement are almost linear and close to zero, which is due to the Tensioned type of platform moorings. Furthermore RAO of the rotational movement initially increases but decreases again after reaching its maximum. In fact the peak RAO of rotating movements occurs in the resonance vicinity where natural and wave frequency are close.

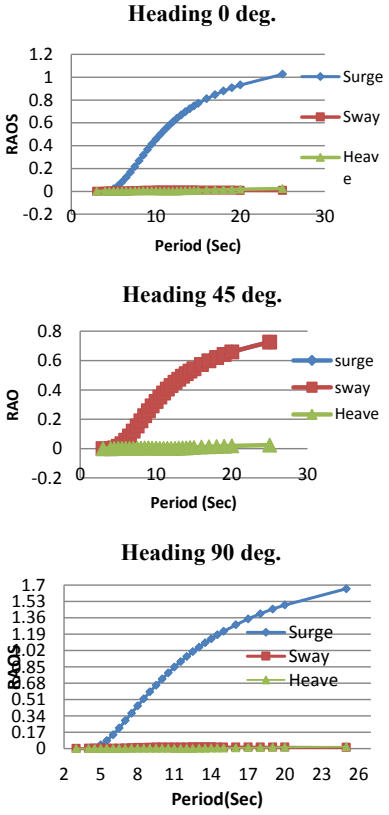

Figure 3. SeaStar Surge, Sway and Heave RAO in different headings

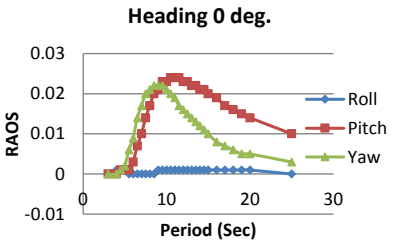

Figure 4. SeaStar Roll, Pitch and Yaw RAO in 0 heading

4. Conclusions

In this paper, the hydrodynamic behavior of the Seastar TLP was studied. The purpose of the study was to investigate the behavior of the platform movements under the impact of collision waves in the Caspian Sea. In order to obtain the amplitude of the response from the 3D-diffraction theory, motions and wave responses are obtained using spectral analysis. The results indicates the proper behavior of the platform in the conditions of the Caspian Sea for operation. Therefore, it is recommended to use this platform at the deep points of the Caspian Sea.

5. References

[1] Kibbee, S., Chianis, J., Davies, K.B., and Sarwono, B.A., The SeaStar Tension Leg Platform, *Offshore Technology Conference*, *OTC 7535*, 1994, pp. 243–256.

[2] Ketabdari, M. J., Alemi Ardakani,and H., Alemi Ardakani, M., "Laboratory Investigation On Response Behaviour Of SeaStar Mini Tension Leg Platformm Against Random Water Waves", 26th International Conference On Offshore Mechanics and Arcitic Engineering, OMAE, 2007.

[3] Battacharyya, S.K., Sreekumar, S., and Idichandy, V.G., Coupled Dynamics of SeaStar Mini Tension Leg Platform, Ocean Engineering 30, 2003, pp. 709-737.

[4] Sreekumar, S., Bhattacharyya, S.K., and Idichandy, V.G., "Coupled dynamics of SeaStar mini tension leg platform using linear diffraction-radiation theory", Offshore Mechanics and Arctic Engineering Conf, 2001.

[5] Tabeshpour, M.R., Golafshani, A.A., and Seif, M.S., "Efficient Numerical Dynamic Analysis of Tension Leg Platforms Under Sea Wave Loads", Journal of Marine Engineering, 3(5).2006, pp.15-30.

[6] Abaiee, M.M., Ketabdari, M.J., Ahmadi, A. and Alemi Ardakani, H., Numerical and Experimental Study on Dynamic Behavior of Sea-star TLP against Regular Waves, Journal of Applied Mechanics and Technical Physics, 57(3), 2015, pp. 510-517.

[7] Iranian National Center for Oceanography, Iranian seas wave modeling – Caspian Sea, Project Report, 1(2), 2005.

ANALYZING THE CURRENT ADVANCES IN HULL CLEANING TECHNOLOGIES

Mohammad Reza Hedayati[1], Mehdi Kamyab Roudsari[2], Mohammad Hossein Amiri[3] and Fatemeh Khodadadi[4]

1) Assistant professor Scientific-Applied Faculty of Post &Comm. Tehran, Iran
2) PhD Research Scaller, Chemical Engineering, Islamic Azad University–Tehran North Branch, Iran
3) MSc student, Islamic Azad University–Tehran North Branch, Iran
4) MSc student, Software Engineering, University of Hertfordshire, Hatfield Hertfordshire, UK

1. Introduction

This paper is part of a collaborative project between ITMO Co. Iranian Sanat Sadaf Co. and Islamic Azad University (North Branch) to study the impact of hull and propeller fouling on vessel's fuel consumption and emissions. It is well known that hull fouling, particularly in case of "hard or shell fouling", can cause detrimental impact to the ship hydrodynamic performance. However, some cleaning practices may also lead to decreased lifetime of the fouling-control coating. The surface covered by sea adherence is about 80% of total ship hull and all sea adherences have to be cleaned before inspection. Underwater cleaning of the hull and the adhesive coating can therefore be performed in between dry-dockings in order to improve the ship's efficiency. Furthermore, hull and propeller cleaning require different time to be performed and imply in distinct costs. Thus, there should be an optimal frequency of maintenance of hull and/or propeller depending on the ship specific fouling condition. The work presented here has consisted in performing several sea trials according to latest standards, in different configurations, in order to isolate the influence of the hull and the propeller underwater cleaning for a crude oil tanker.

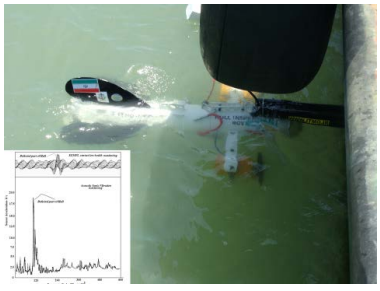

Figure 1 : Specially designed and fabricated robot for hull assessment and cleaning in Iran by authors

This project also is intended to provide a technical assessment of the emerging industry of hull cleaning robots to help the Iran Port and Maritime Organization with their goal of protection and conservation of ports and seawater environments. The project resulted in a comprehensive list of many hull cleaners that identified. In order to obtain effective and usable information for the PMO and the Department of Environment following objectives are defined:

1. Presentation of potential hull cleaning systems and important hull cleaning technologies
2. Study of constraints for evaluating hull cleaning systems
3. Survey on current hull cleaning technologies and ones currently in Development

Besides preventing direct surveying, marine fouling causes a decrease of ship's speed and consequently increases the fuel consumption. For recuperation of ship's performance, it is necessary to dry-dock a ship and to clean off the marine growth on ships hull. This cleaning is always required before any other repairing/maintenance activities can follow on. Nowadays cleaning is done manually in dry-dock with an employment of different adapted methods like grit blasting or water jet. It has to be noticed that, in itself, it is a very contaminant operation (the resulting dust always contains painting particles), it is harmful for human operators health and it is a very uncomfortable job.

The use of the new technical solution allows cleaning a ship from sea adherence without the use of an expensive dry dock. In this case it would be possible to clean a ship much more often, for example, twice a year. Even in the case when it is necessary to make inspection, repair or restoration of a protective coat of a ship in a dry dock, it would be possible to make a ship's hull cleaning out of a dry dock first, which would allow using dry dock more efficiently [1].

A vessel's fuel performance usually begins decreasing after six months from dry-dock and continues to decrease rapidly. Underwater marine growth, barnacles, and/or sea grass can cost a ship-owner millions of extra dollars in time and fuel costs each year. To prevent spending additional dollars for fuel, a ship should be cleaned twice a year. A new VLCC tanker uses approximately 96 tons of bunker fuel per day and 610 barrels of fuel per 24-hour period. The cost per day for fuel alone would be approximately $30,000 with an additional $20,000 for operating expenses per day. On an average 15,000-mile cruise, the VLCC tanker would

make the cruise in about 25 days with a clean hull. If the ship's hull is fouled with marine growth not exceeding 0.5 inch, the same trip would take 28 days. The difference is the loss in speed of over 2 knots, which equates to 3 days. Those additional three days cost $90,000 in fuel consumption alone. The propeller is particularly vulnerable to marine fouling since it is an unpainted surface that must remain clean and shiny for proper operation. The U.S. Navy determined that propeller fouling, despite its small surface area, can generate energy losses amounting to half that of the hull it so maintaining a clean propeller is critical. On military ships, the unpainted surfaces such as propellers, rudders, and sonar domes are cleaned twice as often as the hull surfaces. The propellers are also polished routinely to reduce friction and ensure that the propeller operates at optimum efficiency. Even with routine maintenance, surface roughness can occur as a result of erosion, corrosion etc. This roughness alone can increase fuel consumption up to 10 percent.

2. Hull Cleaning Intervals

The optimum interval between the periodic cleanings and inspections that comprise a preventive maintenance program will vary with the type of vessel, the location of the vessel, and its service profile (speed of operation, idle time, etc.). The type and condition of bottom coatings will also have an effect on the cleaning interval. Large vessels typically have several layers of coatings, up to 6 millimeters thick, and generally operate 4 to 6 months between hull cleanings. The location of the vessel also has a substantial influence on the rate of fouling since marine organisms flourish in warm tropical waters. The U.S. Navy has established geographic fouling zones, indicating the frequency with which the hull and unpainted surfaces (propellers, rudders, and sonar domes) should be cleaned for vessels operating within each geographic zone. In Navy Zones 1 and 3, propeller cleaning is recommended up to six times a year and hull cleaning is recommended up to three times a year.

3. Conclusions

In this paper, observe of main solutions of cleaning a ship is offered, allowing making decision about necessity of underwater ship hull cleaning by robotic devices. Such systems will prolong the service and enable excluding the use of dry dock for performance of this operation that will reduce many times the cost of ship maintenance. This research work examines current motivations and capabilities of hull cleaning robots.

4. References

[1] Cohen, A. N. and J. T. Carlton. 1998. Accelerating Invasion Rate in a Highly Invaded Estuary. Science 279:555-558.

[2]Balashov VS, Gromov BA, Ermolov IL, Roskilly AP (2011) Cleaning by means of the HISMAR autonomous robot. Russian Engineering Research 31(6):589-592.

[3]Coles, S.L., R.C. DeFelice, L.G. Eldredge, and J.T. Carlton. 1999. Historical and recent introductions of non-indigenous marine species into Pearl Harbor, Oahu, Hawaiian Islands. Marine Biology 135(1):147-158.

[4]Chambers, L.D., Stokes, K.R., Walsh, F.C. and R.J.K. Wood. 2006, Modern approaches to marine antifouling coatings. Surface and Coatings Technology, vol. 201, pp. 342–52.

[5] Hopkins GA, Forrest BM, Piola RF, Gardner JPA (2011) Factors affecting survivorship of defouled communities and the effect of fragmentation on establishment success. Journal of Experimental Marine Biology and Ecology 396: 233-243.

THE EFFECTIVENESS OF THE SLIDING ISOLATORSIN CONTROLLING THE DYNAMIC RESPONSES OF THE JACKET TYPE PLATFORMS

Elham Mina[1], Mohammad Taghi Ahmadi [2] and Mehdi shafiee Far[3]

1) Hydraulic Structures , Tarbiat Modarres University,Tehran,Iran, E.mina@modares.ac.ir
2) Hydraulic Structures , Tarbiat Modarres University,Tehran,Iran, mahmadi@modares.ac.ir
3) Marine Structures , Tarbiat Modarres University,Tehran,Iran, shafiee@modares.ac.ir

1. Introduction

Jack platforms have unique features and it is possible to establish a physical link between an oil platform and the seabed in certain areas such as in shallow waters. The greatest advantage of these platforms is their stability, and given the connection between these platforms and the seabed, the exertion of the wind and water forces results in the slight displacement of these platforms. The piers and offshore platforms are affected by complex destructive forces of wind, ocean currents, earthquake, and eddies. These forces result in the considerable displacements in the piers or platforms, which harm the safety and serviceability of the offshore structures in operation. In this research, a hydrodynamics software solution was used to simulate the dynamic interaction between the pier and hydrodynamic forces and to analyze the offshore and structural parameters. The present research objectives were to analyze the sea hydrodynamic parameters and the jacket platform rocking oscillations under the effect of irregular JONSWAP wave torque and to perform a numerical analysis of the seismic isolator performance in the process of controlling the dynamic responses of the offshore jacket platforms and the damped vibrations of the jacket-type platforms. The results were indicative of the effect of the sliding isolator on the offshore jacket platforms and its contribution to the decrease in the effect of vibration caused by waves and other dynamic forces on the superstructure. The sliding isolators considerably increase the energy dissipation capacity without considerably increasing the system hardness and the seismic rehabilitation of the structures is carried out through reducing the lateral earthquake and wind loads.

2. Methodology

In this research, a hydrodynamic software solution and the boundary element method were used to discretize and simulate the equations governing the fluid flow including the continuity and momentum equations. The sea hydrodynamic parameters were also analyzed in the frequency and time domains. In this regard, the effects of the seabed on the structure rocking oscillations and the hydrodynamic characteristics were studied around the given structure using the diffraction and Morrison theories. Moreover, the efficiency of the seismic isolators placed in the supports in controlling and reducing the vibrations of offshore jacket platforms was analyzed and discussed under dynamic loading. The Ansys Transient Structural and Ansys AQWA modules were also used to analyze the sea and structure parameters. In order to analyze the structural response to the irregular waves, the performance of the different wave parameters under hydrodynamic forces was studied along with the response of a four-legged jacket platform using the JONSWAP spectrum parameters. In this research, an offshore jacket platform located in the Persian Gulf was rehabilitated. This platform was situated in the South Pars field and sliding-rubber isolators were placed in the support structure. Sliding isolators(TLD) have been made from 12 to 41 inches in diameter. Slider manufacturing sliders are fabricated with a Teflon disc that mates with a stainless steel sliding surface. The platform is not attached to the soil [1] and wave-induced force is obtained using wave theory [2] to [5] for a regular wave. the environmental specifications and conditions of the region are as follows:

$\rho = 1025\,{}^{kg}/_{m^3},\ g = 9.81\,{}^{m}/_{s^2}, H_0 = 6m,$
$d = 150m,\ T = 8s, \lambda = 100m)$
$k = \frac{2\pi}{\lambda} = 0.062\ m^{-1}, \omega = \frac{2\pi}{T} = 0.7853\ \left(\frac{rad}{s}\right)$

3. Analysis

3.1. Analysis of the Hydrodynamics Structural Response and Wave

The waves were irregular random waves and it was substantially important to perform their time history analyses in assessing the offshore structures. In addition, the time histories of waves have two

major characteristics namely the significant wave height and the frequency content. According to the analysis result of the hydrodynamic force of the Jacket type platforms and the effectiveness of Sliding isolators in controlling the dynamic responses of the Jacket type platforms.

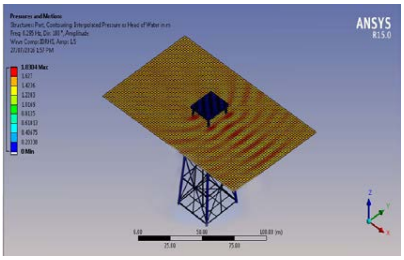

Figure 1. A view of the pressure and diffraction forces in the frequency domain

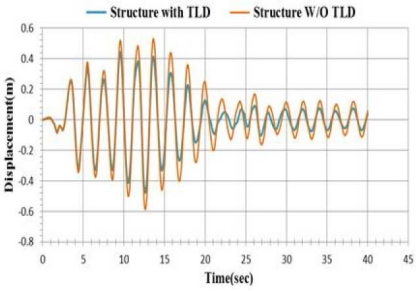

Figure 2. Maximum displacement of total hydrodynamic force of the Jacket type in direction x

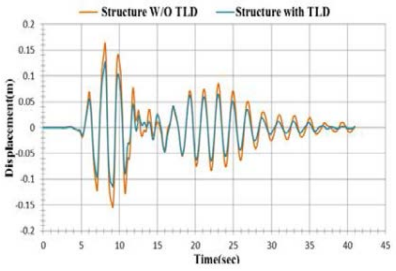

Figure 3. Maximum displacement of total hydrodynamic force of the Jacket type in direction y

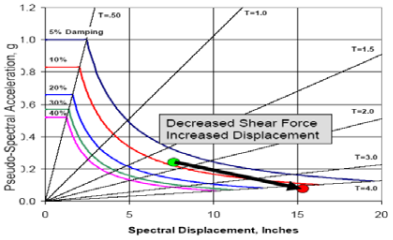

Figure 4. The Sliding isolators effected on displacement of pseudo-spectral

4. Conclusion

Based on the analysis results, the effect of the seismic isolators on the dynamic response of a platform was studied under stimulations caused by the hydrodynamic forces. The effect of the seismic isolator on the dynamic responses suggested that the seismic isolators significantly reduced the dynamic responses and improved the vibration performance of the jacket-type platforms. The decrease corresponding to the maximum displacement of the platform top deck, the maximum base shear of the platform, and the maximum acceleration of the top deck was 38%, and 42%, respectively. also the results showed that with the increasing of the depth, the impact of wave's force and moment on the base of platform are reduced through exponential relationship. The amount of force and total moment are inclined to a fixed value. The reductions are due to the effective depth that is equal to half the wavelength; so that it reduces the amount of force and moment to a small amount.

5. References

[1] Dean, E. T. R., "Offshore Geotechnical Engineering", 1st edition, Thomas Telford Limited, 2010.

[2] Wilson, J. F., "Dynamics of Offshore Structures", John Wiley & Sons, 2003.

[3] McCormick, M. E., "Ocean Engineering Mechanics", Cambridge University Press, 2010.

[4] Abramowitz, M., Stegun, I. A., "Handbook of Mathematical Functions", New York- Dover Publications, 1965.

[5] Mogridge, G. R., Jamieson, W. W., "Wave Forces on Large Circular Cylinders:A Design Method", Hydraulics Laboratory, National Research Council of Canada, Report MH-111, 1976.

AN INVESTIGATION ON RELIABILITY OF FINITE ELEMENT MODELS IN PREDICTING CAPACITY OF TUBULAR JOINTS

Behrouz Asgarian[1] and Vahid Mokarram[2]

1) Professor, K.N. Toosi University of Technology, Tehran, Iran, asgarian@kntu.ac.ir
2) PhD candidate at Department of Civil and Environmental Engineering, Shiraz University, vahid_mokarram@shirazu.ac.ir

1. Introduction

Circular tubular sections are widely used in design and construction of fixed offshore platforms. Code-based load-carrying capacity of tubular joints are dominantly proposed according to experimental tests. However, due to high costs and difficulties attributed to the development of experimental tests, experimental database for predicting capacity of tubular joints are limited.

The engineering community needs to be supported with more insight into how reliable FE models can be developed for predicting the load-carrying capacity of tubular joints. FE models can enhance the database for future code-based capacity formulations. Moreover, FE models can be regarded as a promising tool for evaluating existing fixed offshore platforms. Because, effects of local joint flexibility and brace interaction are automatically incorporated in such models. In this paper, a nonlinear FE model is carefully constructed using shell elements in ANSYS [1] for investigating the pros and cons of such models in evaluating the capacity of unreinforced tubular T-joints subjected to the actions of tensile, compressive and in-plane bending loads of the brace. Finally, a brief discussion on the effects of boundary conditions of the chord on capacity of the joints is presented. The results from FE models shall be compared with recommendations of latest edition of API standard [2].

2. Load-carrying Capacity of Y/T Joints

2.1. Characteristics of the FE Models

Geometrical characteristics of the considered joints considered in this paper are given in Table 1. All joints are modelled with ANSYS [1] Shell93 element, which is an 8-node structural shell element that can incorporate both material and geometrical nonlinearities. The element is particularly suitable for modelling curved shells. Rigid plates are attached to both ends of the chord. Boundary conditions (clamped or pinned ends) are satisfied in the nodes located at the center of these plates.

2.2. Joints Capacity under Axial Tensile Loading

Except for joints with small values of $\beta = D_b/D$ (where D and D_b represent chord diameter and brace diameter, respectively) if crack propagation mechanisms are not incorporated in FE models, the tensile load can be increased to reach a failure due to global plasticity. However, failure mode of such joints is attributed to crack propagations, which eventually result in rupture and separation of the brace form the chord.

2.3. Joints Capacity under Axial Compression Loading

Since crack propagation is not the failure mode of the joints under axial compression loads, FE models yield reliable estimations for load-carrying capacity of such joints. In fact, FE models show that local buckling and plastic deformations of the chord's wall is the main failure mode of Y/T joints under compression.

2.4. Joints Capacity under In-Plane Bending Moment

Figure 1 and Table 2 shows excellent agreements between load-carrying capacities obtained from the FE models and those recommended by API [2]. Joint capacities obtained from API [2] provisions are between 93% (in joint T_5) and 99% (in joint T_2) of those obtained from the FE models. Yura's [3] limit is an experimental deformation-based indicator which is suitable for finding the capacity of joints that have monotonic load-deformation curves. Since the curves corresponding to joints T_2, T_5 and T_8 are monotonic, the non-dimensional $M_{max}/F_{yc}t_c^2D_b$ ratios that are reported in Table 2, have been obtained based on the M_{max} corresponding to Yura's [3] limit (see Figure 1).

By investigating Table 2, it can be confirmed that joints with larger values of γ and smaller values of β had the least local plasticity. In such cases, FE results match the best with capacities obtained from API [2]. Failure of Y/T joints subjected to in-plane bending moments occurs due to (1) failure of the chord's wall under tensile stresses that are exerted on the wall as a result of the bending moment of the brace and, (2) local buckling and plasticity of the chord's wall.

3. Effects of Boundary Conditions on Joints Capacity

In this section, the capacity of joint T_3 for two cases (1) chord with pinned ends, and (2) chord with clamped ends are obtained. The results show that whenever failure modes are not global capacity of the joint, FE results and API's [2] predictions show excellent agreements. However, if the global plasticity of the system is the dominant mode of failure, the FE model yields capacity overestimations in comparison with API [2].

Table 1. Geometric characteristics of the considered T-joints.

Joint ID.	$\gamma = D_c/2t_c$	$\beta = D_b/D$	$\alpha = 2L_c/D$	$\tau = t_b/t_c$	t_c (cm)	L_b (cm)
T1	12	0.25	12	0.8	3.175	200
T2	12	0.5	12	0.8	3.175	200
T3	12	0.75	12	0.8	3.175	200
T4	15	0.25	12	0.8	3.175	200
T5	15	0.5	12	0.8	3.175	200
T6	15	0.75	12	0.8	3.175	200
T7	18	0.25	12	0.8	3.175	200
T8	18	0.5	12	0.8	3.175	200
T9	18	0.75	12	0.8	3.175	200

Note: D, D_b, L_c, L_b, t_c and t_b represent chord diameter, brace diameter, chord length, chord thickness and brace thickness, respectively.

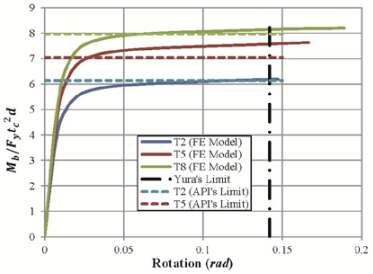

Figure 1. Moment-rotation curves for joints T2, T5 and T8 under in-plane bending moment of the brace along with API [2] and Yura's [3] predictions of the capacity.

Table 2. Capacity of the considered joints under in-plane bending moment.

Joint ID.	API	Nonlinear FE model	
	$\left\|\frac{M_a}{F_{yc}t_c^2D_b}\right\|$	$\left\|\frac{M_{max}}{F_{yc}t_c^2D_b}\right\|$	$\frac{M_{max}}{M_p}$ (%)
T2	6.14	3.09	7.33
T3	9.98	5.33	18.93
T5	7.05	3.29	6.07
T6	11.47	6.12	16.95
T8	7.97	4.07	6.17
T9	12.96	6.71	15.23

Note: M_{max}, M_p and F_{yc} represents the maximum in-plane moment in the intersection region of the joint, plastic moment of the chord section and yield stress of the chord, respectively.

4. Conclusions

Reliability of FE models in predicating load-carrying capacity of tubular T-joints was investigated through considering tubular T-joints with different non-dimensional geometric parameters. Capacity of the considered T-joints were evaluated from FE models and compared against API's predictions for three different loading conditions. For joints under tensile loads, crack propagation and separation of the the brace from the chord is the main failure mode. Hence, findings of this paper suggest that FE models are not unless crack prorogation mechanisms are properly addressed. It was also shown that parameter γ does not affect the capacity of T-joints under tensile actions.

Moreover, the results of this study revealed that FE models are reliable in predicting load-carrying capacity of joints under compressive axial loads and in-plane bending moments. It could be concluded that local buckling and plasticity of joints under compressive actions of the brace could be accurately captured in nonlinear FE models with shell elements. It was also shown that global plasticity is not the failure mode of T-joints under in-plane bending moments. It indicates that, in such cases, FE models can predict the load-carrying capacity with high accuracy. The results presented in this paper show that FE models can effectively estimate load-carrying capacity of tubular joints if local buckling and local plasticity of the chord are the dominant failure mode. This conclusion was also confirmed by investigating the effects of boundary conditions in joint responses.

5. References

[1] ANSYS Inc., ANSYS program. Release 14 user's manual, ANSYS Inc. Canonsburg, Pennsylvania, USA, 2017

[2] American Petroleum Institute. *API RP2A-WSD, Recommended practice for planning, designing and constructing fixed offshore platforms-working stress design*, 22nd ed., 2014.

[3] Yura, J.A., Zettlemoyer, N.A., and Edwards, I.F., "Ultimate capacity equations for tubular joints", in: *Offshore Technol. Conf., Offshore Technology Conference*, Houston, Texas, USA, May 5-8 1980. doi:10.4043/3690-MS.

5

MARINE ENVIRONMENT AND SAFETY

PRIORITIZATION AND DETERMINATION OF THE STRESSORS' INFLUENCE COEFFICIENT ON THE COASTAL ENVIRONMENT AND ITS APPLICATION TO COASTAL ZONE MANAGEMENT

Maryam Yaghoubzadeh[1] and Afshin Danehkar[2]

1) Department of Environmental Science, Gorgan University, Gorgan, Iran, yaghobzadehmaryam@yahoo.com
2) Department of Environmental Science , University of Tehran , Tehran, Iran, danehkar@ut.ac.ir

1. Introduction

Coastal zones usually are exposed by numerous stressors. Waves, tides, winds and storms effect on the shores and will result in increasing coast sensitivity of the coasts. Coastal vulnerability assessment depends on recognition of those factors affecting on the coasts that related to stresses. The concepts of sensitivity and vulnerability have commonly been used as criteria in the identification of areas, where requires special management or protection [1, 2, 3 and 4]. However, the terminology used in these studies lacks common, mutually agreed-upon definitions. In the coastal zones, sensitivity is the degree to which, marine features respond to such stresses and vulnerability is the probability that a feature will be exposed to a stressor to which, it is sensitive [5]. To determine the sensitivity and vulnerability of the coastal zones, the existing stresses must be examined. The purpose of this study is to overview regarding the functional definitions of the sensitivity and vulnerability and also existing stresses in the coastal zones. According to these definitions and terms, a methodology has then been suggested for prioritization of the coefficient of stressors for determination of sensitivity and vulnerability in the coastal zones.

2. Materials and Methods

This paper is based on a literature review, which have been conducted in Iran and other countries. Our findings have been resulted in recognizing and classifying the stressors into 17 groups and following that into 5 main categories. Moreover, 25 stress – exposed environmental resources were studied in both shore and coastal areas. in order to determine the coefficient of stressors, the impact of stress indicators studied at four categories including stress intensity, stress probability, period of exposure, stress impact continuity. It is worthy to note that each of them have been expressed in five categories in term of their importance varying from very high, high, medium, low and very low. out of the influencing factors on 25 stress – exposed environmental resources, 23 sensitive resources have got stressed by one stressor, which has been indicted by Nmax. Five sensitive resources (Nmin) have also got stressed by one stressor. Referring Likret's classification, stress intensity has been determined relying on the range between the Nmax and Nmin. Based on equation 1 and Table 1, Stress intensity (SI) of the stressor was qualitatively and quantitatively determined.

$$SI = \frac{N_{max}\text{-}N_{min}}{C} \quad (1)$$

Table 1 The stressor intensity quality and quantity

Numerical range of stress intensity (SI)	5 - 8.6	8.7 - 12.2	12.3 - 15.8	15.9 - 19.4	19.5 - 23
Statement of stress intensity	Very low	low	medium	high	Very high
Score of stress intensity	1	2	3	4	5

Stress probability (SP) is rate reception sensitive source of exposure to stressor. This indicator is based on the structure and the biological processes of coastal ecosystem and their potential to self-purification, which is expressed in five distinctive classes.

Period of Exposure (PE) refers to exposing duration and were been assessed considering the nature of the stressor. Period of exposure is expressed in five classes and includes very short-time (less than 7 days), short time (less than 1 month), medium (less than 1 season), high (6 month) and very high (1 year or more).

Stress impact continuity (SC) refers to continuum of the effect, which is exposed by stress and was assessed considering the nature of the stress and also national-scale experiences on the coastal zone. Continuum of the impact was divided into five classes including very short-time (less than 7 days), short time (less than 1 month), medium (less than 1 season), high (6 month) and very high (1 year or more).

3. Summary and Conclusion

Coastal zones are geographic space between two ecosystems with properties, which are independent from each other. Protections of these zones are inevitable due to their inherent sensitivities of the coastal zones. Integrated management of the coastal zones is based on site selection of land uses within the coastal zones considering ecological protection frameworks and

conservation of the sensitive and vulnerable zones. Vulnerability is a managerial concept that considers not only natural ecosystems but also human interests, which are related to the coastal zones.

At present study, coastal zones are divided into two divisions, namely shore areas and coastal areas by new approaches. Such an approach was not applied for assessing the vulnerability in other studies. Those studies only focused on the shorelines. Considering the results of the present studies, we have found that geological and climatic factors are of most important criteria and storm; sea-level rise and liquefaction are accounted as the most important sub-criteria, respectively. Moreover, the coefficients of the stressor including sea- level rise assessment are of the most important factor on coastal zones (*Figure 1 and Figure 2*).

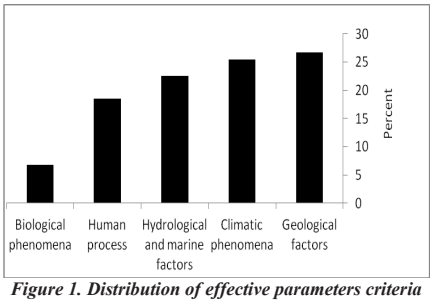

Figure 1. Distribution of effective parameters criteria on coastal zones

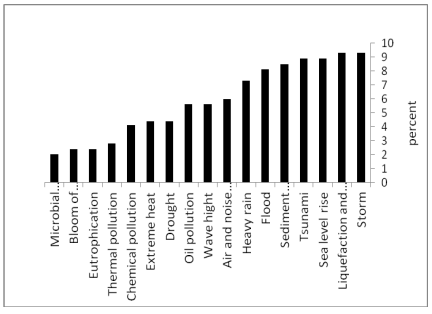

Figure 2. Distribution of effective parameters sub-criteria on coastal zones

4. References

[1]-Amuzu, J., Jallow, B. P., Kabo-Bah, A. T., & Yaffa, S. 2018. The Climate Change Vulnerability and Risk Management Matrix for the Coastal Zone of The Gambia. Hydrology, 5(1), 14.

[2]- Gjerde, K. M. 2002. PSSAs: IMO guidelines. Sea Technology 43: 40 – 46.

[3]- Johnson, D., S. Lewey, P. Park, J. Hoar, M. Pourzanjani, S. Fletcher, *and* S. Tarver. 2001. Particularly sensitive sea areas (PSSA): the Wadden Sea feasibility study. Wadden Sea Newsletter 3: 9 – 12.

[4]- Van Bernem, K. H., B. Bluhm, *and* H. Krasemann. 2000. Sensitivity mapping of particular sensitive areas. *Pages* 229 – 238 *in* G. R.Rodriguez *and* C. A.Brebbia, *editors*. Water studies. 8. Oil and hydrocarbon spills, modelling, analysis and control II. *WIT Press, Southampton , United Kingdom* .

[5]- Zacharias, M.A., E.J. Greger. 2005. Sensitivity and Vulnerability in Marine Environments: an approach to identifying vulnerable marine area. Conservation biology, 19 (1): 86-97.

ENVIRONMENTAL POLLUTION FROM MARITIME TRANSPORTATION AND AIR TRANSPORTATION: CASE STUDY IN IRAN

Vahid Mohamad Taghvaee[1], Abbas Assari Arani[2] and Lotfali Agheli[3]

1) Department of Economic Development and Planning, Tarbiat Modares University, Tehran, Iran, v.taghvaee@modares.ac.ir
2) Department of Economic Development and Planning, Tarbiat Modares University, Tehran, Iran, ASSARI_A@modares.ac.ir
3) Economic Research Institute, Tarbiat Modares University, Tehran, Iran, aghelik@modares.ac.ir

1. Introduction

Maritime transportation plays a dual role in the CO2 emissions. On the one hand, it can rise carbon dioxide emissions due to the highly great amount of cargos which they are transferring, burning an extremely high volume of fuels which leads to considerable CO2 emissions [1]. On the other hand, it might be considered as an CO2 emissions deflator due to its higher capability of carrying bulk cargos [2]. Moreover, it is effective on the economic growth.

In addition to the maritime transportation, the air transportation has its own effects on the environmental pollution and economic growth. It can increase the level of CO2 emissions; and it might heighten the level of economic growth. The environmental and economic effects of air transportation can be compared with the corresponding effects of sea transportation [3, 4].

The main purpose of this study is to compare the maritime transportation effects with air transportation ones on the environment and economy of Iran to discover the most economic and the cleanest transportation mode.

2. Methodology and Model

We compare the environmental and economic effects of maritime and air transportation in short run and long run, in Iran during 1978-2012, using two dynamic log-linear models. Following Farhani, et al., (2014), Taghvaee, et al., (2017), and Taghvaee and Hajiani, (2014) we specify the models below [5, 6, 7].

$$LCO_{2_t} = \alpha_0 + \alpha_1 LM_t + \alpha_2 LA_t + \alpha_3 LY_t + \alpha_4 LCO_{2_{t-1}} + \alpha_5 DW + \varepsilon_t \quad (1)$$

$$LY_t = \beta_0 + \beta_1 LM_t + \beta_2 LA_t + \beta_3 LTR_t + \beta_4 LY_{t-1} + \beta_5 DW + \mu_t \quad (2)$$

where CO2 is Carbon Dioxide emissions; M is maritime transportation; A is air transportation; Y is GDP, and TR is trade volume; "α" and "β" show the parameters of CO2 and GDP models, as the elasticities of environmental pollution and economic growth; DW is the dummy variable which is 0 for the war years (1980-1989) and 1 for the remaining years; L is the natural logarithm; t is year; ε and μ are the residual series; α_1, α_2, and α_3 are the short run elasticities of environmental pollution and β_1, β_2, and β_3 are interpreted as the short run ones of the economic growth. The long run ones are $\alpha_1/1-\alpha_4$, $\alpha_2/1-\alpha_4$, and $\alpha_3/1-\alpha_4$ for the environmental pollution; and $\beta_1/1-\beta_4$, $\beta_2/1-\beta_4$, and $\beta_3/1-\beta_4$ for the economic growth [8]. The estimated residual series are examined for the econometric classical- assumptions for assessing the reliability of the estimated coefficients.

3. Data

The dataset is annual and derived from World Development Indicator [9], except for the maritime and air transportation which are come from the Central Bank of Iran [10]. The per capita sea and air transportation of goods, as the maritime and air transportation proxies, respectively, and measured in ton, are the sea and air transportation of goods divided by the total population, derived from the latter database; the per capita CO2 emissions, measured in metric ton, is the proxy for the environmental pollution; the per capita GDP, measured in the constant 2005 US Dollar, is the proxy for the economic growth; and trade, measured as the percentage of GDP, is the proxy for trade openness. All the data are in natural logarithm.

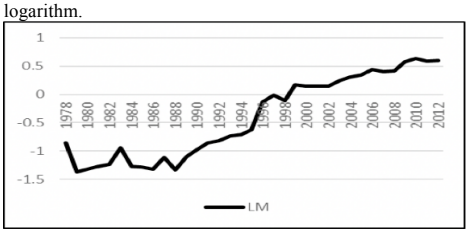

Figure 1. Maritime transportation volume in natural logarithm in Iran.

Figures 1 and 2, respectively, displays the per capita maritime and air transportation volume in natural logarithm in Iran.

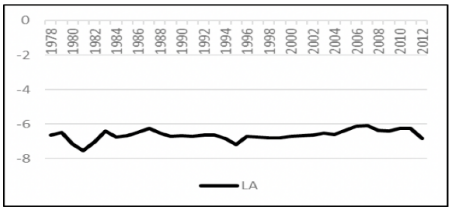

Figure 2. Maritime transportation volume in natural logarithm in Iran.

4. Results

Table 3 represent the resulted coefficients and statistics of the environmental pollution model.

Table 1. Results of the CO2 model estimation.

Variable	Coefficient	t-statistic	Prob.
LM	0.18	4.75	0.00
LA	0.06	1.69	0.10
LY	0.24	2.30	0.02
$LCO2_{t-1}$	0.35	3.09	0.00
$\alpha_1/1-\alpha_4$	0.27		
$\alpha_2/1-\alpha_4$	0.09		
$\alpha_3/1-\alpha_4$	0.36		
DW	0.10	3.10	0.00

Table 4 shows the resulted coefficients and statistics of the economic growth model.

Table 2. Results of the GDP model estimation.

Variable	Coefficient	t-statistic	Prob.
LM	0.05	2.56	0.01
LA	0.10	2.78	0.00
LTR	0.15	3.42	0.00
LY_{t-1}	0.60	9.21	0.00
$\beta_1/1-\beta_4$	0.12		
$\beta_2/1-\beta_4$	0.25		
$\beta_3/1-\beta_4$	0.37		
DW	0.05	2.56	0.01

Table 5 indicates the estimated environmental pollution and economic growth in the short run and long run in Iran, summarily.

Table 3. Estimated elasticities of environmental pollution and economic growth in the short and long run.

Elasticities	**Environmental pollution**		**Economic growth**	
Period	Short	Long	Short	Long
LM	0.18	0.27	0.05	0.12
LA	0.06	0.09	0.10	0.25
LY	0.24	0.36	NA	NA
LTR	NA	NA	0.15	0.37

5. Conclusion and Discussion

This study compares the environmental and economic effects of maritime and air transportation of Iran. The results show the higher maritime transportation elasticities of environmental pollution and lower elasticities in the economic growth, compared with the air transportation. It implies that the maritime transportation is more pollutant and less productive in Iran, in comparison with the air transportation. The policy makers are advised to improve the infrastructure of maritime transportation from both the environmental and economic point of views.

6. Acknowledgment

We express our deep gratitude towards the Department of Economic Development and Planning, Faculty of Management and Economics, Tarbiat Modares University, which supports the research financially and spiritually.

7. References

[1] Taghvaee, V. M., and Hajiani, P., "Environment, energy, and environmental productivity of energy: a decomposition analysis in China and the US ", Second European Academic Research Conference on Global Business, Economics, Finance and Banking, 3-5, July 2015.

[2] International Maritime Organization, 2016, Available at: http://www.imo.org/en/OurWork/Environment/PollutionPreventi on/AirPollution/Pages/Default.aspx

[3] Larkin, A. B., Mander, S. L., Traut, M. B., Anderson, K. L., Wood, F. R., "Aviation and climate change-the continuing challenge", Encyclopedia of Aerospace Engineering, 2016

[4] IATA, International Air Transportation Association, Aviation Economic Benefits, 2014.

[5] Farhani, S., Chaibi, A., and Rault, C., "CO2 emissions, output, energy consumption, and trade in Tunesia", Economic Modelling, 38, 2014, pp 426-434.

[6] Taghavee, V. M., and Hajiani, P., "Price and income elasticities of gasoline demand in Iran: Using static, ECM, and dynamic models in short, intermediate, and long run", Modern Economy, 5, 2014, pp 939-950.

[7] Taghvaee, S.M., Omaraee, B., Taghvaee, V.M., "Maritime transportation, environmental pollution, and economic growth in Iran: using dynamic log-linear model and Granger causality approach", Iranian Economic Review, 21(2), 2017, pp 185-210.

[8] Sene, S. O., " Estimating the demand for gasoline in developing countries: Senegal ", Energy Economics, 2012, pp. 189-194.

[9] World Development Indicator, World Bank, 2014, Available at: http://www.data.worldbank.org

[10] Economic Research and Policy Department of Iran, Central Bank of the Islamic Republic of Iran, Economic Time Series, Database, Available at http://tsd.cbi.ir/

ENVIRONMENTAL EFFECT OF GASES EMITTED FROM SHIP

Reza Tolian[1] and Mohammad Shakibinasab[2]

1) Department of Environmental Pollution, Ahvaz Branch, Islamic Azad University, Ahvaz, Iran.
Gh.tolian@yahoo.com
2) Bushehr Ports & Maritime Organization, Bushehr Port, Iran.
Shakibi_123@yahoo.com

1. Introduction

Nowadays, by increasing human traffic, convenience and attractiveness, as well as cheap and cost-effective shipping, sea transportation has also increased [1]. In fact, shipping is much more efficient than road and rail transport [2]. Projections indicate that without further regulatory action the continued growth in emissions of SOx and NOx from the maritime sector will surpass that of all land-based sources in the EU by 2020[3]. There are more than 450 types of different combinations in smoke of smokestack, 40 of which are known as toxic and dangerous gases and Dangerous for human health [4]. Oceans ship consume more than 4% of global fossil fuels [5]. Annually, oceangoing ships are estimated to emit 1.2–1.6 million metric tons (Tg) of particulate matter (PM) with aerodynamic diameters of 10 μm or less (PM10), 4.7–6.5 Tg of sulfur oxides (SOx as S), and 5–6.9 Tg of nitrogen oxides (NO*x* as N). Some studies have estimated around 15% of global NO*x* and 5–8% of global SO*x* emissions are attributable to oceangoing ships. Given nearly 70% of ship emissions occur within 400 km of land ships have the potential to contribute significant pollution in coastal communities especially for SOx [6]. Also, ships represent 3 to 4 percent of the total CO2 released in the world [5].

2. Current Laws and Regulations

The sixth (VI) Annex to the Marpol Convention, which came into force on May 19, 2005, includes the issue of air pollution from ships. This appendix contains limitations for hazardous gases from ships'emissions. Also based on the MEPC (Marine Environment Pollution Committee) approvals, Vessels must control air pollution in the three periods of time and match themselves to the laws and regulations as described below.

2-1- Nitrogen Oxide Control (NOx)

The IMO program and timetable for reducing NOx are listed in Table 1.

2-2- Sulfur Oxides Control (SOx)

The IMO program and timetable for reducing SOx are listed in Table 2.

Table 1. IMO Schedule for NOx reductions

RPM	Tier I (from 2000.1.1)	Tier II (from 2011.1.1	Tier III (from 2016.1.1
Under 130	17 gr/kWh	14.4 g/kWh	3.4 g/kWh
130~2000	45.0×n (-0.2) g/kWh	44.0×n (-0.23) g/kWh	9×n (-0.2) g/kWh
Over 2000	9.8 g/kWh	7.7 g/kWh	2.0 g/kWh

Table 2. IMO Schedule for SOx reductions

Area	SOx emissions			
	2010	2012	2015	2020
General level	% 4.5	% 3.5		% 0.5
IMO ECA	% 1.5	1% (after 7/2010)		% 0.1
European ports	% 0.1			
USCG (within 24 NM)	% 0.5	% 0.1		

According to the IMO Program and Instructions until 2025, the amount of sulfur in the fuel for ships should be reduced from 3.5% to 0.5% [2]. Of course, for SECA[1] area, namely North America, Baltic Sea, North Sea and Canal Manzé, from the beginning of January 2015, the level of sulfur should be reduced to 0.1%. Scientists have concluded that by reducing the sulfur content of fuel in ships by 0.1 percent, the annual mortality rate in coastal cities will be reduced by more than 45,000 annually[7].

2-3-CO_2 Emissions Control

To measure CO2 emissions, the EEDI[2] factor is defined in formula 1[8]. The purpose of EEDI is reduce CO2 emissions, increase cargo carrying capacity and increase floating performance. This indicatot will lead to different standards for different types of ships. These standards will be developed over time. In such a way that for delivery ships between 2015 and 2019, 10%, from 2020 to 2024, about 20%, and for delivery vessels after 2024, 30% will

[1] Sulphur Emission Control Areas
[2] Energy Efficiency Design Index

be required. The EEDI is a mandatort tool fuel efficiency ship at the design stage of the new ship.

$$EEDI = \frac{\text{CO2 EMMISSIONS}\left(\frac{g}{hr}\right)}{\text{DWT} \times \text{SPEED(ton-knot)}} = \frac{gr}{ton-mile} \quad (1)$$

3. Health and Environmental Effects of Ship Smissions

The harmful compounds and gases of ship emmisions divided into two groups: 1-Primary contaminants that have a direct and immediate impact on health include NOx, SOx, PM, CO, VOC, which causes local effects. 2-Secondary pollutants that include CO2, CH4, HCFC, PAHs. These pollutants are able to travel in long distances and react with other chemical compounds in the air and form secondary pollutants (regional impacts). Scientists forecasted NOx emissions from international shipping in European waters could be equal to that of land-based sources by 2020 [3].

4. Health Effects

There is evidence showing that particulate matter (PM) emissions from shipping are responsible for approximately 60,000 premature deaths annually (Corbett et al., 2007), most of them occurring near populated coastlines in East Asia, South Asia, and Europe[9]. According to the Los Angeles Area Quality Management (AQMD), greenhouse gas emissions from ships that bearthing in ports cause approximately 700 early dead per year.

5. Environmental Impacts and Global Warming

There is another category of ships emission, One category includes gases such as CO_2, chloro-fluorocarbons (CFCs), CH_4, halons that cause global warming and ozone depletion. Other gases such as NOx, SOx, causing acid rain and local health problems. Another category such as NOx and hydrocarbons, produced photochemical oxides such as ozone, which was a greenhouse gas. Its Causing loss and damage to agricultural products and sanitary problems. These pollutants in oceanic environments have created a utrification phenomenon, according to calculations that 2,000 to 800,000 km^3 of sensitive ecosystems in Europe face this phenomenon. It should be noted that 70 to 80 percent of the gases released by the ships penetrate up to 400 km of coastal areas and affect these areas [5].

6. Economic Effects

Air emissions of shipping lead to a lot of hidden and obvious costs calculated for the European Seas the external cost of air pollution from maritime transport at 45 billion euro [9]. Estimated the total external costs of air pollution for 2006 for the EU ocean-going fleet and the world fleet and found them to be 40 billion euro and 184 billion euro respectively [9].

7. Offers

- Use of Cold-ironing technology. Ships use a source of energy in berthing time.
- Instalation of gas absorbing equipment.
- Use of clean and alternative fuels.
- Optimizing the propeller design and stroke to reduce the movement resistance in water. It reduce the fuel consumption.
- Effort to reduce EEDI and carry out some action such as: energy recovery on the ship, reducing the power of machinery, reduce the power requirement of the drift system. Losing weight of the ship using lighter materials such as aluminum.

8. Acknowledgments

Thanks to the Ports and Maritime Organization (this article has been done with the scientific and material support of PMO).

9. References

[1] Butt, N. 2007. The impact of cruise ship generated waste on home ports and ports of call: A study of Southampton. Journal of Marine Policy, 31 (2007), 591–598.

[2] Walker, T. R. Green Marine: An environmental program to establish sustainability in Marine transportation. *Marine Pollution Bulletin*, Vol 105(1), 15 April 2016, PP: 199–207

[3] Ballini, F. and Bozzo, R. Air pollution from ships in ports: The socio-economic benefit of cold-ironing technology .*Research in Transportation Business & Management*, 17 (2015), 92–98.

[4] Bailey, D., and Solomon, G. Pollution prevention at ports: clearing the air. Environmental Impact Assessment Review. 24 (2004), pp.749–774.

[5] Breitling, U. Sustainable Shipping and Port Development. 5th Regional EST Forum in Asia, Bangkok, Thailand, 23-25 August 2010.

[6] Corbett, J. J., Winebreake, J., Green, H, E., Kasibhatla , P., Eyring, V. and Lauer, A. Mortality from Ship Emissions: A Global Assessment. *Environ. Sci. Technol.* 2007**,** *41,* 8512–8518.

[7] Winebreake, J. J., Corbett. J., Green, E. H., Lauer, A., and Eyring, V. Mitigating the health impacts of pollution from oceangoing shipping: an assessment of low-sulfur fuel mandates, Journal of Environmental Science & Technology. 43(13), 2009, PP.4776-4782.

[8] Lloyd, G. "Rules for Guidelines for Determination of the Energy Efficiency Design Index(EEDI)", Rules for Classification and Construction, chapter VI.13.1 (force date:15 sep. 2013).

[9] Chatzinikolaou, S. D ., Oikonomou, S. D ., and Ventikos, N. P. 2015. Health externalities of ship air pollution at port – Piraeus port case study. Transportation Research Part D 40, 2015, pp.155–165.

CLASSIFICATION OF SENSIBILITY OF JAUSK COASTS FOR FINDING A ZONE TO DEVELOP SHIP RECYCLING INDUSTRY

Abdoreza Karbassi[1], Meysam Matinfar[2] and Sepehr Parsa[3]

1) Department of Environmental Engineering, Graduate Faculty of Environment, University of Tehran, Tehran, Iran, akarbasi@ut.ac.ir
2) Department of Environmental Engineering, Graduate Faculty of Environment, University of Tehran, Tehran, Iran, mmatifar@yahoo.com
3) Department of Environmental Engineering, Graduate Faculty of Environment, University of Tehran, Tehran, Iran, sepehrparsa@ut.ac.ir

1. Introduction

Iran's proximity to the Oman Sea and the Persian Gulf and access to the oceans has led to the creation of exceptional opportunities for naval operations and ocean fleets. These ships, in spite of their long and limited lives, should eventually be scraped. Generally, ships have useful lives between 25 and 30 years. As their age grows, their safety factor decreases and their costs of storage and also their environmental hazards increase. therefore, the owners would be obliged to scrap those ships

Over the last few years, this industry has been discussed in most of Iranian maritime communities, but no clear results have yet been obtained. Environmental pollution is the main reason for the opposition against the implementation of this industry, but study on the case of the countries owning this industry shows that, for example in countries such as China and Turkey, the implementation of this industry under international laws and regulations has not led to any environmental pollution, and even caused lots of economic profit [1]. Marine pollution with various metals along with their ecological risks is well discussed and documented [2, 3, 4, 5]. Also the Evaluation of oil pollution dispersion in various media is brought out [6].

One of the determinant factors in the development of ship recycling industry is the coastal location for the operations, meaning that we have to choose a coast which has the least environmental sensitivity for carrying out the activity [7]. Jausk is one of the places with the potential for designing a ship recycling yard

Selection of coastal-marine protected areas as well as coastal-marine sensitive areas is conducted by using criteria of IUCN, IMO [8] and Salm & Price (1995) [9], including 12 main criteria and 20 sub criteria and Each criterion takes a numerical value by adopting a grading method and finally, the right spot for the operation is found. Such studies have been attended by some researchers [10]. This is a very important issue along the Oman and the Persian Gulf where mangroves are found in plenty [11].

In this research, after selecting the main criteria and sub criteria for determining the environmental sensitivity of Jausk coastal areas, each criterion adopts a numerical value by using scoring method. Then, according to the obtained points, the sensitivity of the region will be determined. Finally, coasts with a low sensitivity to work were chosen to organize sunken ships and ships that their life is over. In order to evaluate the environmental sensitivity of the coastal areas of Jausk, the main and secondary criteria were described in Table 1. Accordingly, 12 main criteria and 20 sub criteria were used.

Coastal areas are divided into five sections according to the boundaries of coastal villages. Figure 1 shows these independent evaluation units in the Jausk area. To ensure the comprehensiveness of the identified criteria, each criterion was designed by using an interactive approach and the validity of the assigned values was discussed for each one.

Figure 1. Five evaluating sections of Jausk area

Table 1. Main criteria and sub criteria to evaluate the environmental sensitivity of the coastal areas [8]

	Primary factors	secondary factors	min	max
1	Biological Geography	-	0	5
2	Being pristine	-	0	5
3	uniqueness	-	1	5
4	Affiliation	-	1	5
5	habitat	Value	0	5
6		Variety	1	5
7		Area	1	5
8	Aquatics	Variety	1	5
9		Exposed to Extinction	0	5
10		threatened	0	5
11		Spawning	0	5
12		Place of growth	0	5
13	Birds	threatened	0	5
14		Exposed to Extinction	0	5
15		population	0	5
16		Variety	0	5
17		Regeneration	0	5
18	Sea turtles	Spawning	0	5
19		nourishment	0	5
20	Marine mammals	-	0	5
21	Protection record	-	1	5
22	tourism	Tourism Importance	1	5
23		Tourist facilities	1	5
24		Aesthetics	1	5
25		Historical and cultural monuments	0	5
26	Threat factors	type A	1	5
		type B	1	5
Sum	12	20	11	130

2. Refrences

[1] Hiremath AM, Pandey SK, Asolekar SR. Development of ship-specific recycling plan to improve health safety and environment in ship recycling yards. Journal of Cleaner Production. 2016 Mar 10;116-279-98.

[2] Yılmaz, A. B., Yanar, A., & Alkan, E. N. (2017). Review of heavy metal accumulation on aquatic environment in Northern East Mediterranean Sea part I: some essential metals. Reviews on environmental health, 32(1-2), 119-163.

[3] Gurumoorthi, K., & Venkatachalapathy, R. (2016). Spatial and seasonal trend of trace metals and ecological risk assessment along Kanyakumari coastal sediments, southern India. Pollution 2 (3), 269-287.

[4] Vaezi, A., Karbassi, A., Fakhraee, M., VALIKHANI, S. A., & Heidari, M. (2014). Assessment of sources and concentration of metal contaminants in marine sediments of Musa estuary, Persian Gulf.

[5] Biati, A., Nikoomaram, H., & Karbassi, A. R. (2012). Study of metals concentrations in surface sediments of the Persian Gulf coastal area (Bushehr Province). International Journal of Marine Science and Engineering, 2(1), 75-80.

[6] Abbasi Maedeh, P., Nasrabadi, T., Wu, W., & Al Dianty, M. (2017). Evaluation of oil pollution dispersion in an unsaturated sandy soil environment. Pollution, 3(4), 701-711.

[7] International Maritime Organization (2009): Hong Kong International Convention fot The Safe and Environmentally Sound Recycling of Ships, 2009, International Conference On the Safe and Environmentally Sound Recycling of Ships 19 May 2009

[8] International Maritime Organization (2011): Guidelines for the Development of the Ship Recycling Plan, resolution MEPC.196(62).

[9] Salm, R.V. & A. Price. (1995). Selection of Marine Protected Areas: Principles of Techniques for Management.Edited by Susan Gubby. Chapman and Hall, London.

[10] Nasab, F. N., Karbassi, A. R., & Ghoddousi, J. (2018). Criteria selection for sensitivity evaluation framework in coastal areas; Bushehr Province, Iran. Indian Journal of Geo Marine Sciences, 47(2), 415-425.

[11] Dehghani, M., & Karbassi, A. (2015). Determining environmental sensitivity of mangrove forest at hara protected area. Journal of Biodiversity and Environmental Sciences, 6(1), 480-488.

[12] Assessment EE. ENVIRONMENTAL IMPACT ASSESSMENT & ENVIRONMENTAL MANAGEMENT PLAN.

[13] US EPA – Office of Enforcement and Compliance Assurance: "A Guide for Ship Scrappers – Tips for Regulatory Compliance", EPA 315-B-00-001, Summer 2004

MITIGATION OF WATER QUALITY PROBLEMS BY ENHANCING WATER EXCHANGE RATE: A CASE STUDY (GORGAN BAY)

Mohammad Hassan Ranjbar[1], Majid Jandaghi Alaee[2], Mostafa Nazarali[3] and Mohammad Noori[4]

1) Pouya Tarh Pars Consultant Engineers, Tehran, Iran, m.h.ranjbar@ptpco.com
2) Pouya Tarh Pars Consultant Engineers, Tehran, Iran, m.j.alaee@ptpco.com
3) Pouya Tarh Pars Consultant Engineers, Tehran, Iran, m.nazarali@ptpco.com
4) Golestan Regional Water Authority, Gorgan, Iran, m.noori.t@gmail.com

1. Introduction

Serious concerns have recently been raised about Gorgan Bay due to water quality degradation and eutrophication, which has adversely affected the ecological conditions of the bay and the standard of living of the people inhabiting around it. For example, poor water quality has seriously influenced ecotourism and fishing industries on which the people are dependent for their livelihoods. As a result, a restoration program was set up.

One of the main aims of the project was to propose scenarios facilitating diluting the pollution level inside the bay and flushing pollutants out of it so as to improve water quality. As the ability of a body of water to disperse and flush pollutants is mainly dependent on water input [1], increasing water exchange rate between the bay and Caspian Sea by either opening artificial inlets or dredging existing channels was proposed. The effectiveness of different scenarios was assessed by investigating their impacts on transport time scale, described by residence time, and accumulated water exchange between the sea and the bay [2].

Gorgan Bay, partially bounded by Miankaleh Peninsula, is a semi-enclosed basin located at the southeast of the Caspian Sea, Iran (see Figure 1). It serves as a resting place for migratory birds as well as a spawning habitat for native fish, especially Sturgeon. The bay, having a length of about 60 km, a maximum width of 12 km, and an average depth of 1.8 m, covers an area of about 667 km^2 and has an approximate volume of 1.2 km^3 [3].

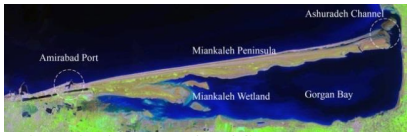

Figure 1. The geography of Gorgan Bay, Iran.

2. Numerical Model

Due to the shallowness, vertical variation of hydrodynamic properties in Gorgan Bay is negligible [3]. Therefore, a 2D coupled model was used to simulate hydrodynamics and dilution of passive dissolved conservative matter in order to estimate residence time of the bay and water exchange under different scenarios. This study employed the MIKE 21 Flow Model FM, developed by the Danish Hydraulic Institute (DHI). Although the model is composed of several modules, only two modules, namely hydrodynamic and transport, were used. The hydrodynamic module provides the current velocity and surface elevation for the transport module, simulating the dispersion of dissolved or suspended substances [4]. Transport module is based on conservation equation defined by

$$\frac{\partial h\bar{C}}{\partial t} + \frac{\partial h\bar{u}\bar{C}}{\partial x} + \frac{\partial h\bar{v}\bar{C}}{\partial y} = hF_C - hk_P\bar{C} + hC_S S \qquad (1)$$

Where t is the time, x and y are the Cartesian coordinates, $\bar{u}$ and $\bar{v}$ are depth-averaged velocity components in x and y directions, h is depth, $\bar{C}$ is depth-averaged concentration of scalar quantity, k_P is linear decay rate of scalar quantity, C_S is concentration of scalar quantity in source, S is magnitude of discharge due to point sources, and F_C is horizontal diffusion term [4].

3. Simulation Setup and Calibration

In this study, the computational mesh, containing 39514 elements, was generated by using MIKE Zero Mesh Generator and the bathymetry data of Gorgan Bay, acquired from Iran National Cartographic Center and local surveys conducted by PTP, Pouya Tarh Pars Consultant Engineers (see Figure 2). Here, the WRF model, Weather Research and Forecasting Model, was used to produce meteorological data, including wind speed, wind direction, and mean sea level pressure. The water level and velocity components in x- and y-directions were specified as the open boundary conditions in the hydrodynamic model.

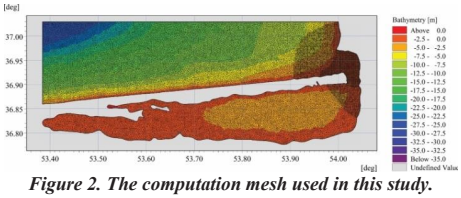

Figure 2. The computation mesh used in this study.

The model was calibrated by comparing the numerical modeling results with the field measurements, including water level and current speed, and adjusting the wind friction coefficient, identified as the most influential parameter on model results at sensitivity analysis stage. The water level and current speed were measured by PTP at 36.900695° N, 54.024822° E and 36.9024° N, 54.02922° E, respectively. After calibration, a correlation coefficient of 0.8 for water level (see Figure 3) and 0.6 for current speed was obtained.

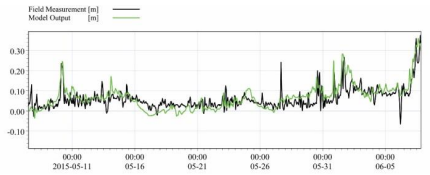

Figure 3. Comparison between the measured and modeled water level.

4. Results and Discussion

The results showed that the domain-averaged residence time in Gorgan Bay was about 340.6 days (see Figure4). A difference, made by different location of open boundaries, was noted between the results of this study and studies conducted previously [3]. In this study, tracer leaving Gorgan Bay was allowed to return the bay if there was a storm surge in the Caspian Sea, which increased the accuracy of the numerical modeling results.

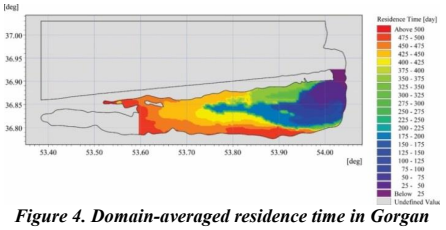

Figure 4. Domain-averaged residence time in Gorgan Bay.

Six scenarios were introduced to mitigate the problems mentioned above. Numerical modeling results revealed that opening an artificial inlet to the northwest of the bay was the most influential way to reduce the residence time and enhance water exchange (see Table 1). Even though this scenario would have the most favorable impact on the residence time, this scenario should not be conducted. It would significantly disrupt physical, chemical and biological processes taking place in the Miankaleh Wetland, located in the western part of the bay, and would have adverse effects on the ecosystem of the wetland. In addition, excavation of a new channel would result in splitting Miankaleh Peninsula, which is an intact habitat of different animals, into two separate lands. Last but not least, opening the inlet would inevitably result in entry of pollutants released from Amirabad Port, located to the west of the bay, to the water body.

Among proposed scenarios, dredging Ashuradeh Channel might have the least adverse effects on the ecosystem of the bay. In economic terms, it would also be effective because it would improve navigability in Gorgan Bay. Finally, it was concluded that the sustainable solution is to control the stressor – pollution coming from Gorgan Bay watershed and discharging into the bay.

Table 1. Domain-averaged residence time in Gorgan Bay after implementing different scenarios.

Scenario	Residence time (day)	Accumulated water exchange (Billion m^3)
Present condition	340.6	5.37
Creating an artificial inlet to the north-west of Gorgan Bay	162.5	7.89
Dredging and restoring Khozeini Inlet and Chapaghli Channel	276.4	7.34
Dredging and restoring Khozeini Inlet	277.4	6.94
Dredging both Chapaghli and Ashuradeh Channels	317	6.09
Dredging Chapaghli Channel	327.5	5.82
Dredging Ashuradeh Channel	331.2	5.69

5. Acknowledgments

We would like to thank Golestan Regional Water Authority for their support of this study.

6. References

[1] Birch, G. F., Evenden, D., and Teutsch, M. E., "Dominance of point source in heavy metal distributions in sediments of a major Sydney estuary (Australia)" *Environmental Geology,*28(4), 1996, pp. 169-174.

[2] Huang, J., Yan, R., Gao, J., Zhang, Z. and Qi, L., "Modeling the impacts of water transfer on water transport pattern in Lake Chao, China" *Ecological Engineering*, 95, 2016, pp. 271-279.

[3] Ranjbar, M. H., and Hadjizadeh Zaker, N., "Numerical modeling of general circulation, thermohaline structure, and residence time in Gorgan Bay, Iran", *Ocean Dynamics,*68(1), 2018, pp. 35-46.

[4] Danish Hydraulic Institute, "MIKE 21 Flow Model User Guide and Scientific Documentation", 2012.

DEVELOPING AN UNMANNED SURFACE VEHICLE FOR HARBOR SURVEY AND SECURITY APPLICATIONS

Rouhollah Goudarzi[1*], Ali Maleki[1] and Ebrahim Alizadeh

1) Malek Ashtar Univ. of Technology, Tehran, Iran, rohadi@mail.com

1. Introduction

Nowadays, the protection and security of civilian harbors, ports and even offshore platforms has received an increasing interest for the related authorities. One of the applicable methods in this area that currently attracts many scientific researchers is the use of Unmanned Surface Vehicle (USV), either in a single or in a group manner. These vehicles could be employed for patrolling purposes, searching of waterways and harbors for suspicious packages or anomalies that might be attached to vessels or dropped to sea bottom, or investigating in hazardous/dangerous situations, which are all of importance as harbor and offshore security becomes increasingly more important. For example, the NATO's Defense against Terrorism (DAT) program [1] has indicated the issue of harbor security as one of the main ten areas of work, where advanced technologies (like efficient sensor networks, electro-optical detectors and unmanned vehicles) can reveal very helpful. An example is given in the development of a family of USVs at the MIT AUV Lab (Manley et al., 2000) since the early 1990's [2].

Owl as one of the first USVs with 3 m length designed by Office of Naval Research (ONR) for special applications such as intelligence, surveillance, and reconnaissance (ISR) and antisubmarine missions [3]. Taiwan Ocean Research Institute (TORI) in cooperated with United Ship Design and Development Center developed a USV named ZhengeHe 101 with integrated surveying equipment for inshore waters surveying to reduce the intervention of human in data acquisition [4].

This paper reviews a preliminary design of a small and light unmanned surface vessel for domestic harbor survey and security applications, with emphasizing on the USV system description and controller design.

2. USV System

The fundamental parts and systems of an unmanned surface vehicle depend on its applications and mission requirements. However, some systems are fundamental for a typical USV and must be considered by a system designer, which includes: Hull and structural system, propulsion and power system, Guidance-Navigation-Control system, Communication system, Data collection and Processing system, Ground Station system and finally Payloads. Figure 1 depicts a typical USV architecture and its components.

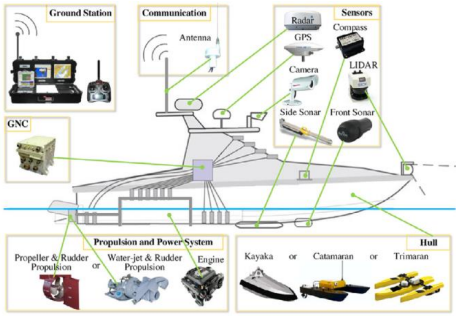

Figure 1. Fundamental architecture of a typical USV [5]

3. USV Dynamic Modeling

Extension of control strategies for USVs especially in the practical mode is related to the kind of operational modes which are categorized into remote control and autonomous control. Nevertheless kinematic and dynamic modeling of a surface vessel was considered as the first steps of studying of USV's behavior. In this paper, dynamic model of rigid body motions of the USV was defined with four degrees freedom in the body coordinate system (C.B) with the surge (u), sway (v), roll (p), and yaw (r) motions as follows:

$$\begin{cases} (m - X_{\dot{u}})\dot{u} = X_H + X_E + X_C \\ (m - Y_{\dot{v}})\dot{v} - (mh_g + Y_{\dot{p}})\dot{p} + (ml_g - Y_{\dot{r}})\dot{r} = Y_H + Y_E + Y_C \\ (I_{xx} - K_{\dot{p}})\dot{p} - (mh_g + K_{\dot{v}})\dot{v} - K_{\dot{r}}\dot{r} = K_H + K_E + K_C \\ (ml_g - N_{\dot{v}})\dot{v} - N_{\dot{p}}\dot{p} + (I_{zz} - N_{\dot{r}})\dot{r} = N_H + N_E + N_C \end{cases} \quad (1)$$

Where m is vessel's mass, *Ixx* and *Izz* are the vessel's roll and yaw inertia moments, lg and hg are longitudinal and vertical distances of the center of gravity to the body coordinate, respectively. X, Y, K and N are the forces and moments exerted to the boat and the subscripts H, E, C denotes hydrodynamic, environmental disturbances and control components, respectively.

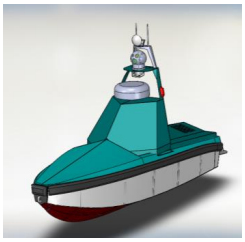

Figure 2. The proposed USV design for harbor surveying

Table 1. Principle characteristic of the proposed USV

Item	Measure	Unit
Displacement	1.5	ton
LOA	6.5	m
Beam	2	m
Draft	0.4	m
Power	150	hp
Range	100	n mile
Speed	30	knot

4. Sensor Systems

Measurement accuracy has noticeable impacts on the performance of the unmanned vehicles. Global Positioning System (GPS), Inertial Measurement System (INS), and Inertial Measurement Unit (IMU) as the most applicable navigational sensing system are utilized to provide position and orientation information and estimate velocity and acceleration based on estimation algorithms.

On the other hand, Radar, Sonar, Lidar, and cameras may be used in order to environmental identification, obstacle detection, target recognizing in operational conditions especially in the presence of environmental disturbances. Also many image processing and vision algorithms has been proposed in the investigations to distinguish objects and targets based on information from Electro-Optic and Infrared sensors and multi-layer sensor fusion.

5. Controller Design

Typically, controller design needs to allocate appropriate structures for actuator inputs. Figure 2 shows a schematic representation of actuators containing the trust force (F_T) and rudder angle (δR).

According to the previous kinematic and dynamical equations of the proposed USV, for control of the USV heading, a state space model can be extracted as follows:

$$\begin{cases} \dot{X}_p = A_p X_p + B_p u_p + D \\ y_p = C_p X_p \end{cases} \quad (2)$$

Where X_p is state variable vector, u_p is control input vector, y_p is output vector and D is effect of environmental disturbances.

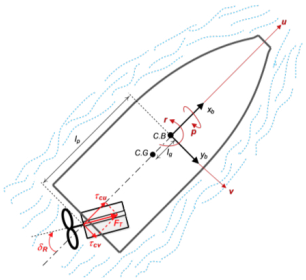

Figure 3. Schematic representation of actuator inputs

Main objective of controller design is tracking of desired inputs in order to follow a predefined path by selection a suitable controller. A state feedback controller has been proposed to achieve the considered goal.

$$u_p = KX_p \quad (3)$$

Also due to high-cost and lacking of some sensors, a Luenberger observer, considered to estimate un-measurable variables. Figure 3 depicts simulation result for motions in U-shape path. This Figure indicates a successful path following based on waypoints.

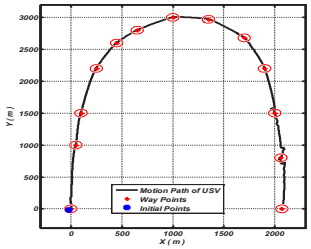

Figure 4. Path following of a typical U-shape path

6. Conclusion

This paper described briefly the architecture and control design of a USV. The proposed USV can be developed for harbor survey and security purposes with the advantage of reduction of personnel and having central control on ports.

7. References

[1] NATO defense against terrorism (DAT) programme (2004). URL *http://www.nato.int/issues/dat/*.

[2] Manley, J.E., Marsh, A, Cornforth, W. and Wiseman, C. "Evolution of the autonomous surface craft AutoCat", *In Proc. of Oceans'00*, 2000, 1:403-408.

[3] V. Bertram, "Unmanned surface vehicles-a survey," presented at the Skibsteknisk Selskab Compenhagen Denmark, 2008.

[4] Yang, W.R, Chen, C.Y, Hsu, C.M, Tseng, C.J, Yang, W.C. 2011. Multifunctional inshore Survey platform with unmanned surface vehicles, In: International journal of automation and smart technology, 19-25.

[5] Z. Liu, Y. Zhang, X. Yu, C. Yuan, "Unmanned surface vehicles: An overview of developments and challenges", *Annual Reviews in Control*, 2016, 1-23

PERFORMANCE EVALUATION OF IACS CLASSIFICATION SOCITIES VS. NON- IACS

Pouria Koulivand[1] and Fardad Fakhr Rahimian[2]

1) Port and Maritime Organization, Tehran , IRAN, Pkoulivand@pmo.ir
2) Port and Maritime Organization, Bandar Imam Khomeini, IRAN, am_rahimian@bik.ir

1. Introduction

When a ship is registered by a flag State, that flag maintains the responsibilities and obligations imposed upon them by International Conventions for ships. The flag State must ensure that these ships comply with the conventions [1].

To achieve this, flag States regularly delegate some or all of the survey, certification and verification functions to Recognized Organizations (RO), most commonly known as Classification Societies. [2].

The main focus of present article is evaluation of performance of Recognized Organizations (IACS members) and comparison with NON-IACS. For this purpose, after introducing required terms, statistics of BIK Port State Control about ROs (2017) will be presented and compared with the other references such as AMSA[1] , Tokyo MOU[2] and IOMOU[3] (2017).

2. Port State Control

Port State Control (PSC) is the inspection of foreign ships in national ports by PSC officers for the purpose of verifying that the competency of the master and officers on board, and the condition of the ship and its equipment comply with the requirements of international conventions (e.g. SOLAS, MARPOL, STCW, etc.) and that the vessel is manned and operated in compliance with applicable international law [3].

Statistics of detention rate by Port State Control is the best way for evaluation of all interested parties, especially ROs (Classification Society).

3. Classification Society

A classification society is a non-governmental organization that establishes and maintains technical standards for the construction and operation of ships and offshore structures. The society will also validate that construction is according to these standards and carry out regular surveys in service to ensure compliance with the standards [4].

It is important to mention that more than 90% of the world's cargo carrying tonnage is covered by Member Societies of IACS[4].

IACS has 12 members that are ABS, BV, CCS, CRS, DNV-GL, IRS, KR, LR, NK, PRS, RINA and RS [5].

4. Statistics of BIK port

Total statistics of BIK port are shown in table 1. Total rate of detention is 14% irrespective of ship's classification society. Other statistics are shown in Figure 1. In 2017 a total of 279 ships with 21 classification societies were inspected [6].

Table 1. Total Statistics of inspection in BIK port.

RO	Total No. of Inspections	Deficiency per inspection	Rate of Detention %
IACS	254	3.5	12
NON IACS	25	9.3	40

Figure 1. Total Statistics of inspection in BIK port.

In present article, detention rate were used for evaluation of classification society performances, and the results have been shown in Top 5 High Performance category. Accordingly these results have been compared with other references, e.g. AMSA, IOMOU and Tokyo MOU.

5. Classification Society Performances

According to statistics of Port state control inspection in BIK port, the performance of classes has been shown in

[1] Australian Maritime Safety Authority.
[2] Tokyo Memorandum of Understanding.
[3] Indian Ocean Memorandum of Understanding.
[4] International Association of Classification Societies.

Figure 2. Performance of classes in IOMOU, Tokyo MOU and AMSA is shown in Figures 3-5. All of figures show the performance of classes in view of Rate of Detention except IOMOU (figure is Detention per RO).

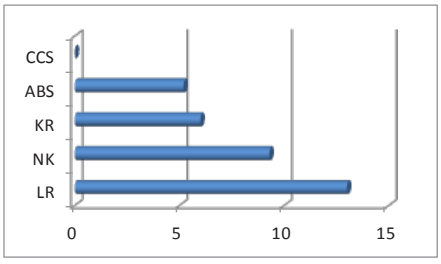

Figure 2. BIK Port 5 Top High Performance classes

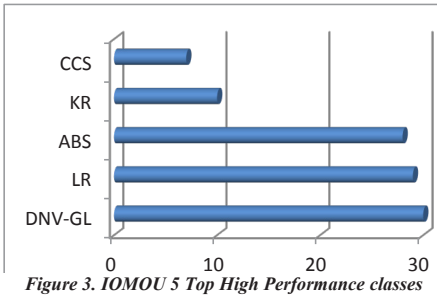

Figure 3. IOMOU 5 Top High Performance classes

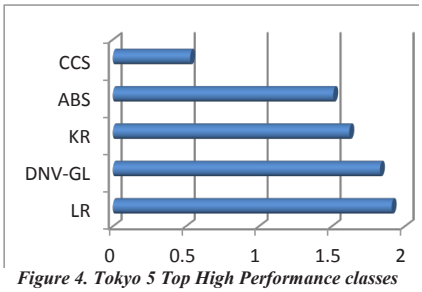

Figure 4. Tokyo 5 Top High Performance classes

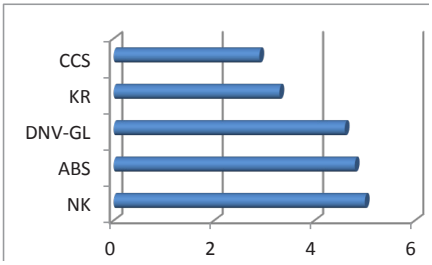

Figure 5. AMSA 5 Top High Performance Classes

According to statistics of BIK port, AMSA and Tokyo MOU, rate of IACS ship inspection, rate of IACS ship detention and rate of NON-IACS ship detention is shown in Figure 6.

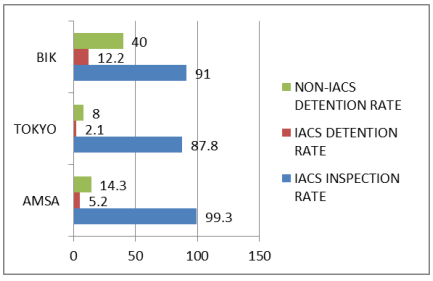

Figure6. Rate of inspection and detention for IACS and NON-IACS ships

6. Results

As shown in above figures following results are obtained:

- The high performance classes in all statistics are IACS members.
- CCS in present article is the best performance RO in all figures.
- In BIK, IOMOU and Tokyo statistics, CCS, KR and ABS are in top 3 high performance ROs.
- In all references NK class had the most inspection rates and medium performance.
- In all references, about 90% of inspections include IACS ships , and detention rate of NON-IACS ships are about three times more than IACS ships.
- BIK Port statistics are in good agreement with other references.
- AMSA has minimum rate of NON-IACS ship for psc inspections (about 0.7%).

7. References

[1] United Nation Convention on the Law of the Sea, Part VII, Article 94, *Duties of Flag State*, 2013, pp 58.

AN EXPLORATORY VIEW OF HEAVY METAL ANALYSIS IN WATER BODY OF MUSA ESTUARY

Seyed Mostafa Haghshenas[1], Ebrahim Akhondi[2] and Hossein Sakhaeinia[3]

1) Department of Chemical Engineering, Central Tehran Branch, Islamic Azad University, Tehran, Iran, smostafah1990@yahoo.com
2) Department of Chemical Engineering, Central Tehran Branch, Islamic Azad University, Tehran, Iran, ebr.akhondi@iauctb.ac.ir
3) Department of Chemical Engineering, Central Tehran Branch, Islamic Azad University, Tehran, Iran, h.sakhaeinia@iauctb.ac.ir

1. Introduction

Estuaries are marine embayments that are significantly diluted by fresh water. They are often preferred sites for shipping corridors and harbour construction. Because of shallow depths, slow currents and long residence times for water, they are prone to accumulation of pollutants. Industrial and domestic waste water flows are two main pollution sources that can affect aquatic life; waste water containing heavy metals can have profound effects on marine life. Current speed and direction, and distance to the pollution sources are two main parameters of pollutant dispersion and accumulation.

The values of heavy metals concentration especially in water bodies could be measured by many different approaches. For gaining a better understanding of these values and the ranges of change in different seas in the world, some studies are mentioned in the following. Many researchers and organizations deal with analysis and monitoring of heavy metals standard levels. Japan International Cooperation Agency (2014) determined acceptable levels of heavy metals in this area. In addition, Jalali *et al*. (2015), Safahieh *et al*. (2013) and Safahieh *et al*. (2011) measured concentrations of some important heavy metals using aquatic organisms as bio indicators in Musa estuary at the northwest corner of the Persian Gulf [2-4]. In the majority of their results, the values were more than standard levels which were issued by WHO; especially, at the end of creeks where residence time of water is long and current speed and direction force pollutants to be accumulated (Payandeh *et al*. 2015) [5].

In this study, we try to make a comprehensive data set of heavy metal concentrations in different parts of an estuary, in order to determine effective parameters and evaluate the level of effectiveness on pollution distribution. We also develop a 2D hydrodynamic model to make a visual analysis of these effective parameters.

2. Case Study

As a case study, Musa Estuary is a semi closed area with shallow depth (-6 - 0 m), very salty water, and intensively hot and humid weather. Extreme water level changes (around 6 m) and presence of tidal current are two significant features of this water body.

Some potentially sensitive points were considered to take surface water samples based on two main criteria: distance to the probable pollution current sources and the effect of extreme current speed. Points 101, 102 and 103 are close to entrance of urban and industrial sewage, point 104 is adjacent to the deepest point of the Persian Gulf with significant current speed, and Control point is considered in a farther location to the pollution sources to monitor changes in concentration values.

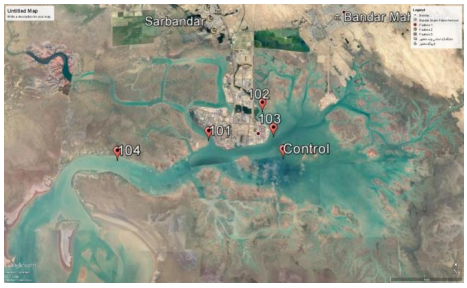

Figure 1. Distribution of sampling points in the study area

After taking three samples of water from each location, concentration values of heavy metals were measured by atomic absorption device for each sample and average of three values was calculated for every sample points. In the next step, values were compared with standard levels which mentioned in the report issued by Japan International Cooperation Agency (2014) (Table 1) [1]. It should be noted in table 1 that arsenic and mercury are not mentioned because the values are not remarkable in comparison with other elements and could be ignored.

To have a better visual understanding of pollution dispersion, concentration data and location of sampling points are defined as information layers in Arc GIS. Then by data interpolation and making a boundary around sampling area the changes in heavy metal levels are illustrated in pictures like Figure 2 for each element of heavy metals.

Table 1. Average concentration values and standard levels of heavy metals

Sample ID	Cd (mg/l)	Cr	Co	Cu	Pb	Ni
Standard	0.01	0.05	0.05	0.05	0.04	0.05
101	0.476	0.307	1.088	0.028	2.077	1.089
102	0.416	0.253	0.949	0.0001	1.895	0.794
103	0.487	0.304	0.948	0.0001	2.083	0.83
104	0.472	0.304	0.966	0.0001	2.057	1.011
Control	0.497	0.312	0.969	0.007	2.223	0.994

Figure 2. Changes in lead concentration along the study area

To set up a 2D hydrodynamic model in Mike- DHI software, different parameters including: bathymetry data and initial and boundary conditions were considered; then the unstructured mesh was applied. For model calibration various sensitivity tests were done to examine roughness heights and eddy viscosity coefficient; then measured and simulated tidal elevation was compared. Finally, daily changes of current direction and speed with a 15-minute time step is shown in the model output (Figure 3).

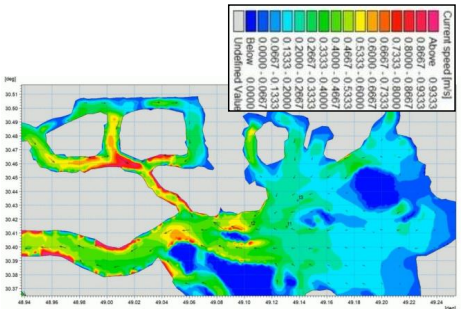

Figure 3. Model output for current speed and direction in the study area

3. Summary

Due to impressive importance of heavy metals in aquatic health, it is vital to gain an appropriate understanding of changes in concentration of elements and, current speed and direction as fundamental parameters to analyze pollutants dispersion. Some of the values reported here are very high. According to Table 1, except arsenic, mercury and copper (just in some locations), all values are extremely more than standards. Focus of accumulation are in two main points, 101 and Control. Point 101 is near to one of the main sources of urban and industrial sewage. High concentration of heavy metal in the Control point which was considered far from pollution sources, could be justified by model output of current (Figure 3). It is visible in this model that the current intensity started to decrease from Control point toward the east of estuary. Furthermore, low pollutant accumulation in point 102, refers to the severe tidal currents which puts pollutants away.

For Control point, it seems a contrast between distance to the pollution source and heavy metal accumulation; although this point is farther, values of chromium, cadmium, and lead are much more compared with other points in the study area which refers to mentioned decrease in the current speed. It is noteworthy that for nickel, copper, and cobalt, pileup occurs around point 101 which is next to one of the main sources.

These high values of heavy metals are very concerning, and suggest that more work needs to be done on upward mobility of metals in the food chain. There could be some serious human health impacts.

4. References

[1] Japan International Cooperation Agency, "The Project for Strengthening Environmental Management in Petroleum Industry in Persian Gulf and Its Coastal Area." 2014.

[2] K Jalali, B Abtahi, K Samaiee. Assessment of cd level in liver and muscle tissues of platycephalus indicus and sediment of musa estuary (northwest of persian gulf). 2015 Jan 1;14(2):0–0.

[3] Safahieh, Babadi, Nabavi, Ronagh, Ghanemi. Assessment of mercury intake through consumption of yellowfin seabream (Acanthopagrus latus) from Musa Estuary. 2013;

[4] Safahieh A, Monikh FA, Ronagh MT, Savari A, Doraghi A. Determination of heavy metals (Cd, Co, Cu, Ni and Pb) in croacker fish (Johnius belangerii) from Musa estuary in the Persian Gulf. Int J Environ Sci Dev Singap. 2011 Dec;2(6):460.

[5] Payandeh A, Zaker NH, Niksokhan MH. Numerical modeling of pollutant load accumulation in the Musa estuary, Persian Gulf. Environ Earth Sci. 2015 Jan 1;73(1):185–96.

COSTS ANALYSIS OF SPILLING A CRUDE OIL BARREL IN OFFSHORE AREA USING EPA BOSCEM METHODS

Mohammadhadi sharafi[1], Mona Yahya[2] and Pegah Moghadam[3]

1) CAPE Group, Tehran, Iran, Sharafi@capegroup.ir
2) CAPE Group, Tehran, Iran, Yahya@capegroup.ir
3) CAPE Group, Tehran, Iran, Pmoghadam@capegroup.ir

1. Introduction

The current global approach to the environmental damages is such that repairs need exorbitant costs and they take lots of time. Furthermore some of the distructions never get restored. To avoid this process, industries in the first step must conduct environmental assessments and scientific methods which evaluate the environmental impacts and afterward participate in payment when environment get contaminate. One of the requirements of this subject is the estimation of environmental damage which there is no guideline as a standard and comprehensive instruction in this context in our country. In this paper counter measure costs of oil spilling is estimated based on EPA BOSCEM method for a crude oil barrel spills. Eventually to compare dimensions of oil spill damage in offshore environment, also the mentioned scenario for oil spills in the oil facilities of operational area (land area) in the same condition is calculated and it is provided. According to results total costs and the damage caused spilling a barrel of oil in offshores and land areas are 13734 and 6085 dollars respectively. In table 1 result shows The Rial equivalent total costs are 550 million and 240 million Rials respectively which are remarkable. Figure1 shows the amount oil spills around the world. Figure 2 shows views of oil spilling in land and sea area.

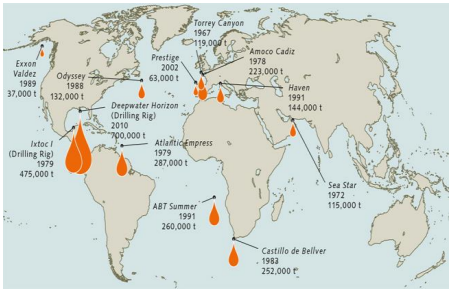

Figure 1. World oil spills

Figure 2. Oil spills in land and sea area

Table 1. Cost estimation of environmental damages caused by spilling one heavy crude oil barrel by using EPA BOSCEM methods

No	Proceedings and damages	Costs based on spills area	
		offshore	land
1	counter measure costs of oil spilling	7623 $	4573.8 $
2	Cost of social economic damages	1575 $	945 $
3	Cost of environmental damages	4536 $	576 $
4	Total costs and damages	13734 $	6085.8 $

2. Estimation Methods of Counter Measure Costs for Oil Spilling

Economic cost of one barrel of heavy crude oil spills was estimated in offshore environment. To confront with this oil spill, it is assumed that to help confronting oil spill specific marine vessels are used. The vessels by use of mechanical equipment, first enclose the oil stain, and then collect upper level of oil. Whatever the dispersions of oil levels are wider the mechanical methods are less efficient and using chemical-biological method such as Dispersants will be much more efficient. Efficiency of mechanical method is 20% and for chemical-biological method is 80% in confronts oil spill

operation. The calculation formula for counter measure costs of oil spilling is as follows:

Counter measure costs of oil spilling =Cost of collecting method × Adjustment Factor× Oil spills volume

3. Calculation Methods for Economic- Social Loss

The amount of Economic- Social loss caused by oil spilling for the amount of less than 500 gallons, it will be equal to 50 dollars. Also adjustment factor based on receiving pollutant environment for onshore and high seas will be equal to 1. The calculation formula for Economic- Social loss is as follows:

The Economic- Social loss of oil spills = economic costs × Adjustment Factor × Oil spills volume

Table 2. The cost of Economic-Social losses for oil spills in terms of dollar per gallons by using EPA BOSCEM method

Oil Type	Volume (gallons)	Base Socioeconomic Cost ($/gallon)
Light Fuels	< 500	$80
	500 – 1,000	$330
	1,000 – 10,000	$500
	10,000 – 100,000	$200
	100,000 – 1,000,000	$100
	> 1,000,000	$90
Heavy Oils	< 500	$150
	500 – 1,000	$600
	1,000 – 10,000	$900
	10,000 – 100,000	$500
	100,000 – 1,000,000	$200
	> 1,000,000	$175
Crudes1	< 500	$50
	500 – 1,000	$200
	1,000 – 10,000	$300
	10,000 – 100,000	$140
	100,000 – 1,000,000	$70
	> 1,000,000	$60
Volatile Distillates	< 500	$65
	500 – 1,000	$265
	1,000 – 10,000	$400
	10,000 – 100,000	$180
	100,000 – 1,000,000	$90
	> 1,000,000	$70

4. Calculation Methods for Environment Loss

According to the assessment form of the accident consequences lead to oil spills, the calculation formula of environment loss in oil spills is as follows:

Environment loss cost of oil spills = environment losses × (wild life Adjustment Factor + sweet water Adjustment Factor) 0.5 × environment oil spill volume.

In this formula, the environment oil spill volume will be 1 barrel or 31.5 gallons. Environment losses per gallon in the amount less than 500 gallons of crude oil are about 90 dollars. The result is based on table 3. Since the oil spill occurs in offshore area, the adjustment factor will be zero.

Table 3. The cost of Environmental losses for oil spills in terms of dollar per gallons by using EPA BOSCEM method

Oil Type	Volume (gallons)	Base Environmental Cost ($/gallon)
Light Fuels	< 500	$85
	500 – 1,000	$80
	1,000 – 10,000	$70
	10,000 – 100,000	$65
	100,000 – 1,000,000	$30
	> 1,000,000	$25
Heavy Oils	< 500	$95
	500 – 1,000	$90
	1,000 – 10,000	$85
	10,000 – 100,000	$75
	100,000 – 1,000,000	$40
	> 1,000,000	$35
Crudes	< 500	$90
	500 – 1,000	$87
	1,000 – 10,000	$80
	10,000 – 100,000	$73
	100,000 – 1,000,000	$35
	> 1,000,000	$30
Volatile Distillates	< 500	$48
	500 – 1,000	$45
	1,000 – 10,000	$35
	10,000 – 100,000	$30
	100,000 – 1,000,000	$15
	> 1,000,000	$10

Contaminated with oil spills, this factor is equivalent to basic value and it will be 1.5. If the industrial confines are contaminated with oil spills and at the same time pollution has entered to rivers and ravines, average of both adjustments factors will be used in calculations. The amount of this average is 0.95.

The adjustment factor of settlement and wildlife damages located in a row of other sensitive settlements and it will be 3.2 in offshore areas such as platforms and marine vessels. Also beaches are located in the row of sensitive settlements.

5. Results and Discussion

According to considered generalities, the cost of one barrel of heavy crude oil spill's collection and its damages are calculated with EPA BOSCEM methods. By considering the results comparison of oil spill damages' dimensions in offshore areas with petroleum installation (land area) oil spills based on described methods will be possible.

6. References

[1] Modeling oil Spill Response & Damage Costs, Dagmar Schmidt Etkin, NY, USA, 2004.
[2] Hypothetical Spill in Etkin et al, 2002-2003 & Oil Fate Modeling by Applied Science Associates' SIMAP in French-McCay et al, 2002
[3] British Oil Spill Control Association (BOSCA). 1993. BOSCA Guide to Suppliers. Response Marketing Group, London, UK.
[4] Elkin, D.S.1998b. Financial Costs of Oil Spills in the United States. Oil Spill Intelligence Report, Cutter Information Corp., Arlington, Massachusetts, USA, 346 pp.
[5] Franken, P.1991.University of Arizona, Department of Economics, Tucson, Arizona, USA, unpublished study.

NUMERICAL SIMULATION OF THE TIDAL DISPERSION OF CONTAMINATION IN A MODEL OF ESTUARY

Maryam Hakimzadeh[1] and Habib Hakimzadeh[2]

1) M.sc Student in Environmental Engineering, Department of Civil Engineering, Sharif University of Technology, Tehran, Iran, Hakimzadeh@mehr.sharif.ir
2) Professor in Coastal Engineering , Faculty of Civil Engineering, Sahand University of Technology , Tabriz, Iran, Hakimzadeh@sut.ac.ir

1. Introduction

Dispersion of contaminated open sea or coastal waters in the estuaries is generally a serious problem for the people who living nearby these tidal basins. Then, daily life of the residents of these regions may gradually and/or abruptly be affected by dispersion of contaminated waters along the estuaries. In addition to human beings, pollution, which is probably the most important threat to quality of water in estuaries, can affect estuarine organisms, such as commercially important fish and shellfish. The most important pollutants that have greatest impacts on the health of estuaries include toxic substances such as chemicals and heavy metals, nutrient pollution and pathogens such as bacteria or viruses [1].

The volume of contamination in the estuary is controlled by two main factors, which are tides and volume of receiving body. Tides are driven by the gravity of Moon and Sun and results in a bulge in the water on the Earth's surface [2].

For this study, numerical code was developed to simulate the tidal dispersion of a contamination in an estuary. The model was first verified for the mass conservation of the contamination in a channel [3].

Therefore, an experimental flume with 20 meters length has been selected as a model estuary. First, it is assumed that there is a steady state current in the flume and the magnitudes of diffusion coefficient and velocity are $0.01 m^2/s$ and 0.05m/s, respectively. In addition to considering constant values for the diffusion and velocity, these parameters have been assumed to be oscillating sinusoidal for the tidal flows. Time period of the sinusoidal oscillation is then assumed to be 60 seconds.

2. Model Verification

The general form of advection-diffusion equation, omitting source and sink terms, is written as:

$$\frac{\partial C}{\partial t} + u_i \frac{\partial C}{\partial x} = D_t \frac{\partial^2 C}{\partial x^2} \quad (1)$$

where $\frac{\partial C}{\partial t}$ is localized changes and $u_i \frac{\partial C}{\partial x}$ and $D_t \frac{\partial^2 C}{\partial x^2}$ are advection and diffusion terms, respectively.

Although there are different methods to discretize this equation, finite difference method has been deployed for this study because of being easily implemented in computational programming. Furthermore, an explicit method rather than implicit one is selected in solving the discretized equation because of its simplicity and being computationally fast. Generally, for the explicit methods, the numerical stability criterion is an important issue that can be achieved through a stability analysis (e.g., von Neumann method). For the adopted explicit method, it is accurate enough to take Δx equal to 0.05 and Δt equal to 0.025. Accordingly, these time and distance steps are taken here. Further details of the numerical schemes and solution process were outlined in [3] and are not given herein for brevity.

In order to verify the numerical model results, mass conservation at the inlet and outlet of the channel has been investigated. Then, the accuracy of mass conservation implies that the model works accurate enough. For instance, by having a concentration pattern equal to C=100mg/l for 30 seconds and calculating the concentration at the outlet, it is derived that mass is equal to 3.0000e+03 at the inlet of the channel and 2.9975e+03 at the outlet of channel, which can validate the accuracy of the model implemented here [3].

3. Application of model to the tidal currents

The model was then run for three tidal cycles and different scenarios. In the following, the produced numerical results are presented. First, the effect of tidal currents is ignored and a steady state flow is assumed to be along the flume (Figure 1 and Figure 2). Then, the effect of tidal current has been investigated in Figure 3 and Figure 4.

In calculating the concentration along the model estuary, it has been assumed that concentration is 100 mg/l at the upstream inlet of flume at all simulation times and is initially equal to zero along the channel. Furthermore, the gradient of concentration at the outlet is set to be zero.

In Figure 1, which is illustrated below, it is first assumed that there is a constant diffusion with zero velocity (no advection). It can be seen from the figures that the contamination could approximately diffuse up to 6m from inlet at 180s.

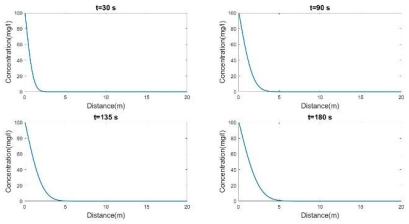

Figure 1 Concentration at different times along the flume (constant diffusion only)

In Figure 2, in addition to a constant diffusion, a constant velocity was assumed along the flume:

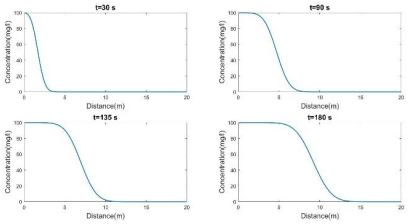

Figure 2 Concentration at different times along the channel (constant diffusion and velocity)

Then, it can be seen from the figures that the contamination could disperse up to about 14m from inlet at 180s. This results show clearly the contribution of the advection term in the abovementioned equation.

Finally, in order to see the effect of tidal currents in the concentration along the flume, an oscillating velocity has been considered at the inlet and along the flume. In the following figures, the velocity has been considered to be equal to 0.05**sin (2πt/T),* in which T is assumed to be 60 seconds. Figure 3 illustrates the concentration along the channel for an oscillating velocity and constant diffusion coefficient.

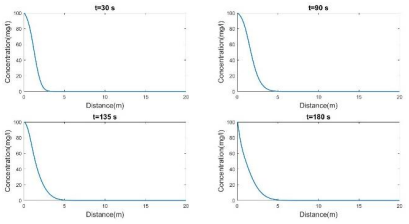

Figure 3 Concentration at different times along the channel (constant diffusion and oscillating velocity)

By comparing the results of this scenario with the previous ones, two important items can clearly be distinguished. First, comparing the results of Figure 1 and Figure 3, shows that the oscillating flow tentatively hinders further diffuse of contamination along the flume. Second, after the lapse of 180s, the advection term of oscillatory flow not only prevents diffuse of the contamination along the flume, but also push it back somewhat.

At last, in addition to the oscillating velocity, it is assumed that the diffusion coefficient is also oscillating according to a sine curve which is reasonable based on turbulent characteristics. The related concentration along the channel is depicted in Figure 4. The numerical results show remarkably even further prevention in comparing with the latter ones.

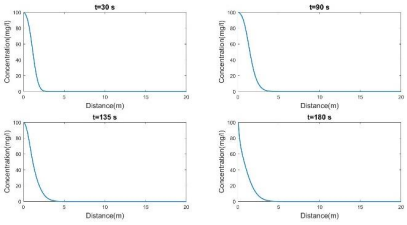

Figure 4 Concentration at different times along the channel (oscillating diffusion and oscillating velocity)

In conclusion, the numerical results of progressive lengths of contaminations up to thousandth of inlet concentration along the flume at different times for the four scenarios are summarized in table 1. According to the table, it can be concluded that at the frame of this study, the progressive of contaminated coastal waters due to tidal currents into the estuaries may not be a serious problem for these tidal basins. Surely, in order to establish a more robust conclusion, further studies must be done for the various kinds of contaminations and diffusion coefficients.

Table 1 Progressive lengths of contamination along the flume at different times

Scenarios/Times	30s	90s	135s	180s
S1	2.60m	4.45m	5.45m	6.25m
S2	3.85m	8.50m	11.65m	14.60m
S3	3.40m	5.25m	5.75m	6.10m
S4	2.85m	4.30m	4.65m	4.85m

4. Reference

[1]https://oceanservice.noaa.gov/education/kits/estuaries/estuaries09_humandisturb.html

[2] Montagna, Paul A., Terence A. Palmer, and Jennifer Beseres Pollack. "Conceptual model of estuary ecosystems." In *Hydrological Changes and Estuarine Dynamics*, pp. 5-21. Springer, New York, NY, 2013.

[3] Hakimzadeh, M., and Hakimzadeh, H., "*Investigation into peak attenuation of the inlet pollution at the outlet of a flume* ", *10th National Congress on Civil Engineering*, Tehran. Iran, April 19-20 2017.

NUTRIENTS AND ORGANIC COMPOUNDS ANALYSIS OF WATER IN WATER BODY OF MUSA ESTUARY

Seyed Mostafa Haghshenas[1], Ebrahim Akhondi[2] and Hossein Sakhaeinia[3]

1) Department of Chemical Engineering, Central Tehran Branch, Islamic Azad University, Tehran, Iran, smostafah1990@yahoo.com
2) Department of Chemical Engineering, Central Tehran Branch, Islamic Azad University, Tehran, Iran, ebr.akhondi@iauctb.ac.ir
3) Department of Chemical Engineering, Central Tehran Branch, Islamic Azad University, Tehran, Iran, h.sakhaeinia@iauctb.ac.ir

1. Introduction

Estuaries are marine embayment which is significantly diluted by fresh water. They are often preferred sites for shipping corridors and harbor construction. Because of shallow depths, slow currents and long residence times for water, estuaries are prone to accumulation of pollutants. Industrial and domestic wastewater flows are two main pollution sources that affect aquatic life; nutrients and organic contents are two important kinds of pollutants including several elements and compounds. Seasonal changes, distance to the pollution sources, and components of the pollution streams, are the main parameters affecting pollution level and accumulation.

The concentration ratio of two elements, nitrogen and phosphorus, indicate biomass productivity and nutrient removal in water treatment. Moreover, the ratio of biological oxygen demand (BOD) and chemical oxygen demand (COD) in waste water, represent the ability of water or wastewater to be purified biologically. For gaining a better understanding of these values and the ranges of change in different seas in the world, some studies are mentioned in the following. Many researchers and organizations deal with analysis and monitoring of nutrients and organic matters standard levels. Japan International Cooperation Agency (2014) determined acceptable levels of nitrogen, phosphorus, and chemical oxygen demand (COD) in this area using standards which was issued by Department of Environment of Iran for ambient water in the Persian Gulf and Oman Sea [1, 5]. In addition, Payandeh *et al*. (2015) developed a 2D hydrodynamic model for nitrogen and phosphorus capacity of Musa estuary [6]. In that study, some scenarios defined for eutrophic zones where remarkable presence of nutrients with high consumption of oxygen occur in different parts of the study area. Furthermore, Z.Wan *et al.* (2011), and Hee Jeong Choi *et al*. (2014) used a criteria for the balance of mass productivity and nutrient removal as the ratio of nitrogen (N) to phosphorus (P) [2, 4]. According to their results, the values between 5-30 of that ratio are acceptable for sea water. In addition, Curtis Deutsch *et al.* (2012) introduced a standard level for N to P ratio around 15 for the oceans. For biological purification ability of water, Khaled Zaher *et al*. (2015) used the ratio of BOD to COD. For values more than 0.6, water can purified biologically, for the values between 0.3 to 0.6 the treatment process rate is slow, and if the ratio is less than 0.3 biological purification do not proceed due to having some toxic components and non-biodegradable substances or water acclimated microorganisms may be required in its stabilization [3].

In this study, we try to make a comprehensive data set of nutrients and organic compounds concentrations in different parts of an estuary, in order to determine effective parameters and evaluate the level of effectiveness on pollution distribution using visual analysis of these effective parameters.

2. Case Study

As a case study, Musa estuary is designated which is a semi closed area with almost shallow depth (-6 - 0 m), very salty water, and intensively hot and humid weather. Extreme water level changes (around 6 m) and presence of tidal current are two significant features of this water body.

Some potentially sensitive points were considered to take surface water samples based on two main criteria: distance to the probable pollution current sources and the effect of extreme current speed. Points 101, 102 and 103 are close to entrance of urban and industrial sewage, point 104 is adjacent to the deepest point of the Persian Gulf with significant current speed, and Control point is considered in a farther location to the pollution sources to monitor changes in concentration values.

Figure 1. Distribution of sampling points in the study area

After taking three water samples from each location, concentration values of nitrogen and phosphorus, and COD values were measured by spectrophotometer device for each sample and average of three values was calculated for every sample points. Also dissolved oxygen (DO) and BOD values are determined by Winkler method. In the next step, the indicator ratios were calculated and values were compared with standard levels which mentioned in the report issued by Japan International Cooperation Agency (2014) (Table 1) [1]. To have a better visual understanding of nutrients and organic matters dispersion, concentration values and location of sampling points are defined as information layers in Arc GIS. Then, by data interpolation and making a boundary around sampling area the changes in elements concentration, N/P ratio, and BOD/COD ratio are illustrated in Figures 2 and Figures 3.

Table 1. Average concentration values and standard levels of heavy metals

Sample ID	Total Nitrogen (ppm)	Total Phosphorus (ppm)	N/P	BOD (mg/l)	COD (mg/l)	BOD/ COD
Standard	0.4	0.045	15	20	5	0.3<
101	0.9	0.27	2.36	4.22	1080	0.003
102	3	0.51	4.16	8.43	570	0.014
103	1.3	0.16	5.75	18.97	1320	0.014
104	0.9	0.1	6.37	39.99	640	0.062
Control	1	0.16	4.42	12.67	1160	0.01

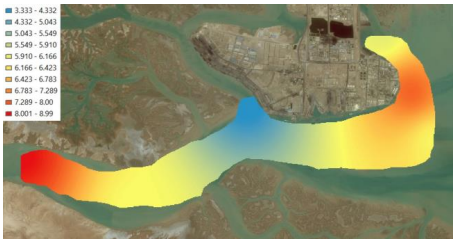

Figure 2. Changes in nitrogen to phosphorus ratio in the study area

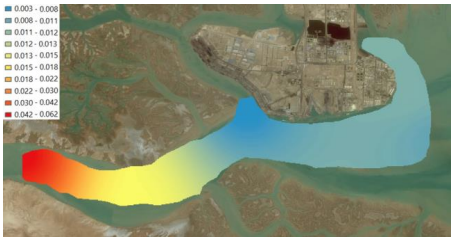

Figure 3. Changes in BOD to COD ratio in the study area

3. Summary

Due to enormous importance of dissolved oxygen in aquatic health, it is vital to provide an appropriate insight into oxygen consumption reactions. The sampling time was end of summer which maximum level of algal bloom and oxygen consumption are expected due to strong sunlight and increasing photosynthesis. However, the oxygen levels seem appropriate in this study (4 to 6 mg/l O_2).

For nitrogen and phosphorus, results show high concentration values and the amounts of N/P factor is lower than standard levels for the oceans which can not satisfy the balance of biomass productivity and nutrients removal [7]. In this study nitrogen is a limited factor due to input huge amount of phosphorus coming industrial and domestic waste water. Furthermore BOD/COD ratio is extremely low for all sampling points showing huge amount of toxic elements which can not to be purified completely by biological reactions.

These high values of organic and toxic matters are very concerning, and suggest that more work needs to be done on upward mobility of toxic elements in the food chain. Presence of heavy metal elements and toxic compounds in sea water can probably cause fundamental destruction of bio cells. Another concern is bio magnification process which is exponentially increase of elements in aquatics body, and in the next step in human body. There could be some serious human health impacts.

4. References

[1] Japan International Cooperation Agency, "The Project for Strengthening Environmental Management in Petroleum Industry in Persian Gulf and Its Coastal Area." 2014.

[2] Z.Wan, L. Jonasson, and H. Bi. N/P ratio of nutrient uptake in the Baltic Sea. 2011.

[3] Khaled Zaher Abdallaa, and Gina Hammamb. Correlation between Biochemical Oxygen Demand and Chemical Oxygen Demand for Various Wastewater Treatment Plants in Egypt to Obtain the Biodegradability Indices. 2014;

[4] Hee Jeong Choi, and Seung Mok Lee. Effect of the N/P ratio on biomass productivity and nutrient removal from municipal wastewater . 2014.

[5] Department of Environment of Iran, Standard for ambient water in Persian Gulf and Oman Sea.

[6] A. Payandeh, N. Hadjizadeh Zaker, and M. H. Niksokhan. Numerical assessment of nutrient assimilative capacity of Khur-e-Musa in the Persian Gulf, 2015.

[7] Curtis Deutsch and ThomasWeber. Nutrient Ratios as a Tracer and Driver of Ocean Biogeochemistry, 2012.

ASSESSING THE AREAS WITH HIGHER PROBABILITY OF BEING AFFECTED BY CONTAMINATION RELEASE, CASE STUDY: PERSIAN GULF

Seyedeh MaryamTabatabaee Samimi [1], Sarmad Ghader[2], Abbasali Aliakbari Bidokhti [3], Abbas Haghshenas[4], Mohammad Hosseiny Bandarabadi[5] and Aref Farhangmehr[6]

1) Institute of Geophysics, Tehran University, Tehran, Iran, maryam.tabatabaee@ut.ac.ir
2) Institute of Geophysics, Tehran University, Tehran, Iran, sghader@ut.ac.ir
3) Institute of Geophysics, Tehran University, Tehran, Iran, bidokhti@ut.ac.ir
4) Institute of Geophysics, Tehran University, Tehran, Iran, sahaghshenas@ut.ac.ir
5) Institute of Geophysics, Tehran University, Tehran, Iran, M.hosseiny@yahoo.com
6) Institute of Geophysics, Tehran University, Tehran, Iran, aref.farhangmehr@gmail.com

1. Introduction

Coastal and marine areas which are habitats for some of the richest but sensitive flora and fauna, are usually not only highly populated but also under increasing anthropogenic pressure in all parts of the world. In order to preserve and conserve these valuable ecosystems, environmental protection should be every government's priority. The ability to predict the path of the pollutants is the key aspect that may assist in controlling/managing the marine pollution problem in case of accidents associated with the release of pollutants.

The study area (Figure 1) includes the Persian Gulf, located in Southwest Asia. This gulf is an extension of the Indian Ocean located between Iran and the Arabian Peninsula.

Figure 1. Persian Gulf, the study area.

There are intense shipping activities in the Persian Gulf, which include massive transport of oil and chemical contaminants. This shows the significance of conducting such a study in this region.

We are interested in finding the areas of the gulf that have higher probability of being affected by contamination after an accident or as a result of a continuous release.

The release may occur during neap or spring tide. Furthermore, two different wind conditions have also been considered: calm and northwest wind.

2. Methodology

In this paper we have employed DHI-Mike Software in order to track the pathways of pollutant particles released into this marine environment.

The method consists of the following steps: (1) velocity field of the sea area obtained from Mike21-FM[1] (2) Lagrangian trajectories of selected particles in the uppermost layer of the sea.

This hydrodynamic model performs integration of the continuity equation and the horizontal momentum equations over depth $h=d+\eta$, namely the following two-dimensional shallow water equations [3]:

$$\frac{\partial h}{\partial t}+\frac{\partial h\bar{u}}{\partial x}+\frac{\partial h\bar{v}}{\partial y}=hS \tag{1}$$

$$\begin{aligned}&\frac{\partial h\bar{u}}{\partial t}+\frac{\partial h\bar{u}^2}{\partial x}+\frac{\partial h\overline{vu}}{\partial y}=f\bar{v}h-gh\frac{\partial \eta}{\partial x}-\frac{h}{\rho_0}\frac{\partial p_a}{\partial x}\\&-\frac{gh^2}{2\rho_0}\frac{\partial \rho}{\partial x}+\frac{\tau_{sx}}{\rho_0}-\frac{\tau_{bx}}{\rho_0}-\frac{1}{\rho_0}\left(\frac{\partial s_{xx}}{\partial x}+\frac{\partial s_{xy}}{\partial y}\right)\\&+\frac{\partial}{\partial x}(hT_{xx})+\frac{\partial}{\partial y}(hT_{xy})+hu_sS\end{aligned} \tag{2}$$

$$\begin{aligned}&\frac{\partial h\bar{v}}{\partial t}+\frac{\partial h\bar{v}^2}{\partial y}+\frac{\partial h\overline{uv}}{\partial x}=-f\bar{u}h-gh\frac{\partial \eta}{\partial y}-\frac{h}{\rho_0}\frac{\partial p_a}{\partial y}\\&-\frac{gh^2}{2\rho_0}\frac{\partial \rho}{\partial y}+\frac{\tau_{sy}}{\rho_0}-\frac{\tau_{by}}{\rho_0}-\frac{1}{\rho_0}\left(\frac{\partial s_{yx}}{\partial x}+\frac{\partial s_{yy}}{\partial y}\right)\\&+\frac{\partial}{\partial x}(hT_{xy})+\frac{\partial}{\partial y}(hT_{yy})+hv_sS\end{aligned} \tag{3}$$

The over-bars indicate depth- averaged values. For example, $\bar{u}$ and $\bar{v}$ are depth-averaged velocities defined by

$$h\bar{u}=\int_{-d}^{\eta}ud_z \tag{4}$$

[1] http://www.mikepoweredbydhi.com/

$$h\bar{v} = \int_{-d}^{\eta} v d_z$$

where η is the surface elevation; d is the still water depth; ρ_0 is the reference density of water; $f = 2\Omega sin\phi$ is the Coriolis parameter (Ω is the angular rate of revolution and ϕ the geographic latitude); s_{xx}, s_{xy}, s_{yx} and s_{yy} are components of the radiation stress tensor; p_a is the atmospheric pressure.

The lateral stresses T_{ij} include viscous friction, turbulent friction and differential advection. They are estimated using an eddy viscosity formulation based on the depth- averaged velocity gradients [3]:

$$T_{xx} = 2A\frac{\partial \bar{u}}{\partial x}$$

$$T_{xy} = A\left(\frac{\partial \bar{u}}{\partial y} + \frac{\partial \bar{v}}{\partial x}\right) \quad (5)$$

$$T_{yy} = 2A\frac{\partial \bar{v}}{\partial y}$$

The area does not experience freezing. Hence, the surface stress $\overrightarrow{\tau_s} = (\tau_{sx}, \tau_{sy})$ is determined by the winds over the surface. The stress is given by the following empirical bulk aerodynamic relation [3]:

$$\overrightarrow{\tau_s} = \rho_a C_d |u_w| \overrightarrow{u_w} \quad (6)$$

where ρ_a is the density of air, C_d is the drag coefficient of air, and $\overrightarrow{u_w} = (u_w, v_w)$ is the wind velocity 10 m above the sea surface.

The particle tracking technique describing transport and dispersion of particles follows the Langevin equation. The equation is written as [4]:

$$dX_t = a(t, X_t)d_t + b(t, X_t)\xi_t d_t \quad (7)$$

Where α is Drift term, b is Diffusion term and ξ is Random number.

3. Results and Discussion

Figure 2 shows the result of the tracking pollutants near Bushehr area after one year. The path of the released pollutants from Bushehr power plant seems to move along the coast, oscillating in the east–west direction with tides. After reaching Damigaz port, part of it extends to the southern part of the gulf entering an anticyclonic circulation.

The movement of the particles is obviously influenced by wind conditions and the tidal state when the release occurs.

Results in Figure 3 indicate that the areas more affected by contamination are located along the coast of Bushehr province. The areas located between Jainak and Ameri ports are more exposed to contamination than other parts.

Such prediction can be useful in any future control of possible accidental release of contaminants in this area.

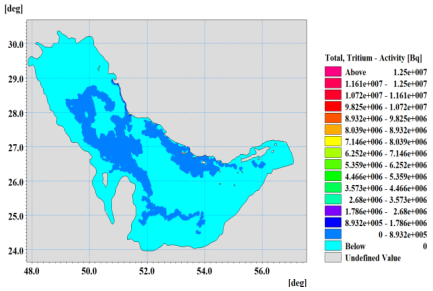

Figure 2. Coasts under threat

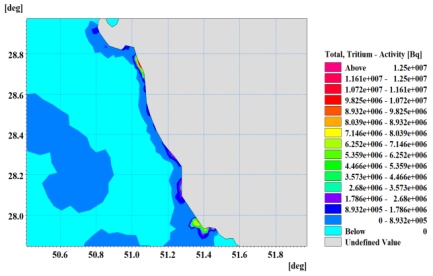

Figure 3. Measured flow tracker data off the coast Bushehr

4. References

[1] Periáñez, R. (2005). Modelling the dispersion of radionuclides in the marine environment. Springer-Verlag Berlin Heidelberg

[2] Breton, M., & Salomon, J. C. (1995). A 2D long term advection dispersion model for the Channel and Southern North Sea. Part A: validation through comparison with artificial radionuclides. *Journal of Marine Systems*, 6, 495-513.

[3] MIKE Powered by DHI. (2014). Hydrodynamic and Transport Module: Scientific documentation.

[4] MIKE Powered by DHI. (2014). Particle Tracking Module: Scientific documentation.

A SEARCH AND RESCUE MODEL FOR TRACING OBJECTS IN THE PERSIAN GULF

Seyed Abbas Jazaeri[1], Kourosh Hejazi[2] and Mehdy Kebriaee[3]

1) Civil Engineering Department, K. N. Toosi University of Technology, Tehran, Iran, A.Jazaeri@email.kntu.ac.ir
2) Civil Engineering Department, K. N. Toosi University of Technology, Tehran, Iran, HejaziK@kntu.ac.ir
3) Ports and Maritime Organization of Iran, Tehran, Iran, Mehdy.kebriaee@gmail.com

1. Introduction

Every year a number of reports about human bodies and boats missing in the Persian Gulf are received. Finding the lost objects was incentive for developing a numerical model for the prediction of their floating motion on the sea. A search and rescue (SAR) Fortran code based on the method proposed by Breivik and Allen [1] has been developed herein.

Many factors such as wind and current fields, release time and position, etc. affect the motion of the objects in the sea. A stochastic model based on the Monte Carlo method has been used to account for the uncertainties in these factors. Search zones for alternative uncertainties are then proposed by the model. The empirical leeway coefficients compiled with the US Coast Guard [2] are used for considering the effect of wind field on the motion of the objects.

2. Forcing Fields

Two forcing fields namely, the current field and the wind field are considered.

The drift associated with the wind force alone on the exposed above-water part of the object is defined as its leeway. It consists of two components: downwind (L_d) and crosswind (L_c) drift. Breivik and Allen [1] have shown that these two components have a linear relation with wind velocity at 10m height above the sea surface, e.g. for the downwind component of leeway, it follows:

$$L_d = a_d \times W_{10} + b_d \quad (1)$$

where a_d and b_d are empirical leeway coefficients determined from the experiments carried out by the U.S. Coast Guard reported for 63 different search objects [2], and W_{10} is the wind velocity at 10m height. The procedure of computing the crosswind component is in the similar way. In the field investigations, it was observed that some of the objects were drifted to the left and others were drifted to the right of the wind direction (Figure 1). Like downwind component, it was observed that in both left-drifted $(L_{C,L})$ and right-drifted $(L_{C,R})$ situations, the relation between crosswind component of leeway and wind velocity was linear. According to the observations, the probability of left and right drifting is almost equal. Thus, a 50/50 distribution is utilized.

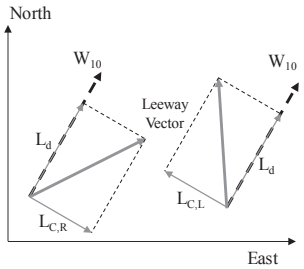

Figure 1. The relation between leeway vector components and wind vector.

The current field used in this study is the simulated results of a 2D horizontal model implemented at a specific depth proportional to the floating depth of the object. It is assumed that in the absence of the wind field, the object is drifted in the same direction of current and in the case of change of the direction of current, the object changes its direction instantly.

3. The Stochastic Model

Several parameters affect the free motion of an object on the sea. The definite impact of these factors is not available. But the search zones, which most likely may host the missing objects, can be estimated by applying the corresponding uncertainties using a stochastic model. In this study a Monte-Carlo stochastic model has been employed.

The Monte Carlo method suggests to perform the simulations for the desired number of similar objects with all affecting parameters perturbed randomly to generate a cloud of possible positions of existence of the objects in the sea. Search zones for alternative percentages of uncertainties are then configured. In this study 500 objects were considered and the model has been simulated to predict their fate.

4. Solution Method

The PMO Dynamics model [3] was used for computing the current field in the Persian Gulf. The wind field was obtained from the WRF wind forecasting model [4].

The governing equation of an object motion on the sea surface includes calculating the arc traced by the leeway vector superposed on the surface current [1] as follows:

$$\mathbf{x}(t)-\mathbf{x}_0=\int_0^t\left[\mathbf{L}(t')+\mathbf{u}_w(t')\right]dt' \qquad (2)$$

Here, $\mathbf{x}(t)$ is the position of the object at time t, $\mathbf{L}$ is the leeway vector that could be calculated with the wind field obtained from WRF model, based on Eq. 1 and $\mathbf{u}_w$ is the current vector computed from the PMO Dynamics model. A second order Runge-Kutta scheme was used for numerically solving Eq. 2. The scheme yields to the following discretized equation:

$$\mathbf{x}(t_0+\Delta t)=\mathbf{x}(t_0)+\Delta t\times \mathbf{V}\left(t_0+\frac{\Delta t}{2},\mathbf{x}(t_0)+\frac{\Delta t}{2}\times\mathbf{V}(t_0,\mathbf{x}(t_0))\right) \qquad (3)$$

where $\mathbf{x}(t_0)$ is the initial position of the object, Δt is the time step and $\mathbf{V}$ is the velocity vector that is the sum of the leeway and surface current. First, the velocity vector in the half of the time step was calculated. Then by substituting the current position, the position of the object at the end of the second half-time-step and for the next time step was computed.

To account for the uncertainties of the release position and time, a range of release locations were used instead of a release point. To implement this range in the model, the location and the time of the start and the end of this range was received as the input data.

The uncertainties of simulated or observed wind and current filed data, and also leeway coefficients applied in the model were based on a normal distribution with 0 average and a variance equal to the variance of the data $N(0,\sigma)$.

Eq. 3 was solved for all 500 particles under perturbed forcing fields. The simulations yielded clouds of particles representing the time evolving candidate positions of drifting object. If the convex hull of alternative number of these positions is drawn, search zones with various percentage of uncertainties are then obtained, e.g. the convex hull of 125 particles defines a search zone with 25% of uncertainties. Based on the cost dedicated to the search operation, alternative number of the particles may be chosen. Increasing the number of particles results in the expansion of the search area.

5. Results

It is assumed that a report about the loss of a human body is received on 2009-08-01T20:30 UTC between Mogham Port and Lavan Island in the Persian Gulf (dropped pin in Figure 2). Here, the range of release time and position includes only one point, where a smaller range results in a more accurate search zone. 500 similar objects start their motion under the current and wind field, for which random uncertainties have been applied. The purple and red points in Figure 2 are particles cloud, 12 and 24 hours after release time, respectively. If the convex hull of all of these particles is drawn, the search zone with considering 100% of uncertainties will be obtained (blue and green hulls for 12 and 24 hours after release time, respectively). As it is expected, the particles cloud after 24 hours covered wider area and therefore, its search zone is more expanded. Also the search zones including different percentages of uncertainties could be obtained by plotting the envelope of certain number of particles. For example, plotting the envelope of 200 particles results in a search zone which 40% of uncertainties. It is clear that smaller percentages of uncertainties correspond to smaller search zones and easier searching field works. The model will be verified in the future based on the hydrodynamics simulations of wind and current and observations about lost objects, but at the moment, it could be intuitively shown that the results are good according to the dominant current and wind fields in the area. Some field experiments to collect data for verification of the model are underway.

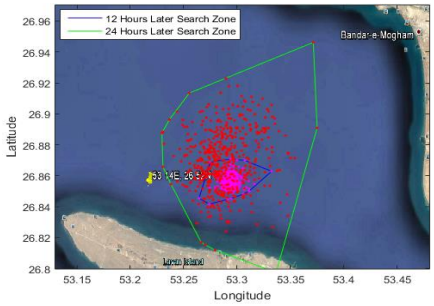

Figure 2. Release position (dropped pin) and search zones after 12 and 24 hours (blue and green polygons respectively). The purple spots are clouds of particles after 12 and the red spots after 24 hours of release time.

6. Acknowledgements

This work was supported by the Ports and Maritime Organization of Iran.

7. References

[1] Breivik, O and Allen, A. A., "An operational search and rescue model for the Norwegian Sea and the North Sea", *ELSEVIER Journal of Marine Systems*, 69, 2008, pp. 99-113.

[2] Allen, A. A. and Plourde, J. V., "Review of Leeway: Field experiments and implementations", *US Coast Guard Research and Development Center*, Report CG-D-08-99, 1999.

[3] Bakhtiari, A., Komijani, F., Allahyar, M. R., Tavakoli, M., Baradaran Ebrahimi, G. and Shoushtari Naseri, A., "Evaluation of Iranian PMO Dynamic model int the Boushehr Bay, Persian Gulf", 10th International Conference on Coasts, Ports and Marine Structures, Nov. 19 2012, Tehran, Iran.

[4] Jimenez, P. A., Dudhia, J., Gonzalez-Rouco, J. F., Montavez, J. P., Garcia-Bustamante, E., Navarro, J., Vila-Guerau de Arellano, J. and Munez-Roldan, A., "An evaluation of WRF's ability to reproduce the surface wind over complex terrain based

BAY CLOSING LINES IN THE PERSIAN GULF AND THE LAW OF THE SEA (CASE STUDY: KUWAIT BAY)

Omran Rasti

Department of Geography, University of Birjand, Birjand, Iran, orasti@birjand.ac.ir

1. Introduction

Baseline is a line in which coastal countries determine their maritime zones (such as the territorial sea, contiguous zone, the exclusive economic zone, the continental shelf and the exclusive fishing zone). In addition, the baseline separates the internal water from the waters of other maritime zones. In the case of the archipelagic countries, it is also considered between the archipelagic waters and the territorial sea. The internal waters and archipelagic waters extend from the baseline to the land and other maritime zones extend from the baseline to the sea [1]

According to the provisions of the Convention on the Law of the Sea, in a general category, the baselines can be divided into three categories: normal baselines follows the low-water line of a coastal state, the geometric or straight baseline divided into several types, and finally archipelagic baseline. The coastal countries did not have the same function in determining the baselines, some have set the normal baselines and some of the straight baseline, some of them including Iran and Kuwait, have combined the normal and the straight baseline along their shores [2]. This article seeks to investigate Kuwaiti's straight baseline and its compliance with the rules of the Convention on the law of the Sea.

2. Straight Baseline of Kuwait

The state of Kuwait uses the system of the straight baseline or bay closing line in front of the Kuwaiti Bay. According to the text of the Kuwaiti Decree No (317) year 2014, Concerning the Delimitation of the Marine Areas Pertaining to the State of Kuwait and its amendment, the designation of the Kuwaiti straight baseline system (which, however, the coordinates of its points have not been announced and publicly released), was approved by Act 12 (1964) regarding the Prevention of oil Pollution of the Navigable Waters and its amending laws. Article 2 (d) of this law stipulates: "In accordance with Annex 3, of the aforementioned act 12 (1964), the baseline of the Bay of Kuwait, shall be the line closing the bay, and the water contained therein shall be considered internal water".

The Kuwaiti Bay in the northwest corner of the Persian Gulf is among the small bays. The Meskan, Faylakah and Awhah Islands are on the front of the mouth of the Kuwaiti Bay. Accordingly, the Kuwaiti Bay can be classified as a bay that has two openings. The closing lines of the Kuwaiti Bay include three straight lines, the total length of the first and second lines, taking into account the beach of the Faylakah Island, over than 18 NM. The first line begins at a distance of 2 NM south of the Bubian Island, with a southeast direction connected to the northern ridges of the Faylakah Island. The second line extends from the eastern tidal elevations of the Faylakah Island and extends to the tidal elevations of the eastern Awhah Islands. Then a 24-mile closing line joins with south-west direction from the end of the Awhah Island to the Mina 'al-Ahmadi on the mainland of Kuwait. Therefore, the complexes of islands in front of the Kuwaiti bay are all located behind the baseline and in the internal waters. (Figure 1 and Figure 2)

Figure 1. The maritime zone the state of Kuwait [4]

3. Kuwait Bay Closing Line and Law of the Sea

Since Kuwait has joined the United Nations Convention on the Law of the Sea (UNCLOS), it is imperative that the adoption of its national laws comply with the provisions of the UNCLOS. In order to verify the conformity or non-compliance closing lines with the provisions of the Convention, one must first answer a few questions:

Is the Kuwaiti Bay among the small bays that can be applied to the closing line system?

Are the closing lines drafted in accordance with the provisions of the UNCLOS?

Have the coordinates of these lines been announced and published officially and internationally?

In response to the question whether the Kuwaiti Bay is a small bay, Article 7 of the 1958 Convention and Article 10 of the 1982 Convention lay down the following geometrical method. First, a line is drawn in the natural mouth, and then a half-circle whose diameter is the same as the line and its area is calculated. Then the area of the water between drawn line and low-water line along the coast is calculated. If the measured water area is greater than the half-circle area, the area is

known as the small bay. Accordingly, if a line is drawn in the natural mouth of the Gulf of Kuwait, the area between the lines is drawn and the low-water line is greater than the half-circle area, so the Kuwaiti Bay can be classified as a small bay.

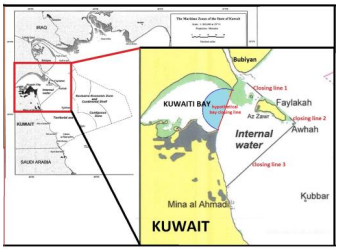

Figure 2. Territoriality in front of Kuwaiti bay

According to [3] from article 10 of UNCLOS, the Bay closing line or the total length of the bay closing lines, where the bay through the islands has more than one mouth, should not exceed 24NM. Accordingly, since the length of the enclosing lines of the Kuwaiti Bay openings is more than 42 nautical miles, it is not in conformity with the provisions of the UNCLOS. The enclosing lines of the two mouths of the Kuwaiti Bay caused the waters in the Kuwaiti Bay and behind the straight baselines to be considered as Kuwait's internal waters.

Another important issue is the declaration of the coordinates of the points of the straight baselines of Kuwait. According to Article 16(1) of the Convention: "The baselines for measuring the breadth of the territorial sea determined in accordance with articles 7, 9 and 10, or the limits derived therefrom, and the lines of delimitation drawn in accordance with articles 12 and 15 shall be shown on charts of a scale or scales adequate for ascertaining their position. Alternatively, a list of geographical coordinates of points, specifying the geodetic datum, may be substituted." Article 16 (2) stipulates that: "The coastal State shall give due publicity to such charts or lists of geographical coordinates and shall deposit a copy of each such chart or list with the Secretary-General of the United Nations." In the case of Kuwait, based on surveys conducted at the Portal of the UNCLOS, this process has not been completed by 2018 at least. And the geographical coordinates of the points of the baselines are not available.

Another item that does not seem to comply with the provisions of the UNCLOS is the placement of the island of Awheh on the back of the straight baseline, while the island is more than 12 miles away from the mainland coast of Kuwait.

Article 7 (1) of the UNCLOS stipulates that: "In localities where the coastline is deeply indented and cut into, or if there is a fringe of islands along the coast in its immediate vicinity, the method of straight baselines joining appropriate points may be employed in drawing the baseline from which the breadth of the territorial sea is measured." In addition, in accordance with Article 4 (2) of the 1958 Convention and Article 7 (3) of the 1982 Convention, "The drawing of straight baselines must not depart to any appreciable extent from the general direction of the coast, and the sea areas lying within the lines must be sufficiently closely linked to the land domain to be subject to the regime of internal waters"[3]. By locating the Faylakah and Awhah Islands behind the straight baseline, this line does not coincide with the general direction of the Kuwait's coastline and its deviation from the Kuwaiti coastline is close to 90 degrees. (Figure 2 and Figure 3)

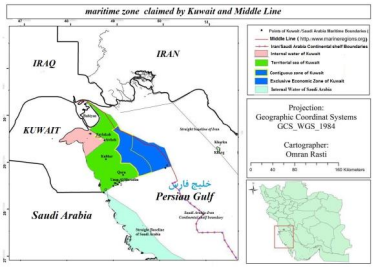

Figure 3. maritime zones claimed by Kuwait

4. Results and Discussion

The present study, with a descriptive-analytical approach and with documentary review, examined the Kuwait's straight baseline. Also in the Arc GIS software, the annexed map of the law has undergone cartographic analysis. Studies and analyzes indicate that the use of straight baselines at the mouth of the Kuwait Bay does not comply with the Convention on the Law of the Sea in the following cases.1) The use of closing lines with a total length of more than 24 nautical miles in the mouth of the Kuwait Bay, 2) No official publication of the geographical coordinates of the points of straight baseline, 3) Insert the Awhah island behind the straight baseline.In summary, the enclosing lines of the Kuwaiti Bay openings are far from the natural course of the shore and have laid a significant level of territorial sea waters in front of the Kuwaiti Bay in the Kuwaiti internal waters, limiting the rights of other countries and free shipping.

5. References

[1] Ranjbarian, A., and Seirafi, S. (2013). Investigating the straight baseline of Iran on the Persian Gulf and Gulf of Oman and other countries protest .The Journal of International Law, 48, 35-64.[In Persian]

[2] Rasti, O., Ashrafi, A. (2017). Claimed territoriality of Coastal Countries and Territories Overlapping (Case Study: The Conflict of Iran and Pakistan on territoriality at the Mouth of Gwadar bay, *Research Political Geography*, *2*(1), 59–86.[In Persian]

[3] Churchill, R., and Lowe,A. (2005). The law of the sea (B.Aghai, Trans.) (3rd ed.).Tehran:Ganj-e Danesh Press. [In Persian]

[4] UN, (2014), Kuwait. Decree No (317) year 2014 Concerning the Delimitation of the Marine Areas Pertaining to the State of Kuwait and its amendment (2014), Retrieved from http://www.un.org/depts/los/legislationandtreaties/pdffiles/deposit/kuwait_decree_317-2014-e.pdf

IRANIAN MODEL FOR OIL SPILL TRACKING IN THE PERSIAN GULF

Ehsan Sarhadizadeh[1], Taher Chegini[2], Kourosh Hejazi[3], Mohsen Soltanpour[4] and Hamid Khalili[5]

1) Department of Civil Engineering, K. N. Toosi University of Technology, Tehran, Iran, sarhadi@gmail.com
2) Department of Civil & Environmental Engineering, University of Houston, United States, taher.chegini@gmail.com
3) Department of Civil Engineering, K. N. Toosi University of Technology, Tehran, Iran, hejazik@kntu.ac.ir
4) Department of Civil Engineering, K. N. Toosi University of Technology, Tehran, Iran, soltanpour@yahoo.com
5) Ports and Maritime Organization, Tehran, Iran, hkhalili@pmo.ir

1. Introduction

Rapid economic growth has caused a significant increase in fossil fuel consumption in recent decades. Exporting oil, especially via marine fleets, and increasing development of petrochemical industry, has caused the marine system to be exposed to severe environmental damages. In the 1991 Persian Gulf (Kuwait) war, oil spill was estimated at 143 billion liters.

The fate and transport of spilled oil is governed by the advection due to current, wave and wind; horizontal spreading of the surface slick due to turbulent diffusion, gravitational, inertia, viscous and surface tension forces; emulsification; weathering processes such as evaporation, dispersion and dissolution; interaction of oil with shoreline; photochemical reaction and biodegradation.

The fate and transport of oil spilled in water is dominated by complex physicochemical processes that depend on oil properties, hydrodynamics and environmental conditions.

2. Oil Spill Processes

The spreading of an oil slick is considered to pass through three phases. In the beginning phase, only gravity and inertia forces are important. In the intermediate phase, the gravity and viscous forces dominate. The final phase is governed by the balance between surface tension and viscous forces.

Evaporation causes a very significant mass loss in many kinds of oil and has a profound effect on density, viscosity and other properties of oil. The most soluble oil components are usually the most toxic. In the present study, the mass of soluble is negligible compared to the dispersed oil droplet near the surface but of the same order of magnitude in the deeper water. The behavior of spilled oil depends not only on the prevailing conditions but also on the physicochemical properties of the oil itself. While the former are site and time dependent, the latter change while interacting with each other with oil movements. The evaporation process, together with dissolution and the mousse formation, leads to an increase in the volume and density respectively.

3. Numerical Modeling

Computations proceed with an Eulerian model on the oil dynamics equations that describe slick advection-spreading on water surface which are given as follows:

$$\frac{\partial h}{\partial t}+\bar{\nabla}\left(h\bar{v}\right)-\bar{\nabla}\left(D\bar{\nabla}h\right)=R_h$$
$$\bar{v}=\left(u_x+\tau_x^w/f\ ,\ u_y+\tau_y^w/f\right) \qquad (1)$$
$$D=gh^2\left(\rho_w-\rho_{oil}\right)/\rho f$$

where h is the oil slick thickness; $\bar{v}$ slick drifting velocity; τ^w/f shear stress due to wind; D slick spreading-diffusion function; f the friction coefficient of oil film-water surface (0.02 kg/ m^{2}s); R_h physical-chemical kinetic terms; g gravity acceleration; $\bar{\nabla}=\left(\partial/\partial x\ ,\partial/\partial y\right)$.

The oil spill model couples with PMO Dynamics (Persian Model for Ocean Dynamics), a 2D hydrodynamic model. An unstructured grid system is used to solve the equations. The oil slick thickness is placed at the vertices of the triangle, while velocity components are placed at the edges of the control volume.

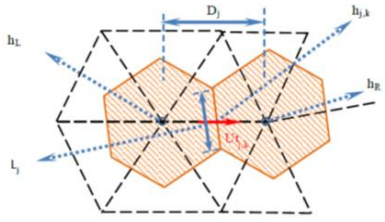

Figure 1. Control volume and normal and tangent velocities on the edge of the triangle

The oil dynamics equations on this grid system (Figure 1) are given as:

$$\frac{\partial h_{oil}}{\partial t}+\bar{\nabla}\left(h\bar{v}\right)-\bar{\nabla}\left(D\bar{\nabla}h\right)=R_{h\,oil} \qquad (2)$$

$$\frac{\partial h_{oil}}{\partial t}+\frac{\partial h_{oil}u_n}{\partial \mathbf{n}}-\frac{\partial}{\partial \mathbf{n}}\left(D\left(\frac{\partial h_{oil}}{\partial \mathbf{n}}\right)\right)=R_{hoil}$$

The equations are solved for advection, horizontal diffusion, and then the weathering of the oil.

$$\frac{{h_{oil}}^{n+1}-{h_{oil}}^{n}}{\Delta t}+div\left(h_{oil}\otimes V\right)^{n}=0$$

$$\frac{{h_{oil}}^{n+1}-{h_{oil}}^{n}}{\Delta t}=div\left[D.grad\left({h_{oil}}^{n}\right)\right] \quad (3)$$

$$\frac{{h_{oil}}^{n+1}-{h_{oil}}^{n}}{\Delta t}=R_{hoil}$$

The discretization of the advection equation can be written using the finite volume method as follows:

$$h_{oilJ}^{n+1}=h_{oilJ}^{n}-\frac{\sum_{k=1}^{nk}\left(Flux_k\times L_j\right)}{Area_j} \quad (4)$$

Validation of the model has been proved through analytical solutions and a laboratory test under controlled conditions [1 and 5].

For the real scale simulation, the model setup was such that the Persian Gulf and part of the Oman Sea formed the computational domain. A high-resolution shoreline data set was implemented using GSHHG; the bathymetry was extracted from ETOPO 2 database and Iranian National Center data. The entire domain comprised of an unstructured triangular 2D mesh with 42,974 cells and an unstructured triangular 3D mesh with 10 layers in the sigma coordinate with 9345 cells.

An unstructured triangular mesh was created on this domain with 42874 nodes. The results of Hybrid Coordinate Ocean Model (HYCOM) were used as initial and boundary conditions for the 2D model. Tidal data based on series of fully global models of ocean tides (TPXO), were used on the open boundaries. To get realistic results, weather conditions were used from the Weather Research and Forecasting (WRF) model. Also, in order to take the effect of waves on the hydrodynamics into account, wave radiation stresses were applied to the model using the full-spectral 3rd generation wave model WAVEWATCH III.

4. Results and Conclusions

Figure 2 shows the temporal growth in areas of the oil slick of thickness greater than 6 µm. in 3 regions after 5 hours.

The present oil model can display the thickness of these pollutants in a spectral manner due to the use of the Eulerian method in solving advection and diffusion equations of oil spill. This continuous spectrum is consistent with the reality.

In this way, the initial thickness of leaked oil can be attributed to 100% probability and, over time, by decreasing the thickness of the slick, the zero thickness attributes to the probability of occurrence of 0%.

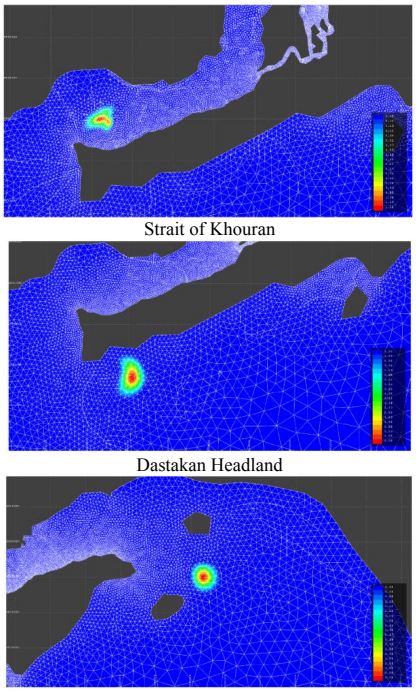

Strait of Khouran

Dastakan Headland

Strait of Hormuz

Figure 2. Model Outputs.

5. Acknowledgment

This study was funded by the Ports and Maritime Organization.

6. References

[1]. Borthwick, A. G. L. and Joynes, S. A. "Laboratory study of oil slick subjected to nearshore circulation," *Journal of Environmental Engineering*, vol. 118, no. 6, pp. 905–922, 1992.

[2]. Fay, J.A., "The Spread of Oil Slick on a Calm Sea", *Hoult, D.P. (Ed.), Oil on the Sea. Plenum Press,* New York, NY, pp. 53–63. 1969.

[3]. Janeiro, J., Zacharioudaki, A., Sarhadi, E., Neves, A., and Martins, F., "Enhancing the management response to oil spills in the Tuscany Archipelago through operational modelling". Marine Pollution Bulletin. Volume 85, Issue 2, Pages 574–589. 2014.

[4]. Mackay, D., "Oil Spill Processes and Models". *Environmental Protection Service*, Canada, 1980.

[5]. Sarhadizadeh E. and Hejazi, K., "Eulerian Oil Spills Model using Finite Volume Method with Moving Boundary and Wet-Dry Fronts", *Journal of Modelling and Simulation in Engineering (Hindawi)*, Computational Fluid Dynamics and Its Applications. 2012.

EXAMINING THE IMPLEMENTATION OF THE OPRC-HNS PROTOCOL AND THE ACCESSION OF IRAN TO THE HNS CONVENTION

Maryam Rasouli[1]

1) Marine Environment Protection Expert , Ports and Maritime Organization (PMO), Tehran, Iran
rasouli.maryam@gmail.com

1. Introduction

Hazardous and noxious chemicals are increasingly being transported by sea. Current estimates indicate some 50000 hazardous and noxious substances (HNS) are carried regularly by sea with bulk trade of 165 million tons per year worldwide. This is a very broad definition and

encompasses chemicals ranging from vegetable oils used in foods and pharmaceuticals through to highly toxic compounds such as corrosive gases (chlorine and ammonia), acids and alkalis (sulphuric acid and sodium hydroxide), and harmful volatile organic compounds (styrene,benzene), all of which have a range of industrial applications.

The OPRC-HNS protocol follows the principles of OPRC, excluding oil products to include all other hazardous and noxious substances. To provide a clear definition of HNS, the issue has to be discussed from different points of view. Many codes and protocols have included definition of HNS, among them OPRC-HNS protocol, MARPOL 73/78, IMDG13 Code, IBC14 Code, and BC15 Code.

The Protocol on Preparedness, Response and Cooperation to Pollution Incidents by Hazardous and Noxious Substances, 2000 (OPRC-HNS protocol) was formally adopted by IMO (OPRC) member States, at a Diplomatic Conference held at the IMO headquarters in London between 9-15 of March 2000. The protocol entry into force was scheduled for 12 months after ratification by fifteen States Parties already members of the OPRC Convention. The fifteenth ratification was filed with IMO on 14 June 2006. The Protocol was therefore entered into force on 14 June 2007. The formal ratification of the OPRC-HNS protocol by the government of Islamic Republic of Iran has started in March 2009. It should be noted that the risks of toxic and hazardous incidents are very different from oil pollution incidents. A chemical incident could include a number of chemicals with different names. Also, a ship can carry a bunch of different chemicals that react to these products with one another, which can have consequences like explosions, fires and environmental pollution. As a result of the safety of individuals and environmental protection and possible compensation of losses due to the immediate effects and serious threats of toxic and dangerous human health in comparison with oil pollution according to the nature of the chemical and type of incident (fire, leakage, ...) Is prioritized. According to the data, the statistics of chemical discharge and loading during the years 1391 to 1395 in our ports were about 2490.79 tons, a considerable amount of which is related to the ports of Mahshahr and Assaluyeh.

2. Implementation of the Hazardous and Noxious Substances (HNS) Of Iran

HNS Activities of I.R. Iran

- Marine pollution study and risk assessment are carried out for the different types of HNS in order to include this information in the National HNS Contingency Plan;
- Development of a Draft HNS National Contingency Plan;
- Establishment of an OPRC-HNS National Steering Committee;
- Extensive laboratory analysis in order to evaluate the extent of HNS damage to the marine environment;
- Study on environmental management aspects of the HNS, conducted for the delivered chemicals in Assaluyeh and Imam Khomeini Ports;
- Classification of chemical substances carried at sea, and provision of the information to the emergency response team to be able to response to any incident based on the information provided to them;
- In general, it is proposed that a database of HNS loaded and discharged in the regional ports be established and included in the present plan. For instance, the chemical propane is produced at the time being in Pars Petrochemical Port in Assaluyeh, and loaded onto chemical carrier vessels.Definition of the role and responsibility of ports and their authorities in case of HNS-release incidents;
- Preparation of a national guideline and action plan to be implemented in ports;
- Include the information in training materials and courses
- Preparation and implementation of pollution response contingency plans and waste management plans by all maritime facilities and industries on Iranian coasts;
- Proper liability insurance coverage for all convention sized and non-convention sized vessels in regard to potential pollution cases; and
- Implementing the MOU for cooperation on marine pollution response between the PMO and Iranian Department of Environment (DOE), 2013.

3. Implementation of HSE Requirements and Regulations

With the promotion and development of chemicals export and import, and development plans of the country, the need for preparedness and response to chemical pollution incidents is felt at the national level.

3.1. National Contingency Plan, Risk Assessment

Marine pollution study and the risk assessment are carried out for the different type of the HNS in order to include the information in the Draft National HNS Contingency Plan, which needs to be approved by the Iranian Parliament.

4. Response to HNS Marine Pollution

Considering the fact that there are more than 8 million chemicals known and 50000 transported on seas, providing response details for every HNS proves to be cumbersome. Therefore, the question is made as how can international experts provide a reasonable set of response techniques and management for HNS transportation and handling on the sea.

Monitoring and Response Capability:

Helicopters, air craft and 9 high-speed boats are available for aerial and surface surveillances for the normal monitoring and during incidents.

Sufficient oil spill response stockpile with the brand new equipment are available along the Iranian coasts. Advanced oil and HNS recovery vessels, 9 scavengers & 7 barges are under construction. Major ports have been equipped with advanced oil spill response equipment the durability of concrete structures, yet decrease their mechanical characteristics.

5. Response Teams and Scientific Support

It is emphasized that a person should be put in charge of a designated safe area for the operation and post operation. The characteristics of such area, the authorized personnel and activities regarding health and safety of response personnel are discussed in detail. Information regarding Personnel Protective Equipment (PPE) is provided in this chapter as well. Decontamination, cleaning processes and disposal of polluted wastes resulted from response operation are also discussed

5.1. Training and Exercises

Technical training departments have been established in major ports and national and regional training workshops are conducted at different levels for the responders with the support of IMO and MEMAC.

5.2. Resources Available

Resources (experts & equipment) are available in case of RSA member states requesting assistance.

6. Conclusion

Despite the fact that the convention has been ratified by a number of countries, the hns convention has not yet entered into force. In view of operational problems that make countries unaffected by the Convention, in 2010, the HNS protocol of 1996 was ratified. In which it referred to three main factors as a barrier to acceptance and membership of the convention by countries.

- It is a duty to report on claims incurred in respect of entitlements. When countries accede to or accede to the Convention, they must report to IMO on their charges received by the country
- Problems in setting up the reporting system for packaging goods, in the 2010 protocol, packaging goods were excluded from the definitions of shipments, and the recipients of such packaged goods would not have a share in the HNS Fund. Although during the events of the goods Packages for which compensation is payable will increase the liability of the ship commander in relation to HNS packaging goods.
- LNG will be difficult for non-member countries. From now on, as stated in the 2010 protocol, the LNG share is the responsibility of the recipient of the goods, apart from the cases where the goods are shipped, the goods are responsible for the goods.

7. Acknowledgement

This paper was scientifically and financially supported by the Ports and Maritime Organization (PMO).

8. References

[1]_www.imo.org/.../protocol-on-preparedness,-response-and-co-operation-to-pollution

[2] P.D.Harold.,H.Brunt.,"Development of risk-based prioritisation methodology to inform public health emergency planning and preparedness in case of accidental spill at sea of hazardous and noxious",Environment Industrial, January 2014,pp137-163

[3] T.neuparth,S.Moreira., "Hazardous and Noxious substances (HNS) in the marine environment: prioritizing HNS that pose major risk in European contact",Marine pollution Bulletin, January 2011,pp21-28

[4] Moujin Lee,Jung-yeal Jung., "Risk assesment and national measure plan for oil and HNS spill accidents near korea",Marine pollution Bulletin,March 2013,pp339-344

[5] HNS Convention,1996 Edition

[6] www.pmo.ir

[7] 2010 HNS Convention Consolidated Text , 2010,HNS Protocol

[8] OPRC-HNS TG14/3

EFFECT OF OIL POLLUTION OF CASPIAN SEA ON HAEMATOLOGICAL RESPONSE OF GREAT STURGEON

Tahereh Bagheri[1] and Seyed Abbas Hosseini[2]

1) Offshore Fisheries Research Center, Iranian Fisheries Science Research Institute, Agricultural Research Education and Extension Organization, Chabahar, Iran, Bagheri1360@gmail.com
2) Offshore Fisheries Research Center, Iranian Fisheries Science Research Institute, Agricultural Research Education and Extension Organization, Chabahar, Iran.

1. Introduction

Caspian Sea, one of the largest lakes in the world, is main habitat of sturgeon species, including beluga (*Huso huso*). Several factors, such as over exploitation and oil spills as a result of inundation of low-lying oil fields along the northeastern coast and offshore drilling activities diminish beluga population [1] Since the study on hematotoxicity and immunotoxicity of diesel on this valuable fish is not well established, a study conducted on Great sturgeon to determine sub-lethal effects of direct diesel oil on hematological and immunological parameters and evaluate their potential toxicity.

2. Material and Methods

Juvenile Beluga, average weight 200 g, submitted to acute doses (5, 10, 20, 40, 100, 500 and 1000 ppm) for 0, 48h and 7 day static toxicity tests in replicate. One control group, exposed only to water (the same as used for acclimation), sampled accompanying with each sampling points. Water quality monitored and controlled. Upon removing fish from test tanks, anesthetized and blood samples taken from the caudal vein. Subsequently, fish were killed by cervical section [2].

3. Results

Fish exposed to crude diesel oil for 48 hour showed a significant elevation in W.B.C, R.B.C, Hb, Ht, M.C.V, M.C.H, M.C.H.C, Neutrophil and Lymphocyte concentration compare to the control ($P\leq 0.05$), whereas among significant indices, W.B.C, M.C.H, M.C.H.C and Neutrophil in fish exposed to crude diesel oil for 48 h were significantly greater compared to the control groups and R.B.C, Hb, Ht M.C.V. and Lymphocyte were significantly lower than control groups ($P\leq 0.05$). Eosinophils did not vary significantly in the groups exposed to 48 h crude diesel oil compare to the control groups ($P> 0.05$)

After 48 h exposure, the correlation between crude diesel oil with all parameters was statistically tested by analyzing the data obtained during the crude diesel oil exposure. Only the R.B.C, Ht and M.C.V levels showed significant correlation ($P<0.05$) with crude diesel oil exposure and all correlation were negative.

Curve estimation regressions data were used to determine the relationship between crude diesel oil concentration with hematological and immunological activity [3]. Only the R.B.C Ht and M.C.V levels showed significant linear regression ($P<0.05$) $Y = a \pm bX$ with crude diesel oil.

Furthermore, 7 day exposures showed a significant change in W.B.C (table 1), M.C.V. and Neutrophil levels, compare to the control treatment ($P\leq 0.05$).

Whereas among significant indices W.B.C. and Neutrophil were significantly greater compare to the control groups ($P\leq 0.05$) and M.C.V. was depleted within the crude diesel oil adjacency. Because of high value of experiment doses (more than LC50), after 7 days exposure there were 100% mortality in 40, 100, 500 and 1000 ppm, and there were no serum samples.

After 7 days exposure, the correlation between crude diesel oil with all parameters was statistically tested through analyzing the data obtained after the crude diesel oil exposure. Only W.B.C, Ht, M.C.V and M.C.H.C levels showed significant correlation ($P<0.05$) with crude diesel oil exposure. W.B.C. and M.C.H.C were positive among that correlation and the other ones were negative.

4. Discussion

Although few studies have used diesel oil exposure to examine the effects of oil contaminants in aquatic organisms [4], the present results showed that under experimental conditions blood parameters were sensitive to different aspects of oil exposure. The major findings of this study could be several changes in hematological and immunological parameters of the studied fish caused through acute diesel oil concentrations; and estimation of these indices, could provide a useful indicator of oil pollution within water bodies [5].

5. Reference

[1] Kaplin, P.A., 1995. Implications of climate change and water-level rise in the Caspian Sea Region. *United Nations Environment Programme.*

[2] Hedayati, Aliakbar ; Safahieh, Alireza. 2011. Serum hormone and biochemical activity as biomarkers of mercury pollution in the Yellowfin seabream Acanthopagrus latus. *Toxicol and Ind Health.*

[3] Brandão, R., Pinto, L., Borges, C., Nogueira W. 2009. Concomitant administration of sodium 2,3-dimercapto-1-propanesulphonate (DMPS) and diphenyl diselenide reduces effectiveness of DMPS in restoring damage induced by mercuric chloride in mice. *Food and Chem Toxicol*. 47. 1771–1778.

[4] Rabitto, I.S., Alves Costa, J.R.M., Silva de Assis, H.C., Pelletier, E., Akaishi, F.M., Anjos, A., Randi, M.A.F., Oliveira Ribeiro, C.A. 2005. Effects of dietary Pb++ and tributyltin on neotropical fish, Hoplias malabaricus: histopathological and biochemical findings. *Ecotoxicol. Environ. Saf*. 60 (2), 147–156.

[5] Hedayati, A., Safahieh, A., Savar, A., Ghofleh Marammazi, J. 2010. Detection of mercury chloride acute toxicity in Yellowfin sea bream (Acanthopagrus latus). *World Journal of Fish and Marine Science.* 2(1): 86-92.

IDENTIFY AND RANK THE RISKS OF DRY BULK DISCHARGING OPERATION OF IMAM KHOMEINI PORT BY FMEA METHOD

Mahmoud Hoseinzadeh

Supervisor of Special terminals, Imam Khomeini Port, Mahshahr, Iran, m.hoseinzadeh59@yahoo.com

1. Introduction

Bulk products are shipped all around the world, in vast tonnages, containing different cargoes. According to UNCTAD in 2016, 7101 billion tone dry bulk cargo discharged in the world [1]. The rate of crew loss in bulk carriers remains almost twice as high as that attributed to piracy, with an average of 24 deaths per year in bulk carrier incidents over the last ten years – a rate which still represents a considerable improvement over earlier years [2].

When bulk cargoes shift, liquefy, catch fire or explode as a consequence of poor loading procedures, the consequences can be massive. Ships may capsize, lose stability or sustain severe structural damage. Such happenings enhance the risks and the occurrence of death, injury, insurance claims, operational delay and considerable expense. Unfortunately, it is often assumed that dry bulk cargoes are less hazardous, and require less expertise [3].

According to Port & Maritime Organization report in 2016, 18 Million tons of Bulk cargo discharged in all of Iranian ports but 13.7 Million tons of Bulk cargo discharged in Imam Khomeini Port. Therefore it is necessary to maintain safety of dry bulk discharging. The main objective of this paper is find the main risks of Dry Bulk Discharging Operation of Imam Khomeini Port by determining the Risk Priority Numbers (RPN) per identified risk.

1-1 Dry Bulk Discharging Operation

Dry Bulk Discharging Operation consists of several steps:

- Close ship to berth by mooring rope
- Start discharging equipment
- Gang present in discharge place to clean berth environment
- Up to foreman to guide discharging equipment operator
- Check of discharging number by captain and agent to balance of the ship
- Present vehicles to move cargo from ship to warehouse or direct transport

2. Literature Review

Most of researches done about liquid bulk cargo and less attention to risks of dry bulk cargo. In this section some of important researches that used in this paper address in Table 1.

Table 1. Briefly of Literature Review

Researcher (s) (Publishing Year)	Result
Grote et al[4]	Unloader Risk
Baur et al[5]	Human Risk
Sayareh et al[2]	Vehicle Risk
INTERCARGO [3]	Cargo Risk
Jafari [6]	Equipment Risk

3. Materials

This research has application nature and in terms of methodology is descriptive-survey method. In this research use FMEA method to analyze risks of dry bulk discharging operation of Imam Khomeini Port. FMEA group include 2 person of HSE, 1 person of Chief Officer of dry bulk carrier, 2 experts of bulk department of the port.

Our research process consists of several steps that can be summarized in the following way:

- Literature review is necessary to study and analyse dry bulk discharging operation risks.
- Use FMEA group viewpoints to determine cause and effect of risk.

FMEA steps applied in this paper consist of:

- Review process of Dry Bulk Discharging Operation
- Hold FMEA group session to determine risk
- Determine severity of the risk
- Determine occurrence probability of the risk
- Determine detention probability of the risk
- Determine RPN on any risk

4. Data Analyze

Results of FMEA technique of Dry Bulk Discharging Operation of Imam Khomeini port show in Table 2.

Table 2. FMEA result.

No	Risk	S	D	O	RPN
1	Falling down cargo on Gang	8	7	4	224
2	Breakdown Grabs	10	4	2	80
3	Falling down Foreman to ship's hatch	10	7	7	490
4	Accident transport vehicle with people on the berth	9	7	5	315
5	Accident vehicle with discharging equipment	7	8	6	336
6	Falling down cargo on the sea	10	8	5	400
7	Tearing of mooring rope	10	4	2	80
8	Unbalancing of ship due to large discharge from one hatch	8	6	5	240
9	Accident unloader arm with ships' keel	10	8	7	560
10	Falling down operator from discharging equipment	10	5	4	200

Refer to result of Table 2, see the risk of accident unloader arm with ships' keel with RPN number 560 is important risk in Bulk Discharging Operation of Imam Khomeini port.

5. Discussion

Imam Khomeini is biggest port of Iran for importing of Dry bulk cargo (75% of total country's import). In this paper we analyze any risks exist in dry bulk Discharging Operation of Imam Khomeini port. To gain this aim, firstly use credit previous research to review dry bulk Discharging Operation and then use FMEA group to identify risk and its features (severity, occurrence and detention probability).

Result of FMEA technique show the risks of Accident unloader arm with ships' keel (560), Falling down Foreman to ship's hatch (490) and Falling down cargo on the sea (400) are important and risks of Breakdown Grabs (80) and Tearing of mooring rope (80) are less important in the operation.

To improve safety dry bulk Discharging operation suggest following solutions:

- Using experienced operators and foreman when apply unloader for discharging of cargo
- Training foreman and gang for traffic on the ship deck and berth in the discharging time
- Use of for reduction falling down cargo on the sea in the discharging time
- Determine traffic line for enhancing safety of operation and reduce delay
- Consistence check discharged cargo from every hatch to keep on ship's balance
- Cleaning berth environment in idle time by gang

6. Acknowledgment

For implementation of the comprehensive scientific plan of the country, Port and Maritime Organization support of this research in terms of scientific and financial due to its role in subjects of port, maritime, shipping and commercial matters.

7. References

[1] UNCTAD., "Review of Maritime Transport 2016". *United Nations Publication*, 2016.

[2] Sayareh, J., Ahouei, V., and Nooramin, A., "Failure Mode and Effect Analysis (FMEA) for Evaluating the Causes of Delays in BIK's Dry Bulk Cargo Operation", *IEEE Transactions on Oceanography*, 2, 6, summer 2011, pp. 7.

[3] INTERCARGO, "Bulk cargo– know the risks", *UK P&I Club*, July, 2013.

[4] Grote, M., Mazurek, N., Grabsch, C., Zeilinger, J., and Floch, S., " Dry bulk cargo shipping- An overlooked threat to the marine environment", M*arine Pollution Bulletin,* Volume 110, Issue 1, 15 September 2016, Pages 511-519.

[5] Baur, X., Budnik, LT., Zhao, Z., Bratveit, M., and Djurhuus, R., "Health risks in international container and bulk cargo transport due to volatile toxic compounds", *Journal of Occupational Medicine and Toxicology*, 2015 May 20; 10:19.

[6] Jafari, H., "Identification and Prioritization of Grain Discharging Operations Risks by Using ORESTE Method", *American Journal of Public Health Research,* 2013, 1 (8), pp 214-220.

THE STUDY OF POLYCYCLIC AROMATIC HYDROCARBONS (PAHS) POLLUTION IN SEDIMENTS OF SOLTANI ESTUARY, USING GAS CHROMATOGRAPHY METHOD

Parisa Ahmadpur[1], Fatemeh Ahmadpur[2], and Mansoureh Hasanzadeh[3]

1) Ports & Maritime Authority, Tehran, Iran, parisaahmadpour78@gmail.com
2) Pars Special Economic Energy Zone, NIOC, Iran,fatima.ahmadpour@gmail.com
3) Ports & Maritime Authority, Bushehr, Iran, mhasanzade@ut.ac.ir

1. Introduction

The Soltani estuary is a unique coastal body which home to special biologic characteristics, water circulation and stimulates primary production. As the main vessel rout, Soltani channel connects Bushehr port to Persian Gulf navigation paths. The geographical position of Bushehr Port turns this region to a heart of marine industries and trade in south of Iran. Therefore, the growth of numerous industries around Soltani estuary causes the spillage of industrial and urban waste water into this semi closed environment. Industrial effluents and accidental oil spillages [4] urban and ecological risk of PAHs [2], emissions from anthropogenic activities predominate; nevertheless, some PAHs in the environment originate from natural sources such as open burning, natural losses or seepage of petroleum or coal deposits, and volcanic activities [1] are considered as the PAHs resources. PAHs are introduced mainly via the inflow of the Vistula and the Oder and through anthropogenic activity, mainly that related to the functioning of ports.

The profile of PAHs showed that the light ones were predominant in water while the heavy ones appeared mostly in sediments. Therefore, monitoring both environmental compartments should be mandatory [5] on the other hands, in order to controlling this problem in 1983 an international convention on the prevention of the contamination of the sea by ships came into force (MARPOL 73/78) [3]. So, this paper tries to investigate the levels of Polycyclic Aromatic Hydrocarbons and also the potential sources of contamination (petrogenic or pyrolitic) of the sediments in the Soltani estuary.

2. Material and method

2.1. Sampling

The locations of sampling stations are shown in fig.1. The positions of sampling sites were recorded using GPS. All sampling was conducted during December 2016. The top (0-5 cm) layers were carefully removed for subsequent analysis. The samples were stored under ice and in the dark boxes during transportation to the laboratory and kept frozen (-20°c) until being analyzed.

2.2- PAHs extraction

The extraction procedure for PAHs was carried out following the method described by Zakaria et al.2002 [7] and Zakaria and Mahat 2006[6]. Briefly, the samples of sediment were taken for dry weight determination.

2.3-Gas Chromatography-Mass spectrometry Analysis

PAHs were analyzed by gas chromatography-mass spectrometry using HP 6890 series gas chromatography with mass detector equipped with a split/split less injector

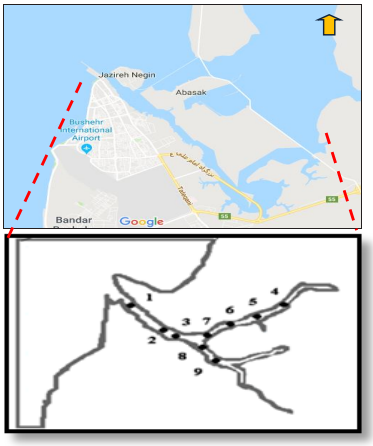

Fig.1-Samplynig sites of Soltani estuary-Bushehr

2.4- Quality control

Quality control study was carried out by monitoring recovery surrogate standards. The five surrogate standards were used for recovery correction of PAHs. The acceptance range of recovery was between 40% and 120%. The relative standard deviation of individual PAHs identified in sample extracts were<10%.

3. Results

The total concentration of 16 compounds of PAHs investigated in surface sediments from Soltani estuary ranged from 13.25 ng/g dw at station 6 to 821.53 ng/g dw at station 8 (Table 1). Antheracene in station 7 and 3 Methylphenantherene were not detected. The highest

concentration levels of PAHs were related to Benzo[e] Pyrene in station 8 and the least was related to Benzo[a] Pyrene in station 4.in all the sampling stations except stations 4 and 5 high molecular weight PAHs were dominated.

Table 1. Measured concentrations of PAH

PAHs compounds	St1	S2	St3	St4
Phenantherene	3/56	5/50	1/85	1/12
Antheracene	8/41	10/15	2/92	1/55
DBT	10/50	7/33	4/05	0/98
2-MethylAntheracene	13/15	12/91	6/10	4/34
1-MetylPhenantherene	16/18	13/02	8/70	2/01
2-MethylPhenanthrene	19/04	16/43	9/35	3/82
3-MethylPhenanthrene	1/97	1/40	3/36	0/86
9-MethylPhenanthrene	3/26	0/60	5/34	0/64
Fluranthrene	27/89	47/21	26/70	2/07
Pyrene	28/13	45/58	29/05	2/23
1-MetylPyrene	37/75	37/20	37/29	2/82
Benzo[a] antheracene	15/06	14/68	16/32	0/26
Chrysene	26/55	28/02	61/55	0/26
Benzo[k] flurantherene	23/41	28/55	66/99	0/36
Benzo[e]pyrene	89/37	68/61	197/01	2/14
Benzo[a]pyrene	17/72	25/00	28/25	0/18
∑PAHs (ng/g D.W)	341/96	362/20	504/82	25/64

Table 2. Measured concentrations of PAH

PAHs compounds	St5	St6	St7	St8	St9
Phenantherene	0/75	1/21	1/63	5/03	17/20
Antheracene	1/62	0/32	Nd	25/71	22/97
DBT	0/94	0/39	0/59	20/16	23/48
2-MethylAntheracene	4/42	1/48	1/32	29/32	44/54
1-MetylPhenantherene	1/97	0/83	1/61	23/45	43/29
2-MethylPhenanthrene	3/97	1/02	2/59	29/62	42/18
3-MethylPhenanthrene	0/55	Nd	0/59	7/61	26/46
9-MethylPhenanthrene	0/46	0/28	0/80	2/32	17/54
Fluranthrene	2/17	1/03	2/28	32/72	11/94
Pyrene	2/24	1/70	2/04	31/32	11/46
1-MetylPyrene	3/12	0/55	1/21	37/05	15/79
Benzo[a]antheracene	0/44	0/34	0/74	14/18	18/13
Chrysene	0/22	0/28	1/05	28/28	27/26
Benzo[k]flurantherene	0/25	0/38	0/63	42/93	32/73
Benzo[e]pyrene	4/20	3/15	16/56	484/77	68/87
Benzo[a]pyrene	0/19	0/29	0/21	7/07	16/39
∑PAHs (ng/g D.W)	27/51	13/25	33/85	821/53	440/23

4. Discussion

A comparison of PAHs concentrations in surface sediments collected from different estuaries and bays is given in Tables 1 and 2. The much more pollution of PAHs in station 8 may be probably due to the vicinity of this station with the barges and boats fuel distribution jetty. Also while ebb tide, 3-4 knot water current washes sediments of Soltani estuary branch line (Lashkari) and pile up the washed sediments in Soltani estuary. Consequently, collected sediments of station 8 may also contain polluted sediments of the secondary branch of Soltani estuary. Phe/Ant<10 and Flu/Pyr>1 indicate that the contamination by PAHs is from a pyrolitic origin, while the PAH from petrogenic is characterized by Phe/Ant>10 and Flu/Pyr<1.our study shows that the surface sediments from Soltani estuary have PAHs from mixed of pyrolitic and petrogenic origin with predominant pyrolitic input at station6.petrogenic sources in this area may be due to discharges of treated and untreated ballast and bilge water from oil tankers and other ships and effluents from oil refineries, while pyrolitic PAHs were be due to activities such as atmospheric deposition and industrial combustion. These two isomeric ratios seem to be inadequate for differentiation of PAHs origins in Soltani estuary. The different results obtained by different molecular ratios are probably due to the different sources of PAHs contamination which Soltani estuary is subjected to. Therefore, by controlling vessels discharges and reducing port traffic, PAH's pollutions at Bushehr port channel could be mitigate significantly.

5. References

[1] Abdel-Shafy, H. I., Mona Mansour,S.M., "A review on polycyclic aromatic hydrocarbons: Source, environmental impact, effect on human health and remediation", Egyptian Journal of Petroleum. 25, 1, 2016, pp 107-123.

[2] Baran A, Tarnawski M, Urbański K, Klimkowicz-PawlasA, Spałek I., "Concentration, sources and risk assessment of PAHs in bottom sediments", Environ Sci Pollut Res Int. 24,29,Oct 2017, PP.23180-23195.

[3] Bartkowski, K., Lewandowska, A., Gaffke, J., Bolałek, J.,"The contamination of bottom sediments in the Southern Baltic with polycyclic aromatic hydrocarbons (PAHs)", Ecocycles, 2,1, 2016,pp. 3-8

[4] Dudhagara DR, Rajpara RK, Bhatt JK, Gosai HB, Sachaniya BK, Dave BP., "Distribution, sources and ecological risk assessment of PAHs in historically contaminated surface sediments at Bhavnagar coast, Gujarat, India". Environmental Pollution, 213, June 2016, PP.338-346.

[5] Sarria-Villa, R., Ocampo-Duque, W., Páez, M., Schuhmacher, M., "Presence of PAHs in water and sediments of the Colombian Cauca River during heavy rain episodes, and implications for risk assessment". Science of the total Environment. 540. 2016.pp. 455–465.

[6] Zakaria, M. P., Mahat, A. A., "Distribution of polycyclic aromatic hydrocarbon (PAHs) in sediments in the Langat Estuary". Coastal marine Science, 30, 1, 2006, pp.387–395.

[7] Zakaria, M. P., Takada, H., Tsutsumi, S., Ohno, K., Yamada, J., Kouno, E., "Distribution of polycyclic aromatic hydrocarbons (PAHs) in rivers and estuaries in Malaysia: a widespread input of petrogenic PAHs". Environtal Science and Technology, 36, 2002, pp. 1907–1918.

INDEX

F

G

H

J

K

L

M

N

O

P

W

Y

Z

Contact Us:
6th Floor, Ports & Maritime Organization, Shahidi St.,
Shahid Haghani highway, Vanaq Sq., Tehran-Iran
Tel: +98 21 84932867
+98 21 84932272

Fax: +98 21 84932279
Email: icopmas@pmo.ir
icopmas@yahoo.com

http://icopmas.pmo.ir